Cyprus University of Technology

Faculty of Geotechnical Sciences and Environmental Management

Doctoral Dissertation

CO_2 Conversion to Acetic Acid by Acetogen-Enriched Microbial Inocula with H_2 Supplied by *In-Situ* Zero-Valent Metal Oxidation

Charis G. Samanides

Limassol, January 2025

CYPRUS UNIVERSITY OF TECHNOLOGY

FACULTY OF GEOTECHNICAL SCIENCES AND ENVIRONMENTAL MANAGEMENT

DEPARTMENT OF CHEMICAL ENGINEERING

Doctoral Dissertation

CO_2 Conversion to Acetic Acid by Acetogen-Enriched Microbial Inocula with H_2 Supplied by In-Situ Zero-Valent Metal Oxidation

Charis G. Samanides

Supervisor

Ioannis Vyrides

Associate Professor

Faculty of Geotechnical Sciences and Environmental Management

Cyprus University of Technology

Limassol, January 2025

Copyrights

The approval of the dissertation by the Department of Chemical Engineering does not necessarily imply the approval by the Department of the writer's views.

ACKNOWLEDGMENTS

I sincerely thank my supervisor, Dr. Ioannis Vyrides, for his continuous support throughout my doctoral studies. I am deeply grateful for the excellent cooperation we shared on various projects and for his unwavering encouragement of my efforts to expand my knowledge through seminars and workshops.

My heartfelt thanks go to Associate Professor Dr. George Konstantinide, Assistant Professor Dr. Loukas Koutsokera, Assistant Professor Dr. Marino Stylianou, and Dr. Maria Patsalou for our collaboration on several research projects.

Finally, I would like to thank the assistant secretary for studies, Mrs. Yiota Themistocleous, who was always willing to assist with any issues, and my fellow lab mates for their collaboration throughout these challenging years.

ABSTRACT

In the last decades, anthropogenic carbon dioxide (CO_2) emissions have increased dramatically, leading to excessive CO_2 levels in the atmosphere. This rise in CO_2 concentration has contributed significantly to global warming. For this reason, the European Union (EU) and the scientific community have been actively seeking solutions.

This study presents an innovative, cost-effective, and sustainable solution for CO_2 mitigation. This gas can be bioconverted into acetic acid by a mixed microbial consortium in a system supplemented with solid metals (zero-valent iron – Fe^0, magnesium – Mg^0, and waste iron – FeW) under mild, anaerobic, and carbonated conditions. The innovation focuses on producing the necessary H_2 gas *in-situ* - which serves as an electron donor and facilitates biological reactions - via the oxidation of metals to eliminate the reliance on external H_2 supply.

The first set of experiments investigates the oxidation of Fe^0 under anaerobic conditions for the production of abiotic H_2 by examining various parameters (temperature, pH, agitation, mechanical action, addition of $NaHCO_3$, etc). Results demonstrated that CO_2 is crucial in Fe^0 oxidation and H_2 generation. Higher H_2 production was observed at elevated temperatures, increased $NaHCO_3$ concentrations, slightly acidic conditions, and with finer Fe^0 particles. Siderite was identified as the primary oxidized product.

The second experimental set-up explored the use of Fe^0 *in-situ* under anaerobic conditions with microbial consortia (anaerobic granular sludge). Methanogenesis was inhibited through various methods, including pH adjustment, thermal sludge pretreatment, and chemical inhibitors [e.g., 2-bromoethanesulfonate (BES) and sodium chlorite]. Results showed that thermal pretreatment (yielding 1286 mg L^{-1} acetic acid after 12 days) and BES (yielding 2028 mg L^{-1} acetic acid after 28 days) effectively suppressed methanogenesis. However, high BES concentrations inhibited acetic acid production. *Clostridium sensu stricto* was the dominant microbial species in the thermally pretreated system.

In the third experimental set-up, the same methodology was applied with minimal alterations as in the second experimental set-up; however, iron was substituted with magnesium ribbon (Mg^0). Results indicated that the thermal pretreatment method effectively inhibited methanogenesis, producing the highest recorded acetic acid

accumulation (2023 mg L^{-1} after 32 days). Additionally, low concentrations of butyric acid were detected. Across all systems, *Methanolinea*, a typical hydrogenotrophic methanogen, was identified as the predominant microbial species.

The fourth experimental set-up expanded the scope by using seven different inocula (two environmental samples and five sludge types) exposed to anaerobic conditions with Fe^0 and low-concentration of BES. The study also compared acetate production by Fe^0-attached, Fe^0-detached, and suspended bacteria. Environmental samples exhibited the highest acetate production rates (maximum: 300 mg L^{-1}). *Acetobacterium* was the most abundant microbial genus. Systems utilizing Fe^0 showed enhanced acetate production, supporting the hypothesis of direct electron donation from solid metals.

The fifth experimental set-up examined acetic acid production in a continuous CO_2-feeding mode using two reactors connected in series and employing waste iron (both *in-situ* and *ex-situ*) within a circular economy framework. The experimental duration was divided into four phases: Phase A: *In-situ* with new waste iron, Phase B: *In-situ* with oxidized waste iron, Phase C: *Ex-situ* with thermally treated reactor with iron, Phase D: *Ex-situ* with uncontaminated new iron. The highest production rate (0.71 g L^{-1}) occurred during Phase A, where new waste iron was used. *Sporomusa* and *Acetobacterium* were the most abundant species. Thermal treatment in Phase C increased the prevalence of spore-forming bacteria like *Clostridium sensu stricto*, leading to the second-highest production rate (0.243 g L^{-1}).

The findings indicate that this innovative CO_2 utilization and value-added chemical production methodology is feasible and surpasses the limitations of conventional Carbon Capture and Utilization and Microbial Electrosynthesis Systems. Integrating sustainable practices, such as using waste metals, further enhances its potential as a viable solution for addressing environmental challenges.

Keywords: Acetic acid and bioethanol production, CO_2 utilization, Iron oxidation derived hydrogen, Magnesium ribbon, Methanogenesis inhibition, Zero valent iron.

TABLE OF CONTENTS

LIST OF TABLES

LIST OF FIGURES

LIST OF ABBREVIATIONS

3,4,5-TMB: 3,4,5-Trimethoxybenzaldehyde

AcCoA: Acetyl-Co-enzyme A (same as: WLP)

Ack: acetate kinase enzyme

Acs: Acetyl-CoA synthase

AD: Anaerobic digestion

Adh: Alcohol dehydrogenase enzyme

AdhE: Bi-functional aldehyde/alcohol dehydrogenase enzyme

Ald: CoA-dependent acetaldehyde dehydrogenase enzyme

AnGrSL: Anaerobic granular sludge

BES: 2-bromoethane sulfonate

BES: Bio-electrochemical system

CHE: Cathodic hydrogen evolution

CoA: Co-enzyme A

CODH: CO-dehydrogenase enzyme

CoFeSP: Corrinoid/Fe-S protein

DIET: Direct interspecies electron transfer

DSMZ: Deutsche Sammlung von Mikroorganismen und Zellkulturen GmbH

(German Collection of Microorganisms and Cell Cultures GmbH)

Ech: Fd-H^+ oxidoreductase complex

EtOH: Ethanol

F_{420}: Flavin 420 coenzyme (oxidized)

$F_{420}H_2$: Flavin 420 coenzyme (reduced)

FAD: Flavin adenine dinucleotide (oxidized)

$FADH_2$: Flavin adenine dinucleotide (reduced)

Fch: Formyl-THF cyclohydrolase

Fd^0 / Fd_{ox}: Ferredoxin (oxidized)

Fd^{2-} / Fd_{red}: Ferredoxin (reduced)

Fdh: Formate-dehydrogenase enzyme

Fe^0: Zero-valent iron

Fh: Formate hydrogenase

FhL: Formate hydrogenlyase

Fhs: Formyl-THF synthetase

Hyd: Hydrogenases

IFT: Interspecies formate transfer

IHT: Interspecies hydrogen transfer

IIET: Indirect interspecies electron transfer

mDIET: Mineral direct interspecies electron transfer

MECs: Microbial electrolysis cells

Mg^0: Zero-valent magnesium

MIET: Mediated interspecies electron transfer

Mthfd: Methylene-THF dehydrogenase

Mthfr: Methylene-THF reductase

mZVI: Micro zero-valent iron

NAD^+: Nicotinamide adenine dinucleotide (oxidized)

NADH: Nicotinamide adenine dinucleotide (reduced)

nZVI: Nano zero-valent iron

OmcS: Outer membrane cytochrome S

ORP: Oxidative-reductive potential

Pta: Phosphotransacetylase enzyme

Rnf: Fd-NAD^+ oxidoreductase

SAOB: Syntrophic acetate-oxidizing bacteria

SAO-HM: Syntrophic acetate-oxidizing bacteria coupled with hydrogenotrophic methanogens

SHE: Standard hydrogen electrode

TDS: Total dissolved sulfide

UASB: Up-flow anaerobic sludge blanket reactor

VFAs: Volatile fatty acids

WLP: Wood-Ljungdahl pathway

ZVI: Zero-valent iron (same as: Fe^0)

1. INTRODUCTION

1.1 Carbon Dioxide: Environmental Challenges and Global Response

Over the past decades, substantial interest has been focused on human activities that negatively affect the climate. Gaseous pollutants, such as carbon dioxide (CO_2), have emerged as a central focus in European Union (EU) discussions due to their significant role as greenhouse gases, affecting climate conditions and significantly impacting sustainability's economic and social pillars.

According to the Intergovernmental Panel on Climate Change (IPCC, 2023) Synthesis Report, during the first two decades of the twenty-first century (2001–2020), the global surface temperature increased by a maximum of 1.10°C compared to temperature data from 1850–1900. The same source indicates that CO_2 concentrations significantly increased from the Industrial Revolution (1750) to the present day, and the anthropogenic origins of CO_2 emissions are now widely recognized. Currently, CO_2 atmospheric levels are reaching 410 parts per million (ppm) based on 2019 data, which is higher than any point in the past two million years.

CO_2 not only contributes to the greenhouse effect but also negatively affects the sustainable development of societies, with both direct and indirect consequences. For instance, the American Chemical Society (ACS, 2023) stated that if greenhouse gas emissions continue to be produced uncontrolled, more extreme weather events will occur globally, exacerbating sea level rise and coastal degradation. Weather patterns will also intensify, affecting transportation and energy infrastructure, disrupting supply chains, and hindering business and industrial productivity. Ecosystems will also be impacted, and ongoing stress on natural resources will affect food and water supply, negatively affecting economies and societies. Furthermore, with higher rates of illness and death, human health will be affected, as well as increased frequency and spread of diseases, which will influence labor productivity.

The European Union (EU), concerned about the noticeable negative impacts on sustainability pillars due to increased levels of CO_2 in the atmosphere, is actively promoting policies and strategies to reduce emissions and mitigate climate change. Under this effort, the European Commission (EC, 2025), on 12th of December 2019, presented the European Green Deal (EGD), a comprehensive strategy aiming to make Europe

climate-neutral by 2050. Under this roadmap, all the 27-EU member states must reduce gas emissions by at least 55% by 2030, compared to 1990 levels, targeting several sectors for emissions reduction, such as aviation, maritime, and industry sectors.

According to Wolf et al. (2021), an analysis of Eurostat data revealed that CO_2 emissions in the EU reached 3.055 Mt in 2018. The authors emphasized that achieving carbon neutrality by 2050 will require a significant reduction in emissions, specifically a decrease of 1.943 Mt — equivalent to a 60% reduction — by 2030. This projection underscores the urgency of developing innovative and sustainable solutions for CO_2 mitigation to address the adverse impacts of rising atmospheric CO_2 levels and to meet the ambitious targets set by the EU.

1.2 Green Alternatives to Fossil Fuels and CO_2 Emission Reduction Strategies

Nowadays, various renewable energy (RE) technologies, such as solar, wind, hydro, and geothermal energy, are increasingly recognized as potential alternatives to fossil fuels. Ang et al. (2022) underscore the increasing attention given to these technologies due to their potential for zero emissions, which is especially critical in the face of the ongoing environmental crisis. However, these technologies also come with several significant challenges. For instance, Osman et al. (2023) stated that studies conducted in China and Europe show that despite using a significant proportion of renewable energy in power generation, the capacity utilization of these plants remains low. Furthermore, they note substantial monthly fluctuations in the energy supply, leading to imbalances in the energy grid on an interannual or seasonal basis. On the contrary, Rahman et al. (2022) delineate various drawbacks linked with renewable energy technologies, encompassing high implementation costs, short lifespans, challenges in energy storage, extensive land requirements, and the emission of CO_2 and toxic substances. Furthermore, Hache et al. (2019) introduce another factor that must be taken into consideration. The need for raw materials in developing RESs. The widespread adoption of low-carbon innovations would reduce reliance on fossil fuels; however, it can give rise to new and unforeseen interdependencies, particularly concerning raw materials — a phenomenon known as "raw material criticality." Al-Shetwi (2022) further underscores the absence of a supporting industry and a large-scale recycling system for these new raw materials, such

as neodymium, dysprosium, cadmium, tellurium, gallium, indium, and selenium, which are recently utilized, and actions are necessary to minimize future negative impacts through the implementation of comprehensive environmental impact assessments.

In addition to the expansion of renewable energy systems, scientists are actively working on strategies for capturing, storing, and utilizing CO_2 emissions from industrial processes. According to Lamberts-Van Assche and Compernolle (2022), these technologies are referred to as "Carbon Capture and Storage" (CCS) and "Carbon Capture and Utilization" (CCU). Using the first technology (CCS), CO_2 can be captured in large quantities at the source point of generation and then permanently injected and stored underground in a geological formation. On the other hand, using the second technology (CCU), the captured CO_2 can be used as a raw material for producing other added-value products. As explained by Park et al. (2022), CCU technologies attract scientific attention because CO_2 can be converted to several carbon-based products such as diamonds, graphene, fullerene, carbon nanotubes (CNTs), porous carbon, and carbon nanofibers (CNFs). However, as stated by the same scientist, this methodology is not as mature as the CCS.

Currently, four primary methods are employed for CO_2 capture: (a) absorption-based, (b) adsorption-based, (c) membrane separation, and (d) chemical looping combustion or reforming - an advanced combustion technology designed to produce energy while inherently capturing CO_2 (Peres et al., 2022; Al-Mamoori et al., 2017). These approaches utilize a range of materials, including solvents (e.g., $Ca(OH)_2$, NaOH, ammonia), porous solids (e.g., zeolites, graphene, carbon nanotubes), polymer-based membranes, and metal oxides (MeO). Despite their potential, these methods face significant challenges, including high implementation costs, material corrosiveness, toxicity, high energy demands for operations, regeneration of solvents or metals, and low CO_2 recovery rates (Peres et al., 2022; Al-Mamoori et al., 2017).

Dubey and Arora (2022) highlighted that the cost of CO_2 capture using these technologies can be up to $200 per ton of CO_2, depending on the application sector. Furthermore, Mikhelkis and Govindarajan (2020), believe that more than 3000 CCS projects must be implemented by 2050 in order to achieve the climate targets and reach sustainable goals.

1.3 Anaerobic Digestion Stages and the Role of Acetogens

Anaerobic digestion (AD) is a biological process where various organic macromolecule materials, such as animal manure, wastewater treatment sludge, energy crops, plant biomass, agricultural residues, and other sources of organic waste are brake down in the absence of molecular oxygen, by the action of a diverse group of bacteria and archaea that promoting the methanation (Fig. 1.1). The methanation process does not produce pure CH_4, but it generates biogas composed of 40% - 60% CH_4 and various other gases. Biogas typically includes 60% - 40% CO_2 and small amounts of hydrogen (H_2), oxygen (O_2), nitrogen (N_2), carbon monoxide (CO), hydrogen sulfide (H_2S), ammonia (NH_3), hydrocarbons, volatile organic compounds (VOCs), and siloxanes. The formation of CH_4-rich biogas is carried out by methanogenic microorganisms under thermophilic (55-60 ºC) or mesophilic (30-40 ºC) conditions. This gas is considered a promising fuel for electricity generation or heating due to its high calorific values, ranging between 21 and 25 MJ m^{-3}. At the end of the AD biochemical process, the remaining solids and organic matter can be used as a bio-fertilizer, known as digestate. This method is not used only for biogas and digestate production but also serves as a waste management and pathogen deactivation procedure, thereby representing a circular bioeconomy approach. (Uddin and Wright, 2023; Harirchi et al. 2022; Zhao et al., 2021; Menzel et al., 2020; Aryal et al., 2018; Bajpai, 2017).

Different types of bacteria work in a symbiotic association to carry out this complex fermentation process to form the final biogas product in AD. The fermentation products of one group of microorganisms can serve as a substrate for another distinct group of microorganisms. For this reason, AD can be divided into four distinct stages: a) hydrolysis, b) acidogenesis, c) acetogenesis/dehydrogenation, and d) methanogenesis (Uddin and Wright, 2023; Bajpai, 2017).

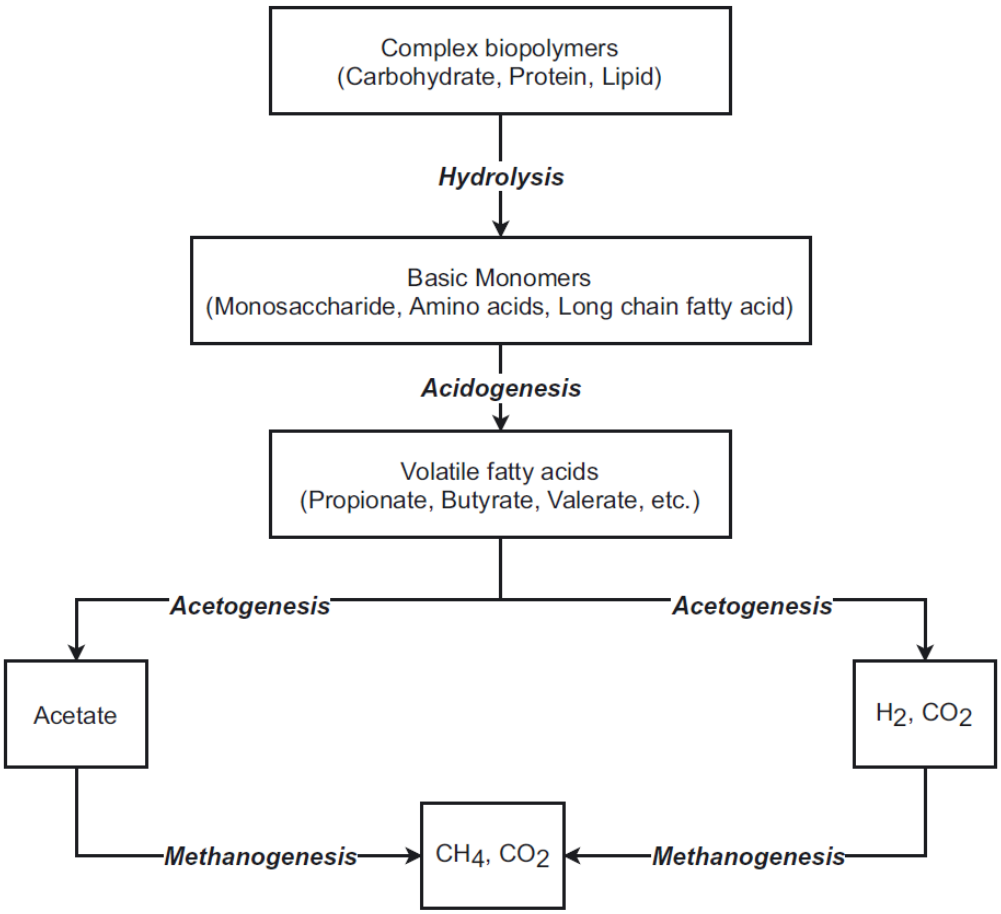

Fig. 1.1: Overview of the four stages of anaerobic digestion (AD) and the roles of bacteria and archaea in degrading complex polymer substrates for the production of acetate, methane, and carbon dioxide (Uddin and Wright, 2023).

During the hydrolysis stage, the complex biopolymers (starches, cellulose, proteins, and fats) are broken down by the action of extracellular enzymes (amylase, cellulase, lipase, protease, and pectinase) in the presence of hydrolytic bacteria. (Uddin and Wright, 2023; Menzel et al., 2020; Bajpai, 2017). However, when high lignocellulosic materials are present in AD, an alkaline pretreatment method, typically involving the use of NaOH, is often applied to enhance nutrient recovery, leading to higher methane production

(Mancini et al., 2018). However, according to Zhang et al. (2020), the addition of NaOH increases Na^+ ions in the AD system, which at low concentrations may stimulate microbial growth but, in excess, can result in severe inhibitory effects on the AD process.

The monomers produced in the previous stage are directed to an acid-forming step called acidogenesis, during which formic, acetic, propionic, butyric, and lactic acids are produced, along with byproducts such as CO_2, H_2, and ammonia (NH_3). During this stage, the pH (5-7) is much lower than the hydrolysis stage due to the production of volatile fatty acids (VFAs), resulting in digester toxicity and methanogenesis inhibition if the AD is left uncontrolled without supervision (Uddin and Wright, 2023; Menzel et al., 2020; Bajpai, 2017). According to Meng et al. (2018), excessive NH_3 production can inhibit methanogenesis; however, appropriate amounts serve as both a nitrogen source for microorganisms and an alkaline buffering agent. Lohani and Havukainen (2017) explain that the hydrolysis of amino acids and the formation of NH_3 enhance the bicarbonate-ammonia buffer, thereby increasing alkalinity. As a result, pH is effectively regulated, countering the acidification caused by the formation of VFAs and stabilizing the AD process. For this reason, alkalinity is considered a more reliable indicator of imbalances in the AD process than pH (Wang et al., 2018).

During the acetogenesis stage, acetogenic and homoacetogenic bacteria act for the transformation of higher organic acids derived from the hydrolysis and acidogenesis stage, into acetate, CO_2, and H_2. Syntrophic acetate-oxidizing bacteria (SAOB) convert acetate into H_2 and CO_2 - however, at standard conditions, this conversion is unfavorable and can be executed only at low H_2 partial pressure - where homoacetogens execute the opposite reaction. (Uddin and Wright, 2023; Pan et al., 2021; Menzel et al., 2020; Cai et al., 2019; Bajpai, 2017). This indicates that homoacetogens can produce acetate autotrophically from H_2/CO_2 in contrast with other VFAs produced at lower concentrations in AD via heterotrophic fermentative processes, which are propionate, isobutyrate, butyrate, and isovalerate (Palacios et al. 2025).

During the last methanogenesis stage, the reactants produced from the previous stage, such as acetate, are consumed by acetoclastic methanogens, and CO_2 and H_2 are consumed by hydrogenotrophic methanogens. Generally, the overall methane production at this stage is attributed to 28% by hydrogenotrophic methanogenesis and 72% by acetoclastic methanogenesis (Harirchi et al., 2022; Uddin and Wright, 2023). According

to Xie et al. (2023), methanogenesis is executed without the addition of H_2. However, the molar ratio of H_2/CO_2 can affect the metabolic pathway, and at elevated H_2 accumulations, the pathway shifts directly to the autotrophic hydrogenotrophic methanogenesis. For this reason, homoacetogens compete with hydrogenotrophic methanogens for autotrophic utilization of CO_2 and H_2 reactants for the production of acetate and syntrophically with acetoclastic methanogens indirectly for the utilization of acetate and methane formation (Xu et al. 2021).

As stated by Uddin and Wright (2023) and Liu et al. (2021), the performance of these stages is influenced by several key parameters, including the microbial species involved, the type of substrate, the temperature, the pH, the H_2 partial pressure in the system, the carbon-to-nitrogen ratio, the organic loading rate (OLR), and the hydraulic retention time (HRT).

1.4 Competitive Interactions Mechanisms Between Acetogens and Methanogens

As shown in Sub-chapter 1.3, methanogenesis activity that utilizes H_2 and acetate as reactants is based on syntrophic collaboration between H_2-producing syntrophic bacteria, homoacetogens, and methanogens. According to Fu et al. (2018), in such microbial population systems, H_2, which is observed to be at low concentration in anoxic systems, plays a crucial and significant ecological role in the coexistence of acetogens and methanogens that compete for H_2 down to the point of bioenergetic limitation. However, as shown in Table 1.1, which includes the primary biochemical reactions among the main microbial partners in AD, methanogenesis appears to be more favorable than acetogenesis/homoacetogenesis based on Gibbs free energy values.

According to Fu et al. (2019) and Zabranska and Pokorna (2018), the competition between homoacetogens and hydrogenotrophic methanogens for CO_2/H_2 utilization in AD systems is affected by temperature, which is the most crucial parameter for the existence of methanogens that influence acetate production or methanogenesis. At elevated temperatures (mesophilic and thermophilic ranges), hydrogenotrophic methanogens are enriched and act as the primary H_2 utilizers (Tsapekos et al., 2022).

Zabranska and Pokorna (2018) stated that this is why typical full-scale anaerobic digesters operate at 35–45 °C (mesophilic conditions), or at 55 °C to enrich thermophilic methanogens, or even higher, at 65 °C, to support hyperthermophilic species. Among these, *Methanosarcinaceae* is the most abundant genus at elevated temperatures. Recently, Laguillaumie et al. (2023) demonstrated that the inhibition of hydrogenotrophic methanogens was possible at 25 °C, enabling the selective enrichment of systems with acetate. On the other hand, hydrogenotrophic methanogens, particularly *Methanobacterium,* were enriched at 35 °C, promoting methane formation. Generally, acetogenesis is favored at lower and moderate temperatures, around 17 °C, as stated by Karekar et al. (2022). The preference for such psychrophilic conditions by homoacetogens is due to the lower energy yield under mesophilic and thermophilic conditions, approximately −18 kJ mol^{-1} to −48 kJ mol^{-1}, compared to hydrogenotrophic methanogens ($\Delta G = -67$ to -98 kJ mol^{-1}).

Regarding pH, hydrogenotrophic methanogens are reported to operate optimally at neutral pH (6–7) or in alkaline environments (8.5–9). In contrast, homoacetogens can function across a wide pH range, with their optimum at slightly acidic conditions (pH ~5.5) (Tsapekos et al., 2022).

Homoacetogens, such as *Acetobacterium wieringae, Acetobacterium woodii, Acetogenium kivui*, *Clostridium aceticum*, *Clostridium thermoautotrophicum,* and *Sulfurovum riftiae,* utilize CO_2 and H_2 to produce acetate (Harirchi et al., 2022). However, the oxidation of H_2 through hydrogenotrophic methanogenesis yields more energy ($\Delta G^o = -135.0$ kJ mol^{-1}) than homoacetogenesis ($\Delta G^o = -104.6$ kJ mol^{-1}) under standard conditions and at low H_2 concentrations. For this reason, CH_4 formation tends to dominate. As a result, the partial pressure of H_2 in the system can drop significantly. Li et al. (2019) reported that under such low-pressure conditions, interspecies hydrogen transfer (IHT) is promoted. Furthermore, the reduced H_2 partial pressure due to hydrogenotrophic methanogenesis facilitates the degradation of intermediates produced during the acidogenesis stage, such as propionate and butyrate (Baek et al., 2019). These degradation reactions are thermodynamically favorable only at very low H_2 pressures ($\sim 10^{-5}$ atm) (Zhu et al., 2020), ensuring optimal anaerobic digestion (AD) performance.

In contrast, elevated H_2 accumulations (>10 Pa) inhibit hydrolytic and fermentative microbial activities (Zhu et al., 2020). If H_2 partial pressure remains high, syntrophic oxidation of volatile fatty acids (VFAs) is thermodynamically unfavorable, leading to VFA accumulation and potential system failure (Zhao et al., 2021; Wang et al., 2021). Under such conditions, homoacetogens are enriched in the system due to their ability to thrive in diverse environmental conditions (Liu et al., 2021). Tsapekos et al. (2022) further explain that under stress and elevated $p(H_2)$ levels, homoacetogenesis becomes more favorable, while methanogens are generally less competitive.

As discussed in Sub-chapter 1.3, during the hydrolysis stage, proteins present in the feedstock of anaerobic digestion (AD) can be converted to ammonia, a chemical recognized as one of the most significant inhibitors in AD (Pan et al., 2021). It has been observed that at low concentrations (50–200 mg L^{-1}), ammonia has a positive effect on AD. This is because ammoniacal nitrogen benefits bacterial growth, not only by providing essential components for bacterial synthesis (e.g., proteins, amino acids, and nucleic acids) but also by acting as a base with a pH-buffering effect, neutralizing organic acids produced by fermentative bacteria (Jiang et al., 2019). However, at elevated concentrations, ammonia inhibits the activity of methanogenic archaea, particularly acetoclastic methanogens, while hydrogenotrophic methanogens are considered less sensitive to ammonia toxicity (Pan et al., 2021). Rocamora et al. (2023) recently explained that the oxidation of volatile fatty acids (VFAs) under high ammonia levels is thermodynamically unfavorable. Methane formation under these conditions is primarily attributed to the activity of syntrophic acetate-oxidizing bacteria (SAOB), which convert acetate into H_2 and CO_2, subsequently consumed by hydrogenotrophic methanogens such as *Methanosarcina*.

Regarding the inhibitory effect of ammonia stress on acetogens, Yang et al. (2024) reported that it is associated with a selective decline in specific acetogenic bacteria, including *Syntrophomonas*, *Syntrophus*, and *Desulfovibrio*. The reduction of *Desulfovibrio*, known for its ability to oxidize propionate and butyrate, leads to the accumulation of these acids in AD systems, further exacerbating methanogenesis inhibition.

In conclusion, homoacetogenesis is enhanced over hydrogenotrophic methanogenesis, which consumes reactants such as H_2 and CO_2, under the application of low temperatures and elevated H_2 pressures in a system with mixed microbial cultures.

Table 1.1: Overview of the main biochemical reactions of bacteria and archaea based on the available substrates under anaerobic conditions (Edited and formatted based on Pan et al., 2021, and Dyksma et al., 2020).

Substrate	Biochemical reactions in AD	ΔG^o (kJ mol^{-1})
Acetogenesis main reactions		
Propionate	$CH_3CH_2COOH + 2H_2O \rightarrow CH_3COOH + 3H_2 + CO_2$	+76.2
Butyrate	$CH_3CH_2CH_2COOH + 2H_2O \rightarrow 2CH_3COOH + 2H_2$	+48.4
Lactate	$CH_3CHOHCOOH + 2H_2O \rightarrow CH_3COOH + HCO_3^- + 2H_2$	-4.2
Ethanol	$CH_3CH_2OH + H_2O \rightarrow CH_3COOH + 2H_2$	+9.6
Homoacetogenesis reaction		
Hydrogen	$4H_2 + 2CO_2 \rightarrow CH_3COOH + 2H_2O$	-104.6
Syntrophic acetate oxidation reaction		
Acetate	$CH_3COOH + 2H_2O \rightarrow 2CO_2 + 4H_2$	+104.6
Methanogenesis main reactions		
Hydrogen	$4H_2 + CO_2 \rightarrow CH_4 + 2H_2O$ From SAOB: $CH_3COO^- + 4H_2O \rightarrow 2HCO_3^- + 4H_2 + H^+$	-135.6 +104.6 Total: -31.0
Acetate	$CH_3COOH \rightarrow CH_4 + CO_2$	-31.0
Formate	$4HCOOH \rightarrow CH_4 + 3CO_2 + 2H_2O$	-304.2
Methanol	$4CH_3OH \rightarrow 3CH_4 + CO_2 + 2H_2O$	-312.8
Ethanol	$2CH_3CH_2OH + CO_2 \rightarrow CH_4 + 2CH_3COOH$	-31.6

It is important to note that methanogenesis can occur not only through utilizing H_2 but also via converting formate to CH_4. Formate, along with H_2, serves as a major interspecies electron carrier in anaerobic digestion systems. Formate utilization pathways represent the more energetically favorable reactions in anaerobic environments (Pan et al., 2021),

as shown in Table 1.1. As Zhang and Zang (2019) explained, this favorable formate consumption by methanogens is attributed to the high solubility of this chemical compound, which demonstrated a concentration difference with H_2 by 1.000-fold, thus promoting long-distance electron transfer. Formate, can be produced during the first fermentation stages of AD (Zhang et al., 2023) as an intermediate product along with acetate and H_2 via propionate and butyrate degradation by syntrophic fatty acid-oxidation bacteria (SFOB) (Lv et al., 2020)

As shown in Fig. 1.2 and Fig. 1.3, for the production of CH_4 through the IFT and IHT, several enzymes are involved in the biochemical reactions of formate diffusion or oxidation to H_2. These enzymes include formate hydrogenase (Fh), formate dehydrogenase (Fdh), and hydrogenases (Hyd), which facilitate the formation of formate/H_2 (Zhang et al., 2023; Lv et al., 2020). The produced formate by the action of Fdh can be consumed by formate-utilizing methanogens (hydrogenotrophic) through the action of formate hydrogenlyase (FhL) (Zhang et al., 2023) that reduces protons to H_2 (Peters and Sargent, 2023). Furthermore, Zhang et al. (2023) stated that in such syntrophic methanogenesis, several redox intermediates evolved for e^- transferred for the production of H_2, such as NAD^+/NADH, FAD/$FADH_2$, and $Fd_{(ox)}$/$Fd_{(red)}$. It is also noted that the produsedby methanogens, coenzyme F_{420}, is involved in electron transfer between compounds within the cells (Grinter and Greening, 2021), and is reduced to $F_{420}H_2$ by the act of the enzymes hydrogenases, dehydrogenases, or alcohol dehydrogenases (Zabranska and Pokorna, 2018).

The IHT and IFT mechanisms described above, which explain the formation of CH_4 from formate/H_2, are both referred to as indirect or mediated interspecies electron transfer (MIET) (Harirchi et al., 2022; Wang et al., 2021). Besides MIET, a new, non-dependent enzymatic reaction mechanism, known as direct interspecies electron transfer (DIET), has also been proposed. According to this theory, electrons can transfer directly between microorganisms, thus promoting the syntrophic association for the formation of CH_4 (Chen et al., 2022).

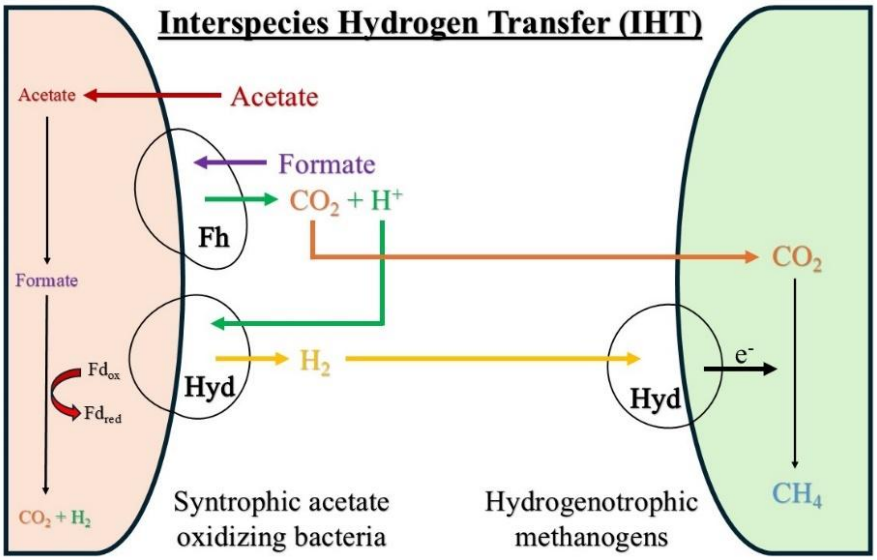

Fig. 1.2: A comprehensive outline of the IHT mechanism theory in CH_4 formation by hydrogenotrophic methanogens, highlighting the role of specific enzymes. (Edited and formatted based on information presented by Weng et al., 2024; Singh et al., 2023; Westerholm et al., 2022; Agne et al., 2021; Pan et al., 2021; Wu et al., 2020).

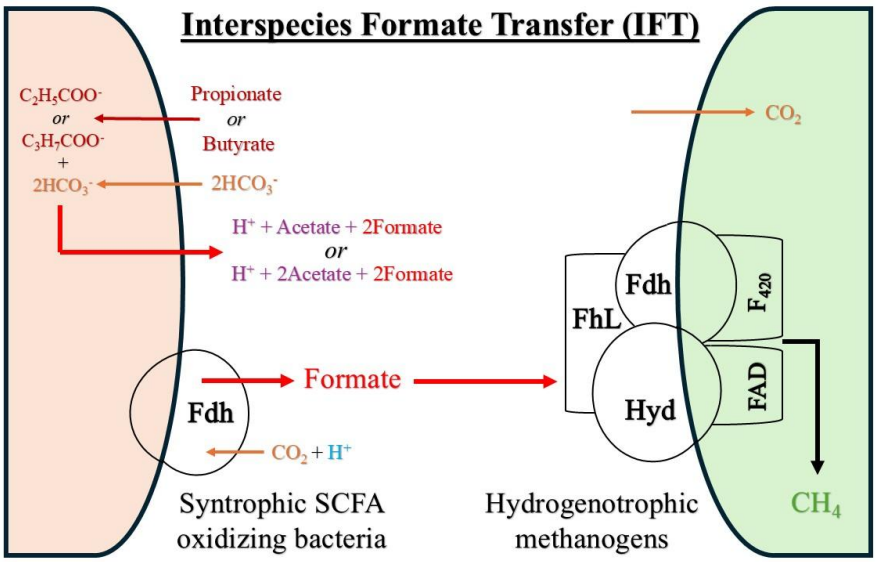

Fig. 1.3: A comprehensive outline of the IFT mechanism theory in CH_4 formation by hydrogenotrophic methanogens, highlighting the role of specific enzymes. (Edited and formatted based on information presented by Weng et al., 2024; Singh et al., 2023; Westerholm et al., 2022; Agne et al., 2021; Pan et al., 2021; Wu et al., 2020).

Several investigators (Harirchi et al., 2022; Wang et al., 2021; Wu et al., 2020; Li et al., 2019) believe that this alternative syntrophic metabolism mechanism based on direct electron connection is executed via 1) electric conductive pili (extracellular electron conduits), 2) c-type iron proteins-cytochrome (OmcS), or 3) conductive materials (Fig. 1.4). Baek et al. (2019), on the other hand, classify the DIET mechanism into two distinct categories. The biological DIET (bDIET), which is executed based on the existence of e-pili or microbial nanowires and through the existence of redox-active proteins as electrical connectors, and the mineral DIET (mDIET), which is executed based on the existence of conductive or semiconductive material complexes such as zero-valent iron (ZVI) or hematite, respectively. However, there is currently no strong evidence conclusively demonstrating this mechanism, and it does not fully explain the observed improvements in AD performance in many cases. Furthermore, there is no direct and clear protocol or combination of methodologies for the investigation and evaluation of the DIET idea in depth and real conditions (Van Steendam et al. 2019)

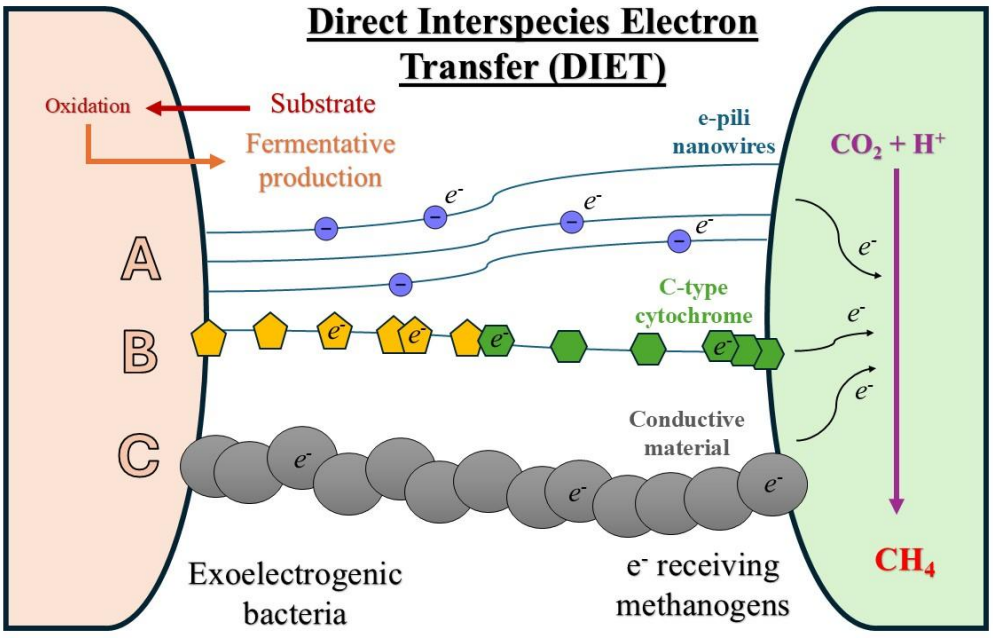

Fig. 1.4: A comprehensive outline of the three electron transfer mechanisms in DIET theory for the production of CH_4 by methanogenic archaea. **A:** electron transfer via conductive pili, **B:** electron transfer via c-type cytochrome, and C: electron transfer via conductive materials (Edited and formatted based on information presented in Sub-chapter 1.4).

When acetate is used as a reactant, the competition is between SAOB and acetoclastic methanogens. As shown in Fig. 1.2, the syntrophic partnership between hydrogenotrophic methanogen and SAOB gives the same stoichiometric energy production as acetoclastic methanogenesis, due to the formation of CH_4. Under these circumstances, hydrogenotrophic and acetoclastic methanogens compete for this small amount of energy (ΔG^o= -31.0 kJ mol^{-1}) and operate near the thermodynamic equilibrium. Under these circumstances, it can be stated that SAOB competes with homoacetogens, which produce acetate. Through the activity of SAOB, acetate is utilized to supply hydrogenotrophic methanogens with the necessary reactants (CO_2 and H_2). As a result, acetate levels decrease in the anaerobic system where these bacteria are present.

However, according to Zhang et al. (2023), CH_4 formation is predominantly driven by acetoclastic methanogens, accounting for 2/3 of the total production in AD. As explained by Pan et al. (2021), the predominance of acetoclastic methanogenesis is attributed to the fact that each microbe has its own energy needs, and the syntrophic association between acetate-oxidizers and hydrogenotrophic methanogens necessitates energetic disadvantages. As a result, acetoclastic methanogens such as *Methanosarcina* and strictly acetate-dependent *Methanosaeta* (Dyksma et al., 2020) can grow faster in the AD system. As highlighted by several investigators (Harirchi et al., 2022; Pan et al., 2021; Dyksman et al., 2020; Conrad, 2020; Lyu et al., 2018), various parameters can differentiate the population of acetoclastic methanogens in AD. For example, at low H_2 levels (consumed by hydrogenotrophic methanogens), acetate formation is promoted, resulting in the acidification of the procedure. Under these elevated VFA conditions, hydrogenotrophic methanogens are inhibited, and acetoclastic methanogens are increased. On the other hand, at elevated temperatures, acetoclastic methanogens are inhibited. Furthermore, substances such as ammonia, sulfide, and heavy metals can also shift the microbial population in AD. Generally, the synergistic association between SAOB, hydrogenotrophic methanogens, and acetoclastic methanogens negatively impacts acetate accumulation in the system.

1.5 The Superior Value of Acetic Acid Compared to Methane

Based on Sub-chapter 1.4, it is clear that AD is a complex process influenced by a range of interdependent factors, including environmental conditions, microbial interactions,

substrate composition, and operational parameters. As shown in Table 1.2, the average market price of methane is approximately 141.40 € ton^{-1}, which is considerably lower than the price of VFAs (such as acetic, propionic, and butyric acids), ranging from 377 to 2357 € ton^{-1}. Even in comparison with ethanol, the average market price of ethanol is about 80% higher than that of methane. Furthermore, a recent study by Castro-Fernandez et al. (2024) demonstrated the economic feasibility of scaling up VFA production through the utilization of food waste (FW). This research, based on an economic comparison between biomethane and VFA production, indicates that the net profit (€ ton^{-1} of FW) for VFA production is approximately 49% higher than that for CH_4 production. In the same manner, Liu et al. (2018) show that by utilizing sewage sludge (SL) in a full-scale project, the net profit (€/m^3 of SL) for VFA production was even higher (59%) than that of methane.

Table 1.2: Overview of primary AD metabolites and their prices, listed from least to most expensive (Rizzioli et al., 2024; Dai et al., 2020).

AD metabolites	Market price (€ ton^{-1})
Methane	94.27 – 188.53
Acetic acid	377.07 – 754.14
Ethanol	471.31 – 942.67
Propionic acid	1178.34 – 1602.55
Hydrogen	754.14 – 1696.81
Lactic acid	942.67 – 1979.62
Butyric acid	1885.35 – 2356.69
Caproic acid	1885.35 – 2356.69
Caprylic acid	3299.36 – 3676.43
Valeric acid	3634.54 – 4049.92

Based on the fact that VFAs are valuable in several industries (chemical, food, and plastic) as a platform chemical, and the significant economic potential that VFAs exhibit, many researchers are now evaluating the suppression of methanogenesis in mixed culture systems to enhance the production of VFAs.

Specifically, acetate (acetic acid), which is one of the main components produced by the fermentation of CO_2 and H_2 as a substrate by acetogens in a methane-inhibited system, is characterized as a bulk chemical (Zhang et al., 2022). Acetic acid, which is an organic acid, is the second simplest and most important carboxylic acid with global economic relevance (Kiefer et al., 2021). Generally, the chemical industry broadly uses it for the production of several added-value products such as vinyl acetate monomer, polyvinyl acetate, cellulose acetate, acetate esters, acetic anhydrate, and mono-chloroacetic acid. Furthermore, it is used even for the production of synthetic fibers and fabrics, as a food additive in the food industry (Mutyala and Kim, 2022), and as a substitute feedstock for the production of biofuels (Kim et al. 2021). According to Mytyala and Kim (2022), acetic acid, as a simple platform chemical, currently attracts scientific interest in synthesizing targeted chemicals through genetic engineering in microbial systems, serving as an alternative feedstock.

In 2019, the global market for acetic acid reached 8.6 billion US$ with 17.3 million tons of production, and it is expected to reach 12 billion US$ with a production of 24.5 million tons by 2025 (Kiefer et al. 2021). According to the Global Acetic Acid Market Report and Forecast for the years 2024-2032 (Polaris Market Research, 2024), the market for acetic acid is expected to grow further by 2032 and will stand at around US$ 36.36 billion. For this reason, LaBelle and May (2017) stated that the scientific community has made significant efforts to enhance the efficiency and production rates of acetic acid through acetogenesis and the utilization of CO_2 and H_2, or via bio-electrochemical methods. Additionally, Mytyala and Kim (2022) note that new large-scale production techniques are being developed to meet market demand and reduce the carbon footprint. Acetate is now selling for between US$ 350 and US$ 450 per ton, which is somewhat less than the price of US$ 500 per ton for glucose (Gu et al., 2024)

Today, approximately 75% of acetate is synthesized chemically via methanol carbonylation, ethylene oxidation, or alkane oxidation (Kim et al. 2021).

1.6 Common Strategies for Methanogenesis Inhibition

As summarized in Table 1.3, various recent methods for enhancing acetate production from CO_2 and H_2 are reviewed. It is evident that BES has been extensively used at different concentrations to inhibit methanogenesis in batch experiments or microbial electrochemical systems (MES). However, no comprehensive studies have been conducted to determine the optimal BES concentration for these systems, which could minimize the use of excess inhibitors and reduce costs. For instance, Lou et al. (2024) and Omar et al. (2018) employed BES at concentrations exceeding 10 g L^{-1} in batch experiments, representing the maximum concentration generally used. In contrast, Tharak et al. (2023) used only 0.2 g L^{-1} of BES in a batch experiment conducted in a single-chamber MES system.

Alternative approaches for methanogenesis inhibition include thermal pretreatment of inoculum at temperatures above 70 °C for durations ranging from 15 minutes to 2 hours, as well as the use of acidic treatments or a combination of these methods. However, some investigators (Chaikitkaew et al., 2024; Wang et al., 2024; Roy et al., 2024; Im et al., 2023; Bayar et al., 2022) have opted to avoid the above methodologies or the use of specific methanogenesis inhibitors altogether by employing pure microbial strains in bottle experiments or MES systems. However, these methodologies pose a significant risk of contamination.

Lou et al. (2024) successfully inhibited methanogenesis by applying approximately 55 mM L^{-1} of BES in batch experiments conducted at pH 7 and 36ºC. The experiments were inoculated with wastewater sludge that had been previously acclimatized in MCFA conditions. Zero-valent iron (ZVI) in various sizes was used as an electron donor. After 70 days, *Romboutsia*, *Clostridium sensu stricto 12*, and *Paraclostridium*, all members of the Firmicutes phylum, were observed as the predominant genera. On the other hand, Tharak et al. (2023), by applying three different methodologies for methanogenesis inhibition (as shown in Table 1.3), found that thermal pretreatment of wastewater sludge resulted in the highest acetate production in batch experiments conducted at pH 7.2. Similarly to Lou et al. (2024), after 47 days, Tharak et al. (2023) identified Clostridia family microbes, with the genus *Clostridium celatum* predominating (37%). *Clostridium butyricum* (7%), *Clostridium perfringens* (3%), and *Clostridium subterminale* (2%) were

also identified. The same Clostridium genus was also identified by He et al. (2022) using thermal pretreatment (90°C for 15 minutes) of anaerobic granular sludge.

Roy et al. (2021) used a two-chambered MEC system to produce acetate at pH 6-7 and 28ºC. The system was inhibited for methanogenesis with approximately 34 mM of BES, and wastewater sludge enriched with *Acetobacterium* (28%) was used as the inoculum. After 29 days, *Acetobacterium*, *Pseudomonas*, *Sulfurospirillum*, and *Desulfovibrio* were the major genera, accounting for 11%, 26%, 13%, and 9%, respectively, with *Acetobacterium* being the only acetogen.

Omar et al. (2018) applied heat pretreatment of sewage sludge at two distinct temperatures (70°C and 90°C for 30 minutes) to inhibit methanogenesis. Batch experiments were inoculated and exposed to pH 6 and 37ºC. After 10 days, *Methanobacterium beijingense 1* (37.9%) and *Methanobacterium formicicum 4* (40.4%) were the most dominant methanogens after the sludge was exposed to 90ºC and 70ºC, respectively. *Desulfovibrio vulgaris* and *Desulfovibrio oxamicus* were also identified at 90ºC and 70ºC, indicating a syntrophic interaction with methanogens. Higher acetate production was observed when the system was exposed to BES, and *Acetoanaerobium noterae 10* (6.37%) was identified as a homoacetogen.

Yang et al. (2021) used acetogen-enriched sludge in an MEC system inhibited with 10 mM of BES and operated at pH 5.5, exposed to different temperatures (12, 25, 35, 55, and 70ºC). They observed that acetogen populations were higher under mesophilic conditions (25°C and 35°C) than in thermophilic (55°C and 70°C) and psychrophilic conditions (10°C). The dominant genera included *Clostridium*, *Treponema*, *Acidithiobacillus*, *Acetobacterium*, and *Acetoanaerobium*.

Based on the experimental observations above, at the class level, Clostridia were the most dominant bacteria, along with *Acetobacterium*, under mesophilic and pH-neutral conditions. BES inhibition was found to be more effective for methanogenesis inhibition compared to the thermal pretreatment method. After thermal treatment, it was observed that methanogenic archaea could survive and become enriched in the systems. However, to date, no one has examined the effect of different concentrations of BES on both methanogenesis and acetogenesis.

Table 1.3: Overview of experimental methodologies for methane inhibition in recent studies aimed at enhancing acetate production.

Implementation	Inoculum	Carbon Source	Electron donor	Methanogenesis inhibition methods	Fermentation products	References
Reactor for immobilization and Batch experiments	*Clostridium thailandense* (free cells and immobilized)	Synthetic biogas (CO_2:CH_4 = 40%:60%)	100% H_2 mixed with biogas H_2:CO_2 = 2:1	**Use of a pure acetogenic strain**	Acetate	Chaikitkaew et al., 2024
Batch experiments and bioreactor	1: *Acetobacterium woodii* (DSM 1030) 2: *Megasphaera hexanoica* (DSM 106893)	CO_2 (1 bar) Lactic acid: 10 g L^{-1}	Batch experiment - ZVI (149-297 µm): 1, 3, 5, 10 g L^{-1} Bioreactor - ZVI (149-297 µm): 3 g L^{-1}	**Use of a pure acetogenic strain**	Acetate Butyrate caproate	Wang et al., 2024
Batch experiments	*Fonticella tunisiensis* HN43	CO: 40% CO_2: 40%	12.5 g L^{-1} ZVI (1-2mm)	**Use of pure strain**	Acetate Butyrate Methane	Im et al., 2023
Batch experiments and bioreactor	1: *Clostridium aceticum* (DSM 1496) *2: Clostridium carboxidivorans* (DSM 15243)	CO_2: 0.5-4 bar	Batch set 1 & 2: 25 g L^{-1} ZVI Reactor: 50 & 75 g L^{-1} ZVI	**Use of a pure acetogenic strain**	Acetate Ethanol	Bayar et al., 2022
Batch experiments	Wastewater mixed culture (60 days acclimatized in MCFAs)	CO_2: 20%	10 g L^{-1} ZVI (75µm, 250µm) 0.12 mol L^{-1} Sodium acetate 0.36 mol L^{-1} Ethanol	**BES: 10.5 g L^{-1}**	Caprylate Butyrate Caproate	Lou et al. 2024

Implementation	Inoculum	Carbon Source	Electron donor	Methanogenesis inhibition methods	Fermentation products	References
Batch experiments and single-chamber MES system	Anaerobic consortia from sewage treatment plant	Batch experiments - CO_2:H_2 = 1:4 MES system - CO_2: 0.6 ml min^{-1}	Batch experiment: H_2 MES system: electrode	**Batch experiment - BES: 0.2 g L^{-1}** **Pretreatment - Heat-shook 80°C for 2 h, and Acid-shook with H_3PO_4 (pH 3) for 10 h**	Acetate	Tharak et al., 2023
Batch experiments and two-chamber MES system	1: Enriched wastewater sludge 2: *Clostridium ljungdahlii* (DSM13528)	1: Industrial CO_2 (97.91%) with O_2 (0.356%) or pure CO_2 2: CO_2:H_2 = 1:2	Electrode	**BES: 6.4 g L^{-1}**	Acetate	Roy et al., 2021
Batch experiments	Sewage sludge	H_2:CO_2:CH_4 = 1,2,3,4:1:1.5	H_2	**Enrichment stage - BES: 10.40 g L^{-1}** **Heat-shock 70°C and 90°C for 30 min** **Experimental stage - BES: 10.40 g L^{-1}**	Acetate	Omar et al., 2018
Batch experiments and bioreactor	Batch exp. - Waste water anaerobic consortium Reactor exp. - Homoacetogen enriched anaerobic consortium	Batch exp. - CO_2:H_2 = 20%:80% Reactor exp. - CO_2:H_2 mixture at 2 bars	H_2	**Batch experiment –** **1: Heat-shock 80°C for 2 h** **2: Acid-shock with H_3PO_4 (pH3) for 24 h** **3: Acid + Head shock**	Acetate Butyrate	Modestra et al., 2020
Batch enrichment: H2 MES system: electrode	Enrichment stage: anaerobic sludge Acetogenic enriched inoculum	Enrichment stage - CO_2:H_2 = 20%:80% CO_2: 10ml min^{-1}	Batch enrichment - H_2 MES system - electrode	**BES: 2.08 g L^{-1}**	Acetate	Yang et al., 2021

Implementation	Inoculum	Carbon Source	Electron donor	Methanogenesis inhibition methods	Fermentation products	References
Two-chamber MES system - Continuous	Homoacetogenic enriched inoculum	3.68 gr $NaHCO_3$ in total at each phase	Phase 1-Stage 2: 5 g L^{-1} nZVI (100 nm) Phase 2: 7.5 g L^{-1} nZVI (100 nm)	**BES: 2 g L^{-1}**	Acetate Butyrate Caproate	Wu et al., 2023
Semi-continuous fed-batch bioreactor	Acetogen-enriched anaerobic granular sludge	CO_2:H_2 = 80%:20% 100% H_2 Flow rate: 10 ml min^{-1}	H_2 Tungsten: 1.84 mg L^{-1}	**Heat-shock 90°C for 15 min**	Acetate Butyrate Propionate Caproate Valerate Ethanol	He et al., 2022
Batch experiments	Anaerobic granular sludge	CO_2:H_2 = 20%:80% CO_2:H_2 = 20%:80% + 2.1 g L^{-1} $NaHCO_3$	H_2	**Heat-shock 90°C for 15 min.**	Acetate Ethanol	He et al., 2021

1.7 Acetogens: Carbon Bio-Fixation to Acetic Acid and Biofuels via the Wood-Ljungdahl Pathway.

Despite the various strategies proposed nowadays for energy transition, the production of CO_2 remains inevitable, persisting at high concentrations in the atmosphere with a negative impact on the climate, as elucidated in Sub-chapter 1.1. Hence, CO_2 emissions will remain a challenge for a few more decades. Therefore, new challenges emerge in identifying innovative and cost-effective approaches that utilize CO_2 as a complementary feedstock to support future decarbonization efforts.

To achieve the above objective, an alternative possibility is leveraging the metabolic pathways of specific bacteria as an economically sustainable process for CO_2 valorization into bio-commodities and/or biofuels. This dissertation proposed the use of Acetogenic bacteria that can reduce two mol of CO_2 with co-enzyme A (CoA) to give one mol of acetyl-CoA, which is further converted to acetyl-phosphate, which can be further converted to C2-products like acetic acid or ethanol while simultaneously oxidizing inorganic electron donors such as H_2 (Kremp et al., 2022; Katsyv and Müller, 2020).

According to Ruiz-Fernández et al. (2020), nowadays, six distinguished autotrophic carbon fixation pathways are recognized, such as: 1) the Calvin-Benson-Bassham cycle (CBB), 2) the reductive tricarboxylic acid cycle (TCA), 3) the 3-hydroxypropionate bicycle (3HP), 4) the 3-hydroxypropionate/4-hydroxybutyrate cycle (3HP/4HB), 5) the dicarboxylate/4-hydroxybutyrate cycle (DC/4HB), and 6) the reductive Acetyl-CoA or Wood-Ljungdahl pathway (AcCoA - WLP). The CBB cycle is considered the most common process conducted by photo-synthesizers, where the CO_2 relates to a reactive group (carboxylation) and is then reduced, producing organic compounds. More than 90% of CO_2 is fixed through this cycle, contributing to the global synthesis of organic matter (Feng et al., 2023; Ruiz-Fernández et al., 2020; Lemaire et al., 2020). On the other hand, WLP is the only linear pathway that reduces CO_2 before carboxylation for AcCoA. Hence, this pathway is considered to be the most efficient, simplest, and non-photosynthetic CO_2-fixing pathway despite operating on the verge of thermodynamic feasibility (Yang et al., 2021; Lemaire et al. 2020; Valgepea et al. 2017). Igarashi and Kato (2017) highlighted that acetogens can serve as biocatalysts for converting CO_2 into valuable organic compounds, owing to the energy efficiency superiority of their pathway compared to others. Furthermore, Litty and Müller (2021) noted that specific strains of

acetogens not only contribute positively to carbon capture and storage but also represent promising candidates for H_2 production or storage.

Acetogenic bacteria, or Acetogens, are phylogenetically diverse, omnipresent, strictly anaerobic bacteria (Litty and Müller, 2021) that are represented by 29 genera, and more than 100 different species account for this group. This kind of bacteria is known for its ability to produce acetate via acetogenesis, as indicated by its name. Generally, due to most of these microorganisms can produce only acetate as their fermentation product, sometimes referred to as Homoacetogens (Kim et al., 2023). The acetogenesis was first introduced by F. Fischer and associates back in 1932, who discovered that microbial consortium present in sewage can utilize H_2 and CO_2 to acetate, where the first mesophilic strain (*Clostridium aceticum*) isolated from soil and was published by K. T. Wieringa in 1936. In 1942, the second thermophilic acetogen was isolated (*Clostridium thermoaceticum*) from horse manure by F. E. Fontaine and associates. Both strains are spore-forming bacteria. However, they can utilize different substrates to produce acetate (Drake et al., 2008), as indicated in Eqs. 1 and 2 (Ragsdale and Pierce, 2008).

$$2CO_2 + 4H_2 \underset{\text{aceticum}}{\overset{\text{Clostridium}}{\rightleftharpoons}} CH_3COO^- + H^+ + 2H_2O \quad \Delta G^o = -95 \text{ kJ mol}^{-1} \qquad \text{(Eq. 1)}$$

$$C_6H_{12}O_6 \xrightarrow[\text{thermoaceticum}]{\text{Clostridium}} 3CH_3COO^- + 3H^+ \quad \Delta G^o = -310.9 \text{ kJ mol}^{-1} \qquad \text{(Eq. 2)}$$

As stated by Kim et al. (2023) and supported by the above ability to utilize different substrates, acetogenic bacteria demonstrate adaptability to distinct environmental conditions. They can survive under different temperatures and a broad range of pH levels. According to Drake et al. (2002), Acetogens, due to their versatility to service under a wide range of conditions, can inhabit several environments. Hence, it is often difficult to detect them, as they occupy niches that are frequently overlooked, suggesting that acetogens may be more ubiquitous than previously recognized, influencing various habitats.

To date, acetogens have been discovered in a variety of environments. For instance, bacteria utilizing the WLP have been isolated from WWTP samples, soils, hypersaline

waters, rivers, compost samples, animal rumen fluids, and termites, mostly using H_2 and CO_2 as substrates. Acetogenic bacteria were isolated even from metallic iron, which is used by bacteria (MIC) as an electron donor (Table 1.4).

Table 1.4: Overview of Acetogenic bacteria isolated from diverse sources.

Isolated strains			
Sp.	**Source**	**Substrate**	**Ref.**
Terrisporobacter	Horse feces, river sediment, digest sludge, and compost	$H_2 : CO_2$	Böer et al., 2024
Acetoanaerobium	Digested sludge		
Clostridium	Rumen fluid samples of Murrah buffaloes	$H_2 : CO_2$	Choudhury et al., 2023
Eubacterium limosum			
Acetobacterium woodii			
Clostridium muellenanum	Old hay	$CO : CO_2$, $H_2 : CO_2$	Doyle et al., 2022
Clostridium thailandense	Peatland soil	$H_2 : CO_2$	Chaikitkaew et al., 2024
Natranaerofaba carboxydovora	Hypersaline soda lake	CO	Sorokin et al., 2020
Clostridium	WWTP – sewage sludge	Wastewater sludge	Huang et al., 2020
Acetobacterium malicum	DSMZ	Fe^0, CO_2	Philips et al., 2019
Acetobacterium wieringae			
Sporomusa sphaeroides			
Clostridium carboxidivorans	Agricultural settling lagoon	CO, $H_2 : CO_2$	Liou et al., 2005
Treponema primitia	Termite hindguts	$H_2 : CO_2$	Graber and Breznak, 2004
Acetobacterium tundrae	Tundra soil	$H_2 : CO_2$	Simankova et al., 2000
Sporomusa	Anoxic Rice soil	Ethylene glycol, 2,3-butanediol, 3,4,5-TMB	Rosencrantz et al. 1999

As indicated in Table 1.4, Acetogens can utilize several substrates, and as highlighted by Schuchmann and Müller (2016), this ability of WLP to be combined with a wide range of electron donors gives the Acetogens the ecological and energetic advantage through the redox balancing compared to classical fermentation. However, it predominantly

grows chemolithoautotrophically by using CO_2 or HCO_3^- as a carbon source (electron acceptor) and H_2 as the energy source (Frolov et al., 2023). Acetogens also develop heterotrophic capabilities. Organic substrates such as alcohols, organic acids, sugars, aldehydes, and aromatic compounds can be utilized by Acetogens. Furthermore, it can also use alternative electron acceptors such as Fe^{3+}, sulfate, thiosulfate, nitrate, nitrite, perchlorate, dimethylsulfoxide, fumarate, and others. The ability of acetogens to utilize several organic substrates makes them an essential part of anaerobic digestion (AD). They work synergistically with microbial communities such as methanogens, which use the produced acetate, the end product of acetogenesis (Frolov et al., 2023).

1.7.1 The Wood-Ljungdahl Pathway (WLP)

According to Appel et al. (2013), WLP is used by both methanogenic archaea and bacteria for anabolic (biosynthesis) and catabolic (energy) purposes through the use of CO_2 and the synthesis of acetyl-CoA. The utilization of CO_2 can be achieved through two steps of reduction. The first step is associated with the reduction of CO_2 to formate through the catalytic action of the formate-dehydrogenase enzyme (Fdh), and the second step involves the action of the CO-dehydrogenase enzyme (CODH) for the reduction of CO_2 to CO.

These two distinguishing steps included in the linear pathway are referred to as methyl and the carbonyl branch, respectively (Takors et al., 2018). Sometimes referred to as the eastern and western branches, both combined to produce a central intermediate acetyl-CoA, a precursor for acetate formation as the end product (Karekar et al., 2022).

As shown in Fig. 1.5, the eastern or methyl branch starts with the action of the formate dehydrogenase enzyme that utilizes NAD(P)H as a reducer (electron donor) for the reduction of CO_2 to formate (Debabov, 2021; Litty and Müller, 2021).

Müller (2019) proposed that during autotrophic growth, the electron-bifurcating hydrogenase is involved in the activation of H_2 and, as a result, NAD(P)H and reduced ferredoxin (Fd_{red} or Fd^{2-}) are produced (Frolov et al., 2023).

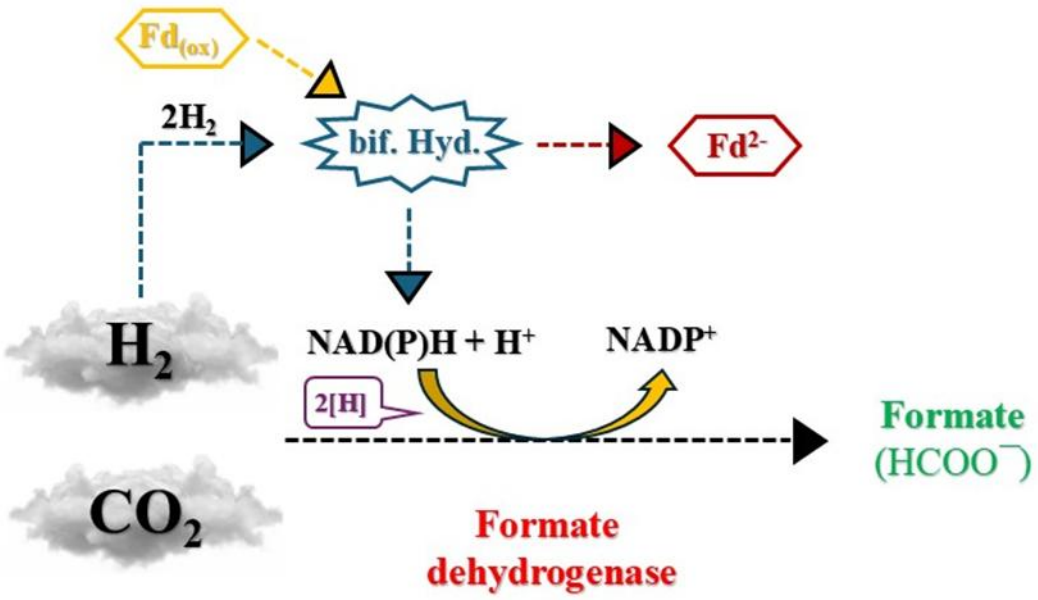

Fig. 1.5: Graphic representation of the methyl (eastern) branch of the Wood–Ljungdahl pathway up to the point of formate production.

Subsequently, the produced formate (formyl group), through the action of formyl-THF synthetase (Fhs), binds to a C1-carrier tetrahydrofolate (THF) and formyl-tetrahydrofolate is produced. Conversely, one ATP molecule is hydrolyzed to carry out the above reactions (Kim et al., 2023; Debabov, 2021; Yang et al., 2021; Katsyv and Müller, 2020; Litty and Müller, 2021; Esposito et al., 2019) as shown in Fig. 1.6.

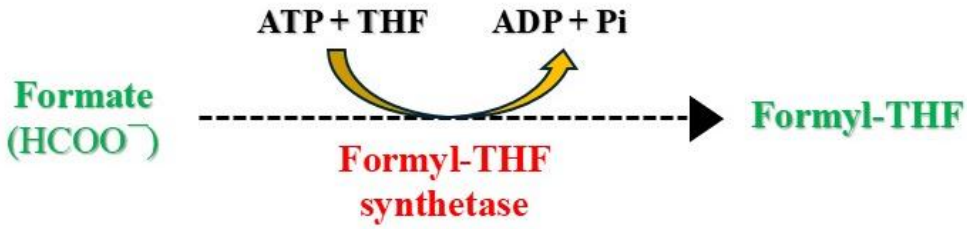

Fig. 1.6: Graphic representation of the formate condensation with THF in the methyl (eastern) branch of the Wood–Ljungdahl pathway for the generation of formyl-THF.

Subsequently, in the sequence of reactions, the formyl-THF cyclohydrolase enzyme (Fch) is involved, and Formyl-THF is further metabolized to Methenyl-THF through water release. Following, methenyl-THF is catalyzed by methylene-THF dehydrogenase (Mthfd), and NAD[P]H is used as an electron donor. Then, through the action of methylene-THF reductase (Mthfr) the methylene-THF is reduced to methyl-THF. Acetogens to catalyze the THF-bound methylene group used electrons derived via reduced ferredoxin produced at the first step of methyl (eastern) branch by electron bifurcating hydrogenase or can use NADH as an electron donor. Generally, four hydrogen equivalents are necessary for the reduction reactions of the methenyl-THF to methyl-THF. Finally, the methyl group is transferred onto a specific protein that contains iron-sulfur clusters and cobalamin (corrinoid/Fe-S protein - CoFeSP) by the action of the methyl transferase enzyme, as shown in Fig. 1.7 (Frolov et al., 2023; Kim et al., 2023; Debabov, 2021; Yang et al., 2021; Katsyv and Müller, 2020; Litty and Müller, 2021; Esposito et al., 2019).

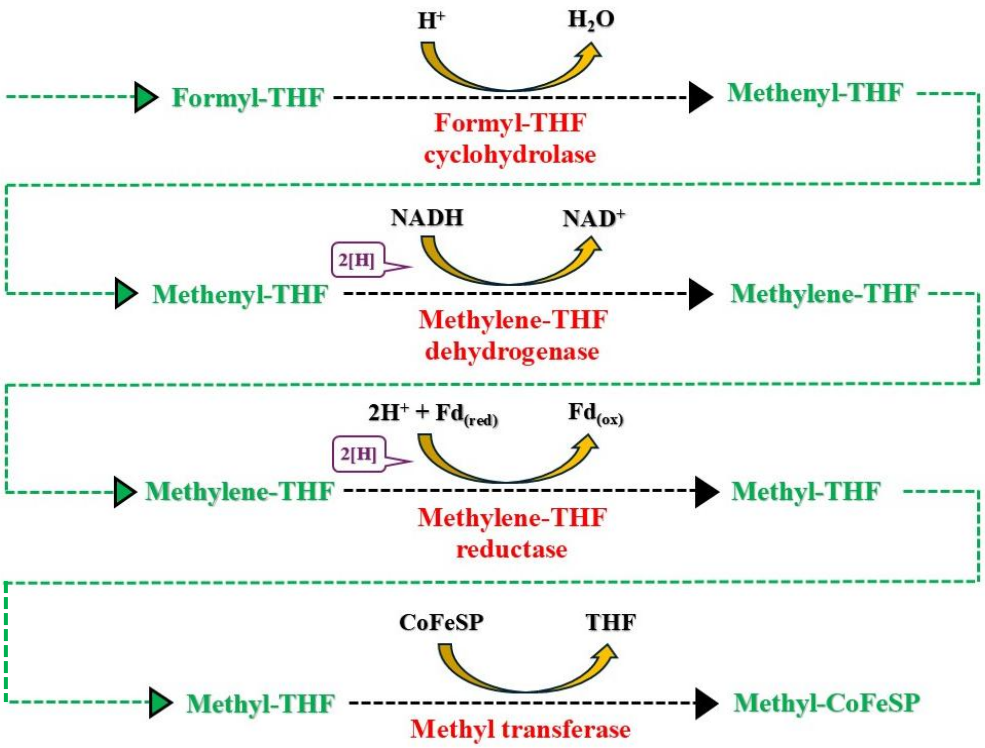

Fig. 1.7: Graphic representation of the tetrahydrofolate pathway reactions in the methyl (eastern) branch of the Wood–Ljungdahl pathway.

The methyl branch with the corrinoid iron-sulfur protein (Methyl-CoFeSP) can be transmitted to the last step, where a central intermediate, called Acetyl-CoA, is produced. This enzyme is a precursor for the synthesis of bacterial anabolic biomass.

At this point, the western or carbonyl branch of the WLP, contributes to the formation of acetyl-CoA by utilizing a second CO_2 molecule. During this reaction, the carbon monoxide dehydrogenase enzyme (CODH) reduces the CO_2 to CO. The already produced Methyl group (Methyl-CoFeSP) by the eastern branch, along with the CO produced by the western branch in the presence of coenzyme A (CoA), are catalyzed by the CODH and acetyl-CoA synthase (Acs) enzymes (Fig. 1.8). These two stable complex enzymes are characterized as the key enzymes of all WLP. Most acetogens utilize acetyl-CoA not only for anabolic biomass synthesis but also for producing bio-commodities and biofuels through catabolic processes (Frolov et al., 2023; Debabov, 2021; Yang et al., 2021; Katsyv and Müller, 2020; Litty and Müller, 2021; Esposito et al., 2019; Schoelmerich and Müller, 2019; Schuchmann and Müller, 2016).

.

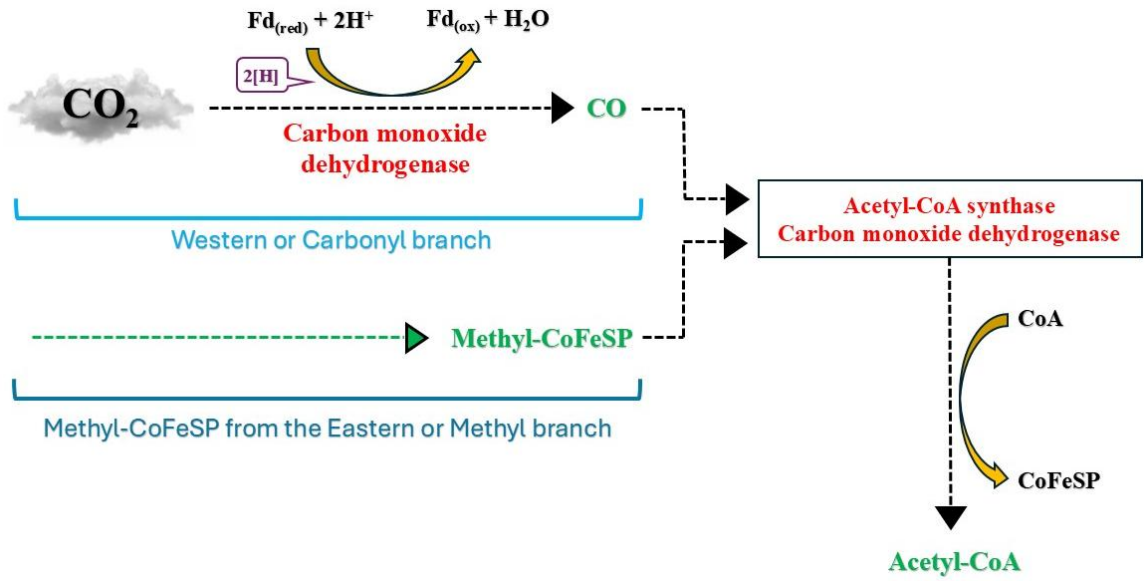

Fig. 1.8: Graphic representation of the Acetyl-CoA production by catalyzing the methyl group and CO that are produced by the methyl (eastern) and carbonyl (western) branches of the Wood–Ljungdahl pathway, respectively, by the action of acetyl-CoA synthase and carbon monoxide dehydrogenase.

As demonstrated in Eqs. 3 and 4, the utilization of CO in the WLP is more favorable.

$$2CO_2 + 4H_2 \rightarrow CH_3COOH + 2H_2O \quad (\Delta G° = -95 \text{ kJ mol}^{-1}) \qquad \text{(Eq. 3)}$$

$$4CO + 2H_2O \rightarrow CH_3COOH + 2CO_2 \quad (\Delta G° = -175.0 \text{ kJ mol}^{-1}) \qquad \text{(Eq. 4)}$$

However, due to the very low solubility of CO in aqueous solutions, the reactions shift to Eq. 3 (Bae et al., 2022; Debabov, 2021; Takors et al., 2018).

Once acetyl-CoA is formed as a key precursor, it can either be utilized by bacteria as an organic substrate for biomass synthesis or be catabolically converted into acetate through the final two reactions catalyzed by phosphotransacetylase (Pta) and acetate kinase (Ack). As shown in Fig. 1.9, acetyl-CoA can be converted by phosphotransacetylase to acetyl-phosphate, followed by the release of the CoA. Thereafter, acetate kinase catalyzes the conversion of acetyl phosphate to acetate in the presence of ADP. At this last enzymatic reaction, one mol of ATP is generated and immediately utilized to activate formate to formyl-THF in the methyl branch. Hence, the WLP does not result in a net increase in ATP production, which is characterized as a neutral pathway. However, in WLP, energy was released by reacting four H_2 molecules with two CO_2 molecules, producing acetate. (Debabov, 2021; Katsyv and Müller, 2020; Litty and Müller, 2021).

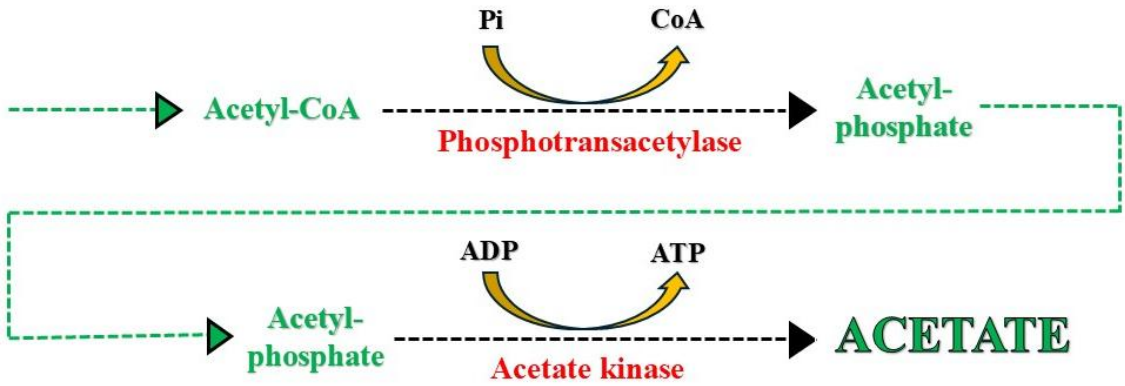

Fig. 1.9: Graphic representation of the acetyl-CoA conversion to acetate with the release of one mole of ATP via phosphotransacetylase and acetate kinase.

As previously shown in Fig. 1.6, the WLP requires only one molecule of ATP for C1 gas fixation. Its minimal energy requirements distinguish the WLP compared to other metabolic pathways. This, combined with the ability of acetogens to utilize CO_2 and CO (C1 gases), has sparked significant interest in employing these bacteria as efficient biocatalysts for fixing industrial waste gases (Lee et al., 2022). CO_2 and CO are also present in syngas as a mixture of gases containing H_2 in its composition (CO_2: 15-35%, CO: 20-100%, H_2: 5-30%). Many industrial processes mainly produce this gas as a waste by-product or emerge from the thermal gasification of several materials such as coal, biomass, cellulose, and agricultural wastes (He et al., 2022; Lee et al., 2022).

In conclusion, Esposito et al. (2019) highlighted three main advantages of the WLP: a) versatility, b) modularity, and c) flexibility. These key benefits stem from the pathway's ability to connect with methanogenesis, convert energy through the generation of electrochemical gradients, channel electrons produced via fermentation even when partially utilizing the WLP, employ different coenzymes and/or electron carriers depending on the species, and reverse the pathway to produce energy in the form of molecular hydrogen and carbon dioxide.

1.8 Evaluating Hydrogen Production Methods for Enhanced Acetogen Performance

As discussed in Sub-chapter 1.7.1 on the WL pathway, hydrogen is a vital component supporting anaerobic bacteria's survival. It plays a crucial role in their metabolic processes as an electron donor and reducing agent for the biological fixation of CO_2 due to its redox potential (Igarashi and Kato, 2017), fueling the bacteria with high chemical energy to carry out the metabolic reactions for their energy production (Martin and Thauer, 2017).

Hydrogen its carbon-free fuel combined with an exceptional calorific value of 140.4 MJ kg^{-1}, which is approximately 3-4 times higher than that of hydrocarbon fuels like coke and gasoline, hydrogen and is considered as an environmentally friendly energy option (Xu et al., 2022) and a vital alternative in our efforts to combat rising global temperatures as discussed in Sub-chapter 1.1. Despite its abundance, accounting for around 90% of the universe, managing it in its elemental state is challenging (Abdin et al., 2020).

Hydrogen can be produced by various sources, encompassing both renewable and non-renewable options, each associated with differing costs and carbon dioxide emissions. According to Zhang et al. (2016), these wide feedstock production sources include water, coal, natural gas, biomass, hydrogen sulfide, boron hydrides, and more, using various methods such as thermal, electrolytic, or photolytic processes. However, as stated by Nikolaides and Poullikkas (2017), fossil fuels still dominate the world's hydrogen supply due to the strong correlation between production costs and fuel prices, and Salkuyeh et al. (2017) believe that despite the recent crude oil price fluctuations, hydrogen production from this sector has not altered notably. More than 80% of the hydrogen produced today is derived from a long-standing and common method, steam methane reforming (SMR). SMR contributes 48% to hydrogen production, whereas oil fraction and coal gasification contribute around 30% and 18%, respectively. Due to low hydrogen production yields, electrolysis contributes only 4% (Younas et al., 2022). In Europe, approximately 50% of the produced hydrogen is driven to refineries, 40% is used for ammonia production, and only 10% is used for methanol synthesis and other uses (Abdin et al., 2020). As stated by Khaleel et al. (2024), fossil fuel-dependent hydrogen production contributes to the climate with around 830 million tons of CO_2 emissions per year.

The hydrogen produced by technologies that are free of carbon dioxide emissions is known as "green hydrogen" and is typically produced via electrolysis using renewable electricity. However, compared to hydrogen derived from fossil sources, it remains relatively costly, with a price range of approximately $2.28 to $7.43 per Kg. This cost surpasses that of both black hydrogen (produced from coal) and grey hydrogen (produced from natural gas) (Yu et al., 2021). According to Roy and Pramanik (2024), this kind of hydrogen is related to high production costs, so currently, only a small amount is produced by this method.

A more economical hydrogen production method compared to “green” uses non-renewable sources such as natural gas and is based on the steam-methane reforming (SMR) process. This hydrogen is referred to as "Blue hydrogen" and is accompanied by the release of carbon dioxide in the process. To address this, pollution control technologies known as "Carbon Capture Use and Storage" (CCUS) methods are complemented. However, this method is also related to costs and expenses associated

with capturing, reusing, or storing carbon dioxide, and it is predominantly influenced by the price of coal or natural gas (Roy and Pramanik, 2024; Yu et al., 2021).

When hydrogen production occurs within an unrecoverable oil reserve well, avoiding carbon dioxide emissions into the atmosphere, this hydrogen is referred to as "aqua hydrogen". In the future, it can contribute to a low-carbon hydrogen economy, but now it is still in the pilot production phase, facing three main challenges: scaling up production, addressing environmental concerns, and gaining public acceptance (Ajanovic et al., 2022; Yu et al., 2021).

Recent research has introduced two new categories for hydrogen nomenclature: “aquamarine hydrogen” and “white hydrogen”. These designations proposed by Boretti (2021a; 2021b) aim to describe more environmentally friendly approaches that eliminate the need for CCS technologies. However, the method relies on concentrated solar energy (CSE) systems and thermal energy storage (TES) availability and production, which occurs at high temperatures (1000°C) in the presence of a catalyst. It is projected that more than eight hundred million dollars of investment will be made by 2059.

In recent decades, considerable scientific attention has been directed towards "biohydrogen" production. Biohydrogen is generated from diverse biomass sources through microbial activity that transforms organic waste into hydrogen. This microbial conversion process can occur under different conditions, including with or without light, known as photo-fermentation and dark fermentation.

According to Cheng et al. (2022), the process of photo-fermentation utilizes facultative purple non-sulfur photosynthetic bacteria (PNSB) to decompose waste organic materials into CO_2 and H_2 by harnessing light energy. On the other hand, dark fermentation occurs in the absence of light and relies on hydrogen-generating microorganisms, such as facultative anaerobes and obligate anaerobes, that utilize waste biomass for biohydrogen production. According to Jain et al. (2024), the initial stages of AD (hydrolysis and acetogenesis) include dark fermentation, a process where microorganisms produce the necessary H_2 for the system. For this reason, the relative abundance of bacteria in the initial inoculum can significantly impact overall biohydrogen production. It has been observed that in mixed microbial cultures, *Clostridium* species are the primary H_2-producing bacteria, with *Clostridium butyricum*, *Clostridium saccharobutylicum*, and *Clostridium pasteurianum* being the most dominant under mesophilic conditions.

Additionally, *Bacillus* and *Enterobacter* species have been identified. Under thermophilic conditions, species of *Thermoanaerobacterium* have been observed. However, the H_2 produced by these species is consumed by homoacetogens and methanogens, as elaborated in Sub-chapter 1.3, interrupting bio-H_2 production. To address this, methanogens, which are non-sporulating microorganisms, can be eliminated by applying heat treatment to the medium (100 °C for 10 minutes) to selectively favor spore-forming, hydrogen-generating microbes. However, as *Clostridium* species also belong to homoacetogenic bacteria, the heating method is not fully effective for eliminating H_2-consuming bacteria. Based on these conditions, acetate may accumulate in the system.

Both methods (photo, dark fermentation) face several challenges, including substrate pretreatment, reactor design, bacterial activity, the availability of light, operational parameters such as pH, temperature, the presence of oxygen and volatile fatty acids, and hydraulic retention time (HRT), as well as scalability concerns. Despite these challenges, these methods generate CO_2 and other trace gases such as CH_4, CO, and H_2S. The separation of biohydrogen from this gas mixture remains a significant challenge and a key concern within the scientific community (Putatunda et al., 2023; Sarangi and Nanda, 2020). In a recent study by Putatunda et al. (2023), the capital investment costs for microbial fermentation (photo and dark fermentation) methods were estimated at approximately $182.5 million.

Hence, it can be concluded that almost all the hydrogen production methods exhibit significant disadvantages, such as increased impurity levels in the generated hydrogen, environmental issues stemming from elevated pollution levels, substantial energy consumption, and suboptimal conversion efficiency (Zhang et al., 2021). In addition, Capurso et al. (2022) highlight safety considerations associated with hydrogen use, the significant water requirements for its production, and the risks posed to life by its release into the atmosphere. Compared to a decade ago, hydrogen levels in the atmosphere have increased by 4%.

1.9 Hydrogen Supply and Electron Donation, Driven by Zero-Valent Metals

Based on the information presented in Sub-chapter 1.8, it is evident that there is an imperative need to develop cost-effective methodologies for hydrogen production, as it is

crucial for its use in microbial systems along with CO_2. As discussed in Sub-chapter 1.7 and demonstrated in Eq. 1, for the production of 1 mol of acetic acid by acetogens, it is required 4 mol of molecular H_2. In order to address the challenges posed by current hydrogen production methods, instead of using exogenous explosive hydrogen gas in acetogenic enriched systems, an alternative and economical approach is proposed: the use of metals, such as iron or magnesium, within microbial systems (*in situ*).

1.9.1 Zero-Valent Iron (ZVI-Fe^0)

Iron (Fe), as a chemical element, is the most prevalent element in the Earth's core, comprising about 85.5 wt%, and was a vital component of the early Earth's electron supply before O_2 began to accumulate in the sea and atmosphere. Pushcharovsky, 2019; Tosca et al., 2019). Iron has been recognized as an essential element for life, but also plays a significant role for many microorganisms inhabiting water, soil, and sediment (Weber et al., 2006).

In recent decades, iron, in the form of zero-valent iron (ZVI -Fe^0), has attracted scientific interest for its environmental and biological applications. Several studies released (Zhou et al., 2022; Galdames et al., 2020; Sun et al., 2016; Guan et al., 2015; Fu et al., 2014) summarize the applications of ZVI, showing significant potential for remediating and treating groundwater and wastewater contaminated with a broad spectrum of pollutants such as antibiotics, halogenated organics, volatile organic chlorides (VOCl), various halogenated aliphatic hydrocarbons, nitroaromatics, dyes, phenolic compounds, heavy metals etc. Ken and Sinha (2020) also stated that ZVI also exhibits a bactericidal effect against both Gram-positive and Gram-negative bacteria, including *Bacillus subtilis*, *Escherichia coli*, and *Pseudomonas fluorescens*.

Sun et al. (2016) explain that the versatility of ZVI relies on its ability to function as a reductant of contaminants due to surface-bound Fe^{2+} acting as a sorbent for other metals via the iron (hydr)oxide layer, and a coagulant for various anions present in contaminated media. ZVI is also characterized as an environmentally friendly material with minimal secondary pollution dynamics (Zhou et al., 2022; Tang et al., 2021). The number of atoms presented at the ZVI surface is proportionally increased as the ZVI particle size decreases as a way for charge stabilization (Mukherjee et al., 2016). So smaller particle sizes

demonstrated higher reductive efficiency due to the greater effective surface area (Liu and Wang, 2019), when examined under similar environmental conditions (Galdames et al., 2020).

According to Liu and Wang (2019) ZVI may be separated into two categories: micro-scale (mZVI) and nano-scale (nZVI, particle size: 1–100 nm), with the second to exhibit an increased number of active sites and, most crucially, a distinct core-shell structure (Tang et al., 2021).

ZVI was not only tested for environmental remediation but also for indirect H_2 production. As stated by Malik and Kumar (2021), through the reaction of ZVI with water, H_2 gas can be generated according to the general Eq. 5.

$$ZVI + 2H_2O \rightarrow Fe^{2+} + 2OH^- + H_2 \quad \text{(Eq. 5)}$$

However, limited scientific studies have investigated H_2 production via ZVI oxidation under anaerobic conditions (Table 1.5).

Table 1.5: Overview of different Fe^0 types (sizes, concentrations) used for abiotic H_2 production under ambient conditions.

Type of Iron	Concentration ($g\ L^{-1}$)	Condition	Duration (h)	H_2 production (mmol)	References
mFe^0 (2-5 μm) nFe^0 (60 nm)	0.5-50	Anaerobic (N_2)	119-259	1.34-3.03	Chen et al., 2011
Fe (300 – 1300 mm) Fe [D10, D50, D90] – 41, 98, 162 (μm) nFe (D50 < 0.07)	4.74-50.04	Anaerobic (N_2)	528-2520	$3.47x10^{-1}$ - $7.73x10^{-2}$ ($ml\ day^{-1}$)	Velimirovic et al., 2014
nZVI	1	Anaerobic (N_2)	168	1.34	Eljamal et al., 2018

Fe (27.82 mm)	16-224	Anaerobic (CO_2)	744	0.42-4.97	Khemkhao et al., 2024
mFe^0 (3-5 µm)	14.28	Anaerobic (CO_2)	10	~100% at elevated temperature (60ºC)	Eba et al., 2020
mFe^0 (3-5 µm)	~22	Anaerobic (CO_2)	16	19.3	Michiels et al., 2015

As summarized in Table 1.5, various sizes of iron, ranging from millimeter scale to nanoscale, have been utilized at different concentrations and experimental durations. Anaerobic conditions were typically achieved using an inert gas such as N_2. Despite these efforts, the experimental setups generally yielded low H_2 concentrations, typically on the millimolar scale.

Eba et al. (2020) and Michiels et al. (2015) investigated H_2 production through the oxidation of ZVI (zero-valent iron) under elevated temperatures in the presence of CO_2. Eba et al. (2020), for instance, examined H_2 production by supplementing a system with ZVI-Fe^0 under anaerobic conditions and 1 bar of CO_2. Six separate systems with identical conditions were exposed to varying temperatures (10, 25, 40, 50, and 60°C). Despite the decrease in CO_2 solubility with increasing temperature, Eba et al. (2020) demonstrated that at elevated temperatures (60°C), nearly all the CO_2 was consumed within 3 hours, with the system's headspace replaced by almost 100% H_2 gas. In contrast, at room temperature (25°C), only half of the CO_2 was utilized. This is due to the acceleration of reactions at high temperatures.

Michiels et al. (2015) explored H_2 production from ZVI-Fe^0 under even higher temperatures (140, 160, 180, and 200°C) and pressures (6 bar). Their experiments were conducted in a reactor containing ZVI-Fe^0, 1 M potassium hydroxide solution, and CO_2 gas that was injected into the system at 6 bars. The maximum H_2 accumulation (19.3 mmol) was achieved among the tested conditions at 160°C and 25 bar. The potassium hydroxide solution was employed to absorb CO_2, forming carbonate ions (CO_3^{2-}), which played a key catalytic role in facilitating H_2 production from iron.

More recently, Khemkhao et al. (2024) examined the effects of varying ZVI-Fe^0 concentrations at ambient temperature (35°C) in systems pressurized with CO_2 at 1.5 bar. Their findings indicated that higher concentrations of ZVI led to greater H_2 production.

Both Eba et al. (2020) and Michiels et al. (2015) identified siderite ($FeCO_3$) and magnetite (Fe_3O_4) as by-products in their systems. Conversely, Khemkhao et al. (2024) observed the formation of FeOOH, Fe_2O_3, and Fe_3O_4. As explained by Wang et al. (2021), siderite formation occurs due to the reaction of ZVI-Fe^0 with water, producing Fe^{2+} and $2e^-$. Subsequent H_2 generation results from the combination of $2H^+$ with the electrons from the cathodic reaction under anaerobic conditions in the presence of CO_2, as depicted in Fig. 1.10.

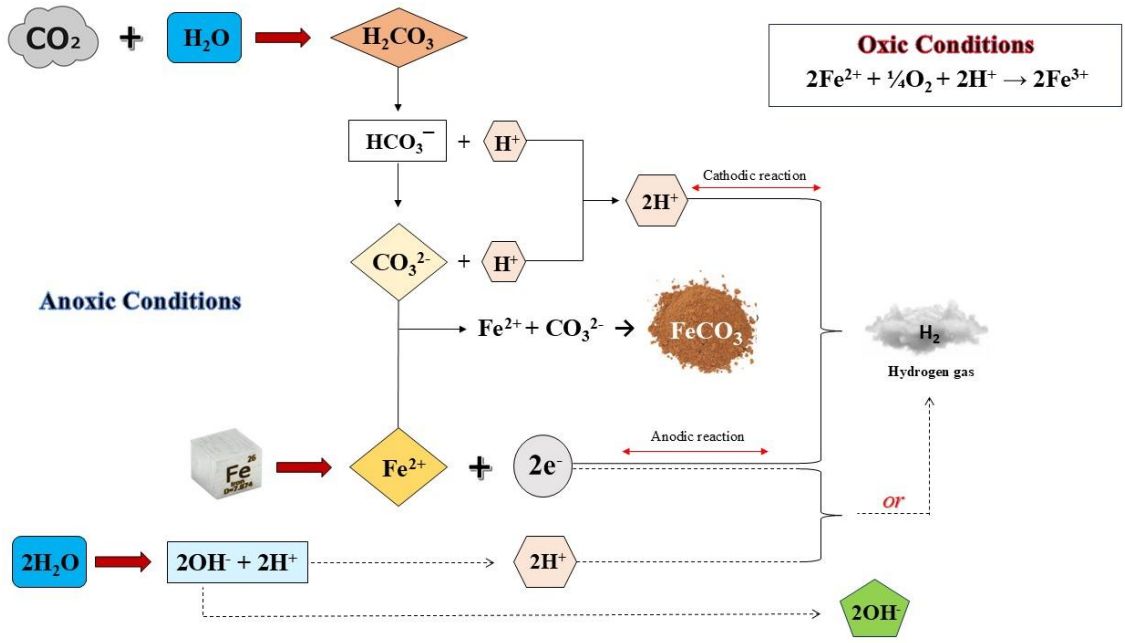

Fig. 1.10: A comprehensive overview of key reactions and the crucial involvement of HCO_3^- and CO_3^{2-} in the process of siderite formation and hydrogen production under anoxic conditions (Edited and formatted according to the information presented in Sub-chapter 3.1.13.1).

The identification and formation of other iron oxides, according to Eba et al. (2020), is attributed to the secondary decomposition of $FeCO_3$ under atmospheric and moisture conditions.

The limited availability of scientific articles addressing this topic provided additional motivation for including it in this study. Accordingly, this research explores abiotic H_2 production through iron oxidation, expanding the range of previously examined experimental parameters, such as pH, temperature, exposure to various gases, and more, as detailed in Sub-chapter 2.1

1.9.2 Zero-Valent Iron Addition to AD

As discussed in Sub-chapter 1.9.1, ZVI is extensively used for remediating and treating groundwater and wastewater contaminated with a broad spectrum of pollutants. According to Ye et al. (2021), its low electrode potential (E^o = -0.44 V) establishes it as a material with strong reduction ability. Combined with its low toxicity and chemical stability, ZVI presents a promising sustainable strategy for enhancing AD when used in situ. The application of ZVI in AD to enhance CH_4 production by methanogens was first described by Daniels et al. (1987), and it has been widely investigated in recent years.

The methodology of implementing ZVI in AD plays a multifaceted role, and several researchers (Kong et al., 2023; He et al., 2022; Kong et al., 2021; Charalambous and Vyrides, 2021; Zhang, 2020; Xu et al., 2017) investigate various parameters enhanced or positively affected by this approach. Key factors include boosting enzyme activity, promoting abiotic H_2 production, altering the oxidative-reductive potential (ORP), buffering pH, and mitigating ammonia toxicity.

ZVI, as a trace element donor, contributes to the growth of ZVI-related microorganisms such as methanogens. As noted by He et al. (2022), iron participates in the synthesis of critical electron transfer proteins and enzymes. For instance, c-type cytochromes and $F_{420}H_2$ oxidase are promoted in the presence of ZVI, accelerating overall methanogenesis. Additionally, Zhong et al. (2022) suggest that ZVI creates an optimal environment for obligatory anaerobic microbes, enhancing the activity of enzymes involved in the hydrolysis and acidogenesis stages of AD, thereby expediting the process.

The Fe^{2+} released from ZVI can further enhance and promote the activities of specific enzymes, such as formate dehydrogenase, carbon monoxide dehydrogenase, alcohol dehydrogenase, and coenzyme F_{420} (He et al., 2022). More specifically, Wang et al. (2021) demonstrated that Fe^{2+} stimulates pyruvate formate-lyase, which is involved in the

production of formic acid. Zhou et al. (2020) also reported that Fe^{2+} enhances the activity of pyruvate-ferredoxin oxidoreductase, an enzyme containing Fe-S clusters that facilitate propionate decomposition.

As Palacios et al. (2019) explain, Fe^{2+} can stabilize extracellular enzymes. For example, hydrogenases, which are released into the extracellular milieu by dying cells, can utilize electrons generated during ZVI oxidation to convert protons in the solution into H_2. Although hydrogenases are typically functional for only a few days, their activity can be extended in the presence of Fe^{2+}.

According to Zhang et al. (2020) and Dong et al. (2019), the Fe^{2+} ions required for enzyme enhancement can be generated within the system through the abiotic oxidation of ZVI, as illustrated in Eq. 6

$$2H_2O + Fe^0 \rightarrow Fe^{2+} + H_2 + 2OH^- \quad (\Delta G^0 = -5.02 \text{ kJ mol}^{-1}) \qquad \text{(Eq. 6)}$$

However, along with Fe^{2+}, hydrogen is also generated and can serve as an electron donor for both autotrophic and heterotrophic bacteria (Xu et al., 2017). According to Kong et al. (2021), the abiotic H_2 produced from ZVI can be utilized by hydrogenotrophic methanogens, along with CO_2, for methane production, as shown in Eq. 7.

$$4H_2 + CO_2 \xrightarrow[\text{methanogens}]{\text{Hydrogenotrophic}} CH_4 + 2H_2O \quad (\Delta G^0 = -139 \text{ kJ mol}^{-1}) \qquad \text{(Eq. 7)}$$

Based on the above equation, Kong et al. (2021) highlight the enhancement of biochemical methane potential (BMP) in AD when ZVI is used. The elevated CH_4 yield has been confirmed in several AD systems supplemented with ZVI, treating waste sludge, domestic wastewater, food waste, and poultry waste. High CH_4 production is attributed to hydrogenotrophic methanogens, with *Methanosarcina* spp. believed to play a major role (Zhang et al., 2020). Furthermore, Vyrides et al. (2018) demonstrated that hydrogenotrophic methanogens are present in systems supplemented with ZVI where CO_2 is used as the sole carbon source. As explained by Zhou et al. (2020), the H_2 produced by ZVI not only accelerates the conversion of CO_2 into CH_4 by hydrogenotrophic

methanogens, as indicated in Eq. 7, but also facilitates the breakdown of organic materials in AD through hydrolysis.

Dong et al. (2019) emphasize that the use of ZVI in AD can also indirectly and positively affect CH_4 production. In the presence of ZVI, homoacetogenic bacteria such as *Clostridium* and *Sporomusa* can utilize CO_2 to produce acetic acid (CH_3COOH). This acetic acid can then be further utilized by acetoclastic methanogens such as *Methanosaeta* or *Methanosarcina* for the production of CH_4 and CO_2, as shown in Eq. 8 and Eq. 9.

$$2CO_2 + 4H_2 \rightarrow CH_3COOH + 2H_2O \quad (\Delta G0 = -95 \text{ kJ mol}^{-1}) \qquad \text{(Eq. 8)}$$

$$CH_3COOH \rightarrow CH_4 + CO_2 \quad (\Delta G0 = -75.5 \text{ kJ mol}^{-1}) \qquad \text{(Eq. 9)}$$

According to He et al. (2022), another vital parameter in AD is the oxidative-reductive potential (ORP), which is influenced by ZVI. ORP serves as an indicator for determining the types of acidification fermentation, as it depends on redox balance. Baek et al. (2019) explain that the redox properties of ZVI can effectively and directly lower the ORP, thereby creating better conditions for the survival and growth of not only methanogens but also other obligatory anaerobic microorganisms. According to Kong et al. (2023), under these low ORP conditions, not only is methanogenesis enhanced, but the acetification of propionic acid and the production of VFAs or medium-chain fatty acids are also promoted. For instance, as stated by Ye et al. (2021), such low ORP levels not only improve methanogenesis by increasing hydrogenotrophic methanogens but also enhance butyric acid production. The formation of caproate, which can be used as biofuel, has also been reported (He et al., 2022).

Furthermore, the H_2 produced by ZVI in microbial systems can serve as an electron transport carrier between substrate-oxidizing syntrophic bacteria and H_2-utilizing methanogens, promoting interspecies hydrogen transfer (IHT) -as explained in the sub-chapter - on syntrophic metabolism of propionate and/or butyrate. In contrast, Zhu et al. (2020) refer to ZVI as a conductive material capable of acting as an electron bridge in direct interspecies electron transfer (DIET). However, as mentioned in Sub-chapter 1.4, the DIET theory is not supported by all scientists.

Another parameter that can be altered in AD by the addition of ZVI is pH. According to Kong et al. (2023), VFA production and accumulation in AD is an undesirable phenomenon that can lead to acidification of the system and a drop in pH. Consequently, CH_4 production is inhibited, and the AD system may collapse. The addition of ZVI in AD results in the production of hydroxide ions, as shown in Eq. 6, through the oxidation of ZVI under anaerobic conditions. On the other hand, the reduction of H^+ by ZVI for the formation of H_2 leads to an increase in OH^- ions in the system. As a result, pH is neutralized, and methanogenesis can continue (He et al., 2022).

The addition of ZVI not only mitigates pH inhibition in AD but also addresses high ammonia accumulation, which, according to Zhang et al. (2020), can block acetate metabolism and lead to system instability. Ye et al. (2021) stated that microorganisms in the presence of ZVI can resist high ammonia concentrations. As explained by Kong et al. (2021), this is because ammonia can be absorbed and co-sedimented, driven by ZVI oxidation. On the other hand, Xu et al. (2017) suggest that ammonia reduction occurs due to improved biological denitrification facilitated by ZVI. The H_2 produced by ZVI oxidation supports the activity of denitrifying bacteria, enhancing nitrate removal.

Based on the above, the combined positive effects clearly highlight the potential of ZVI to optimize AD processes and enhance methane yield.

1.9.3 Magnesium (Mg^0) as a Hydrogen Source

Magnesium is the 3rd most abundant dissolved element in the sea and, on the earth's crust, accounts for approximately 2.35%, ranking as the 8th most abundant among the other elements (Sun et al., 2018). Due to their specific physicochemical characteristics (environmentally friendly, lightweight, energy-efficient, low density of 1.74 g cm^{-3}, and theoretical hydrogen storage capacity of 7.6 wt %), Mg and Mg-based alloys are used in several sectors (transportation, aerospace, medical material, battery applications, corrosivity detectors), offering an exceptional opportunity for practical implementation (Wu et al., 2021; Ouyang et al., 2020; Cao et al., 2020; Sun et al., 2018).

Nowadays, Mg metal is attractive for H_2 production due to its high reactivity properties, high H_2 gas productivity (921 L for every Kg of Mg powder used at standard conditions via hydrolysis), and low cost (Xiao et al., 2024). This high reactivity and H_2 immediate productivity of Mg, when supplemented in water, as Lorowitz et al. (1992) showed, compared to Fe^0 under anaerobic conditions, can be explained by the different standard reduction potentials (SRP) of the two metals. During Mg corrosion, two electrochemical reactions contribute to the anodic (Eq. 10) and cathodic processes (Eq. 11) (Song and Atrens, 2023).

$$Mg \rightarrow Mg^{2+} + 2e^- \quad \text{(Eq. 10)}$$

$$H_2O + e^- \rightarrow OH^- + \tfrac{1}{2}H_2 \quad \text{(Eq. 11)}$$

It is observed in experiments that the hydrogen evolution (HE) rate increases along with the potential. For this reason, it is believed that Mg does not form divalent Mg ions as dissolved but exists as an Mg^+ intermediate. Then, this Mg fraction travels from the metal surface to the aqueous solution and hence is homogeneously oxidized, producing H_2, as shown in Eqs. 12 and 13 (Frankel et al., 2013).

$$Mg \rightarrow Mg^+ + e^- \quad \text{(Eq. 12)}$$

$$Mg^+ + H_2O \rightarrow Mg^{2+} + \tfrac{1}{2}H_2 + OH^- \quad \text{(Eq. 13)}$$

Based on Eq. 13, hydroxides were produced from the oxidation of Mg, leading to increased pH in the supplemented system. According to Song and Atrens (2023), the pH value can increase rapidly to more than 10, which is attributed to the low solubility of $Mg(OH)_2$ that can be formed due to Mg hydrolysis and has to do with the equilibrium between water (H_2O), H^+ and OH^- ions as shown in Eq. 14.

$$Mg^{2+} + 2OH^- = Mg(OH)_2 \quad \text{(Eq. 14)}$$

Based on the standard reduction potential of the two-electron oxidation of elemental Fe and Mg, it is evident that Mg is more reactive than Fe at standard conditions. As shown in Eq. 10 and Eq. 15, Mg demonstrated a high negative reduction potential compared to Fe, indicating high reactivity and easy electron loss and driving protons to hydrogen reduction (Esmaily et al., 2017; Bae and Hanna, 2015; Crane and Scott, 2012; Sun et al., 2006).

$$Mg \rightarrow Mg^{2+} + 2e^- \quad E^0 = -2.37 \text{ V vs SHE} \quad \text{(Eq. 10)}$$

$$Fe \rightarrow Fe^{2+} + 2e^- \quad E^0 = -0.44 \text{ V vs SHE} \quad \text{(Eq. 15)}$$

Considering the standard hydrogen electrode (SHE) potential (Eq. 16) and the reduction potential for the half-reaction of water (Eq. 17), the overall E^0 for Fe and Mg when exposed to water can be represented in Eq. 18 and Eq. 19, respectively indicated that both metals can react with water producing H_2.

$$2H^+ + 2e^- \rightarrow H_2 \quad E^0 = 0 \text{ V} \quad \text{(Eq. 16)}$$

$$2H_2O + 2e^- \rightarrow H_2 + 2OH^- \quad E^0 = -0.83 \text{ V} \quad \text{(Eq. 17)}$$

$$Fe^0 + 2H_2O \rightarrow Fe^{2+} + 2OH^- + H_2 \quad E^0 = -0.39 \text{ V} \quad \text{(Eq. 18)}$$

$$Mg + 2H_2O \rightarrow Mg^{2+} + 2OH^- + H_2 \quad E^0 = -1.54 \text{ V} \quad \text{(Eq. 19)}$$

The use of magnesium in a closed system, due to its reactivity and the significant amount of hydrogen it can produce, can lead to an increase in the partial pressure of H_2 within the system. According to Braga Nan et al. (2020), this phenomenon can alter the metabolic equilibrium in AD, as discussed in Sub-chapter 1.4.

Lorowitz et al. (1992) investigated the effects of magnesium supplementation in a system inoculated with *Methanobacterium thermoautotrophicum* under anaerobic conditions. Their experiments demonstrated significantly higher methane production and an increase in cell density compared to the control systems. The same researcher stated that this is attributed to the ability of magnesium to completely oxidize abiotically, producing higher amounts of hydrogen than iron and requiring less time for the reaction with water. The above observations indicate that magnesium can be used as a novel source for autotrophic growth, not only for methanogens but also for acetogens, due to its excellent electron donor.

1.10 Current Experimental Approaches for Acetic Acid Production Through CO_2 Utilization

To date, the production of acetate via the microbial bioconversion of CO_2 has been examined in only a few scientific studies, primarily involving systems supplemented with exogenously produced H_2 gas. These studies utilized either pure microbial strains or mixed microbial inocula for the execution of the biochemical reactions. In an alternative approach, limited research has investigated the use of ZVI as an *in-situ* H_2 source, where the oxidation of ZVI generates H_2 to fuel these systems. Additionally, more complex configurations, such as microbial electrosynthesis systems (MES), have been employed for CO_2 utilization and H_2 generation. In MES, the produced H_2 can subsequently be used by methanogens or acetogens to synthesize acetic acid. Both methodologies present distinct advantages and limitations that merit further investigation.

1.10.1 Microbial Electrosynthesis Systems for Acetate Production

Microbial Electrolysis Cells (MECs), a type of Bio-electrochemical System (BES), have shown significant promise for CO_2 utilization. These MEC systems typically consist of one or two-chamber reactors interconnected by an ion exchange membrane and are equipped with electrodes (anode and cathode). They can effectively operate with various microbial compositions, including pure strains, co-cultures, and mixed strains. The electrons generated by electrodes flow through the system's chambers via an external circuit under an external potential, facilitating hydrogen production that is consumed by microorganisms. Compared to one chamber, Dual-chamber MECs present a more complex scaling process, with the potential for hydrogen consumption by hydrogenotrophic microorganisms in the anode chamber. Scientists try to optimize this process for large-scale field applications. However, several challenges need to be addressed, including electrode cost and modulation, the incorporation of affordable anodes and cathodes instead of the use of noble metals like platinum, gold, or palladium, reactor configuration, effective removal of gaseous pollutants such as CO_2 electricity prices, the cost of ion exchange membranes, which can constitute up to 40% of total reactor expenses, initial investment, maintenance, and disposal expenses of ion exchange membranes. All the above factors collectively pose significant challenges to the widespread adoption of this method on a large scale (Lee et al., 2022; Murugaiyan et al., 2022; González-Pabón et al., 2021).

In addition to the above, Ferraren-De Cagalitan and Abundo (2021) furthermore highlighted that the commercialization of MECs is a challenge due to the precise mechanisms governing electron transfer between microorganisms involved and electrodes remaining partially understood. Furthermore, the methanogenic activity of archaea presented in these systems, along with bacteria in both the anode and cathode, not only compete with electroactive bacteria (EAB) for organic substrates but also consume reactants to produce methane, resulting in lower hydrogen and acetate production yields. Consequently, further research must be done concerning the methanogenic activity inhibition strategies in such systems for commercial-scale production of added-value products through MECs. While chemical inhibitors have shown promise in suppressing methanogens, they also add to operational costs.

The production of acetate by microorganisms utilizing CO_2 in MEC systems was first introduced in the mid-1990s, and then pure acetogenic strains such as *Sporomusa* and *Clostridium* spp. were used in such systems for the bioconversion of CO_2 to acetate due to these strains are able to harvest electrons directly from the system's cathode (Aryal et al., 2018). Hengsbach et al. (2022) also stated that the inoculation of such systems with acetogens not only offers the production of acetate but also the formation of platform chemicals in a sustainable way. As shown in Table 1.6, the production of acetate from CO_2 in MEC systems predominantly involves the use of pure strains such as *Sporomusa* or *Clostridium* as inocula, typically without the addition of methanogenesis inhibitors. Furthermore, anaerobic consortia have also been cited as viable options; however, it is generally observed that pre-enriched acetogenic microbial inocula are preferred. These inocula are often pretreated with acid to minimize methanogenic activity or supplemented with BES inhibitors to suppress methanogenesis. Such pretreatment reduces the acclimatization time required for the inocula, enabling faster acetate production by the microbial cells. According to Hengsbach et al. (2022), acetate production using mixed microbial cultures in MEC systems heavily depends on biofilm formation on the cathode. In response, Krige et al. (2021) developed a laboratory method to synthetically produce biofilms using the *Sporomusa* strain, addressing the slow biofilm formation in natural settings, which requires extra effort.

Most scientific studies utilize two-chamber MECs separated by proton exchange membranes. CO_2 is commonly supplied to the microbial cell in a continuous mode, often using peristaltic pumps, with gas introduced from external reservoirs. Roy et al. (2021) uniquely used real industrial CO_2 waste gas in their MEC systems, demonstrating the feasibility of incorporating industrial waste streams. Noteworthy experimental results presented by Liu et al. (2018), conducted with the MEC system, demonstrated low acetic acid production under 100% CO_2. However, by experimenting with varying concentrations of H_2 in batch mode, experiments show that by using a gas mixture of CO_2:H_2 at a 10%:80% ratio, a significantly higher acetate production can be achieved compared to systems with lower H_2 content (10%). By using mixed gas with low H_2 concentrations, the system showed a more than 70% drop in acetate accumulation. These findings highlight the critical role of H_2 gas as an electron donor for the bioconversion of CO_2 during acetogenesis.

Despite the potential of MEC systems, their complex configurations pose significant challenges, as already mentioned. These include the need for advanced cell designs, a reliable electrical supply, sophisticated electrodes for microbial immobilization, and costly proton exchange membranes. Additionally, several operational parameters further hinder MEC performance. Hengsbach et al. (2022) identified key issues, such as the temperature-dependent solubility of reactant gases (CO_2/H_2), bubble formation leading to H_2 losses at high hydrogen evolution reaction (HER) rates, electrode passivation influenced by pH, and the need for innovative electrode materials or coatings. Other challenges include slow biofilm formation, high energy demands for electrochemical H^+ reduction, and prolonged system startup times. Based on the above, MEC systems remain in the experimental phase and have not yet been scaled up for industrial applications.

Table 1.6: Overview of scientific studies reporting acetate formation via CO_2 utilization in microbial electrolysis cell (MEC) systems.

Inoculum	Carbon source	Electron donor	Inhibition	Exp. mode	Duration	Acetate production	References
Acetobacterium-enriched mixed culture	CO_2: 95% (with 1% of O_2)	Electrode (graphite plate) - 0.8 V, -1 V, -1.2 V vs Ag/AgCl	x	Two-chamber MES system with Nafion 117 membrane	≈78 days (with -1 V) 20 days (with -8 V) 20 days (with -1.2 V)	CO_2 flow rate 0.3 L day^{-1} → 1.94 g L^{-1} CO_2 flow rate 0.4 L day^{-1} → 4.9 g L^{-1} CO_2 flow rate 0.7 L day^{-1} → 6.6 g L^{-1} (after 20 days with -1 V) CO_2 flow rate 0.9 L day^{-1} → 5.5 g L^{-1} (after 18 days with -1 V) CO_2 flow rate 0.7 L day^{-1} and -0.8 V Max: 1.1 g L^{-1} (at day15) CO_2 flow rate 0.7 L day^{-1} and -1.2 V 4.7 g L^{-1} (at day 20)	Roy et al., 2024
Mixed culture from anaerobic fermenter	CO_2: 1.2-1.3 bar	Electrode (carbon cloth) - 0.8 V vs. SHE	x	Two-chamber MES system with CMX Nenosepta membrane	60 days	Chamber 1 → 12.90 g L^{-1} Chamber 2 → 11.87 g L^{-1}	Romans-Casas et al., 2023

Inoculum	Carbon source	Electron donor	Inhibition	Exp. mode	Duration	Acetate production	References
Anaerobic consortia from sewage treatment plant	CO_2: 0.6 ml min^{-1}	Electrode (carbon clothe) -0.4 V, -0.6 V vs Ag/AgCl	Acid-pretreated inoculum with H_3PO_4 (pH 3) for 10 h	Single-chamber MES	40 days - 8 cycles with -0.4 V (retention time of each cycle: 5 days) 40 days - 8 cycles with -0.6 V (retention time of each cycle: 5 days)	0.7 g L^{-1} (cycle 8, -0.4 V) and 1.2 g L^{-1} (cycle 8, -0.6 V)	Tharak et al., 2023
1: Enriched wastewater sludge 2: *Clostridium ljungdahlii* (DSM13528)	Industrial CO_2 (97.91%) with O_2	Electrode (graphite plate) Mix culture: -0.84 V vs Ag/AgCl Pure culture: -1 V vs Ag/AgCl	BES: 6.4 g L^{-1}	Two chambers MES system with Nafion 117 membrane	mix culture → 29 days (Cycles 1,2,3 : 10, 10, 9 days) pure culture → 23 days (Cycles 1,2,3 : 5, 8, 10 days)	Mix culture: 1.8 g L^{-1} with industrial CO_2 (on day 7 - cycle 3) Pure culture: 1.1 g L^{-1} with industrial CO_2	Roy et al., 2021

Inoculum	Carbon source	Electron donor	Inhibition	Exp. mode	Duration	Acetate production	References
Acetogenic enriched inoculum	CO_2: 10 ml min^{-1}	Electrode (graphite felt) -0.9 V vs Ag/AgCl	BES: 2.08 g L^{-1}	Two chambers MES system with Nafion 117 membrane	10 °C: ≈24 days 25 °C: ≈20 days 35 °C: ≈11.5 days 55 °C: ≈11.5 days 70 °C: ≈8.5 days	10 °C: 70.53 mg L^{-1} (day 24) 25 °C: 525.84 mg L^{-1} (day 20) 35 °C: 468.51 mg L^{-1} (day10) 55 °C: 309.59 mg L^{-1} (day10) 70 °C: 193.04 mg L^{-1} (day 4)	Yang et al., 2021
Sporomusa ovata (SSM 2662) (Synthetic biofilm)	CO_2: 6 ml min^{-1}	Electrode (graphite rob) -0.8 V vs Ag/AgCl	x	Single-chamber MES	≈240 days	Max: 3.45 g L^{-1}	Krige et al., 2021
Clostridium ljungdahlii	CO_2: 3 ml min^{-1}	Electrode (Ni-P modified carbon felt)	x	Two chambers MES system with Nafion 117 membrane	7 days	Max: 1.18 g L^{-1}	Wang et al., 2020

Inoculum	Carbon source	Electron donor	Inhibition	Exp. mode	Duration	Acetate production	References
Acetogenic-enriched anaerobic sludge from MES	CO_2: 10 ml min^{-1}	Electrode (graphite stick) -1 V vs Ag/AgCl	x	Two-chamber MES system with Nafion 117 membrane	116 days	First batch (0-54 days) → 5.66 g L^{-1} after 26 days without power interruption 6.20 g L^{-1} after 56 days with 3 power interruptions Second batch (54-116 days) 50% of the growth medium was replaced→ 1.14 g L^{-1} after 5 days without power interruption 3. 97 g L^{-1} after 62 days with 3 power interruptions	Rojas et al., 2018
Clostridium scatologenes	CO_2:H_2= 10%:80% CO_2:H_2:N_2 =10%:10% :80%	Electrode (carbon felt) -0.6, -1.2 V vs Ag/AgCl	x	Two-chamber MES system with Nafion 117 membrane	28 days	Max: 1.25 g L^{-1} with CO_2:H_2 for 6 days 0.362 g L^{-1} with CO_2:H_2:N_2 for 2 days MES system-Max: 0.44 g L^{-1} with 100% CO_2 at -1.2 V	Liu et al., 2018

1.10.2 Acetate Production from CO_2 and H_2 in Batch and Reactor Systems

Another straightforward methodology for producing acetate, avoiding the complex configuration of MEC systems, involves using H_2 gas instead of electrodes. H_2 gas can be introduced exogenously into anaerobic systems as an electron donor for the bioconversion of CO_2 to acetate. However, only a few scientific reports have investigated this approach. As shown in Table 1.7, different types of inocula can be used for the biological reactions. These include not only pure strains, but also acetogenic-enriched sludge or sludge derived from wastewater treatment plants, in contrast to MEC systems, where pure strains or acetogenic-enriched inocula are preferred. When a mixed microbial consortium was used, a pretreatment method must be applied prior to inoculation to prevent the consumption of reactants (CO_2/H_2) by methanogenic archaea. Generally, three methods are employed to inhibit methanogenesis: applying a heat shock, an acid shock, or using a specific methanogenesis inhibitor such as BES, or a combination of these methods.

Chaikitkaew et al. (2024) examined the use of synthetic biogas mixed with H_2 gas for acetate production instead of pure CO_2/H_2 gas. Zhou et al. (2024) suggest that using homoacetogens for simultaneous biogas upgrading and the production of value-added products is a promising technology. However, to date, this methodology has demonstrated low acetate production rates.

He et al. (2022) studied the interruption of CO_2 in a system inoculated with acetogenic-enriched sludge after a period of supplementation with a CO_2/H_2 gas mixture. When only H_2 gas was introduced, acetate production declined by 94%, highlighting the importance of both gas reactants in the system. In contrast, Omar et al. (2018) examined the transient increase of H_2 concentration in a biogas mix used in a system inoculated with sewage sludge. They observed that increasing the H_2 concentration stimulated acetic acid production.

Furthermore, He et al. (2022) also investigated the addition of $NaHCO_3$ to a system utilizing anaerobic granular sludge. They found that the presence of HCO_3^- ions significantly accelerated acetate production due to the high availability of carbonate ions for bacteria in the aqueous solution. Some reports have demonstrated that maximum acetate production is observed under ambient conditions.

Table 1.7: Overview of scientific studies reporting acetate formation via biological CO_2/H_2 utilization.

Inoculum	Carbon source	Electron donor	Inhibition	Exp. mode	Duration	Acetate production	References
Clostridium thailandense (free cells and immobilized)	Synthetic biogas $CO_2:CH_4$ = 40%:60%	100% H_2 mixed with biogas $H_2:CO_2$ = 2:1	x	Batch experiments Reactor for immobilization	7 days	Free cells: 732.91 mg L^{-1} Active carbon: 939.8 mg L^{-1} Expanded clay: 879.2 mg L^{-1} Coir: 869.6 mg L^{-1}	Chaikitkaew et al., 2024
Acetogen-enriched anaerobic granular sludge	$CO_2:H_2$ = 80%:20% 100% H_2 Flow rate: 10 ml min^{-1}	H_2	Heat-shock at 90°C for 15 min	Semi-continuous fed-batch bioreactor	Stage 1: 26 days (with $CO_2:H_2$ = 80%:20% - pH 6) Stage 2: 23 days (days 27-50) (with H_2 = 100% - pH 4.5-5)	Stage 1 → Acetate: 2 g L^{-1} (on day 26) Stage 2 → Acetate: Decline (- 1.89 g L^{-1} on day 33)	He et al., 2022

Inoculum	Carbon source	Electron donor	Inhibition	Exp. mode	Duration	Acetate production	References
Anaerobic granular sludge	CO_2:H_2 = 20%:80% CO_2:H_2 = 20%:80% + 2.1 g L^{-1} $NaHCO_3$	H_2	Heat-shock at 90°C for 15 min	Batch experiments	Temperature examination: 10 days pH examination: 24 days	Temper.: Max acetate: 1783.49 mg L^{-1} (at 25°C with CO_2:H_2, pH 6) Max acetate: 7365.14 mg L^{-1} (at 25°C with CO_2:H_2 + HCO_3^-, pH6) pH: Max acetate: 3920.27 mg L^{-1} (at 25°C with CO_2:H_2, pH 7)	He et al., 2021
Stage 1 → Wastewater anaerobic consortium Stage 2 → Homoacetogen-enriched consortium	Batch exp.: CO_2:H_2 = 20%:80% Reactor exp.: CO_2:H_2 mixture at 2 bars	H_2	1: Heat-shock at 80°C for 2 h, 2: Acid-shock 3: Acid + Head shock	Batch experiments and Reactor	Stage 1 → 10 cycles (48h each) Stage 2 → 6 cycles (72h each)	Batch → (non-specified in which cycle) Heat: Acetate: 410 mg L^{-1} (after 48h) Acid: Acetate: 320 mg L^{-1} (after 48h) Heat+Acid: Acetate: 543 mg L^{-1} (after 48h) Reactor → (non-specified in which cycle) Acetate: 1234 mg L^{-1} (after 72h) (control: 1013 mg L^{-1})	Modestra et al., 2020

Inoculum	Carbon source	Electron donor	Inhibition	Exp. mode	Duration	Acetate production	References
Sewage sludge	Enrichment stage → H_2:CO_2:CH_4 = 2:1:1.5 (biogas mixture 1.5 bar) Experimental stage → H_2:CO_2:CH_4 = 1:1:1.5 H_2:CO_2:CH_4 = 2:1:1.5 H_2:CO_2:CH_4 = 3:1:1.5 H_2:CO_2:CH_4 = 4:1:1.5	H_2	Enrichment stage → BES: 10.40 g L^{-1} 1: Heat-shock 70°C for 30 min 2: Heat-shock 90°C for 30 min Experimental stage → BES: 10.40 g L^{-1}	Batch experiments	Enrichment stage: 4 days Experimental stage: 10 days	Enrichment stage → Acetate: 291 mg L^{-1} Experimental stage → H_2:CO_2:CH_4 = 1:1:1.5 Acetate: 142 mg L^{-1} (day 10) H_2:CO_2:CH_4 = 2:1:1.5 Acetate: 288 mg L^{-1} (day 2) H_2:CO_2:CH_4 = 3:1:1.5 Acetate: 287 mg L^{-1} (day 6) H_2:CO_2:CH_4 = 4:1:1.5 Acetate: 358 mg L^{-1} (day 4)	Omar et al., 2018

1.10.3 Acetate Production from CO_2 and H_2 Generated via *In-Situ* ZVI Oxidation

As highlighted in Sub-chapter 1.10.2, limited scientific reports address acetate production from CO_2 and H_2 gas. However, the aforementioned methodological approach relies on the continuous supplementation of H_2 gas, which is both hazardous and explosive, requiring careful handling and an external source. As an alternative, zero-valent iron (ZVI) can be used *in-situ* alongside microbial inocula to continuously supply the necessary H_2 gas.

As summarized in Table 1.8, ZVI has primarily been used in batch experiments or added to reactors inoculated with pure microbial strains, typically without any pretreatment of the initial inoculum source. In these studies, CO_2 gas or $NaHCO_3$ has been utilized as a carbon source. The supplementation of ZVI in MES systems has not been widely implemented due to the reliance on electrodes in such setups to supply the necessary electrons or hydrogen to microbes. Wu et al. (2023) remains the only study to date that mentions the use of ZVI in such systems as part of their methodology

For acetate production via ZVI oxidation *in-situ*, various concentrations of ZVI have been used, ranging from 1 g L^{-1} to 75 g L^{-1}, and in different particle sizes in batch experiments or reactors. However, these studies primarily focused on pure, strictly acetogenic, or non-strictly acetogenic bacterial strains. No studies have investigated acetate production in systems supplemented with ZVI and inoculated with a mixed bacterial consortium while applying different methanogenesis inhibition methods.

For instance, Wang et al. (2024) investigated CO_2 utilization in both batch experiment systems and reactors by supplementing these systems with various concentrations of ZVI ranging from 1-10 g L^{-1}. Two pure acetogenic strains were used as co-cultures to examine the acetate production potential. The systems were incubated at 35-37 ºC, and the initial pH was adjusted to 7. After a 14-day experimental duration, the maximum acetate production was observed on day 11 using 5 g L^{-1} ZVI. However, at a lower concentration of ZVI (3 g L^{-1}), caproate was identified, reaching its maximum on day 13 at ≈1.75 g L^{-1}. At the end of the experiment, butyric acid was measured at a concentration of ≈1.6 g L^{-1} in all systems.

On the other hand, the bioreactor supplemented with 3 g L^{-1} ZVI exhibited lower acetate production compared to the batch experiments. However, higher butyrate and caproate accumulations were observed, accounting for 2.88 g L^{-1} and 1.84 g L^{-1}, respectively, at the end of the experiment. It is important to mention that both systems (batch experiment and reactor) were also implemented with lactic acid at a concentration of 10 g L^{-1}.

Under the same concept, Im et al. (2023) used a pure strain, *Fonticella tunisiensis*, for acetate production in a batch system supplemented with 12.5 g L^{-1} of ZVI. Im et al. (2023) investigated not only the utilization of CO_2 but also the consumption of CO at low concentrations in the systems (only 40% in the headspace). The batch systems were incubated at mesophilic conditions (35ºC), and the initial pH was adjusted to 6. After 8 days, only 295 mg L^{-1} of acetic acid and 87 mg L^{-1} of butyrate were produced by utilizing CO_2. The use of CO accelerated the formation of acetate (1594 mg L^{-1}) and butyrate (104 mg L^{-1}), and methane accumulation (1.2%) was identified in the headspace of the batch systems. This phenomenon is attributed to the thermodynamically favorable nature of CO utilization, as elaborated in Sub-chapter 1.7.1.

Bayar et al. (2022) also examined two pure strains of *Clostridium*, separated and used as co-cultures in batch experiments and in bioreactors, both supplemented with elevated ZVI concentrations compared to the above studies. The systems were incubated at 30ºC, with the pH varying according to the experimental set (1st batch set: pH 8, 2nd batch set: pH 8.5, and bioreactor: pH 6.9). The first batch set lasted for 16 days, while the second batch set ran for 30 days. The reactor operated for 36 days. After the experimental duration, high acetate production was observed in all systems, ranging between 1178 mg L^{-1} and 2113 mg L^{-1}. It is important to mention that the higher ZVI concentrations did not positively affect acetate production; however, at 75 g L^{-1} of ZVI, ethanol formation was observed at 125 mg L^{-1}.

Based on the above, it is evident that until now, only pure strains have been examined for acetate production, and no study has investigated this concept using mixed cultures where methanogens were inhibited. The scientists above used pure strains to avoid pretreatment methods for methane inhibition, but the use of pure strains poses the risks of contamination and requires well-sterilized equipment. This dissertation addresses this gap by investigating acetate production using mixed inocula under various conditions with ZVI as an electron donor, where methanogenesis is inhibited.

Table 1.8: Overview of scientific studies reporting acetate formation via biological CO_2/H_2 utilization.

Inoculum	Carbon source	Electron donor	Inhibition	Exp. mode	Duration	Acetate production	References
Acetobacterium woodii *Megasphaera hexanoica* As a co-culture	CO_2 (1 bar) Lactic acid: 10 g L^{-1}	Batch exp.: ZVI (149-297 µm): 1, 3, 5, 10 g L^{-1} Bioreactor: ZVI (149-297 µm): 3 g L^{-1}	x	Batch experiments and reactor	Batch experiment: 14 days Bioreactor: 14 days	Batch experiment → ≈2.6 g L^{-1} (5 g L^{-1} ZVI, on day 11) Bioreactor → ≈1.87g L^{-1} on day 14	Wang et al., 2024
Fonticella tunisiensis HN43	CO: 40% CO_2: 40%	12.5 g L^{-1} ZVI (1-2mm)	x	Batch experiments	≈ 8 days	CO: ≈1594 mg L^{-1} (CO) CO_2: ≈ 295 mg L^{-1} (CO_2)	Im et al., 2023
Clostridium aceticum *Clostridium carboxidivorans*	1st set: 1.5 bar in total - (*C. aceticum*) 2nd set: 4 bars in total - (*C. aceticum* & *carboxidivorans*) Reactor: 0.5 bar in total - (*C. aceticum*)	Batch set 1 & 2: 25 g L^{-1} ZVI Reactor: 50 & 75 g L^{-1} ZVI	x	Batch experiments and reactor	Batch 1st set: 16 days Batch 2nd set: 30 days Reactor: 36 days	1st set: 1178 mg L^{-1} (*C. aceticum*) 2nd set: 1400 mg L^{-1} (*C. aceticum*) & 2000 mg L^{-1} (*C. Carboxidivorans*) Reactor → 2113 mg L^{-1} (ZVI 50 g L^{-1}) 2050 mg L^{-1} (ZVI 75 g L^{-1})	Bayar et al., 2022

1.11 Aim and Objectives of the Study

This doctoral thesis aims to bioconvert CO_2 into acetic acid using a homoacetogen-enriched microbial consortium. The process is studied in systems supplemented with zero-valent metals, which oxidize under anaerobic conditions, providing the necessary H_2 for microbial reactions while operating under methane-inhibited conditions.

The innovation of this study lies in the *in-situ* use of zero-valent metals as electron donors in microbial systems for CO_2 fixation (as an electron acceptor). This approach is cost-effective and sustainable, aligning with the principles of the circular economy for the production of the required H_2. Instead of relying on electrodes or exogenous supplementation of H_2 gas, the study suggests the *in-situ* utilization of zero-valent metals or waste metals. Under anaerobic conditions, these materials oxidize, generating abiotic H_2 through (bio)corrosion processes. For instance, the corrosion of zero-valent iron (ZVI), waste iron, or magnesium in CO_2-enriched systems provides hydrogen gas, which, along with CO_2, is consumed by the microbial consortia used as inoculum.

As highlighted in Sub-chapter 1.10, existing scientific reports on the bioconversion of CO_2 to acetate predominantly focus on microbial electrosynthesis cells (MECs), a highly complex system configuration, and only a few studies have successfully produced acetate from CO_2 and H_2 gas. In contrast, the use of *in-situ* metal to drive microbial reactors has been examined in limited reports, which have predominantly focused on pure acetogenic strains. No studies have explored acetate production from CO_2 and zero-valent metals utilizing mixed microbial consortia as inoculum.

However, the effectiveness of this process is hindered by methanogenic archaea, which compete with acetogenic bacteria for these reactants. Consequently, the inhibition of methanogenesis is essential to ensure that acetogenic microorganisms utilize CO_2 and H_2 for the production of acetic acid.

As mentioned above, only limited scientific studies have investigated the *in-situ* application of zero-valent metals for CO_2 utilization and acetic acid production using mixed microbial cultures. This highlights the necessity for further in-depth exploration of this promising hypothesis.

To investigate the hypothesis outlined, the experimental framework was divided into five distinct experimental groups, each targeting specific objectives and methodologies:

- ***First Experimental Set-up:***

The first group focused on elucidating the mechanisms of iron oxidation for the production of abiotic H_2. Key parameters such as the influence of N_2 and CO_2 gases, pH levels, sodium bicarbonate addition, temperature, agitation mode, iron concentration, and particle size were systematically examined. Sodium hydroxide solutions were also tested for CO_2 capture and subsequently integrated into systems containing iron. To manage the formation of siderite ($FeCO_3$) - a byproduct of CO_2 and iron reactions - weak acid (citric acid) was employed to treat oxidized iron.

- ***Second Experimental Set-up:***

Building upon the findings of the first group, the second group explored the feasibility of utilizing such systems in the presence of a microbial consortium as a proof of concept. To inhibit methanogenesis, various methods were tested, including pH reduction, heat-shock inoculum treatment prior to inoculation, and the use of a specific inhibitor, 2-bromoethanesulfonic acid (BES). As an economical alternative, sodium chloride was also investigated. To minimize costs, six low concentrations of BES were evaluated to determine their methane inhibition potential and their impact on acetogenesis.

- ***Third Experimental Set-up:***

The third experimental group built upon the methane inhibition strategies established in the second group, incorporating magnesium ribbons (Mg^0) as the hydrogen-producing electron donor. Minimal methodological modifications were made to accommodate the high reactivity of magnesium in aqueous solutions, which generates H_2 rapidly under elevated pressures. This experimental group evaluated the potential for acetic acid production under these conditions. BES was utilized as a chemical inhibitor at an optimized concentration of 4 mM, previously demonstrated to effectively inhibit methanogenesis without significantly impacting acetogenesis. For comparison, control experiments were conducted with systems designed to produce methane.

- ***Fourth Experimental Set-up:***

The fourth experimental group was designed to expand upon the findings highlighted in Sub-chapter 1.7. To date, scientific implementations for CO_2 utilization to produce acetic acid have primarily employed mixed microbial consortium sludge, often derived from wastewater. In this group, five different inocula were investigated alongside two

environmental samples collected from a river and a constructed wetland. The aim was to assess the potential of these seven inocula to produce acetic acid under anaerobic conditions, with CO_2 serving as the sole carbon source.

Zero-valent iron (ZVI) was used as the electron donor, while methanogenesis was inhibited using BES at a concentration of 4 mM. Additionally, the experimental design included a protocol to differentiate the contributions of suspended bacteria, bacteria detached from ZVI, and bacteria firmly attached to ZVI in acetic acid production.

Furthermore, the influence of varying CO_2 supplementation strategies was examined, focusing on frequent feeding versus low or high pressurized concentrations. These approaches aimed to evaluate their impact on the productivity of the inocula and the microbial system's response to different CO_2 supplementation conditions.

- ***Fifth Experimental Set-up:***

The fifth experimental group was focused on evaluating the potential of waste iron as a sustainable alternative to zero-valent iron in a circular economy framework for the production of acetic acid and ethanol under continuous operation by using bioreactors. This group utilized a two-stage bioreactor system connected in series, with the most productive mixed microbial consortium from the fourth experimental group serving as the inoculum. The experiments were structured into four distinct phases, each designed to test specific variables and operational strategies:

Phase A: The acetic acid and ethanol performance of the bioreactors was assessed by using newly introduced waste iron (*in situ*), where methanogenesis was inhibited with BES.

Phase B: The focus shifted to the reuse of previously oxidized waste iron with fresh growth medium. This phase tested the ability of the system to maintain productivity with recycled materials, aligning with circular economy principles.

Phase C: The productivity of the bioreactor was examined with the supplementation of H_2 gas produced externally from a hydrogen-produced reactor supplemented with waste iron. This phase provided insights into how externally supplied hydrogen impacts system efficiency compared to in situ-generated hydrogen.

Phase D: A bioreactor supplemented with hydrogen derived from a hydrogen-producing reactor containing double the amount of waste iron as in phase C. This phase aimed to explore the scalability and interconnected operation of multiple reactors for maximizing hydrogen and acetic acid production.

For all experimental groups, X-RD analysis was conducted to identify oxidation products formed on iron/waste iron surfaces. DNA extractions were also performed to analyze the microbial communities involved, providing insights into which species contributed to acetic acid production and how methanogenic activity was suppressed under each condition.

2: RESEARCH METHODOLOGY

2.1 Experimental Set-Up 1: Hydrogen Production Through Carbon Dioxide (CO_2) Reaction with Zero-Valent Iron (Fe^0) or Waste Iron (Fe-W)

This chapter employs different methods to examine several variables, as detailed below, that may affect the generation of abiotic H_2 from Fe^0, or Fe-W reacted with CO_2 under anaerobic mild operation conditions.

2.1.1 Experimental Set-Up 1: Experimental Implementation and Analyses.

All batch laboratory-scale experiments were conducted using 160 mL glass serum bottles. Two types of serum bottles were employed: clear glass sloping shoulder flat bottles and standard round clear glass borosilicate crimp top serum bottles. The dimensions and orientations of the two types of bottles facilitate the creation of a distinct air-water interface, with horizontal cross-sections measuring approximately 75 and 28 cubic meters, respectively. In all experiments, carbonate-buffered water with varying concentrations of $NaHCO_3$ was used to fill the serum bottles, reaching a working volume of either 64 mL or 48 mL, depending on the specific experiment.

Five different types of iron were utilized, including two commercial iron powders with distinct particle sizes: 10 μm and 800 μm. (sourced from Sigma Aldrich, for analysis reduced, particle size 10 μm EMSURE®, CAS No. 7439-89-6; Carlo Erba, Iron powder RPE for analysis, No. 451377). The other three types of iron were waste materials originating from the wood and machinery industry, and each had distinct characteristics. These comprised steel wool and two additional iron wastes with varying sizes (0.5 mm x 0.1 mm and 10 mm x 0.5 mm). The bottles were sealed using a butyl septum and an aluminum crimp. To create anoxic conditions, 99.99% N_2 and/or 99.99% CO_2 gases (supplied by: Linde – Hadjikyriakos Gas Ltd; Cyprus) were used. This was achieved by flashing the liquid phase of the experiments for 3 min, using a fine needle, which effectively removed oxygen from the headspace of the serum bottles. The main experiments were conducted at 33°C with continuous agitation at 100 rpm, and the initial pH was set to 6, as explained in sub-chapter 2.7.7.

The gas composition in all experiments was monitored and quantified over time in the headspace of the serum bottles using the methodology outlined in sub-chapter 2.7.1. Gas measurements are expressed as percentages (%). However, for calculating the number of moles of H_2, the ideal gas law equation (Eq. 20) was used:

$$pV=nRT \quad \text{(Eq.20)}$$

p: is the absolute pressure of the gas (atm),

V: is the volume of the gas (L),

n: is the number of moles of a gas,

R: is the gas constant, equal to the product of the Boltzmann constant and the Avogadro constant (0.082 L atm K^{-1} mol^{-1}), and

T: temperature in Kelvin.

Initially, the volume of gas produced in the headspace of the serum bottles was calculated by multiplying the headspace volume by the gas percentage (%) in order to convert the percentage into liters (L). Subsequently, the total amount of H_2 in moles was calculated using the ideal gas law.

2.1.2 Experimental Set-Up 1: Experimental Strategies - Investigating Hydrogen Evolution from Fe^0 Using Various Approaches.

2.1.2.1 Impact of N_2 and CO_2 gases on Fe^0 - Experiment 1

In this experimental setup, 25 g L^{-1} of Fe^0 was introduced into deionized water. A designated group, denoted as Group A, was created. Within Group A, two sub-groups were created, labeled A1(a,b,c) and A2(a,b,c). To establish anoxic conditions, the headspaces of Sub-groups A1 and A2 were purged with N_2 and CO_2 gas, respectively. The experiments were conducted in triplicate, spanning a total of 75 h. After the experimental period, X-ray diffraction (X-RD) analysis was performed to examine the resulting products of the reaction.

The primary focus of this experiment was to investigate the influence of N_2 and CO_2 gases on the oxidation of iron and the concurrent production of H_2, along with the resulting oxidation products. All the parameters of the experiment are summarized in Table 2.1.

2.1.2.2 Influence of $NaHCO_3$ at Different Concentrations on Fe^0 - Experiment 2

In this experimental setup, 25 g L^{-1} of Fe^0 was introduced into deionized water, which had been buffered with $NaHCO_3$ at different concentrations. A designated group, denoted as Group B, was created. Within Group B, two sub-groups were created based on the gas purged into the headspace of the serum bottles for the creation of anoxic conditions. Sub-group B1-B5 [$NaHCO_3$ concentrations - $B1_{(a,b,c)}$: 2 g L^{-1}; $B2_{(a,b,c)}$: 4 g L^{-1}; $B3_{(a,b,c)}$: 6 g L^{-1}; $B4_{(a,b,c)}$: 8 g L^{-1}; $B5_{(a,b,c)}$: 10 g L^{-1}] were utilized N_2 gas to establish anoxic conditions, while sub-group B6-B10 [$NaHCO_3$ concentrations - $B6_{(a,b,c)}$: 2 g L^{-1}; $B7_{(a,b,c)}$: 4 g L^{-1}; $B8_{(a,b,c)}$: 6 g L^{-1}; $B9_{(a,b,c)}$: 8 g L^{-1}; $B10_{(a,b,c)}$: 10 g L^{-1}] were utilized CO_2 gas for the same purpose. The experiments were conducted in triplicate, spanning a total of 75 h. Sub-groups $A1_{(a,b,c)}$ and $A2_{(a,b,c)}$ from experiment 1 were used as a control sample. After the experimental period, X-RD analysis was performed on samples $B5_{(a,b,c)}$ and $B10_{(a,b,c)}$ to analyze the resulting corrosion products from the reaction between Fe^0 and 10 g L^{-1} of $NaHCO_3$ under N_2 and CO_2 environments. The primary focus of this experiment was to investigate the influence of $NaHCO_3$ at different concentrations on Fe^0 under N_2 and CO_2 environments and its concurrent effect on hydrogen production. All the parameters of the experiment are summarized in Table 2.1.

2.1.2.3 Influence of Temperature on a Fe^0-$NaHCO_3$ System - Experiment 3

This experiment involved introducing 25 g L^{-1} of Fe^0 into deionized water buffered with 10 g L^{-1} $NaHCO_3$. A designated group, denoted as Group C, was created. Within Group C, five serum bottles, labeled C1-C5, were prepared, and each incubated at a different temperature [$C1_{(a,b,c)}$: 2 °C; $C2_{(a,b,c)}$: 20 °C; $C3_{(a,b,c)}$: 33 °C; $C4_{(a,b,c)}$: 40 °C; $C5_{(a,b,c)}$: 50 °C]. To establish anoxic conditions, CO_2 gas was purged into the serum bottles. The experiments were conducted in triplicate, spanning a total of 93 h.

The primary objective of this experiment was to investigate the influence of temperature on Fe^0 under $NaHCO_3$-buffered conditions and its concurrent effect on hydrogen production. A summary of all experiment parameters is provided in Table 2.1.

2.1.2.4 Influence of pH on a Fe^0-$NaHCO_3$ System - Experiment 4

This experiment involved introducing 25 g L^{-1} of Fe^0 into deionized water buffered with 10 g L^{-1} $NaHCO_3$. A designated group, denoted as Group D, was created. Within Group D, five serum bottles, labeled D1-D5, were prepared using CO_2 gas to establish anoxic conditions. Each sample was adjusted to different pH values [$D1_{(a,b,c)}$: pH 4; $D2_{(a,b,c)}$: pH 5; $D3_{(a,b,c)}$: pH 6; $D4_{(a,b,c)}$: pH 7; $D5_{(a,b,c)}$: pH 8] and incubated at the same conditions. The experiments were conducted in triplicate, spanning a total of 91 h.

The primary focus of this experiment was to investigate the influence of pH on Fe^0 under $NaHCO_3$-buffered conditions and its concurrent effect on hydrogen production. All the parameters of the experiment are summarized in Table 2.1.

2.1.2.5 Evaluation of Different Agitation Modes - Experiment 5

This experiment involved the introduction of 25 g L^{-1} of Fe^0 into deionized water buffered with 10 g L^{-1} $NaHCO_3$. A designated group, denoted as Group E, was created. Within Group E, three serum bottles, labeled E1-E3, were prepared and each sample was incubated at 33 °C under a distinct agitation mode [$E1_{(a,b,c)}$: 0 rpm; $E2_{(a,b,c)}$: 100 rpm; $E3_{(a,b,c)}$: 200 rpm]. The experiments were conducted in triplicate, spanning a total of 107 h.

The primary focus of this experiment was to investigate the effect of agitation mode on Fe^0 under $NaHCO_3$-buffered conditions and its concurrent effect on hydrogen production. All the parameters of the experiment are summarized in Table 2.1.

2.1.2.6 H_2 Generation Across Varied Fe^0 Concentrations - Experiment 6

This experiment involved the introduction of various concentrations of Fe^0 into deionized water buffered with 10 g L^{-1} $NaHCO_3$. A designated group, denoted as Group F, was created. Within Group F, four groups of serum bottles, labeled F1-F4, [Fe^0 concentration

- $F1_{(a,b,c)}$: 5 g L^{-1}; $F2_{(a,b,c)}$: 10 g L^{-1}; $F3_{(a,b,c)}$: 25 g L^{-1}; $F4_{(a,b,c)}$: 50 g L^{-1};] were prepared, utilizing CO_2 gas and incubated at 33 °C with an agitation mode of 100 rpm. The experiments were conducted in triplicate, spanning a total of 107 h.

The primary focus of this experiment is to extract data regarding the yield of produced H_2 over time under different concentrations of Fe^0. All the parameters of the experiment are summarized in Table 2.1.

2.1.2.7 Impact of Fe^0 Particle Sizes - Experiment 7

This experiment involved the introduction of various concentrations of Fe^0 into deionized water buffered with 10 g L^{-1} $NaHCO_3$. In contrast to other experiments utilizing 10 μm-sized Fe^0 particles, this study employed Fe^0 particles with a size of 800 μm. The serum bottles used in the experiments were incubated under identical conditions as the other experiments (33 °C, 100 rpm). To facilitate comparison with experiments involving fine-grained Fe^0, a control sample was prepared using 10 μm Fe^0 particles at a concentration of 25 g L^{-1}. A designated group, denoted as Group G, was created. Within Group G, two sub-groups were created based on the Fe^0 particle sizes and concentration. Sub-group G1-G3 represent systems prepared using 800 μm-sized Fe^0 particles at different concentrations [$G1_{(a,b,c)}$: 25 g L^{-1}; $G2_{(a,b,c)}$: 100 g L^{-1}; $G3_{(a,b,c)}$: 200 g L^{-1}] while Sub-group G4 represents systems that prepared using 10 μm-sized Fe^0 particles at a concentration of $G4_{(a,b,c)}$: 25 g L^{-1}. All samples utilized CO_2 gas to establish anoxic conditions. The experiments were conducted in triplicate, spanning a total of 115 h.

The primary focus of this experiment is to examine the role of iron particle size in the production of H_2 over time. All the parameters of the experiment are summarized in Table 2.1.

2.1.2.8 Impact of *In-Situ* Mechanical Action on Fe^0 - Experiment 8

This experiment involved the introduction of 25 g L^{-1} of Fe^0 into deionized water buffered with 10 g L^{-1} $NaHCO_3$. Additionally, to induce a mechanical effect on the iron, glass beads and boiling chips were added to the bottles (sourced from: Merck, Glass beads, Anti-bumping granules, diam. ~5 mm, CAS No. 18406; Merck, Boiling chips granules,

size 2-8 mm, CAS No. 1.07913). A control sample was prepared without the addition of any mechanical disruptor material.

A designated group, denoted as Group H, was created. Within Group H, three sub-groups were created based on the disruptor material that was used. Sub-groups H1 and H2 represent the systems that glass beads and boiling chips were used *in-situ* respectively [$H1_{(a,b,c)}$: 145 g L^{-1} glass beads; $H2_{(a,b,c)}$: 145 g L^{-1} boiling chips] and sub-group H3 represents the sample without the use of any mechanical disruptor *in-situ*. All samples utilized CO_2 gas to establish anoxic conditions. The experiments were conducted in triplicate, spanning a total of 115 h.

The primary focus of this experiment is to investigate the effect of the mechanical action of specific materials (*in-situ*) on iron and the resulting H_2 production over time under $NaHCO_3$-buffered conditions. All the parameters of the experiment are summarized in Table 2.1.

2.1.2.9 Impact of Air-Water Interface Area Size - Experiment 9

This experiment involved the introduction of 25 g L^{-1} of Fe^0 into deionized water buffered with 10 g L^{-1} $NaHCO_3$. Two different types of systems, each with distinct air-water interface areas, were employed. A designated group, denoted as Group I was created. Within Group I, two groups of serum bottles, labeled I1 -I2, [$I1_{(a,b,c)}$: 25 cm^2 interface area; $I2_{(a,b,c)}$: 75 cm^2 interface area], were prepared. To establish anoxic conditions, CO_2 was used in all experimental systems. The experiments were conducted in triplicate, spanning a total of 115 h.

The primary focus of this experiment is to investigate whether the size of the air-water interface area affects the utilization of CO_2 and, consequently, leads to an increase in the production of H_2 over time. All the parameters of the experiment are summarized in Table 2.1.

2.1.2.10 Waste Iron Materials (Fe-W) Evaluation with Different Particle Sizes - Experiment 10

In this experiment, three distinct types of waste iron materials were used, obtained from the wood and machinery industry. These waste iron materials were added to deionized water buffered with 10 g L^{-1} $NaHCO_3$ at two different concentrations, namely 25 g L^{-1} and 100 g L^{-1}. Three groups, denoted as J, were created. Sub-groups J1-J2, J3-J4, and J5-J6 were prepared, with each group representing scrap iron particles possessing surface areas of 0.05 mm², 5 mm², and steel wool, respectively, at the two concentrations mentioned above [$J1_{(a,b,c),\ (25\ g\ L^{-1}\ Fe^0)}$ - $J2_{(a,b,c),\ (100\ g\ L^{-1}\ Fe^0)}$: 0.05 mm^2; $J3_{(a,b,c),\ (25\ g\ L^{-1}\ Fe^0)}$ – $J4_{(a,b,c),\ (100\ g\ L^{-1}\ Fe^0)}$: 5 mm^2; $J5_{(a,b,c),\ (25\ g\ L^{-1}\ Fe^0)}$ – $J6_{(a,b,c),\ (100\ g\ L^{-1}\ Fe^0)}$: Steel wool]. CO_2 was employed in all experimental groups to establish anoxic conditions. The experiments were conducted in triplicate, spanning a total of 139 h.

The primary objectives of this experiment were to explore the potential of waste iron materials for hydrogen production, assess the influence of varying surface area in scrap iron particles on hydrogen generation, and evaluate the role of scrap iron concentration in the gradual production of H_2. A comprehensive summary of the experiment's parameters can be found in Table 2.1.

Table 2.1: Overview of experimental parameters and conditions of experiments 1-10 of the experimental set-up 1.

Experiments - Groups	Exp. 1: Group A		Exp. 2: Group B		Exp. 3: Group C	Exp. 4: Group D	Exp. 5: Group E	Exp. 6: Group F	Exp. 7: Group G		Exp. 8: Group H			Exp. 9: Group I	Exp. 10: Group J		
Sub-Groups	**A1**	**A2**	**B1-B5**	**B6-B10**	**C1-C5**	**D1-D5**	**E1-E3**	**F1-F4**	**G1-G3**	**G4**	**H1**	**H2**	**H3**	**I1-I2**	**J1-J2**	**J3-J4**	**J5-J6**
Fe° Concentration (g L^{-1})	25		25		25	25	25	**5; 10; 25; 50**	**25; 100; 200**	**25**	25			25	**25; 100 (Waste Iron)**		
Fe° Size (µm or mm^2)	10 µm		10 µm		10 µm	10 µm	10 µm	10 µm	**800 µm**	**10 µm**	10 µm			10 µm	**0.05 mm^2**	**5 mm^2**	**Steel Wool**
Fe° Pretreatment	No		No		No	No	No	No	No		No			No	No		
Addition of $NaHCO_3$ (g L^{-1})	No		**2; 4; 6; 8; 10**		10	10	10	10	10		10			10	10		
Gas Purging Injection	**N_2**	**CO_2**	**N_2**	**CO_2**	CO_2	CO_2	CO_2	CO_2	CO_2		CO_2			CO_2	CO_2		
Temperature (C°)	33		33		**2; 20; 33; 40; 50**	33	33	33	33		33			33	33		
pH	6		6		6	**4; 5; 6; 7; 8**	6	6	6		6			6	6		
Agitation (rpm)	100		100		No	100	**0; 100; 200**	100	100		100			100	100		
Total / Working Volume (mL)	160/64		160/64		160/48	160/48	160/48	160/48	160/48		160/48			160/48	160/48		
Mechanical Action	No		No		No	No	No	No	No		**Glass beads**	**Boiling chips**	**No**	No	No		
Gas - Water Interface Area (cm^2)	28		28		28	28	28	28	28		28			**28; 75**	28		
Duration (h)	75		75		93	91	107	107	115		115			115	139		

2.1.2.11 Impact of $NaHCO_3$ Solutions Generated Through CO_2 Capture in NaOH Solutions on Fe^0 - Experiment 11

This experiment involved introducing two distinct types of waste Fe^0 materials: Fe-W (0.05 mm²) and Fe-W (Steel Wool), each at a concentration of 100 g L^{-1}. Instead of employing deionized water buffered with $NaHCO_3$, an alternative methodology was applied. For the preparation of the $NaHCO_3$ solution, two distinguished solutions with concentrations of 0.25 M and 0.75 M NaOH were prepared and exposed to CO_2 gas at 25°C. The solutions underwent flashing with N_2:CO_2 (31.5%:68.5%) for 25 min and 55 min, respectively, at a constant flow rate of 3 L min^{-1}, following the procedure outlined by Yoo et al. (2013). As a result, three sub-groups, denoted as K, were created. Sub-groups K1 and K2 represent waste Fe^0 with a particle size of 0.05 mm^2 and steel wool, respectively, introduced into the $NaHCO_3$ solution resulting from the reaction between NaOH (0.25 M) and CO_2 [$K1_{(a,b,c)}$: 0.05 mm^2 Fe^0 – 0.25 M NaOH; $K2_{(a,b,c)}$: Steel wool – 0.25 M NaOH]. Sub-groups K3 and K4 represent the same iron waste as K1 and K2, introduced into the $NaHCO_3$ solution resulting from the reaction of NaOH (0.75 M) and CO_2 [$K3_{(a,b,c)}$: 0.05 mm^2 Fe^0 – 0.75 M NaOH; $K4_{(a,b,c)}$: Steel wool – 0.75 M NaOH]. The last sub-groups, K5 and K6, represent the same iron wastes as the previous sub-groups; however, no $NaHCO_3$ solution was used, but only deionized water flashed with CO_2 for 25 min at the same flow rate described above [$K5_{(a,b,c)}$: 0.05 mm^2 Fe^0 – water; $K6_{(a,b,c)}$: Steel wool – water]. The experiments were conducted in triplicate, spanning a total of 164 h.

The primary objective of this experiment was to explore the potential of waste iron materials for hydrogen production. This was achieved using $NaHCO_3$ solutions of varying concentrations, which were created by capturing CO_2 in a NaOH solution. Furthermore, it aimed to assess the influence of varying surface areas of scrap iron particles on hydrogen generation. A comprehensive summary of the experiment's parameters can be found in Table 2.2.

2.1.2.12 Impact of $NaHCO_3$ Solutions Generated Through CO_2 Capture in NaOH Solutions on Oxidized or Pretreated Waste Iron Materials - Experiment 12

This experiment utilized waste Fe^0 materials obtained from Experiment 11. The previously processed waste Fe^0 materials (Fe-W: 0.05 mm² and steel wool) were subsequently employed in a new batch experiment, following the same methodology as in Experiment 11. The $NaHCO_3$ solutions used resulted from the reaction of two distinct concentrations of NaOH (0.25 M and 0.75 M) with CO_2 using the same processes as described in Experiment 11. The processed oxidized waste Fe^0 materials were used as-is from Experiment 11, at a concentration of 100 g L^{-1} for the conduction of the experiment. Furthermore, based on the X-RD results from Experiments 1 and 2, to eliminate the $FeCO_3$ formed on the surface of the waste Fe^0 materials, another 100 g L^{-1} of the aforementioned oxidized Fe^0 was separately subjected to a weak acid for 3 h for the dissolution of the oxidized layer covering the Fe^0 samples. A citric acid solution at a concentration of 0.5 M was used for oxide dissolution. Consequently, six sub-groups, denoted as L, were created.

Sub-groups L1-L2, L3-L4, and L5-L6 were prepared, with each group representing the systems with oxidized 0.05mm^2 Fe^0 and oxidized steel wool separately subjected to distinguished solutions with different concentrations of $NaHCO_3$ (NaOH 0.25 M and 0.75 M) and water, respectively, without previously undergoing an acid pretreatment [$L1_{(a,b,c)}$: 0.05 mm^2 Fe^0 – No pretreatment – NaOH (0.25M); $L2_{(a,b,c)}$: Steel wool – No pretreatment – NaOH (0.25M)], [$L3_{(a,b,c)}$: 0.05 mm^2 Fe^0 – No pretreatment – NaOH (0.75M); $L4_{(a,b,c)}$: Steel wool – No pretreatment – NaOH (0.75M)], [$L5_{(a,b,c)}$: 0.05 mm^2 Fe^0 – No pretreatment – Water; $L6_{(a,b,c)}$: Steel wool – No pretreatment – Water].

For the preparation of the other three sub-groups, L7-L8, L9-L10, and L11-L12, the same oxidized waste Fe^0 material was used by applying the same methodology as above; however, the oxidized Fe^0 samples were previously pretreated with citric acid. [$L7_{(a,b,c)}$: 0.05 mm^2 Fe^0 – Citric acid – NaOH (0.25M); $L8_{(a,b,c)}$: Steel wool – Citric acid – NaOH (0.25M)], [$L9_{(a,b,c)}$: 0.05 mm^2 Fe^0 – Citric acid – NaOH (0.75M); $L10_{(a,b,c)}$: Steel wool – Citric acid – NaOH (0.75M)], [$L11_{(a,b,c)}$: 0.05 mm^2 Fe^0 – Citric acid – Water; $L12_{(a,b,c)}$: Steel wool – Citric acid –Water].

To establish anoxic conditions, CO_2 gas was purged in the headspace of the serum bottles. The experiments were conducted in triplicate, spanning a total of 138 h.

The primary objectives of this experiment were to investigate the potential of oxidized waste iron materials for hydrogen production under different concentrations of $NaHCO_3$ solution created by capturing CO_2 in a NaOH solution. Additionally, it aimed to evaluate the influence of citric acid treatment on the oxidized surface of waste iron particles and its impact on hydrogen generation. A comprehensive summary of the experiment's parameters can be found in Table 2.2.

Table 2.2: Overview of experimental parameters and conditions of experiments 11 & 12 of the experimental group 1.

Experiments- Groups	Exp. 11: Group K			Exp. 12: Group L					
Sub-Groups	K1 -K2	K3-K4	K5-K6	L1-L2	L3-L4	L5-L6	L7-L8	L9-L10	L11-L12
Fe° Concentration (g L^{-1})	100 (Waste Iron)			100 (Oxidized waste Iron)					
Fe° Size (µm or mm^2)	0.05 mm^2; Steel Wool			0.05 mm^2 iron; Steel wool					
Fe° Pretreatment	No			No			Citric acid (0.5 M)		
Addition of $NaHCO_3$ (g L^{-1})	NaOH (0.25 M) + CO_2	NaOH (0.75 M) + CO_2	H_2O + CO_2	NaOH (0.25 M) + CO_2	NaOH (0.75 M) + CO_2	H_2O + CO_2	NaOH (0.25 M) + CO_2	NaOH (0.75 M) + CO_2	H_2O + CO_2
Gas Purging Injection	CO_2			CO_2					
Temperature (C°)	33			33					
pH	6			6					
Agitation (rpm)	100			100					
Total / Working Volume (mL)	160/48			160/48					
Mechanical Action	No			No					
Gas - Water Interface Area (cm^2)	28			28					
Duration (h)	164			138					

2.2 Experimental Set-Up 2: Bioconversion of Carbon Dioxide (CO_2) to Volatile Fatty Acids (VFAs) Using Anaerobic Granular Sludge (AnGrSL) With Zero-Valent Iron (ZVI - Fe^0) in Methanogenesis-Inhibited Systems.

This chapter delves into a novel proof of concept for CO_2 utilization in the production of value-added products such as carboxylic acids, featuring carbon atoms ranging from 1 to 5 (including formic, acetic, propionic, butyric, iso-butyric, and valeric acid). These short-chain fatty acids (SCFAs) can be generated under aquatic ambient conditions within a system employing anaerobic granular sludge (AnGrSL) and CO_2 as the sole carbon source (electron acceptor) for the microbial consortium of the AnGrSL. Instead of utilizing exogenous H_2 gas (electron donor) for the microbial reactions, a Zero-valent Iron (ZVI - Fe^0) was employed *in-situ* in the systems that under anaerobic and carbonate aqueous environment oxidized, producing H_2, thereby mitigating safety concerns associated with the use of exogenous H_2 gas supplier. In these systems involving CO_2, H_2, and untreated bacterial population consortia, methanogenesis is thermodynamically favored over acetogenesis, with methanogens competing with Acetogens for H_2 utilization. Hence, the primary aim of these experimental setups was to delineate various strategies for inhibiting or eliminating methanogens in an AnGrSL-CO_2-ZVI (Fe^0) system, thereby enriching the system with Acetogens or spore-forming bacteria to facilitate the production of acetic acid or other volatile fatty acids (VFAs). These strategies include a) lowering the pH of the systems, b) using both specific and non-specific inhibitors, such as 2-bromoethanesulfonate (BES) and sodium chlorite (NaCl), at various concentrations, and c) applying thermal shock to the anaerobic granular sludge (AnGrSL) before inoculation, as detailed in Sub-chapter 2.2.2.

2.2.1 Experimental Set-Up 2: Experimental Implementation and Analyses.

For the experimental setup, anaerobic granular sludge (AnGrSL) was utilized as the inoculum. This sludge was obtained from a mesophilic up-flow anaerobic sludge blanket bioreactor (UASB) treating dairy wastewater with a pH range of 6.8–7.3. Before its application, AnGrSL underwent a pre-treatment process to eliminate any residual organic substrates. This involved washing the AnGrSL with a phosphate buffer (20 mM) and sieving it through a #18 mesh (with a pore diameter of 1,000 μm). The sieved sludge was

then divided into two 1 L bottles containing a phosphate buffer solution (20 mM), sealed with screw caps fitted with rubber septa, and flushed with CO_2. Following this, the pH of the two bottles was adjusted to 5-6 and 6-6.5, respectively, and the bottles were incubated at 33°C and 100 rpm for 3 days.

All batch laboratory-scale experiments were conducted using 250 mL glass serum bottles. Each serum bottle was inoculated with 100 g L^{-1} of wet AnGrSL, which had been treated with phosphate buffer, and exposed to 100 g L^{-1} of ZVI - Fe^0 obtained from Sigma Aldrich (reduced for analysis, particle size 10 μm EMSURE®, CAS No. 7439-89-6). Subsequently, the serum bottles were filled with a bacterial growth medium following the protocol proposed by Angelidaki et al. (2009) as described in Sub-chapter 2.6, albeit without the addition of $Na_2S \cdot 9H_2O$, resulting in a working volume of 100 mL. The serum bottles were then sealed with rubber septa and screw caps. To create anaerobic conditions, the bottles were flushed with 99.9% CO_2 (supplied by Linde – Hadjikyriakos Gas Ltd; Cyprus) for 5 minutes using a fine needle through the rubber septa. Following this, CO_2 was injected into the serum bottles, serving as the sole carbon source, using a glass syringe equipped with a fine needle until a pressure of 0.5 bar was achieved in the headspace of the bottles. Moreover, control samples were prepared for all experimental systems, omitting ZVI (Fe^0). Subsequently, all systems were incubated at 33°C with agitation at 100 rpm.

Gas composition in the headspace of the serum bottles from bacterial reactions (CO_2 and H_2 utilization; CH_4 production) was analyzed using gas chromatography, as detailed in sub-chapter 2.1. Concentrations of metabolites (volatile fatty acids - VFAs) resulting from CO_2/H_2 bacterial utilization were determined via high-performance liquid chromatography, as described in Sub-chapter 2.7.2. X-ray diffraction (X-RD) patterns of selected ZVI specimens (both non-exposed and exposed to a CO_2 environment with bacteria) were obtained following the procedure outlined in sub-chapter 2.7.5. pH and pressure levels during the experiments were monitored, as explained in Sub-chapters 2.7.7 and 2.7.8, respectively. Upon completion of the experiments, DNA extraction was performed for Next-Generation Sequencing analysis to identify the bacterial profile, as outlined in Sub-chapter 2.7.4, for the following samples: a) the initial inoculum of AnGrSL, b) the control system with 50 mM of BES, c) the system utilizing heat pre-treated AnGrSL operating at pH 6 - 6.5, d) the systems utilizing AnGrSL exposed to ZVI

– Fe^0 and 50 mM of BES, operating at pH 5 - 6 and pH 6 - 6.5, and e) the system utilizing AnGrSL exposed to ZVI – Fe0 and NaCl (60 g L-1), operating at pH 5 - 6. The same procedure was also conducted to identify the archaeal profile for the following samples: a) the control system with 50 mM of BES, b) the system utilizing AnGrSL exposed to ZVI - Fe^0 and 50 mM BES, operating at pH 5 - 6, and c) the system utilizing heat pre-treated AnGrSL, operating at pH 6 - 6.5.

2.2.2 <u>Experimental Set-Up 2:</u> Experimental Strategies: Investigating Methane Inhibition Through Various Approaches for VFA Production.

2.2.2.1 Impact of Low pH on Methane Inhibition in an AnGrSL-ZVI (Fe^0) System - Experiment 1

In this experimental setup, a mixture comprising 100 g L^{-1} of AnGrSL and 100 g L^{-1} of ZVI (Fe^0) was introduced into a growth medium. A set of triplicate bottles was prepared and designated as Group A. The experiment spanned 15 days and was segmented into two cycles. To establish anaerobic conditions, the headspaces of the Group A bottles were purged with CO_2 gas. Then, CO_2 gas was injected into the serum bottles as the sole carbon source for the bacterial consortia until the pressure reached approximately 0.5 bar. This process was conducted on Day 0 and Day 7. During cycle 1, which extended over 7 days (Day 0-7), no methanogenesis inhibition strategy was implemented, allowing the systems to generate methane while maintaining a daily pH regulation at 5. In cycle 2, spanning 8 days (Day 7-15), the pH was daily reduced below 3 using HCl as described in Sub-chapter 2.7.7 as a methanogenesis inhibition method.

The primary aim of this experiment was to examine the impact of pH reduction in an AnGrSL-ZVI (Fe^0) system as a strategy for methane inhibition and to enhance VFA production. All experimental parameters are summarized in Table 2.3.

2.2.2.2 Evaluation of Utilizing Thermally Pre-treated AnGrSL in a ZVI (Fe^0) System for VFAs Production - Experiment 2

In this experimental setup, 100 g L^{-1} of thermally pre-treated AnGrSL (Fig. 2.1) and 100 g L^{-1} of ZVI (Fe^0) were introduced into a growth medium. A set of triplicate bottles was prepared and designated as Group B. Within Group B, two sub-groups, labeled $B1_{(a,b,c)}$ and $B2_{(a,b,c)}$, were created according to the pH adjustments (pH working values) which were 5-6 and 6-6.5 respectively. The experiment spanned 12 days and was conducted in one cycle. To establish anaerobic conditions, the headspaces of the Group B bottles were purged with CO_2 gas. Then, CO_2 gas was injected into the serum bottles as the sole carbon source for the bacterial consortia until the pressure reached approximately 0.5 bar. This process was conducted on Day 0 and Day 8. To impede methanogenesis, AnGrSL was subjected to a heat pre-treatment method at 95°C for 30 minutes before the inoculation, aiming to foster the enrichment of spore-forming bacteria within the systems, as depicted in Fig. 2.1. The pH of the systems was adjusted daily using HCl.

The primary objective of this experiment was to investigate the elimination of methane-producing bacteria by applying a short thermal treatment methodology to AnGrSL before the inoculations as a strategy to enhance the production of acetic acid. All experimental parameters are summarized in Table 2.3.

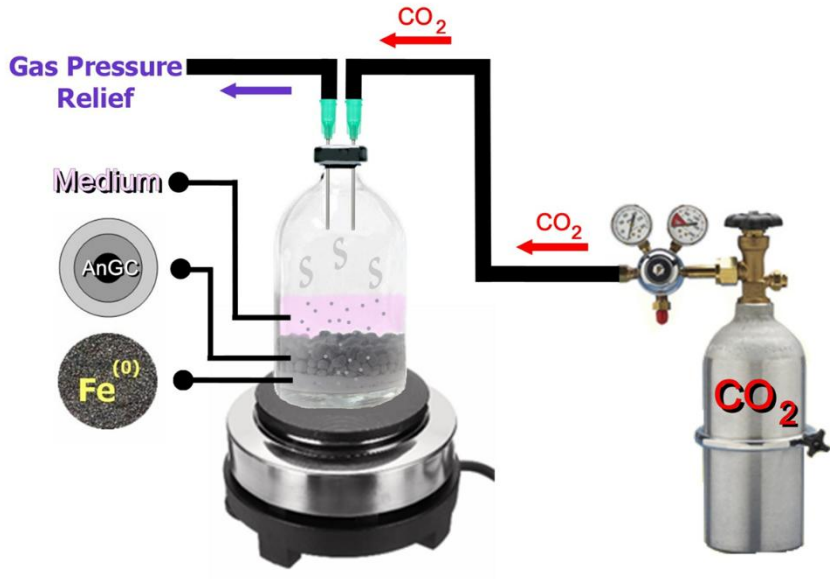

Fig. 2.1: Thermal treatment methodology applied on AnGrSL-ZVI (Fe^0) system for methane inhibition.

2.2.2.3 Impact of 50 mM of Sodium 2-bromoethanesulfonate (BES), on Methane Inhibition in an AnGrSL-ZVI (Fe^0) system - Experiment 3

In this experimental setup, a mixture comprising 100 g L^{-1} of AnGrSL and 100 g L^{-1} of ZVI (Fe^0) was introduced into a growth medium. A set of triplicate bottles was prepared and designated as Group C. Within Group C, two sub-groups, labeled $C1_{(a,b,c)}$ and $C2_{(a,b,c)}$, were created according to the pH adjustments (pH working values) which were 5-6 and 6-6.5 respectively. The experiment spanned 27 days and was segmented into two cycles. To establish anaerobic conditions, the headspaces of the Group C bottles were purged with CO_2 gas. Then, CO_2 gas was injected into the serum bottles as the sole carbon source for the bacterial consortia until the pressure reached approximately 0.5 bar. This process was conducted on Days 0, 7, 15, and 23. During cycle 1, spanning 15 days (Day 0-15), a specific inhibitor (50 mM of BES) was introduced in the systems as a methane inhibition strategy on day 0. Upon completion of cycle 1, 90% of the growth medium was replaced with fresh medium in the serum bottles while retaining the AnGrSL and ZVI (Fe^0). Subsequently, cycle 2 commenced, lasting for 12 days (Day 15-27), without the addition of a further BES inhibitor. The pH of the systems was adjusted daily using HCl.

The primary objective of this experiment was to investigate methane inhibition within an AnGrSL-ZVI (Fe^0) system utilizing the chemical BES at a high concentration commonly reported in international literature. Additionally, the study aimed to evaluate the efficacy of maintaining methane inhibition upon removal of BES and introducing a fresh growth medium without further BES supplementation in the systems. These strategies were implemented to enhance acetic acid production. All experimental parameters are summarized in Table 2.3.

2.2.2.4 Assessment of the Methane Inhibitory Effect of BES at Various Low Concentrations (1-10 mM) - Experiment 4

In this experimental setup, a mixture comprising 100 g L^{-1} of AnGrSL and 100 g L^{-1} of ZVI (Fe^0) was introduced into a growth medium. A set of triplicate bottles was prepared and designated as Group D. Within Group D, six sub-groups, labeled $D1_{(a,b,c)}$, $D2_{(a,b,c)}$, $D3_{(a,b,c)}$, $D4_{(a,b,c)}$, $D5_{(a,b,c)}$, and $D6_{(a,b,c)}$ were created based on the concentration of the specific inhibitor used. The experiment spanned 22 days and was segmented into two

cycles. To establish anaerobic conditions, the headspaces of the Group D bottles were purged with CO_2 gas. Subsequently, CO_2 gas was then injected into the serum bottles as the sole carbon source for the bacterial consortia until the pressure reached approximately 0.5 bar. This process was conducted on Days 0, 8, 11, and 15. During cycle 1, spanning 15 days (Day 0-15), a specific inhibitor at various concentrations (1, 2, 4, 6, 8, and 10 mM of BES) was introduced in the systems as a methane inhibition strategy on day 0. Upon completion of cycle 1, 90% of the growth medium was replaced with fresh medium in the serum bottles while retaining the AnGrSL and ZVI (Fe^0). Subsequently, cycle 2 commenced, lasting for 7 days (Day 15-22), without the addition of further BES inhibitor. The pH of the systems was adjusted daily at 5-6 using HCl.

The primary objective of this experiment was to investigate methane inhibition within an AnGrSL-ZVI (Fe^0) system utilizing varying low concentrations of BES. The aim was to minimize the usage of this chemical while identifying the optimal concentration of BES that achieves maximum methane inhibition with minimal impact on acetogens and maximal acetic acid production. Additionally, the study evaluated the efficacy of maintaining methane inhibition upon removal of these low concentrations of BES and the introduction of a fresh growth medium without further BES supplementation in the systems. All experimental parameters are summarized in Table 2.3.

2.2.2.5 Effect of NaCl at Various Concentrations on Methane Inhibition When Employed in an AnGrSL - ZVI (Fe^0) System - Experiment 5

In this experimental setup, a mixture comprising 100 g L^{-1} of AnGrSL and 100 g L^{-1} of ZVI (Fe^0) was introduced into a growth medium. A set of triplicate bottles was prepared and designated as Group E. Within Group E, three sub-groups, labeled $E1_{(a,b,c)}$, $E2_{(a,b,c)}$, $E3_{(a,b,c)}$ were created based on the concentration of the non-specific inhibitor used. The experiment spanned 24 days and was segmented into one cycle. To establish anaerobic conditions, the headspaces of the Group E bottles were purged with CO_2 gas. Subsequently, CO_2 gas was injected into the serum bottles as the sole carbon source for the bacterial consortia until the pressure reached approximately 0.5 bar. This process was conducted on Days 0, 3, 10, and 17. To impede methanogenesis, AnGrSL was exposed to various concentrations of NaCl ($E1_{(a,b,c)}$ 30 g L^{-1}; $E2_{(a,b,c)}$ 60 g L^{-1}; $E3_{(a,b,c)}$ 90 g L^{-1}). The pH of the systems was adjusted daily at 5-6 using HCl.

The primary objective of this experiment was to investigate methane inhibition within an AnGrSL-ZVI (Fe^0) system using a non-specific inhibitor, such as NaCl, at three distinct concentrations. The aim was to identify an economically viable alternative to using BES, aiming to minimize methane production without adversely affecting acetogenesis. All experimental parameters are summarized in Table 2.3.

Table 2.3: Overview of parameters and conditions of experiments 1-5 of experimental set-up 2.

Experiments - Groups	Exp. 1: Group A		Exp. 2: Group B		Exp. 3: Group C		Exp. 4: Group D						Exp. 5: Group E		
Sub-Groups	$A_{(a,b,c)}$		**$B1_{(a,b,c)}$**	**$B2_{(a,b,c)}$**	**$C1_{(a,b,c)}$**	**$C2_{(a,b,c)}$**	**$D1_{(a,b,c)}$**	**$D2_{(a,b,c)}$**	**$D3_{(a,b,c)}$**	**$D4_{(a,b,c)}$**	**$D5_{(a,b,c)}$**	**$D6_{(a,b,c)}$**	**$E1_{(a,b,c)}$**	**$E2_{(a,b,c)}$**	**$E3_{(a,b,c)}$**
Cycles	**1: Day 0-7**	**2: Day 7-15**	**1:** Day 0-12		**1:** Day 0-15; **2:** Day 15-27 (New growth medium)		**1:** Day 0-15; **2:** Day 15-22 (New growth medium)						**1:** Day 0-24		
Duration	15 days		12 days		27 days		22 days						24 days		
Starting point	Day 0		Day 0		Day 0		Day 0						Day 0		
CO_2 flashing	CO_2 at day 0 & 7 (3 min.)		CO_2 at day 0 & 7 (3 min.)		CO_2 at day 0, 7, 15 & 23 (3 min.)		CO_2 at day 0, 8, 11 & 15 (3 min.)						CO_2 at day 0, 3, 10 & 17 (3 min.)		
Carbon Source	CO_2 at ~ 0.5 bar (day 0 & 7)		CO_2 at ~ 0.5 bar (day 0 & 7)		CO_2 at ~ 0.5 bar (day 0, 7, 15 & 23)		CO_2 at ~ 0.5 bar (day 0, 8, 11 & 15)						CO_2 at ~ 0.5 bar (day 0, 3, 10 & 17)		
H_2 supply	100 g L^{-1} Fe^0 Added on day 0		100 g L^{-1} Fe^0 Added on day 0		100 g L^{-1} Fe^0 Added on day 0		100 g L^{-1} Fe^0 Added on day 0						100 g L^{-1} Fe^0 Added on day 0		
Fe° Size (µm)	10		10		10		10						10		
Methanogenesis Inhibition	**X**	**AnGrSL exposed to acid for 8 days (Day 7-15)**	**AnGrSL thermally pre-treated (95 °C for 30 min) (Day 0)**		**AnGrSL exposed to 50 mM of BES (Day 0)**		**1 mM BES (Day 0)**	**2 mM BES (Day 0)**	**4 mM BES (Day 0)**	**6 mM BES (Day 0)**	**8 mM BES (Day 0)**	**10 mM BES (Day 0)**	**30 g L^{-1} NaCl (Day 0)**	**60 g L^{-1} NaCl (Day 0)**	**90 g L^{-1} NaCl (Day 0)**
pH	**5**	**3**	**5-6**	**6-6.5**	**5-6**	**6-6.5**	5-6						5-6		
Temperature (C°)	33		33		33		33						33		
Agitation (rpm)	100		100		100		100						100		
Total / Working Volume (mL)	250/100		250/100		250/100		250/100						250/100		

2.3 Experimental Set-Up 3: Bioconversion of Carbon Dioxide (CO_2) to Volatile Fatty Acids (VFAs) Using Anaerobic Granular Sludge (AnGrSL) With Magnesium Ribbon (Mg^0) in Methanogenesis-Inhibited Systems

The aim of this experimental set-up is to examine the bioconversion of CO_2 into acetic acid under aquatic ambient conditions within systems employing anaerobic granular sludge (AnGrSL) and CO_2 as the sole carbon source (electron acceptor) for the microbial consortium of the AnGrSL. However, as an electron donor (H_2) for the microbial reactions, instead of using ZVI -$Fe^{0,}$ as demonstrated in experimental group 2, magnesium ribbon (Mg^0) was employed *in-situ* in the systems, avoiding the exogenous H_2 supply of the systems. Magnesium is also oxidized under anaerobic and carbonate aqueous environments, producing H_2 as ZVI. However, a significantly lower concentration was required. In these AnGrSL-CO_2- Mg^0 systems, methanogenesis was inhibited by applying several strategies, as done in the experimental group 1 with minimal alteration, so that the reactants (CO_2 and H_2) increased and thereby enriched the system with Acetogens to facilitate the production of acetic acid or other VFAs. These strategies include a) the use of a specific inhibitor (4 mM BES), b) the use of a non-specific inhibitor (NaCl), at various concentrations, and c) applying thermal shock (95 °C for 30 min) to the anaerobic granular sludge (AnGrSL) before the inoculation, as illustrated in Fig. 2.1.

2.3.1 Experimental Set-Up 3: Experimental Implementation and Analyses

For the experimental setup, anaerobic granular sludge (AnGrSL) was used as the inoculum. This sludge was obtained from a mesophilic up-flow anaerobic sludge blanket bioreactor (UASB) treating dairy wastewater with a pH range of 6.8 to 7.3. Before its application, AnGrSL underwent a series of preparatory processes, as described in sub-chapter 2.2.1, including washing, sieving, and deposition in a 2 L bottle containing a phosphate buffer solution (10 mM). The bottle was then sealed with screw caps fitted with rubber septa and flushed with CO_2 to mitigate background CH_4 production. Subsequently, the pH of the bottle was adjusted to 6.5 and stored in a shaking incubator (100 rpm) at 33 °C for 3 days.

All batch laboratory-scale experiments were conducted using 250 mL glass serum bottles. Each serum bottle was inoculated with wet pre-cleaned AnGrSL (8% w/v) and exposed

to Mg^0 (≥ 99.5%, Sigma Aldrich, CAS Number: 7439-95-4) (8% w/v). Subsequently, the serum bottles were filled with a carbonate-buffered mineral medium prepared following the protocol proposed by Schink (1994) as described in Sub-chapter 2.6., without adding $Na_2S \cdot 9H_2O$, reaching the working volume of 120 mL. The serum bottles were then sealed with rubber septa and screw caps and, for the creation of the anaerobic conditions, were flushed with 99.9% N_2 (supplied by Linde – Hadjikyriakos Gas Ltd; Cyprus) for 3 minutes using a fine needle through the rubber septa. Following this, as an electron acceptor, 60 mL of CO_2 (Linde – Hadjikyriakos Gas Ltd; Cyprus) was injected into the bottles with a glass syringe, achieving a gauge pressure of 0.5 bar within the serum bottles. Moreover, control samples were prepared in triplicate. Control systems containing AnGrSL and growth medium without an electron donor (H_2 from Mg^0) were prepared, as summarized in Table 2.4. Additionally, abiotic control systems consisting only of Mg^0 and growth medium, without the addition of AnGrSL, were prepared. The temperature used for all incubations (samples & controls) was 33 °C at 100 rpm.

Gas composition in the headspace of the serum bottles from bacterial reactions (CO_2 and H_2 utilization; CH_4 production) was analyzed using gas chromatography, as detailed in Sub-chapter 2.7.1. Concentrations of metabolites (volatile fatty acids - VFAs) resulting from CO_2/H_2 bacterial utilization were determined via high-performance liquid chromatography, as described in Sub-chapter 2.7.2. pH and pressure levels during the experiments were monitored following Sub-chapters 2.7.7 and 2.7.8, respectively. Upon completion of the experiments, DNA extraction was performed for Next-Generation Sequencing analysis to identify the archaea profile, as outlined in Sub-chapter 2.7.4, for the following samples: a) the initial inoculum of AnGrSL, b) all the control systems with AnGrSL, thermal pre-treated AnGrSL, AnGrSL with 4 mM of BES, and AnGrSL with 70 g L^{-1} NaCl. The same procedure was also conducted to identify the bacterial profile of all the above-mentioned samples.

2.3.2 Experimental Set-Up 3: Experimental Strategies: Investigating Methane Inhibition Through Various Approaches for VFA Production.

2.3.2.1 Impact of 4 mM of Sodium 2-bromoethanesulfonate (BES), on Methane Inhibition in an AnGrSL-Mg^0 system - Experiment 1

In this experimental setup, a mixture comprising 80 g L^{-1} of AnGrSL and 4 g L^{-1} of Mg^0 was introduced into a growth medium. A set of triplicate bottles was prepared and designated as Group A. The experiment spanned 32 days and was segmented into 7 cycles. To establish anaerobic conditions, the headspaces of the Group A bottles were purged with N_2 gas. Then, 60 mL of CO_2 gas was injected into the serum bottles as the sole carbon source for the bacterial consortia, and the pressure reached approximately 0.5 bar at the beginning of the experiment (day 0). Following, 6 more CO_2 refeeds of 60 mL were done on Days 3, 8, 14, 21, 25, and 28, corresponding to the beginning of each cycle 2, 3, 4, 5, 6, and 7, respectively. On Day 0, a specific inhibitor (4 mM of BES) was introduced into the systems as a methane inhibition strategy. The pH of the systems was adjusted daily using HCl.

The primary objective of this experiment was to investigate methane inhibition within an AnGrSL-Mg^0 system to enhance acetic acid production by utilizing the chemical BES at a low concentration (4 mM). The selected concentration of 4 mM was based on the results extracted from experimental set-up 2 (Sub-chapter 2.2.2.4), where maximum acetic acid production was observed at this concentration. All experimental parameters are summarized in Table 2.4.

2.3.2.2 Evaluation of Utilizing Thermally Pre-treated AnGrSL in a Mg^0 System for VFAs Production - Experiment 2

In this experimental setup, a mixture comprising 80 g L^{-1} of thermally pre-treated AnGrSL and 4 g L^{-1} of Mg^0 was introduced into a growth medium. A set of triplicate bottles was prepared and designated as Group B. The experiment spanned 32 days and was segmented into 7 cycles. To establish anaerobic conditions, the headspaces of the Group A bottles were purged with N_2 gas. Then, 60 mL of CO_2 gas was injected into the serum bottles as the sole carbon source for the bacterial consortia, and the pressure

reached approximately 0.5 bar at the beginning of the experiment (day 0). Following, 6 more CO_2 refeeds of 60 mL were done on Days 3, 8, 14, 21, 25, and 28, corresponding to the beginning of each cycle 2, 3, 4, 5, 6, and 7, respectively. To impede methanogenesis, AnGrSL was subjected to a heat pre-treatment method at 95°C for 30 minutes before the inoculation, aiming to foster the enrichment of Acetogens or spore-forming bacteria within the systems. The pH of the systems was adjusted daily using HCl.

The primary objective of this experiment was to investigate the elimination of methane-producing bacteria by applying a short thermal treatment methodology to AnGrSL before the inoculation as a strategy to enhance the production of acetic acid. All experimental parameters are summarized in Table 2.4.

2.3.2.3 Effect of NaCl at Various Concentrations on Methane Inhibition When Employed in an AnGrSL - Mg^0 System - Experiment 3

In this experimental setup, a mixture comprising 80 g L^{-1} of AnGrSL and 4 g L^{-1} of Mg^0 was introduced into a growth medium. A set of triplicate bottles was prepared and designated as Group C. Within Group C, three sub-groups, labeled $C1_{(a,b,c)}$, $C2_{(a,b,c)}$, $C3_{(a,b,c)}$, were created based on the concentration of the non-specific inhibitor used. The experiment spanned 32 days and was segmented into 7 cycles. To establish anaerobic conditions, the headspaces of the Group C bottles were purged with N_2 gas. Then, 60 mL of CO_2 gas was injected into the serum bottles as the sole carbon source for the bacterial consortia, and the pressure reached approximately 0.5 bar at the beginning of the experiment (day 0). Following, 6 more CO_2 refeeds of 60 mL were done on Days 3, 8, 14, 21, 25, and 28, corresponding to the beginning of each cycle 2, 3, 4, 5, 6, and 7, respectively. To impede methanogenesis, AnGrSL was exposed to various concentrations of NaCl ($C1_{(a,b,c)}$: 50 g L^{-1}; $C2_{(a,b,c)}$: 70 g L^{-1}; $C3_{(a,b,c)}$: 90 g L^{-1}). The pH of the systems was adjusted daily using HCl.

The primary objective of this experiment was to investigate methane inhibition within an AnGrSL-Mg^0 system using a non-specific inhibitor, such as NaCl, at three distinct concentrations. The aim was to identify an economically viable alternative instead of using BES, aiming to minimize methane production without adversely affecting acetogenesis. All experimental parameters are summarized in Table 2.4.

2.3.2.4 Evaluation of Methane Production Potential in AnGrSL Exposed to Mg^0 Without a Methanogenesis Inhibitor – Experiment 4

In this experimental setup, a mixture comprising 80 g L^{-1} of AnGrSL and 4 g L^{-1} of Mg^0 was introduced into a growth medium. A set of triplicate bottles was prepared and designated as Group D. The experiment spanned 32 days and was segmented into 7 cycles. To establish anaerobic conditions, the headspaces of the Group C bottles were purged with N_2 gas. Then, 60 mL of CO_2 gas was injected into the serum bottles as the sole carbon source for the bacterial consortia, and the pressure reached approximately 0.5 bar at the beginning of the experiment (day 0). Following, 6 more CO_2 refeeds of 60 mL were done on Days 3, 8, 14, 21, 25, and 28, corresponding to the beginning of each cycle 2, 3, 4, 5, 6, and 7, respectively. The pH of the systems was adjusted daily using HCl.

The primary objective of this experiment was to investigate the CH_4 productivity of an AnGrSL-Mg^0 system without using any methane inhibitors. The aim was to identify the maximum accumulation of CH_4 produced throughout the cycles for CH_4 comparison reasons with both the methane-inhibited and control systems. All experimental parameters are summarized in Table 2.4.

Table 2.4: Overview of parameters and conditions of experiments 1-4 of experimental set-up 3.

Experiments - Groups	Exp. 1: Group A	Exp. 2: Group B	Exp. 3: Group C			Exp. 4: Group D
Sub-Groups	$A_{(a,b,c)}$	$B_{(a,b,c)}$	$C1_{(a,b,c)}$	$C2_{(a,b,c)}$	$C3_{(a,b,c)}$	$D_{(a,b,c)}$
Cycles	**Cycle 1** (days: 0-3); **Cycle 2** (days: 3-8); **Cycle 3** (days: 8-14); **Cycle 4** (days:14-21); **Cycle 5** (days 21-25); **Cycle** 6 (days: 25-28); **Cycle 7** (days: 28-32)	**Cycle 1** (days: 0-3); **Cycle 2** (days: 3-8); **Cycle 3** (days: 8-14); **Cycle 4** (days:14-21); **Cycle 5** (days 21-25); **Cycle** 6 (days: 25-28); **Cycle 7** (days: 28-32)	**Cycle 1** (days: 0-3); **Cycle 2** (days: 3-8); **Cycle 3** (days: 8-14); **Cycle 4** (days:14-21); **Cycle 5** (days 21-25); **Cycle** 6 (days: 25-28); **Cycle 7** (days: 28-32)			**Cycle 1** (days: 0-3); **Cycle 2** (days: 3-8); **Cycle 3** (days: 8-14); **Cycle 4** (days:14-21); **Cycle 5** (days 21-25); **Cycle** 6 (days: 25-28); **Cycle 7** (days: 28-32)
Duration	32 days	32 days	32 days			32 days
Starting point	Day 0	Day 0	Day 0			Day 0
CO_2 flashing	N_2 at day 0 (3 min.)	N_2 at day 0 (3 min.)	N_2 at day 0 (3 min.)			N_2 at day 0 (3 min.)
Carbon Source	60 mL of CO_2 in each cycle (total 420 mL of CO_2 – 7 cycles)	60 mL of CO_2 in each cycle (total 420 mL of CO_2 – 7 cycles)	60 mL of CO_2 in each cycle (total 420 mL of CO_2 – 7 cycles)			60 mL of CO_2 in each cycle (total 420 mL of CO_2 – 7 cycles)
H_2 Supply	4 g L^{-1} Mg^0 Added on day 0	4 g L^{-1} Mg^0 Added on day 0	4 g L^{-1} Mg^0 Added on day 0			4 g L^{-1} Mg^0 Added on day 0
Mg° Size (mm)	3 x 1.5 mm	3 x 1.5 mm	3 x 1.5 mm			3 x 1.5 mm
Methanogenesis Inhibition	**4 mM BES (Day 0)**	**AnGrSL thermally pre-treated (95 °C for 30 min) (Day 0)**	**50 g L^{-1} NaCl (Day 0)**	**70 g L^{-1} NaCl (Day 0)**	**90 g L^{-1} NaCl (Day 0)**	**X (Methane production system)**
pH	6.5- 7.5	6.5- 7.5	6.5- 7.5			6.5- 7.5
Temperature (C°)	33	33	33			33
Agitation (rpm)	100	100	100			100
Total / Working Volume (mL)	250/120	250/120	250/120			250/120
Control Systems	**4 mM BES + AnGrSL No electron donor (Mg^0 or H_2)**	**AnGrSL thermally pre-treated No electron donor (Mg^0 or H_2)**	**X**	**70 g L^{-1} NaCl + AnGrSL No electron donor (Mg^0 or H_2)**	**X**	**AnGrSL No electron donor (Mg^0 or H_2)**

2.4 Experimental Set-Up 4: Production of Acetic Acid and Other VFAs by Seven Different Biological Inoculum Systems Exposed to ZVI and BES.

This group of experiments explores the production of acetic acid in systems utilizing seven different inocula separately: river sludge, wetland sludge, anaerobic granular sludge, compost sludge, anaerobic sludge from WWTP, activated sludge, and drilling cuttings sludge. This experimental implementation expands the limited range of inocula previously examined for acetic acid production under mild aquatic anaerobic conditions. Additionally, the influence of various CO_2 feeding regimes—including frequent CO_2 feeding, one-time CO_2 feeding, and high-pressure CO_2 feeding—on experimental systems exposed to ZVI and BES was investigated. This investigation aims to assess the potential impact of CO_2 on both H_2 production by ZVI and acetic acid production by Acetogens. Furthermore, this chapter includes additional batch experiments to evaluate the roles of suspended microorganisms derived from the main experiments in acetic acid production. Similarly, these batch experiments also investigate the acetic acid production potential of microorganisms attached to and detached from ZVI.

2.4.1 Experimental Set-Up 4: Experimental Implementation and Analyses

To develop an efficient bacterial consortium enriched in Acetogens for this experimental setup, seven different types of sludge/solids were used as inocula. The origin and specific characteristics of these inocula, including structure, composition, granule size, and initial pH, are provided in Table 2.5. Before inoculation, the AnGr-SL sample was washed with a phosphate buffer (20 mM), and large granules (approximately 0.3–0.4 cm) were collected by sieving. Samples Anaer.-SL and Activ.-SL were collected from a municipal wastewater treatment facility after initial settling. Samples Comp.-SL and Dr.Cuts-SL were obtained from a digester at a company that implements treatment methods for hazardous industrial wastes. No pretreatment procedure was applied for the environmental sludge samples, River-SL and Wetland-SL.

Table 2.5: Summary of initial inocula characteristics and sample codes.

Inoculum Code	Physical Structure	Composition	Sample Origin	Size (cm)	Initial pH
River-SL	Slurry	Soil, Water	Germasogia river - Limassol	~0,01-0,1	7.3
Wetland-SL	Slurry	Soil, Wastewater	Constructed wetlands for wastewater treatment – Choletria - Paphos	~0,01-0,1	7.1
AnGr-SL	Granular	Anaerobic granular sludge, Cheese whey wastewater	Up-flow anaerobic sludge blanket treatment reactor (UASB) (Industry)	~0,3-0,4	6.8 - 7.3
Comp.-SL	Solid	Leaves (25 Kg), Pruning (16 kg), Grass (15 Kg), Sawdust (10 Kg), Food Waste Digestate (25 Kg)	Hazardous Wastes Treatment Company - Limassol	~0,3-1,0	8.6
Anaer.-SL	Slurry	Urban wastewater sludge	Sewerage Board of Limassol - Amathus (SBLA)	~0,01	7.5
Activ.-SL	Slurry	Urban wastewater sludge	Sewerage Board of Limassol - Amathus (SBLA)	~0,01	8.4
Dr. Cuts-SL	Solid	Drilling Cuts (250 Kg), Pruning (150 kg), Sewerage sludge (50 Kg)	Hazardous Wastes Treatment Company - Limassol	~0,2-1,0	6.5

All batch laboratory-scale experiments were conducted using 500 mL glass serum bottles. For the enrichment and screening of Acetogens, a carbonate-buffered mineral liquid substrate was employed in the screw cap serum bottles, following the protocol proposed by Schink (1994) as described in Sub-chapter 2.6, without the addition of $Na_2S \cdot 9H_2O$. Experimental systems were prepared in triplicate, each supplemented with a distinct inoculum source (Table 2.5) and filled with growth medium to achieve a working volume of 250 mL. As an electron donor, ZVI obtained from Sigma Aldrich (reduced for analysis, particle size 10 μm EMSURE®, CAS No. 7439-89-6) was added at the beginning of the experiments at a concentration of 80 g L^{-1}. The serum bottles were then sealed with rubber septa and screw caps and, for the creation of the anaerobic conditions, were flushed with 99.9% CO_2 or 99.9% N_2 (supplied by Linde – Hadjikyriakos Gas Ltd; Cyprus) for 3 minutes using a fine needle through the rubber septa. Following this, as an electron acceptor, CO_2 gas (Linde – Hadjikyriakos Gas Ltd; Cyprus) was injected into the bottles with a glass syringe at a specific amount, as described in Table 2.6. The experiment was divided into two cycles based on the growth medium replacement (90%) with a new one after 56 days, as detailed in Table 2.6. To inhibit methanogenesis, 4 mM BES was employed at the beginning of Cycle 1 (day 0) and 10 mM BES at the beginning of Cycle 2. Control samples were also prepared in triplicate for each inoculum without adding ZVI and were maintained under identical conditions to the experimental setups, specifically at 33 °C and 100 rpm.

The experiments related to the roles of a) suspended, b) detached bacterial communities from the ZVI, and c) ZVI-attached microbial communities in acetic acid production were evaluated. These batch experiments were conducted in triplicate using 160 mL glass serum bottles. Each bottle was filled with 80 mL of growth medium (as proposed by Schink, 1994) and sealed with a rubber septum and aluminum cap. Anaerobic conditions were established by purging the headspace with 99.99 % CO_2 using a fine needle. As an electron donor, exogenous H_2 gas was supplied by a glass syringe to the systems, ensuring that the CO_2:H_2 ratio was approximately 40:60 in the headspace of the serum bottles and achieving a final gauge pressure of roughly 1.5 bars. Three H_2 re-feeds were performed during a 45-day experimental period, as detailed in Table 2.7.

Gas composition in the headspace of the serum bottles from bacterial reactions (CO_2 and H_2 utilization; CH_4 production) was analyzed using gas chromatography, as detailed in

Sub-chapter 2.7.1. Concentrations of metabolites (volatile fatty acids - VFAs) resulting from CO_2/H_2 bacterial utilization were determined via high-performance liquid chromatography, as described in Sub-chapter 2.7.2. X-ray diffraction (X-RD) patterns of ZVI specimens (from all systems) were obtained following the procedure outlined in sub-chapter 2.7.5. pH and pressure levels during the experiments were monitored following Sub-chapters 2.7.7 and 2.7.8, respectively. DNA extraction was performed for Next-Generation Sequencing analysis to identify the bacteria profile, as outlined in Sub-chapter 2.7.4, for the following samples: a) all the initial inoculums, b) all systems inoculated with sludges and exposed to BES at the end of cycle 1 (Day 58), c) at the end of cycle 2 (Day 112), and d) All Control systems at the end of cycle 2 (Day 112). The same procedure was also conducted to identify the archaeal profile of a) All Control systems at the end of cycle 2 (Day 112) and b) all systems inoculated with sludges and exposed to BES at the end of cycle 2 (Day 112).

2.4.2 <u>Experimental Set-Up 4:</u> Experimental Strategies: Influence of Various CO_2 Feeding Regimes on Different Inoculum Systems Exposed to Fe^0 and the Role of Suspended, Detached, and Firmly Attached to ZVI Bacteria.

2.4.2.1 Influence of Frequent CO_2 Supplementation Regimes on Acetic Acid Production

In these experimental configurations, seven groups of triplicate bottles were prepared, filled with growth medium, and supplemented with 80 g L^{-1} of ZVI-Fe^0. Each triplicate was inoculated with a distinct inoculum sample as described in Table 2.5 and sealed with a rubber septum and screw cap. All systems then proceeded to Cycle 1, which spanned 56 days. Cycle 1 was segmented into two sub-cycles (Day 0–15 and Day 15–56) based on the implementation of CO_2 flashing. To establish anaerobic conditions, the headspaces of the triplicate bottles were purged with CO_2 gas at the beginning of the experiment on Day 0 (Sub-cycle: Day 0–15). As the sole carbon source for the bacterial consortia, an intensive CO_2 feeding plan (240 mL of CO_2) was applied on days 0, 5, 9, and 12, reaching a gauge pressure of approximately 0.7 bar in the systems. Based on the second CO_2 flashing on Day 15, the second sub-cycle began (Day 15–56), with three additional CO_2

feedings implemented on days 15, 26, and 30. As a methanogenesis inhibition strategy, 4 mM of BES was introduced to the systems at the start of the experiments on Day 0. However, during the first sub-cycle (Day 0–15), the system inoculated with AnGr-SL demonstrated high CH_4 production. To prevent the consumption of the reactants by methanogens (CO_2 and H_2), an additional 6 mM of BES was introduced to the AnGr-SL systems only.

The primary aim of this cycle was to examine the influence of the intensive CO_2 feeding plan on acetic acid production by the bacterial consortium and assess the impact of CO_2 flashing in the medium on the regeneration of ZVI-Fe^0 and, subsequently, the production of H_2. All experimental parameters are summarized in Table 2.6.

2.4.2.2 Influence of Low and High Concentrations of CO_2 on Acetic Acid Production

At the end of Cycle 1, 90% of the growth medium in all systems was replaced with fresh medium, while the previously processed ZVI-Fe^0 from Cycle 1 was retained. Based on the methane observations from Cycle 1, 10 mM of BES was introduced to the systems alongside the new growth medium as a methane inhibition strategy. All systems then proceeded to Cycle 2, which spanned 56 days and was segmented into two sub-cycles (Day 56–86 and Day 86–112) based on the implementation of flashing with N_2 or CO_2 and the CO_2 feeding plan. To establish anaerobic conditions, the headspaces of the triplicate bottles were purged with N_2 gas at the beginning of Cycle 2 on Day 56 (Sub-cycle: Day 56–86), followed by a single CO_2 feeding of 240 mL, reaching a gauge pressure of approximately 0.7 bar in the systems. In the second sub-cycle (Day 86–112), the systems were flashed with CO_2, and one CO_2 feeding was performed on Day 86. However, this time, CO_2 was injected into the systems at a higher concentration (720 mL of CO_2), reaching a high pressure of 2 bar within the systems.

The primary aim of this cycle was to examine the influence of low CO_2 concentration and compare it with high-pressure CO_2 implementation concerning H_2 production and VFA enhancement. All experimental parameters are summarized in Table 2.6.

Table 2.6: Overview of experimental parameters and conditions for acetic acid production of experimental set-up 4.

Experimental - Cycles	**Cycle 1**		**Cycle 2**	
Duration – Sub-cycles	**Day 0-15**	**Day 15-56**	**Day 56-86**	**Day: 86-112**
Starting Point	Day 0		Day 56	**Day 86**
Duration	32 days		32 days	32 days
Starting Point	Day 0		Day 0	Day 0
CO_2 or N_2 Flashing	CO_2 at day 0 & 15 (3 min.)	CO_2 at day 15 (3 min.)	N_2 at day 56 (3 min.)	CO_2 at day 86 (3 min.)
Feeding Plan	Day: 0, 5, 9, 12, 15, 26, 30		Day: 56	Day: 86
Carbon Source	240 mL CO_2 each feed Pressurized at ≈ 0.7 bar		240 mL CO_2 Pressurized at ≈ 0.7 bar	720 mL CO_2 Pressurized at ≈ 2 bar
H_2 Supply	80 g L^{-1} Fe^0 Added on day 0		80 g L^{-1} Fe^0 – Processed From cycle 1	80 g L^{-1} Fe^0 – Processed From cycle 1
Methanogenesis Inhibition	**4 mM BES (Added on Day 0) Plus 6 mM BES for AnGr-SL (Added on Day 15)**		**New growth medium (90%) 10 mM BES (Added on Day 56)**	**No further addition of BES 10 mM BES (Added on Day 56)**
pH	6-6.5		7	6-6.5
Temperature (C°)	33		33	33
Agitation (rpm)	100		100	100
Total / Working Volume (mL)	500/250		500/250	500/250

2.4.2.3 Assessment of Acetic Acid Production by Freely Suspended, Detached, and Firmly Bounded to ZVI Bacteria

After 112 days of the main experiments described in Sub-chapters 2.4.2.1 and 2.4.2.2, one system was selected from those with different inocula based on the highest acetic acid productivity for further experimentation. The River-SL system was chosen to evaluate the performance of a) suspended bacterial communities, b) bacterial communities detached from the ZVI, and c) ZVI-bound microbial communities in acetic acid production. Liquid samples and processed ZVI were obtained from this system for the following analysis:

A) Suspended Biomass Performance Investigation:

The process involved extracting 20 mL of liquid from the River-SL system on day 112, followed by centrifugation at 14.500 rpm for 15 minutes. After centrifugation, the supernatant was discarded, and the microbial pellets were transferred into sterile 160 mL bottles containing 80 mL of growth medium using a sterile pipette (Table 2.7).

B) Performance of Bacterial Communities Detached from ZVI:

Approximately 10% of the processed ZVI was extracted from the River-SL system using a sterile Pasteur glass pipette after day 112. Two grams of processed ZVI were transferred into a sterile Falcon tube with 3 mL of sterile growth medium and vortexed for 5 minutes. After vertexing, the supernatant (3 mL) was carefully transferred into sterile bottles containing growth medium, assuming that the firmly attached to the ZVI bacteria had detached from the ZVI surface (Table 2.7).

C) ZVI-bound Bacterial Communities:

The processed ZVI with bacteria attached to its surface was used directly as an inoculum without further processing. To achieve this, 2 g L^{-1} of the processed ZVI was carefully extracted from the River-SL system using a sterilized Pasteur glass pipette after day 112. This portion of processed ZVI was then transferred into sterilized bottles containing growth medium using a sterilized pipette to serve as inoculum for further analysis (Table 2.7).

These experiments were conducted over 45 days, and three H_2 feed implementations were done on days 0, 14, and 24. The triplicate groups were incubated at 33 °C and 100 rpm.

Table 2.7: Acetic acid performance evaluation of suspended, detached, and firmly bounded ZVI bacteria - Overview of experimental parameters and conditions.

Investigation	A) Suspended Biomass	B) Bacterial Communities Detached from ZVI	C) ZVI-bound Bacterial Communities
Duration	45 Days		
Starting Point	Day 0 (After 112 Days of the main experiments)		
CO_2 Flashing	Day 0		
Inoculum	River-SL (After the initial experiments – Day 112)		
Feeding Plan	Day: 0, 14, 24		
Carbon Source	40% in the headspace of the serum bottles		
H_2 Supply	Exogenous H_2 supply – 60% in the headspace of the serum bottles		
Pressure after CO_2:H_2 feeding	≈ 1.5 bar		
Methanogenesis Inhibition	X		
pH	5.5-6.5		
Temperature (C°)	33		
Agitation (rpm)	100		
Total / Working Volume (mL)	160/80		

2.5 Experimental Set-Up 5: Acetic Acid Production Utilizing Waste Iron (Fe-W) and Acetogen-Enriched Inoculum in a Continuous CO_2 Feeding Bioreactor System

This group of experiments examines the production of acetic acid using waste iron (Fe-W) in two parallel-connected reactors inoculated with river sludge. In previous experimental groups, ZVI-Fe^0 or processed ZVI-Fe^0 was used in the systems to evaluate the potential of bacterial consortia to produce acetic acid and other volatile fatty acids (VFAs) by utilizing CO_2 and H_2 that were derived from the *in-situ* oxidation of ZVI-Fe^0. This experimental implementation expands upon the concept of using ZVI-Fe^0 by replacing it with waste iron (Fe-W) derived from the machinery industry. This approach aligns with the circular economic concept, utilizing Fe-W in reactors to produce the necessary abiotic H_2 (electron donor) for bacterial reactions. The acetic acid productivity of the reactor/bioreactors was enhanced by using bio-carriers, potentially allowing for the immobilization of microorganisms. The productivity of the reactors/bioreactors was evaluated under mild aquatic anaerobic conditions at atmospheric pressure, with the experiments segmented into four phases reflecting different experimental alterations.

2.5.1 Experimental Set-Up 5: Experimental Implementation and Analyses

In this setup, an environmental sample derived from the Germasogia River (Limassol district of Cyprus) was used as an inoculum for the experimental operation of continuous anaerobic bioreactors. The aqueous slurry inoculum sample, with a pH value of 6.9, was used fresh without any pretreatment methods, such as heat or acid shock, to prevent methane formation. Before inoculation, DNA extraction of the sample was performed for 16S rRNA sequence analysis to investigate the initial microbial community and the evolution of the consortium during the experiment.

Two bioreactors were used to investigate the bioconversion of CO_2 to volatile fatty acids (VFAs) and the enrichment/screening of Homoacetogenic bacteria in the presence of waste iron metal (Fe-W). The custom-designed glass reactors, with a total and working volume of 3500 mL and 3000 mL, respectively, were equipped with an airtight lid and tubing connectors. For gas fermentation analysis, the lid was fitted with a rubber septum. A flexible silicone rubber tube was used to connect the two reactors in series, as shown in Table 2.8.

For the enrichment of Homoacetogens, a mineral growth medium was used in both reactors, as described by Schink (1994), though $Na_2S \cdot 9H_2O$ was not added. To facilitate the reaction of CO_2 to solventogenesis by Homoacetogens, Fe-W was used as a source for the production of abiotic hydrogen (as an electron donor) *in-situ* and *ex-situ* for Phases A, and B, Phases C and D, respectively, as detailed in Tables 2.8-2.11. CO_2 gas (Linde - Hadjikyriakos Gas Ltd, Cyprus) was used as an electron acceptor in a continuous mode at a flow rate of 0.08 L min^{-1}. To prevent the consumption of the reactants and bioproducts (CO_2, H_2, VFAs) by methanogens, 2-bromoethanesulfonate (BES) at a concentration of 4 mM was used as an inhibition strategy in all phases of the experiment.

For the immobilization of microorganisms responsible for the bioconversion of CO_2 to acetic acid, 22 mm Mutag BioChips with a surface area of 3.450 m^2/m^3 were used at a concentration of 50 g L^{-1}. The inoculated reactors were incubated vertically in a water bath at 33 °C to enrich and grow bacteria with the shaking mode disabled.

Gas composition in the headspace of the reactors/bioreactors, specifically H_2 and CH_4 production, was analyzed using gas chromatography as detailed in Sub-chapter 2.7.1. Metabolite concentrations, particularly volatile fatty acids (VFAs) resulting from CO_2/H_2 bacterial utilization, were determined via high-performance liquid chromatography, as described in sub-chapter 2.6.2. The bioethanol content in the reactors/bioreactors was also analyzed through gas chromatography, as outlined in Sub-chapter 2.7.3. X-ray diffraction (X-RD) patterns of selective Fe-W specimens were obtained following the procedure outlined in sub-chapter 2.7.5. SEM images at various magnifications were captured for selected Fe-W and bio-carrier specimens, following the methodology detailed in Sub-chapter 2.7.6. Throughout the experiments, pH was monitored, as explained in Sub-chapter 2.7.7.

Upon completion of each experimental phase, DNA extraction was conducted for Next-Generation Sequencing analysis to identify the bacterial profile, as described in Sub-chapter 2.7.4. The samples analyzed included: a) bacterial processed Fe-W, b) suspended bacteria in the growth medium, and c) biocarriers.

2.5.2 <u>Experimental Set-Up 5:</u> Experimental Strategies: Reactor/Bioreactor - 4 Phases Operation Modes

A four-phase (A-D) experimental methodology was conducted using two bioreactors (R-A and R-B) connected in series to investigate the chemosynthetic fixation of CO_2 by Homoacetogenic bacteria enriched in the reactors in the presence of waste iron metal (Fe-W). The reactors operated in continuous mode. The biological and non-biological reactions that occurred in the reactors led to the generation of value-added products, such as acetic acid and bioethanol, through the inhibition of methanogenesis. The phases were carried out as follows:

<u>Phase-A:</u> This Cycle was conducted to investigate the enrichment of Homoacetogens and to examine the productivity of both reactors in acetic acid accumulation. The two reactors (Reactor-A, Reactor-B) were inoculated with the same environmental sample (River-SL) and filled with 2 L of growth medium and 2 kg of Fe-W. For methanogenesis inhibition, 4 mM of BES was used in both reactors. Reactor-A, connected with a CO_2 bottle, and through a gas flow regulator for small volumes, CO_2 was introduced into Reactor-A. Reactor-A was followed in series by Reactor-B through silicone tubing, and the unconsumed reactants (CO_2 and H_2) from Reactor-A ended up in Reactor-B, where the same procedures were exhibited as in Reactor-A. Phase A lasted for 60 days. At the end of the cycle, two samples (Fe-W, medium) from Reactor A and one sample (Fe-W with liquid) from Reactor B were collected. These samples were then processed for DNA extraction for 16S rRNA sequence analysis (Table 2.8).

<u>Phase-B:</u> This cycle was conducted to further enrich Homoacetogens within the reactors for acetic acid production. It followed the same procedure as Phase-A, with the primary difference being the replacement of 1900 ml of the old medium with fresh medium containing 4 mM of BES in both reactors. Additionally, bio-carriers (50 g L^{-1}) were introduced into the second reactor (Reactor-B) to facilitate the immobilization of bacteria. The same processed waste iron metal was used for abiotic hydrogen production without removal or pretreatment for the dissolution of siderite, which had formed on the iron surface due to the reaction with CO_2. Phase B lasted for 60 days. At the end of the cycle, one sample (Fe-W with liquid) from Reactor A and two samples (Fe-W with liquid and biocarriers) from Reactor B were collected. These samples were then processed for DNA extraction for 16S rRNA sequence analysis (Table 2.9).

Phase-C: This cycle was designed to enable Reactor-A to function as the abiotic H_2 producer. The H_2 *ex-situ* produced from Reactor-A, along with CO_2, was then used to feed Reactor-B. To inhibit methanogenesis in the ex-situ H_2 producer Reactor-A, a thermal pretreatment was applied instead of using a chemical inhibitor. Before the thermal pretreatment, the growth medium in Reactor-A was discarded and subjected to an additional 2 kg of fresh Fe-W, without removing the 2 kg of processed Fe-W previously used in Phase B, and 1400 ml of water. Then, the reactor was autoclaved for 15 minutes at 121 ºC and 1 atm. At this stage, only Reactor-B was inoculated with a Homoacetogenic-enriched sample (100 ml of medium and 20 g of carriers) collected from Phase B and Reactor-B. Reactor B was used for CO_2 and H_2 (the *ex-situ* produced from Reactor-A) utilization for acetic acid production. To prevent reactant (H_2 and CO_2) consumption by methanogens, 4 mM of BES was used in Reactor B. Phase C lasted for 60 days. At the end of the cycle, one sample (Fe-W with liquid) from Reactor A and two samples (medium and bio-carriers) from Reactor B were collected. These samples were then processed for DNA extraction for 16S rRNA sequence analysis (Table 2.10).

Phase-D: This cycle was conducted in the same concept as Phase C. Reactor A was designed as the abiotic H_2 producer. However, instead of applying thermal inhibition at reactor A, at this phase, a new uncontaminated glass reactor was used and implemented with 4 kg of new Fe-W and filled with 1400 ml of water as the *ex-situ* H_2 supplier to reactor B. Reactor-B was filled with new growth medium (with 4 mM of BES) and inoculated with homoacetogenic enriched sample from Phase-C (100 ml medium and 20 gr carriers) and Reactor-B. Phase D lasted for 60 days. At the end of the cycle, samples of the medium and bio-carriers from Reactor B were collected and subjected to DNA extraction for 16S rRNA sequencing analysis (Table 2.11).

Table 2.8: Overview of experimental parameters and conditions of Phase-A.

Cycle	**Phase-A**	
Reactor	**Reactor A**	**Reactor B**
Inoculum	Germasogia river sludge (River-SL)	
Growth Medium	2000 mL	
Connection	In series	
Electron Donor (H_2)	2 Kg Fe-W (each reactor)	
Electron Acceptor	**Continuous CO_2 feeding (0.08 L min^{-1})**	**CO_2 feeding (≈0.08 L min^{-1}) from Reactor A**
Methanogenesis Inhibition	4 mM of BES (each reactor)	
Bio-carriers	No	
Days	60	
DNA Extraction	At the end of Phace-A (Day 60) Samples: 1) Initial Inoculum; 2) Reactor A (medium and Fe-W); 3) Reactor B (medium and Fe-W)	
Schematic Representation of the Experimental Setup	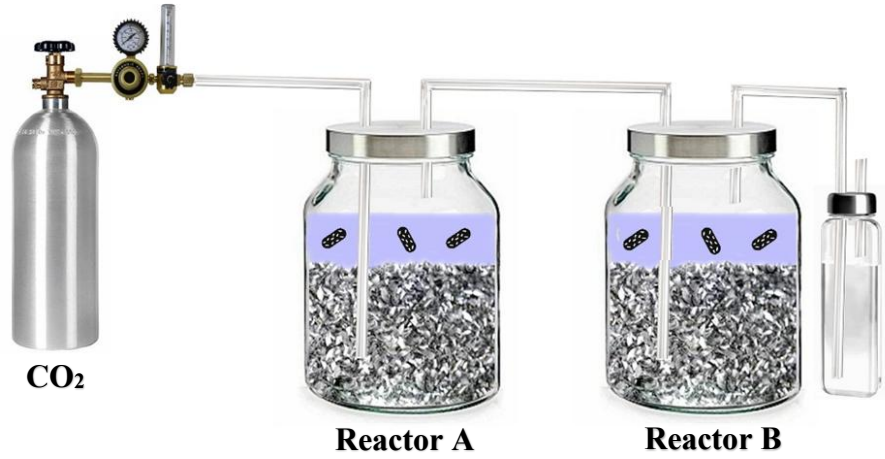	

Table 2.9: Overview of experimental parameters and conditions of Phase-B.

Cycle	**Phase-B**	
Reactor	**Reactor A**	**Reactor B**
Inoculum	**Homoacetogen enriched sample from Phase-A, Reactor A**	**Homoacetogen enriched sample from Phase-A, Reactor B**
Growth Medium	**1900 mL - New Medium**	
Connection	In series	
Electron Donor (H_2)	2 Kg Fe-W - Already processed Fe-W from Phase – A (each reactor)	
Electron Acceptor	**Continuous CO_2 feeding (0.08 L min^{-1})**	**CO_2 feeding (≈0.08 L min^{-1}) from Reactor A**
Methanogenesis Inhibition	4 mM of BES (each reactor)	
Bio-carriers	**No**	**50 g L^{-1}**
Days	60	
DNA Extraction	At the end of Phace-B (120 days from Phase-A) Samples: 1) Reactor A (medium and Fe-W); 2) Reactor B (medium); 3) Reactor B (biocarriers)	
Schematic Representation of the Experimental Setup	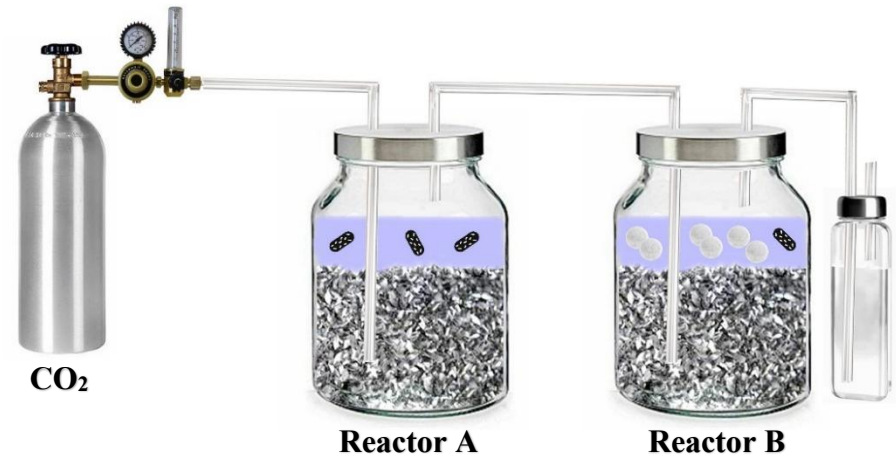	

Table 2.10: Overview of experimental parameters and conditions of Phase-C.

Cycle	**Phase-C**	
Reactor	**Reactor A**	**Reactor B**
Inoculum	**No**	**Homoacetogen enriched sample from Phase-B, Reactor B**
Growth Medium	**1400 mL Water**	**1900 mL - New Medium**
Connection	In series	
Electron Donor (H_2)	**2 Kg Fe-W (Processed from Phase – B) + 2 Kg Fe-W (New)**	**No**
Electron Acceptor	**Continuous CO_2 feeding (0.08 L min^{-1})**	**CO_2 feeding (≈0.08 L min^{-1}) from Reactor A**
Methanogenesis Inhibition	**Thermal Inhibition**	**4 mM of BES**
Bio-carriers	**No**	**20 g (From Phase-B, Reactor B)**
Days	60	
DNA Extraction	At the end of Phace-C (180 days from Phase-A) Samples: 1) Reactor A (medium); 2) Reactor A (Fe-W); 3) Reactor B (medium); Reactor B (biocarriers)	
Schematic Representation of the Experimental Setup		

Table 2.11: Overview of experimental parameters and conditions of Phace-D.

Cycle	**Phase-D**	
Reactor	**Reactor A**	**Reactor B**
Inoculum	**No**	**Homoacetogen enriched sample from Phase-C, Reactor B**
Growth Medium	**1400 mL Water**	**1900 mL - New Medium**
Connection	In series	
Electron Donor (H_2)	**4 Kg Fe-W (New)**	**No**
Electron Acceptor	**Continuous CO_2 feeding (0.08 L min^{-1})**	**CO_2 feeding (≈0.08 L min^{-1}) from Reactor A**
Methanogenesis Inhibition	**No (New uncontaminated reactor)**	**4 mM of BES**
Bio-carriers	**No**	**20 g (From Phase-C, Reactor B)**
Days	60	
DNA Extraction	At the end of Phace-D (240 days from Phase-A) Samples: 1) Reactor B (medium); 2) Reactor B (biocarriers)	
Schematic Representation of the Experimental Setup		

2.6 Preparation of Bacterial Growth Medium.

In order to enhance the growth of anaerobic bacteria, two distinct growth media were used with different chemical components, including minerals, micronutrients, and vitamins. These essential components are crucial in facilitating anaerobic bacteria's optimal growth and metabolic processes. Some experiments were conducted using a growth medium, as proposed by Angelidaki et al. (2009). The Angelidaki et al. protocol required the creation of 5 different stock solutions diluted in distilled water and consisting of the mineral medium, the trace-metal and selenite solution, the vitamin mixture solution, the resazurin solution, the cysteine hydrochloride/sodium bicarbonate, (sodium sulfide nonahydrate solution excluded). Furthermore, in certain experiments, $NaHCO_3$ was omitted to enhance the bacteria's CO_2 gas consumption.

Owing to the intricacy of the Angelidaki et al. protocol, certain experiments were conducted using a growth medium as recommended by Schink (1994). The selection of the Schink protocol was based on its ability to support the growth and proliferation of targeted Homoacetogenic bacteria strains and its capacity to create an optimal environment conducive to achieving the desired outcomes. For the enrichment of mesophilic Homoacetogenic bacteria strains, the following minerals: KH_2P0_4, 0.2 g; NH_4CI, 0.5 g; NaCI, 1.0 g; $MgCI_2$ x 6 H_2O, 0.4 g; KCI, 0.5 g; $CaCI_2$ x 2 H_2O, 0.15 g, was used for the preparation of 1 L. It should be noted that the protocol stated the use of 2 mL of 0.5 M Na_2S x 9 H_20 solution and 0.5 mL of tenfold concentrated. However, these chemicals were not used. The trace element solution SL-10 was prepared based on the DSMZ company (Germany) protocol. For the preparation of a 1 L stock solution, the following chemicals were used: HCl (25%; 7.7 M), 10.00 mL; $FeCl_2$ x 4 H_2O, 1.50 g; $ZnCl_2$, 70.00 mg; $MnCl_2$ x 4 H_2O, 100.00 mg; H_3BO_3, 6.00 mg; $CoCl_2$ x 6 H_2O, 190.00 mg; $CuCl_2$ x 2 H_2O, 2.00 mg; $NiCl_2$ x 6 H_2O, 24.00 mg; Na_2MoO_4 x 2 H_2O, 36.00 mg, was used. Not all acetogenic bacteria strains necessitate a combination of vitamins, and for both economic and practical purposes, vitamins were not used.

2.7 Analytical Techniques

2.7.1 Gas Composition Measurements

The compositional analysis of the gas (H_2, O_2, N_2, CH_4, and CO_2) used in all experiments or produced under different experimental procedures was conducted using gas chromatography. An Agilent Technologies System (7820A GC) was used, coupled with a thermal conductivity detector (TCD). Argon was used as the carrier gas. The Injector operated at a constant temperature of 125 °C, and the detector at a constant temperature of 250 °C. The oven temperature was maintained at 60 °C for 2 min, then the temperature was raised to 160 °C with a rate of 20 °C min^{-1}. A ShinCarbon ST 50/80 mesh column (Restek Corporation, Bellefonte, PA, USA) was employed to separate gas molecules. For gas analysis, 1 mL of a gas mixture sample was withdrawn from the headspace of the serum bottles through a rubber septum and injected into the system. A previously defined calibration curve was used to calculate the concentration of gases.

2.7.2 Determination and Concentration Measurement of Organic Acids

Short-chain volatile fatty acids (SCFAs), including specific volatile fatty acids (VFAs) such as acetate, formate, iso-butyrate, butyrate, propionate, and valerate, were identified and quantified using High-Performance Liquid Chromatography (HPLC). A Shimadzu system (LC-20AD) equipped with a Shimadzu SPD-20A UV/VIS detector was used. All samples were centrifuged at 13000 rpm for 3 minutes and filtered with a 0.22 μm syringe filter before being loaded into the autosampler (Shimadzu, SIL-20A HT). Organic acids were separated and analyzed using the RezexTM ROA-Organic Acid H+ (8%) column (Phenomenex®, LC column 150 x 7.8 mm). The column was operated isocratically at 55 °C with a flow rate of 0.7 mL min^{-1}, using a mobile phase of 5 mM H_2SO_4. The injection volume was set at 1 μL, and the UV detector was set at 210 nm, as described by Vyrides and Stuckey, 2009.

2.7.3 Determination and Concentration Measurement of Ethanol

The ethanol content of the samples was analyzed through Gas Chromatography. A Shimadzu GC-2014 (Shimadzu, Milton Keynes, UK) was coupled with a 30 m long

Zebron ZB-5 capillary column with a 0.25 mm internal diameter from Phenomenex (Macclesfield, UK) that ended in a flame ionization detector. Nitrogen was used as the mobile phase, while the column's stationary phase was composed of 95% dimethylpolysiloxane and 5% phenyl. All samples were centrifuged for 10 min at 13000 rpm, and ethanol was extracted after vortexing 1 mL of the filtered liquid sample (0.2 μm) with 2 mL of the Hexane solvent for 1 minute. Approximately 1 μL of the extract was injected into the GC, and the column's temperature was maintained at 40 °C for 2.5 min before rising to 160 °C (with a step of 30 °C min^{-1}) and remaining there for an additional 5 min. A previously defined calibration curve was used to calculate the concentration of ethanol.

2.7.4 DNA Extraction and Sequence Analysis

Wet sludge samples from the experiments (200–300 mg) were obtained from the investigated systems at the end of the batch experiments for DNA extraction. Two different DNA extraction kits were used to implement DNA extraction for 16S rRNA gene amplicon sequencing analysis targeting the bacterial and archaeal variable region V3-V5. The total genomic DNA of the samples was extracted using the reagents and components included in the kits, following the extraction protocols provided by the manufacturers. The QIAGEN DNeasy PowerSoil Pro Kit and MP Biomedicals FastDNA Spin Kit for Soil DNA Extraction were employed.

The extracted genomes from the samples were sent to two bioinformatics companies. Some samples were prepared and analyzed by Novogene (Beijing, China), while others were handled by DNASense Apps Company (Denmark) following the most recent research standards. The abundance of the operational taxonomic units (OTUs) was exported as raw data and analyzed manually using Microsoft Excel Spreadsheet Software.

2.7.5 X-RD

Iron samples (Fe^0, Fe-W) and processed iron samples were subjected to X-ray diffraction (X-RD) analysis to determine the purity of the iron samples and identify any secondary crystalline structures that may have formed after the iron was processed under anoxic/anaerobic conditions. All measurements were performed, and patterns were

recorded using a multi-purpose diffractometer (Ultima IV, Rigaku). The diffractometer was equipped with a Cu tube operating at 40 kV and 40 mA, and the incident beam was conditioned to parallel mode using a multilayer mirror and partially monochromatized Cu Ka (λ = 0.15418 nm). To mitigate the strong fluorescence of the iron samples, a graphite monochromator was employed, positioned on the receiving side of the optics directly in front of the detector. X-RD patterns were recorded in the range of 20° to 85° 2-theta, with a step size of 0.05° and a scanning speed of 0.5° min^{-1}.

2.7.6 SEM

A Quanta 200 (FEI, Hillsboro, Oregon, USA) scanning electron microscope (SEM) was used at various accelerating voltages to examine the microstructural oxidation features and screen for possible micro-organisms immobilized on the iron samples (Fe^0, FeW) processed under anoxic/anaerobic conditions in the presence of bacteria. The SEM was also used to identify bacteria attached to the biocarriers used in the experiments for immobilization. Before imaging, all samples underwent sputter coating with a thin layer of gold (a few nm) to enhance sample conductivity and minimize surface charging effects. In conjunction with imaging, energy-dispersive X-ray spectroscopy analysis (EDS) was conducted to provide insights into the elemental composition of the processed iron samples.

2.7.7 pH monitoring and measurements

All pH measurements were carried out using a Mettler Toledo FiveGo portable pH meter equipped with a probe specifically designed for small liquid volumes. The monitoring process involved extracting approximately 1 mL from each experimental system (serum bottles or bioreactors) and measuring it in a 5 mL clean and sterilized beaker. The pH of the samples was regulated by using 3M HCl and 2M NaOH buffers.

2.7.8 Pressure monitoring and measurements

To monitor and measure the absolute gas pressure within the serum bottles used in all experimental procedures, a KELLER – LEO1 (Switzerland) manometer was used. The

manometer was equipped with a syringe luer lock, facilitating the secure attachment of a fine needle. This arrangement enabled precise and reliable pressure measurements through the rubber septum of the serum bottles while ensuring safety during the process.

3: RESULTS AND DISCUSSION

3.1 Experimental Set-Up 1: Hydrogen (H_2) Production Through Carbon Dioxide (CO_2) Reaction with Zero-Valent Iron (Fe^0) or Waste Iron (Fe-W)

Based on the findings from the literature review presented in the introduction (Chapter 1), 95% of H_2 production through conventional methods contributes to CO_2 emissions, while unconventional methods are often associated with high costs. This chapter has two primary aims. First, to explore an alternative approach that simultaneously addresses CO_2 utilization while generating abiotic H_2. This is achieved by reacting CO_2 with iron under aqueous anaerobic conditions. The phenomenon of iron corrosion in a CO_2 environment has primarily been studied in the oil and gas industry, mainly to assess steel corrosion rates in pipelines. According to Askary et al. (2019), CO_2 is an acid gas, and due to its solubility in water, it can corrode steel—a process known as "sweet corrosion"—promoting the formation of $FeCO_3$ and H_2.

This phenomenon has mostly been examined from the perspective of carbonate scale formation and pipeline failure threats, with little focus on H_2 production. For this reason, this chapter employs various methods to examine multiple variables that may affect the generation of abiotic H_2 from Fe^0 or Fe-W reacted with CO_2 under anaerobic, mild operating conditions. Second, based on the results, this study aims to assess the potential of using H_2 derived from Fe^0-oxidation in two ways. Using H_2 to supply an anaerobic bacterial consortium system externally (*ex-situ*) or by inoculating the H_2-producing system directly (*in-situ*) with bacteria to achieve the bioconversion of this gas into a sustainable, safe liquid energy form.

3.1.1 Impact of N_2 and CO_2 gases on Fe^0

As depicted in Fig. 3.1, in an environment primarily composed of N_2, minimal abiotic-H_2 production was observed, with concentrations reaching only 0.65% in the headspace of the bottles after a 75-hour duration. In contrast, within systems where a total of ~4 mmol of CO_2 was introduced with a fine needle through the rubber septum, a notably higher production of H_2 was observed. In this CO_2-rich system, H_2 production reached approximately 93%, representing a substantial increase of 99.33% compared to the N_2 systems.

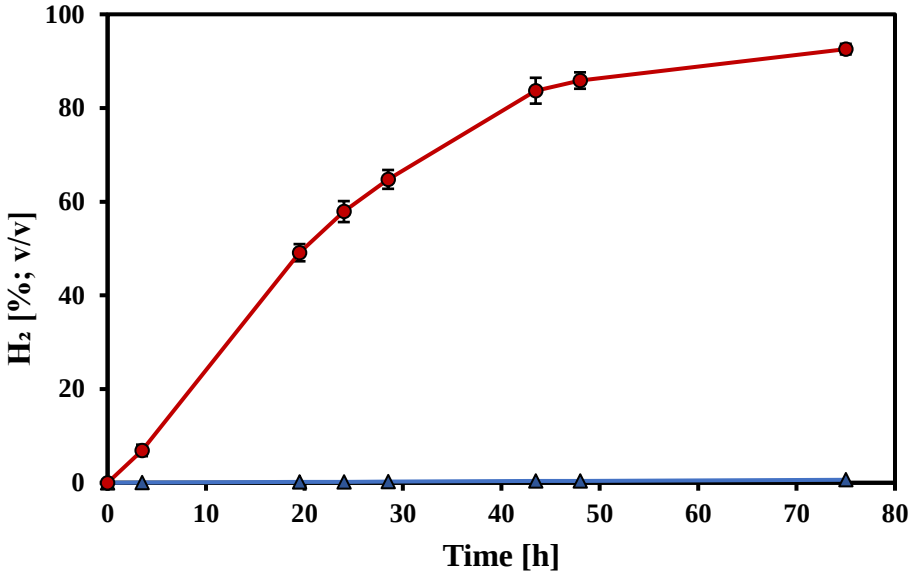

Fig. 3.1: Abiotic H_2 production over time, in a system with deionized water and 25 gr L^{-1} of Fe^0, under N_2 and CO_2 environment, respectively.

: H_2 accumulation in Fe^0-N_2 system; : H_2 accumulation in Fe^0-CO_2 system.

As indicated in Table 3.1, the CO_2-enriched system generated 3.715 mmol of H_2 after 75 h, while the N_2-enriched system produced only 0.025 mmol of H_2 over the same period, representing a 99.33% increase in H_2 production when CO_2 was used.

Table 3.1: H_2 accumulation in mmol over time in sub-groups A1 and A2.

mmol of H_2								
Time [h]	**0**	**3.5**	**19.5**	**24**	**28,5**	**43.5**	**48**	**75**
A1: Fe^0-N_2 system	0	0.00204	0.00685	0.00811	0.00924	0.01507	0.01622	0.02475
A2: Fe^0-CO_2 system	0	0.267	1.897	2.236	2.501	3.264	3.364	3.715

Regarding the pH, the two systems (N_2 and CO_2) exhibited notable differences in pH values over time, as shown in Fig. 3.2. Initially, both systems were set to a pH of approximately 6. The N_2-enriched system showed no significant change in pH throughout the experiment. In contrast, the CO_2-enriched system demonstrated a decline in pH during the first 3.5 h, followed by a significant increase of 1.64 units, ultimately reaching a pH of 7.19 after 75 h.

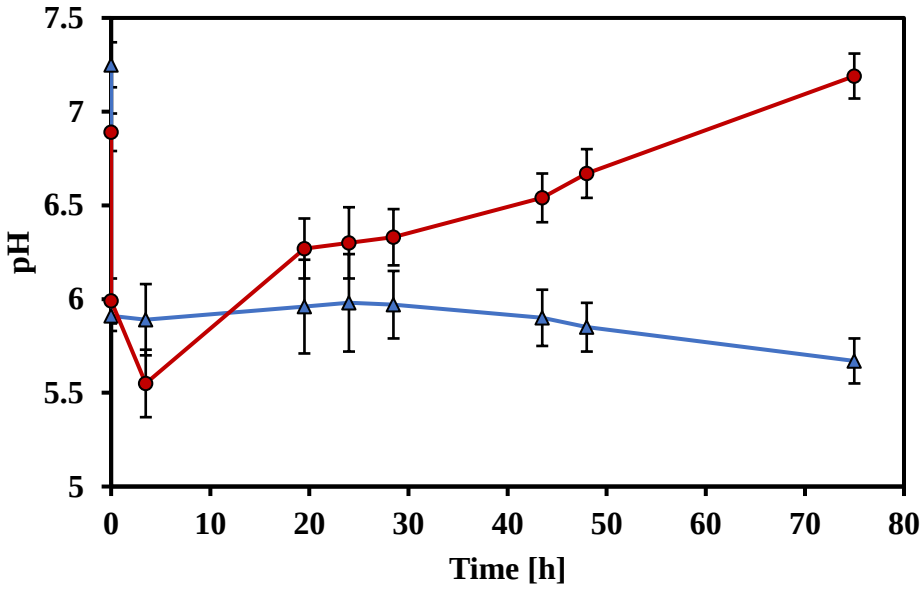

Fig. 3.2: The pH monitoring of the N_2-enriched and CO_2-enriched systems over time.

: Fe^0-N_2 system; : Fe^0-CO_2 system.

The CO_2 utilization and changes in headspace pressures (absolute) for both systems (N_2 and CO_2) are illustrated in Appendix I (Suppl. Info. Figs. 3.1 & 3.2).

At the end of the experiment (after 75 h), the processed Fe^0 samples from both the Fe^0-N_2 and Fe^0-CO_2 systems were subjected to X-RD analysis to identify crystalline structures formed due to the oxidation of Fe^0 under anoxic conditions. To facilitate comparisons of X-RD patterns of the samples, unprocessed pure Fe^0 was also analyzed.

As illustrated in the X-RD pattern in Fig. 3.3, sample A1, corresponding to Fe^0 exposed to deionized water under an N_2 environment, exhibited a prominent peak indicative of Fe^0, along with lower-intensity peaks identified as the crystal structures of magnetite (Fe_3O_4). In contrast, sample B, representing Fe^0 exposed to deionized water under a CO_2 environment, displayed a distinct X-RD pattern. Weak intensity peaks were identified as the crystal structures of goethite (ferric oxyhydroxide; α-FeOOH) and siderite ($FeCO_3$).

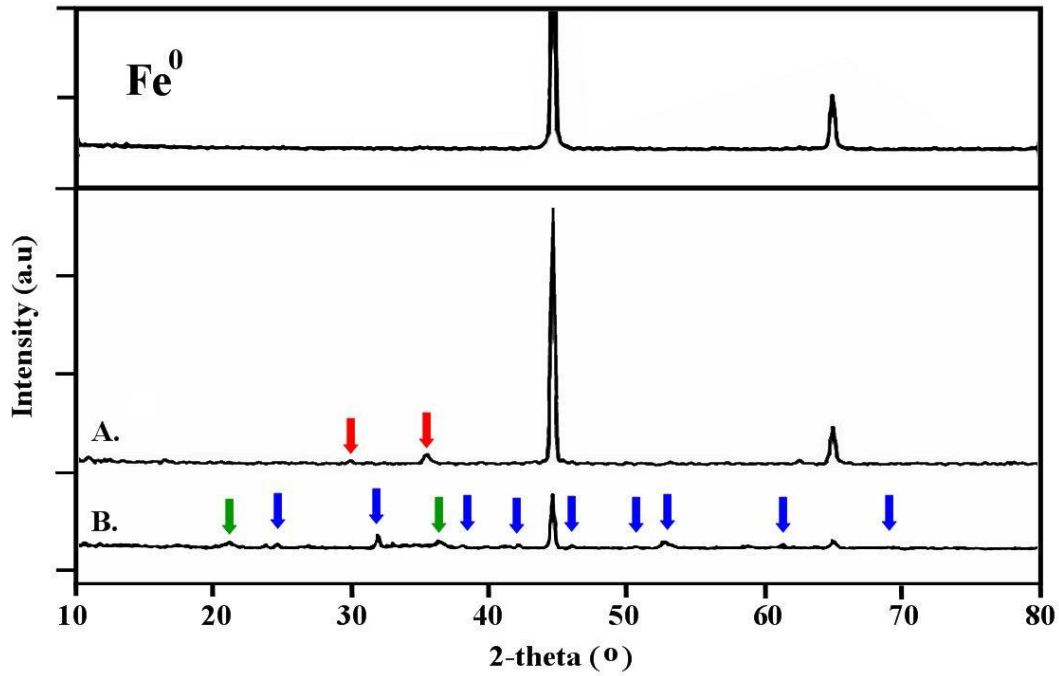

Fig. 3.3: X-ray diffraction pattern of **A.:** Fe^0 with deionized water exposed to N_2 environment and **B.:** Fe^0 with deionized water exposed to CO_2 environment.

: Magnetite (Fe_3O_4); : Goethite (α-FeOOH); : Siderite ($FeCO_3$).

3.1.2 Influence of $NaHCO_3$ at Different Concentrations

In both systems, Fe^0-N_2 and Fe^0-CO_2, exposed to varying concentrations of $NaHCO_3$, H_2 concentrations ranging from 30% to 98%, were identified in the headspace of the serum bottles, as illustrated in Fig. 3.4 (A. & B.). Upon analyzing the average H_2 production of each system, it was observed that the Fe^0-N_2 system exhibited 50% less H_2 production

than the system purged with CO_2. Specifically, under N_2-environment, the lowest H_2 accumulation was identified in the system where Fe^0 was exposed to 2 g L^{-1} of $NaHCO_3$, reaching 30%. This percentage gradually increased by adding 4, 6, 8, and 10 g L^{-1} of $NaHCO_3$, reaching the maximum H_2 production of 61% at 10 g L^{-1} of $NaHCO_3$ after 75 h (Fig. 3.4; A.). Contrastingly, the system exposed to CO_2 exhibited significantly higher accumulations of H_2, surpassing 96% in the headspace of the serum bottles after 75 h. This trend remained consistent across all concentrations of $NaHCO_3$ studied in the Fe^0-CO_2 system (Fig. 3.4; B.).

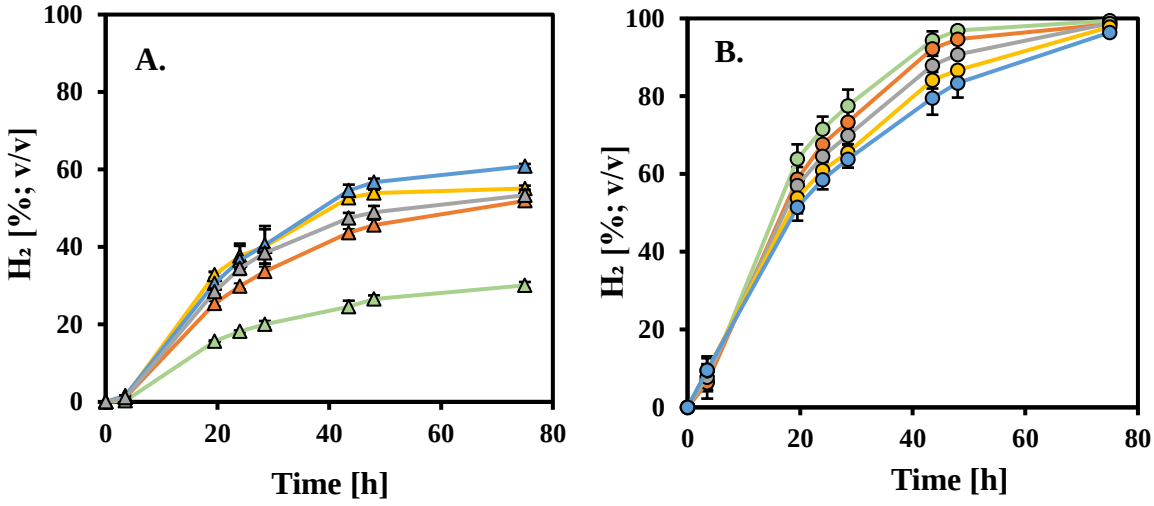

Fig. 3.4: The evolution of H_2 production by Fe^0 exposed to different concentrations of $NaHCO_3$. **A.:** H_2 produced under N_2-environment. **B.:** H_2 produced under CO_2-environment.

: 2 g L^{-1} $NaHCO_3$; : 4 g L^{-1} $NaHCO_3$; : 6 g L^{-1} $NaHCO_3$;

: 8 g L^{-1} $NaHCO_3$; : 10 g L^{-1} $NaHCO_3$.

The pH of both systems was initially set to approximately 6. As shown in Fig. 3.5, pH was increased in both the N_2 and CO_2 systems over the experimental period. However, the N_2 systems exhibited a more significant rise in pH after 75 h, reaching levels between 8 and 9 across the different Fe^0 concentrations. In contrast, the CO_2 systems displayed pH values ranging from 6.8 to 8.88, with a more pronounced variation between Fe^0 concentrations. Overall, after 75 hours, the pH increase was generally proportional to the $NaHCO_3$ concentrations in the serum bottles in both systems.

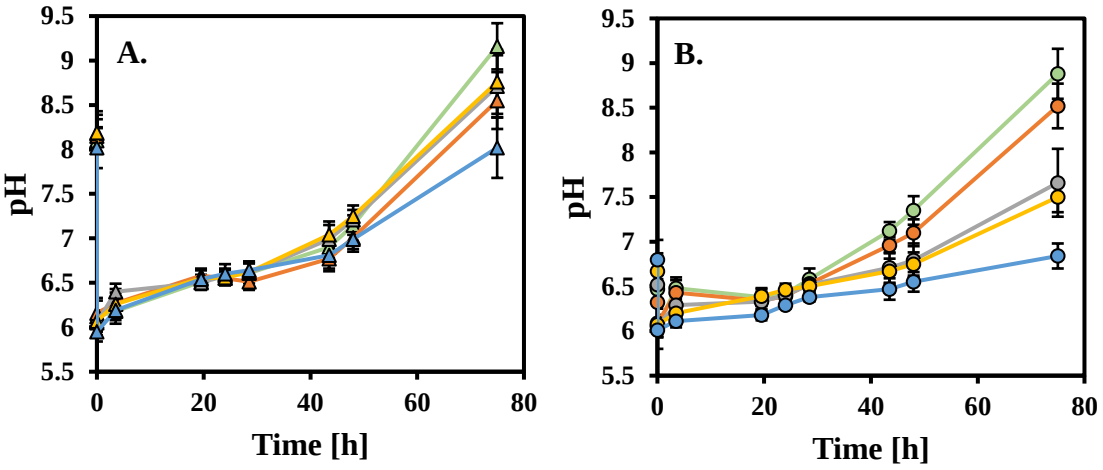

Fig. 3.5: Variations in pH during the experimental duration in both **A.:** N_2-environment and **B.:** CO_2-environment.

: 2 g L^{-1} $NaHCO_3$; : 4 g L^{-1} $NaHCO_3$; : 6 g L^{-1} $NaHCO_3$;

: 8 g L^{-1} $NaHCO_3$; : 10 g L^{-1} $NaHCO_3$.

Regarding the accumulations of H_2 in mmol, as presented in Table 3.2, for the Fe^0-N_2 system, by adding 2 g L^{-1} of $NaHCO_3$, the concentration of H_2 after 75 h was identified to be 1.59 mmol. With the addition of 4, 6, 8, and 10 g L^{-1} of $NaHCO_3$, the accumulation of H_2 increased in each sample, with increments of 1.33, 0.77, 0.91, and 1.13 mmol, respectively, by comparing each system with the previous one that having a lower $NaHCO_3$ concentration, at the end of the experiment. Sample $B5_{(a,b,c)}$, where the $NaHCO_3$ was used in a concentration of 10 g L^{-1} demonstrated the maximum H_2 accumulations reaching 5.73 mmol after 75 h.

Table 3.2: H_2 accumulation in mmol observed over time in sub-groups B1 – B5 by adding different concentrations of $NaHCO_3$.

mmol of H_2								
Time [h]	**0**	**3,5**	**19,5**	**24**	**28,5**	**43,5**	**48**	**75**
B1: Fe^0-N_2 system + 2 g L^{-1} $NaHCO_3$	0	0.0123	0.710	0.9104	1.0079	1.2827	1.3970	1.5930
B2: Fe^0-N_2 system + 4 g L^{-1} $NaHCO_3$	0	0.0562	1.3441	1.6157	1.8471	2.4129	2.5559	2.9242
B3: Fe^0-N_2 system + 6 g L^{-1} $NaHCO_3$	0	0.0718	1.8284	2.2456	2.5306	3.2278	3.3524	3.6919
B4: Fe^0-N_2 system + 8 g L^{-1} $NaHCO_3$	0	0.0924	2.4825	2.8740	3.0927	4.1600	4.2815	4.6020
B5: Fe^0-N_2 system + 10 g L^{-1} $NaHCO_3$	0	0.1242	2.7449	3.2865	3.6782	5.0491	5.2905	5.7262

On the other hand, the Fe^0-CO_2 system exhibited a significant differentiation in H_2 production across all $NaHCO_3$ concentrations compared to the Fe^0-N_2 system. Filling the headspace of the serum bottles with only ~0.4 mmol of CO_2 resulted in a 68%, 48%, 44%, 41%, and 36% increase in H_2 production, respectively, compared to H_2 accumulation observed in the Fe^0-N_2 system samples after 75 h. As indicated in Table 3.3, Fe^0 exposed to 2 g L^{-1} of $NaHCO_3$ produced 4.93 mmol of H_2 after 75 h. With the addition of 4, 6, 8, and 10 g L^{-1} of $NaHCO_3$, the accumulation of H_2 increased in each sample, with increments of 0.70, 0.98, 1.19, and 1.16 mmol, respectively, comparing each system with the previous one that having a lower $NaHCO_3$ concentration, at the end of the experiment. Similarly to the system with N_2, Sample $B10_{(a,b,c)}$, where Fe^0 was exposed to 10 g L^{-1} $NaHCO_3$, demonstrated the maximum H_2 accumulation, reaching 8.96 mmol after 75 h.

Table 3.3: H_2 accumulation in mmol observed over time in sub-groups B6 – B10 by adding different concentrations of $NaHCO_3$.

mmol of H_2								
Time [h]	**0**	**3,5**	**19,5**	**24**	**28,5**	**43,5**	**48**	**75**
B6: Fe^0-CO_2 system + 2 g L^{-1} $NaHCO_3$	0	0.2583	2.5629	2.9517	3.3184	4.3964	4.6178	4.9274
B7: Fe^0-CO_2 system + 4 g L^{-1} $NaHCO_3$	0	0.2679	2.6867	3.1760	3.5235	4.7786	4.9784	5.6283
B8: Fe^0-CO_2 system + 6 g L^{-1} $NaHCO_3$	0	0.3562	2.9126	3.4449	3.8859	5.0869	5.3203	6.6072
B9: Fe^0-CO_2 system + 8 g L^{-1} $NaHCO_3$	0	0.4987	3.3002	3.9422	4.3352	5.6925	5.9971	7.8000
B10: Fe^0-CO_2 system + 10 g L^{-1} $NaHCO_3$	0	0.6642	4.1043	4.7334	5.2130	6.8868	7.2486	8.9605

The CO_2 utilization and changes in headspace pressures (absolute) for both systems (N_2 and CO_2) are illustrated in Appendix I (Suppl. Info. Figs. 3.3 & 3.4).

At the end of the experiment (after 75 h), the processed Fe^0 with the maximum concentration of $NaHCO_3$ (10 g L^{-1}) from both Fe^0-N_2 and Fe^0-CO_2 systems were subjected to X-RD analysis. As illustrated in the X-RD pattern in Fig. 3.6, both systems exhibited a prominent peak indicative of siderite ($FeCO_3$). However, upon comparison, it is evident that the Fe^0-CO_2 system exhibited more intense peaks for siderite ($FeCO_3$).

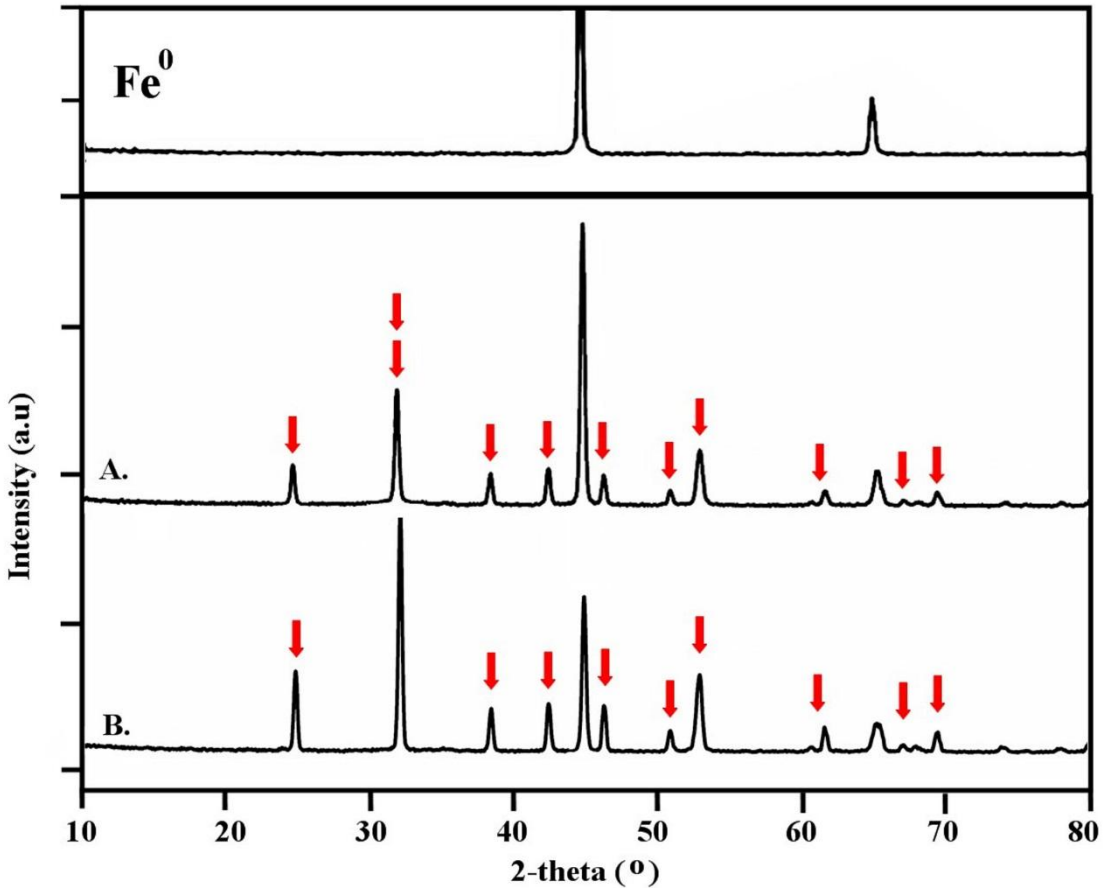

Fig. 3.6: X-ray diffraction pattern of **A.:** Fe^0 with deionized water exposed to N_2 and 10 g L^{-1} $NaHCO_3$ and **B.:** Fe^0 with deionized water exposed to CO_2 and 10 g L^{-1} $NaHCO_3$.

➡ : Siderite ($FeCO_3$).

3.1.3 Influence of Temperature on a Fe^0-$NaHCO_3$ System

As illustrated in Fig. 3.7 (A.), H_2 production increased with the rise in the system's temperature. The system exposed to 50 °C exhibited the maximum H_2 production, reaching 98% in the headspace of the serum bottles after 93 h. Conversely, the minimum H_2 production was observed in the system exposed to 2 °C, measuring 41% in the headspace. The pattern of CO_2 consumption followed the reverse trend of H_2 production, with the highest carbon dioxide consumption occurring in systems where elevated accumulations of H_2 were identified (Fig. 3.7; B.).

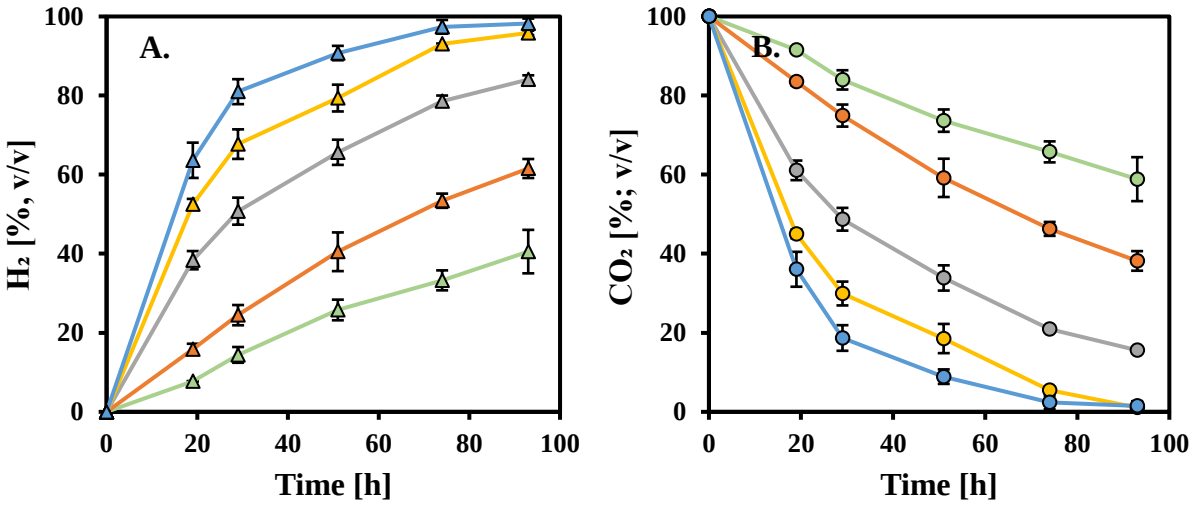

Fig. 3.7: Variations in H_2 and CO_2 gas composition in systems under different temperatures over time. **A.:** H_2 evolution under CO_2-environment. **B.:** CO_2 utilization.

: 2 °C; : 20 °C; : 33 °C; : 40 °C; : 50 °C

The pH of the systems was initially set to approximately 6. As shown in Fig. 3.8, the systems exposed to lower temperatures (2 ºC and 20 ºC) exhibited minimal changes in pH, with an increase of approximately 0.6 after 93 h. However, as the temperature increased, a corresponding rise in pH values was observed across the systems during the experiment. The systems exposed to 50 ºC showed a more significant pH alteration, reaching approximately 7.5 after 93 h.

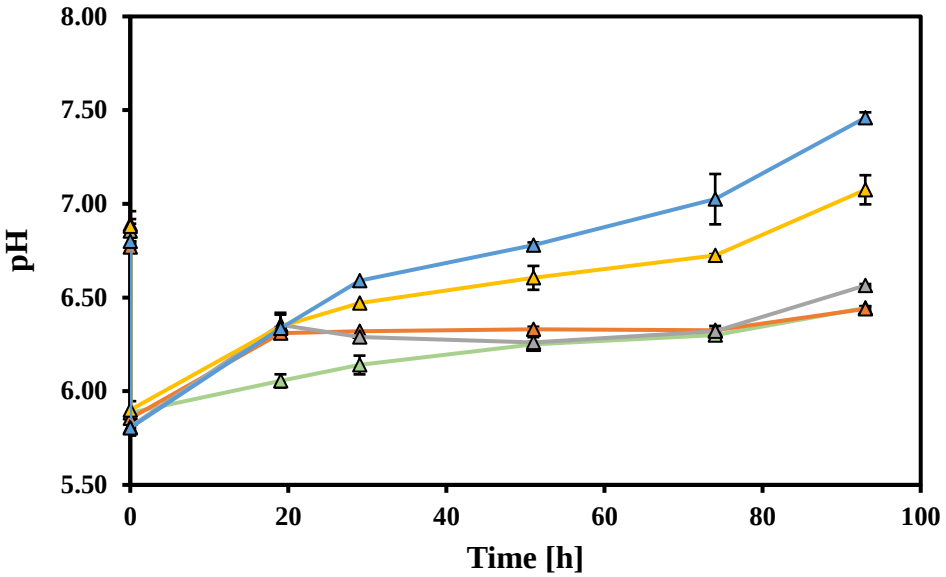

Fig. 3.8: Variations in pH during the experimental duration in sup-groups C1-C5 at various temperatures.

: 2 °C; : 20 °C; : 33 °C; : 40 °C; : 50 °C

Table 3.4 presents the accumulation of H_2 across systems incubated at various temperatures. As detailed, the system exposed to 2 °C produced a H_2 concentration of 2.51 mmol after 93 h. In contrast, increasing the temperature to 50 °C (25 times higher) resulted in a 75% rise in H_2 accumulation, reaching 9.97 mmol after the same duration.

Table 3.4: H_2 accumulation in mmol observed over time in sub-groups C1-C5 exposed to various temperatures.

Time [h]	0	19	29	51	74	93
C1: Fe^0-$NaHCO_3$-CO_2 system at 2 °C	0	0.4693	0.8792	1.5850	2.0620	2.5128
C2: Fe^0-$NaHCO_3$-CO_2 system at 20 °C	0	1.0843	1.7694	3.0684	4.2929	5.0748
C3: Fe^0-$NaHCO_3$-CO_2 system at 33 °C	0	3.1302	4.3207	5.8335	7.1035	7.6725
C4: Fe^0-$NaHCO_3$-CO_2 system at 40 °C	0	4.4168	5.8095	7.0142	8.3027	8.6360
C5: Fe^0-$NaHCO_3$-CO_2 system at 50 °C	0	6.1396	7.9492	9.0595	9.8030	9.9688

The changes in headspace pressures (absolute) within the systems are illustrated in Appendix I (Suppl. Info. Fig. 3.5).

3.1.4 Influence of pH on a Fe^0-$NaHCO_3$ System

All systems adjusted to different pH values on day 0 displayed a consistent H2 production and CO2 utilization pattern, as illustrated in Fig. 3.9 (A. & B.). The percentage of H_2 in the headspace of the serum bottles varied between 79% and 97%, while the CO_2 levels decreased from an initial 100% to nearly 0%, with a maximum observed CO_2 concentration of only 18% after 91 h.

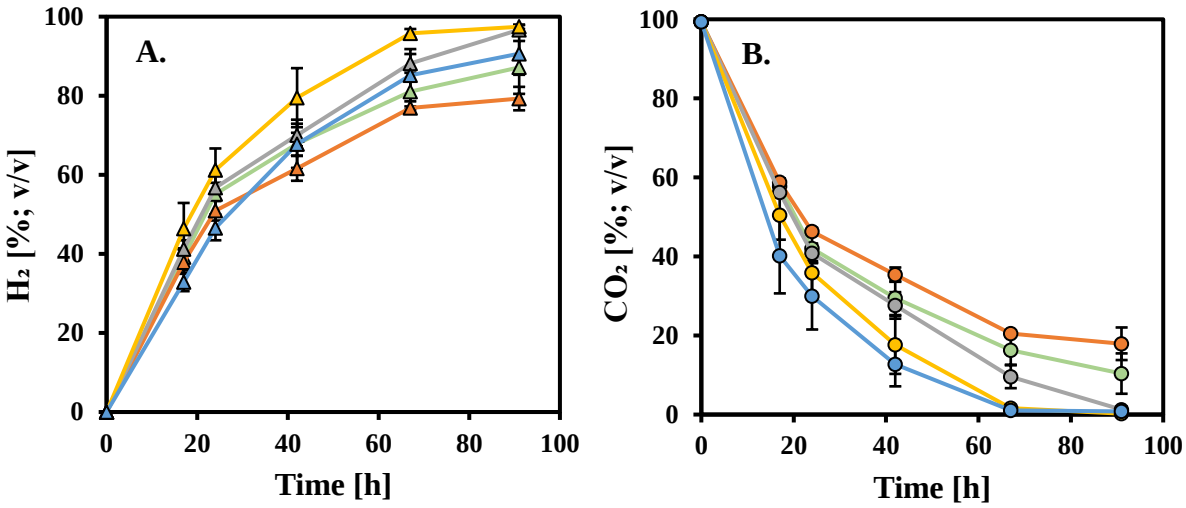

Fig. 3.9: Variations in H_2 and CO_2 gas composition in systems under different temperatures over time. **A.:** H_2 evolution under CO_2-environment. **B.:** CO_2 utilization.

: 4 pH; : 5 pH; : 6 pH; : 7 pH; : 8 pH

It is observed that the production and increase of H_2 in the systems do not exhibit a proportional relationship with the rise in pH, like the observations with temperature in Sub-chapter 3.1.3. As depicted in Table 3.5, the highest concentration of H_2 was observed in the system where the pH was adjusted to 6 on day 0, reaching 7.55 mmol after 91 h. Following the system where the pH was regulated at 5 on day 0, producing 7.52 mmol of H_2 after 91 h. Conversely, systems with pH adjustments to 7 and 8 on day 0 exhibited lower H_2 productivity, measuring 5.98 and 4.08 mmol, respectively. By increasing the pH by only 2 units, from 6 to 8, the productivity of H_2 was inhibited and decreased by almost 46%.

Table 3.5: H_2 accumulation in mmol observed over time in sub-groups D1-D5 adjusted at different pH values on day 0.

Time [h]	0	17	24	42	67	91
D1: Fe^0-$NaHCO_3$-CO_2 system at pH 4	0	3.0089	4.4492	5.6556	6.8659	7.4190
D2: Fe^0-$NaHCO_3$-CO_2 system at pH 5	0	3.3185	4.5559	5.6665	7.1898	7.5165
D3: Fe^0-$NaHCO_3$-CO_2 system at pH 6	0	2.9633	4.1589	5.2549	6.8064	7.5488
D4: Fe^0-$NaHCO_3$-CO_2 system at pH 7	0	2.4800	3.3485	4.4223	5.6224	5.9775
D5: Fe^0-$NaHCO_3$-CO_2 system at pH 8	0	1.4810	2.0973	3.0518	3.8379	4.0835

The pH of each system was initially adjusted to five different values ranging from 4 to 8. As depicted in Fig. 3.10, after 17 h, all systems exhibited stabilization within the pH range of 6 to 7.5. Following this stabilization period, systems initially set to pH 6, 7, and 8 showed an increase in pH, with those initially adjusted to pH 7 and 8 reaching approximately pH 9 after 91 h. Systems with initial pH values of 4 and 5 displayed minimal changes in pH throughout the experimental period.

The changes in headspace pressures (absolute) within the systems are illustrated in Appendix I (Suppl. Info. Fig. 3.6).

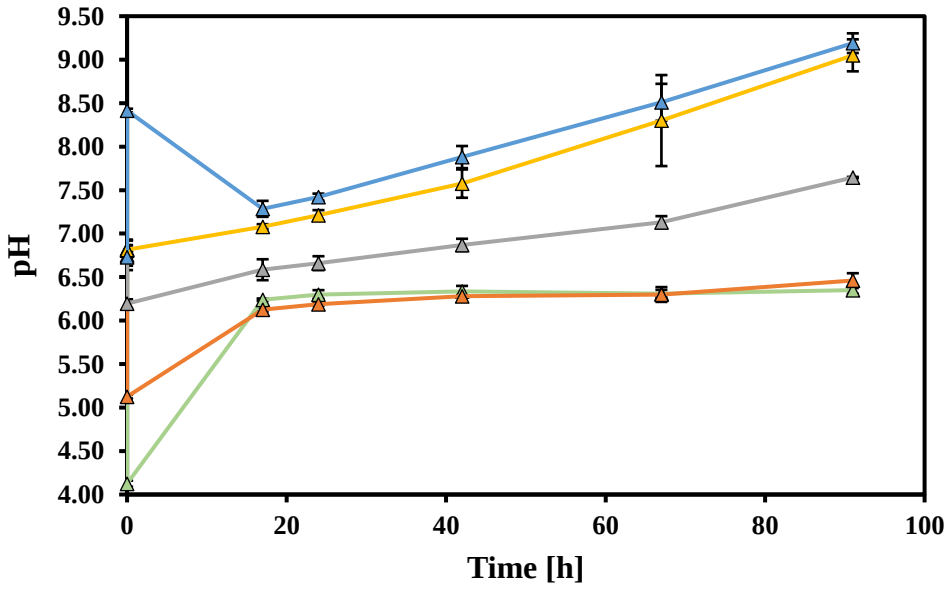

Fig. 3.10: pH fluctuations over the experimental period in Sub-groups D1-D5 with varied initial pH settings.

: 4 pH; : 5 pH; : 6 pH; : 7 pH; : 8 pH

3.1.5 Evaluation of Different Agitation Modes

All systems subjected to various agitation modes throughout the experimental duration (107 h) demonstrated a consistent trend in H_2 production, with the percentage ranging between 81% and 90% in the headspace of the serum bottles. Regarding CO_2 utilization, the system under 200 rpm agitation demonstrated the highest efficiency at 91%. The utilization percentages were 86% at 100 rpm and 81% when no agitation was applied, as illustrated in Fig. 3.11 (A.&B.).

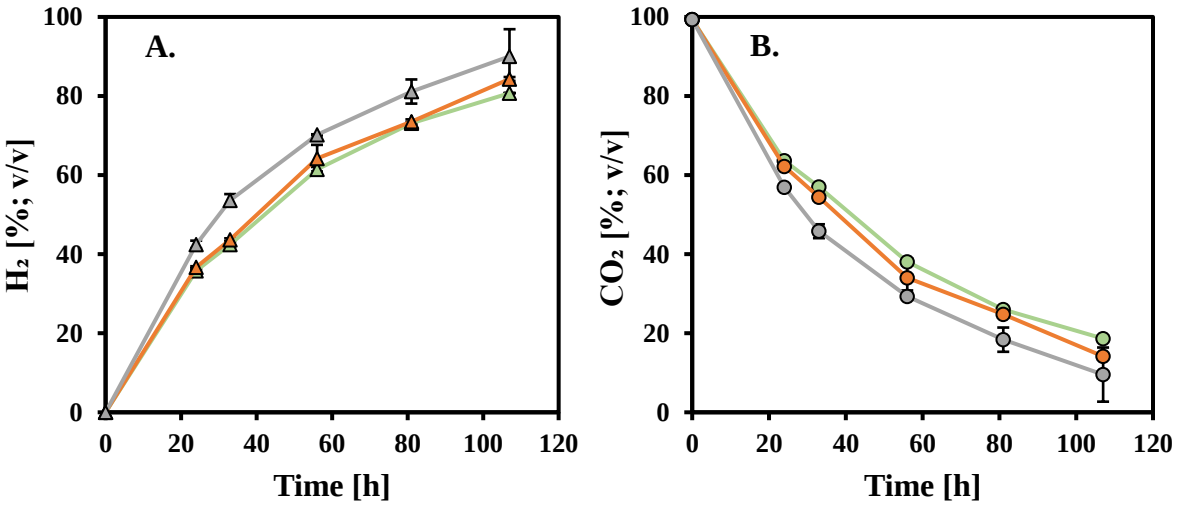

Fig. 3.11: H_2 and CO_2 gas evolution in systems subjected to different agitation modes over time. **A.:** H_2 evolution under CO_2-environment. **B.:** CO_2 utilization.

: 0 rpm; :100 rpm; : 200 rpm

As illustrated in Table 3.6, the system subjected to agitation at 200 rpm exhibited the highest H_2 concentration, reaching 8.69 mmol after 107 h. In contrast, after the same duration, the systems exposed to 0 and 100 rpm showed similar H_2 production, with values of 7.58 mmol and 7.51 mmol, respectively. The influence of agitation mode on the percentage of H_2 produced by the systems was minimal, showing a modest increase from 0 rpm to 200 rpm, reaching ≈13%.

Table 3.6: H_2 accumulation in mmol over time in Sub-groups E1-E3 under varied agitation modes.

Time [h]	0	24	33	56	81	107
E1: Fe^0-$NaHCO_3$-CO_2 system at 0 rpm	0	2.9495	3.7240	5.6116	6.7901	7.5825
E2: Fe^0-$NaHCO_3$-CO_2 system at 100 rpm	0	2.7816	3.6467	5.7055	6.5691	7.5106
E3: Fe^0-$NaHCO_3$-CO_2 system at 200 rpm	0	3.6329	4.8710	6.6222	7.7457	8.6943

The pH of the systems was initially set to 6. As shown in Fig. 3.12, all systems exhibited a consistent pattern in pH increase, with minimal variation during the experimental period, reaching pH values between 6.6 and 6.7 after 107 h.

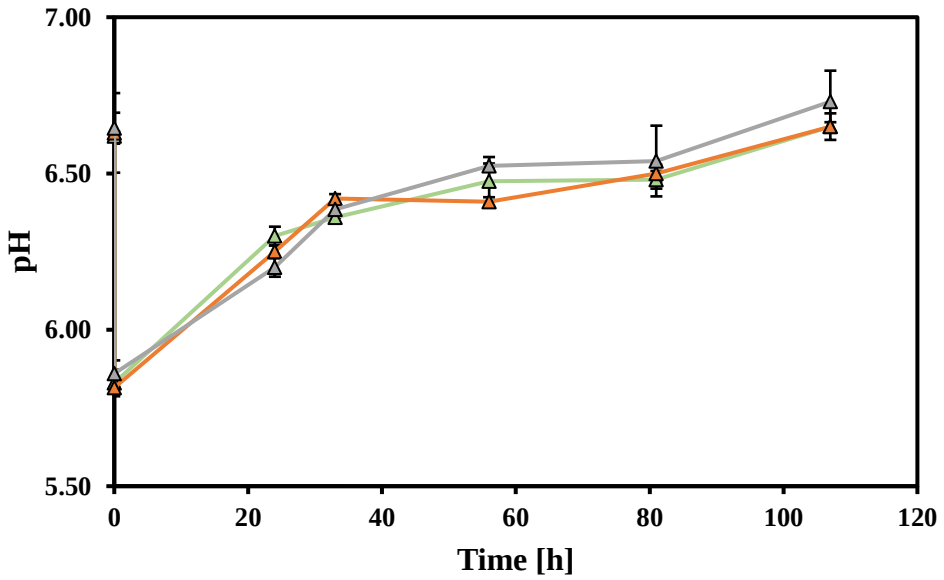

Fig. 3.12: pH fluctuations over the experimental period in Sub-groups E1-E3 exposed to varied agitation speeds.

: 0 rpm; : 100 rpm; : 200 rpm

The changes in headspace pressures (absolute) within the systems are illustrated in Appendix I (Suppl. Info. Fig. 3.7).

3.1.6 H_2 Generation Across Varied Fe^0 Concentrations

As depicted in Fig. 3.13 (A.), the evolution of H_2 substantially increased with the rise in Fe^0 concentration in the systems over time. The system with the highest Fe^0 concentration (50 g L^{-1}) exhibited the maximum H_2 accumulation, reaching 99 % in the headspace of the serum bottles after 107 h, while the minimum production was observed in the system with only 5 g L^{-1}, producing approximately 35 %. The ratios between consecutive H_2 results were approximately 1.59 when doubling the amount of Fe^0 in the system from 5 g L^{-1} to 10 g L^{-1}. However, doubling the amount of Fe^0 in the system from 25 g L^{-1} to 50 g L^{-1} resulted in a lower ratio of 1.18. The pattern of CO_2 consumption followed the reverse trend of H_2 production, with the highest CO_2 consumption occurring in systems where higher amounts of Fe^0 were used (Fig. 3.13; B.).

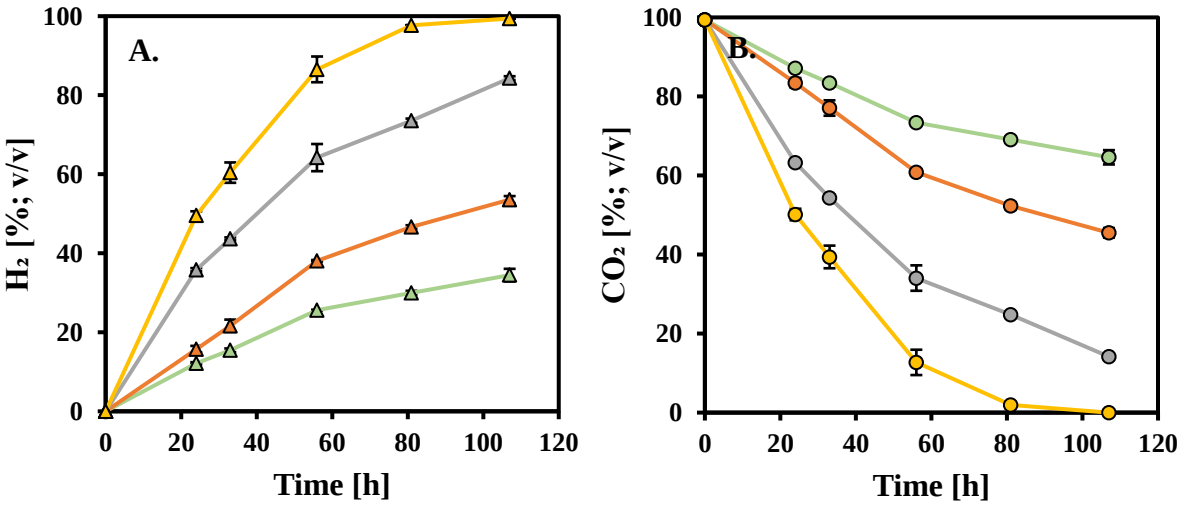

Fig. 3.13: H_2 and CO_2 gas evolution over time in systems with varied concentrations of Fe^0.

A.: H_2 evolution under CO_2-environment. **B.:** CO_2 utilization.

: 5 g L^{-1}; : 10 g L^{-1}; : 25 g L^{-1}; : 50 g L^{-1}

As illustrated in Table 3.7, the lowest H_2 accumulations were identified in the system where only 5 g L^{-1} of Fe^0 was used, reaching only 2.72 mmol after 107 h, while the maximum was observed to be 10.30 mmol in the system where 50 g L^{-1} of Fe^0 was used. By increasing the concentration of Fe^0 by 2, 5, and 10 times, the accumulations of H_2 increased by 39%, 64 %, and 74%, respectively. Increasing the Fe^0 concentration does not result in a proportional increment in H_2 production.

Table 3.7: Accumulation of H_2 in mmol over time in Sub-groups F1-F4, featuring varied concentrations of Fe^0.

Time [h]	0	24	33	56	81	107
F1: $NaHCO_3$-CO_2 system with 5 g L^{-1} Fe^0	0	0.8709	1.1776	1.9774	2.3424	2.7210
F2: $NaHCO_3$-CO_2 system with 10 g L^{-1} Fe^0	0	1.1458	1.6905	3.1089	3.8484	4.4658
F3: $NaHCO_3$-CO_2 system with 25 g L^{-1} Fe^0	0	2.7336	3.6467	5.7055	6.5691	7.6220
F4: $NaHCO_3$-CO_2 system with 50 g L^{-1} Fe^0	0	4.1750	5.5275	8.6805	10.0377	10.2991

As in the previous experiments, the pH was initially adjusted to approximately 6. As shown in Fig. 3.14, the systems utilizing 5, 10, and 25 g L^{-1} of Fe^0 exhibited minimal changes in pH throughout the experimental duration. However, at a higher concentration, the system with 50 g L^{-1} of Fe^0 showed a significant increase in pH, reaching nearly 9 after 107 h.

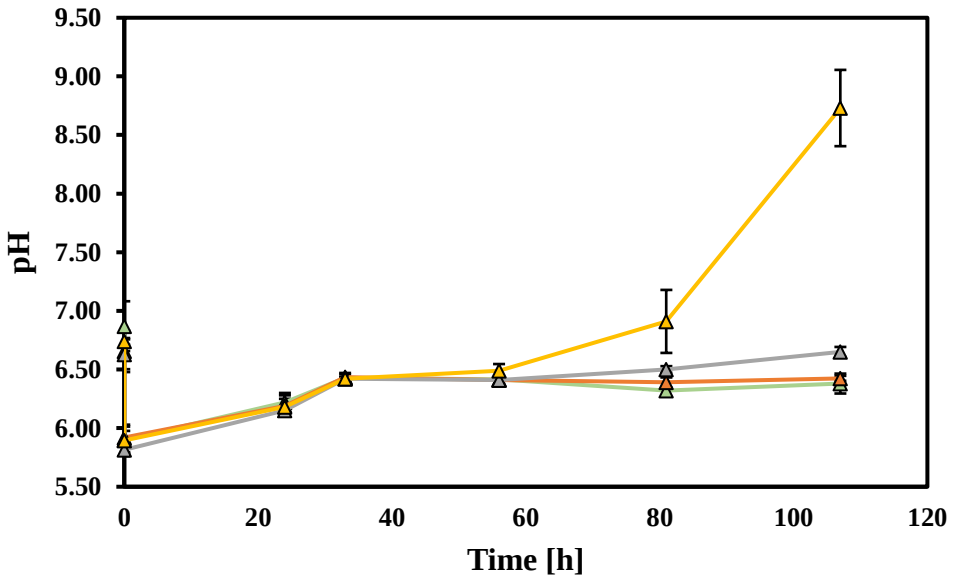

Fig. 3.14: pH fluctuations over the experimental period in Sub-groups F1-F4, which were subjected to different concentrations of Fe^0.

:5 g L^{-1}; :10 g L^{-1}; :25 g L^{-1}; :50 g L^{-1}

The changes in headspace pressures (absolute) within the systems are illustrated in Appendix I (Suppl. Info. Fig. 3.8).

3.1.7 Impact of Fe^0 Particle Sizes

As illustrated in Fig. 3.15 (A.), using coarse-grained Fe^0 in abiotic H_2 production is significantly less effective than fine-grained Fe^0. A comparison of systems with the same Fe^0 concentration (25 g L^{-1}) but differing particle sizes of 800 µm and 10 µm (Control) [Fig. 3.15 (A.) – Black lines] reveal a notable increase of approximately 87% in H_2 production after 115 hours when the particle size is reduced by 80 times.

For systems utilizing 800 µm-sized Fe^0 at varying concentrations (25, 100, 200 g L^{-1}), a pattern similar to that observed in systems with fine-grained Fe^0 (10 µm) at different concentrations, as discussed in sub-chapter 3.4.6, was evident, though with lower percentages in the headspace of the serum bottles. Among the systems using 800 µm-sized Fe^0, the highest H_2 accumulation occurred in the system with 200 g L^{-1} Fe^0, reaching 48%, while the systems with 100 g L^{-1} and 25 g L^{-1} Fe^0 showed accumulations of 31% and 13%, respectively, in the headspace of the serum bottles after 115 hours.

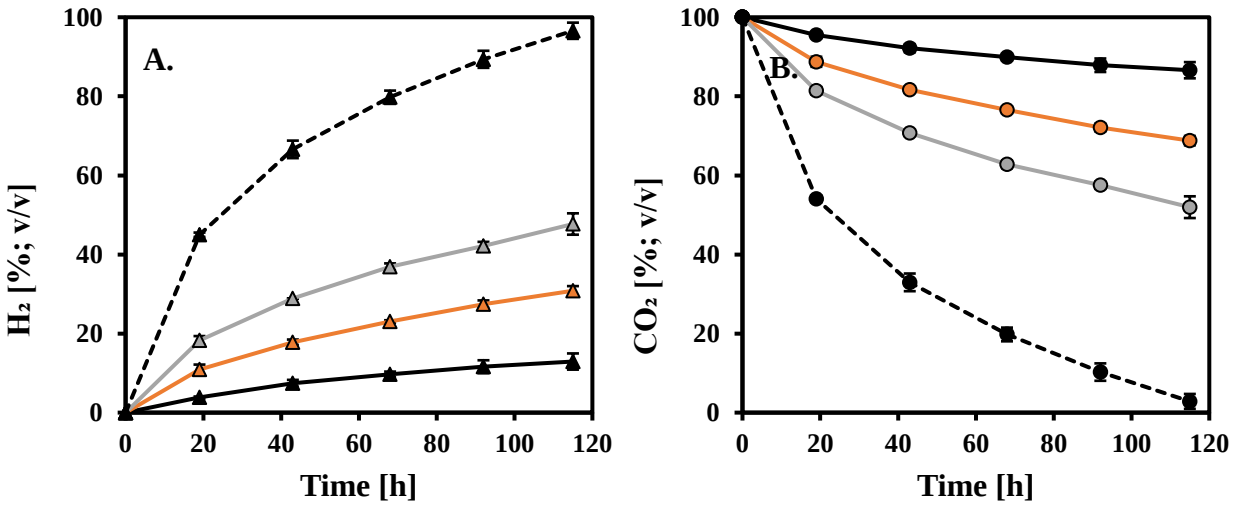

Fig. 3.15: H_2 evolution and CO_2 utilization over time in systems employing the same amount of Fe^0 (25 g L^{-1}) with different particle sizes and with varying concentrations of Fe^0, featuring a particle size of 800 µm.

A.: H_2 evolution under CO_2-environment. **B.:** CO_2 utilization.

: 25 g L^{-1} – 800 µm Fe^0; : 25 g L^{-1} – 10 µm Fe^0 (Control).

: 100 g L^{-1} – 800 µm Fe^0; : 200 g L^{-1} – 800 µm Fe^0.

The trend in CO_2 utilization followed an inverse pattern to H_2 production [Fig. 3.15 (B.)]. It was also observed that CO_2 utilization increased not only with higher Fe^0 concentrations used in the systems but also accelerated when finer Fe^0 particles were used. A comparison of CO_2 utilization between systems with the same Fe^0 concentration (25 g L^{-1}) but different particle sizes (800 µm and 10 µm – Black lines) revealed a difference of 84% [Fig. 3.15(B.)]

Regarding H_2 production in mmol (Table 3.8), the highest H_2 accumulation among systems using Fe^0 at various concentrations (G1-G3) with a particle size of 800 µm was observed in the system with 200 g L^{-1} Fe^0, reaching 4 mmol after 107 hours. This was followed by the system with 100 g L^{-1} Fe^0, which produced nearly half the amount at 2.43 mmol. At the lowest Fe^0 concentration (25 g L^{-1}), only 1 mmol was quantified. When comparing systems that use the same amount of Fe^0 (25 g L^{-1}) but with different particle sizes (G1: 800 µm Fe^0 and G4: 10 µm Fe^0), there was an 89% increase in H_2 production when fine-grained Fe^0 (10 µm) was used. The above observations suggest that to produce an equivalent amount of H_2, a substantially greater concentration of coarse-grained Fe^0 is necessary compared to the use of fine-grained Fe^0.

Table 3.8: Accumulation of H_2 in mmol over time in Sub-groups G1-G3 and G4, with varying concentrations of 800 µm Fe^0 and the control system (25 g L^{-1} - 10 µm Fe^0), respectively.

Time [h]	0	19	43	68	92	115
G1: $NaHCO_3$-CO_2 system with 25 g L^{-1} Fe^0 - 800 µm	0	0.3055	0.6063	0.7744	0.9022	0.9975
G2: $NaHCO_3$-CO_2 system with 100 g L^{-1} Fe^0 - 800 µm	0	0.9234	1.4726	1.8867	2.1847	2.4272
G3: $NaHCO_3$-CO_2 system with 200 g L^{-1} Fe^0 - 800 µm	0	1.6197	2.5194	3.1897	3.6098	4.0607
G4: $NaHCO_3$-CO_2 system with 25 g L^{-1} Fe^0 - 10 µm (Control)	0	3.8190	6.0777	7.4924	8.5117	9.2845

The initial pH of all systems was adjusted to 6. As shown in Fig. 3.16, a significant variation in pH was observed after 115 hours between systems utilizing the same amount of Fe^0 (25 g L^{-1}) but with different particle sizes. The system supplemented with 10 µm Fe^0 (Control) exhibited an increase in pH of approximately 1 unit. In contrast, the systems supplemented with 800 µm Fe^0 showed minimal alteration in pH across all concentrations (25, 100, 200 g L^{-1}).

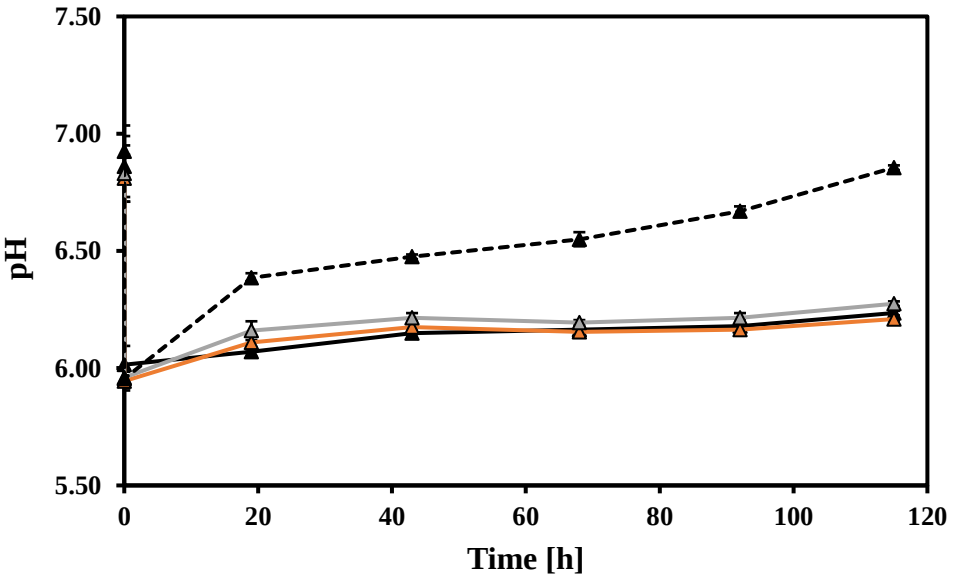

Fig. 3.16: pH fluctuations over the experimental period in sub-groups G1-G3 (800 µm Fe^0) and G4 (10 µm Fe^0).

: 25 g L^{-1} – 800 µm Fe^0 (G1); : 25 g L^{-1} – 10 µm Fe^0 (Control – G4).

: 100 g L^{-1} – 800 µm Fe^0 (G2); : 200 g L^{-1} – 800 µm Fe^0 (G3).

The changes in headspace pressures (absolute) within the systems are illustrated in Appendix I (Suppl. Info. Fig. 3.9).

3.1.8 Impact of *In-Situ* Mechanical Action on Fe^0

Figure 3.17 (A. & B.) illustrates that the H_2 percentage in the headspace of the serum bottles reached approximately 97% over the 115-hour experimental period. There was no notable difference between the two systems, which were subjected to different mechanical disruptions (glass and boiling beads), and the control system, without any solid substrate *in-situ*. The pattern of CO_2 consumption followed an inverse trend to H_2 production, with a reduction of nearly 97%.

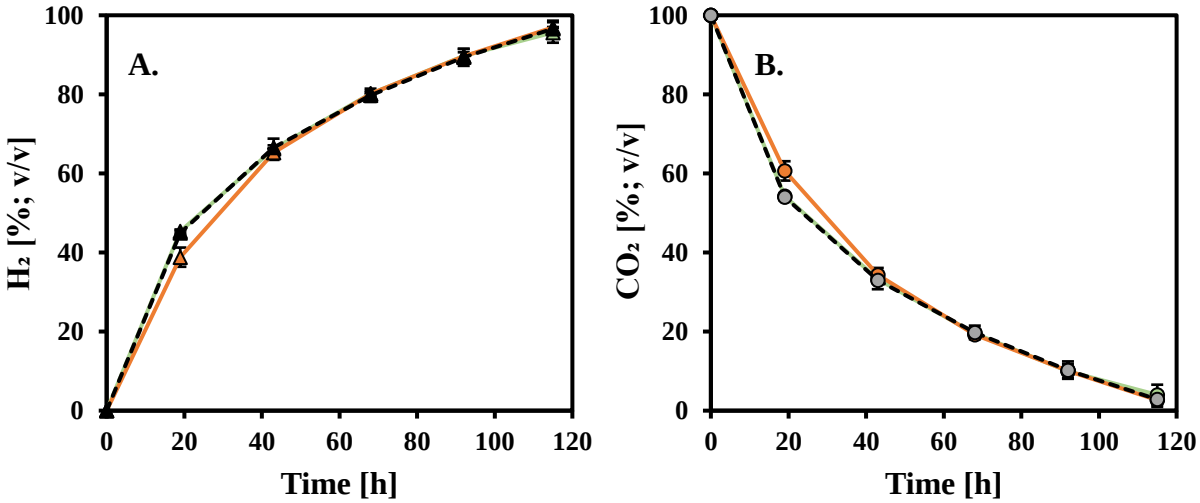

Fig. 3.17: Evolution of H_2 and CO_2 gases over time in systems subjected to *in situ* mechanical disruption and no disruption. **A.:** H_2 evolution under CO_2-environment. **B.:** CO_2 utilization.

: Glass beats (145 g L^{-1}); : Boiling chips (145 g L^{-1}); : Control (no mechanical action).

Concerning H_2 accumulation, all systems demonstrated similar H_2 production, reaching approximately 9.5 mmol of H_2 after 115 h, as shown in Table 3.9, with negligible variation. This suggests that solid mechanical disruptors had a minimal impact on system productivity under the proposed methodology.

The pH of the systems was initially adjusted to 5.5-6, and, after the experimental duration (115 h), increased to approximately 6.8 with no significant variation between the systems and the control. Furthermore, no variation of headspace pressures was observed among

systems where the absolute pressure was measured at 2.20 bar at the end of the experiment, as illustrated in Appendix I (Suppl. Info. Fig. 3.10).

Table 3.9: Accumulation of H_2 in mmol over time in Sub-groups H1, H2, and H3 with and without solid mechanical disruptors.

Time [h]	0	19	43	68	92	115
H1: Fe^0-$NaHCO_3$-CO_2 system with glass beads (*in-situ*)	0	4.2016	6.2230	7.6689	8.6665	9.3844
H2: Fe^0-$NaHCO_3$-CO_2 system with boiling chips (*in-situ*)	0	3.3558	6.1016	7.7242	8.6550	9.4033
H3: Fe^0-$NaHCO_3$-CO_2 system. Control (no mechanical disruptors)	0	3.8190	6.0777	7.4924	8.5117	9.2845

3.1.9 Impact of Air-Water Interface Area Size

As depicted in Fig. 3.18 (A. & B.), the use of narrow (I1) or wide (I2) serum bottles with distinct gas-water interface areas had minimal impact on the evolution of H_2. Both systems exhibited similar percentages in the headspace of the serum, reaching 97 % after 115 h. The pattern of CO_2 utilization followed the reverse trend of H_2 production, also reaching approximately 98 %.

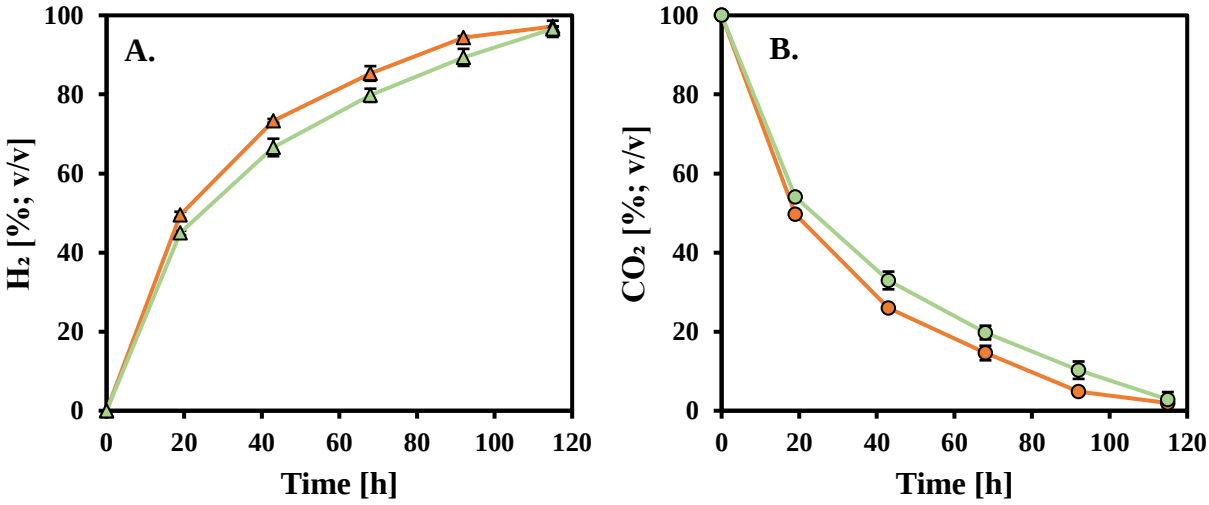

Fig. 3.18: Evolution of H_2 and CO_2 gases over time in serum bottles with distinct gas-water interface areas. **A.:** H_2 evolution under CO_2-environment. **B.:** CO_2 utilization. : 28 cm^2 interface area; : 75 cm^2 interface area.

Concerning H_2 accumulation, an alteration of 5% between the systems after 115h was observed, as shown in Table 3.10. The narrow serum bottle systems produced nearly 9.28 mmol of H_2, while the wide ones produced almost 9 mmol of H_2 after 115 hours.

Table 3.10: Accumulation of H_2 in mmol over time for the systems with narrow (I1) and wide (I2) serum bottles, respectively.

Time [h]	0	19	43	68	92	115
I1: Fe^0-$NaHCO_3$-CO_2 system. Gas-water interface area: 28 cm^2	0	3.8190	6.0777	7.4924	8.5117	9.2845
I2: Fe^0-$NaHCO_3$-CO_2 system. Gas-water interface area: 75 cm^2	0	3.9642	6.4671	7.6182	8.3677	8.8071

The pH of the systems was initially adjusted to 6 and at the end of the experiment (115 h) increased only by almost 1 unit without any variation between the systems. Similarly, no pressure variations were observed between systems. After the experimental duration absolute pressure increased by one unit (2 bar) in both systems as illustrated in Appendix I (Suppl. Info. Fig. 3.11).

3.1.10 Waste Iron Materials (Fe-W) Evaluation with Different Particle Sizes

As illustrated in Fig. 3.19 (A. & B.), the various types of waste Fe^0 materials displayed different patterns of H_2 production. It was observed that a reduction in the specific surface area of the Fe^0 resulted in increased H_2 evolution.

Waste iron particles, with sizes of 0.05 mm^2 and 5 mm^2, exhibited H_2 generation reached 22 % and 12 %, respectively. In comparison, steel wool demonstrated a higher H_2 generation of 59 % in the headspace of the serum at 139 h, utilizing a concentration of 25 g L^{-1} of waste Fe^0 [Fig. 3.19 (A.)]. A similar trend persisted with the increase in waste Fe^0 concentration to 100 g L^{-1}. However, quadrupling the concentration of waste Fe^0 resulted in an average increase of 45 % in H_2 accumulation across all systems. The H_2 accumulations in the serum bottle headspaces reached 43%, 21%, and 100% after 139 h when waste iron particles with sizes of 0.05 mm^2, 5 mm^2, and steel wool were utilized, respectively [Fig. 3.19 (B.)].

The pattern of CO_2 utilization mirrored the inverse trend of H_2 production for both concentrations of waste Fe^0. At a concentration of 25 g L^{-1}, the CO_2 utilization ranged from 13 % to 60 % [Fig. 3.19 (C.)]. With a fourfold increase in the concentration of waste Fe^0 to 100 g L^{-1}, the utilization subsequently increased, ranging from 22 % to 100 % [Fig. 3.19 (D.)].

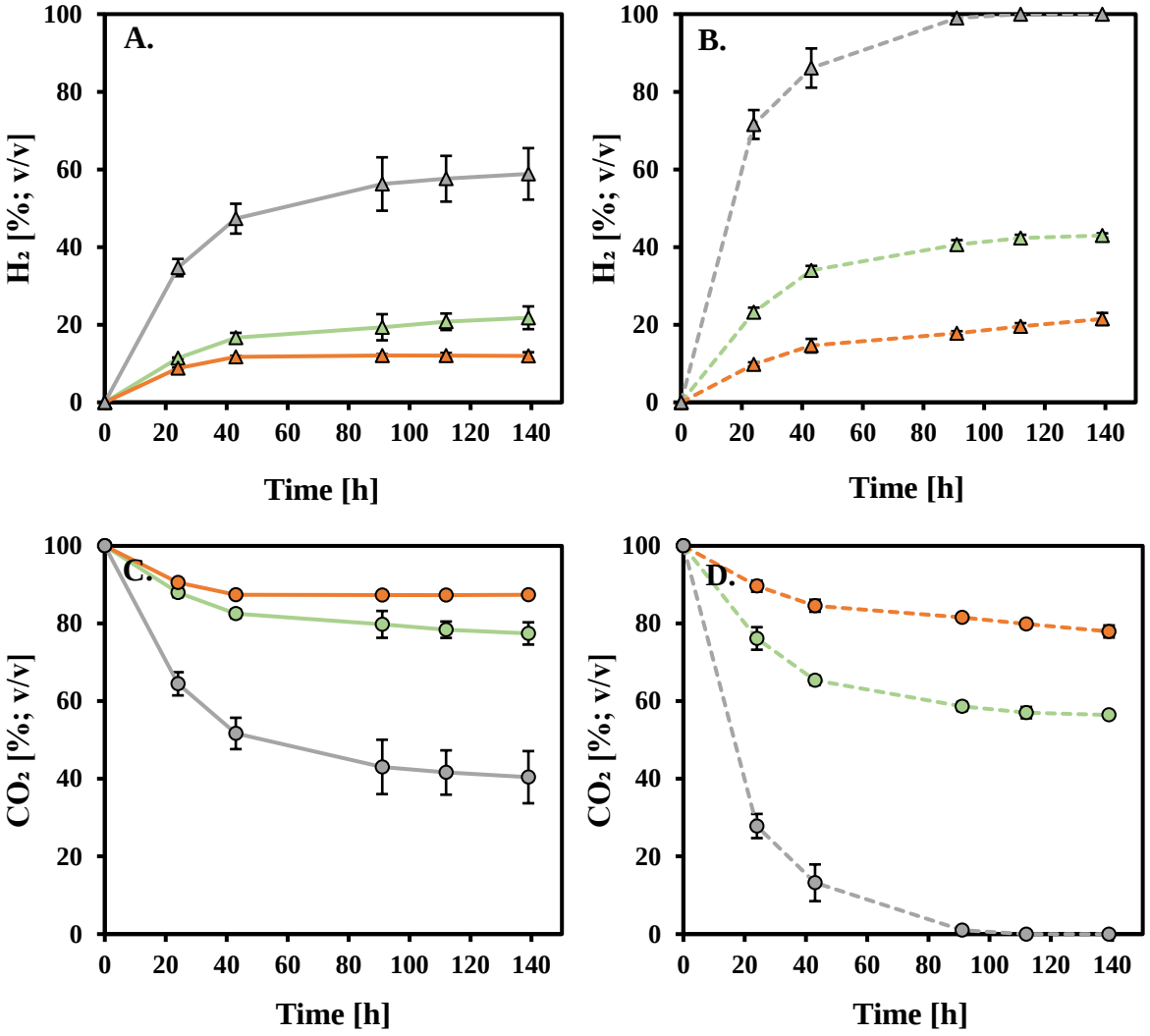

Fig. 3.19: Evolution of H_2 and CO_2 gases over time in systems exposed to various waste Fe^0 materials at two distinguished concentrations.

A. & B.: H_2 evolution under CO_2-environment. **C. & D.:** CO_2 utilization.

: 25 g L^{-1} waste Fe^0; : 100 g L^{-1} waste Fe^0

: 0.05 mm^2; : 5 mm^2; : Steel wool

As illustrated in Table 3.11, the maximum H_2 accumulation in mmol, exhibited in the system where steel wool was used at both concentrations, 25 g L^{-1} and 100 g L^{-1}, reached 5.84 mmol and 11.24 mmol, respectively, at 139 h. This represents an increase of almost 48%, with a fourfold increase in the concentration of waste Fe^0. On the other hand, the waste Fe^0 with a specific area of 5 mm^2 demonstrated lower H_2 accumulations, reaching 0.96 mmol and 1.79 mmol when using 25 g L^{-1} and 100 g L^{-1} of waste Fe^0, respectively. By increasing the specific surface area of the waste Fe^0 by 100 times (0.05 mm^2), the accumulations of H_2 increased by 46 % and 55 % when using 25 g L^{-1} and 100 g L^{-1} of waste Fe^0, respectively, corresponding to 1.78 mmol and 4 mmol of H_2.

The pH was initially adjusted to 6 for both systems using different waste Fe^0 at two distinct concentrations. After 139 h, no significant variation in pH was observed in systems using Fe-W at a concentration of 25 g L^{-1}, with the pH increasing by only approximately 0.30 across all systems [Fig. 3.20 (A.)]. Similar observations were made for systems utilizing Fe-W at a concentration of 100 g L^{-1}. However, the system using steel wool at a concentration of 100 g L^{-1}, which demonstrated the maximum H_2 production, exhibited a different pattern in pH, as shown in Fig. 3.20 (B.). The pH increased by more than 2.5 units from the initial adjustment, reaching 8.6 after 139 h.

Table 3.11: Accumulation of H_2 in mmol over time for systems exposed to various types of waste Fe^0 materials and two distinguished waste Fe^0 concentrations.

Time [h]	Fe^0 conc.	0	24	43	91	112	139
J1: $NaHCO_3$-CO_2-Waste Fe^0 Size: 0.05 mm^2	25 g L^{-1}	0	0.8306	1.3303	1.5608	1.6840	1.7770
J3: $NaHCO_3$-CO_2-Waste Fe^0 Size: 5 mm^2	25 g L^{-1}	0	0.6145	0.8949	0.9388	0.9438	0.9564
J5: $NaHCO_3$-CO_2-Waste Fe^0 Size: steel wool	25 g L^{-1}	0	3.0157	4.3183	5.4554	5.6628	5.8375
J2: $NaHCO_3$-CO_2-Waste Fe^0 Size: 0.05 mm^2	100 g L^{-1}	0	1.8129	2.9303	3.7010	3.8968	3.9986
J4: $NaHCO_3$-CO_2-Waste Fe^0 Size: 5 mm^2	100 g L^{-1}	0	0.6947	1.1199	1.4394	1.6149	1.7902
J6: $NaHCO_3$-CO_2-Waste Fe^0 Size: steel wool	100 g L^{-1}	0	6.9744	8.9025	10.9066	11.1539	11.2419

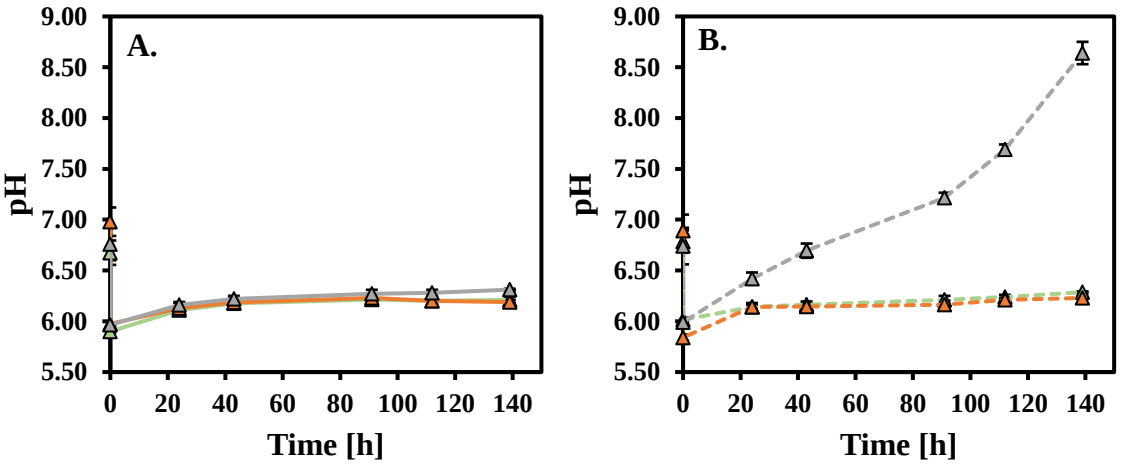

Fig. 3.20: pH fluctuations in systems exposed to various waste Fe^0 materials over the experimental period at two distinguished concentrations.

A.: ▬ - $NaHCO_3$-CO_2 system using 25 g L^{-1} of waste Fe^0 (J1; J3; J5)

B.: ▬▬▬ - $NaHCO_3$-CO_2 system using 100 g L^{-1} of waste Fe^0 (J2; J4; J6)

▭ : 0.05 mm^2; ▭ : 5 mm^2; ▭ : Steel wool

Changes in headspace pressures (absolute) within the systems during the experimental period were also monitored and are illustrated in Appendix I (Suppl. Info. Fig. 3.12).

3.1.11 Impact of $NaHCO_3$ Solutions Generated Through CO_2 Capture in NaOH Solutions on Waste Iron Materials

In line with the observations from Experiments 7 (Sub-chapter 3.1.7) and Experiment 10 (Sub-chapter 3.1.10), it becomes evident that the size of Fe^0 particles significantly influences H_2 evolution. Finer particles are more reactive for H_2 production within a $NaHCO_3$ buffered solution under a CO_2 environment. To delve deeper into this H_2 evolution pattern, various waste Fe^0 materials with distinct particle sizes were examined in a solution generated by reacting different NaOH concentrations with CO_2, all within a CO_2 environment. As shown in Fig. 3.21 (A. & B.), steel wool demonstrated higher H_2 accumulation compared to coarse-grain Fe^0 particles with a surface area of 0.05 mm^2,

even when these two distinct systems were separately exposed to $NaHCO_3$ solutions derived from 0.25 M and 0.75 M NaOH, respectively.

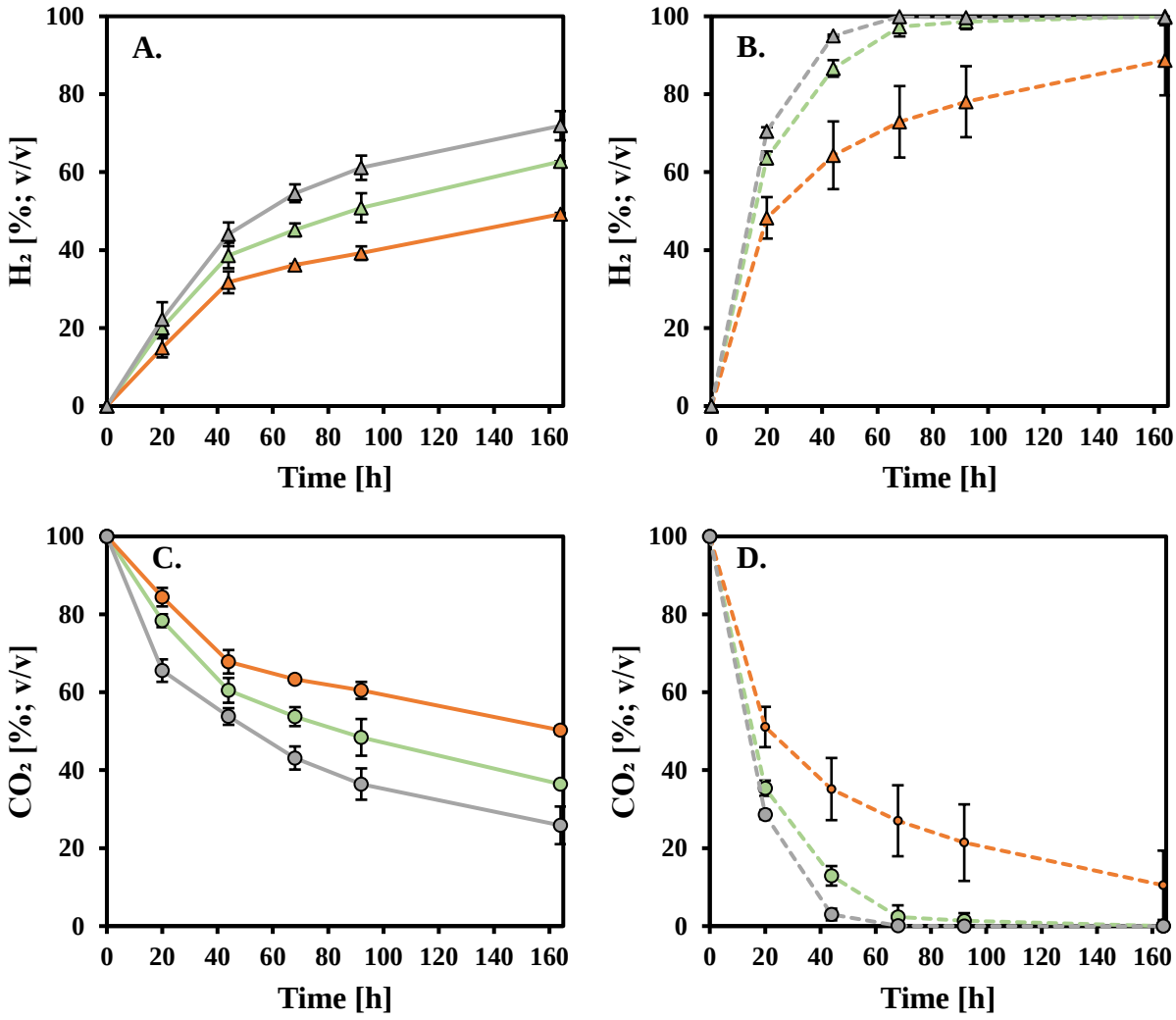

Fig. 3.21: Evolution of H_2 and CO_2 utilization over time in systems exposed to various waste Fe^0 materials and different NaOH solutions used for CO_2 capture. **A. & B.:** H_2 evolution under CO_2-environment. **C. & D.:** CO_2 utilization.

: 100 g L^{-1} waste Fe^0 (0.05 mm^2); : 100 g L^{-1} waste Fe^0 (steel wool)

: NaOH (0.25 M); : NaOH (0.75 M); : Water

However, it's essential to note that the percentage of H_2 in the system where water was used and exposed to CO_2 exhibited higher, albeit fictional, percentages due to the nearly zero relative pressure within the serum bottles compared to the other systems that

exhibited higher pressures, as indicated in Suppl. Info. Fig. 3.13. The pattern of CO_2 utilization mirrored the inverse trend of H_2 production for both concentrations of waste Fe^0 under varying $NaHCO_3$ concentration solutions [Fig. 3.21 (C. & D.)].

As illustrated in Table 3.12, and by comparing the waste Fe^0 particle sizes used, the maximum H_2 accumulations were observed in the system where steel wool was used, quantified at 10.6 mmol, 11.3 mmol, and 6.5 mmol using NaOH solutions at concentrations of 0.25 M, 0.75 M, and water, respectively, at 164 h.

The system demonstrated a similar pattern of H_2 mmol fluctuations, where waste Fe^0 particle sizes of 0.05 mm^2 were used with the same order of NaOH solutions and water, quantified at 5 mmol, 4.9 mmol, and 3.2 mmol, respectively. These observations suggest that elevating NaOH concentration in the CO_2 capture solution and prolonged reaction times enhance H_2 production when the resulting $NaHCO_3$ solution is used in a system with Fe^0.

Table 3.12: Accumulation of H_2 in mmol over time for systems exposed to various types of waste Fe^0 materials and two distinguished waste Fe^0 concentrations.

Time [h]	Solution	0	20	44	68	92	164
K1: 100 g L^{-1} Waste Fe^0 (Size: 0.05 mm^2**) – CO_2 environment**	NaOH (0.25 M) + CO_2	0	1.5215	3.0503	3.5873	4.0394	5.0106
K3: 100 g L^{-1} Waste Fe^0 (Size: 0.05 mm^2**) – CO_2 environment**	NaOH (0.75 M) + CO_2	0	1.3921	3.1419	3.6102	3.9258	4.9283
K5: 100 g L^{-1} Waste Fe^0 (Size: 0.05 mm^2**) – CO_2 environment**	H_2O + CO_2	0	1.0047	1.9850	2.4594	2.7546	3.2404
K2: 100 g L^{-1} Waste Fe^0 (steel wool**) – CO_2 environment**	NaOH (0.25 M) + CO_2	0	6.1887	9.0706	10.2322	10.3709	10.5815
K4: 100 g L^{-1} Waste Fe^0 (steel wool**) – CO_2 environment**	NaOH (0.75 M) + CO_2	0	5.8111	8.0543	9.1937	9.8783	11.2620
K6: 100 g L^{-1} Waste Fe^0 (steel wool**) – CO_2 environment**	H_2O + CO_2	0	3.7646	5.8683	6.2629	6.2886	6.4692

The pH was initially adjusted to 6 for both systems using two distinct $NaHCO_3$ solutions. After 164 h, no significant variation in pH (~ 0.5 increasing) was observed in systems utilizing various Fe-W and exposed to $NaHCO_3$ solution resulting from the reaction of NaOH 0.25 M with CO_2, as shown in Fig. 3.22 (A.). Similar observations were made when $NaHCO_3$ solution was used, resulting from the reaction of NaOH 0.75 M with CO_2. However, the system using steel wool exhibited a different pattern in pH, as shown in Fig. 3.22 (B.). The pH increased almost 3 units from the initial adjustment, reaching 9 after 164 h.

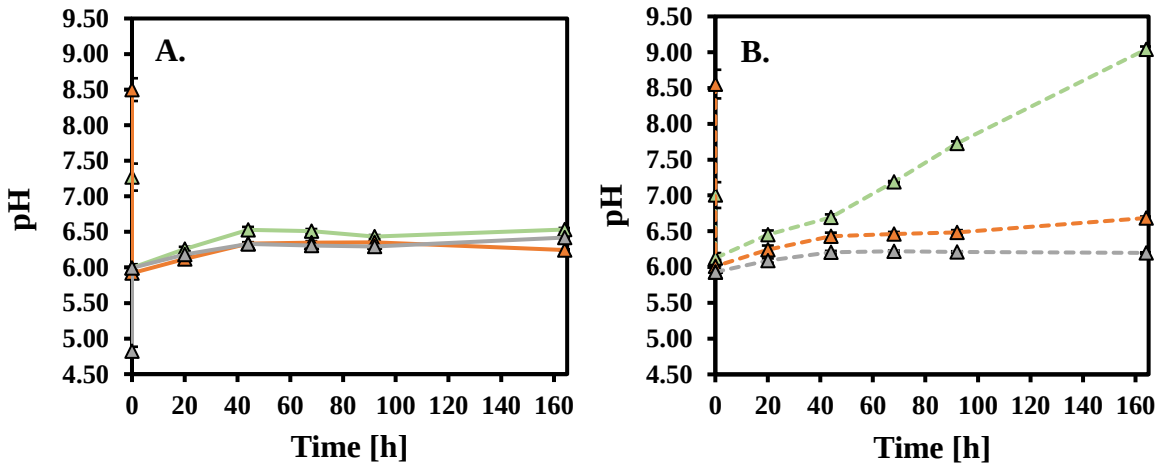

Fig. 3.22: pH fluctuations in systems exposed to various waste Fe^0 materials and different NaOH solutions over the experimental period.

A.: ▬ - NaOH-CO_2 system using 100 g L^{-1} waste Fe^0 (0.05 mm2) (K1; K3; K5)

B.: ▬▬ - NaOH-CO_2 system using 100 g L^{-1} waste Fe^0 (steel wool) (K2; K4; K6)

▭ : NaOH (0.25 M); ▭ : NaOH (0.75 M); ▭ : Water

Changes in headspace pressures (absolute) within the systems during the experimental period were also monitored and are illustrated in Appendix I (Suppl. Info. Fig. 3.13).

3.1.12 Impact of $NaHCO_3$ Solutions Generated Through CO_2 Capture in NaOH Solutions on Oxidized or Pretreated Waste Iron Materials

The processed waste Fe materials from the previous experiment (Experiment 11 – Sub-chapter 3.1.11) were reused here to evaluate the potential of H_2 evolution of the already oxidized Fe. As illustrated in Fig. 3.23, the already processed Fe materials exhibit H_2 productivity when exposed to new $NaHCO_3$ solutions. It is observed that the core Fe^0 material (0.05 mm^2) demonstrates lower H_2 accumulations in the headspace of the serum bottles, as discussed previously, compared to the fine Fe^0 material (steel wool) [Fig. 3.23 (A.)].

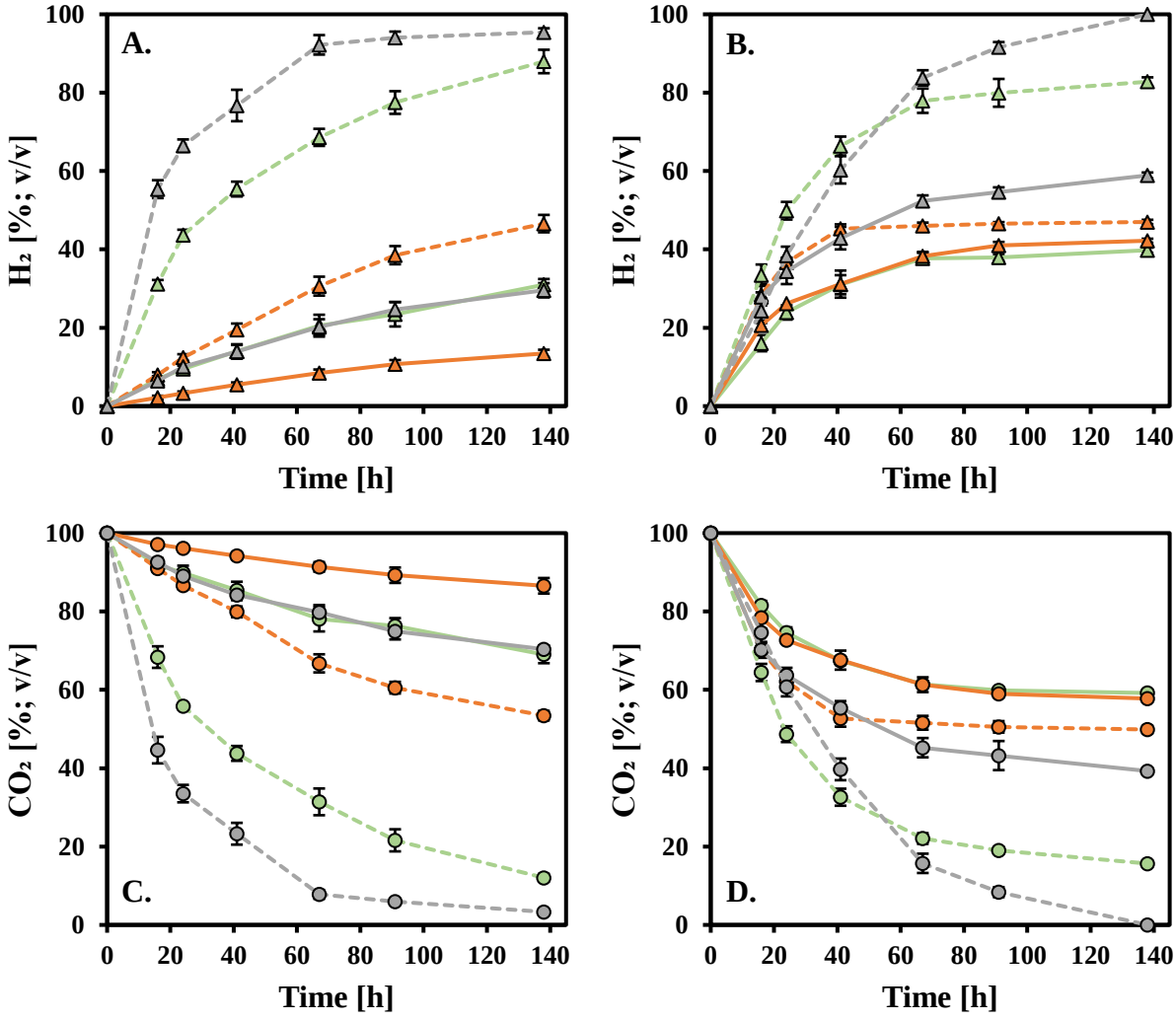

Fig. 3.23: Evolution of H_2 and CO_2 gases over time in systems where various oxidized waste Fe^0 materials and pre-treated oxidized waste Fe^0 materials were exposed to different NaOH solutions used for CO_2 capture.

A. & B: H_2 evolution of oxidized waste Fe^0 materials (A.) and pre-treated oxidized waste Fe^0 materials (B.), respectively, under CO_2-environment. **C. & D.:** CO_2 utilization in systems with oxidized waste Fe^0 materials (C.) and pre-treated oxidized waste Fe^0 materials (D.), respectively.

: 100 g L^{-1} oxidized waste Fe^0 (0.05 mm^2); : 100 g L^{-1} oxidized waste Fe^0 (steel wool)

: NaOH (0.25 M); : NaOH (0.75 M); : Water

The same patterns regarding the correlation between Fe^0 particle sizes and H_2 evolution were also exhibited when the oxidized waste Fe^0 materials were pre-treated with citric acid [Fig. 3.23 (B.)]. By comparing the percentage of H_2 in the headspace of the serum bottles, it is evident that there is a decrease across the systems in the order of unprocessed Fe^0, processed Fe^0, and pre-treated Fe^0. The pattern of CO_2 utilization mirrored the inverse trend of H_2 production for both processed and pre-treated waste Fe^0 under different $NaHCO_3$ solutions [Fig. 3.23 (B. & C.)].

Regarding the calculated H_2 accumulations in mmol, the maximum H_2 productions were observed in the systems where a $NaHCO_3$ solution was used, prepared from NaOH solution of 0.25 M and CO_2 gas, in both oxidized waste Fe^0 materials (0.05 mm_2 Fe^0 and steel wool), quantified at 2.80 mmol and 9.11 mmol, respectively, at 138 h (Table 3.13). However, after the pre-treatment with citric acid, the 0.05 mm^2 Fe^0 particle sizes demonstrated higher H_2 accumulations when a $NaHCO_3$ solution was used, which resulted from 0.75 M NaOH and CO_2, reaching 5.34 mmol. After the pretreatment, the steel wool exhibited higher H_2 accumulation when exposed to a $NaHCO_3$ solution that resulted from 0.25 M NaOH and CO_2, reaching 8.18 mmol at 138 h. It's worth mentioning that the system where 0.05 mm^2 Fe^0 particles were exposed to a solution resulting from water exposed to CO_2 gas exhibited low H_2 production (~1.40 mmol); however, after the pre-treatment of Fe^0 with citric acid, the production increased by over 62 %, reaching 3.70 mmol of H_2 at 138 h (Table 3.13).

The pH was initially adjusted to between 5.5 and 6 in all systems at the beginning of the experiment. After 138 h, no significant variation in pH was observed, with an increase of approximately 0.5 in all systems, as shown in Fig. 3.24.

Table 3.13: Accumulation of H_2 in mmol over time for systems where various oxidized waste Fe^0 materials and pre-treated oxidized waste Fe^0 materials were exposed to different NaOH solutions for CO_2 capture.

Time [h]	0	16	24	41	67	91	138
Oxidized Waste Fe^0 Materials (100 g L^{-1})							
L1: Fe^0 (Size: 0.05 mm^2) – **CO_2 environment** NaOH (0.25 M) + CO_2	0	0.6207	0.8511	1.2693	1.8647	2.1197	2.8009
L3: Fe^0 (Size: 0.05 mm^2) – **CO_2 environment** NaOH (0.75 M) + CO_2	0	0.2730	0.4129	0.6871	1.0644	1.3449	1.6827
L5: Fe^0 (Size: 0.05 mm^2) – **CO_2 environment** H_2O + CO_2	0	0.3166	0.4995	0.6837	0.9719	1.1663	1.3714
L2: Fe^0 (steel wool) – **CO_2 environment** NaOH (0.25 M) + CO_2	0	2.8432	4.1172	5.3743	6.8652	7.8921	9.1139
L4: Fe^0 (steel wool) – **CO_2 environment** NaOH (0.75 M) + CO_2	0	0.8908	1.3962	2.2034	3.5101	4.4335	5.3598
L6: Fe^0 (steel wool) – **CO_2 environment** H_2O + CO_2	0	2.9585	3.7270	4.4366	5.5752	5.8094	6.0216
Pre-treated Waste Fe^0 Materials (100g L^{-1}) With Citric Acid							
L7: Fe^0 (Size: 0.05 mm^2) – **CO_2 environment** NaOH (0.25 M) + CO_2	0	1.4096	2.1721	2.8693	3.4756	3.4775	3.6153
L9: Fe^0 (Size: 0.05 mm^2) – **CO_2 environment** NaOH (0.75 M) + CO_2	0	2.5963	3.3607	4.0086	4.9069	5.2278	5.3407
L11: Fe^0 (Size: 0.05 mm^2) – **CO_2 environment** H_2O + CO_2	0	1.5381	1.9751	2.5169	3.1183	3.3022	3.6902
L8: Fe^0 (steel wool) – **CO_2 environment** NaOH (0.25 M) + CO_2	0	2.9462	4.7720	6.4693	7.7673	7.9681	8.1780
L10: Fe^0 (steel wool) – **CO_2 environment** NaOH (0.75 M) + CO_2	0	3.4600	4.5199	5.6247	5.7363	5.7865	5.8219
L12: Fe^0 (steel wool) – **CO_2 environment** H_2O + CO_2	0	1.1279	1.8504	3.1682	4.8066	5.5801	6.5308

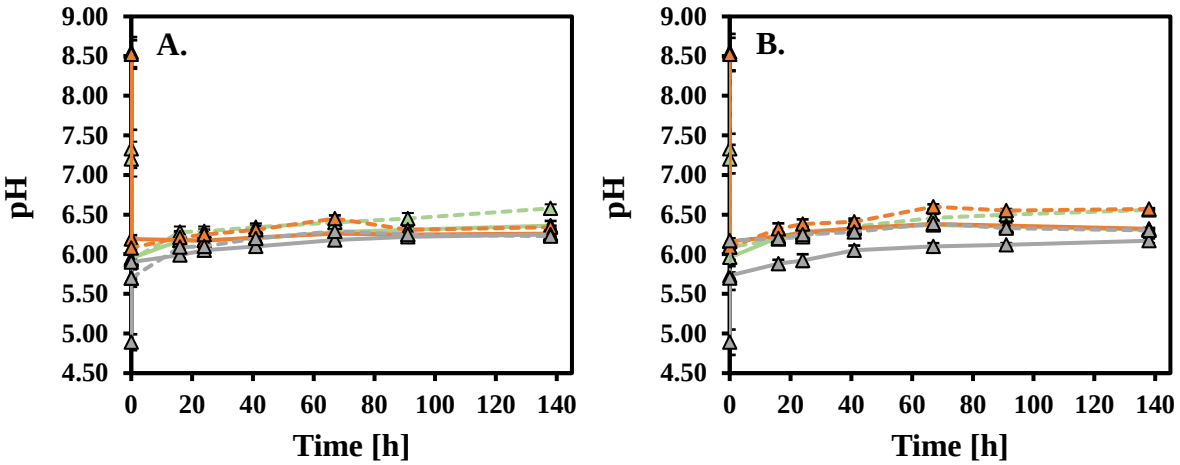

Fig. 3.24: pH fluctuations over the experimental period in systems where various untreated and pre-treated oxidized waste Fe^0 materials were exposed to different NaOH solutions used for CO_2 capture.

A.: pH fluctuations of systems utilizing untreated oxidized waste Fe^0 materials (L1-L6)

B.: pH fluctuations of systems utilizing pretreated oxidized waste Fe^0 materials (L7-L12)

: 100 g L^{-1} oxidized waste Fe^0 (0.05 mm^2); : 100 g L^{-1} oxidized waste Fe^0 (steel wool)

: NaOH (0.25 M); : NaOH (0.75 M); : Water

Changes in headspace pressures (absolute) within the systems during the experimental period were also monitored and are illustrated in Appendix I (Suppl. Info. Fig. 3.14).

3.1.13 Discussion of Experimental Set-Up 1

3.1.13.1 Mechanisms of Fe^0 Oxidation Under Anaerobic Conditions

The observations extracted from Sub-chapters 3.1.1 and 3.1.2 underscore the significant role of CO_2-enriched environments in Fe^0 corrosion, leading to the production of abiotic H_2. The process commences with the dissolution of CO_2 in water (Eq. 21). Upon CO_2 hydration, carbonic acid (H_2CO_3) forms, which is a weak acid (Eq. 22). Then H_2CO_3 dissociates in water, resulting in the generation of bicarbonate (HCO_3^-) and further carbonate ions (CO_3^{2-}), accompanied by the release of hydrogen protons (H^+) (Eq. 21 - 24) (Taramura et al., 2017).

$$CO_{2\,(g)} \rightleftharpoons CO_{2\,(aq)} \quad \text{(Eq. 21)}$$

$$CO_{2\,(aq)} + H_2O_{\,(l)} \rightleftharpoons H_2CO_{3\,(aq)} \quad \text{(Eq. 22)}$$

$$H_2CO_{3\,(aq)} \rightleftharpoons HCO_3^-{}_{(aq)} + H^+_{\,(aq)} \rightarrow \quad \text{(Eq. 23)}$$

$$HCO_3^-{}_{(aq)} \rightleftharpoons CO_3^{2-}{}_{(aq)} + H^+_{\,(aq)} \quad \text{(Eq. 24)}$$

However, the solubility of CO_2 is negligible at highly acidic values, and elevated pH levels promote the dissociation of H_2CO_3. As depicted in Fig. 3.25, representing the mole fractions of a carbonate system as a function of pH, at lower pH values (around pH 4), a more significant fraction of H_2CO_3 only partially dissociates in an aqueous solution. As the pH is elevated from 5 to 8, the proportion of CO_2 in the form of HCO_3^- increases, reaching its maximum at approximately pH 8.2, where all the $H_2CO_{3(aq)}$ dissociates to HCO_3^- as shown in Eq. 23. At higher pH levels (pH 8.2–14) apply, the system becomes enriched with CO_3^{2-} until the pH reaches around 14, where the only species present is CO_3^{2-} (Eq.24).

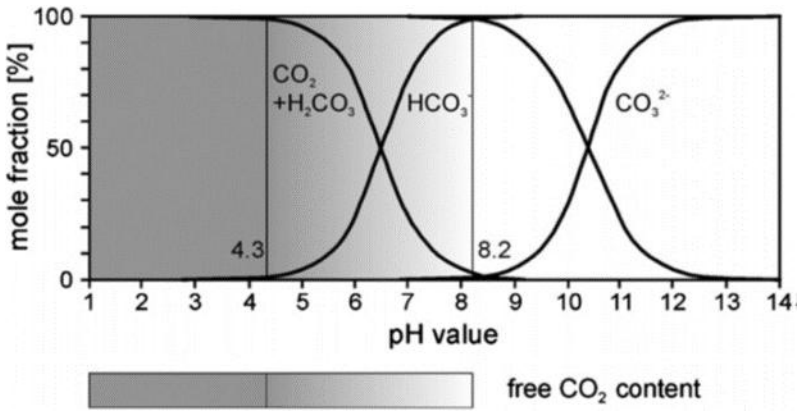

Fig. 3.25: Fractions identified in a carbonate system under varied pH conditions (The figure herein has been directly sourced from scholarly work authored by Zosel et al., 2011).

As shown in Fig. 3.2 (Sub-chapter 3.1.1), the Fe^0-CO_2 system exhibited a decline in pH within the initial 3.5 hours, which can be attributed to the dissolution of CO_2 into water and the formation of H_2CO_3. This dissolution of CO_2 is reflected in the monitoring of system pressure. As illustrated in the Suppl. Info. Fig. 3.2, during the first 3.5 hours, the headspace of the CO_2 system exhibited a negative relative pressure of -0.28 bar (absolute pressure 0.72). Furthermore, the pH decline is also due to the "buffering effect" caused by the dissociation of H_2CO_3 (Basilico et al., 2021), as shown in Eqs. 23 and 24. Throughout this process, the pH of the CO_2 system can decrease due to the high accumulation of H^+ ions produced.

Several additional reactions can occur when Fe^0 is introduced into an aqueous medium saturated with CO_2. Fe^0 can dissolve directly into ferrous ions (Fe^{2+}) (Eq. 25). The bicarbonate (HCO_3^-) and carbonate (CO_3^{2-}) ions produced from the earlier reactions (Eq. 26 & 27) can act as catalysts for the formation of a corrosion scale ($FeCO_3$) during the anodic reaction process (Eq. 26 - 28) (Wang et al., 2020).

<u>Anodic reactions:</u>

$$Fe^0 \rightarrow Fe^{2+} + 2e^- \quad \text{(Eq. 25)}$$

$$Fe^{2+} + CO_3^{2-} \rightarrow FeCO_{3\,(s)} \quad \text{(Eq. 26)}$$

$$Fe^0 + HCO_3^- \rightarrow FeCO_{3\,(s)} + 2e^- + H^+ \quad \text{(Eq. 27)}$$

$$Fe^0 + CO_3^{2-} \rightarrow FeCO_{3(s)} + 2e^- \quad \text{(Eq. 28)}$$

During the well-established cathodic reaction process (Eq. 29), H_2 gas is generated from hydrogen protons (H^+) and electrons (e^-), which result from the dissociation of H_2CO_3 and the anodic reactions, respectively (Kahyarian and Nesic, 2020; Kahyarian and Nesic, 2019). This leads to an increase in pH due to deprotonation and the enrichment of the system with OH^-, which aligns with our findings. As the anodic and cathodic reactions progressed, the pH of the Fe^0-CO^2 system increased as shown in Fig. 3.2.

Cathodic reaction:

$$2H^+ + 2e^- \rightarrow H_{2\ (gas)} \quad \text{(Eq. 29)}$$

Apart from the proposed mechanism based on the dissociation of $H_2CO_{3(aq)}$ and $HCO_3^-{}_{(aq)}$, several corrosion studies on steel within the pH range of 6–8 (Cole et al., 2011; Han et al., 2011) have suggested that bicarbonate HCO_3^-acts as an electrochemically active species, undergoing reduction reactions on the iron substrate's surface (Eqs. 30 & 31)

$$2H_2CO_{3(aq)} + 2e^- \rightarrow H_{2(g)} + 2HCO_3^- \quad \text{(Eq. 30)}$$

$$2HCO_3^-{}_{(aq)} + 2e^- \rightarrow H_{2(g)} + 2CO_3^{2-} \quad \text{(Eq. 31)}$$

There is an ongoing debate in steel corrosion studies regarding the role of H_2CO_3 in the cathodic reduction process—whether it occurs through direct reduction or via H^+ release (Alsalem et al., 2023)

The aforementioned theoretical framework aligns with our findings, indicating that under high concentrations of CO_2 and/or $NaHCO_3$, Fe^0 corrosion is governed by high H_2 gas accumulation compared with systems that have no or low concentrations of CO_2 and/or $NaHCO_3$, as covered by the overall reaction as indicated in Eq. 32.

$$Fe^0{}_{(s)} + HCO_3^-{}_{(aq)} + H^+{}_{(aq)} \rightarrow FeCO_{3\ (s)} + H_{2\ (g)} \quad \text{(Eq. 32)}$$

The X-RD pattern analysis revealed the presence of a corrosion scale identified as siderite ($FeCO_3$) under a CO_2 environment (non-saturated systems), as shown in Fig 3.3. However, goethite (α-FeOOH) was also detected. This observation can be attributed to the small amount of oxygen quantified in the Fe^0-CO_2 system (approximately 8%).

This small amount of O_2 penetrates the septum stopper due to the negative relative pressures (~ -0.3 bar) developed by the system after the dissolution of CO_2 gas into water. Under these conditions, Fe^{3+} is produced, and the ratio of Fe(II)/Fe(III) diversifies, promoting the creation of different iron species and shifting the reactions towards more thermodynamically stable crystalline structures such as goethite, as shown in Eqs. 33 & 34 (Xiao et al., 2021; Bricker et al., 2004).

$$Fe^{2+} + 1/4\ O_2 + 5/2\ H_2O \rightarrow Fe(OH)_3 + 2H^+ \quad \text{(Eq. 33)}$$

$$Fe(OH)_3 \rightarrow FeOOH_{(goethite)} + H_2O \quad \text{(Eq. 34)}$$

However, the X-RD pattern analysis of the systems buffered with $NaHCO_3$ and exposed to a CO_2 environment (saturated systems) (Fig. 3.6) clearly shows the formation of $FeCO_3$, as indicated by Eq. 32.

With respect to the Fe^0-N_2 system, minimal alterations were observed in the system's pH (Fig. 3.2), which was initially adjusted to ~6 and pressure (Suppl. Info. Fig. 3.2). The X-RD analysis (Fig. 3.3) shows that Fe^0 corroded to Magnetite (Fe_3O_4). The formation of $Fe(OH)_2$ from Fe^0 (Eq. 35) in a wet environment is characterized as a metastable solid (Rovira et al., 2007), which, according to Melchers (2014), under anoxic conditions and normal low temperatures, can be transformed to Fe_3O_4 at a very low rate (Eq. 36). This can also explain the small amounts of H_2 (0.025 mmol) quantified in the system. Thus, these observations confirm the hypothesis that CO_2 plays a significant role in iron oxidation.

$$Fe + 2H_2O \rightarrow Fe(OH)_2 + H_{2(g)} \quad \text{(Eq. 35)}$$

$$3Fe(OH)_2 \rightarrow Fe_3O_{4(s)} + 2H_2O + H_{2(g)} \quad \text{(Eq. 36)}$$

Hence, under high CO_2 concentrations in a Fe^0-water system, a higher amount of H_2 is produced. However, a recent study by Zhu et al. (2024) highlighted that increased HCO_3^- concentration in a system can lead to the formation of a protective film, resulting in the "passivation" of Fe^0. Moreover, Mishra et al. (2020) demonstrated that the thickness of the 'passivation' carbonate layer is inversely proportional to its porosity after exposing carbon steel to a 1M $NaHCO_3$ solution with an initial pH of 8.1 at 25°C. A greater passivation layer resulted in lower porosity, thus lower reaction rates between Fe^0 and CO_3^{2-}. This can explain the decline in the production rates after 19.5 h in our experiments. Furthermore, Zhu et al. (2024) explain that, under pH higher than 7 and elevated bicarbonate (HCO_3^-) concentrations surpassing 0.05 M, there is a pronounced enhancement in the density of the protection layer and the crystal nucleation, resulting in the formation of a dense $FeCO_3$ grain. The above observations were made after experimentally exposing carbon steel to various $NaHCO_3$ solutions (up to 1 M, pH ~7.7) at 50°C under anaerobic conditions (CO_2). The above scientific studies assert the absence of direct contribution of H_2CO_3 and HCO_3^- into H_2 evolution, particularly at low pH levels (4-6), suggesting that contributions occur solely through dissociation reactions. Moreover, it has been indicated that H_2CO_3 can serve as a pH buffer, facilitating the dissolution of additional CO_2 in the system, even in the presence of a high concentration of HCO_3^- (Alsalem et al., 2023; Teramura et al., 2017). This observation aligns with our results, wherein the Fe^0-N_2-$NaHCO_3$ systems displayed higher initial pH values than the Fe^0-CO_2-$NaHCO_3$ system, as illustrated in Fig. 3.7.

3.1.13.2 Temperature and pH Effects on Hydrogen Evolution by Fe^0

The findings presented in Sub-chapters 3.1.3 (Fig. 3.7 & Table 3.4) highlight the significant impact of increased temperature on abiotic H_2 production in CO_2-enriched Fe^0 systems. When the temperature was raised from 2°C to 50°C, a notable ~75% increase in H_2 production was observed after 93 hours. This enhancement is attributed to the accelerated electrochemical reaction rates at the Fe^0 surface, which facilitate mass transfer and the dispersion of electroactive Fe species at higher temperatures (Elgaddafi et al., 2021). In our CO_2-Fe^0 systems, the applied temperatures were kept below 60°C. According to Rizzo et al. (2020) and Li et al. (2019), at temperatures below 60°C, corrosion products such as $FeCO_3$, which form from the reaction between CO_2 and carbon

steel, may not effectively develop. This is due to the porous nature of $FeCO_3$ under these conditions and its increased solubility, preventing the formation of a protective layer on the steel surface (Rizzo et al., 2020; Li et al., 2019). Sun et al. (2009) reported that the solubility of $FeCO_3$, formed from the reaction between steel and CO_2 at room temperature (25 °C), ranges from 3.72×10^{-11} to 9.33×10^{-12} mol^2/L^2. Neerup et al. (2023) highlighted that there was negligible temperature dependency in the $FeCO_3$ solubility. However, because the rate constant for the dissolution of $FeCO_3$ increased with temperature, kinetics were impacted by temperature. Hence, this can explain the higher H_2 accumulations in our experiments at elevated temperatures over time.

Eba et al. (2020) similarly observed an increase in abiotic H_2 production by Fe^0 at elevated temperatures. In their study, 14.29 g L^{-1} of pure iron powder with particle sizes of 3-5 μm was exposed to carbonated water under 1 bar of CO_2, and as the temperature increased from 10°C to 60°C with 2000 rpm agitation, a rise in bottle pressure indicated H_2 production. This finding aligns with the pressure data recorded in our study, as shown in Suppl. Info. Fig. 3.5.

However, numerous studies (Elgaddafi et al., 2021; Rizzo et al., 2020; Hua et al., 2019) have emphasized that at elevated temperatures, depending on the specific operating conditions, $FeCO_3$ can form and become more adherent and denser as the temperature exceeds 60°C. This layer serves as an effective barrier between the metal and the electrolyte, reducing the corrosion rate of Fe^0 and enhancing surface protection. Furthermore, at higher temperatures, the solubility of CO_2 significantly decreases, leading to the formation of various other iron oxide and hydroxide compounds such as Fe_2O_3, $Fe(OH)_2$, and Fe_3O_4. Additionally, temperature elevation affects the ionization of carbonic acid, thereby influencing the solution's pH (Elgaddafi et al., 2021; Hua et al., 2019).

Regarding the pH factor, the collective findings from various studies emphasize the intricate interplay between pH and environmental conditions with Fe^0 corrosion behavior. According to Barker et al. (2018), pH is a critical variable influencing the rate of $FeCO_3$ precipitation. An elevated pH results in a lower Fe^{2+} concentration required to significantly exceed $FeCO_3$ solubility (from 3.72×10^{-11} mol^2/L^2 to 1.17×10^{-11} mol^2/L^2 at 25 °C), which encourages the development of a protective film.

As shown in Table 3.5, the lowest H_2 accumulations were observed in the systems with elevated pH values of 7 and 8, measured at 5.98 and 4.08 mmol, respectively, after 91 h. According to Zosel et al. (2011), at elevated pH values, particularly between 7 and 10, the HCO_3^- ion is the predominant species in aqueous solution. As a result, at a pH of 8, Eq. 27 is fueled with HCO_3^- ions, leading to the formation of $FeCO_3$. Based on the above and the fact that at elevated pH levels, the availability of H^+ ions is negligible, this can explain the low accumulation of H_2 in a system with a pH value of 8. Kahyarian et al. (2017) believe that the iron dissolution reactions at such high pH values were in the passivation and *trans*-passivation range, also referring to the creation of $Fe(OH)_2$ and Fe_2O_3 layers. However, De Motte et al. (2020) also stated the same observations at higher temperatures. Experiments revealed that carbon steel corrosion under a CO_2 environment was rapidly inhibited when exposed to high pH values (exceeding 6) at 80 °C. $FeCO_3$ was identified as the main component. However, Chuckanovite [$FeCO_3(OH)_2$] was also recognized. The above-proposed mechanisms can explain the low H_2 accumulations in our systems at high pH.

On the other hand, the systems that were adjusted at lower pH values, 6 and 5, demonstrated higher H_2 accumulation, reaching 7.55 mmol and 7.52 mmol, respectively, as shown in Table 3.5, after 91 h. At low pH, the total carbonates exist as free dissolved CO_2 in the solution (Zosel et al., 2011). As a result, the formation of $FeCO_3$ crystal structures is not favorable on carbon steel, leading to more unprotected areas. This is because carbonate ion concentrations are low and do not exceed the solubility limit required for the formation of $FeCO_3$ (De Motte et al., 2018). Experiments conducted by Kahyarian et al. (2017) on mild steel corrosion under a CO_2 environment revealed that the corrosion rates, based on exchange current density values, are higher at pH 5 than pH 4 when the iron is exposed under 1 bar pressure of CO_2 and at a temperature of 30ºC. This can explain the slightly increased H_2 accumulation in our experiments at pH 5 compared to systems with pH 4 under similar temperatures and pH conditions. Hence, in an acidic environment (pH<4), the anodic reaction (Eq. 25) of iron dissolution is predominated buffering the systems with e^-. Then, under these conditions, the cathodic reaction (Eq. 29) process takes place, and H_2 is produced by the cathodic reduction of H^+ due to its high concentration (Barker et al., 2017; Nazari et al., 2010). Kahyarian and Nesic (2019) believe that the H_2CO_3 concentration is just a small portion of the H^+ concentration at pH

4 and 1 bar CO_2, and even H_2CO_3 exhibits electrochemical activity, its predicted little contribution to the total cathodic current. This can explain the production of H_2 in our system adjusted to pH 4 with HCl.

In addition to the reactions of Eq. 25 and Eq. 29, one more reaction is involved, the reduction of carbonic acid (Eq. 30), which can contribute more to the evolution of H_2 (Barker et al., 2017), since at the range of pH 4-6, the CO_2 concentrations can affect the anodic dissolution (Fazal et al. 2022) reactions (Eq. 27).

3.1.13.3 Effects of Agitation Mode, Mechanical Action, and Air-Water Interface Area of the systems on Fe^0

As shown in Table 3.6, the Fe^0-CO_2 systems exhibited minimal variation in H_2 evolution under different agitation modes (0, 100, 200 rpm). However, increasing the agitation speed from 100 rpm to 200 rpm resulted in approximately 1 mmol more H_2 accumulation after 107 hours. As explained by Soosaiprakasam and Veawab (2008), in higher agitation modes, the density of cathodic currents increased, leading to a higher reduction rate of the oxidizing agent (CO_2).

Using different types of serum bottles to accelerate the CO_2 dissolution in an aqueous solution and consequently to increase H_2 production by Fe^0 was not a sufficient methodology.

In the context of adding mechanical disruptors to a Fe^0-CO_2 system, there was minimal alteration in H_2 accumulation when comparing the effects of glass beads and boiling chips. This is despite some scientific reports indicating that particles present in fluids can increase corrosion rates when interacting with steel in a CO_2 environment, a common scenario in the oil and gas industry (Senatore et al., 2021).

3.1.13.4 Role of Fe (Fe^0 or Fe-W) Concentration and Particle Size in H_2 Evolution

The findings in Sub-chapters 3.1.6 and 3.1.7 underscore the significant impact of Fe particle sizes and concentrations on H_2 evolution. As illustrated in Table 3.7 (Sub-chapter 3.1.6), increasing the Fe^0 concentration led to higher H_2 accumulations in the Fe^0-CO_2 systems compared to systems with lower Fe^0 concentrations.

The extracted experimental data aligns with recent scientific reports regarding the H_2 accumulations. As stated by Khemkhao et al. (2024), increasing the concentration of Fe^0 in a CO_2 system positively affected H_2 accumulation. The experiments were conducted in serum bottles with a total/working volume of 120mL/45mL, and several concentrations of ZVI were examined (32, 64, 96, and 224 g L^{-1}) in the same manner as our experiments. For the creation of anaerobic conditions, CO_2 gas was purged into the bottles until a pressure of 1.5 bar was reached. The systems were incubated at 120 rpm and 35 ºC. It was highlighted that Fe^0 oxidation correlated with the surface area, which increased with the concentration of iron. However, it was also stated that at extreme concentrations, the dissolution of Fe^0 can be suppressed by the increased pH, resulting in the inhibition of H_2 production.

Velimirovic et al. (2014) also made similar observations when examining the corrosion rates of microscale Fe^0 particles for H_2 production. They found that such systems demonstrated versatility, with the H_2 production influenced by varying Fe^0 concentrations, particle size, and the specific brand of manufactured iron used.

Regarding the particle sizes, as revealed by the experimental results of Sub-chapter 3.17 (Table 3.8), the efficacy of fine-grained Fe^0 (10 μm) is notably superior to that of coarse-grained Fe^0 (800 μm) concerning abiotic H_2 production. The advantage of the high specific surface area of Fe^0 used was underscored by several investigators in environmental remediation applications. For example, Li et al. (2019) emphasized that the active surface, associated with the active sites of solid iron, significantly influences processes such as transformation, adsorption, and co-precipitation, irrespective of the contaminant's nature. Generally, it is acknowledged that an increase in the surface area of Fe^0 leads to accelerated rates of contaminant removal. Presently, various artificial techniques, such as the use of sodium borohydride, have been devised to generate Fe^0 nanoparticles, altering their surface characteristics to enhance their effectiveness for field distribution and reactions (Sun et al., 2006). Ken and Sinha (2020) explained that nanoscale (1−100 nm) particle size, due to the high specific area, exhibits stronger reducing and adsorption properties and superior mobility than microscale Fe^0 particles.

However, only a few scientific articles have focused on H_2 production from Fe^0. Chen et al. (2011), experimenting with different concentrations and particle sizes of Fe^0, showed that the average H_2 production rate of nanoFe^0 is 5.05 E-2 (g H_2 / kg Fe^0 • h), which is

50-100 times higher than the rates exhibited by microFe^0 with production rates of 5.23 E-4 to 1.02 E-3. On the other hand, Velimirovic et al. (2014) managed to produce 4.34 E-2 (ml day^{-1}) of H_2 using coarse-grained Fe^0. Khemkhao et al. (2024) demonstrate a maximum H_2 production of 8 mmol after 744 h by using Fe^0 with a particle size of ≈30 mm (Table 3.14).

Our experiment demonstrates that employing smaller Fe^0 particle sizes within the micro-scale range (10 μm and 800 μm) can result in higher H_2 production, as depicted in Table 3.14.

However, by calculating the production rates between the two concentrations (25 g L^{-1} and 200 g L^{-1}) of 800 μm iron, a noticeable trend is observed. A slight increase in production rate occurs with a decrease in the concentration of Fe^0 with a particle size of 800 μm from 200 g L^{-1} to 25 g L^{-1} (production rate: from 14.6E−6 to 7.42×10−6 gH_2 / gFe^0 • h). This phenomenon can be attributed to embedding, wherein adding more Fe^0 leads to the formation of additional layers. These upper layers undergo corrosion, forming iron oxides that act as barriers, inhibiting the corrosion of the underlying iron and consequently reducing H_2 production in the lower layers. Furthermore, this reduction in H_2 production may also be attributed to the compaction caused by the weight of iron.

Table 3.14: Overview of various Fe^0 types (sizes, concentrations, Fe^0 with other metals) investigating H_2 production under different environments and experimental durations.

Reference	Chen et al., 2011				Velimirovic et al., 2014			Eba et al., 2020	Khemkhao et al., 2024	Present study	
Particle size	mFe^0 (2-5 µm)	mFe^0 (2-5 µm)	nFe^0 (60 nm)	Bimetallic nFe^0 (Fe/Ni)	Fe (300 – 1300 mm)	Fe [D10, D50, D90] – 41, 98, 162 (µm)	nanoFe D50 < 0.07	mFe^0 (3-5 µm)	Fe (27.82 mm)	mFe^0 (10 µm)	mFe^0 (800 µm)
Conc. (g L^{-1})	20	50	0,5	0,5	50,04	49,97	4.74	14.28	16, 32, 64, 96, and 224	25	25
Exp. duration (h)	259	119	147	46	2520	2520	528	10	744	115	115
Addition of $NaHCO_3$	No	No	No	No	No	No	No	No	No	10 g L^{-1}	10 g L^{-1}
Gas purging	N_2	N_2	N_2	N_2	N_2	N_2	N_2	CO_2	CO_2	CO_2	CO_2
Temperature °C	26	26	26	26	12	12	12	60	35	33	33
H_2 production	1.34 mmol	3.03 mmol	1.84 mmol	4.15 mmol	4,34 E-2 (ml day^{-1})	7.73 E−2 (ml day^{-1})	3.47 E−1 (ml day^{-1})	100 % H_2	≈ >3 mmol (16 g L^{-1} Fe) ≈ >5 mmol (32 g L^{-1} Fe) ≈ >7 mmol (64, 96 g L^{-1} Fe) ≈ 8 mmol (224 g L^{-1} Fe)	9.28 mmol	1 mmol
Production rate	5,23 E-4 (gH_2 $kg^{-1}Fe^0$ h^{-1})	1,02 E-3 (gH_2 $kg^{-1}Fe^0$ h^{-1})	5,05 E-2 (gH_2 $kg^{-1}Fe^0$ h^{-1})	3,65 E-1 (gH_2 $kg^{-1}Fe^0$ h^{-1})	x	x	x	x	1,12903E-05 (16 g L^{-1} Fe) 9,4086E-06 (32 g L^{-1} Fe) 6,58602E-06 (64 g L^{-1} Fe) 4,39006E-06 (96 g L^{-1} Fe) 2,15054E-06 (224 g L^{-1} Fe) (gH_2 g^{-1} h^{-1})	1.36 E-4 (gH_2 $g^{-1}Fe^0$ h^{-1})	1.46 E-5 (gH_2 $g^{-1}Fe^0$ h^{-1})

3.1.13.5 Impact of $NaHCO_3$ Solution from CO_2 Capture on Fe (Fe^0- oxidized Fe and Pretreated Fe^0)

Nowadays, solid and liquid CO_2 adsorbents are recognized as promising materials to address challenges associated with climate change, as indicated in the introduction. Our research proposes the utilization of the $NaHCO_3$ solution resulting from the reaction between NaOH solution and CO_2 in a system with Fe^0 for H_2 production under ambient conditions. As illustrated in Fig. 3.21 (C. & D.), the CO_2 injected into the serum bottles was continuously utilized, even if the NaOH solution may be saturated, maximizing CO_2 mitigation. As indicated by Yoo et al. (2013), to compensate for the lack of physically unabsorbed CO_2 in the water throughout the process, a small quantity of CO_2 may be additionally absorbed.

As shown in Table 3.12, the production of abiotic H_2 is affected by the specific surface areas of Fe-W materials, as detailed in Sub-chapter 3.1.13.4. Systems employing both coarse-grained Fe-W (0.05 mm^2) and fine-grained Fe-W (steel wool), supplemented with $NaHCO_3$ solution - resulting from higher concentrations of NaOH reacted with CO_2 - exhibited more significant accumulations of H_2. This effect is attributed to the elevated NaOH concentration, which enhances CO_2 absorption. The resulting $NaHCO_3$ solution provides a higher concentration of HCO_3^- ions in the system, which then react with Fe-W to produce H_2. As Sibhat et al. (2024) explain, NaOH in water ionizes into Na^+ and OH^- ions, resulting in a highly alkaline aqueous solution. Under these conditions, CO_2 dissolves in the solution and reacts with hydroxide ions to form bicarbonates.

In comparison, control systems where core-grained Fe-W (0.05 mm^2) and fine-grained Fe-W (steel wool) were exposed to H_2O under a CO_2 environment produced only 3.24 mmol and 6.47 mmol of H_2, respectively. These values are significantly lower than those observed in systems using $NaHCO_3$ solutions derived from both 0.25 M and 0.75 M NaOH solutions. The low H_2 accumulation in the control systems is due to the lack of HCO_3^- saturation, which limits the reaction efficiency with the Fe-W materials.

A different pattern was observed when processed and already oxidized Fe-W was subjected to the same procedure and used in systems containing $NaHCO_3$ solutions derived from both 0.25 M and 0.75 M NaOH solutions with CO_2, without any pretreatment. As indicated in Table 3.13, there was a decrease in average H_2 production

for both core-grained Fe-W (0.05 mm²) and fine-grained Fe-W (steel wool) compared to unoxidized Fe-W systems. This reduction may be attributed to the previous formation of a corrosive $FeCO_3$ layer. However, $NaHCO_3$ solutions derived from 0.25 M NaOH demonstrated higher H_2 accumulations. This is likely due to the inhibition of H_2 production by the higher concentrations of HCO_3^- present in $NaHCO_3$ solutions derived from 0.75 M NaOH, which may have facilitated the faster formation of $FeCO_3$ on the already oxidized Fe-W.

When the oxidized Fe-W materials were subjected to pretreatment with citric acid and then exposed to $NaHCO_3$ solutions derived from both 0.25 M and 0.75 M NaOH solutions with CO_2, alterations in the results were observed. As shown in Table 3.13, core-grained Fe-W (0.05 mm²) exhibited increased H_2 production in both NaOH concentrations compared to the previous experiment. This enhancement may be attributed to the dissolution of the outer $FeCO_3$ layer, which exposed the internal, unaffected iron. However, no significant change in H_2 production was observed in systems utilizing fine-grained Fe-W (steel wool), likely due to the depletion of the fine-grained Fe.

First, Brannon and Asmus (1981) proposed the mechanism underlying the anti-corrosion properties of citric acid ($C_6H_8O_7$). Since then, aqueous solutions of citric acid have been conventionally used for effective rust removal while preserving the integrity of the base metal. According to Jiand-Xue et al. (2019), its scientific interest has increased due to its non-hazardous nature, biodegradability, efficient rust removal, corrosion inhibition, and natural occurrence as a metabolic product in organisms. Additionally, Ashassi-Sorkhabi et al. (2014) highlighted its role in eliminating lime deposition in boilers and evaporators, as well as its use in water softening for the production of laundry detergents and soaps. The same report also indicates its effectiveness as a corrosion inhibitor for carbon steel exposed to cooling water.

In the study by Nguyen et al. (2016), the dissociation of citric acid in solutions was described, as shown by Eqs. 37 to 39.

$$H_3Cit \rightleftharpoons H^+ + H_2Cit^- \quad \text{(Eq. 37)}$$

$$H_2Cit^- \rightleftharpoons H^+ + HCit^{2-} \quad \text{(Eq. 38)}$$

$$HCit^{2-} \rightleftharpoons H^+ + Cit^{3-} \quad \text{(Eq. 39)}$$

As described, the H_2Cit^-, $HCit^{2-}$, and Cit^{3-} anions can react with divalent and trivalent Fe for the formation of various complexes, as shown in Eqs. 40 to 43.

$$Fe^{2+} + HCit^{2-} \rightleftharpoons FeHCit \quad \text{(Eq. 40)}$$

$$Fe^{2+} + Cit^{3-} \rightleftharpoons FeCit^- \quad \text{(Eq. 41)}$$

$$Fe^{3+} + HCit^{2-} \rightleftharpoons FeHCit^+ \quad \text{(Eq. 42)}$$

$$Fe^{3+} + Cit^{3-} \rightleftharpoons FeCit \quad \text{(Eq. 43)}$$

The Cit^{3-} anion, resulting from the dissociation of citric acid, can bind to the Fe^{2+} ions produced during the anodic reaction process, leading to the formation of a ferrous citrate complex, as shown in Eq. 43. This binding of Fe ions inhibits the formation of $FeCO_3$ due to the reduced availability of Fe ions reacting with bicarbonate ions (Eq. 32). Consequently, H_2 evolution is attributed to the execution of the cathodic reaction, as indicated in Eq. 29.

However, Ashassi-Sorkhabi et al. (2014) explain that under stagnant conditions in a system with Fe and citric acid, the surface citrate ions prefer to form soluble complexes with produced Fe ions, as shown in Eqs. 40 to 43, rather than adsorbing on the metal surface. This results in low corrosion inhibition efficiencies. However, Saji (2019) argues that the type and characteristics of the rust layer (total adherent rust, rust film thickness, rust structure, and composition, etc.) must also be taken into consideration, along with the physicochemical abilities of the rust-converting compound (structure, concentration, solubility, pH, capacity to chelate with ferric ions, etc.), to determine the effectiveness of a rust conversion therapy.

Furthermore, citric acid is utilized as a green corrosion inhibitor to address environmental concerns. For instance, Yang et al. (2019) successfully created carbon dots based on citric acid and imidazole ionic liquids, with a size range of 3 – 5.5 nm. The maximum corrosion inhibitory effect was observed when exposing carbon steel to 1 M HCl.

3.1.14 Conclusions of Experimental Set-Up 1

The experiments provided compelling evidence that CO_2 can be effectively utilized in a system involving iron for the production of H_2, revealing a promising avenue for sustainable energy production. The outcomes suggest a notable potential for H_2 evolution through the interaction of waste iron materials with CO_2, especially when employing $NaHCO_3$ solutions created by capturing CO_2 in NaOH. Until now, the production of abiotic hydrogen by the oxidation of Fe^0 has been examined under anaerobic conditions by using N_2 or CO_2 gas, and no one has examined the effect of HCO_3^- ions (addition of $NaHCO_3$) along with CO_2 in the acceleration of H_2 production. The results show that the addition of $NaHCO_3$ in a system supplemented with Fe^0 under anaerobic conditions leads to high accumulation and production rates of H_2 compared to reports where no $NaHCO_3$ was used. Despite these encouraging findings, it is crucial to acknowledge that further in-depth investigations are warranted to fully comprehend the underlying mechanisms, optimize the process parameters, and address any potential challenges. Using waste iron materials under mild conditions contributes to the principles of the circular economy, waste-to-energy conversion, and sustainability. The siderites produced through this process can be reduced using weak acids like citric acid or repurposed as a raw material in the steel or cement industry, or as a fertilizer. In conclusion, the following observations were obtained:

A system containing 25 g L^{-1} of Fe^0 exposed to water in a CO_2 environment produced 3.72 mmol of H_2 after 75 h. In contrast, negligible H_2 production was observed when the same amount of Fe^0 was exposed to water in an N_2 environment, highlighting the crucial role of CO_2 in the abiotic production of H_2 from Fe^0. When 25 g L^{-1} of Fe^0 was exposed to $NaHCO_3$-buffered water (10 g L^{-1}) under a CO_2 environment, 8.96 mmol of H_2 was produced after 75 h. A 36% decrease in H_2 production (5.73 mmol) was observed under similar conditions with N_2 after the same duration. X-RD analysis identified siderite ($FeCO_3$) as the corrosion product of Fe^0.

In systems where 25 g L^{-1} of Fe^0 was exposed to water and CO_2 and incubated at varying temperatures (2°C – 50°C), the maximum H_2 production of 5.8 mmol was observed at 50°C, while at 2°C, production declined by 75% (2.51 mmol) after 93 h. Although higher temperatures accelerate H_2 production reactions, energy consumption must be considered, particularly in systems involving bacteria or archaea. Altering the pH in

systems (pH 4 – pH 8) with 25 g L^{-1} Fe^0 in water under CO_2, the highest H_2 accumulation was observed under slightly acidic conditions (pH 5-6), demonstrating a production of 7.55 mmol after 91 h. The lowest H_2 production (4.08 mmol) occurred at pH 8, representing a 46% reduction.

Systems with 25 g L^{-1} of Fe^0 exposed to the same conditions and incubated at different agitation speeds (0 – 200 rpm) showed a slight increase in H_2 production from 7.58 mmol to 8.69 mmol after 107 h when the agitation speed increased from 0 rpm to 200 rpm. Increasing the concentration of 10 μm Fe^0 by tenfold (from 5 g L^{-1} to 50 g L^{-1}) under CO_2 conditions resulted in a 73.6% increase in H_2 production (from 2.72 mmol to 10.30 mmol) after 107 h. Conversely, decreasing the Fe^0 surface area by 80 times (from 10 μm to 800 μm) led to an 89-fold increase in H_2 production (from 1 mmol to 9.28 mmol) after 115 hours under CO_2 conditions.

Using mechanical disruptors *in-situ* within systems utilizing 25 g L^{-1} of Fe^0 exposed to water and CO_2 had minimal impact on H_2 production, with negligible differences compared to control systems without mechanical disruptors. Similarly, negligible changes in H_2 production were observed when the same amount of Fe^0 was introduced into bottles with varying air-water interface areas (28 cm^2 – 75 cm^2) sparged with CO_2.

Using waste Fe^0 materials, H_2 production was observed, although at lower concentrations. For instance, 100 g L^{-1} of fine-grained Fe-W exposed to water in a CO_2 environment produced nearly 84% more H_2 (5.84 mmol) than coarse-grained Fe-W (0.96 mmol) after 139 h. When 100 g L^{-1} of Fe-W was exposed to $NaHCO_3$ solution derived from 0.75 M NaOH under CO_2 conditions, H_2 production was observed. Fine-grained Fe-W in this solution resulted in 11.26 mmol of H_2 after 164 hours, while coarse-grained Fe-W under the same conditions exhibited a 56% decrease in H_2 production (4.93 mmol) over the same duration.

When oxidized Fe-W was used instead of new Fe-W at the same concentration (100 g L^{-1}) under $NaHCO_3$ conditions, H_2 production occurred at lower rates. However, using $NaHCO_3$ solution derived from 0.25 M NaOH led to higher H_2 production compared to systems utilizing $NaHCO_3$ solution derived from 0.75 M NaOH under the same conditions. Fine-grained Fe-W in $NaHCO_3$ solution derived from 0.25 M NaOH produced 9.11 mmol of H_2 after 164 hours, while coarse-grained Fe-W produced 2.80 mmol after the same time.

When citric acid was used to dissolve the $FeCO_3$ corrosion product from oxidized Fe-W, an increase in H_2 production was observed only in coarse-grained Fe-W exposed to $NaHCO_3$ solution derived from 0.75 M NaOH. This resulted in a nearly 68.5% increase in H_2 production after 138 hours.

3.2 Experimental Set-Up 2: Bioconversion of Carbon Dioxide (CO_2) to Volatile Fatty Acids (VFAs) Using Anaerobic Granular Sludge (AnGrSL) With Zero-Valent Iron (ZVI - Fe^0) in Methanogenesis-Inhibited Systems.

Despite the substantial efforts to achieve a more sustainable and cleaner environment through the adoption of new technologies like Renewable Energy Systems (RES) and the production and use of hydrogen (H_2), concerns have been raised regarding implementation costs, safety, and environmental impacts, as discussed in Chapter 1 of the introduction. Moreover, despite the various strategies proposed for energy transition, CO_2 production remains unavoidable, leading to its continued high concentration in the atmosphere and a detrimental impact on the climate. Therefore, there is an urgent need to explore new, cost-effective, and innovative methods for CO_2 utilization for the production of chemicals that could support the development of alternative energy technologies.

This group of experiments explores an innovative proof of concept for CO_2 utilization and the production of value-added products such as carboxylic acids with carbon chain numbers ranging from 1 to 5 (including formic, acetic, propionic, butyric, iso-butyric, and valeric acid). These short-chain fatty acids (SCFAs) can be synthesized under aquatic, ambient conditions in a system utilizing bacteria and CO_2 as the sole carbon source (electron acceptor). However, in such anaerobic systems, H_2 is necessary as an electron donor for the bioconversion of CO_2 to volatile fatty acids (VFAs). Instead of using external H_2 gas for microbial reactions, iron (Fe) can be used within these systems (*in-situ*).

As demonstrated in Sub-chapter 3.1, iron oxidizes and produces H_2 under anaerobic and carbonate aqueous conditions, enabling the *in-situ* use of Fe and mitigating safety concerns associated with using exogenous H_2 gas. The findings from experimental set-up 1 (Sub-Chapter 3.1) indicate that iron materials with a higher specific surface area exhibit greater H_2 productivity. Consequently, zero-valent iron (ZVI-Fe^0) with a particle size of 10 μm was chosen for the experiments in this chapter. Anaerobic granular sludge (AnGrSL) was used as the inoculum, consisting of several layers that house acidogens, hydrogenogens, syntrophic bacteria, and methanogens from the outer to inner layers, respectively (Tang et al., 2021). However, in systems containing CO_2, H_2, and AnGrSL, methanogenesis is thermodynamically more favorable than acetogenesis, with

methanogens competing with acetogens for H_2 utilization (Modestra et al., 2020; Pan et al., 2021).

As shown by Vyrides et al. (2018), systems supplemented with zero-valent iron (ZVI-Fe^0) and inoculated with anaerobic granular sludge (AnGrSL) under aquatic, ambient, and anaerobic conditions resulted in methane (CH_4) production. The H_2 produced abiotically by the ZVI and CO_2 can be utilized by hydrogenotrophic methanogens present in AnGrSL, to produce CH_4, as represented in Eq. 44.

$$4H_2 + CO_2 \rightarrow CH_4 + 2H_2O \ (\Delta G° = -131 \text{ kJ mol}^{-1}) \quad \text{(Eq. 44)}$$

Additionally, acetic acid is naturally produced by acetogens, which are also present in AnGrSL. This acetic acid can subsequently be utilized in a different metabolic pathway involving acetoclastic methanogens to produce CH_4, as illustrated in Eqs. 45 and 46.

$$4H_2 + 2CO_2 \rightarrow CH_3COO^- + H^+ + 2\ H_2O \ (\Delta G° = -95 \text{ kJ mol}^{-1}) \quad \text{(Eq. 45)}$$

$$CH3COO^- + H^+ \rightarrow CH_4 + CO_2 \ (\Delta G° = -75.7 \text{ kJ mol}^{-1}) \quad \text{(Eq. 46)}$$

However, CH_4 is a potent greenhouse gas (GHG) with a significantly higher global warming potential than CO_2. It also presents safety and environmental risks due to its explosive nature under certain conditions and the production of CO_2 upon combustion. Given these concerns, the primary aim of this study was to investigate various strategies (such as heat treatment, low pH exposure, and the use of chemicals) to inhibit or eliminate methanogens in an AnGrSL-CO_2-ZVI (Fe^0) system. This approach aims to enhance the system's enrichment with acetogens or spore-forming bacteria, thereby improving the efficiency of Eq. 45 and increasing the production of acetic acid or other volatile fatty acids (VFAs).

3.2.1 Impact of Low pH on Methane Inhibition in an AnGrSL-ZVI (Fe^0) System

As illustrated in Fig. 3.26, during cycle 1 (Days 0-7), when no methanogenesis inhibition method was applied, methane accumulation in the headspace of the AnGrSL–ZVI (Fe^0) system increased linearly, corresponding with the consumption of H_2 and CO_2. Initially, H_2 accumulation rose over the first 3 days due to the abiotic H_2 produced by the ZVI (Fe^0) under anaerobic and carbonated conditions. After 3 days, a decline in H_2 levels was observed, attributed to the enrichment of the system with hydrogenotrophic methanogens. By the end of cycle 1, CH_4 had accumulated to nearly 50% in the headspace, while approximately 80% of CO_2 had been utilized within 7 days.

At the onset of cycle 2, on day 7, the systems were re-flushed with CO_2, and the pH was lowered to 3 to inhibit methanogenesis. However, due to the reactions depicted in Equations 32 and 29, the production of H_2 via the oxidation of ZVI (Fe^0) requires the capture of H^+ ions, leading to an increase in OH^- ions in the systems and a subsequent rise in pH. Therefore, daily monitoring and pH adjustments became necessary. Despite 8 days of daily pH regulation during cycle 2, methanogenesis persisted, unaffected by the acidic environment due to the continuous rise in pH (Suppl. Info. Fig. 3.15). By the end of the experiment on day 15, CH_4 had reached 43% in the headspace. Adjusting the pH to 3 reduced methane production by only 7% compared to cycle 1. Furthermore, CO_2 utilization decreased by 28% compared to cycle 1, attributable to the daily pH adjustments.

Regarding the VFAs (Fig. 3.27), minimal accumulation was observed during the first cycle, with concentrations below 50 mg L^{-1}. These findings align with those reported by Vyrides et al. (2018) in their research on CO_2 utilization and methane production using anaerobic granular sludge (AnGrSL) and zero-valent iron (ZVI, Fe^0). During the second cycle, where the pH was adjusted to 3 daily, the systems showed a similar pattern in VFA production, with a notable increase in propionic acid concentration, reaching nearly 230 mg L^{-1} by the end of cycle 2 on day 15.

Changes in headspace pressures (absolute) within the systems during the experimental period were also monitored and are illustrated in Appendix I (Suppl. Info. Fig. 3.16).

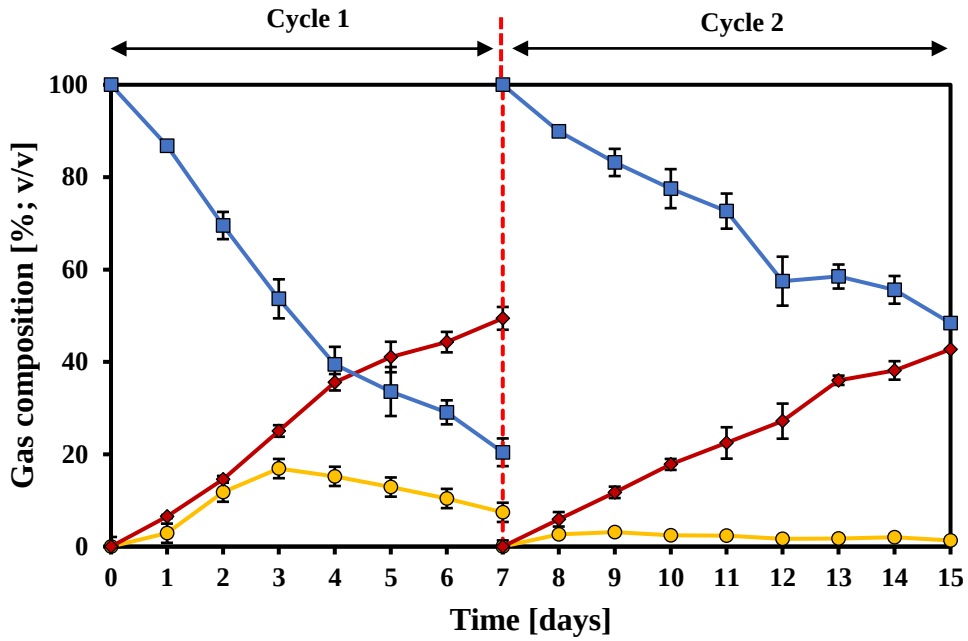

Fig. 3.26: Utilization of H_2 and CO_2 gases and the evolution of CH_4 over time in an AnGrSL – ZVI (Fe^0) system at pH 5 (cycle 1) and pH 3 (cycle 2).

: CO_2 utilization; : H_2 evolution and utilization; : CH_4 productivity.

: CO_2 gas purging.

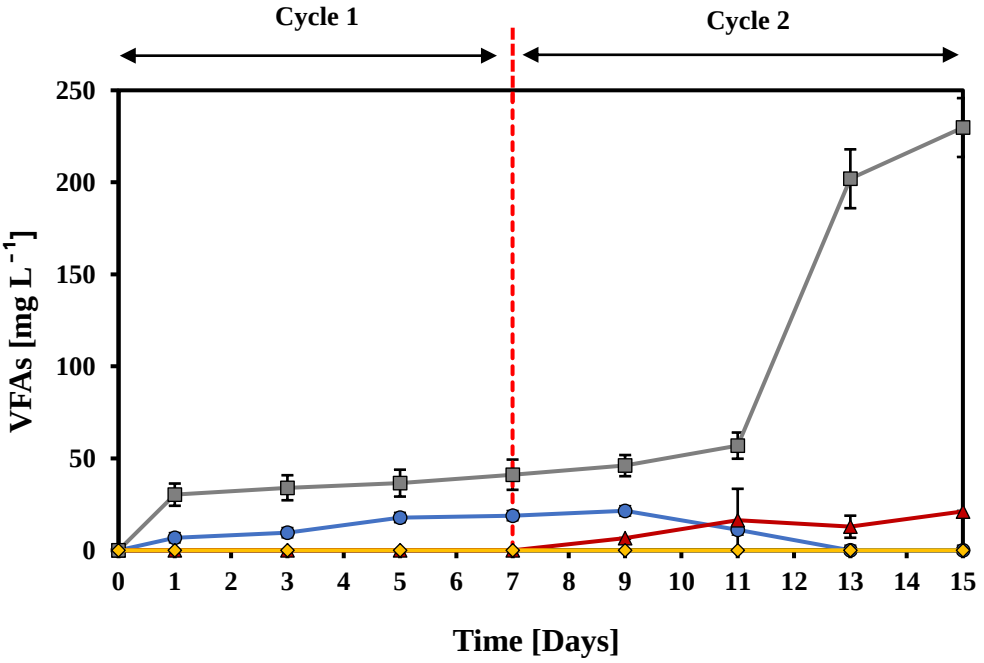

Fig. 3.27: VFAs production over time in an AnGrSL – ZVI (Fe^0) system at pH 5 (cycle 1) and pH 3 (cycle 2).

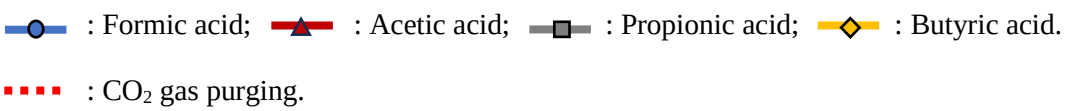

The control systems consisted solely of AnGrSL exposed to anaerobic conditions (CO_2 gas) and underwent the same methodology as the experimental systems. These control systems exhibited a negligible alteration in CO_2 utilization and CH_4 production (< 3%), with minimal changes in pH and pressure. The minimal decline in CO_2 observed in the control systems can be attributed to the small amount of CO_2 dissolved in the aqueous growth medium. Additionally, negligible VFA productivity was observed in the control systems (< 20 mg L^{-1}) (data not shown).

To enhance VFA production in a system, inhibition of acetoclastic and hydrogenotrophic methanogens is necessary. Methanogenic archaea typically produce CH_4 under neutral conditions, with a pH range between 6.5 and 7.2 during anaerobic digestion (Neri et al., 2023). In contrast, inhibition can occur at lower pH levels (5.5 to 6.25) (Staley et al., 2011). It is noted that low pH values can adversely affect the enzymatic activities of methanogens. Membrane-permeable free acid molecules in high concentrations can inhibit the methanogenic consortium in a system (Han et al., 2019). In a recent study by Qiu et al. (2023), it was elucidated that at extreme pH values, particularly low ones, the quantity or activity of the enzymes involved in the acetoclastic methanogenesis pathway decreases, and as a result, the depletion of acetoclastic methanogens. Conversely, facultative hydrogenotrophic and obligatory hydrogenotrophic methanogens may be enhanced even if essential enzymes decrease under low pH experimental conditions. The enzyme reduction results in ATP synthesis and electron transportation deceleration. Low levels of ATP may lead to damage or malfunction in specific metabolic processes, such as microbial disintegration and decay, as higher ATP levels are required to pump excess protons out of cells and maintain a neutral pH. The methodology of lowering the pH for methanogenesis inhibition proved ineffective in a system utilizing ZVI (Fe^0). However, propionic acid was found to be the predominant VFA at lower pH values. Similar findings were reported by Latif et al. (2017), which showed that by lowering the pH (< 5.5) in a continuously stirred (250 rpm) tank reactor with a total/working volume of 1.5 L/1L

utilizing waste-activated sludge under mesophilic (37 ºC) and anaerobic conditions (N_2), propionic acid was found to be increased (370 - 430 mg L^{-1}) in the reactor.

3.2.2 Evaluation of Utilizing Thermally Pre-treated AnGrSL in a ZVI (Fe^0) System for VFAs Production

As depicted in Fig. 3.28, during the initial 8 days, the accumulation of H_2 gas in the headspace of both sub-groups, B1 (pH adjusted between 5 - 6) and B2 (pH adjusted between 6 - 6.5), increased to 65% and 67%, respectively. Concurrently, the CO_2 accumulations decreased by approximately 70% in both sub-groups. Methanogenesis was fully inhibited during this period. Following a CO_2 re-flash on day 8 and until the experiment's conclusion on day 12, distinct patterns emerged in the two sub-groups. The H_2 accumulation in the headspace of sub-group B2 (pH 6 - 6.5) remained below 1%, whereas in sub-group B1 (pH 5 - 6), H_2 levels initially increased until day 11, then began to decline, measuring 21% by the experiment's end. Moreover, differences were observed in CO_2 utilization between the two sub-groups. Sub-group B2, with higher pH values, exhibited greater CO_2 utilization at 51%, while sub-group B1 achieved a utilization rate of 31%. CH_4 production remained negligible for both sub-groups until day 12, when CH_4 began to be produced (2%).

Regarding the VFAs (Fig. 3.29), during the initial 6 days, all VFAs remained below 316 mg L^{-1}. Subsequently, there was an acceleration in acetic acid production in both sub-groups, attributable to the enrichment of Acetogens. Sub-group B2 (pH 6 - 6.5) exhibited higher acetic acid production, reaching 1285 mg L^{-1} by day 12, compared to Sub-group B1 (pH 5 – 6), which produced only 650 mg L^{-1}. By the end of the experiment on day 12, other VFAs (formic, propionic, and butyric) were measured to be lower than 129 mg L^{-1} in both sub-groups.

The pH adjustments and changes in the headspace pressure (absolute) of the systems during the experimental period were also monitored and illustrated in Appendix I (Suppl. Info. Figs. 3.17 and 3.18).

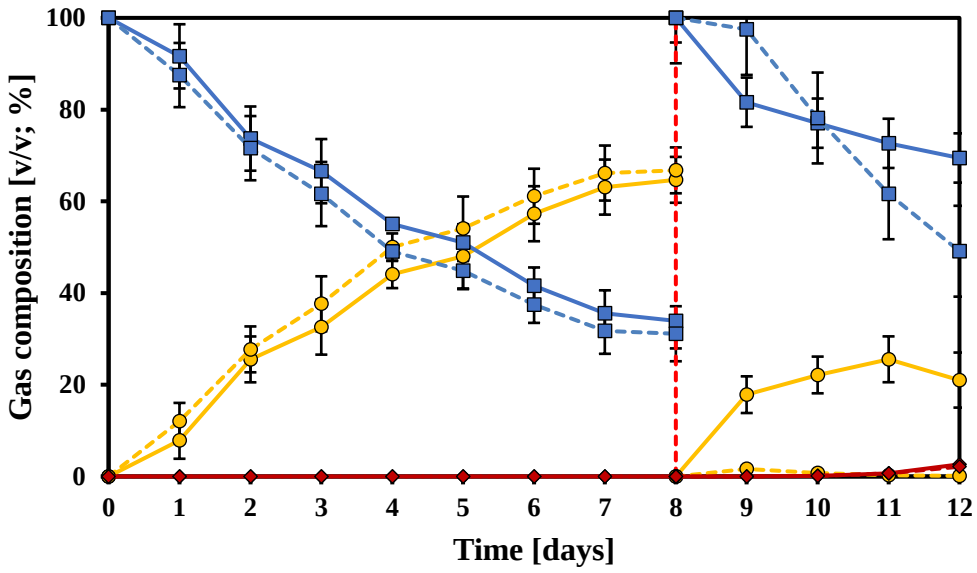

Fig. 3.28: Gas compositional alteration in the headspace of the systems over time inoculated with thermally pre-treated AnGrSL.

: Sub-group B1 operated at pH 5 – 6; : Sub-group B2 operated at pH 6 – 6,5.

: CO_2 utilization; : H_2 evolution and utilization; : CH_4 productivity.

: CO_2 gas purging.

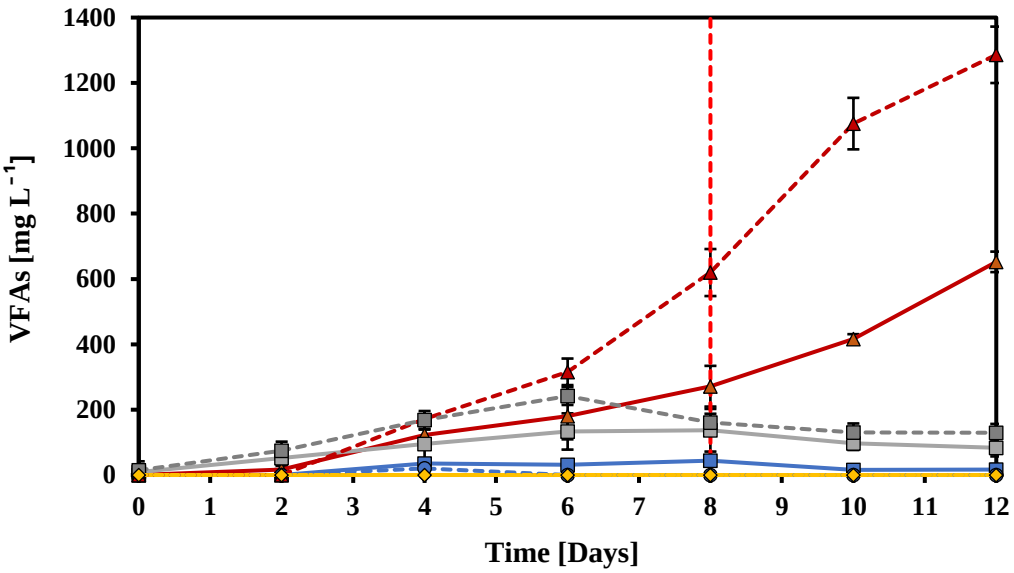

Fig. 3.29: VFAs productivity over time in systems that inoculated with thermally pre-treated AnGrSL.

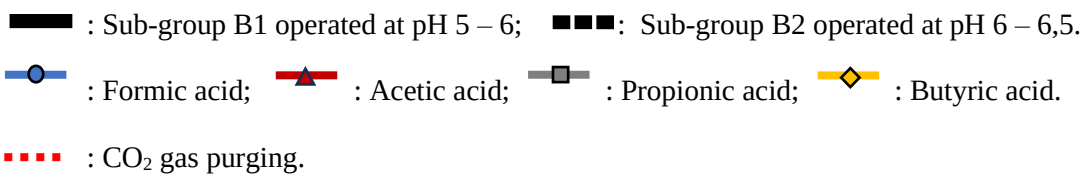

The control systems consisted solely of thermally pre-treated AnGrSL exposed to anaerobic conditions (CO_2 gas) and underwent the same methodology as the experimental systems. These control systems exhibited minimal alteration in CO_2 utilization and CH_4 production (< 7 %), with minimal changes in pH and pressure. Regarding the VFAs, Sub-group B1 (pH 5 - 6) demonstrated a total of 395 mg L^{-1}, while Sub-group B2 (pH 6 – 6.5) generated 289 mg L^{-1}. This productivity of the control systems accounts for approximately 26% and 37% of the total VFAs generated by the experimental systems consisting of ZVI (Fe^0) and heat-treated AnGrSL, likely due to AnGrSL degradation (data not shown).

According to Mockaitis et al. (2020), a heat-pretreatment method for methane inhibition poses a significant advantage due to its versatility across various anaerobic microbial consortia. Through the thermal pre-treatment, microbial communities that use the same metabolic pathways can be enriched; hence, the metabolism can be maximized, and the microbial inoculum can be shifted for the production of any desired products from certain substrates. More specifically, Singh and Singh (2021) describe that the heat shock treatment can be beneficial at temperatures ranging from 65 °C to 121 °C, applied for 20 min to 24 h. Spore-forming bacteria can survive at these harsh temperature conditions, while H_2-consumer non-spore formers, such as methanogens, can be eliminated. Pendyala et al. (2012) elucidated that high temperatures destroy enzymes such as [NiFe]-hydrogenases, crucial for mediating the conversion of H_2 and CO_2 to CH_4 by hydrogenotrophic methanogens, thereby inhibiting methanogenesis.

He et al. (2021) adopted a similar approach, yielding 1783 mg L^{-1} of acetic acid over a 10-day period in a setup employing thermally pre-treated AnGrSL. In contrast to utilizing ZVI in situ (which typically undergoes oxidation under anaerobic conditions, producing H_2), they employed a commercial mixture of H_2 and CO_2 gas in an 80:20 ratio. This gas

blend was introduced into the system at an initial pressure of 1.8 bar. The pH was initially adjusted to 6 and remained unregulated throughout the incubation period, conducted under sub-mesophilic conditions (25°C). Notably, no data on the VFA productivity of the control sample was provided.

3.2.3 Impact of 50 mM of Sodium 2-bromoethanesulfonate (BES), on Methane Inhibition in an AnGrSL-ZVI (Fe^0) system

As shown in Fig. 3.30, during the initial 7 days of cycle 1, the accumulation of H_2 gas in the headspace of both sub-groups, C1 (with pH adjusted between 5 - 6) and C2 (with pH adjusted between 6 - 6.5), increased to 74 % and 83 %, respectively. Meanwhile, the CO_2 decreased by approximately 84 % for both sub-groups over the same period. Following a CO_2 re-flashing on day 7 and until the conclusion of cycle 1 on day 15, distinct patterns emerged in the two sub-groups. In sub-group C2 (pH 6 - 6.5), the H_2 accumulation in the headspace peaked at nearly 60 % on day 12, followed by a gradual reduction, measured at 7% by the end of cycle 1 (day 15). This decline (88%) can be attributed to favorable conditions and the enrichment of the system with Acetogens, which utilize H_2 along with CO_2 for the production of acetic acid, as depicted in Eq. 45. Conversely, sub-group C1 (pH 5 - 6) exhibited negligible gas changes (H_2 and CO_2) from day 7 to day 15, compared to the experimental period from day 0 to 7.

To investigate if BES permanently affected AnGrSL, a partial replacement of the growth medium with a fresh one without additional methane inhibitors was done. Thus, on day 15, while retaining the AnGrSL and ZVI (Fe^0), 90 % of the growth medium was replaced with fresh medium, and CO_2 gas was sparged into the system to commence cycle 2. During the first 8 days of cycle 2 (day 15-23), sub-group C1 (pH 5 - 6) exhibited similar gas patterns as observed in cycle 1. However, in sub-group C2 (pH 6 - 6.5), the H_2 accumulations in the headspace increased only 20 % on day 17 and then decreased nearly to zero by day 23. Sub-group C2 displayed a dynamic pattern of H_2 utilization, similarly observed during the second CO_2 re-flashing on day 23 of cycle 2. From day 23 until the experiment's conclusion on day 27, a negligible H_2 concentration was measured in the headspace of the systems. Conversely, in sub-group C1, by the end of the experiment, the H_2 accumulation was identified at 28 %, indicating a lower H_2 consumption than Sub-

group C2. This suggests that under these conditions (pH 5-6), Acetogens require a longer period for adaptation and H_2 consumption to be accelerated.

Adding 50 mM of BES at day 0 resulted in the complete inhibition of methanogenesis for both cycles and sub-groups. Only a negligible concentration of CH_4 was detected (< 1.28%) at the beginning of the experiment (day 0 – 4) for both sub-groups.

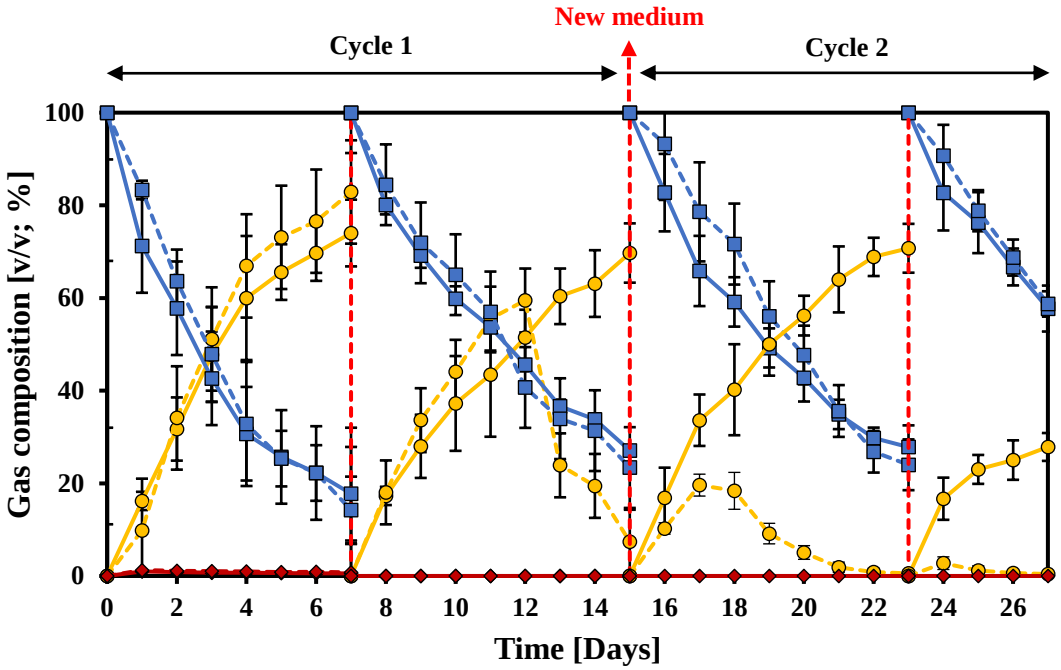

Fig. 3.30: Changes in gas composition in the headspace of AnGrSL - ZVI (Fe^0) systems exposed to BES, over time.

: Sub-group B1 operated at pH 5 – 6; : Sub-group B2 operated at pH 6 – 6,5.

: CO_2 utilization; : H_2 evolution and utilization; : CH_4 productivity.

: CO_2 gas purging.

Regarding the VFAs (Fig. 3.31), during the initial 7 days of cycle 1, all VFAs remained below 534 mg L^{-1}, with formic acid being the dominant VFA in both sub-groups. Subsequently, there was an acceleration in acetic acid production after the CO_2 re-flashing on day 11, particularly in sub-group C2 (pH 6 - 6.5), consistent with the observed increase in H_2 utilization (Fig. 3.30). At the end of cycle 1 (day 15), sub-group C2 (pH 6 - 6.5) demonstrated high acetic acid production, reaching 1736 mg L^{-1}, whereas sub-group C1 (pH 5 - 6) exhibited a slower but steady acetic acid production, reaching 614 mg L^{-1} at

the end of cycle 1. Propionic acid was detected as the second-highest VFA at the end of cycle 1, reaching almost 500 mg L^{-1} and 226 mg L^{-1} in sub-group C2 (pH 6 - 6.5) and sub-group C1 (pH 5 - 6), respectively. Butyric acid and formic acid were quantified at 157 mg L^{-1} and 4 mg L^{-1}, respectively, in sub-group C2 (pH 6 - 6.5), whereas in sub-group C1 (pH 5 - 6), they were quantified at 156 mg L^{-1} and 98 mg L^{-1}, respectively, at the end of cycle 1 (day 15).

After the introduction of the new medium into the systems, a high acceleration in acetic acid production was demonstrated by sub-group C2 (pH 6 - 6.5), reaching 2028 mg L^{-1} at the end of cycle 2 (day 27), whereas the other VFAs were identified to be lower than 250 mg L^{-1}. Regarding the productivity of sub-group C1 (pH 5 - 6), it was lower than that of sub-group C2 (pH 6 - 6.5), and an acceleration in acetic acid was observed on day 23, coinciding with the increase in rates of H_2 utilization, which reached 671 mg L^{-1} at the end of cycle 2 (day 27).

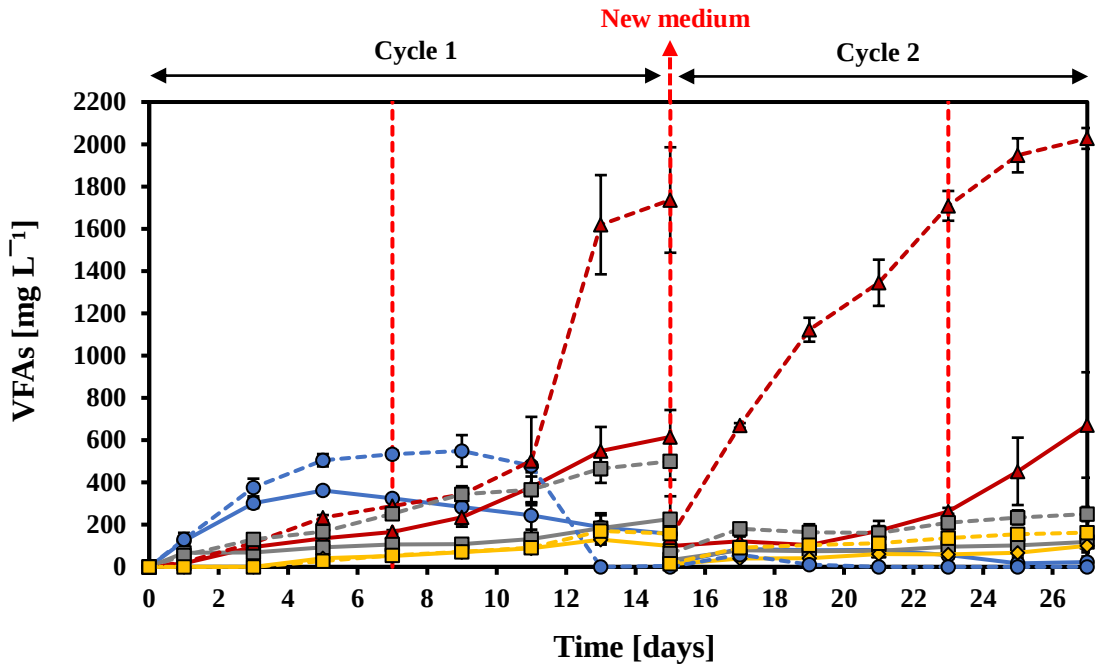

Fig. 3.31: VFAs productivity in AnGrSL - ZVI (Fe^0) systems exposed to BES, over time.

: Sub-group B1 operated at pH 5 – 6; : Sub-group B2 operated at pH 6 – 6,5.

: Formic acid; : Acetic acid; : Propionic acid; : Butyric acid.

: CO_2 gas purging.

The pH adjustments and changes in the headspace pressure (absolute) of the systems during the experimental period were also monitored and illustrated in Appendix I (Suppl. Info. Figs. 3.19 and 3.20).

The control systems were comprised solely of AnGrSL exposed to anaerobic conditions (CO_2 gas) and underwent the same methodology as the experimental systems. These control systems exhibited minimal alteration in CO_2 utilization and CH_4 production (< 8%), with negligible changes in pH and pressure (data not shown).

Regarding the VFAs of the control systems, the results indicated that during the first cycle, the VFAs were lower than 253 mg L^{-1}, whereas, during the second cycle, they were lower than 180 mg L^{-1} for both sub-groups (Suppl. Info. Figs. 3.21). It was calculated that the total VFAs (day 27) attributed to soluble microbial products (controls) accounted for approximately 36% on average for both cycles, of the total VFAs produced by AnGrSL in the presence of ZVI (Fe^0) under a CO_2 environment (CO_2 as the only external carbon source) for sub-group C1 (pH 5 - 6). Sub-group C2 (pH 6 - 6.5) demonstrated an even lower percentage, averaging 9% for both cycles. These findings indicate that the primary cause of VFAs generation from CO_2 by AnGrSL was attributed to the addition of ZVI (Fe^0), rather than cell lysis of the AnGrSL.

In this experiment, a specific methanogenic inhibitor (BES) was used at a concentration of 50 mM, a choice informed by prior studies (Schmidt et al., 2018; Omar et al., 2018; Xiao et al., 2018). According to Liu et al. (2011), such "specific" inhibitors selectively affect methanogenic archaea while leaving non-methanogenic bacteria unaffected. Hence, this specific inhibitor can be applied not only in systems featuring methanogenic cultures but also in those with mixed microbial consortia (Logroño et al., 2022). Due to its effectiveness, BES has been utilized in various bioreactors (Qiu et al., 2023), where inhibition of acetoclastic and hydrogenotrophic methanogens is required to promote the production of VFAs, acetate, and H_2, thereby preventing the development of syntrophic bacteria (Wang et al., 2021), especially at elevated BES concentrations (Zinder et al., 1984).

However, despite these applications, there are conflicting opinions regarding the effectiveness of BES-based methanogenesis inhibition. Qiu et al. (2023) highlight the unclear mechanism by which BES suppresses methanogenesis in relation to methanogen metabolism and community organization in microbial systems. Some studies primarily

observe BES's negative impact on acetoclastic methanogenesis due to its dominance in pathways. Additionally, BES has been used in pure hydrogenotrophic systems to reduce reactant consumption, such as H_2 and CO_2, although Wang et al. (2018) suggest that hydrogenotrophic methanogens may be less susceptible to BES than acetoclastic ones.

Therefore, further research must be done investigating different parameters, including the expression of genes encoding enzymatic characteristics of microbes, to elucidate the impact of BES on electron distribution between system bacteria, energy metabolism, and the optimal concentration required for complete methanogenesis inhibition across various inoculum systems.

3.2.4 Assessment of the Methane Inhibitory Effect of BES at Various Low Concentrations (1-10 mM)

As depicted in Fig. 3.32 (A), during the initial 15 days of cycle 1, each system underwent exposure to varying low concentrations of BES, resulting in diverse levels of acetic acid accumulations. Initially, all systems exhibited acetic acid production below 174 mg L^{-1} for the first 7 days. This initial low acetic acid concentration could be attributed to the utilization of acetic acid by acetoclastic methanogens, as supported by the methane productivity observed during the same period [Fig. 3.33 (B)]. However, a buildup of H_2 in the systems during this period suggests severe inhibition of hydrogenotrophic methanogens by the BES inhibitor [Fig. 3.33 (A)].

Following the CO_2 re-flashing on day 8, a significant acceleration in acetic acid accumulations was observed across all systems, persisting after the subsequent CO_2 re-flashing on day 11. This acceleration indicated enrichment of the systems with Acetogens, corroborated by gas composition analyses showing low H_2 accumulation and minimal CH_4 production from day 8 to day 15.

By the end of cycle 1 (day 15), the systems exposed to 4 mM and 2 mM of BES exhibited the highest acetic acid production, yielding 1558 mg L^{-1} and 1509 mg L^{-1}, respectively. The system subjected to 6 mM of BES demonstrated a production of 1026 mg L^{-1}. Conversely, the system exposed to 10 mM of BES displayed the lowest production, with acetic acid reaching only 503 mg L^{-1}.

To further investigate the effect of BES on AnGrSL, a partial replacement of the growth medium with fresh medium without adding extra BES was conducted on day 15 while retaining the AnGrSL and ZVI (Fe^0) to commence cycle 2. From day 15 to 22, all systems demonstrated lower acetic acid accumulations than in cycle 1. At the end of cycle 2 (day 22), the system exposed to 4 mM of BES exhibited the highest acetic acid concentration, reaching 1263 mg L^{-1}.

However, the system exposed to 2 mM of BES showed a significant drop in acetic acid by almost 69% compared to cycle 1, producing only 471 mg L^{-1}. This decline is attributed to the enrichment of the system with methanogens, as evidenced by CH_4 accumulation in the headspace of the serum bottles starting from day 19 and reaching 7.5% by the end of the experiment on day 22.

The system exposed to 1 mM of BES exhibited the lowest acetic acid accumulations at the end of cycle 2 (day 22), reaching only 158 mg L^{-1}. However, this system demonstrated the highest CH_4 production, reaching 28% in the headspace of the serum bottles by the end of cycle 2 [Fig. 3.33 (B)].

Regarding the other VFAs, it is observed that formic acid reached its maximum accumulation in the systems between days 7 and 9, with the highest concentration measured in the system exposed to 10 mM of BES on day 9 at 360 mg L^{-1}. Subsequently, formic acid declined in all systems until the end of cycle 1. A similar pattern was observed during cycle 2, but at a lower concentration compared to cycle 1. Formic acid reached its maximum accumulation in the systems between days 18 and 20, with the highest concentration measured in the system exposed to 2 mM of BES on day 18 at 163 mg L^{-1} [Fig. 3.32 (B)].

A different pattern was observed for propionic acid, which increased in all systems during cycle 1, especially after the CO_2 re-feeding on day 8, reaching its maximum concentration between 219 mg L^{-1} and 358 mg L^{-1} on day 15. During cycle 2, systems exhibited minimal alteration compared to the beginning of cycle 2, with the maximum measured accumulation being 151 mg L^{-1} [Fig. 3.32 (C)].

Regarding the butyric acid, during the first 7 days, no production was observed on all systems. Following the CO_2 re-feeding on day 8, an acceleration in production was observed for all systems, with the maximum concentration measured at 124 mg L^{-1}. A similar pattern was observed during cycle 2, with the maximum butyric acid concentration measured at 151 mg L^{-1} [Fig. 3.32(D)].

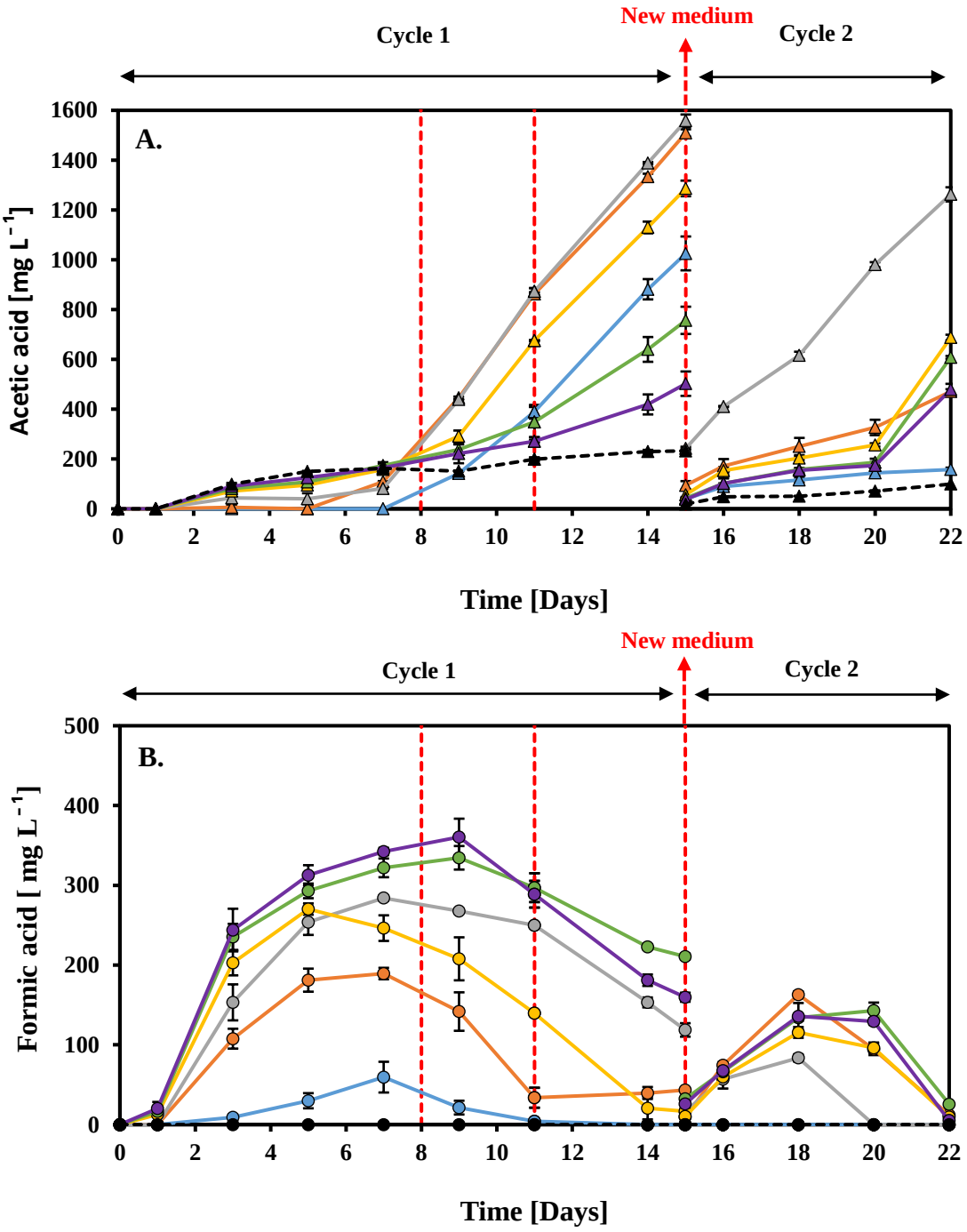

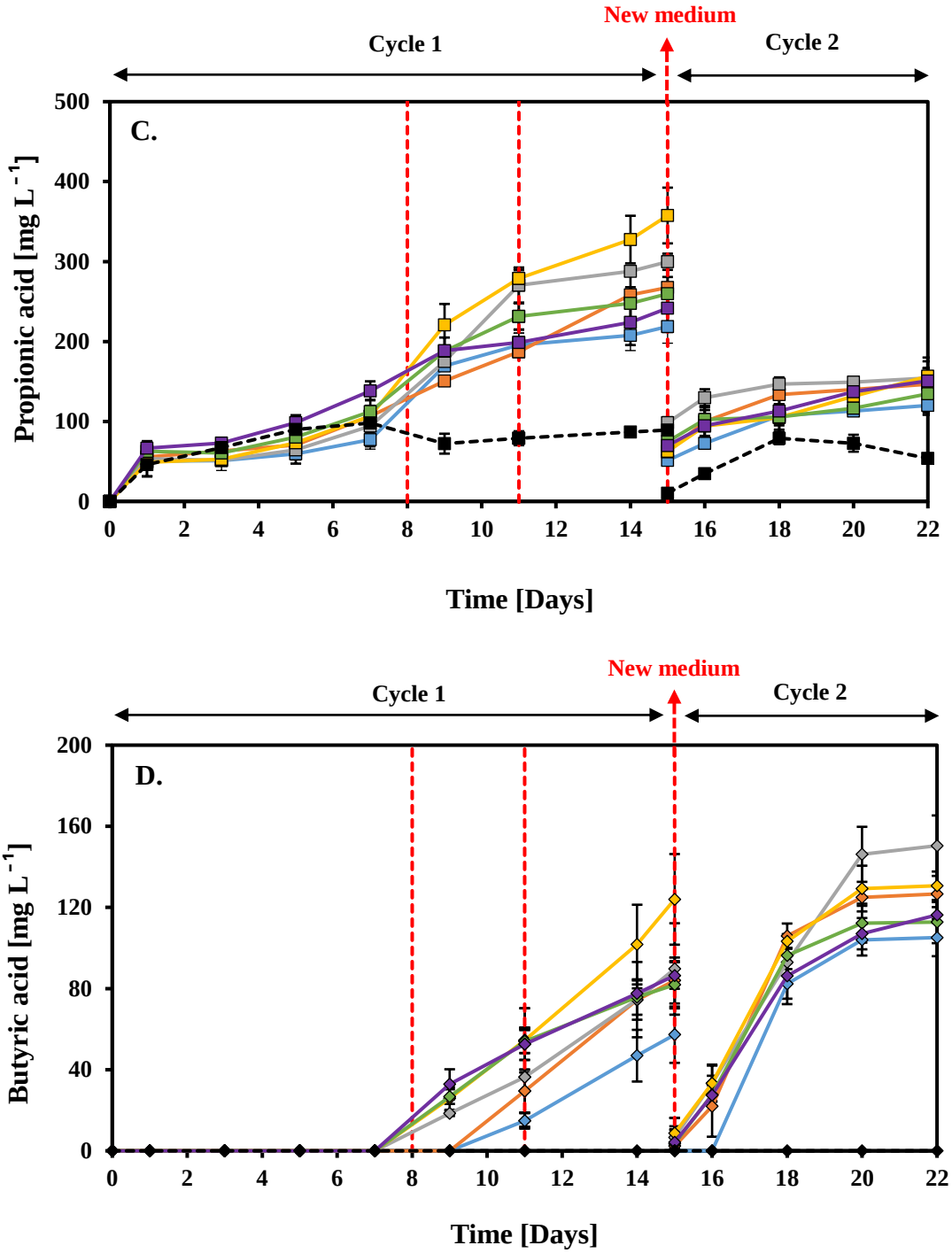

Fig.3.32: VFAs productivity over time in AnGrSL - ZVI (Fe^0) systems exposed to various low concentrations of BES. (A): Acetic acid, (B): Formic acid, (C): Propionic acid, (D): Butyric acid.

: 1 mM BES; : 2 mM BES; : 4 mM BES; : 6 mM BES; : 8 mM BES; : 10 mM BES; : Control; : CO_2 gas purging.

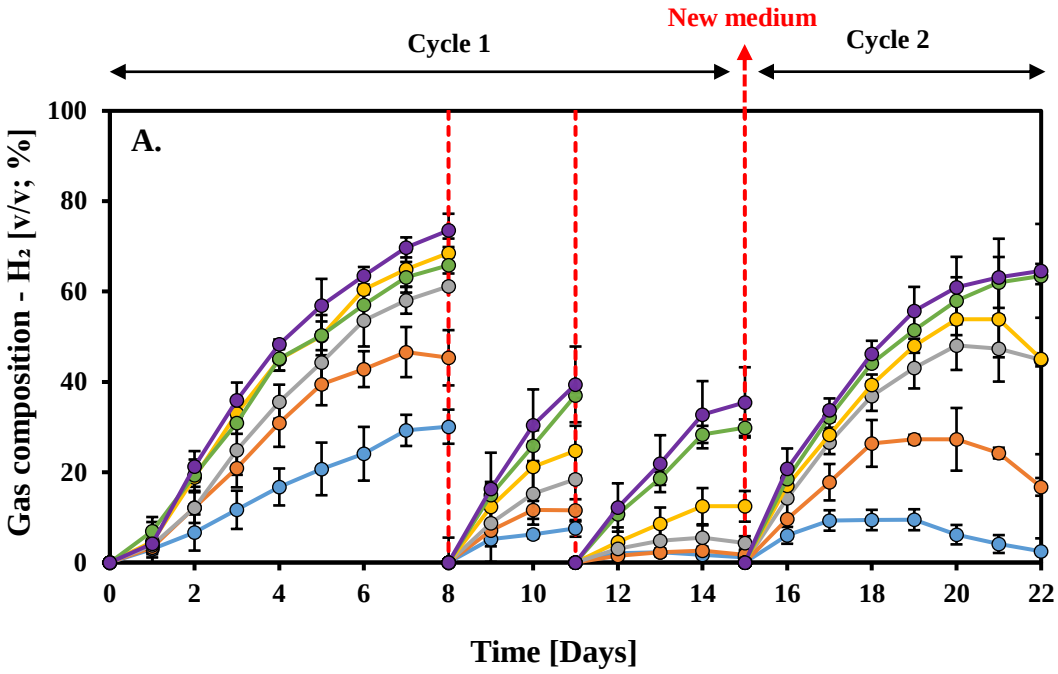
New medium
Cycle 1
Cycle 2
A.
Gas composition - H₂ [v/v; %]
Time [Days]

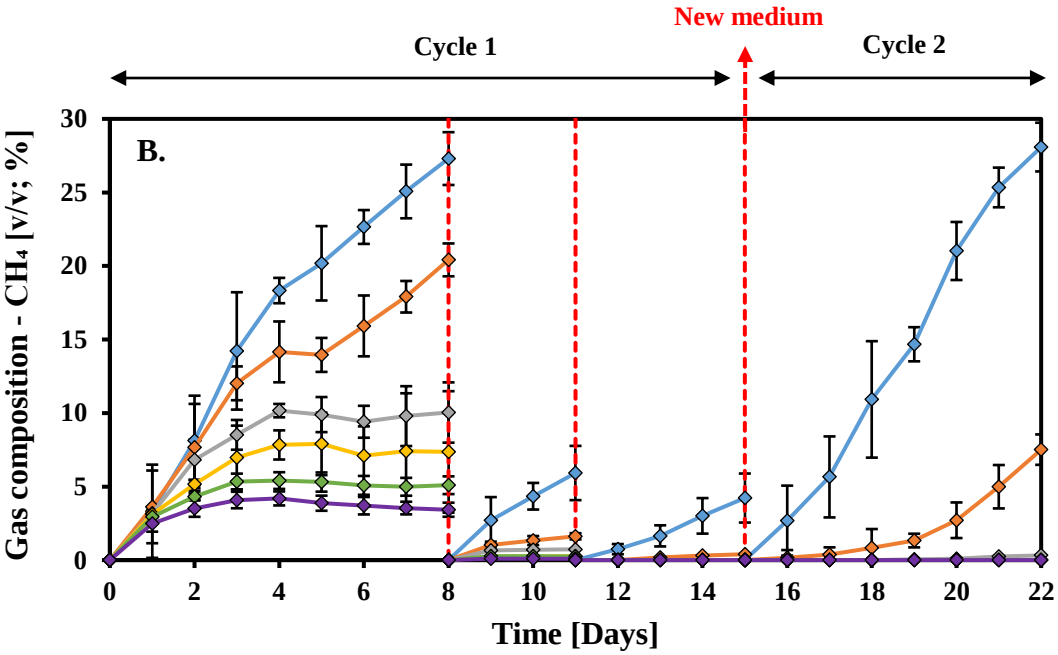
New medium
Cycle 1
Cycle 2
B.
Gas composition - CH₄ [v/v; %]
Time [Days]

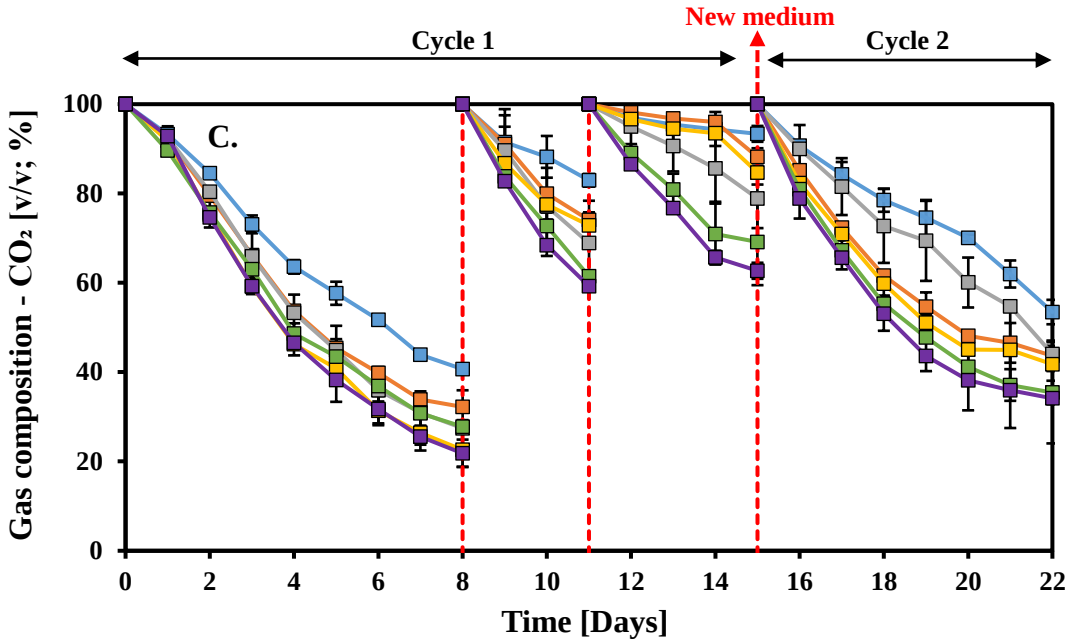

Fig. 3.33: Changes in gas composition in the headspace of AnGrSL - ZVI (Fe^0) systems exposed to various low concentrations of BES. (A): H_2 evolution and consumption, (B): CH_4 production, (C): CO_2 utilization.

: 1 mM BES; : 2 mM BES; : 4 mM BES; : 6 mM BES; : 8 mM BES; : 10 mM BES; : CO_2 gas purging.

The pH adjustments and changes in the headspace pressure (absolute) of the systems during the experimental period were also monitored and illustrated in Appendix I (Suppl. Info. Figs. 3.22 and 3.23).

The control systems consisted solely of AnGrSL exposed to anaerobic conditions (CO_2 gas) and underwent the same methodology as the experimental systems. These control systems exhibited a negligible alteration in CO_2 utilization and CH_4 production (< 1.5 %), with minimal changes in pH and pressure. The slight decline in CO_2 observed in the control systems can be attributed to the small amount of gas sampled from the serum bottle headspace for analysis. Additionally, negligible VFA productivity was observed in the control systems (< 5 mg L^{-1}) (data not shown).

The sodium salt of 2-BES stands out as the most widely utilized compound in various applications, exhibiting a complete inhibition effect on methanogenesis in microbial

consortium systems at an optimal concentration of approximately 50 mM (Eryildiz and Taherzadeh, 2020). As noted by Omar et al. (2018), treatment with BES at this concentration significantly enhances the efficiency of VFA generation compared to alternative treatments. However, the high cost associated with this chemical poses a challenge to its widespread commercial application in large-scale bioreactors (Shrestha et al., 2023). For instance, the utilization of 50 mM of BES equates to approximately 10.66 grams of the chemical per liter. Based on data obtained from Merch (https://www.sigmaaldrich.com), this amount translates to a cost of 14.28 euros (BES, ≥ 98%, CAS Number: 4263-52-9, €33.50 per 25 grams) per liter.

Recent reports by Serna-García et al. (2023) and, Lopes and Ahring (2023) have demonstrated that even lower concentrations of BES (10 mM) can achieve complete inhibition of methanogenesis in batch systems inoculated with sludge enriched with hydrogenotrophic methanogens exposed to H_2/CO_2 gas, or in bioreactors inoculated with sludge enriched with Homoacetogens. Additionally, it has been reported that 10 mM BES is also effective in inhibiting methanogenesis in rice root systems under anaerobic conditions (Conrad et al., 2000).

The present study highlights that even lower concentrations of BES can positively impact acetic acid production while maintaining the inhibition of CH_4. As explained by Lins et al. (2015), BES not only inhibits methanogenic archaea but also has the potential to affect non-methanogenic bacteria. However, this effect on non-methanogens is not considered significant, primarily altering generation time or increasing the lag phase. The current research demonstrates that a mere 4 mM of BES (0.85 g L^{-1}) effectively inhibits methanogenesis in an AnGrSL - ZVI (Fe^0) system, resulting in a cost of 1.14 € L^{-1}, representing a significant cost reduction (92%) compared to the use of 50 mM of BES. Furthermore, by minimizing the use of chemical inhibitors, not only are cost savings achieved, but also environmental impacts are reduced. Sing and Sing (2021) express concerns regarding such inhibitors, noting their potentially hazardous ecological effects if present in effluents.

Based on experimental and literature findings, it is imperative to thoroughly evaluate the overall performance of systems inoculated with a microbial consortium utilizing BES to identify optimal inhibitory doses based on the specific application system. Additionally, a combination of parameters such as pH and temperature must be considered to ensure

the enrichment of systems with appropriate bacteria for producing specific metabolites such as acetic acid. Jadhav et al. (2019) advocate combining methanogen inhibition methods to improve overall metabolite yields and extend operation times, thereby creating cost-efficient conditions for scale-up configurations. Furthermore, additional parameters must be considered. For instance, Laguillaumie et al. (2023) report that BES may degrade over time, necessitating periodic additions to the application system. Conversely, Shrestha et al. (2023) suggest that BES may be consumed by sulfate-reducing bacteria, such as *Desulfovibrio* spp., as an electron acceptor for their growth. Zhang et al. (2019) reported that several bacteria, including root bacteria like *Azospira oryzae*, can consume BES under anaerobic conditions. Moreover, Harirchi et al. (2022) propose that the inability of BES to inhibit methanogenesis could be attributed to resistance or adaptation by hydrogen-consuming microorganisms (HCM) at high dosages of BES.

3.2.5 Effect of NaCl at Various Concentrations on Methane Inhibition When Employed in an AnGrSL - ZVI (Fe^0) System

As illustrated in Fig. 3.34 (A.), employing NaCl as a strategy for inhibiting methanogenesis led to reduced accumulations of acetic acid in the systems throughout the experimental duration, compared to experiments conducted with BES.

It is observed that increasing the concentration of NaCl from 30 g L^{-1} to 60 g L^{-1} and 90 g L^{-1} inhibits acetic acid production in the systems, with the highest accumulation exhibited by the system with 30 g L^{-1}, reaching 414 mg L^{-1} after 17 days. However, after day 17, acetic acid declined in the 30 g L^{-1} NaCl system, possibly due to acetoclastic methanogens adapting to salinity and utilizing acetic acid for CH_4 production, which reached 28% in the headspace of the systems by the experiment's end (day 24), as depicted in Fig. 3.35 (B.). Additionally, the system with 30 g L^{-1} NaCl exhibited complete H_2 utilization from day 10, indicating the presence of hydrogenotrophic methanogens [Fig. 3.35 (A.)].

Subsequently, the system with 60 g L^{-1} NaCl exhibited the highest accumulation of acetic acid after 17 days, reaching 209 mg L^{-1}, with lower CH_4 accumulation (6%) compared to the 30 g L^{-1} NaCl system [Fig. 3.35 (B.)]. Conversely, the system with 90 g L^{-1} NaCl demonstrated a distinct pattern, with acetic acid accumulations steadily increasing and

reaching a maximum at the experiment's end (day 24), at 164 mg L^{-1}, with zero CH_4 accumulation in the headspace. The systems with 60 g L^{-1} and 90 gr L^{-1} NaCl exhibited low H_2 consumption, which increased in the headspace to 61% and 81%, respectively, indicating hydrogenotrophic methanogen inhibition [Fig. 3.35 (A.)].

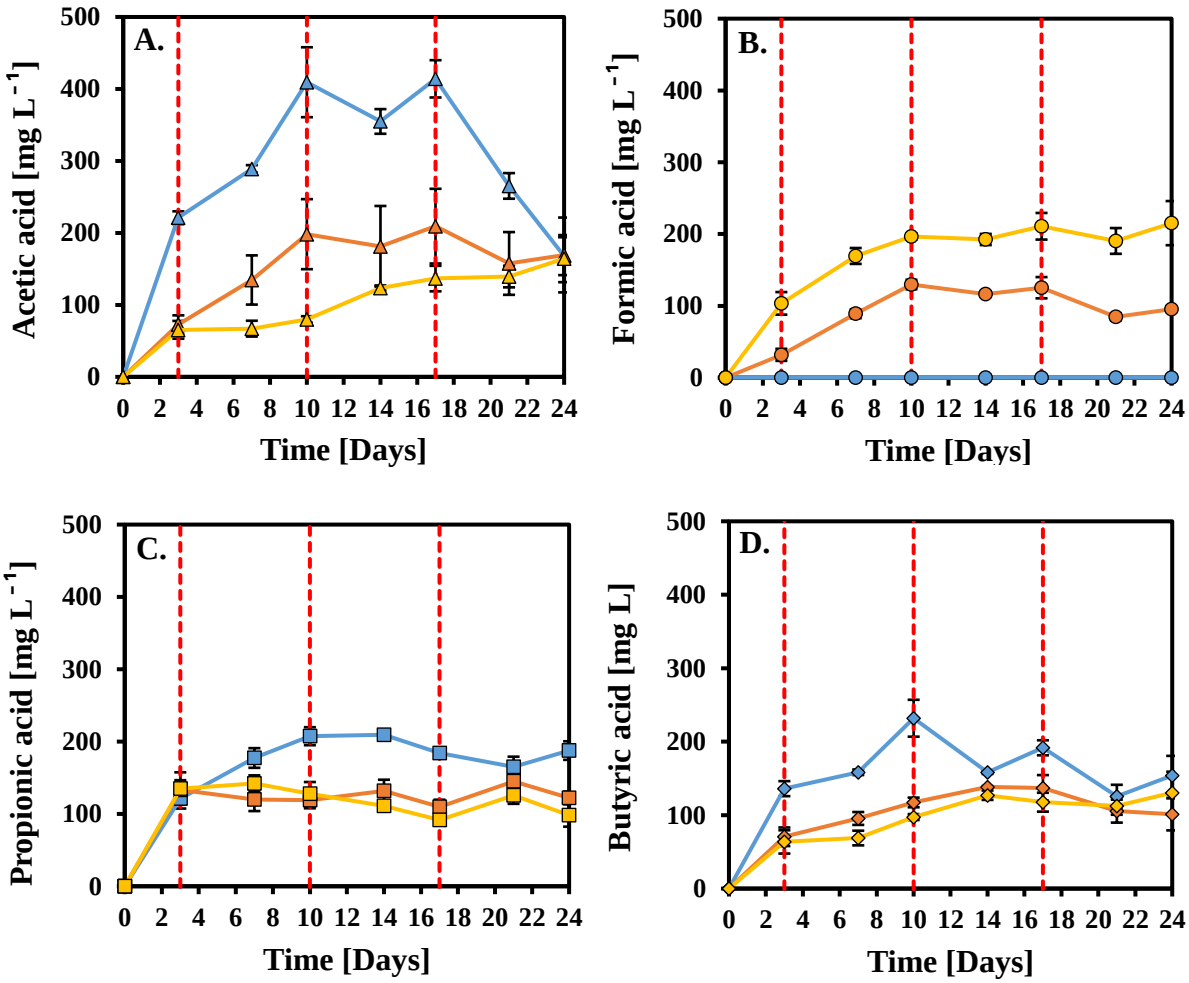

Fig. 3.34: VFAs productivity over time in AnGrSL - ZVI (Fe^0) systems exposed to various concentrations of NaCl. (A): Acetic acid, (B): Formic acid, (C): Propionic acid, (D): Butyric acid.

: 30 gr L^{-1} NaCl; : 60 gr L^{-1} NaCl; : 90 gr L^{-1} NaCl; : CO_2 gas purging.

Thus, at 30 g L^{-1} NaCl exhibited a simultaneous generation of CH_4 and VFAs by AnGrSL exposed to ZVI (Fe^0) utilizing CO_2 as the only carbon source. Interestingly, a similar trend (in both VFAs and gas composition) was observed when sterilized seawater was used instead of 30 g L^{-1} NaCl (data not shown). Based on the above observation, the same configuration potentially may find application in sea vessels for CO_2 utilization, where CO_2 can be first adsorbed in a reactor with seawater, and then the CO_2-saturated seawater to be used in a system of AnGrSL and ZVI.

Propionic acid and butyric acid accumulations ranged between 98-188 mg L^{-1} and 101-154 mg L^{-1} at the experiment's end (day 24) for all systems [Fig. 3.34 (C.) & (D.)]. The maximum concentration of formic acid, reaching 215 mg L^{-1}, was observed in the system using the highest NaCl concentration (90 g L^{-1} NaCl) at the end of the experiment (day 24) [Fig. 3.34 (B.)].

The control systems consisted solely of AnGrSL exposed to anaerobic conditions (CO_2 gas) and underwent the same methodology as the experimental systems (with 30 g L^{-1} and 90 g L^{-1} NaCl). These control systems exhibited a negligible alteration in CO_2 utilization and CH_4 production (< 1.22 %), with minimal changes in pH and pressure (data not shown). The slight decline in CO_2 observed in the control systems can be attributed to the small amount of gas sampled from the serum bottle headspace for analysis. The VFAs productivity of the control samples (30 g L^{-1} and 90 g L^{-1} NaCl) are depicted in Suppl. Info. Fig. 3.24 (A. & B.).

The pH adjustments and changes in the headspace pressure (absolute) of the systems during the experimental period were also monitored and illustrated in Appendix I (Suppl. Info. Figs. 3.25 and 3.26).

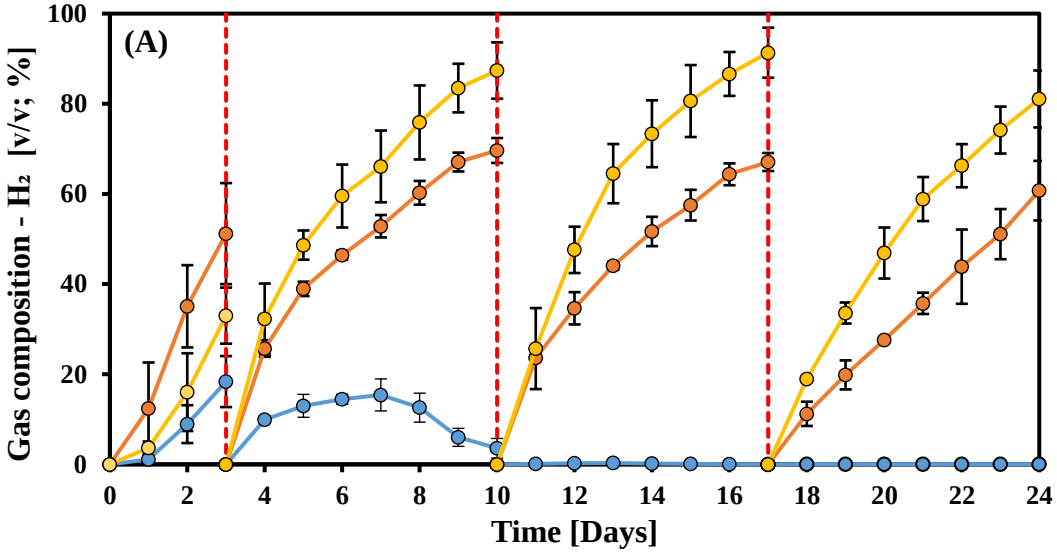
(A)
Gas composition - H₂ [v/v; %]
Time [Days]

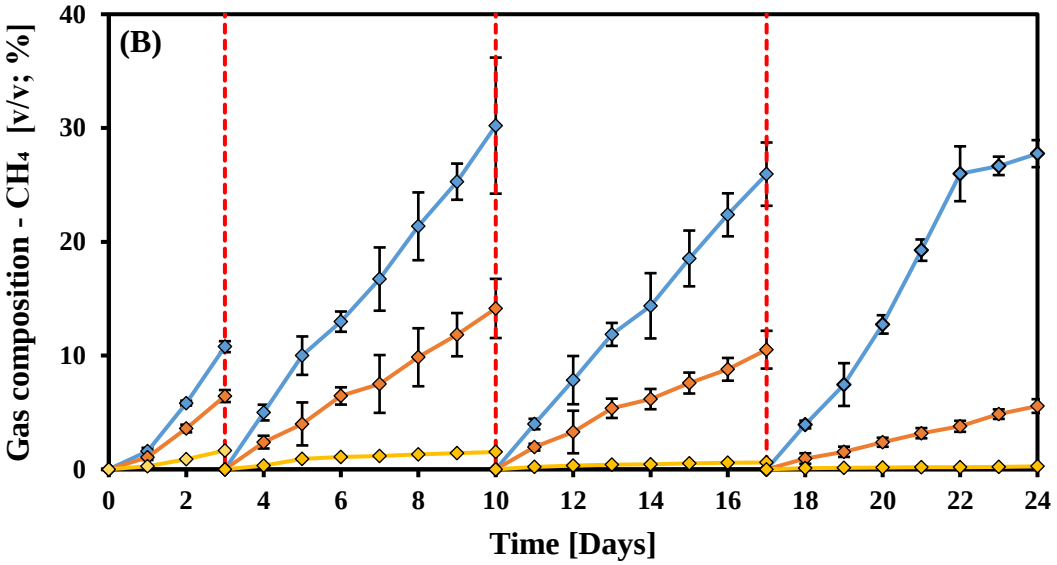
(B)
Gas composition - CH₄ [v/v; %]
Time [Days]

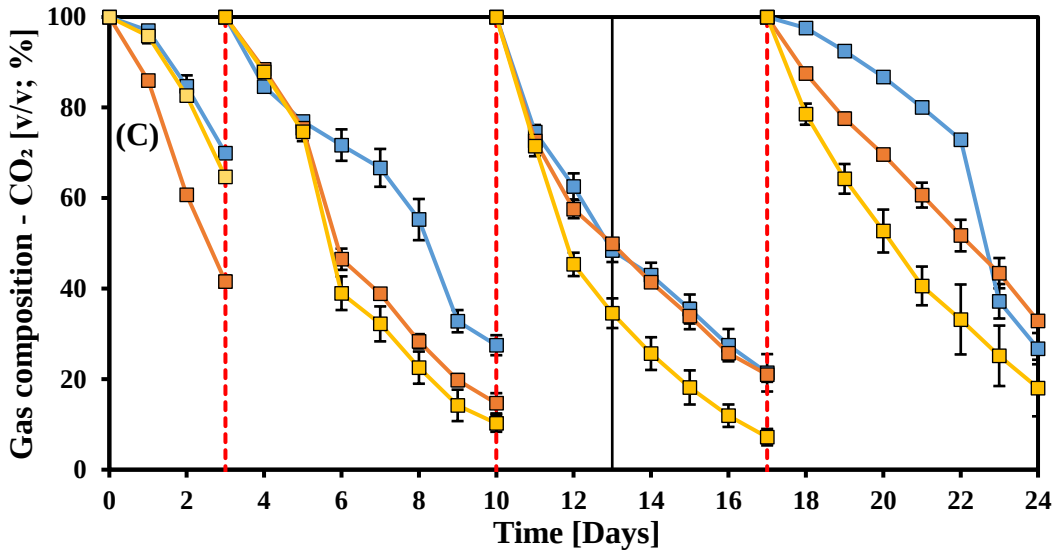
(C)
Gas composition - CO₂ [v/v; %]
Time [Days]

Fig. 3.35: Changes in gas composition in the headspace of AnGrSL - ZVI (Fe^0) systems exposed to various concentrations of NaCl. (A): H_2 evolution and consumption, (B): CH_4 production, (C): CO_2 utilization.

: 30 gr L^{-1} NaCl; : 60 gr L^{-1} NaCl; : 90 gr L^{-1} NaCl ; : CO_2 gas purging.

The salt content (salinity) in a microbial system can negatively influence its performance or be beneficial at specific concentrations for the growth of microorganisms. As stated by Yin et al. (2022) and Oliveira et al. (2021), low concentrations of sodium cations (Na^+) are involved in the oxidation of NADH and can be coupled with Na^+-dependent membrane-bound ATP synthase for the formation of adenosine triphosphate (ATP), which plays a crucial energy role in the metabolism and proliferation of microorganisms. However, elevated salinity results in high sodium cation content, which acts as a stressor for microbial activity in anaerobic digestion (AD) processes. Several investigators (Guan et al., 2023; Zupančič et al., 2023; Liu et al., 2019) have explained that high salinity inhibits important enzymes, disturbs metabolic processes, and exerts osmotic stress on the cell walls of microorganisms, resulting in inhibited cell growth. Elevated salinity causes an increase in osmotic pressure, leading to dehydration of microbial cells, plasmolysis, desiccation, and ultimately cell death, which in turn leads to the failure of the AD process.

Salinity also affects and alters the microbial community structure in a system. Low salinity can suppress methanogenesis while promoting hydrolysis and acidification processes in AD. Conversely, elevated salt levels significantly impede these processes (hydrolysis-acidification) due to the sensitivity of methanogens to environmental stresses such as salinity. Salinity toxicity affects methanogens in the reactant-consuming pathway, shifting from acetoclastic to hydrogenotrophic methanogenesis (Liu et al., 2019). Several factors contribute to this phenomenon. Chen et al. (2020) attributed it to the fact that acetoclastic methanogens cannot withstand environmental stresses since they cannot synthesize CoM independently and require extracellular absorption, unlike hydrogenotrophic methanogens. Furthermore, the acetoclastic methanogens unique cell wall structure makes them vulnerable to toxic compounds that easily penetrate the cells. Hydrogenotrophic methanogens, on the other hand, may obtain more energy for growth

and maintenance due to the higher Gibbs free energy of hydrogenotrophic methanogenesis compared to acetoclastic methanogenesis, aiding in their ability to withstand high salt stress. Yin et al. (2022) and Zhang et al. (2020) correlate the alteration and inhibition of methanogens to the inhibition of the F_{420} enzyme, which progressively declines as salinity levels rise. Gao et al. (2022) stated that F_{420} might be used as H_2 carriers in the hydrogenotrophic methanogenic pathway, and F_{420}-reducing hydrogenase's catalysis is an essential part of the H_2 transfer process.

Liu and Boone (1991) experimentally showed that increasing NaCl concentration from 0 gr L^{-1} to 87.66 gr L^{-1} (5 M) inhibits bacteria in the following order: 1. bacteria that break down lignocelluloses, 2. bacteria that utilize acetate, 3. bacteria that utilize propionate, and 4. organisms that utilize H_2/CO_2. However, even at high salinity and anoxic environments, methanogens can be detected based on their degree of tolerance (Christman et al., 2020). Several scientific reports mention different NaCl concentrations for methane inhibition, examining various AD systems and operational parameters such as initial inocula, bioreactor type, substrate type, and operating temperature.

For instance, Ogata et al. (2016) reported methanogenesis inhibition at 35 mS cm^{-1} electrical conductivity, approximately 22 gr L^{-1} NaCl, in a system with organic waste under mesophilic conditions. Zupančič et al. (2023) reported 28.2 g L^{-1} NaCl inhibition in thermophilic anaerobic digestion of organic waste. According to Chen et al. (2008), mild AD inhibition occurs at Na^+ concentrations between 3.5 and 5.5 gr L^{-1} (8.88 g L^{-1} and 13.97 g L^{-1} NaCl), with severe methanogen inhibition observed at Na^+ values over 8.0 g L^{-1} (20.34 g L^{-1} NaCl). Zhang et al. (2020) demonstrated only a 42% CH_4 inhibition using 30 g L^{-1} NaCl and found that such concentrations reduced F_{420} and CoM enzymes by 60.62% and approximately 38%, respectively, under mesophilic conditions and by utilizing organic waste. They also reported that *Methanosaeta* and *Methanosarcina* could adapt to high-salinity environments. Kallistova et al. (2020) stated that acetoclastic methanogenesis is inhibited at NaCl concentrations above 40 g L^{-1}, while Sorokin et al. (2016) noted that acetate might still be indirectly converted to methane via bacterial syntrophy at Na^+ concentrations higher than 3M (175.32 g L^{-1} NaCl). Zhang et al. (2022) achieved 81.1% CH_4 inhibition using 85 gr L^{-1} NaCl with anaerobic granular sludge utilizing wastewater under mesophilic conditions. Yin et al. (2022) observed reductions in VFAs and CH_4 by 13.4% and 72.3%, respectively, in a system with anaerobic granular

sludge utilizing wastewater under mesophilic conditions at 52 g L^{-1} NaCl, with increased butyric acid accumulations between 13 g L^{-1} and 52 g L^{-1} NaCl. Conversely, Sarkar et al. (2020) observed increased butyric (3.04 g L^{-1}) and acetic acid (1.17 g L^{-1}) accumulations in a system utilizing organic food waste inoculated with anaerobic sludge under mesophilic conditions at 40 g L^{-1} NaCl. Zeb et al. (2019) reported 83% methanogenesis inhibition at 48 g L^{-1} NaCl in a system with dairy wastewater under mesophilic conditions. Oliveira et al. (2021) fully inhibited methanogenesis at 50 g L^{-1} NaCl using anaerobic granular sludge with poultry slaughterhouse wastewater under mesophilic conditions.

Besides microbial inhibition under high salinity, several other factors must be considered for the optimal operation of systems under high salinity. When AnGrSL is used as inoculum, elevated salinity can cause flocs and granules to disintegrate, resulting in a noticeable biomass wash-out, and sludge granulation is challenging to complete successfully at high salinities (Sierra et al., 2019). Li et al. (2022) highlighted the impact of salinity beyond CH_4 inhibition when using a bio-electrochemical system, indicating that high salinity is connected with high solution conductivity, which substantially negatively impacts system performance. Gagliano et al. (2017) stated that the genus *Methanosaeta*, which dominates in saline environments and forms advantageous cohesive and coordinated functional communities (biofilms) up to 50 g L^{-1} NaCl, is inhibited at higher concentrations.

Generally, Andrei et al. (2012) categorize methanogenic archaea into three major groups: 1. methanogens that use substrates such as H_2 + CO_2 and formate for CH_4 production, which can grow at elevated salinity of 120 g L^{-1} NaCl; 2. methanogens that utilize compounds such as methanol, trimethylamine, dimethylsulfide, and some alcohols such as isopropanol, which can survive at elevated salinity of 270 g L^{-1} NaCl; and 3. methanogens that use acetate as a primary substrate, which can survive at elevated salinity of 40 g L^{-1} NaCl.

These scientific findings align with the results presented in this sub-chapter. The increase in formic, acetic, and butyric acid, along with high H_2 accumulations in the high-salinity system (90 g L^{-1}), indicates the inhibition of group 1 and group 3 methanogens. At 60 g L^{-1} NaCl, methanogenesis occurred, with CH_4 levels at 14% on day 10 in the headspace, declining to 6% by the end of the experiment on day 24. The observed CH_4 accumulations at these high salinity levels can be explained by partial acclimatization of the AnGrSL

obtained from a reactor treating cheese whey wastewater containing NaCl. The decrease in CH_4 accumulations during the experimental duration aligns with the findings of Zeb et al. (2019), who observed that over time, digesters with salinity-acclimated inoculum produced less CH_4 compared to those with unacclimated inoculum, which exhibited higher CH_4 production at the initial stage. All the above findings strongly indicate that each system operating under specific parameters must be examined independently to determine the salinity stress it can withstand. The optimal salinity concentration for methane inhibition varies depending on the desired output results and operational limitations. Therefore, no single salinity concentration is ideal for methane inhibition across all systems.

3.2.6 Next-generation sequencing and microbial population analysis

The bacterial microbial profile at phylum and genus levels examined after the end of the experimental duration for systems B2 (thermal inhibition), C1 (BES inhibition; pH 5-6), C2 (BES inhibition; pH 6-6.5), and E3 (high salinity inhibition) along with bacteria relative abundance of the initial inoculum as shown in Table 2.3.

As depicted in Fig.3.36, the thermal pre-treated AnGrSL (system B2) that was exposed to ZVI (Fe^0) under anaerobic conditions (CO_2) exhibited an increase in Firmicutes, were identified at 65.9%, compared with the initial inoculum (7%) and control system (29%) The main genera level identified at system B2 (thermal inhibition) was *Clostridium sensu stricto* which did not detected in the initial inoculum and only 7% was detected in the control systems. *Clostridium sensu stricto* also appeared in C1 (BES inhibition; pH 5-6), C2 (BES inhibition; pH 6-6.5) systems with high relative abundances of 22% and 24%, respectively. Vyrides et al. (2018) similarly identified *Clostridium sensu stricto* as one of the dominant genera in AnGrSL exposed to ZVI (Fe^0) under anaerobic conditions (CO_2). Philips et al. (2019) reported a 10% relative abundance of *Clostridium sensu stricto* in an anoxic corrosion crust sample enriched with ZVI (Fe^0). Further, studies by Huang et al. (2019) using micron-sized ZVI (Fe^0) and by Yin and Wang (2019) using ZVI (Fe^0) nanoparticles in anaerobic digesters treating swine manure and macroalgae, respectively, also identified *Clostridium sensu stricto* among the anaerobic bacteria.

Furthermore, a significant increase in the *Syntrophobacter* genus was observed in systems C1 (BES inhibition; pH 5-6), and C2 (BES inhibition; pH 6-6.5), representing 14.3% and 8.7%, respectively, compared with the initial inoculum and control system (2%). Also, *Syntrophorhabdus* increased in the above systems at approximately 4%. The same genus, *Syntrophobacter*, and *Syntrophorhabdus*, were also identified in system E3 (high salinity inhibition) at 14% and 3% respectively. *Syntrophobacter* plays a significant role in anaerobic digestion and positively correlates with methanogenesis. Characterized as propionate-oxidizing bacteria and through the utilization of substrates such as propionate and butyrate, can be found with other methanogenic archaea (acetoclastic) in syntrophic cooperation (Li et al., 2022; Pan et al., 2019). Worm et al. (2011) also reported that this genus requires low formate and H_2 concentrations. So, hydrogen-consuming partners are required (methanogens) to maintain a low hydrogen partial pressure, making propionate oxidation thermodynamically favorable. Under the influence of ZVI (Fe^0), the elevated H_2 partial pressure might facilitate the microbial reduction of CO_2 to butyric and/or propionic acid. These acids can then be further degraded by *Syntrophobacter* and Homoacetogenic bacteria (such as *Clostridium sensu stricto* or others) into acetic acid. *Syntrophbacter* and *Syntrophorhabdus*, which are crucial for the breakdown of VFAs (butyrate and propionate) and for supplying enough substrates for methanogens throughout the AD process, were also identified by Pan et al. (2019) in systems exposed to elevated nZVI (Fe^0) dosed along with the H_2-producing acetogenic bacteria such as *Syntrophus* that utilize butyric acid. As mentioned by Kong et al. (2018), exposing the inoculant to ZVI (Fe^0) has a favorable impact on the syntrophic bacteria in AD.

Methanogens were also analyzed at the end of the experiment to identify the genera that survive under these conditions and potentially reduce system performance by consuming acetic acid and/or H_2. As shown in Fig. 3.37, exposure of AnGrSL to ZVI (Fe^0) and BES resulted in a decrease in the *Methanosaeta* genus to 29.7% compared to 52.1% in the control, while the *Methanobacterium* genus significantly increased to 38.6% compared to 3.3% in the control. This aligns with the findings of Xu et al. (2010), who reported that acetoclastic methanogens are more sensitive to BES than hydrogenotrophic methanogens. Conversely, thermal pre-treatment of AnGrSL led to a significant increase in *Methanosaeta* species to 74.4% compared to 52.1% in the control. This could be due to the high concentrations of acetic acid available under these conditions and the heat

resistance of the *Methanosaeta* genus, which is attributed to their thick, relatively impervious S-layers that form a protective sheath around the cell wall (Bhattad et al., 2017).

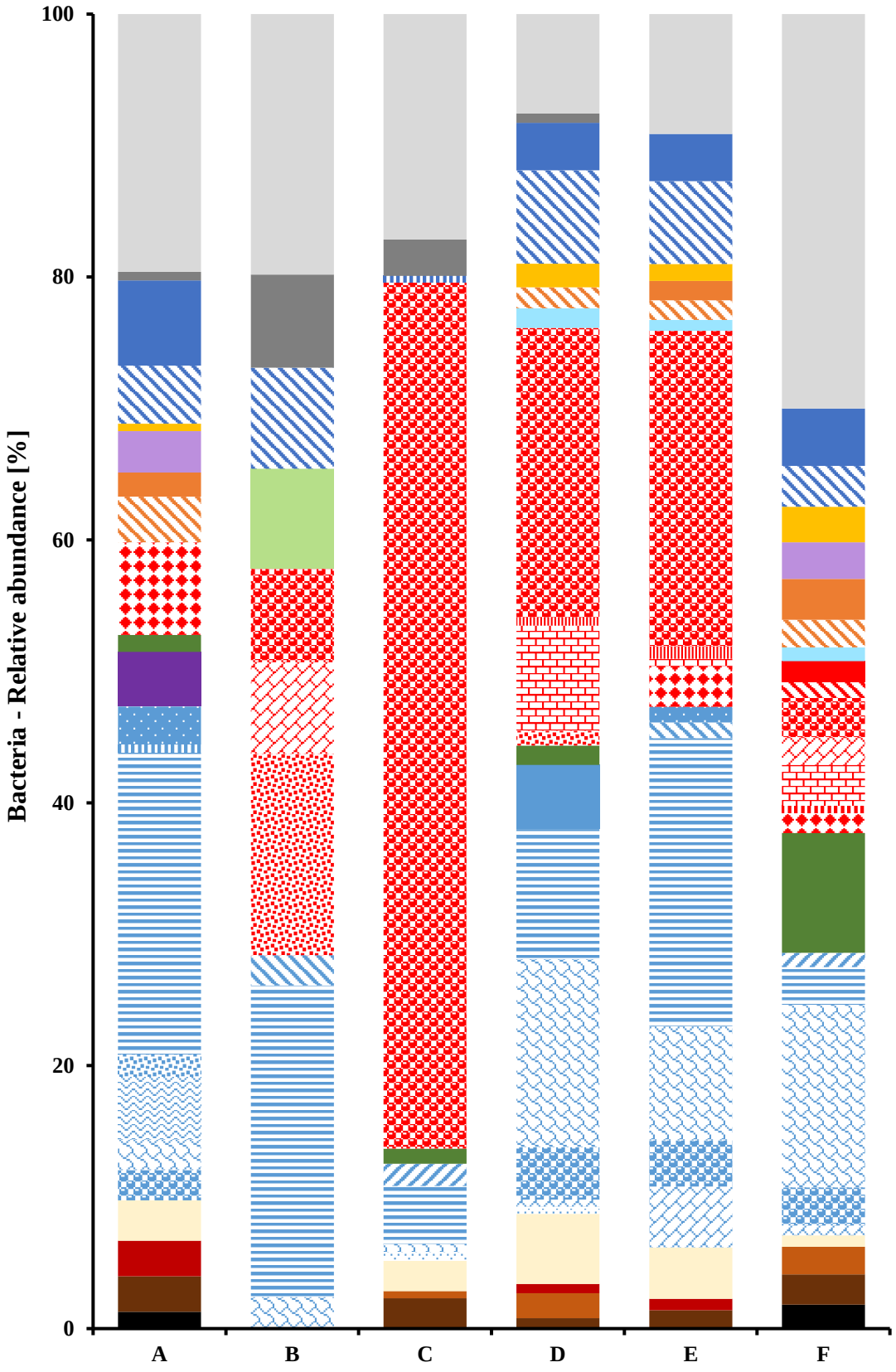
Bacteria - Relative abundance [%]
100
80
60
40
20
0
A
B
C
D
E
F

Fig. 3.36: Bacteria relative abundance [%] at phylum and genera level, at the end of the experimental duration.

A: Initial inoculum – AnGrSL; **B:** Control system (BES 50 mM); **C:** Heat pre-treated AnGrSL – systems B2; **D:** AnGrSL exposed to ZVI (Fe^0) and BES (50 mM) and operated at pH 5-6 – systems C1; **E:** AnGrSL exposed to ZVI (Fe^0) and BES (50 mM) and operated at pH 6-6.5 – systems C2; **F:** AnGrSL exposed to ZVI (Fe^0) and NaCl (60 g L^{-1}) and operated at pH 5-6 – system E2.

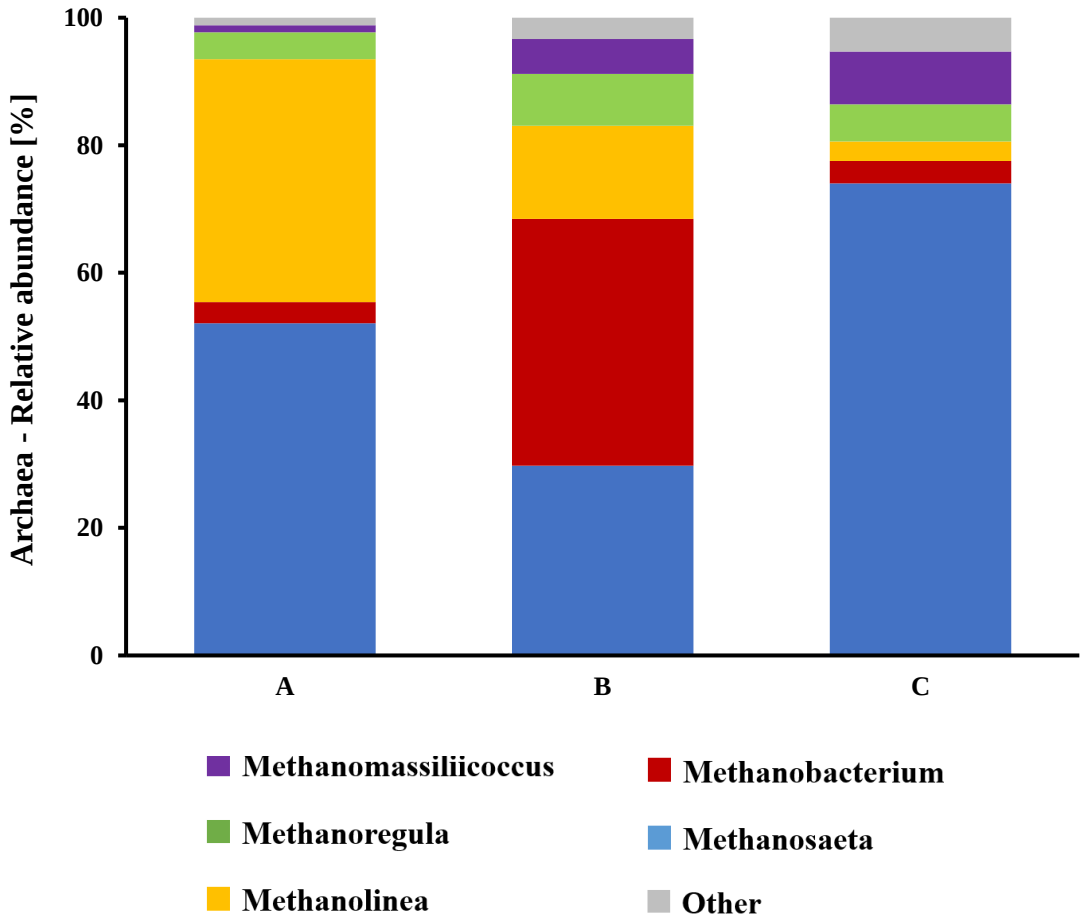

Fig. 3.37: Archaea relative abundance [%] at the general level at the end of the experimental duration.

A: Control system (BES 50 mM); **B:** AnGrSL exposed to ZVI (Fe^0) and BES (50 mM) and operated at pH 5-6 – systems C1; **C:** Heat pre-treated AnGrSL – systems B2.

3.2.7 Structural characterization of ZVI (Fe^0) before and after exposure to AnGrSL and CO_2

As illustrated in Fig. 3.38, the ZVI (Fe^0) powder before use exhibits three diffraction peaks at 2θ = 44.7°, 65.0°, and 82.3°, corresponding to the body-centered cubic (BCC) crystalline alpha phase of iron (α-Fe), commonly known as ferrite [Fig. 3.38 (A.) – black line]. The absence of additional peaks confirms the purity of the iron and the lack of iron oxides or other crystalline impurities in the initial material. Conversely, the ZVI (Fe^0)

sample was exposed to the BES inhibitor (50 mM) after 27 days of the anaerobic process [Fig. 3.38 (B.) – red line], shows peaks primarily associated with siderite ($FeCO_3$) and pure α-Fe. The siderite peaks result from oxidation products under aquatic carbonate anaerobic conditions, as described by Eq. 32. At the same time, the presence of Fe^0 indicates the unreacted portion of ZVI, suggesting incomplete transformation after 27 days. Additionally, a minor amount of magnetite (Fe_3O_4) is present, indicated by the peak at $2\theta = 35.4°$, suggesting it as a secondary oxidation product. The X-RD pattern of the ZVI sample exposed to the NaCl inhibitor (60 g L^{-1}) after 24 days of the anaerobic process [Fig. 3.38 (C.) – green line] also shows peaks of $FeCO_3$ and pure Fe^0, similar to the ZVI exposed to the BES inhibitor, with insignificant Fe_3O_4 formation. Moreover, two minor NaCl peaks are observed, likely due to residual NaCl crystals that remained undissolved or unreacted.

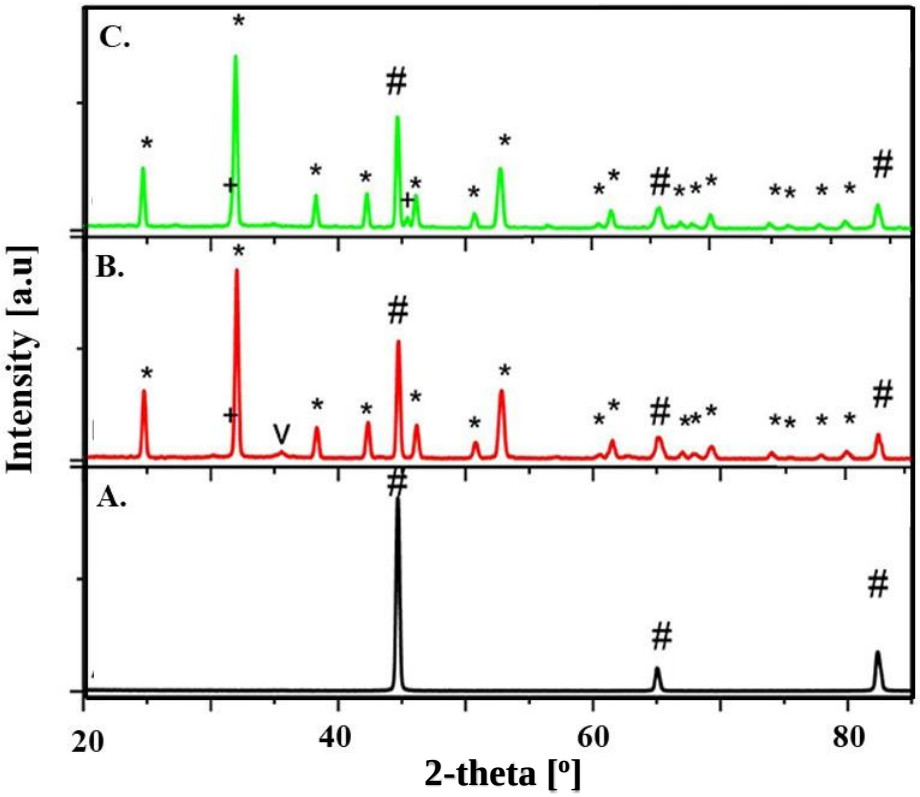

Fig. 3.38: X-RD patterns of the processed ZVI (Fe^0) in the presence of BES and NaCl inhibitors, under anaerobic conditions.

Symbols: #: Fe; +: NaCl; V: Magnetite; *: Siderite.

A.: Unprocessed ZVI (Fe^0); **B.:** Processed ZVI (Fe^0) exposed to 50 mM of BES under anaerobic conditions; **C.:** Processed ZVI (Fe^0) exposed to 60 gr L^{-1} of NaCl under anaerobic conditions.

3.2.8 Discussion of Experimental Set-Up 2

The experiments provide compelling evidence that CO_2 can be effectively utilized and bioconverted to acetic acid and other VFAs in a system inoculated with AnGrSL, involving ZVI (Fe^0) and various methanogenesis inhibition strategies. This reveals a promising avenue for sustainable CO_2 utilization and the production of platform chemicals.

To date, various physicochemical technologies have been developed for CO_2 mitigation (Muñoz et al., 2015). Alternatively, chemoautotrophic microbes can convert CO_2 into CH_4 or other valuable products under mild operational and environmental conditions (Angelidaki et al., 2018). Specifically, microbial power-to-gas technologies utilize hydrogenotrophic methanogens to convert H_2 and CO_2 to CH_4 in either *in-situ* or *ex-situ* biological processes. Moreover, microbial electrosynthesis (MES) has been used to reduce CO_2 to carboxylic acids (Prévoteau et al., 2020; Jiang et al., 2019). However, recent reviews (Prévoteau et al., 2020; Jiang et al., 2019; Bajracharya et al., 2017) indicate that no pilot or full-scale MES studies have been reported, with cost reduction remaining a significant challenge (Jiang et al., 2019).

This proof-of-concept study demonstrates that using ZVI (Fe^0) in a system with AnGrSL under anaerobic conditions and feeding the system with CO_2, allows for the conversion of CO_2 to carboxylic acids without the complex configurations required for microbial electrosynthesis (MES) systems, such as electrodes, proton exchange membranes, and power supply connections. The study shows that a system with AnGrSL, ZVI (Fe^0), and BES can produce 4,837 mg L^{-1} of total VFAs after 27 days. A system with heat-treated AnGrSL and ZVI (Fe^0) can also produce 1,415 mg L^{-1} of total VFAs after 12 days. Furthermore, AnGrSL exposed to ZVI (Fe^0) and 30 g L^{-1} NaCl produced over 800 mg L^{-1} of total VFAs after 10 days, with about 30% of the system headspace consisting of CH_4. This trend was consistent when seawater was used instead of 30 g L^{-1} NaCl,

suggesting potential applications in marine vessels for CO_2 utilization or industries generating high CO_2 levels near the coast.

This study highlights several factors to consider before scaling up the process: the cost of BES or sludge pre-treatment, VFA recovery costs, and ZVI regeneration. During the experiments, it was observed that ZVI (Fe^0) retained its activity over 27 days of CO_2 re-feeding, consistent with previous studies (Vyrides et al., 2018), where a single addition of ZVI sustained CH_4 production over two CO_2 re-feedings for 67 days. As indicated by X-RD patterns, the initially high concentration of ZVI (100 gr L^{-1}) was not fully oxidized to siderite, thus retaining part of its activity. Future studies should investigate the conversion of oxidized ZVI (mainly siderite) back to ZVI to enhance sustainability, an area where limited research exists. For instance, Jin et al. (2011) regenerated oxidized $Fe(OH)_3$ to ZVI using glycerin at 280 °C in the presence of NaOH. Other studies (Jin et al., 2014; Steinfeld, 2002) proposed using concentrated solar energy for the reduction of oxidized metals (ZnO) to native metals (Zn^0). The synthesis of nano-ZVI from iron ions using plant-derived polyphenols or agro-waste under ambient conditions has also been explored as a cost-effective and sustainable method (Stefaniuk et al., 2016; Herlekar et al., 2014; Hoag et al., 2009). However, Mystrioti et al. (2015) noted that the synthesis of nano-ZVI from plant or biomass extracts can be limited due to the formation of mixtures of other iron compounds, such as iron oxides or iron hydroxides. Another cost-reduction strategy could involve using scrap ZVI, which is cheaper than new ZVI and has been shown to enhance methane production in laboratory anaerobic bioreactors for waste treatment (Wang et al., 2017; Zhen et al., 2015).

Using ZVI in an anaerobic system also offers advantages for H_2 solubilization. Unlike power-to-gas systems, where H_2 must cross the gas-liquid interface to become available to microorganisms, ZVI naturally releases H_2 within the liquid phase (Maegaard et al., 2019; Angelidaki et al., 2018; Tirunehe and Norddahl, 2016). Additionally, anaerobic microorganisms can form biofilms on ZVI or attach to it (Philips et al., 2018), enhancing H_2 utilization efficiency compared to power-to-gas systems. It is suggested that Fe^0 corrosion under microbial anaerobic conditions is hydrogen-dependent, possibly due to extracellular components such as hydrogenase enzymes and low H_2 concentrations maintained by cells attached to Fe^0 (Philips et al., 2018). In this study, a low H_2 composition in the system's headspace correlated with high acetic acid concentrations,

likely due to H_2 and CO_2 utilization by homoacetogens. Other researchers have also reported that anaerobic microorganisms might directly utilize electrons from ZVI to generate acetic acid from CO_2 (Kato, 2016), although a detailed understanding of the extracellular electron mechanisms of acetogens remains lacking (Kato, 2016; Philips et al., 2018).

Notably, strategies for long-term methanogenesis inhibition should be established to improve efficiency and scale up such systems (ZVI, AnGrSL, and CO_2 as the sole carbon source). Targeting other products like butyric acid or ethanol, which have a higher value than acetic acid (Jiang et al., 2019), could also increase profitability. Additionally, comparing the proposed system's performance and cost with systems providing H_2 externally to anaerobic biomass and/or using microbial electrosynthesis could help evaluate the strengths and limitations of this metal-bioprocess approach.

3.2.9 Conclusions of Experimental Set-Up 2

Based on the experimental results, it is clear that CO_2 can be effectively utilized in a system containing AnGrSL and ZVI to produce acetic acid and siderite when methanogenesis inhibition strategies are implemented.

Applying a low pH to an AnGrSL and ZVI system proved ineffective for inhibiting methanogenesis due to the continuous increase in pH caused by the oxidation of ZVI. As a result, these systems exhibited 43% CH_4 in the headspace and produced only 21 mg L^{-1} of acetic acid after 15 days.

AnGrSL systems exposed to ZVI performed optimally at nearly neutral pH values (pH 6-6.5) for both methanogenesis inhibition methods tested (heat shock and BES). The system using heat-pretreated AnGrSL at pH 6-6.5 produced 1286 mg L^{-1} of acetic acid after two cycles and 12 days, whereas the system at pH 5 produced only 652 mg L^{-1} of acetic acid over the same period. The system exposed to 50 mM BES at pH 6-6.5 produced 2028 mg L^{-1} of acetic acid after two cycles and 27 days, while the system at pH 5 yielded only 671 mg L^{-1} of acetic acid in the same timeframe.

High concentrations of BES (50 mM) can inhibit methanogenesis and enhance acetogenesis; however, by comparing different low concentrations of BES (2, 4, 6, 8, and 10 mM), it is evident that by increasing the concentration of BES not only methanogenesis

inhibited but also VFA production by Acetogens affected. The maximum acetic acid concentration (1263 mg L^{-1}) was observed in systems exposed to 4 mM BES after two cycles and 22 days.

AnGrSL can adapt to high salinity. AnGrSL-ZVI systems exposed to 30 g L^{-1} of NaCl produced 414 mg L^{-1} of acetic acid after 17 days (with a total experimental duration of 24 days) and 28% CH_4 in the headspace, indicating partial methanogen inhibition. However, at elevated salinity (90 g L^{-1}), methanogenesis was fully inhibited, leading to the production of a more diverse range of VFAs due to increased H_2 pressure in the systems.

After the experimental period, the formation of siderite was observed in systems exposed to 50 mM BES and 60 g L^{-1} NaCl.

Heat-pretreated AnGrSL exposed to CO_2 and ZVI resulted in an increase of *Clostridium sensu stricto* to 65.9%. The same genus also increased when AnGrSL was exposed to BES and ZVI (~23%).

These observations and results from international literature suggest that there is no ideal methanogenesis inhibition strategy. Optimizing acetic acid production requires different inhibition methods or chemical concentrations depending on the system parameters, such as initial inoculum, temperature, and pH.

3.3 Experimental Set-Up 3: Bioconversion of Carbon Dioxide (CO_2) to Volatile Fatty Acids (VFAs) Using Anaerobic Granular Sludge (AnGrSL) With Magnesium Ribbon (Mg^0) in Methanogenesis-Inhibited Systems

This experimental set-up explores a novel metal bioprocess for CO_2 utilization in a system with AnGrSL for producing acetic acid and other volatile fatty acids (VFAs) under aquatic, ambient conditions in the presence of metal. In this process, CO_2 serves as an electron acceptor and the sole carbon source for the microbial consortium in systems (AnGrSL).

As explained in Sub-chapter 3.2, methanogenic bacteria present in AnGrSL dominated over acetogenic bacteria, which were also present in AnGrSL. These methanogens consumed reactants such as H_2 and CO_2 and utilized the acetic acid produced by acetogens in the systems, leading to CH_4 production, as depicted in Eq. 44 and Eq. 46. However, this study's primary aim is to produce VFAs, specifically acetic acid. Therefore, several strategies were investigated to inhibit methanogens, such as heat treatment and the use of chemicals, to enhance the reaction described by Eq. 45 by enriching the systems with acetogens. This approach follows the same concept as in Sub-chapter 3.2, with minimal alterations to the experimental configurations.

However, H_2 gas is required as an electron donor for the bioconversion of CO_2 to acetic acid by Acetogens. In these experiments, instead of using Fe^0 for H_2 production, magnesium ribbon (Mg^0) was used within the systems (*in-situ*). This substitution was made for the same reason outlined in Sub-chapter 3.2: to avoid the use of exogenous, dangerous, and explosive H_2 gas. Under aqueous anaerobic and carbonate conditions, Mg^0 oxidizes, generating magnesium hydroxide and H_2, as demonstrated in Eq. 47:

$$Mg_{(s)} + 2H_2O \rightarrow Mg(OH)_{2(aq)} + H_{2(g)} \ (\Delta G° = -295.1 \text{ kJ mol}^{-1}) \qquad \text{(Eq. 47)}$$

Due to its superior H_2 storage capacity — pure Mg^0 can theoretically store up to 7.6% by weight of H_2 — and the fact that it is a widely available and cost-effective resource, comprising approximately 2.35% of the Earth's crust and ranking as the eighth most abundant element (Ouyang et al., 2020), Mg^0 can be considered a feasible alternative to

Fe^0 for practical application in such microbial anaerobic systems. Additionally, it can be used at significantly lower concentrations than Fe^0.

3.3.1 Gas Composition Dynamics Across Various Strategies for Methanogenesis Inhibition

Fig. 3.39 illustrates the gas evolution (H_2, CH_4, and CO_2) over time in the headspace of all experimental setups containing AnGrSL and Mg^0, which were subjected to various conditions for inhibiting methanogenesis, as detailed in Table 2.4.

To inhibit methanogenesis, NaCl was tested at various concentrations as a cost-effective alternative method. As shown in Fig. 3.39 (A.), the highest amount of H_2 was observed in the system where AnGrSL was exposed to 90 g L^{-1} NaCl (System C3), reaching 74.3% in the headspace of the bottles on day 25. This high percentage of H_2 is attributed to the significant inhibition of H_2 utilizers (homoacetogens and hydrogenotrophic methanogens) at elevated salinity levels. The system with AnGrSL exposed to 70 g L^{-1} NaCl (System C2) exhibited a similar trend to the 90 g L^{-1} NaCl system but showed lower H_2 accumulation in the headspace of the bottles, with a maximum percentage of 66.3% on day 14.

In contrast, AnGrSL exposed to a lower NaCl concentration (50 g L^{-1}) (System C1) resulted in even lower H_2 accumulation identified in the headspace of the bottles, with a peak of only 14.6% on day 31. However, the system exposed to 50 g L^{-1} NaCl demonstrated higher CH_4 accumulation compared to the systems with 90 and 70 g L^{-1} NaCl. At high NaCl concentrations (70 and 90 g L^{-1}), CH_4 production remained below 4.8% and 0.7%, respectively, while at the lower NaCl concentration (50 g L^{-1}), CH_4 accumulation reached 25.2%. This is due to the reduced toxicity of sodium to homoacetogens and methanogens at lower NaCl concentrations [Fig. 3.39 (B.)].

High concentrations of NaCl not only inhibited methanogenesis but also acetogenesis, resulting in reduced H_2 consumption in the systems. This is consistent with the high absolute pressures observed in the bottles over time, as shown in the Suppl. Info. Fig. 3.27, and the low acetic acid accumulation quantified in the systems exposed to NaCl, as presented in Sub-chapter 3.3.2.

The system that utilizes thermally pretreated AnGrSL (System B) and the systems exposed to 4 mM BES (System A) demonstrated different H_2 patterns compared to those exposed to NaCl.

As shown in Fig. 3.39 (A.), these systems demonstrated high H_2 consumption. Initially, H_2 reached its maximum percentage in the headspace of both systems during cycle 2, between days 3 and 8. The system using thermally pretreated AnGrSL showed the highest H_2 accumulation, reaching 56.1% in the headspace of the bottle on day 7 of cycle 2, before drastically decreasing in cycles 3 and 4. In contrast, the systems exposed to 4 mM BES also showed maximum H_2 evolution during cycle 2, similar to the thermally pretreated AnGrSL system, but the amount of H_2 generated was eight times lower. From cycles 3 to 7, the percentage of H_2 in the headspace of the triplicates remained below 2%. These low percentages of H_2 can be attributed to its consumption, along with CO_2, by hydrogenotrophic methanogens and homoacetogens.

Regarding CH_4 [Fig. 3.39 (B.)], System B (Thermal inhibition) demonstrated an increase in CH_4 accumulation during cycles 5 to 7, coinciding with the complete decrease in H_2 and CO_2 consumption by both homoacetogens and methanogens. In contrast, System A (4 mM BES) exhibited a maximum CH_4 accumulation of 23% in the headspace of the bottles during cycle 3, which remained relatively stable at around 20% until the end of cycle 7. In the system where no methanogenesis inhibition strategy was applied (System D), the CH_4 accumulation increased significantly, reaching a maximum of 42.7% in the headspace on day 21.

Regarding the CO_2, a total of 7 cycles were conducted, with approximately 60 ml of CO_2 injected into each system for every cycle, amounting to a total of 420 ml of CO_2 used throughout the experiment for each system. As depicted in Fig. 3.39 (C.), CO_2 levels decreased across all systems, with the highest utilization occurring during cycle 3. Systems B (Thermal inhibition) and System A (4 mM BES) showed the greatest CO_2 utilization during the first 5 cycles. A similar pattern was observed in System D (No inhibition), where CO_2 utilization ranged from 100% to 71.6% until cycle 5 (Suppl. Info. Fig. 3.28).

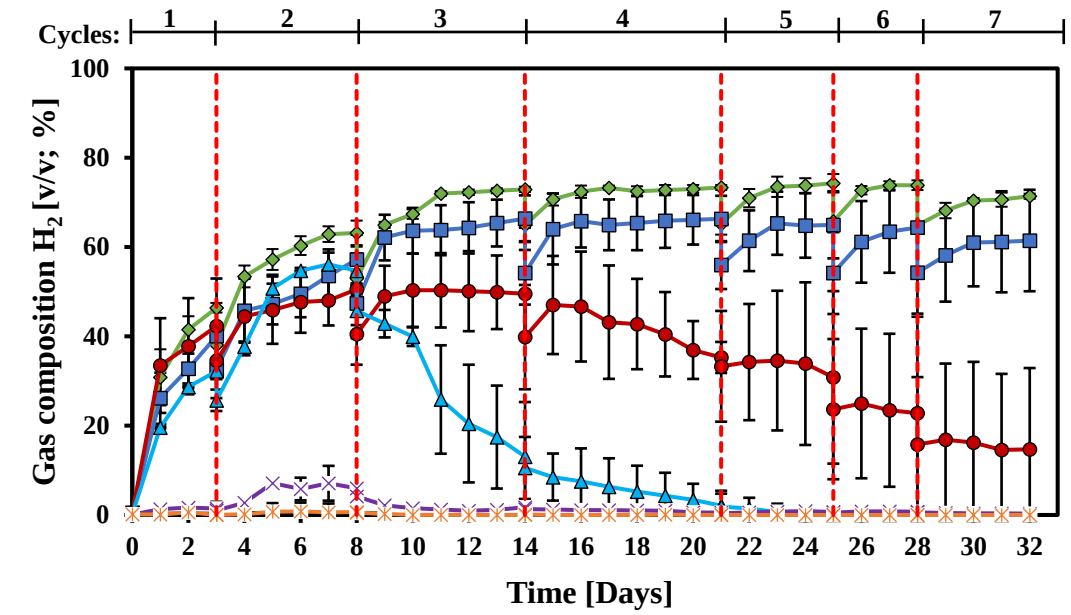
Cycles:
1
2
3
4
5
6
7
Gas composition H_2 [v/v; %]
Time [Days]

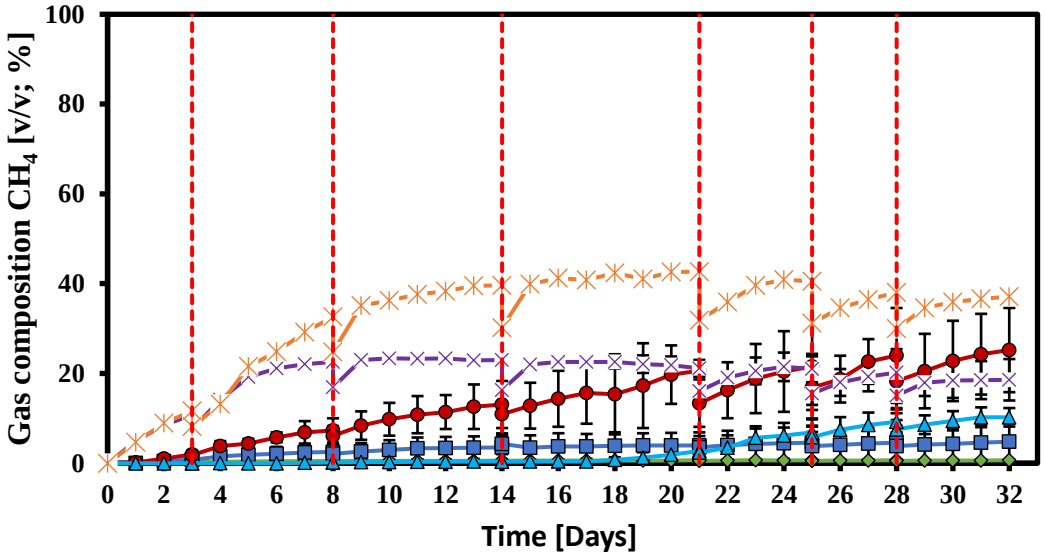
Gas composition CH_4 [v/v; %]
Time [Days]

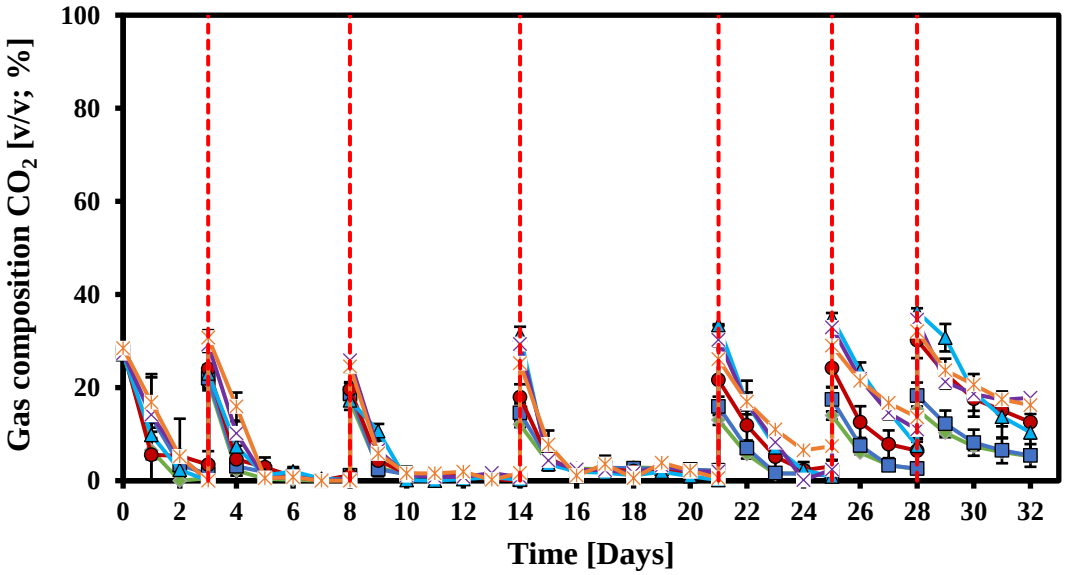
Gas composition CO_2 [v/v; %]
Time [Days]

Fig. 3.39: Changes in gas composition in the headspace of AnGrSL – Mg^0 systems exposed to various methanogenesis inhibition strategies. (A.): H_2 evolution and consumption, (B.):CH_4 production, (C.): CO_2 utilization.

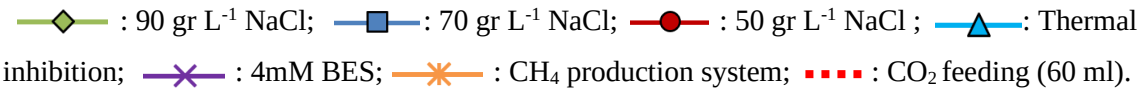

The reduction of CO_2 in the bottles was likely due to its diffusion from the gas phase into the liquid phase, where it was then utilized by homoacetogens and hydrogenotrophic methanogens. Additionally, a portion of the dissolved CO_2 and H^+ reacted with the Mg^0, which caused the pH to rise to around 8-9 (Suppl. Info. Fig. 3.29). As a result, the pH of the systems was monitored and adjusted to maintain a range of 6.5-7.5. During cycles 6 and 7, the rate of CO_2 absorption slowed (Suppl. Info. Fig. 3.28) compared to previous cycles due to the depletion of the reaction described in Eq. 46 and the maintenance of a neutral pH. In the control samples, where no Mg^0 was added, there was no significant change in CO_2 utilization (data not shown).

3.3.2 Production of Acetic Acid and Other VFAs in Systems Exposed to Various Methanogenesis Inhibition Strategies

As shown in Fig. 3.40, System B, which used thermally pretreated AnGrSL (at 95°C for 30 minutes) and was exposed to CO_2 and Mg^0, demonstrated the highest accumulation of acetic acid during cycle 7, producing approximately 2023 mg L^{-1}. In this system, the H_2 generated by Mg^0 increased in the bottles during the first 2 cycles, as illustrated in Fig. 3.39 (A.), indicating a phase of Homoacetogen enrichment. During the 3rd cycle (after 13 days), the system achieved its peak production rate of 235 mg L^{-1} per day, resulting in a total of 1537 mg L^{-1} of acetic acid. Between cycles 4 and 7, there was only a slight increase in acetic acid due to the consumption of H_2 by hydrogenotrophic methanogens, as discussed in Sub-chapter 3.3.3. Additionally, acetoclastic methanogens may have utilized some of the acetic acid generated by homoacetogens. The reduced acetic acid production during cycles 4 to 7 could also be attributed to decreased H_2 production by magnesium, likely due to partial passivation of the magnesium ribbon (Andronikou et al., 2022).

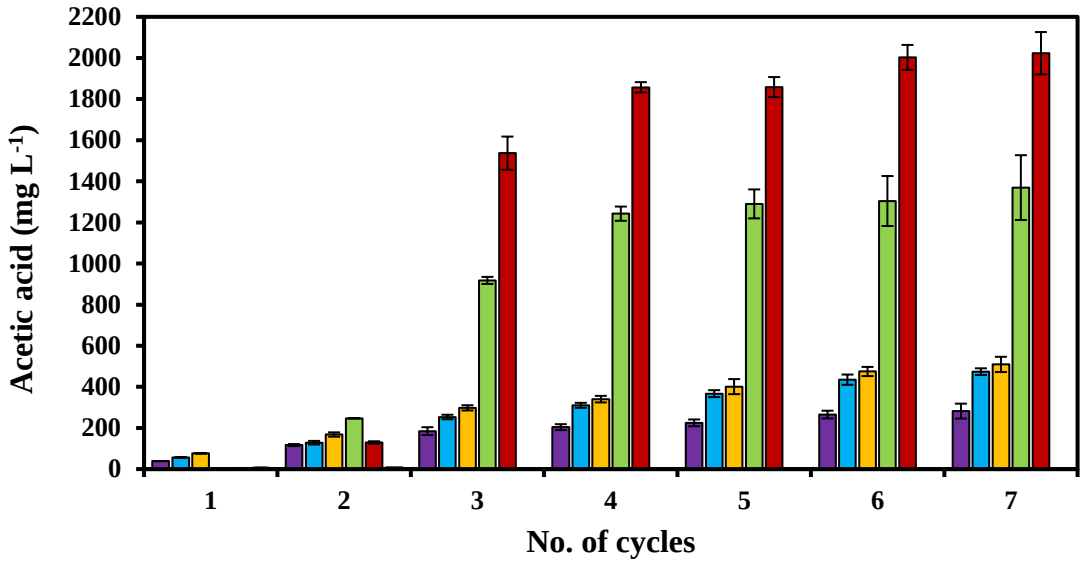

Fig. 3.40: Accumulation of acetic acid across all systems during cycles 1–7.

: 90 gr L^{-1} NaCl; : 70 gr L^{-1} NaCl; : 50 gr L^{-1} NaCl; : Thermal inhibition; : 4mM BES; : CH_4 production system.

In System A, where AnGrSL was exposed to CO_2, Mg^0, and 4 mM BES as an alternative approach for inhibiting methanogenesis and enhancing homoacetogens, the second-highest accumulation of acetic acid was observed, reaching approximately 1369 mg L^{-1} during cycle 7 (Fig. 3.40). This system achieved its peak production rate of 111 mg L^{-1} per day (totaling 918 mg L^{-1} of acetic acid) during the 3rd cycle (after 14 days). Following the 3rd cycle, the pattern of acetic acid accumulation resembled that of System B (Thermal inhibition), with a gradual increase followed by relative stability until the conclusion of the experiment. The factors contributing to the stability of acetic acid levels between cycles 4 and 7 are similar to those described for System B (Thermal inhibition).

Fig. 3.41, which presents data on other volatile fatty acids, indicates that in System B (Thermal inhibition), formic acid, identified during cycle 2, decreased during cycles 3 to 7. Concurrently, there was a notable appearance of isobutyric acid and an increase in propionic acid. A similar trend in the reduction of formic acid over the cycles was observed in System A (4 mM BES). By cycle 7, formic acid levels had dropped to zero,

while isobutyric acid and butyric acid were detected during cycles 5 to 7 and 6 to 7, respectively.

In contrast, the control samples of system B and system A (Table 2.4), where Mg^0 was not used, produced approximately 450 mg L^{-1} and 83 mg L^{-1} of acetic acid, respectively, by the end of cycle 7. Consequently, the net acetic acid production in System B (Thermal inhibition) and System A (4 mM BES) was approximately 1573 mg L^{-1} and 1287 mg L^{-1}, respectively, by the end of the experiment on Day 32.

The systems employing NaCl at concentrations of 50 g L^{-1}, 70 g L^{-1}, and 90 g L^{-1} exhibited varying patterns in acetic acid production. The highest accumulation of acetic acid was observed in System C1, which used 50 g L^{-1} NaCl, reaching 509 mg L^{-1} by cycle 7. This was followed by System C2, which used 70 g L^{-1} NaCl, with an accumulation of approximately 474 mg L^{-1}, and System C3, which used 90 g L^{-1} NaCl, yielding about 282 mg L^{-1} by the end of cycle 7 (Fig. 3.40).

Regarding the production of formic, propionic, isobutyric, and butyric acids (Fig.3.41), systems exposed to 90 g L^{-1} and 70 g L^{-1} NaCl showed a similar trend in the production of these carboxylic acids. Formic acid was predominantly produced at these concentrations, followed by propionic acid, with lower concentrations of isobutyric and butyric acids. In contrast, at 50 g L^{-1} NaCl, a similar pattern was observed, albeit with reduced formic acid levels, likely due to decreased inhibition of hydrogenotrophic methanogens under these conditions. The elevated levels of formic acid could be attributed to the activity of formate hydrogen lyase, an enzyme complex associated with the membrane that converts H_2 and soluble CO_2 into formic acid (Stams and Plugge, 2009; Thiele and Zeikus, 1988), as described in Eq. 48. This reversible reaction is also influenced by pH and temperature (Voolapalli and Stuckey, 2001).

$$H_2 + CO_2 \leftrightarrow HCOO^- + H^+ \ (\Delta G^0 = -1.3 \text{ kJ mol}^{-1}) \qquad \text{(Eq. 48)}$$

Additionally, some formic acid may be produced through abiotic reactions involving magnesium, bicarbonate, and water. Recent research by Rawool et al. (2021) demonstrated that formic acid can also form under abiotic conditions in systems containing magnesium nanoparticles, CO_2, and water. In the present study, elevated

salinity levels were observed to inhibit the activity of homoacetogens and hydrogenotrophic methanogens that metabolize H_2 and CO_2, as well as certain species of hydrogenotrophic methanogens that utilize formic acid. Consequently, formic acid accumulation was observed. However, when methane levels increased (after the 3rd cycle), formic acid concentrations decreased, suggesting its utilization by hydrogenotrophic methanogens.

The control system, which comprised only AnGrSL without Mg^0 and utilized 70 g L^{-1} NaCl and CO_2, produced 161 mg L^{-1} of acetic acid.

In System D, which did not implement any methanogenesis inhibition strategies and consisted of AnGrSL and Mg^0, acetic acid production was minimal and was only detected during cycle 2. This low level of acetic acid can be attributed to its rapid consumption by acetoclastic methanogens for CH_4 production. Additionally, H_2 was used and converted into CH_4 along with CO_2 by hydrogenotrophic methanogens, which compete with homoacetogens. This trend is consistent with Fig. 3.39 (A.), which shows a marked decrease in H_2, dropping to near-zero levels during cycles 3 through 7. Regarding the other volatile fatty acids, propionic acid was the predominant compound, reaching a maximum concentration of approximately 61 mg L^{-1} by cycle 7.

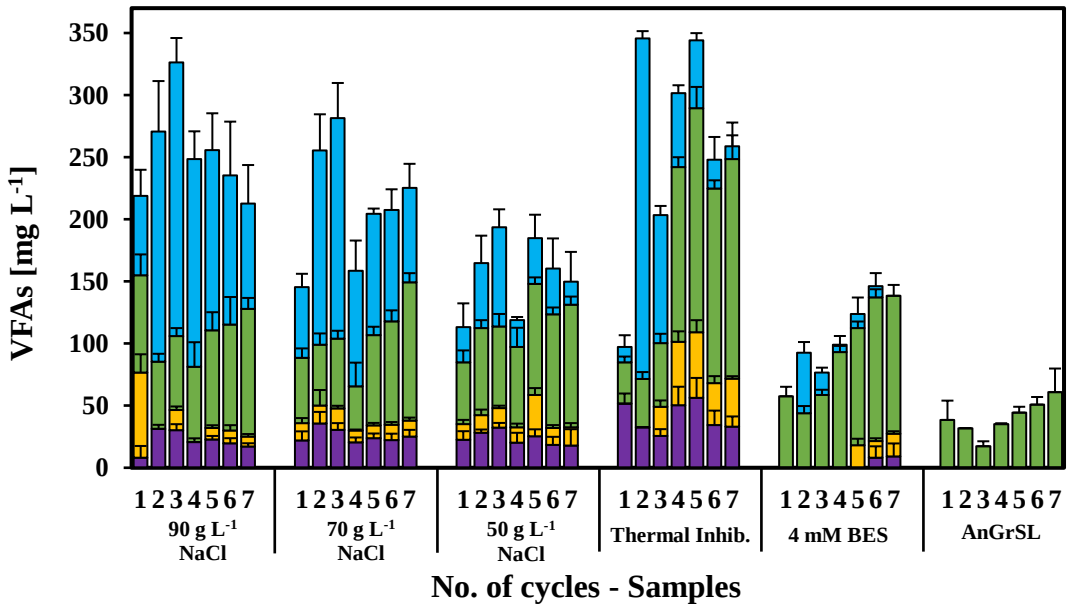

Fig. 3.41: Accumulations of formic, propionic, isobutyric, and butyric acid during cycles 1 to 7 for all systems.

: Formic acid; : Propionic acid; : Isobutyric acid; : Butyric acid.

3.3.3 Next-generation Sequencing and Microbial Population Analysis

Fig. 3.42 presents the bacterial microbial profile at the phylum and genus levels at the end of cycle 7. The predominant phyla identified in the systems included *Actinobacteria, Bacteroidetes, Chloroflexi, Firmicutes, Nitrospirae, Patescibacteria, Proteobacteria, Spirochaetes, Synergistetes,* and *TA06*. At the genus level, *Desulfobulbus, Syntrophobacter, and Syntrophorhabdus* were notably present in System B (Thermal inhibition) and System A (4 mM BES). The absence of homoacetogenic bacteria at the genus level can be attributed to the timing of DNA extractions, which were conducted at the end of the experiments (cycle 7), by which time hydrogenotrophic methanogens had become more prevalent and homoacetogens likely decreased due to the reduced availability of reactants (H_2 and CO_2). According to Tsapekos et al. (2022), hydrogenotrophic methanogens are the primary consumers of H_2 in systems containing homoacetogens, which explains the predominance of syntrophic bacteria. This finding correlates with the gas composition results [Fig. 3.39 (B.)], where CH_4 accumulations were 10.4% and 18.6% in the headspace of System B (Thermal inhibition) and System A (4 mM BES), respectively, at cycle 7, and acetic acid reached its peak concentration at cycle 3 before slightly increasing until cycle 7.

Regarding the archaeal communities (Fig. 3.43), Euryarchaeota appeared to be the most diverse phylum across all systems. At the genus level, *Methanolinea*, a typical hydrogenotrophic methanogen, was the most dominant in System B (Thermal inhibition) and System A (4 mM BES), accounting for 67% and 70% of the archaea, respectively. Franchi et al. (2020) indicated that *Methanolinea* can utilize formic acid, along with H_2 and CO_2, to produce CH_4. This finding is consistent with the data presented in Fig. 3.39 (A.), which demonstrated a significant decrease in H_2 levels in both System B (Thermal Inhibition) and System A (4 mM BES). *Methanolinea* also dominated in Systems where AnGrSL was exposed to various NaCl concentrations (90, 70, and 50 g L^{-1}) and Mg^0. It has been noted that high Na+ concentrations have a more significant inhibitory effect on acetoclastic methanogens compared to hydrogenotrophic methanogens (Charalambous et al., 2020).

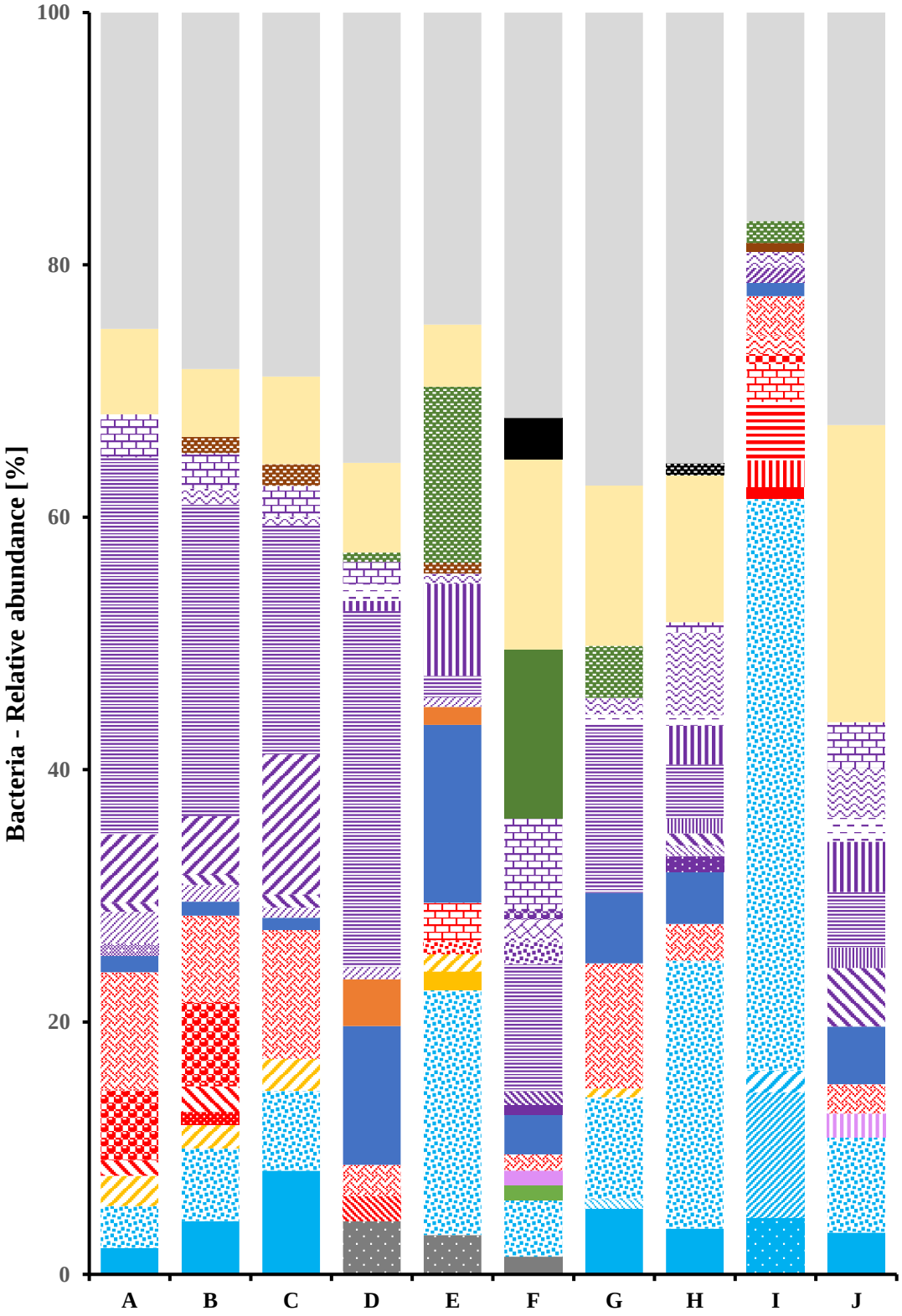
Bacteria - Relative abundance [%]
100
80
60
40
20
0
A
B
C
D
E
F
G
H
I
J

Fig. 3.42: Bacteria relative abundance [%] at phylum and genera level, at the end of the experimental duration.

A: 50 g L^{-1} NaCl; **B:** 70 g L^{-1} NaCl; **C:** 90 g L^{-1} NaCl; **D:** 4 mM BES; **E:** Thermal inhibition;

F: Methane production system (No inhibition); **G:** Control - 70 g L^{-1} NaCl; **H:** Control – 4 mM BES; **I:** Control – Thermal inhibition; **J:** Control – AnGrSL.

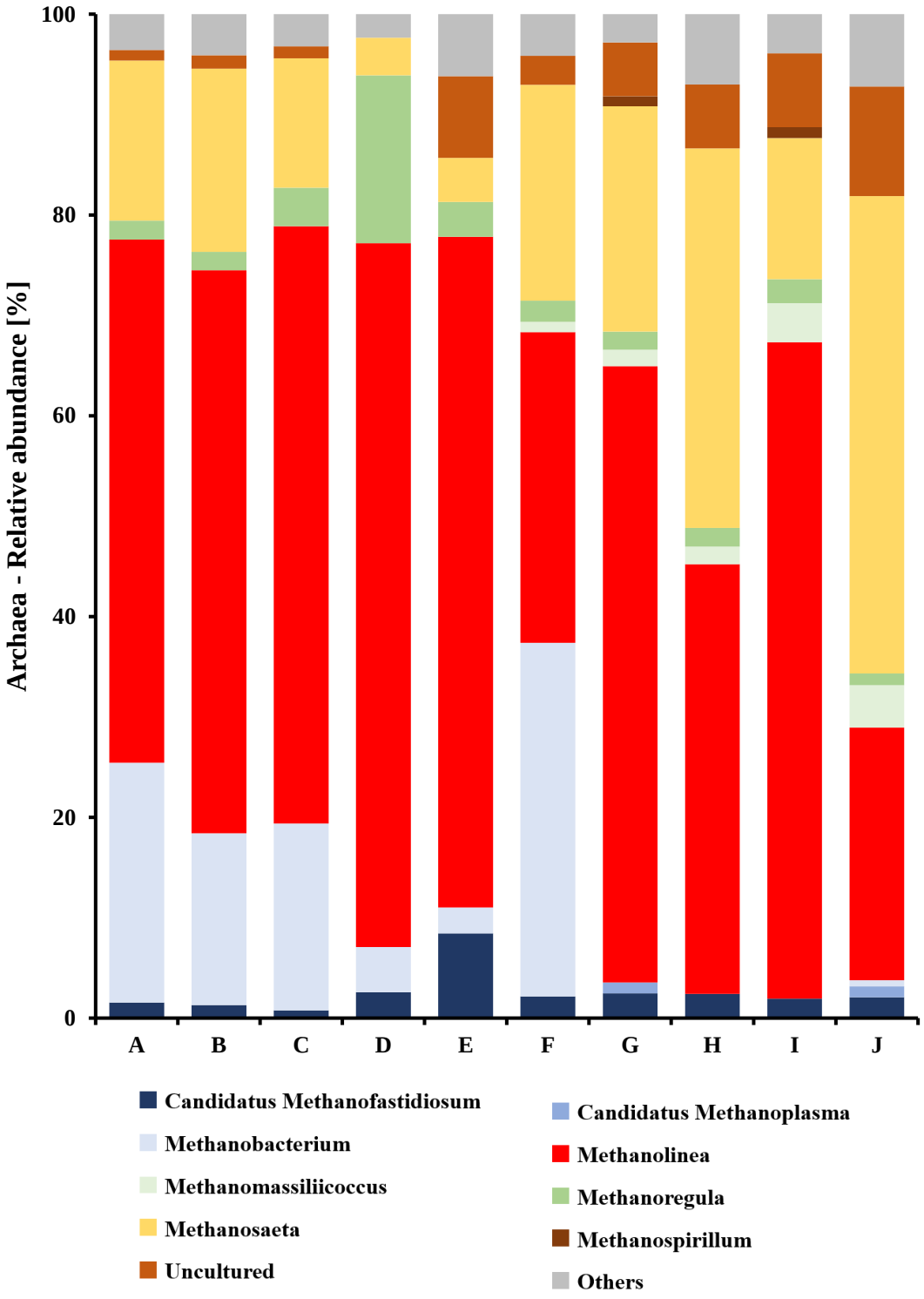

Fig. 3.43: Archaea relative abundance [%] at genera level, at the end of the experimental duration.

A: 50 g L^{-1} NaCl; **B:** 70 g L^{-1} NaCl; **C:** 90 g L^{-1} NaCl; **D:** 4 mM BES; **E:** Thermal inhibition;

F: Methane production system (No inhibition); **G:** Control - 70 g L^{-1} NaCl; **H:** Control – 4 mM BES; **I:** Control – Thermal inhibition; **J:** Control – AnGrSL.

3.3.4 Discussion of Experimental Set-Up 3

This study introduces a novel and sustainable approach for utilizing CO_2 (as the sole carbon source) for the production of VFAs, specifically acetic acid, using a mixed culture (AnGrSL) and magnesium ribbon (Mg^0) under ambient conditions. The metal bioprocess is described by Eq. 49:

$4Mg^0 + 6HCO_3^- + 6H^+ \rightarrow CH_3COOH + 4MgCO_3 + 4H_2O$ ($\Delta G° = -466.65$ kJ mol^{-1}) (Eq. 49)

In this hybrid metal-biological process, CO_2 is converted to acetic acid, with H_2 being generated *in-situ* by the abiotic reaction of Mg^0, eliminating the need for external H_2 addition. The use of magnesium ribbon simplifies handling and transportation compared to the addition of H_2 gas from an external source. Additionally, H_2 produced *in-situ* by Mg^0 is likely utilized more rapidly by microbes than H_2 introduced from an external source. Furthermore, this process offers several advantages over microbial electrolysis systems (MES) as it does not require costly external materials or equipment such as electrodes or ion exchange membranes. In single-chamber MES without a proton exchange membrane, O_2 produced at the anode can inhibit oxygen-sensitive homoacetogens, thereby reducing the overall efficiency of the process (Georgiou et al., 2022; Gidding et al., 2015).

The maximum net accumulation of acetic acid was observed in the system utilizing thermally pretreated AnGrSL, reaching up to 1573 mg L^{-1} by cycle 7 (day 32), followed by AnGrSL exposed to 4 mM BES, which reached up to 1287 mg L^{-1} by cycle 7 (day 32). This was achieved using only 4 g L^{-1} of Mg^0, which is significantly less than the zero-valent iron (ZVI) amounts (50–100 g L^{-1}) used by Bayar et al. 2022 and Samanides et al. 2020.

Modestra et al. (2020) demonstrated that pretreatment of anaerobic sludge with a combination of acid and heat resulted in the highest acetic acid production compared to the control in anaerobic reactors fed with a commercial H_2 and CO_2 gas mixture in an 80:20 ratio (Table 3.15).

Table 3.15: An overview of acetic acid production using ZVI or H_2 and CO_2.

Carbon source - Electron donor	Microbial Inoculum	Methanogenesis inhibition method	Acetic acid production (Max)	Ref.
100 % CO_2 100 g L^{-1} ZVI	Anaerobic granular sludge	2-bromoethanosulfonate (50 mM BES) Heat-shock (95°C for 30 min)	**Acetic acid:** **BES** → 1st batch: 1736 mg L^{-1} (15 days) - *Control: ≈0 mg L^{-1}* **BES** → 2nd batch: 2020 mg L^{-1} (12 days) - *Control: 51 mg L^{-1}* **Heat** →1290 mg L^{-1} (12 days) - *Control: 395 mg L^{-1}*	Samanides et al., 2020
20% CO_2 80% H_2	Homoacetogen enriched wastewater	Heat-shock (80-90 °C for 1-2 hours) and Acid-shock (H_3PO_4- pH 3)	**Acetic acid:** **H+A** → Stage 1: 543 mg L^{-1} (2 days) - *Control: 241 mg L^{-1}* **H+A** → Stage 2: 1234 mg L^{-1} (3days) - *Control: 1013 mg L^{-1}*	Modestra et al., 2020
20% CO_2 80% H_2	Anaerobic granular sludge	Heat-shock (90°C for 15 min)	**Acetic acid:** **Heat** → 1783mg L^{-1} (10 days) - *Control: No*	He et al., 2021
0.5 bar CO_2 75 g L^{-1} ZVI	*Clostridium aceticum* (DSM 1496)	Pure culture	**Acetic acid:** 2113 mg L^{-1} (36 days) *Control: No*	Bayar et al. 2022
420 ml CO_2 4 g L^{-1} Mg^0	Anaerobic granular sludge	2-bromoethanosulfonate (4 mM BES) Heat-shock (95°C for 30 min)	**Acetic acid:** **BES** → 1369 mg L^{-1} (32 days) **Max Prod. Rate: 111 mg L^{-1} day^{-1}** (14 days) *Control: 83 mg L^{-1}* **Heat** → 2023 mg L^{-1} (32 days) **Max Prod. Rate: 235 mg L^{-1} day^{-1}** (14 days) *Control: 450 mg L^{-1}*	Present study

In this study, using NaCl to inhibit methanogens resulted in lower acetic acid productivity compared to the other two inhibition methods (thermal shock and BES inhibitor). However, it led to the production of a wider variety of VFAs, such as formic acid, as shown in Fig. 3.41. One potential solution to enhance acetic acid production under these conditions is to employ halophilic homoacetogens, which can perform better in high-salinity environments.

He et al. (2021) used AnGrSL as an inoculum for ethanol and VFA production from H_2/CO_2 at various temperatures (18, 25, and 30 ºC). To inhibit methanogenesis, the AnGrSL was thermally treated at 90 ºC for 15 minutes. The highest acetic acid production was observed at 1783 mg L^{-1} (29.7 mM) after 240 h at 25 ºC (Table 3.15).

Samanides et al. (2020) employed ZVI (100 g L^{-1}) in systems (*in-situ*) and introduced CO_2 gas within to produce VFAs on a batch laboratory scale. AnGrSL was used as the inoculum, and several strategies were implemented to suppress methanogens: a) heat pre-treatment, b) acid pre-treatment, c) NaCl (30, 60, 90 g L^{-1}), and d) BES (1-10 mM, 50 mM). The highest acetic acid concentrations after 12 days were achieved using 50 mM of BES and thermal shock pre-treated AnGrSL, reaching 2020 mg L^{-1} and 1290 mg L^{-1}, respectively (Table 3.15).

Recently, Bayar et al. (2022) used pure cultures of *Clostridium aceticum* and *Clostridium carboxidivorans* instead of a microbial consortium (AnGrSL) to avoid the need for methanogenesis inhibition pretreatments. Various concentrations of ZVI (0, 25, 50, 75 g L^{-1}) were used as an H_2 source in the presence of CO_2 gas in batch experiments. The *Clostridium aceticum* strain achieved maximum acetic acid accumulation (2113 mg L^{-1}) after 36 days (Table 3.15). Using pure strains instead of pretreated mixed cultures combined offers another approach to promote homoacetogenesis. However, maintaining sterile conditions and preventing contamination remain significant challenges with this method.

Andronikou et al. (2022) recently explored using Mg^0 and AnGrSL for converting CO_2 to CH_4. According to Chen et al. (2022), VFAs have a higher market value in the EU (1800–2500 €/ton) compared to CH_4 (1.8 €/m^3). Additionally, acetic acid has broader potential applications than CH_4 and can serve as a precursor for the microbial production of other high-value products (Pandey et al., 2022). In the present study, starting with

AnGrSL, methanogens were inhibited, and the process was directed towards homoacetogenesis to produce acetic acid (Eq. 49). For an effective CO_2 bioconversion process, it is essential to consider several factors, including pH, CO_2 addition, Mg^0 dosage, potential uses of magnesium carbonate, and the type of initial inoculum.

3.3.5 Conclusions of Experimental Set-Up 3

This study presents a novel and effective method for producing acetic acid through the use of Homoacetogens, employing magnesium ribbon *in-situ* as a H_2 source and CO_2 as the sole carbon source in a system containing AnGrSL. The *in-situ* use of Mg^0 increased the availability of H_2 as an electron donor, facilitating the utilization of CO_2 by homoacetogens to synthesize VFAs under ambient conditions. Selective acetate production by homoacetogen-enriched sludge was achieved by inhibiting methanogenesis through various strategies, including the application of different NaCl concentrations (50, 70, and 90 g L^{-1}), the use of a specific inhibitor (4 mM BES), and heat-shock pre-treatment.

Among the three methanogenesis inhibition methods tested, heat pre-treatment proved to be the most effective, yielding 2023 mg L^{-1} of acetic acid by the end of the experiment (Cycle 7, Day 32) with a maximum production rate of 235 mg L^{-1} day^{-1} observed during the third cycle (Day 14). This was followed by the system using the BES inhibitor, which produced 1369 mg L^{-1} of acetic acid (Cycle 7, Day 32) and reached a peak production rate of 111 mg L^{-1} day^{-1} in the third cycle (Day 14). Although all systems utilizing Mg^0 showed significant improvements in acetic acid production compared to the control samples, the use of NaCl inhibited both methanogenesis and acetogenesis due to the presence of sodium (Na^+) ions. Among the NaCl concentrations tested, 50 g L^{-1} NaCl was the most effective, resulting in the production of 509 mg L^{-1} of acetic acid and 25% CH_4 by the end of Cycle 7 (Day 32).

CH_4 accumulation was observed in all systems at the conclusion of the seventh cycle (Day 32), likely due to the enrichment of the system with *Methanolinea* (52%–70%), a typical hydrogenotrophic methanogen.

3.4 Experimental Set-Up 4: Production of Acetic Acid and Other VFAs by Seven Different Biological Inoculum Systems Exposed to ZVI and BES.

As highlighted in the Introduction (Chapter 1) and Sub-chapter 3.3, many studies have focused on microbial electrosynthesis systems (MES) or the direct use of H_2 gas in systems inoculated with mixed anaerobic cultures for the bioconversion of CO_2 into other products. However, limited research has explored using ZVI (Fe^0) within these systems as a method for *in-situ* H_2 supply. The studies that do address MES systems or configurations using externally supplied H_2 gas often rely on a narrow range of inocula, primarily obtained from anaerobic bioreactors or digesters that treat wastewater, or they use pure microbial strains, as shown previously in Table 3.15.

This chapter investigates acetic acid production in systems utilizing seven different inocula separately: river sludge, wetland sludge, anaerobic granular sludge, compost sludge, anaerobic sludge from wastewater treatment plants (WWTP), activated sludge, and drilling cuttings sludge. Each system independently employed these microbial inocula, which were exposed to ZVI (Fe^0). To inhibit methanogenesis, 4 mM of BES was used, as depicted in Eq. 50, in order to enhance the biological acetogenesis reaction, as described in Eq. 51, by increasing the population of acetogens within the systems. The concentration of BES was selected based on the findings presented in Sub-chapter 3.2.

$$4H_2 + HCO_3^- + H^+ \rightarrow CH_4 + 3H_2O \ (\Delta G^\circ = -135.5 \text{ kJ mol}^{-1}) \quad \text{(Eq. 50)}$$

$$4H_2 + 2HCO_3^- + H^+ \rightarrow CH_3COO^- + 2H_2O \ (\Delta G^\circ = -104.6 \text{ kJ mol}^{-1}) \quad \text{(Eq. 51)}$$

The experimental approach outlined in this chapter broadens the limited range of inocula previously examined for acetic acid production under mild aquatic anaerobic conditions. Over a 112-day period, the study evaluated the effectiveness of these inocula in utilizing CO_2 and producing acetic acid, exploring different CO_2 feeding strategies—frequent CO_2 feeding, single CO_2 feeding, and high-pressure CO_2 feeding—to optimize the process. Additionally, the experimental methodology assessed the impact of these CO_2 feeding strategies on H^2 production by ZVI (Fe^0). Additional batch experiments were conducted to assess the contributions of suspended microorganisms from the primary experiments

to acetic acid production. These experiments also aimed to evaluate the acetic acid production potential of microorganisms both attached to and detached from ZVI.

3.4.1 Production of Acetic Acid and Other VFAs in Systems Exposed to Zero-Valent Iron and Biological Inocula

Acetic acid was the predominant VFA produced across all seven inocula throughout the experiments. Fig. 3.44 (A. and B.) shows acetic acid production over 112 days in systems inoculated separately with different sludges and exposed to ZVI and BES, as well as the acetic acid production of control systems, respectively. The control systems consisted of the same inocula as in the experimental setup, but without adding ZVI. Notably, the River-SL inoculum achieved the highest net concentration of acetic acid, reaching 5238 mg L^{-1} by the end of cycle 1, after 56 days. The Wetland-SL inoculum followed with the second-highest net acetic acid concentration, peaking at 4620 mg L^{-1} within the same period. In contrast, the Anaer.-SL and AnGr-SL systems exhibited the lowest net acetic acid concentrations, recording 3026 mg L^{-1} and 2592 mg L^{-1}, respectively, over the 56 days of cycle 1. The systems inoculated with Dr.Cuts-SL, Activ.-SL, and Comp.-SL had net acetic acid concentrations of 4070 mg L^{-1}, 3910 mg L^{-1}, and 3498 mg L^{-1}, respectively. The River-SL inoculum exhibited the highest maximum rate of acetic acid production at 300 mg L^{-1} per day, followed by Wetland-SL at 269 mg L^{-1} per day at the beginning of the first cycle. Among the other sludges, AnGr-SL had the highest maximum production rate, recorded at 150 mg L^{-1} per day.

Control systems (no ZVI added) demonstrated a significantly lower concentration of acetic acid, as depicted in Fig. 3.44 (B.). During the first 56 days of cycle 1, the system inoculated with Activ.-SL produced approximately 578 mg L^{-1} of acetic acid. This was followed by the Anaer.-SL, AnGr-SL, and Comp.-SL systems, which generated between 280 and 312 mg L^{-1}. The system inoculated with Dr.Cuts-SL yielded around 131 mg L^{-1}. Meanwhile, the systems containing River-SL and Wetland-SL produced no detectable acetic acid. These findings can be attributed to the hydrolysis of solid organic compounds present in the inocula, which, under anaerobic conditions, leads to the production of acetic acid and CH_4 as shown in the Suppl. Info. Fig. 3.30 (C.)

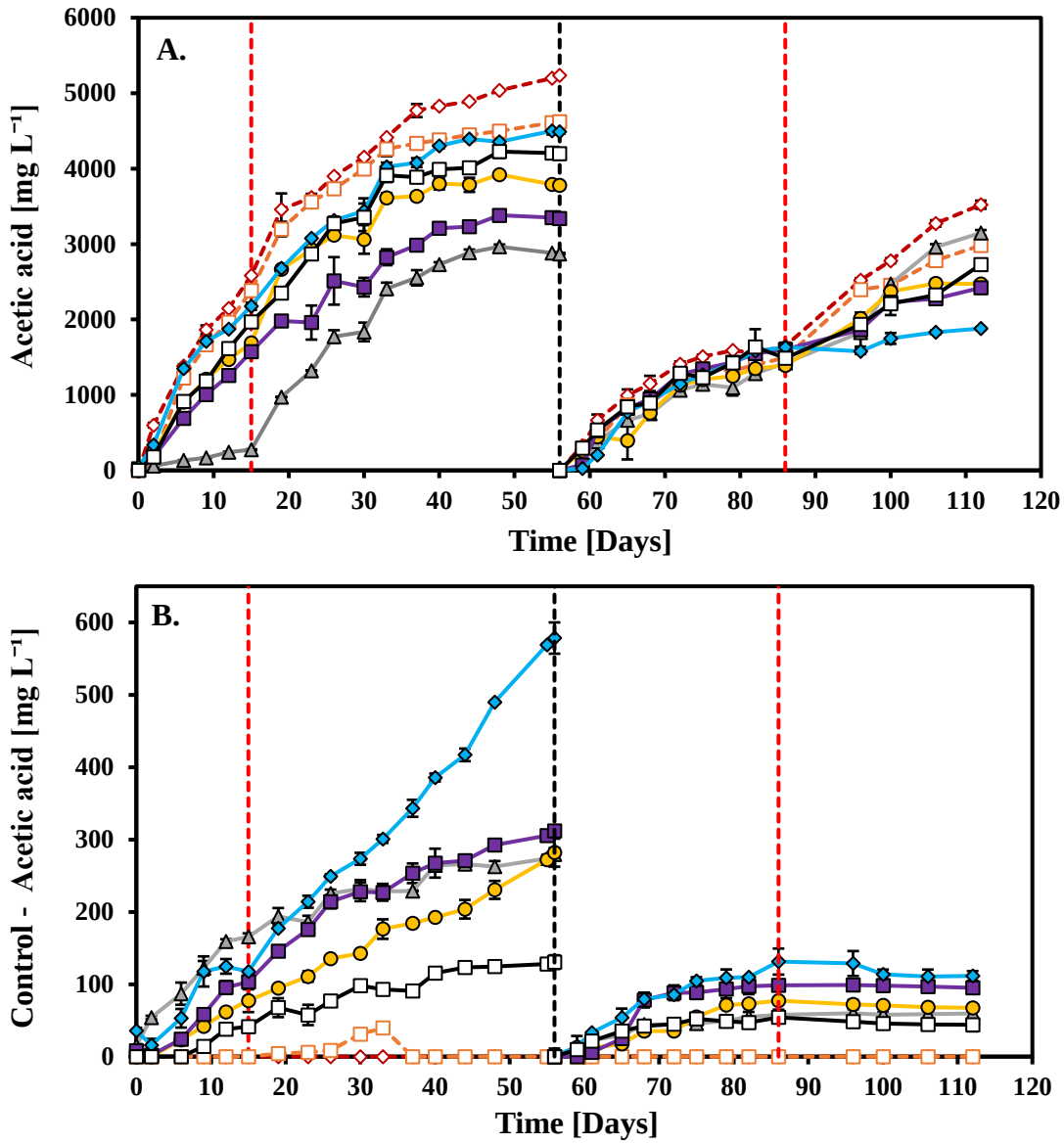

Fig. 3.44: Accumulation of Acetic Acid During Cycles 1 and 2 in Seven Inoculum Systems. (A.) Acetic acid production in all systems exposed to ZVI and BES, (B.) Acetic acid production in control systems without ZVI.

: River-SL; : Wetland-SL; : AnGr.-SL; : Comp.-SL;

: Anaer.-SL; : Actv.-SL; :Dr.Cuts-SL.

: CO_2 flashing / CO_2 feeding; : CO_2 flashing / CO_2 feeding.

All systems, which were inoculated with seven different sludges separately and exposed to ZVI, followed by a CO_2 flushing on day 0 of cycle 1, showed a significant peak in H_2 accumulation in the headspace of the bottles by day 2. These accumulations gradually decreased until the start of the next sub-cycle. The systems inoculated with River-SL, Wetland-SL, and Activ.-SL exhibited higher H_2 levels, ranging from 79% to 94%, as pH increased, as indicated in Suppl. Info. Fig. 3.31. After the second CO_2 flushing on day 15, a similar trend in peak H_2 levels was observed in the systems' headspace by day 19, although at reduced levels due to H_2 consumption by the predominant Homoacetogens [Fig. 3.45 (B.)]. Additionally, on day 15, 6 mM of BES was added to the AnGr-SL system to inhibit methanogenesis. The dense structure of anaerobic granular sludge likely protected the methanogens located in the core of AnGr-SL from BES inhibition, unlike other biomass types. This addition of BES effectively suppressed methanogen activity, resulting in CH_4 production of less than 1% until the end of cycle 1. Similarly, CH_4 levels below 1% were observed in the headspace of the River-SL and Activ.-SL systems at the end of cycle 1 (day 56). In contrast, the Wetland-SL, Anaer.-SL, Comp.-SL, and Dr.Cuts-SL systems exhibited CH_4 levels of 14%, 9%, 7%, and 2%, respectively [Fig. 3.45(A.)].

During cycle 2, H_2 produced by ZVI (Fe^0) in the systems after CO_2 feeding on day 56 and between days 56-86 was observed to be lower than the H_2 accumulations observed in the systems after CO_2 feeding on day 56 than that recorded H_2 accumulations after CO_2 flashing and CO_2 feeding on day 86 and between days 86-11. This difference was due to CO_2 flushing and pressurized CO_2 feeding on day 86, compared to N_2 flushing on day 56. Between days 56 and 86, acetic acid concentrations were lower than in cycle 1, primarily because of the reduced CO_2 gas concentration in the systems and the partial passivation of ZVI over time, as noted by Constantinou et al. (2023). After the introduction of pressurized CO_2 on day 86, reaching nearly 2 bar (relative pressure), an increase in acetic acid production was observed, which continued until the end of the experiment on day 112. Similar to cycle 1, the system inoculated with River-SL showed the highest net acetic acid concentration at the end of cycle 2 (day 112), reaching 3522 mg L^{-1}.

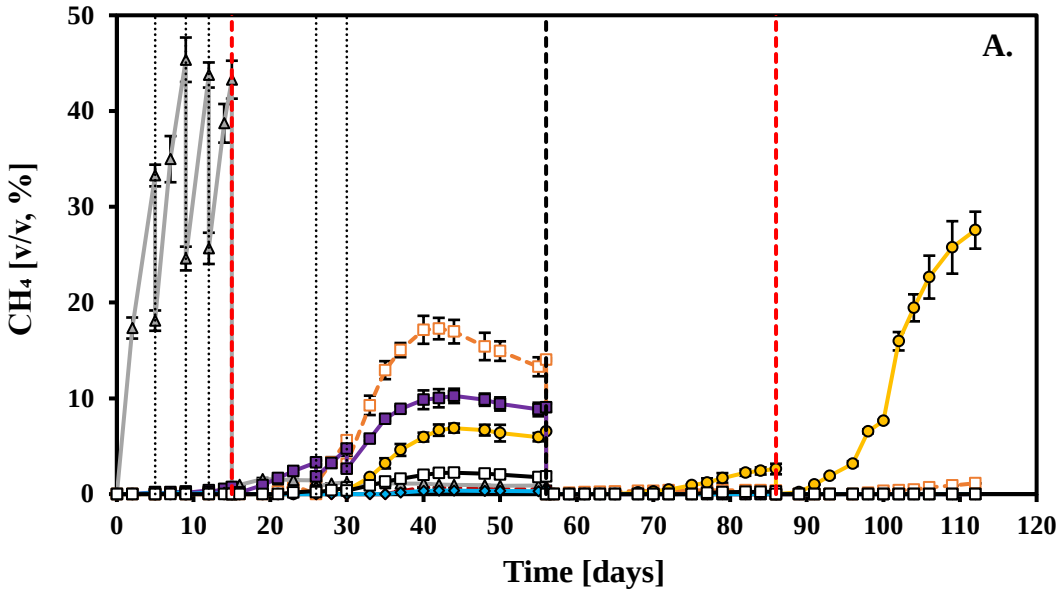
A.
CH₄ [v/v, %]
Time [days]

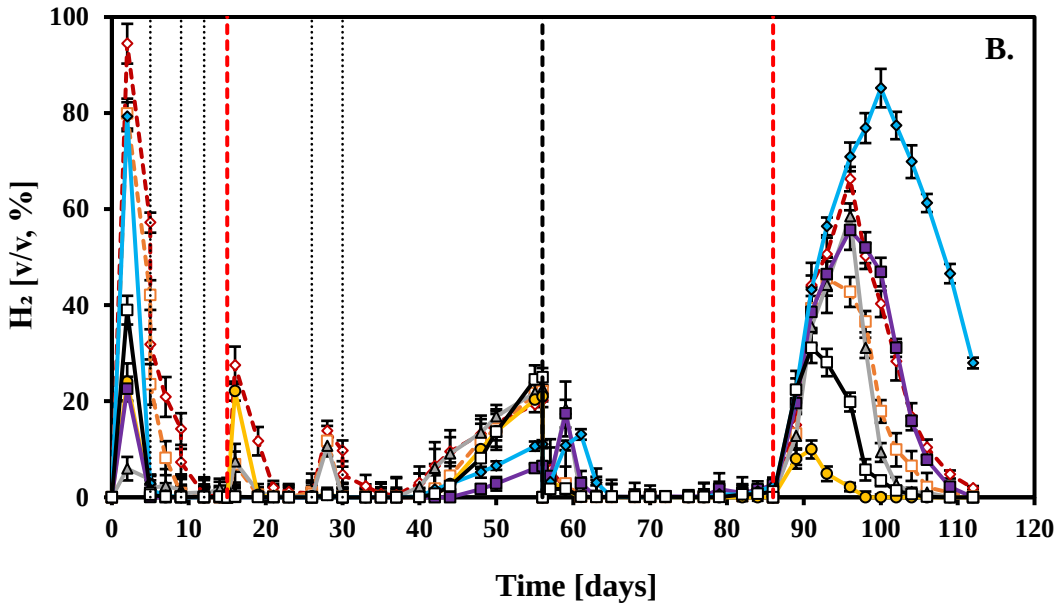
B.
H₂ [v/v, %]
Time [days]

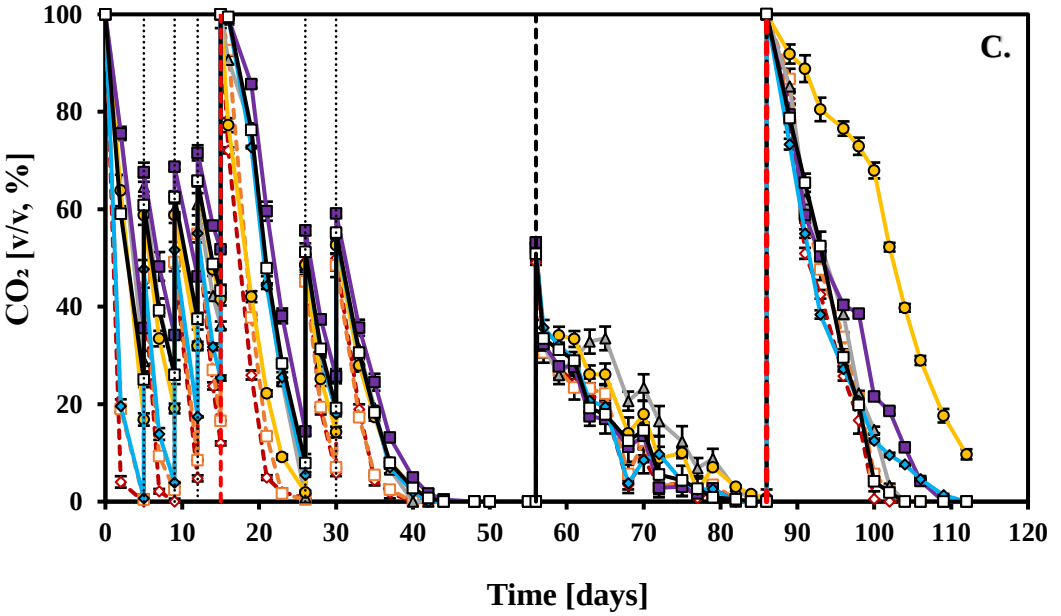
C.
CO₂ [v/v, %]
Time [days]

Fig. 3.45: Gas composition over time of all systems where various inoculums were exposed to ZVI and BES: (A.) CH_4 productivity of the systems (B.) H_2 production by ZVI, and the simultaneous consumption by the systems, and (C.) CO_2 utilization by the systems.

: River-SL; : Wetland-SL; : AnGr.-SL; : Comp.-SL; : Anaer.-SL; : Actv.-SL; : Dr.Cuts-SL; : CO_2 flashing / CO_2 feeding; : N_2 flashing / CO_2 feeding; : CO_2 feeding.

This was followed by AnGr-SL and Wetland-SL, which produced 3088 mg L^{-1} and 2983 mg L^{-1}, respectively [Fig. 3.44 (A.)]. The concentration of CO_2 in the systems impacts both the production of abiotic H_2 by ZVI (Fe^0), as shown in Sub-chapter 3.1.1, and acetogenesis. The addition of 10 mM BES at the start of cycle 2 on day 56 effectively inhibited methanogenesis in most inocula, with relatively higher CH_4 levels (27.5%) observed only in the Comp.-SL system [Fig. 3.45 (A.)]. Control systems exhibited negligible levels of acetic acid in all systems, as shown in Fig. 3.44 (B.). At the end of cycle 2 (day 112), the control systems inoculated with River-SL and Wetland-SL still showed zero concentrations of acetic acid, while the other systems had even lower acetic acid concentrations than in cycle 1, ranging from 44 to 111 mg L^{-1}.

Regarding other VFAs, formic acid showed low accumulation across most systems. The highest concentrations were recorded after the CO_2 purging and pressurized CO_2 feeding on day 86, at 186 mg L^{-1} and 184 mg L^{-1} on days 96 and 100, respectively, in systems inoculated with AnGr-SL and Actv.-SL as shown in Fig. 3.46 (A.). These levels of formic acid observed under these conditions may be attributed to the activity of formate hydrogen lyase, a membrane-associated enzyme complex that can convert H_2 and soluble CO_2 into formic acid, as described by Samanides and Vyrides (2023). Additionally, the formic acid was rapidly consumed, likely because methanogens prefer to utilize formic acid over H_2, given its availability in the aqueous solution as an electron donor. The control systems showed no formic acid production.

Regarding propionic acid, all systems exhibited negligible concentrations. In the first cycle, propionic acid levels were low across all systems, ranging from 22 mg L^{-1} to 97 mg L^{-1}. This trend continued into the second cycle, with both the experimental and control systems [Suppl. Info. Fig. 3.32 (A.)] maintaining low concentrations of propionic acid.

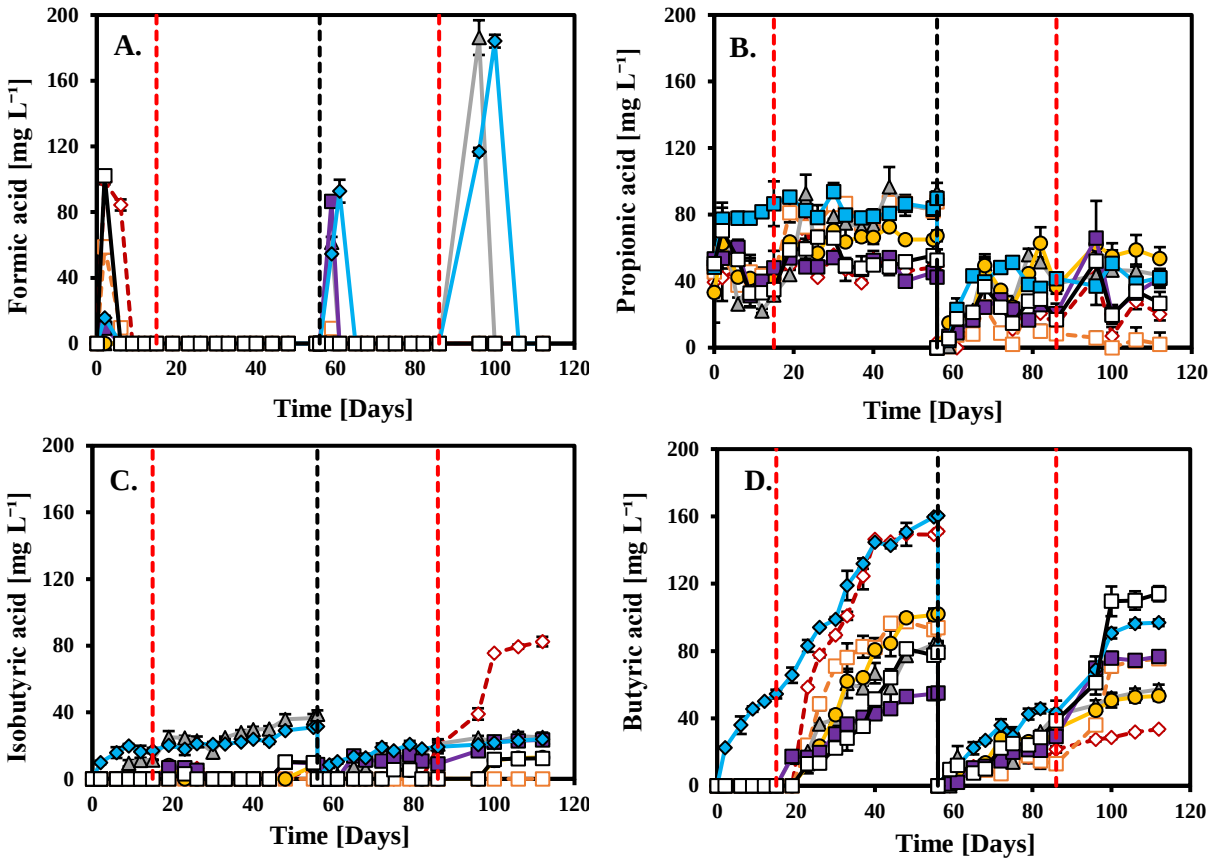

Fig. 3.46: Accumulations of (A.) formic, (B.) propionic, (C.) isobutyric, and (D.) butyric acid, observed in all systems exposed to ZVI and BES, over time.

: River-SL; : Wetland-SL; : AnGr.-SL; : Comp.-SL;

: Anaer.-SL; : Actv.-SL; : Dr.Cuts-SL;

: CO_2 flashing / CO_2 feeding; : N_2 flashing / CO_2 feeding.

Concerning isobutyric acid, all systems showed low accumulation levels, staying below 39 mg L^{-1} throughout cycle 1 and the initial 56-day period. By the end of cycle 2, on day 112, the system inoculated with River-SL reached a maximum concentration of 82 mg L^{-1}. At the same time, other inocula primarily produced butyric acid, with concentrations ranging from 33 mg L^{-1} to 114 mg L^{-1}, as shown in Fig. 3.46 (C.). In contrast, the control systems produced negligible amounts of isobutyric acid, peaking at 27 mg L^{-1} during cycle 1 [Suppl. Info. Fig. 3.32 (B.)].

Regarding butyric acid produced during cycle 1, the systems inoculated with Actv.-SL and River-SL demonstrated the highest concentrations, reaching 160 mg L^{-1} and 149 mg L^{-1}, respectively, at the end of cycle 1 (day 56). The remaining systems showed butyric acid concentrations between 55 mg L^{-1} and 102 mg L^{-1}, as shown in Fig. 3.46 (D.). In the control systems, butyric acid concentrations were minimal, with the Activ.-SL and AnGr-SL systems reaching only 13 mg L^{-1} [Suppl. Info. Fig. 3.32 (C.)]. It is important to note that valeric acid was not detected in any of the systems.

The identification of VFAs other than acetic acid is influenced by the type of inoculum and the H_2 partial pressure, which depends on bicarbonate concentration and ZVI. However, the concentrations of these VFAs are significantly lower, ranging from 10 to 25 times less than that of acetic acid in all inocula, due to the enrichment of homoacetogens (see Sub-chapter 3.4.2). Homoacetogens utilize the Wood-Ljungdahl pathway (the reductive acetyl-CoA pathway) to produce acetic acid from CO_2 and H_2.

The utilization of CO_2 by the systems was monitored [Fig. 3.45 (C.)], and pressure (absolute) readings were taken across the seven inocula [Suppl. Info. Fig. 3.33 (A.)]. Both pressure and CO_2 concentrations exhibited a similar trend across all seven inocula. Initially, introducing CO_2 led to an increase in pressure, followed by a significant decrease due to the consumption of CO_2 by homoacetogens. Another contributing factor to the decline in CO_2 and pressure is likely the precipitation on the ZVI surface and the formation of siderite and H_2, as outlined in Eq. 23. In contrast, the control samples exhibited a more gradual pressure decrease, likely due to CO_2 dissolving and sample withdrawals, without the sharp fluctuations observed in the experimental setups [Suppl. Info. Fig. 3.33 (B.)].

3.4.2 Microbial Profile Analysis of the Seven Systems Inoculated with Various Sludges

The study also investigates microbial diversity across different systems, highlighting substantial initial differences among phyla. The introduction of ZVI and BES and elevated CO_2 levels led to a notable increase in the Firmicutes phylum in all systems. This shift was apparent across every setup, reflecting a significant and consistent alteration in microbial composition. By day 56, Firmicutes emerged as the dominant phylum, representing 29% to 75% of the microbial community, with the highest proportions found in the Wetland-SL, River-SL, and AnGr-SL systems. During the second cycle, from days 56 to 112, the continued presence of BES and high CO_2 levels further boosted the abundance of Firmicutes, which reached 58% to 87% of the microbial community by the end of the cycle, signifying a marked increase in this phylum over time. In contrast, on day 112, the control systems (without ZVI) showed Firmicutes constituting only 0.5% to 7.5% of the microbial community, with a greater variety of phyla observed across all samples, as shown in Fig. 3.47. Initially, Firmicutes were present in minimal amounts, and a diverse array of phyla was identified in the initial inocula as demonstrated in Fig. 6.48.

Exposure of various biomasses to ZVI and BES from days 1 to 56, combined with multiple CO_2 feeding regimes detailed in Table 2.6, led to a notable increase in *Acetobacterium* across all systems, with growth ranging from 27% to 71% as shown in Fig. 3.47. Particularly, the highest levels were observed in systems inoculated with Wetland-SL and River-SL, where *Acetobacterium* abundance reached 71% and 65.5%, respectively. These systems also produced the highest amounts of acetic acid during this period. From days 56 to 112, further growth medium replacement, BES addition, and sustained high CO_2 exposure continued to elevate *Acetobacterium* levels across all systems. By day 112, systems inoculated with Activ.-SL, Anaer.-SL, Comp.-SL, and Dr.Cuts-SL displayed *Acetobacterium* levels between 41% and 56%. The highest abundances were found in systems inoculated with River-SL, Wetland-SL, and AnGr-SL, reaching 85%, 75%, and 69%, respectively (Fig. 3.47). The increase in *Acetobacterium* in these inocula was closely associated with the highest acetic acid production observed during both cycles [Fig. 3.44 (A.)]. In contrast, the control systems showed varied microbial compositions with a minimal abundance of *Acetobacterium* and inconsistent

acetic acid productivity throughout the experiment. However, under conditions of ZVI, BES, and high CO_2 levels, a consistent enrichment of *Acetobacterium* was noted across all systems.

The analysis of archaeal profiles within the initial inocula revealed a significant prevalence of *Methanosarcina* in Dr.Cuts-SL (74%), while *Methanosaeta* was the dominant genus in Actv.-SL (22%), Anaer.-SL (34%), AnGr-SL (44%), and Wetland-SL (50%). Comp.-SL primarily consisted of *Candidatus Nitrocosmicus* (83.8%) as shown in Fig. 3.49. After the growth media was replaced and BES was added on day 56 (marking the start of cycle 2), a notable shift in microbial dominance occurred, particularly among methanogens. By the end of cycle 2 on day 112, systems inoculated with Comp.-SL, which contained 98% hydrogenotrophic methanogens (*Methanobacterium*), produced a substantial amount of CH_4 (27.5%) as shown in Fig. 3.45 (A.). In contrast, Wetland-SL, which had 95% *Methanobacterium*, produced only 1.12% CH_4. *Methanobacterium* also dominated in Dr.Cuts-SL (81%) and River-SL (33%), yet these systems did not produce CH_4. *Methanosaeta* was predominant in Activ.-SL (64%), AnGr-SL (69%), and Anaer.-SL (83%), but no CH_4 accumulation was observed. These results indicate a potential correlation between high *Methanobacterium* abundance and CH_4 production, likely due to its resistance to BES inhibition.

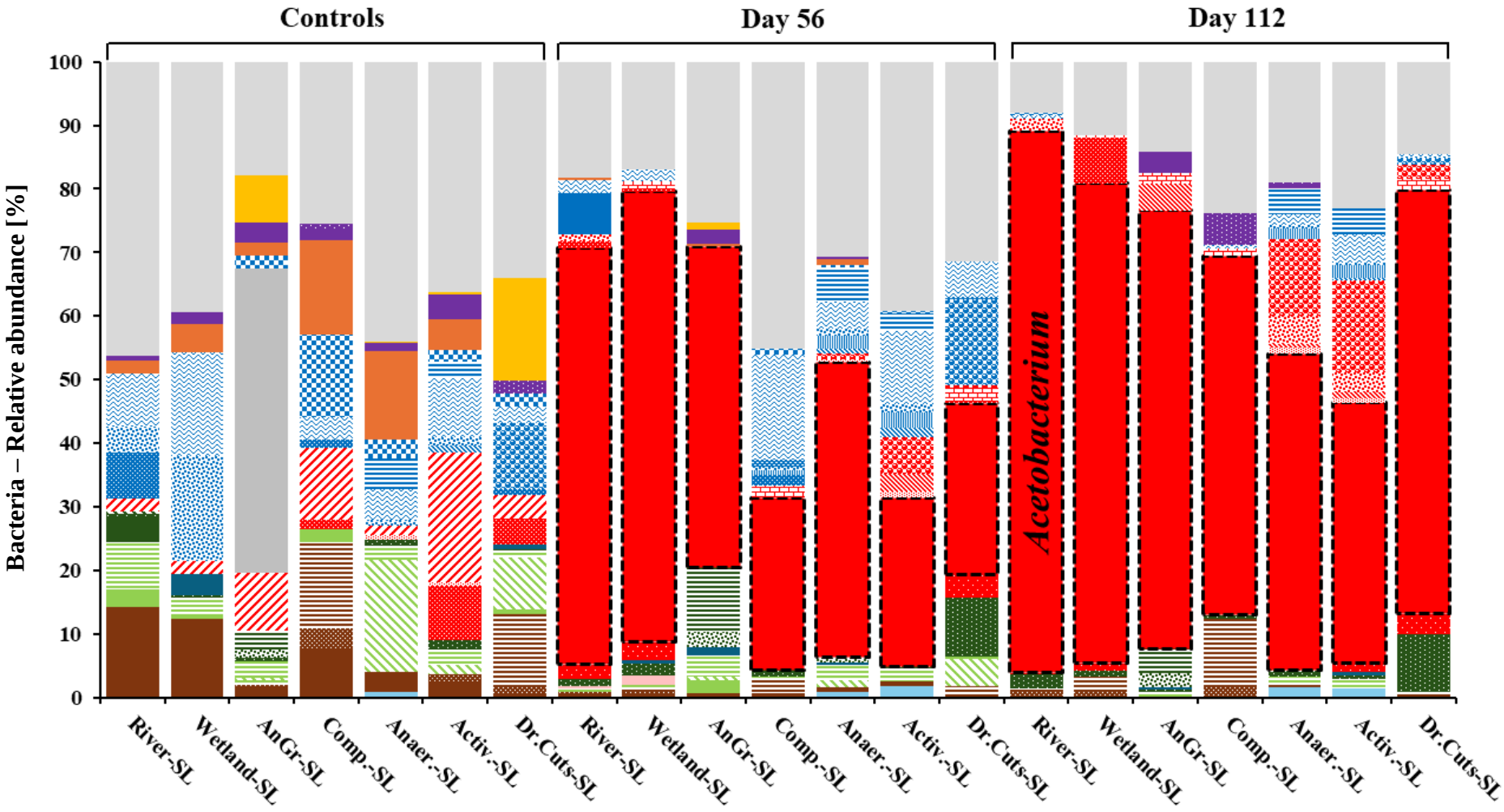
Controls
Day 56
Day 112
Bacteria – Relative abundance [%]
100
90
80
70
60
50
40
30
20
10
0
Acetobacterium
River-SL
Wetland-SL
AnGr-SL
Comp.-SL
Anaer.-SL
Activ.-SL
Dr.Cuts-SL

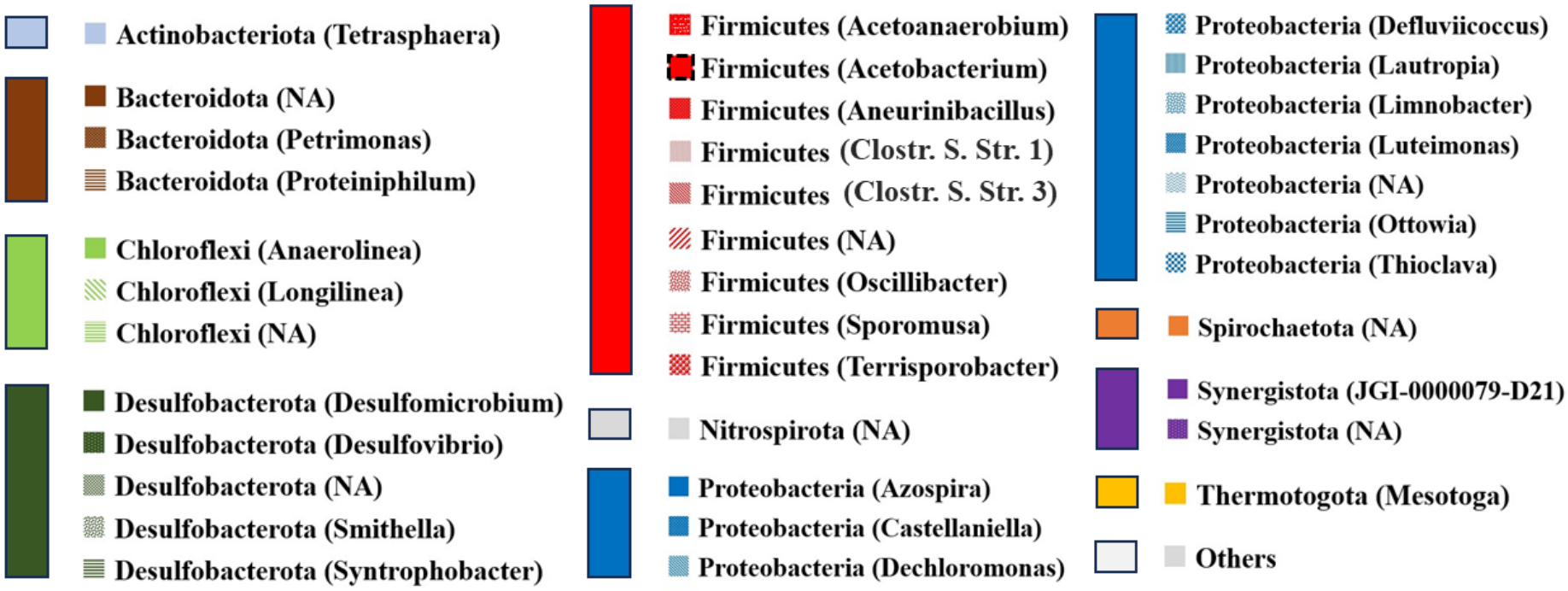

Fig. 3.47: Relative abundance of cultivated bacteria (%) at phylum and genus levels.

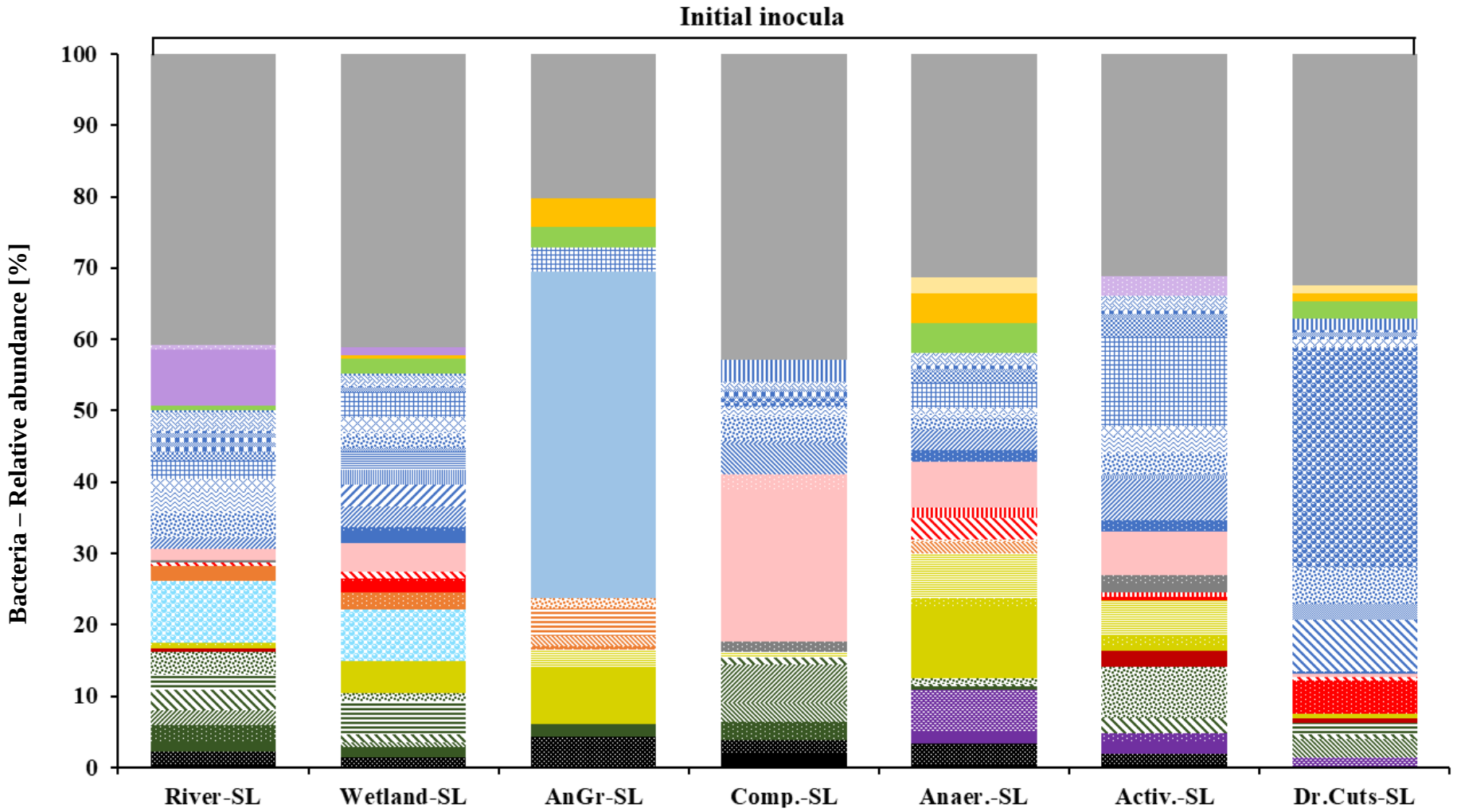
Initial inocula
Bacteria – Relative abundance [%]
100
90
80
70
60
50
40
30
20
10
0
River-SL
Wetland-SL
AnGr-SL
Comp.-SL
Anaer.-SL
Activ.-SL
Dr.Cuts-SL

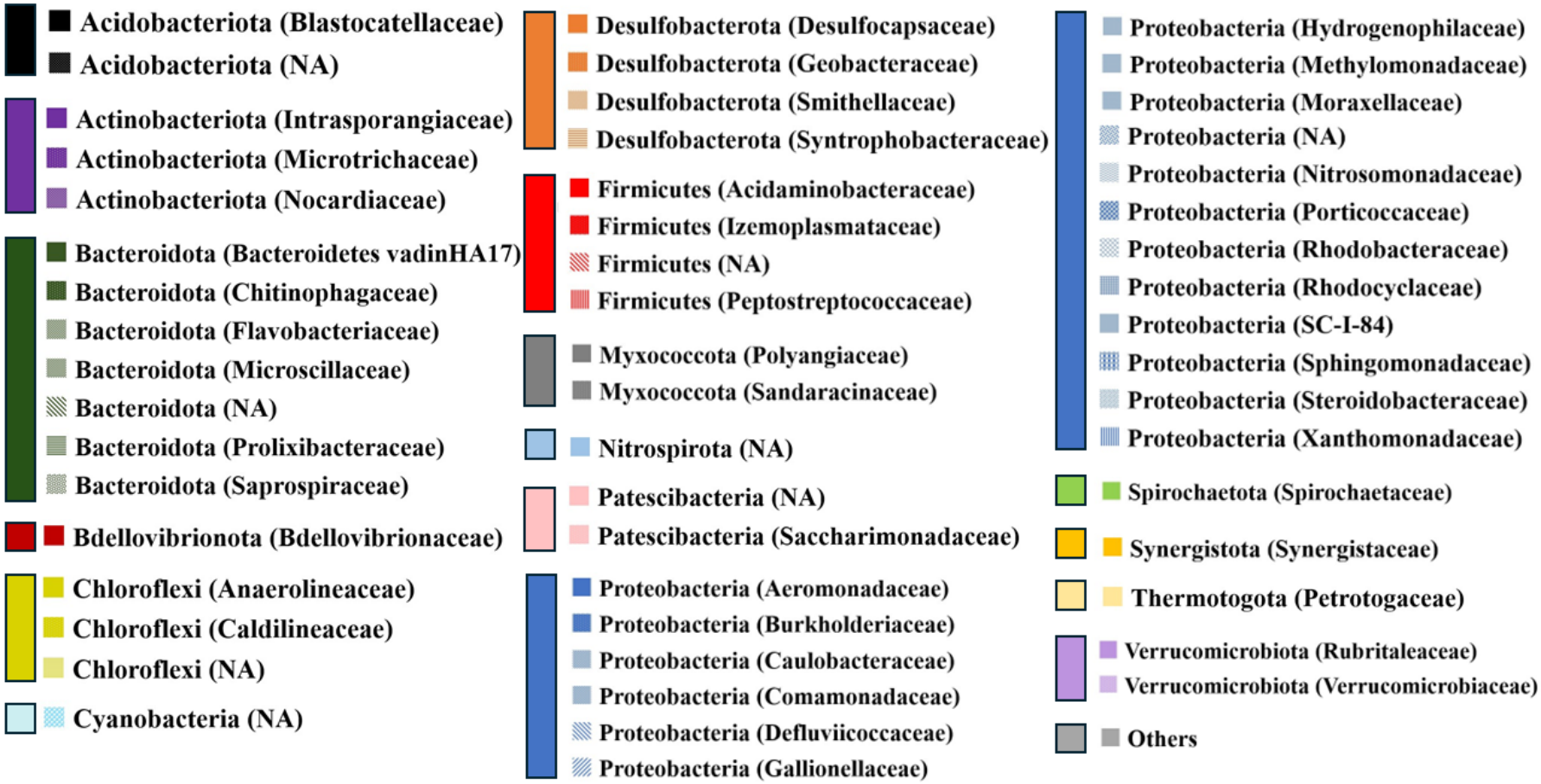

Fig. 3.48: Relative abundance of bacteria (%) at phylum and genus levels of the initial inoculum.

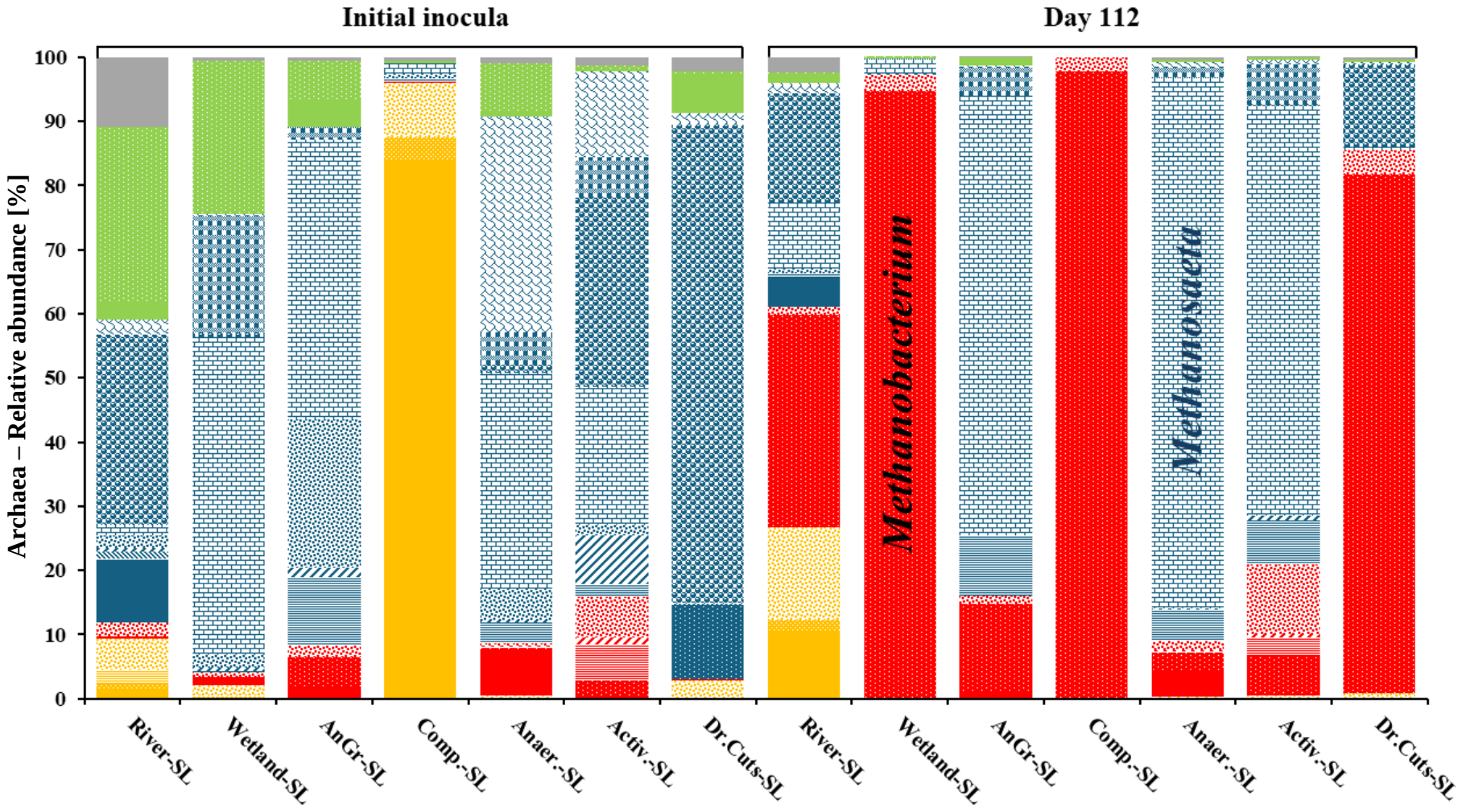
Initial inocula
Day 112
Archaea – Relative abundance [%]
100
90
80
70
60
50
40
30
20
10
0
Methanobacterium
Methanosaeta
River-SL
Wetland-SL
AnGr-SL
Comp.-SL
Anaer.-SL
Activ.-SL
Dr.Cuts-SL
River-SL
Wetland-SL
AnGr-SL
Comp.-SL
Anaer.-SL
Activ.-SL
Dr.Cuts-SL

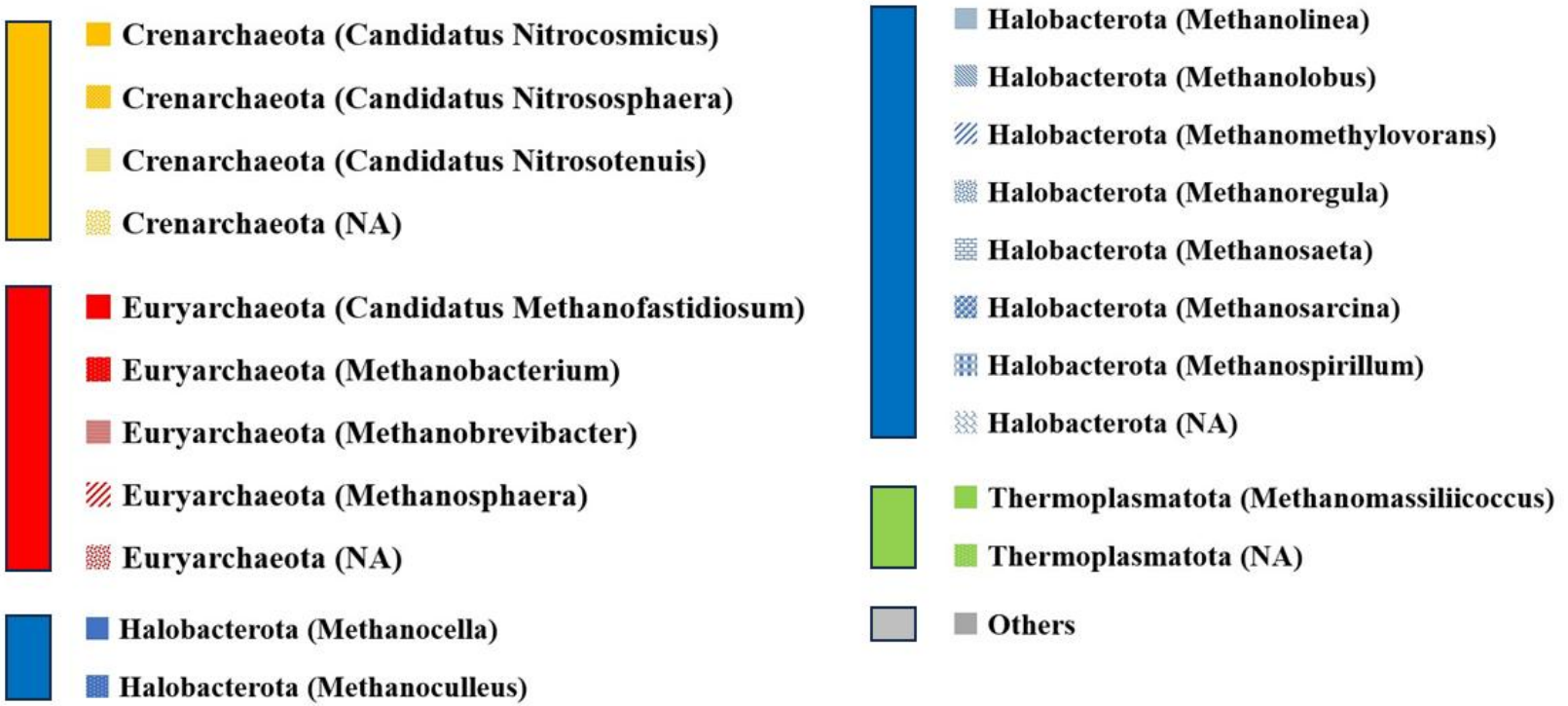

Fig. 3.49: Relative abundance at phylum and genus levels of the cultivated archaea (%) and archaea presented in the initial inoculum.

3.4.3 Structural Characterization of ZVI (Fe^0) After Exposure to CO_2 in Systems Inoculated with Seven Different Microbial Consortia Separately

The same ZVI (Fe^0) used in Experimental set-up 2 was utilized for the experiments conducted in this set-up. The X-RD patterns of ZVI (Fe^0) (data not shown) confirmed the absence of iron oxides or other crystalline structures, with three prominent diffraction peaks (44.7°, 65.0°, and 82.3°), indicating the high purity of the iron used. Following an experimental duration of 112 days, ZVI samples obtained from the seven systems, each inoculated with different inocula, were subjected to X-RD analysis. The experiments, conducted in a CO_2-enriched environment, as detailed in Table 2.6, yielded consistent X-RD patterns across all systems. As illustrated in Fig. 3.50, the observed peaks primarily corresponded to pure α-Fe (~45°), siderite ($FeCO_3$) (~32°), and magnetite (Fe_3O_4) (~35°). The mechanisms underlying the formation of siderite and magnetite from ZVI under anaerobic conditions are discussed in detail in Sub-chapter 3.1.13.1.

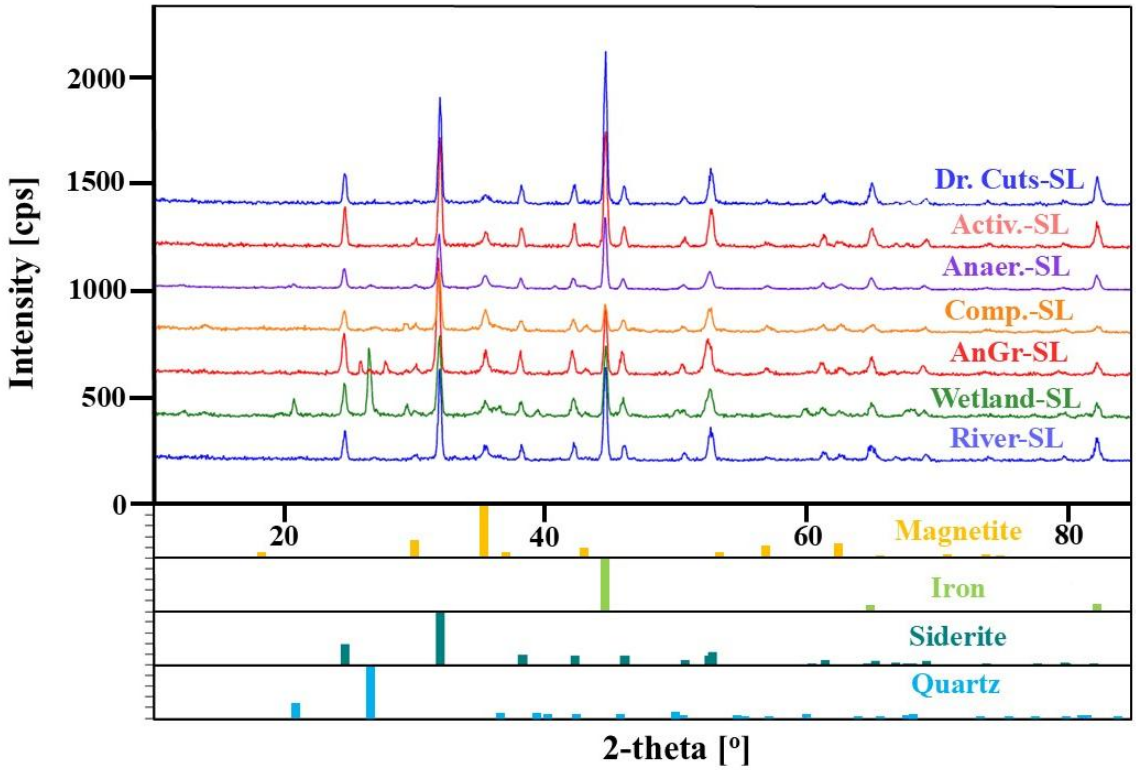

Fig. 3.50: X-RD patterns of the processed ZVI (Fe^0) in the presence of BES under anaerobic conditions derived from the seven systems, each inoculated with distinct inoculum.

However, the X-RD pattern for ZVI obtained from the system inoculated with wetland-derived samples (Wetland-SL system) revealed additional peaks (~21° and ~26°) associated with the crystalline structure of quartz. The presence of quartz is attributed to the inclusion of siliceous rocks collected along with the microbiological sample from the wetland environment.

3.4.4 Response of Suspended, ZVI-attached, and ZVI-detached Bacteria in Acetic Acid Production Under a CO_2:H_2 Environment

Fig. 3.51 presents the accumulation of acetic acid by three types of bacterial biomass derived from the River-SL system: freely suspended biomass, biomass detached from ZVI, and biomass firmly attached to ZVI, when exposed to H_2 and CO_2. The suspended biomass and ZVI-detached biomass systems initially showed slow H_2 consumption and low acetic acid production, with concentrations around 237 mg L^{-1} after 14 days [Fig 3.51 (A. and B.)].

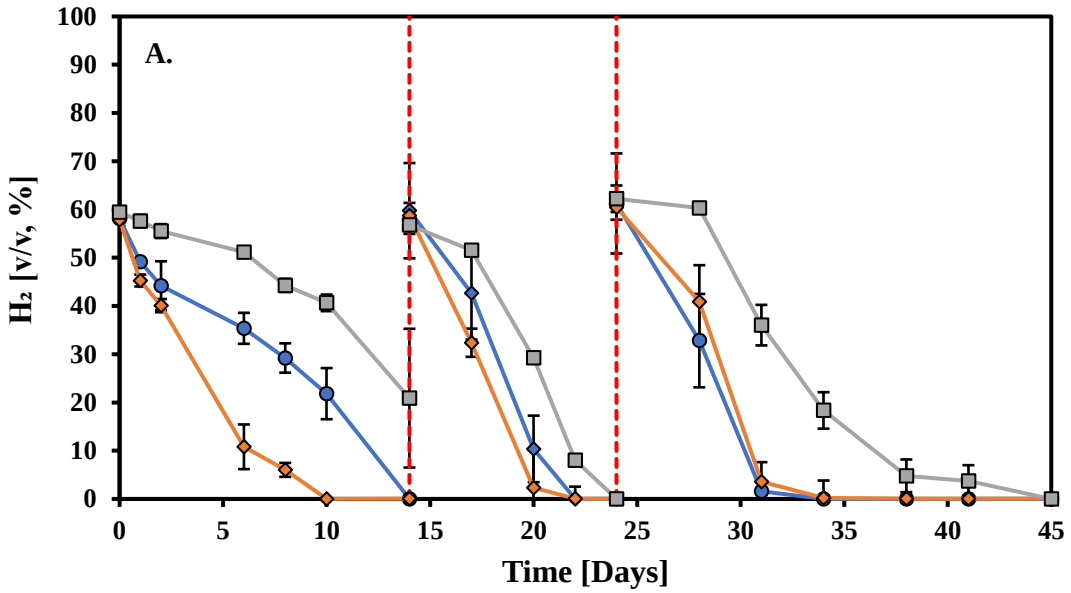

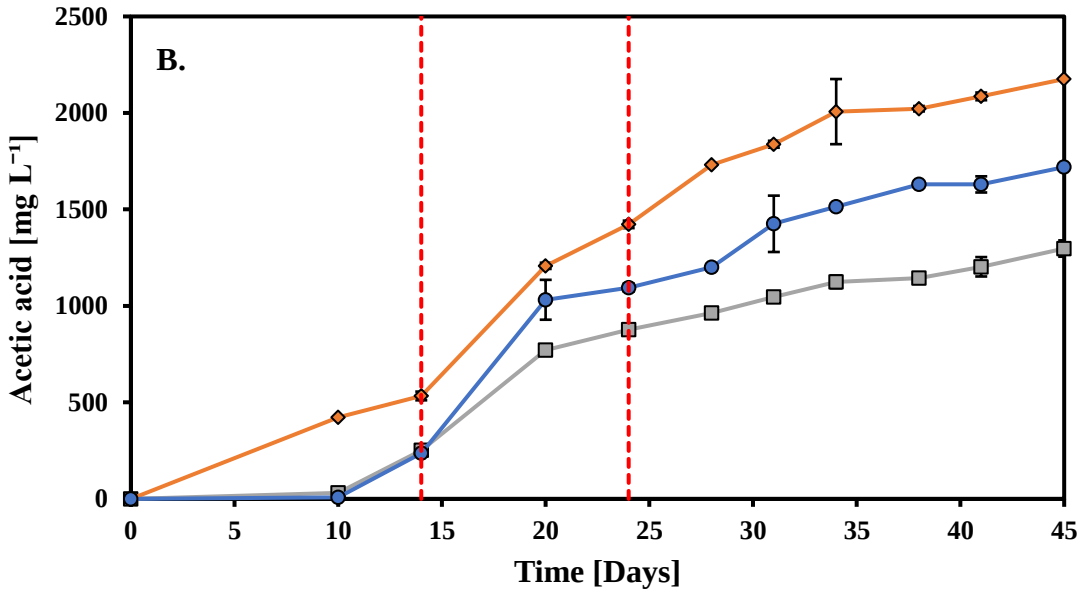

Fig. 3.51: Response of suspended, firmly attached, and detached bacteria to (A.) H_2 utilization and (B.) acetic acid production under an anaerobic environment.

: Suspended bacteria; : ZVI firmly attached bacteria;

: ZVI detached bacteria; : H_2 feeding.

In contrast, the bacteria attached to the ZVI exhibited the most rapid H_2 consumption and acetic acid production. Following an additional H_2 injection on day 14, the suspended biomass system produced 877 mg L^{-1} of acetic acid by day 24. In contrast, the ZVI-detached biomass system accumulated 1095 mg L^{-1}, and the bacteria attached to ZVI achieved the highest acetic acid production at 1422 mg L^{-1}. This trend persisted, with the ZVI-attached bacteria consistently leading to acetic acid production. By day 45, the systems with ZVI-attached, detached, and suspended biomass produced 2175 mg L^{-1}, 1719 mg L^{-1}, and 1297 mg L^{-1} of acetic acid, respectively.

3.4.5 Discussion of Experimental Set-Up 4

This study examined acetic acid production by seven different inocula exposed separately to ZVI (Fe^0) and CO_2 as the sole carbon source, exploring a novel and sustainable method for VFA production under ambient conditions. The results showed that inocula from environmental samples, such as river sludge [River-SL (5,200 mg L^{-1} of acetic acid after

56 days)] and constructed wetland sludge [Wetland-SL (4,620 mg L^{-1} of acetic acid after 56 days)] had the highest acetic acid production rates, reaching 300 mg L^{-1} day^{-1} and 269 mg L^{-1} day^{-1}, respectively. Numerous scientific studies have examined the efficiency of converting CO_2 to acetate in microbial electrochemical systems (MES) inoculated with bacterial communities, as reviewed by Hengsbach et al. (2022). Compared to the production rates reviewed by Hengsbach et al. (2022), this study's river sludge production rate of 300 mg L^{-1} day^{-1} ranks among the highest observed under batch conditions. Furthermore, most studies reviewed by Hengsbach et al. (2022) utilized pure bacterial strains or inocula from wastewater treatment plants (WWTPs) and bioreactors, with experiments lasting less than 30 days. In contrast, this study lasted longer and included a broader range of inocula, including natural samples from rivers and wetlands.

Roy et al. (2021) demonstrated, for instance, that by using a two-chamber MES system separated by a 117 Nafion proton exchange membrane, operated at 28–30°C and pH 7, 1800 mg L^{-1} of acetic acid was produced after 27 days over three cycles. The production rate was calculated at 260 mg L^{-1} day^{-1}, using anaerobic sludge enriched with 26% *Acetobacterium* and feeding the system daily with 20 mL of unpurified industrial CO_2 as the sole carbon source. Methanogenesis was inhibited using 34 mM L^{-1} of BES. Additionally, the same configuration was tested with pure strains of *Clostridium ljungdahlii*, resulting in 1100 mg L^{-1} of acetic acid after 21 days (three cycles), with a production rate of 138 mg L^{-1} day^{-1} at pH 6.

Mohanakrishna et al. (2020) also used a two-chamber MES system with a Nafion 117 membrane, achieving 368 mg L^{-1} of acetic acid and a production rate of 24.53 mg L^{-1} day^{-1} after 84 days over seven cycles. The system was inoculated with acetogen-enriched granular-activated sludge previously adapted to high bicarbonate concentrations. The system operated with the addition of 15 g HCO_3^- L^{-1} at 22–24°C, with an initial pH set to 7.

Similarly, Yang et al. (2021) managed to produce 525.84 mg L^{-1} of acetic acid with a production rate of 49.2 mg L^{-1} day^{-1} after 20 days in a two-chamber MES system under mesophilic conditions (25°C and 37°C). In this case, a CMI 7000 ion exchange membrane was used. Methanogenesis was inhibited with 20 mM L^{-1} of BES, and the system was inoculated with mixed culture WWTP sludge. In contrast, without using methane inhibition measures, Mateos et al. (2019) achieved maximum acetic acid accumulations

of 1687 mg L^{-1} after 56 days without a CO_2 recirculation loop and 1957 mg L^{-1} after 92 days with a CO_2 recirculation loop, with a peak production rate of 261 mg L^{-1} day^{-1}.

Based on the acetic acid production rates from various scientific reports, it is evident that the methodology proposed in this chapter outperforms the complex MES configurations, which typically require expensive materials such as electrodes and ion exchange membranes. Additionally, the proposed methodology surpasses the acetic acid accumulations observed in other batch experiments, including those utilizing systems directly fed with H_2 gas or *in-situ* metals (Fe^0 or Mg^0) that oxidize anaerobically to produce H_2.

For instance, Modestra et al. (2020) employed a CO_2:H_2 gas mixture at a 1:4 ratio (v/v) in a system utilizing wastewater anaerobic consortia pretreated with heat and exposed to low pH for methanogenesis inhibition. Under initial pH of 6.5 and 30-32 °C, acetic acid accumulation reached 1234 mg L^{-1} after three days (stage 2), while control systems produced 1013 mg L^{-1}. Omar et al. (2018), on the other hand, produced 358 mg L^{-1} of acetic acid after four days utilizing wastewater anaerobic consortia exposed to BES (50 mM) under anaerobic conditions with a CO_2:H_2 gas ratio of 1:4 (v/v) at pH 6 and 37°C. Similarly, He et al. (2021) used anaerobic granular sludge as inoculum and supplied the system with a similar CO_2:H_2 gas ratio and HCO_3^- at 25 °C, achieving a maximum acetic acid production rate of 217 mg L^{-1} day^{-1}. Roy et al. (2021) utilized an anaerobic mixed culture in a system with a total volume of 100 mL and a working volume of 40 mL, injecting 55 mL of unpurified industrial CO_2 and 110 mL of H_2. This setup produced 1300 mg L^{-1} of acetic acid after 13 days, with a production rate of 185 mg L^{-1} day^{-1}. Additional experiments were conducted using a pure strain of *Clostridium ljungdahlii*, which yielded 430 mg L^{-1} of acetic acid after 14 days, with a production rate of 60 mg L^{-1} day^{-1}. Similar mixed culture and pure strain experiments were also performed using pure CO_2 gas in a CO_2:H_2 gas ratio of 20%:80%, achieving production rates of 113 mg L^{-1} day^{-1} and 100 mg L^{-1} day^{-1}, respectively.

Instead of using H_2 gas, Samanides et al. (2020) employed ZVI at a concentration of 100 g L^{-1}, along with AnGrSL as inoculum, in a system with BES (50 mM) to facilitate *in-situ* CO_2 conversion to VFAs on a laboratory scale. The maximum production rate achieved with AnGrSL was approximately 168 mg L^{-1} day^{-1}. In a later study, Samanides and Vyrides (2023) replaced ZVI with magnesium ribbon and found that heat pre-

treatment of AnGrSL resulted in an acetic acid production rate of 235 mg L^{-1} day^{-1}. Bayar et al. (2022) used a pure culture of *Clostridium aceticum* in a system with ZVI (75 g L^{-1}), producing approximately 2113 mg L^{-1} of acetic acid after 36 days under 0.5 bar of CO_2, without the need for methanogenesis inhibition. However, the use of pure cultures poses a risk of system contamination. As Tsapekos et al. (2022) noted, the accumulation of other VFAs, such as butyric, isobutyric, and propionic acids, in anaerobic inocula systems can be attributed to increased H_2 partial pressure.

Regarding the behavior of suspended, ZVI-attached, and ZVI-detached bacteria in acetic acid production under a CO_2 environment, Palacios et al. (2019) documented a similar trend in H_2 consumption by bacteria detached from ZVI. Their study focuses on Baltic Sea sediments and enriched acetogens with ZVI and BES over eight cycles. They found that when Acetogens, predominantly Sporomusa, were separated from ZVI and exposed to H_2, there was a five-day lag before H_2 utilization began. In another study, Laguillaumie et al. (2023) emphasized the significance of temperature and mass transfer limitations in the competition between homoacetogenic microbes and hydrogenotrophic methanogens in a microbial enrichment culture. Under batch conditions, when hydrogenotrophic methanogens were inhibited using BES, homoacetogens began consuming H_2 after delays of 3 and 6 days at temperatures of 25°C and 35°C, respectively. The above findings and the current study highlight the delayed H_2 consumption by suspended homoacetogenic bacteria.

Bacteria attached to ZVI, however, did not exhibit any delay in hydrogen utilization. The ZVI-acetogen system typically achieves a balance between abiotic H_2 production and its microbial consumption by homoacetogens, resulting in ZVI oxidation and acetic acid production. If this balance is disrupted, homoacetogens may require an adaptation period to resume efficient H_2 utilization. The H_2 threshold, as described by Philips (2020), is a critical parameter influencing acetogenesis. It represents the partial pressure of H_2 below which acetogenesis becomes thermodynamically unfavorable. During the main experiments, the acetic acid production rate in the 1st cycle was significantly higher when bacteria were exposed to ZVI than when H_2 gas was supplied externally. Although it is possible that ZVI generated some H_2 in the attached bacteria system, however, no detectable increase in H_2 was observed, likely due to immediate consumption by the bacteria attached to ZVI or partial ZVI oxidation. The finding that attached bacteria were

primarily responsible for acetic acid production is advantageous for studies focused on CO_2 utilization but may be problematic in research concerning microbial corrosion.

3.4.6 Conclusion of Experimental Set-Up 4

This study highlights the significant role of CO_2 in enhancing H_2 evolution by ZVI (Fe^0) in systems employing various microbial consortia for VFA production. It is demonstrated that increased CO_2 levels substantially boost H_2 production, which concurrently elevates acetic acid yields. The study assessed the acetic acid production performance of seven different inocula (river, constructed wetland, anaerobic granular, compost, anaerobic, activated, and drilling cut sludges) individually exposed to ZVI (Fe^0) and 4 mM BES under anaerobic conditions, with CO_2 as the sole carbon source at varying concentrations. Results showed acetate as the dominant VFA across all systems. River and constructed wetland sludges exhibited the highest production rates, reaching 300 mg $L^{-1}day^{-1}$ and 269 mg $L^{-1}day^{-1}$, respectively. CO_2-enriched environments, particularly in the river and wetland sludges, significantly promoted the growth of *Acetobacterium*, reaching 85% and 75 %, respectively. Additionally, ZVI-attached bacteria demonstrated faster H_2 consumption and acetic acid production compared to their free-floating or ZVI-detached counterparts when H_2 was supplied externally. X-RD analysis shows the formation of siderite in all systems. The study emphasizes the beneficial effect of high soluble CO_2 concentrations, which serve both as a reactant for ZVI-driven hydrogen production and as a substrate for homoacetogens, resulting in enhanced acetic acid generation.

3.5 <u>Experimental Set-Up 5:</u> Acetic Acid Production Utilizing Waste Iron (Fe-W) and River Sludge in a Continuous CO_2 Feeding Bioreactors System

Building on the findings of the previous chapters, this section explores the potential of acetogen-enriched inoculum to produce acetic acid or other VFAs in a continuous CO_2-feeding bioreactor system exposed to waste iron (Fe-W) derived from a machinery industry.

As demonstrated in experimental set-ups 2 and 4 (Sub-chapters 3.2 and 3.4), systems inoculated with microbial consortia, and exposed to anaerobic conditions using ZVI (Fe^0) or processed ZVI (Fe^0) can achieve high acetic acid concentrations under aqueous ambient conditions by utilizing CO_2 as the sole carbon source and H_2, which is abiotically produced through *in-situ* ZVI (Fe^0) oxidation. As shown in Sections 3.1.6 and 3.1.10, ZVI (Fe^0) not only generates abiotic H_2 in anaerobic, carbonated conditions, but it is also feasible to produce H_2 from waste iron materials under certain conditions. Therefore, this chapter explores the substitution of ZVI (Fe^0) with waste iron (Fe-W) in alignment with the circular economy concepts. However, as concluded in Section 3.1.13.4, fine-grained iron exposed to anaerobic conditions produces more abiotic H_2 than coarse-grained iron due to its larger specific surface area. Consequently, coarse-grained iron (0.05 mm^2) requires higher concentrations to produce sufficient abiotic H_2 as an electron donor for bacterial reactions. Hence, two reactors with a total volume of 3500 mL were used in this experimental group, connected in parallel as described in Sub-chapter 2.5. The experimental implementations were divided into four phases, as outlined in Tables 2.8–2.11 in Sub-chapter 2.5.

In Phase A (Table 2.8), both reactors (A and B) were filled with Fe-W (2 Kg), inoculated with a river microbial consortium, and continuously fed with CO_2. Acetic acid production was monitored in both reactors. In Phase B (Table 2.9), to enrich homoacetogenic bacteria, the old growth medium was replaced while retaining the previously processed Fe-W. Subsequently, Reactor B was supplemented with biocarriers to enhance acetic acid production by potentially immobilizing microorganisms. For Phases A and B, 4 mM of BES was used to inhibit methanogenesis.

In Phases C and D (Table 2.10 & 2.11), Reactor A was designated as the *ex-situ* H_2 producer, using double the concentration of Fe-W (4 kg) from previous phases, and supplied H_2 to Reactor B, where the microbial consortium was present. In Phase C,

Reactor A underwent thermal pretreatment to eliminate microbial communities and prevent H_2 consumption. In Phase D, Reactor A continued to serve as the ex-situ H_2 producer for Reactor B, but with new Fe-W in an uncontaminated reactor. In Phases C and D, 4 mM of BES was used in Reactor B.

3.5.1 Acetic Acid Productivity of Reactors Under Continuous CO_2 Feeding

The data obtained from VFA monitoring in reactors inoculated with river sludge under continuous CO_2 supply reveal that acetic acid was the only VFA detected throughout the experimental period across all four phases. Formic, propionic, isobutyric, butyric, and valeric acids were not identified.

As shown in Fig. 3.52, during Phase-A, both reactors, supplemented with Fe-W and inoculated with river sludge, exhibited significant acetic acid accumulation. By the end of Phase-A, on day 60, Reactor-A, which received the initial CO_2 supply, demonstrated an acetic acid concentration of 4722 mg L^{-1}. At the same time, Reactor-B recorded an acetic acid concentration exceeding 7050 mg L^{-1} on the same day, with a production rate of 350 mg L^{-1} day^{-1} during days 28-37. The elevated acetic acid levels align with the gas composition measurements, indicating that bacteria fully utilized the abiotically produced H_2 from *in-situ* Fe-W. However, the 33% lower acetic acid accumulation in Reactor-A may be attributed to the removal of trace amounts of H_2 due to the passage of CO_2, which resulted in Reactor-B being supplied with both CO_2 and unconsumed H_2 from Reactor-A. The increased H_2 availability in Reactor-B facilitated the activity of methanogenic bacteria, which utilized the reactants (H_2 and acetic acid) to produce CH_4. As shown in Fig. 3.53 (B.), by day 56, Reactor-B had 4.5% CH_4 in its headspace, while Reactor-A exhibited CH_4 accumulation of less than 1%.

During Phase-B, the growth media was replaced with a fresh medium on day 60, while the same pre-processed Fe-W from Phase-A was reused. Both reactors exhibited a similar pattern of acetic acid production as in Phase-A, though at lower concentrations. As shown in Fig. 3.52, Reactor B consistently produced higher amounts of acetic acid, reaching 5440 mg L^{-1} (3957 mg L^{-1}net acetic acid) by the end of Phase-B on day 120, compared to Reactor A, which reached 4246 mg L^{-1} (3018 mg L^{-1} net acetic acid) during the same period. The 24% lower acetic acid production in Reactor-A can be attributed to the

previously mentioned factors. The overall decrease in acetic acid production during Phase-B may be due to using the already processed Fe-W from Phase-A. As discussed in Sub-chapter 3.1.13.1 and as noted by Zhu et al. (2024), high concentrations of HCO_3^- resulting from continuous CO_2, feeding can lead to the formation of a protective film, "passivating" the Fe-W and inhibiting H_2 production. Additionally, during Phase-B, CH_4 accumulation in the headspace of Reactor-B increased to nearly 12% by day 120. In comparison, CH_4 levels in Reactor-A remained low (1%), possibly due to insufficient H_2 remaining in the reactor (Fig. 3.53).

During Phase-C, a different approach was implemented. Reactor-A now serves as an *ex-situ* H_2 producer and supplier for Reactor-B. The growth medium in Reactor-A was replaced with water, retaining the previously processed Fe-W from the earlier phase. Instead of using a chemical inhibitor to deactivate methanogens, Reactor-A underwent thermal inhibition treatment, and an additional 2 kg of new Fe-W was introduced, bringing the total Fe-W to 4 kg. As illustrated in Fig. 3.52, Reactor A, acting as the *ex-situ* H_2 producer, showed no acetic acid production during the first 8 days. However, after day 8, acetic acid levels in Reactor-A increased significantly, surpassing those in Reactor-B, reaching 4497 mg L^{-1} by the end of Phase-C on day 180. In contrast, Reactor-B showed lower acetic acid accumulation, reaching only 1668 mg L^{-1} (1500 mg L^{-1} net acetic acid) during the same period.

As indicated by the relative abundance analysis in Sub-chapter 3.5.2, the high acetic acid concentration observed in Reactor-A was attributed to the cultivation of *Clostridium sensu stricto* in the system. This observation aligns with the findings of Samanides et al. (2020), where thermal pretreatment of a microbial consortium (AnGrSL) exposed to ZVI (Fe^0) also identified the same genus. Regarding the gas composition, by supplementing Reactor-A with double the amount of Fe-W used in Phases A and B, higher H_2 accumulations were observed in the headspace, peaking at 38% on day 166. Based on the H_2 values obtained from Reactors A and B, as shown in Fig. 3.53, the H_2 consumption of Reactor-B was recorded to be approximately 1%–6%, determined by subtracting the values of the reactors during Phase-C. Regarding CH_4 accumulations, the thermal treatment (Reactor-A) and the use of 4mM of BES (Reactor-B) were sufficient methods fully inhibited the methanogenesis.

During Phase D, the same approach as Phase C was applied, but a new, uncontaminated reactor was used, supplemented with 4 kg of fresh Fe-W as the ex-situ H_2 producer. The data presented in Figs. 3.52 and 3.53 indicate that using new Fe-W and exposing it to CO_2, abiotic H_2 accumulations increased within the system. The uncontaminated Reactor-A, which continuously produced abiotic H_2, showed a consistent increase throughout the 60-day experimental period of Phase-D, reaching a peak of 63% H_2 in the headspace by the Phase end. The abiotic H_2 produced by Reactor-A was supplied to Reactor-B, where approximately 3% of the H_2 was utilized, resulting in the production of 3245 mg L^{-1} of acetic acid by the end of Phase D on day 240. Methanogenesis was fully inhibited in both reactors.

No other VFAs (formic acid, propionic acid, isobutyric acid, butyric acid, and valeric acid) were identified during the experimental duration.

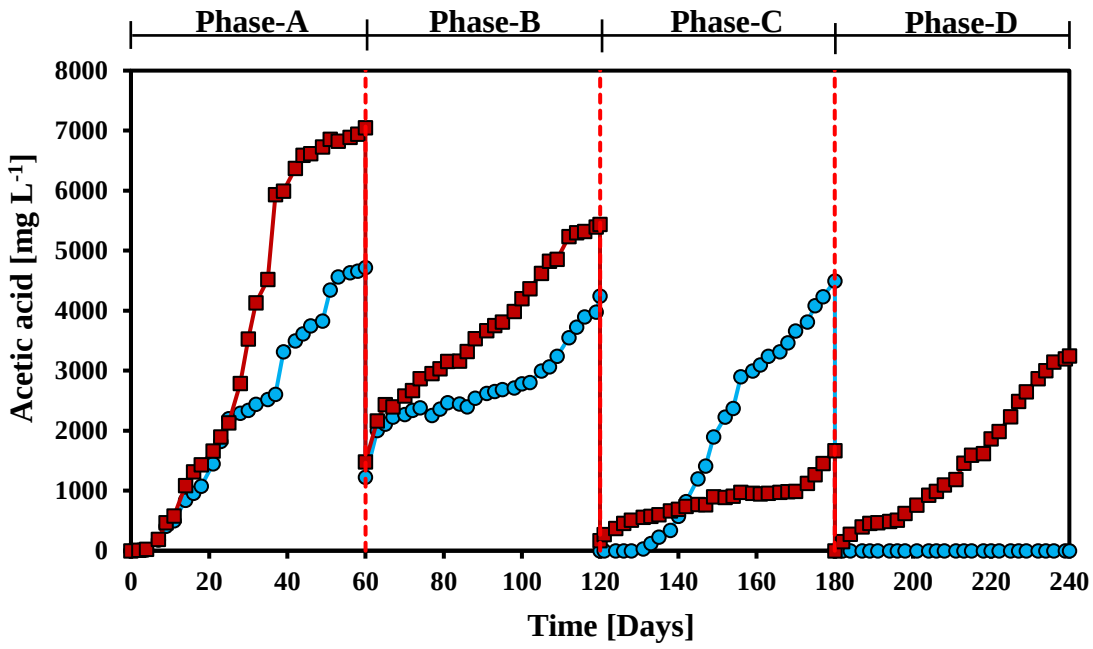

Fig. 3.52: Acetic acid production in Reactors A and B during the 240-day experimental period.
: Reactor-A; :Reactor-B.

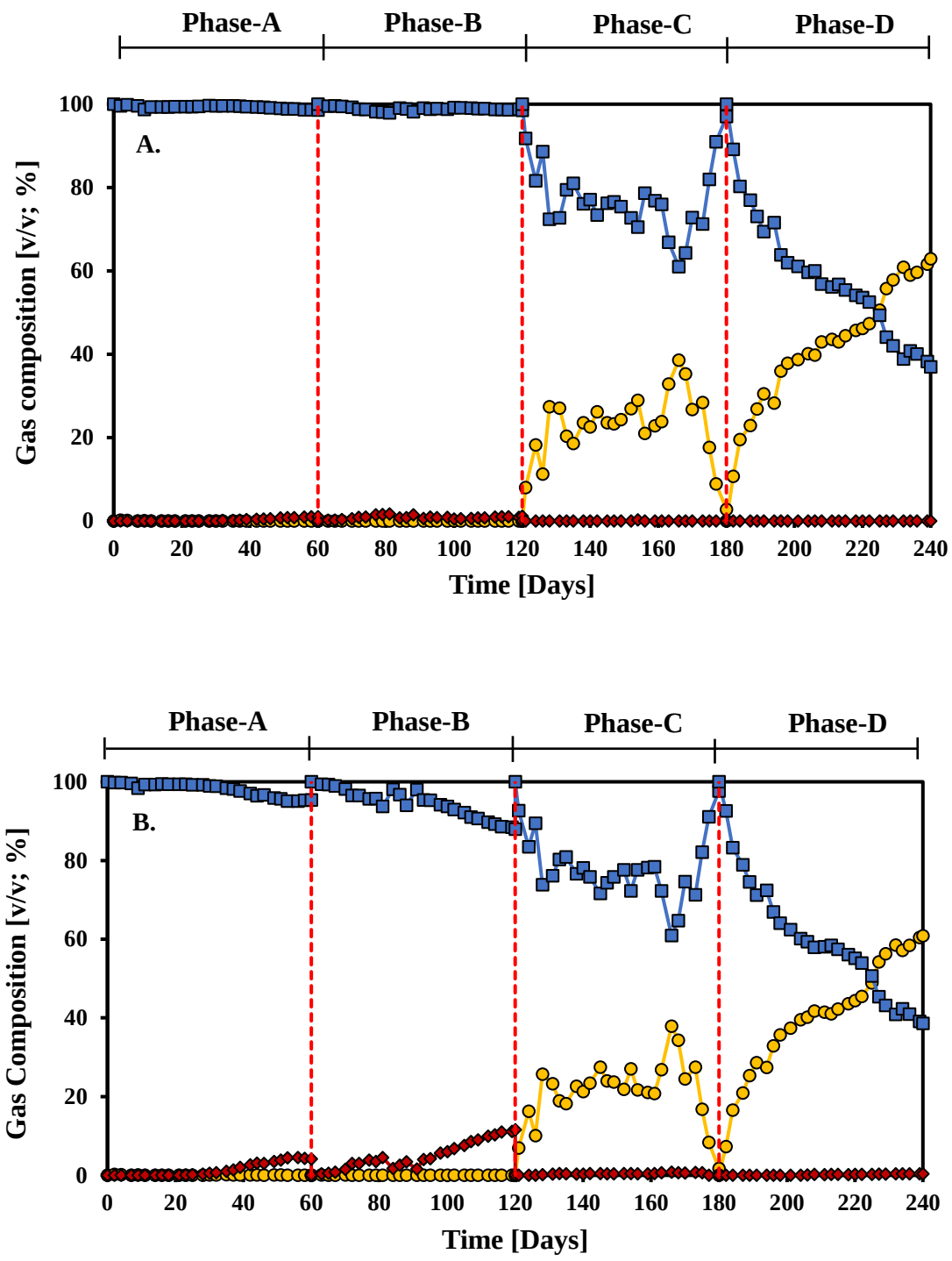

Fig. 3.53: Gas composition in the Reactors' headspace throughout the experimental duration's four phases. **A.:** Reactor-A; **B.:** Reactor-B.

: CO_2 utilization; : H_2 evolution and utilization; : CH_4 productivity.

Regarding pH monitoring, the data indicates that during each phase of the experimental period, the pH declined to approximately 5.5 from the initial adjustment range of 6-7 (Fig. 3.54). This decline is attributed to the high accumulation of acetic acid produced in the reactors, as shown in Fig. 3.52. On the other hand, the continuous CO_2 feeding feature of the system contributes to pH stabilization due to the presence of carbonate ions, which act as part of a buffering mechanism to regulate pH levels as explained in Sub-chapter 3.1.13.1.

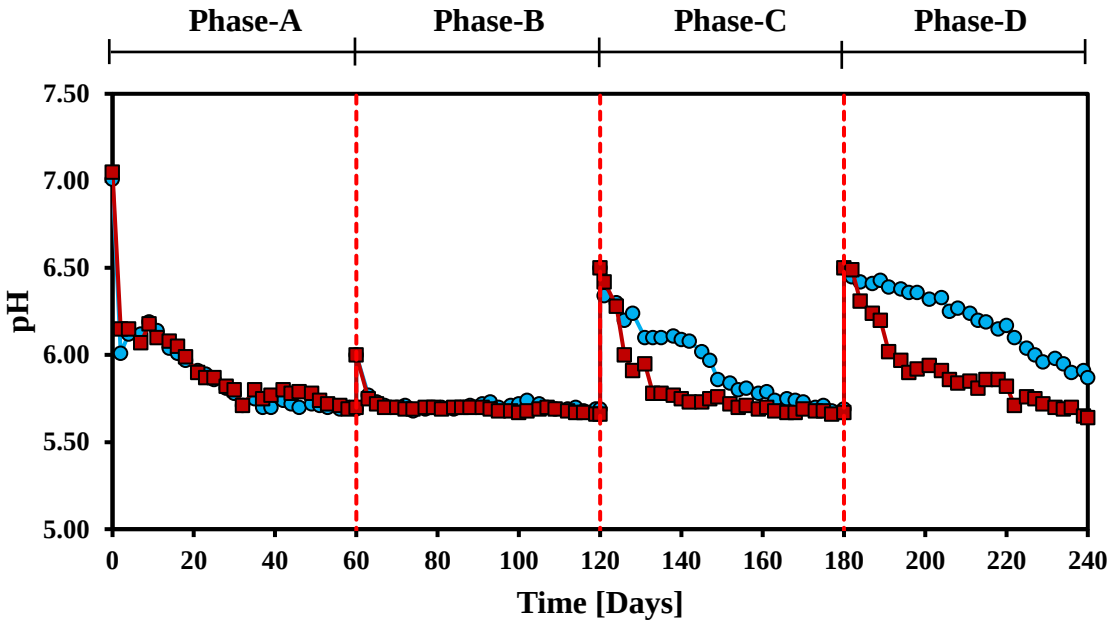

Fig. 3.54: Reactors' pH fluctuations throughout the experimental duration's four phases.
: Reactor-A; :Reactor-B.

3.5.2 Bioethanol Production via Solventogenesis

This study mainly targets acetic acid production, which, as indicated in Fig. 3.52, is the primary metabolic pathway yielding high accumulations. However, at the end of Phase-A and Phase-B, where the availability of H_2 in both reactors was minimal, along with the stabilization of acetic acid production, ethanol (EtOH) was also detected. As shown in Fig. 3.55, at the end of Phase-A, bioethanol production was measured at 1.10 g L^{-1} and 1.12 g L^{-1} in Reactors A and B, respectively, after 60 days. By the end of Phase-B (120 days), when the oxidized Fe-W from Phase-A was reused for an additional 60 days,

ethanol biosynthesis increased by 14% in Reactor A and 26.8% in Reactor B. After 120 days, Reactor A exhibited bioethanol production of 1.28 g L^{-1}, while Reactor B achieved 1.53 g L^{-1}.

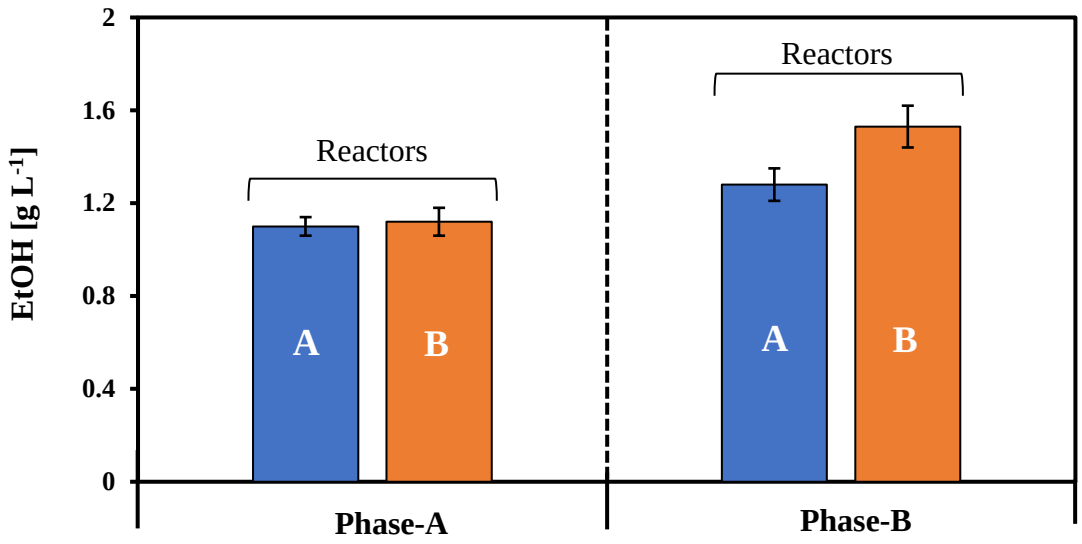

Fig. 3.55: Bioethanol production in Reactors A and B at the end of Phase-A and Phase-B, with each phase lasting 60 days.

3.5.3 Microbial Profile Analysis of Selected Samples from Reactors Throughout the Four Stages

In this study, bacterial diversity was analyzed across multiple samples (Fe-W, growth medium, and biocarrier) obtained from each reactor (A and B) at the end of each phase. The relative abundance analysis of bacteria, as shown in Fig. 3.56, reveals significant differences at both the phylum and genus levels compared to the initial inoculum (Fig. 3.49 – River-SL), which displayed a noticeably greater variety of phyla. The use of Fe-W in two parallel reactors exposed to BES and supplied with continuous CO_2 led to a marked increase in the Firmicutes phylum in both reactors (A and B) throughout the experiment, compared to the initial inoculum, where Firmicutes made up only 1.31% of the microbial community.

After 60 days, at the end of Phase-A, two different samples were taken from Reactor-A for DNA extraction: one consisting solely of Fe-W and the other a liquid sample collected

from the aqueous phase to analyze both suspended and Fe-W-attached bacterial communities. From Reactor-B, a single sample of Fe-W was collected. Sequence analysis revealed that Firmicutes increased in Reactor-A to approximately 44-52%. Both Reactor-A samples (Fe-W and liquid) showed strong similarities, with the *Sporomusa* genus being the most dominant at 31.57% and 27.60%, respectively. The *Acetobacterium* genus was present at lower levels, around 4% in both samples. The sample from Reactor-B showed an even higher abundance of Firmicutes, reaching 71%. Additionally, *Acetobacterium* significantly increased in Reactor-B, representing 55.86% of the community. This high *Acetobacterium* abundance likely explains the higher acetic acid accumulation observed in Reactor-B compared to Reactor-A. Both *Acetobacterium* and *Sporomusa* are homoacetogenic bacteria capable of growing autotrophically on an H_2/CO_2 substrate via the acetyl-CoA pathway (Karekar et al., 2022). However, the high relative abundance of *Acetobacterium* in Reactor-B is attributed to the specific design of the reactors, which are connected in parallel, with Reactor-B receiving the unconsumed trace amounts of H_2 from Reactor A. As Philips et al. (2019) stated, several homoacetogenic bacteria, including *Acetobacterium* species, do not strictly rely on iron-induced corrosion, unlike *Sporomusa*. Abiotic H_2 produced in Reactor-A was transferred to Reactor-B due to the continuous CO_2 feeding mode. As a result, Reactor B was supplemented with H_2, which accumulated and combined with the abiotic H_2 produced in situ. As Laura and Jo (2023) highlighted, *Sporomusa* strains have a lower H_2 threshold than *Acetobacterium*, which requires higher H_2 supply rates. On the other hand, *Acetobacterium* exhibited higher relative abundance in enrichments, and until now, only a pure strain of *Sporomusa* (*S. ovata*) has demonstrated high acetic acid production. This explains the elevated relative abundance of *Acetobacterium* and the higher acetic acid concentrations in Reactor B.

At the beginning of Phase-B, the old growth medium was replaced with a fresh medium, and Reactor-B was supplemented with biocarriers. After 120 days, at the conclusion of Phase-B, one sample was collected from Reactor A, consisting of Fe-W, while two samples were obtained from Reactor-B, including Fe-W and biocarriers, which were subjected to DNA extraction. The relative abundance analysis revealed that the medium replacement resulted in a significant increase in *Acetobacterium* in Reactor-A by approximately 14% (overall percentage: ~18%), accompanied by a reduction in the *Sporomusa* genus by approximately 13.5% (overall percentage: ~16.11%). During Phase-

A, *Sporomusa* exhibited an elevated relative abundance of 29.6%. The same genus was also identified by Philips et al. (2018) in an anaerobic system, where CO_2 was the sole carbon source, supplemented with ZVI (Fe^0) under conditions similar to those of our experiments. In their study, H_2 gas was detected at extremely low concentrations, and acetate was the only VFA that increased almost linearly in the reactors.

A similar observation was also reported by Kato et al. (2020), who found that when H_2 concentrations were low, these two genera predominated. However, the decrease in *Sporomusa* may be attributed to several factors. As explained by Philips et al. (2018), *Sporomusa* relies heavily on elemental H_2. During Phase-B, already oxidized and passivated iron was used, leading to lower H_2 production by Fe-W. This may explain the increase in the *Acetobacterium* genus (Laura and Jo, 2023) due to its ability to survive and adapt to varying H_2 concentrations.

On the other hand, as stated by Madjarov et al. (2022), *Sporomusa* does not appear to form biofilms. The sample from Reactor-B containing Fe-W displayed similarities to Reactor A in terms of bacterial communities. However, *Acetobacterium* was the most dominant genus, representing 27.26%, followed by *Sporomusa* at 16.81%. However, the biocarriers in Reactor-B exhibited a markedly higher abundance of *Acetobacterium*, reaching 53.32%. This substantial increase in *Acetobacterium* immobilized in biocarriers may explain the higher acetic acid production. Ameen et al. (2019) recognized the ability of *Acetobacterium* to form biofilms in MES systems.

At the beginning of Phase-C, the growth medium in Reactor-A was replaced with water, and an additional 2 Kg of fresh Fe-W was introduced while retaining the 2 Kg of Fe-W from the previous phase. This material underwent sterilization (thermal treatment - 121ºC for 15 min) to inhibit bacterial and archaeal activity, with the goal of making Reactor-A an exclusive hydrogen producer and supplier for Reactor-B. However, the sterilization process, while effective at inhibiting methanogenesis, was insufficient to prevent acetogenesis, as shown in Fig. 3.53. The thermal treatment applied to Reactor-A led to a substantial increase in *Clostridium sensu stricto*, which rose by nearly 60%, suppressing acetic acid production that had been observed in Reactor-B during Phases A and B. Analysis of the two samples from Reactor-B —one from the liquid phase and one from the biocarrier—revealed strong similarities in bacterial abundance, with *Acetobacterium* being the most dominant, reaching 55% and 54% in each sample, respectively.

Sporomusa was present at a relative abundance of 4.05% in the liquid samples, while biocarrier samples showed a relative abundance of 2.46%

After Phase-D, during the final experimental phase, only two samples were collected from Reactor-B, one from the liquid phase and one from the biocarrier. No samples were taken from Reactor-A, which was equipped with new, sterilized, and uncontaminated materials designed to function as the H_2 producer and supplier to Reactor-B. Replacing the old growth medium in Reactor-B increased Firmicutes in the liquid phase to over 83%. *Acetobacterium* remained the most abundant genus, representing 68.49% and 45.10% of the liquid and biocarriers population, respectively. *Sporomusa* was also identified in Phase-D, representing 9.89% in the liquid samples, while biocarrier samples showed a relative abundance of 9.83%. It is evident that during the experimental duration, *Acetobacterium* is responsible for the production of acetic acid in Reactor-B, whereas no acetic acid production was detected in Reactor-A. The same observation, where *Acetobacterium* became the predominant species, was also reported by Aryal et al. (2017) in MES systems, where environmental samples were used in methanogenesis-inhibited systems, and CO_2 served as the electron acceptor.

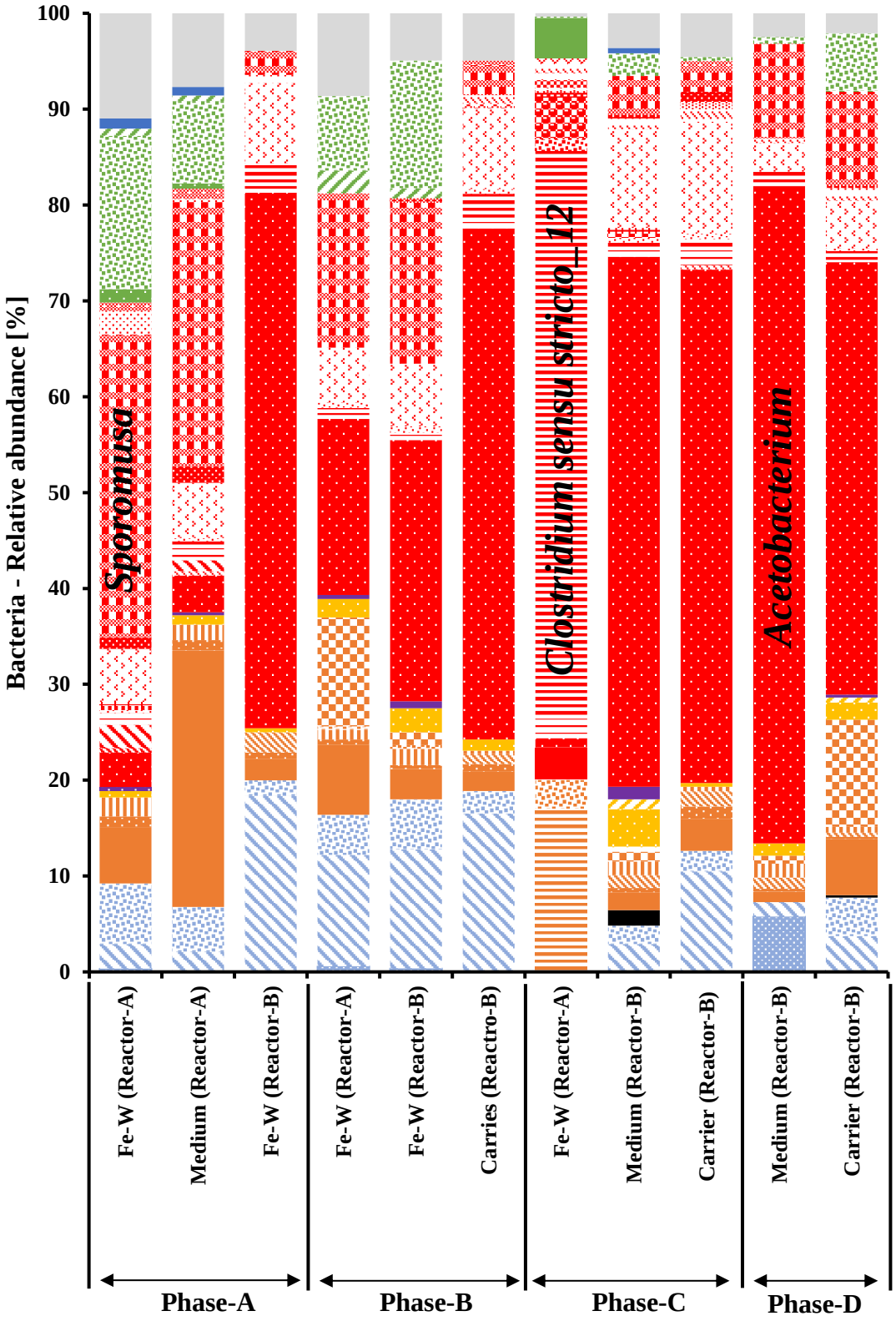
Bacteria - Relative abundance [%]
100
90
80
70
60
50
40
30
20
10
0
Sporomusa
Clostridium sensu stricto_12
Acetobacterium
Fe-W (Reactor-A)
Medium (Reactor-A)
Fe-W (Reactor-B)
Fe-W (Reactor-A)
Fe-W (Reactor-B)
Carries (Reactro-B)
Fe-W (Reactor-A)
Medium (Reactor-B)
Carrier (Reactor-B)
Medium (Reactor-B)
Carrier (Reactor-B)
Phase-A
Phase-B
Phase-C
Phase-D

Fig. 3.56: Relative abundance of bacteria (%) at phylum and genus levels at the end of each experimental phase.

3.5.4 Structural Evolution of Processed Fe-W Material

The structural changes of Fe-W particles used in (bio)reactors were assessed by analyzing the X-RD patterns and SEM images of selective specimen samples taken at different phases of the experiment.

Four Fe-W samples were subjected to X-RD analysis to examine their structural characteristics. In order to investigate the purity and the absence of iron oxides or other crystalline phases of the Fe-W derived from the machinery industry, unprocessed Fe-W before the implementation was analyzed. Additional two Fe-W samples were collected from Reactor A and Reactor B at the conclusion of Phase-B, following 120 days of continuous CO_2 feeding, and were also analyzed. Furthermore, at the end of phase-D, Fe-W sample was obtained from the ex-situ H_2-producing Reactor A where double the amount of Fe-W was utilized for the reaction with CO_2 driven for analysis.

As illustrated in Fig. 3.57, the unprocessed Fe-W (blue line) displays three dominant diffraction peaks at 44.7°, 65.0°, and 82.3°, confirming that the Fe-W used was new and unoxidized.

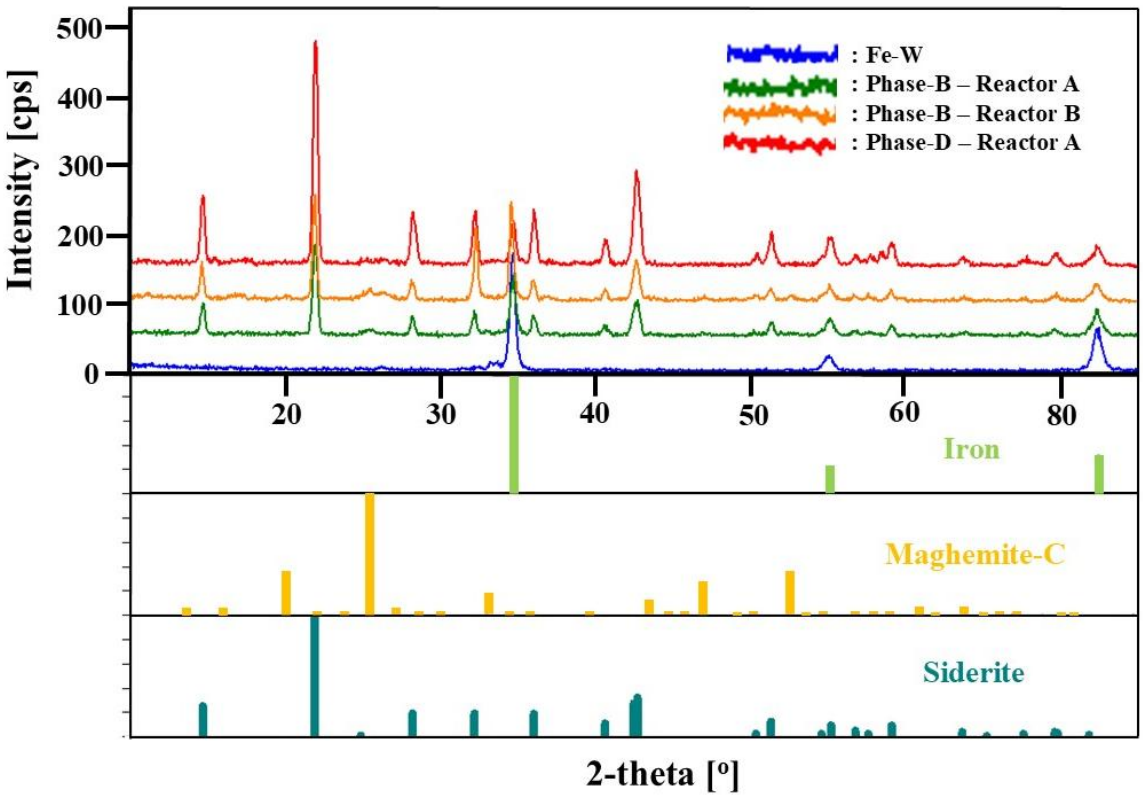

Fig. 3.57: X-RD patterns of unprocessed and processed Fe-W samples supplemented in reactors operating under continuous CO_2 feeding mode.

On the other hand, the Fe-W supplemented in continuous fed-batch reactors inoculated with a microbial consortium and inhibited with 4 mM of BES exhibited a distinct pattern. The processed Fe-W demonstrated a prominent peak (~20°), indicating the formation of siderite ($FeCO_3$). The same observation of siderite formation was noted when ZVI was exposed to low and high carbonated conditions, as shown in Sub-chapters 3.1.1 and 3.1.2, and when ZVI was exposed to the same conditions in the presence of bacteria, as shown in Sub-chapter 3.2.7. As highlighted by Wang et al. (2020), when iron is exposed to CO_2-saturated conditions, the carbonate ions produced by the hydrolysis of carbonic acid in the aqueous solution, where CO_2 is dissolved, combine with ferrous ions to form siderite.

Additionally, a weak peak corresponding to maghemite (γ-Fe_2O_3) was identified. The sample derived from Phase-D showed the same X-RD pattern.

The corroded by-products of distinguished prosed Fe-W samples harvested from the reactors at the end of all phases were also qualitatively investigated by analyzing SEM images of the samples. As shown in Fig. 3.58, SEM images between selected samples do not vary significantly, and the mineralogical structure of the formatted corrosion by-product of Fe-W substrate indicates the formation of well-structured trigonal crystals typical for siderite. This observation is direct evidence of the formation and the existence of siderite, thus enhancing the results of the analysis conducted with X-RD. The uncontaminated Fe-W samples collected at the end of Phase-D (*ex-situ* Reactor A) and subjected to SEM show the formation of siderite crystals (Fig. 3.58 – Image A.). On the other hand, SEM images of Fe-W contaminated by bacteria, derived from Phase A and Phase B, not only reveal the formation of siderite but also illustrate bacterial activity on the siderite crystals and their chemical corrosion induced by the production of acetic acid. (Fig. 3.58 – Image D.). Additionally, fossilized bacteria (Fig. 3.58 – Image C.) and their imprints were also identified (Fig. 3.58 – Images B. and D.). Fe-W samples derived from reactors (A & B) at Phase-A and Phase-B exhibited the same patterns regarding the formation and observation of siderite crystals. At the end of Phase-B, biocarriers were also collected from Reactor-B and were driven for SEM imaging analysis (Fig. 3.58 – Image F.). The images from SEM reveal the formation of siderite crystals; however, they are not well-structured. Samples of Fe-W derived from the *ex-situ* Reactor A at the end of Phase-C were also analyzed. The SEM images (Fig. 3.58 – Image E.) show a distinguished pattern compared to the images from Phase-D. A well-structured siderite

crystal was identified along with needle-like iron oxide/hydroxide crystals. This is attributed to adding extra new Fe-W at the beginning of Phase-C, fueling the system with iron ions. After the liquid sample was exposed to air, secondary iron oxide crystals were formed.

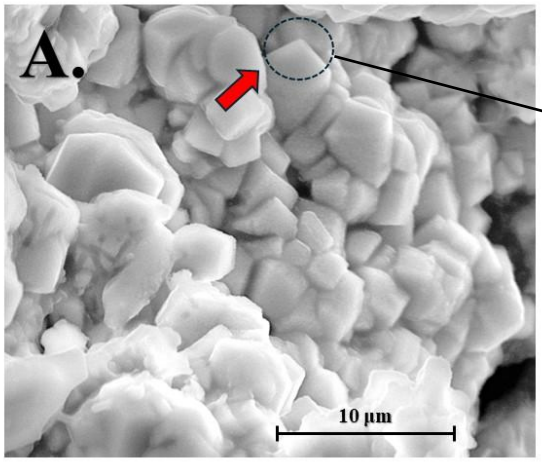

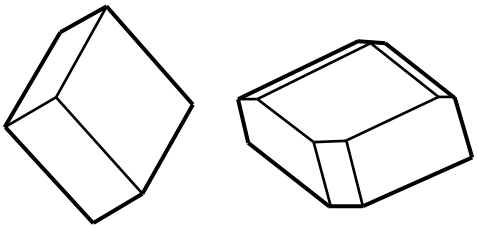

Crystal System: Trigonal-Rhombohedral

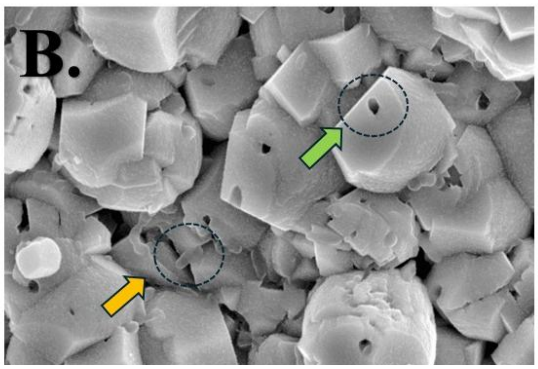

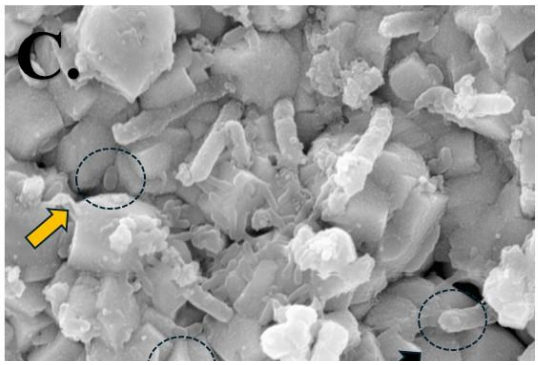

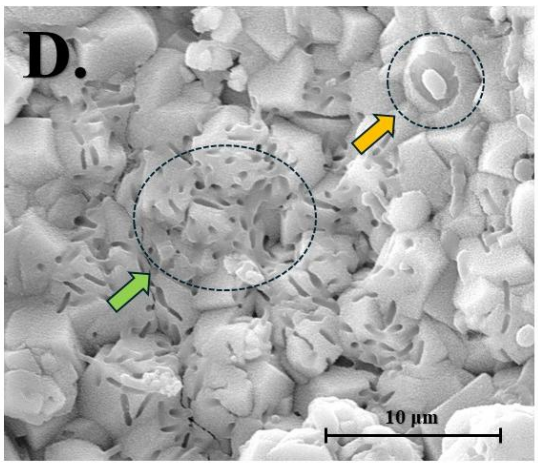

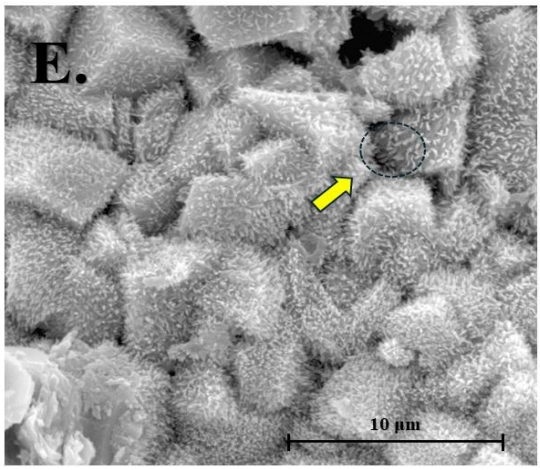

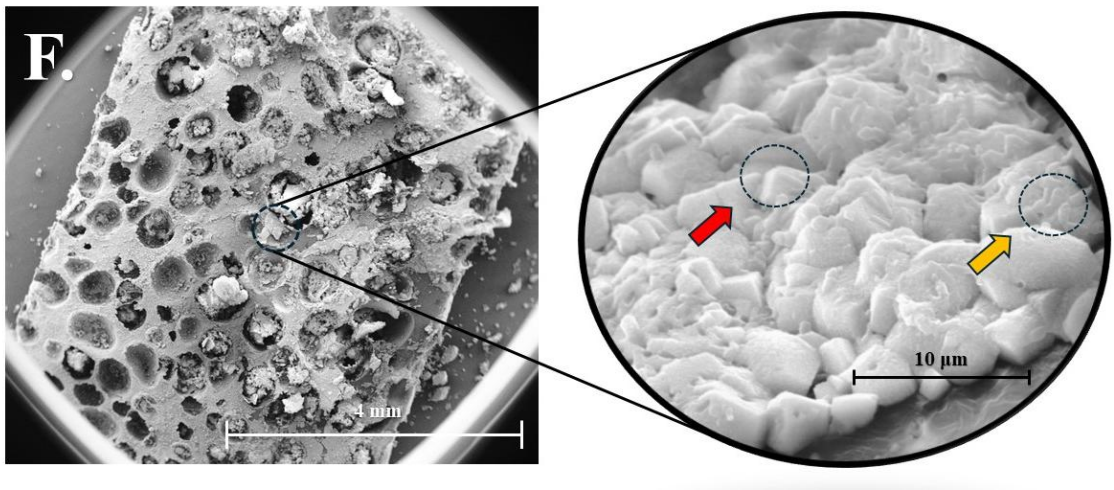

Fig. 3.58: Micrograph SEM images of Fe-W substrate utilized in reactors and the appearance of the corrosion product. **A.:** SEM images of Fe-W samples derived from the *ex-situ* Reactor A at the end of the experimental duration (60 days) of Phase-D (after 240 days); **B. & C.:** SEM image of Fe-W contaminated by bacteria, collected from reactors at the end of the experimental duration (60 days) of Phases A (after 60 days); **D.:** SEM image of Fe-W contaminated by bacteria, collected from reactors at the end of the experimental duration (60 days) of Phases B (after 120 days); **E.:** SEM image of Fe-W samples derived from the *ex-situ* Reactor A at the end of the experimental duration (60 days) of Phase-C (after 180 days); **F.:** SEM image of biocarrier sample derived from Reactor B at the end of the experimental duration (60 days) of Phase-B (after 120 days).

: Crystal structure of siderite; : Rod-shaped bacteria; : Bacteria imprints;

: Fossilized bacteria; : Iron oxide/hydroxide needle-like crystal formation.

3.5.5 Discussion of Experimental Set-Up 5

This study examined a new sustainable approach for CO_2 utilization by using bioreactor systems cabled with a continuous CO_2 feeding system that utilizes waste iron fillings (Fe-W) from a machinery industry in a circular economy concept. In this bioreactor system, CO_2 is bioconverted into acetic acid, an important platform chemical highly demanded in industry.

The results indicate high acetic acid production throughout the experimental duration, particularly during the first 60 days, corresponding to Phase-A. This is attributed to the high relative abundance of *Sporomusa* in Reactor A and *Acetobacterium* in Reactor B, two acetogenic strains capable of lithotrophic growth by utilizing CO_2 and H_2. The continuous CO_2 flow in the reactor system facilitated H_2 outflow, resulting in low H_2 concentrations within the system. Under these conditions, bacteria could utilize only low concentrations of H_2 gas, which explains the high relative abundance of *Sporomusa* in Reactor A.

Laura and Jo (2023) confirmed that *Sporomusa* strains have an H_2 threshold two orders of magnitude lower than those of *Acetobacterium* and *Clostridium* strains. Consequently, in Reactor B, *Acetobacterium* thrived due to the relatively higher availability of H_2. Furthermore, as noted by Liu et al. (2020) and Kotsyurbenko et al. (2001), under conditions of low H_2 pressure and concentration, acetogenic reactions become more thermodynamically favorable in mixed microbial cultures. This observation also explains the high accumulation of acetic acid during Phase-A, particularly in Reactor B.

It is important to note that *Sporomusa* was present during all experimental phases of this study. Experiments conducted by Igarashi and Kato (2021) demonstrated that *Sporomusa* species can transform iron and facilitate the dissolution and alteration of Fe(III) oxides. This finding aligns with the formation of maghemite (γ-Fe_2O_3), as identified through X-RD analysis. Moreover, it has been reported that Homoacetogens possess the ability to actively dissolve insoluble Fe(III), including crystalline Fe(III) oxides, to acquire the iron necessary for their metabolic processes.

During Phase-B, a similar pattern in acetic acid production was observed, with the same strains contributing to the system, albeit with lower acetate accumulations. This reduction is attributed to the use of already oxidized Fe-W from Phase-A. The formation of siderite, as confirmed by X-RD analysis, acted as a passivating corrosion scale, inhibiting the production of abiotic H_2. Furthermore, the relative abundance of *Acetobacterium* increased during this phase due to its ability to adapt to different H_2 concentrations, as explained in Sub-chapter 3.5.3.

At the end of both Phase-A and Phase-B, low ethanol accumulation was measured. This may be attributed to the pH levels at which the reactors operated. As stated by Arslan et al. (2019), pH plays a critical role in determining the end products of acetogenic bacteria. Generally, higher pH levels favor biomass formation and acid production, while lower

pH levels promote solventogenesis. This observation aligns with the pH operating parameters and ethanol formation in this study. During Phase-A and Phase-B, the reactors operated at average pH levels of 5.7, under mildly acidic conditions, as shown in Fig. 3.54, where ethanol production was observed. As highlighted by Romans-Casas et al. (2023), several studies show that at pH levels below 5.4, and always in the presence of acetic acid, ethanol can be formed at approximately 1 g L^{-1}, an observation that aligns with our results. In contrast, during Phase-C and Phase-D, when the reactors operated at higher pH values (6.0–6.5), bioethanol production was not detected.

As stated by Romans-Casas (2023), bioethanol can also be produced through the reduction of acetate, with H_2 serving as an electron donor for aldehyde:ferredoxin oxidoreductase activity. Katsyv and Müller (2020) describe that both acetate and acetaldehyde (a precursor to ethanol formation) have a highly negative redox potential (E_0' = −580 mV). Consequently, a low-potential electron donor such as ferredoxin is required, along with the activity of monofunctional alcohol dehydrogenase for the further reduction of acetaldehyde to ethanol.

He et al. (2022) explain an additional mechanism that accelerates bioethanol formation. At low pH levels, the concentration of undissociated acids increases, enabling these acids to penetrate bacterial cells. To prevent damage caused by intracellular pH reduction, bacteria convert these acids into neutral ethanol, ensuring their survival. This mechanism aligns with our pH monitoring data (Fig. 3.54), which shows that reactors operated at the lowest pH values (below 6) during Phase-B. Furthermore, Ammam et al. (2016) demonstrated the positive effect of iron ions on ethanol production acceleration in *Sporomusa* species.

The formation of ethanol from acetate through the chain elongation mechanism is described in Eq. 52 (Rovira-Alsina et al., 2022).

$$CH_3COO^- + H^+ + 2H_2 \rightarrow CH_3CH_2OH + H_2O \ (\Delta G^\circ = -10.50 \text{ kJ mol}^{-1}) \quad \text{(Eq. 52)}$$

During Phase-C, Reactor A, which served as an exogenous hydrogen producer and was supplemented with Fe-W, along with Fe-W itself, were subjected to thermal pre-treatment, leading to the observation of a distinctive bacterial species. *Clostridium sensu stricto 12* was enriched in Reactor A, with higher accumulations of acetic acid (4497 mg

L^{-1}) compared to Reactor B (1500 mg L^{-1}) was observed due to the utilization of Fe-W derived H_2. According to Wu et al. (2020), these Gram-positive anaerobic bacteria exhibit significant biocatalytic diversity and have the ability to form spores.

Pyne et al. (2014) characterized Clostridium as "truly ubiquitous," highlighting their ability to resist thermal shock and survive under various conditions, including elevated oxygen levels, acidity, the presence of alcohols, subjected to desiccation, and under ammonia stress (Wang et al., 2022). Due to these robust characteristics, *Clostridium* is currently being investigated for its high application potential in biotechnological fields, including medical and industrial sectors (Pyne et al., 2014).

The same genus was identified by Samanides et al. (2020) in experiments where anaerobic granular sludge underwent thermal pre-treatment before inoculation into an anaerobic system supplemented with ZVI. The Clostridium genus has also been identified in microbial electrosynthesis (MES) systems. For example, Mateos et al. (2019) found *Clostridium* to be responsible for acetic acid production, accounting for over 67% of the microbial community, along with *Sporomusa* (41.5%), in a continuous CO_2 feeding mode without applying any inhibition methods. Similarly, Rojas et al. (2018) identified *Clostridium* (24.5%) and *Sporomusa* (56.5%) in an MES system under continuous CO_2 feeding without inhibition.

Li et al. (2023), in their study on anaerobic fermentation consortia acclimatized to acetate and ethanol for the production of medium-chain fatty acids (MCFAs) through the chain elongation process, found that *Clostridium sensu stricto 12* predominated in the system (45.4%). The same researchers concluded that *Clostridium sensu stricto 12*, which was also identified in our systems, is a relatively slow consumer of H_2. This finding aligns with our results. During Phase-C, in addition to the elevated concentrations of acetic acid in Reactor A, H_2 gas was detected (up to 35%), whereas during Phase-A and Phase-B, H_2 gas was not observed.

The elevated relative abundance of the *Clostridium sensu stricto* genus may not only be attributed to spore formation during heat pre-treatment but also to electron uptake from solid metals. Pan et al. (2021) emphasized that *Clostridium sensu stricto* can be enhanced in systems with ZVI due to the potential for DIET.

Lastly, during Phase-D, Reactor A, which supplied exogenous H_2 to Reactor B, was supplemented with double the amount of Fe-W compared to the previous phases. As a result, higher concentrations of H_2 were produced and detected in the reactors, reaching

up to 61%. This observation supports the hypothesis that Acetogens perform optimally under low H_2 concentrations and can directly utilize electrons from solid materials.

Regarding the analysis of SEM images revealed the formation of well-structured rhombohedral crystals, indicative of siderite formation, during all experimental phases. Similar well-defined siderite crystals have also been observed by Matamoros-Veloza et al. (2020) and Joshi et al. (2018). These studies investigated the corrosion of carbon steel pipelines transporting NaCl brine in a CO_2 environment and the corrosion of iron substrates exposed to CO_2-saturated water at elevated temperatures, respectively. This phenomenon, referred to as "pseudo-passivation," may explain the lower acetic acid accumulations observed during Phase-B compared to Phase-A.

According to Joshi et al. (2018), the rhombohedral morphology of siderite results from the initial nucleation of amorphous ferrous carbonate (AFC) on the corroding substrate when the system's solution is near surface supersaturation with ionic $Fe^{2+}_{(aq)}$ and $CO_3^{2-}{}_{(aq)}$. However, by the end of Phase-C, the Fe-W sample exhibited distinctive SEM characteristics. In addition to siderite crystals, needle-like or nanorod-shaped crystals were also synthesized as a secondary corrosion scale. During Phase-C, the ex-situ Reactor A was supplemented with fresh Fe-W, introducing unstable Fe^{2+} ions into the system. Subsequently, at the end of Phase-C, aqueous Fe-W samples were extracted from Reactor A for SEM analysis. The Fe^{2+} species underwent rapid oxidation upon exposure to atmospheric conditions, producing iron hydroxides when Fe-W samples were extracted for analysis. The resulting Fe^{3+} ions formed various iron morphologies, including FeOOH species (Pullin et al., 2017). This process explains the formation of needle-like goethite (α-FeOOH) crystals (Fig. 3.58 – E).

The dual confirmation of siderite formation through X-RD and SEM analysis suggests that CO_2 is not only consumed by bacteria but is also catalytically transformed on the surface of Fe-W. This corrosion bioproduct can be treated with weak acids for regeneration, as extensively detailed in Sub-chapters 3.1.12 and 3.1.13.5, or utilized directly in various applications aligned with circular economy principles.

For example, Zhu et al. (2020) proposed the use of siderite as an innovative reductant for environmentally friendly processing of low-grade refractory iron ore via magnetization roasting coupled with low-intensity magnetic separation technology. Additionally, Van Beek et al. (2021) demonstrated its potential for controlling iron (II) concentrations in

fresh groundwater, while Yang et al. (2018) highlighted its capability for the simultaneous removal of nitrate and phosphate from wastewater.

Moreover, as evidenced in this study, siderite can serve as a substrate for the formation of α-FeOOH. Li et al. (2022) and Fang et al. (2020) emphasize the significance of this mineral, citing its unique chemical and physical properties, such as chemical stability, high specific surface area, and fine particle size, which render it suitable for various industrial applications.

This study investigates acetic acid production through the utilization of CO_2, supplemented in a system in continuous mode. Until now, this methodology has been investigated only by a few scientists, especially in MEC systems where electrodes were used as electron donors and not iron.

The production of acetic acid under continuous CO_2 recirculation feeding was also investigated by Mateos et al. (2019) by using a two-chambered MES without ZVI and inoculated with enriched anaerobic sludge. The experiments were performed in two sets. During the first set, an average acetic acid production rate of 61 mg L^{-1} d^{-1}, with a peak concentration of 1687 mg L^{-1}. At the end of the second set, a higher average production rate of 109 mg L^{-1} d^{-1} and a maximum acetic acid concentration of 1957 mg L^{-1} were observed. However, these reported values do not account for the acetic acid already present in the system from previous batches, which were approximately 1200 mg L^{-1} in the first set's initial batch and 1100 mg L^{-1} in the final batch of the second set, as detailed in Table 3.16.

In contrast, the findings of this study, demonstrate higher acetic acid production after 21 days of continuous CO_2 feeding, even during the initial enrichment phase (Phase A). Reactor A reached 1450 mg L^{-1}, while Reactor B achieved 1665 mg L^{-1}, corresponding to production rates of 76 mg L^{-1} d^{-1} and 87 mg L^{-1} d^{-1}, respectively. These results were achieved without needing a complex setup involving electrodes, an electrical supply, ion exchange membranes, or a prolonged sludge acclimation phase.

Bajracharya et al. (2017) also use the MES system for the production of acetic acid at a continuous CO_2 feed mode. However, the experimental setup involved multiple pre-treatment and enrichment stages. These included thermal pre-treatment of anaerobic sludge at 90 °C for 1 hour, regrowth of bacteria in a glucose-supplemented system with 2 mM BES under a CO_2:H_2 (20%:80%) environment, and transfer of the enriched culture to the MES system. For the startup phase, *Clostridium ljungdahlii* and 2 mM of fructose

were supplemented. The experiments were conducted in three batches, with the maximum acetic acid production rate of 400 mg L^{-1} d^{-1} observed during the second batch. The highest concentrations were measured on day 332, reaching 7 g L^{-1}, with bioethanol accumulation reaching 0.19 g L^{-1}. In contrast, our study demonstrates higher acetic acid production over shorter durations and a more straightforward setup. At the end of Phase-A (60 days), without requiring extensive pre-treatments, long inoculum preparations, or expensive ion exchange membranes, by using only 4 mM BES to inhibit methanogenesis, Reactor A produced 4.7 g L^{-1} of acetic acid. At the same time, Reactor B achieved 7 g L^{-1}. Additionally, both reactors produced approximately 1 g L^{-1} of bioethanol.

Although Bajracharya et al. (2017) reported high acetic acid production rates, these values reflect short intervals during batch operations, often with fluctuations in acetic acid output during the experiment. In contrast, our process demonstrated steady increases in acetic acid production across all experimental phases without significant fluctuations. Consequently, while our calculated production rates may appear lower, they reflect sustained performance over time.

In a different approach, Ntagia et al. (2021) produce acetic acid from CO_2/H_2 by implementing a highly complex bioreactor configuration utilizing mixed microbial culture. As detailed in Table 3.16, the process utilized an electrochemical cell to generate H_2 gas. During the 168-day experimental period, the maximum acetic acid production rate was recorded on day 43, reaching 0.8 g L^{-1} d^{-1}. However, adding 1.3 mM of total dissolved sulfide (TDS) to the system led to a significant drop in production to 0.1 g L^{-1} d^{-1} over the subsequent 20 days, during the inhibition event from days 43 to 63.

In contrast, our study achieved a maximum acetic acid production rate of 0.71 g L^{-1} d^{-1} during the experiment's first phase (days 35–37) in Reactor B using a straightforward continuous CO_2 feed bioreactor. Unlike the Ntagia et al. (2021) approach, our setup did not require electrical energy to operate pumps or an electrochemical cell. Their reliance on such cells for H_2 production posed risks of electrode corrosion at high electrical currents, necessitating electrode replacements.

Furthermore, the operation of their gas fermentation column required amounts of KOH and NaOH for pH adjustments. In contrast, our bioreactors achieved high acetic acid accumulation without pH adjustments, as the dissolution of CO_2 in the aqueous solution generated carbonic acid, acting as a buffer. This natural buffering mechanism countered

pH increases caused by electron utilization and H_2 formation by Fe-W, as discussed in Sub-chapter 3.1.13.1.

In a different concept, Riegler et al. (2019) investigated various parameters for acetic acid production from CO_2 and H_2 in a continuous mode, including gas dilution rates, gas pressures, and gas or liquid flow rates, using two modified tank bioreactors (Pached-bed and trickle-bed biofilm reactor) inoculated with pure culture of *Clostridium aceticum* (DSM 1496) immobilized on Sera Siporax™ carriers. Maximum acetate production was achieved by using Trickle-bed bioreactor at a concentration of 8.8 g L^{-1} (Production Rate: 0.80 g L^{-1} h^{-1}) with liquid flow rate set at 1.03 ml min^{-1} (Table 1.16).

This experimental setup used pure strain to utilize CO_2 and H_2 gases. However, Dessì et al. (2021) noted that using pure strains presents several challenges. The process requires a complex start-up procedure, a specific growth medium, and sterilization to prevent contamination. It is sensitive to fluctuations in system conditions and vulnerable to oxygen exposure. Furthermore, a preliminary period was also required for biofilm formation on the carrier materials. In contrast, our experimental setup, in continuous mode with a constant CO_2 flow rate of 0.08 L min^{-1}, produced a maximum acetic acid concentration of 7 g L^{-1} after 60 days without the need for complex procedures, sterilization or gas filtration prior to introducing the gases into the reactors as was done by Riegler et al. (2019)

Rojas et al. (2018) also investigated acetic acid production in a two-chamber MES system. The acetogenesis was carried out using a pre-enriched Homoacetogenic culture. The results showed a maximum acetic acid concentration of 5656 mg L^{-1} without any electrical supply interruptions. However, with electrical interactions, acetate levels dropped in the systems to 4912 mg L^{-1}. These observations indicate that continuous electrical supplementation is essential to maintain acetate production. However, when the electrical supply was disconnected, acetate was not produced, and acetate-consuming bacteria utilized the accumulated acetate in the system. This highlights the necessity of using microbial inhibitors to deactivate acetate-consuming microbes.

Our experiments demonstrated the production of more than 7000 mg L^{-1} (Max prod. rate 709 mg L^{-1} – during Phase-A) of acetic acid (Phase-A, Reactor B) after 60 days without requiring an electrical supply configuration. The inhibition of acetate-consuming archaea was achieved using only 4 mM of BES. Our acetic acid accumulation surpassed the concentrations reported by Rojas et al. (2018), even when the system utilized a processed

Fe-W (3957 mg L^{-1} during Phase-B, Reactor B). Additionally, higher acetate accumulation was observed when Reactor A was thermally pretreated during Phase C, reaching 4497 mg L^{-1}.

Based on the above, it is evident that acetate can be produced at elevated concentrations without the need for complicated and expensive configurations, utilizing only waste iron under ambient conditions and within a circular economy framework. Higher acetic acid production rates were observed during Phase A, reaching 354 mg L^{-1} between days 37–39 in Reactor A and 709 mg L^{-1} between days 35–37 in Reactor B. These findings indicate a promising alternative route for acetate production compared to conventional methods.

Table 3.16: An overview of acetic acid and/or bioethanol production in continuous CO_2 feeding systems.

Inoculum	Carbon source	Electron donor	Inhibition	Exp. mode	Duration	Acetate production	References
Mixed microbial community	100% CO_2 (flow rate 12 ml min^{-1}) CO_2:H_2 = 2:1	H_2 gas from electrochemical cell operated between 0.001A and 4A (Electro Syn cell)	Total dissolved sulphide (TDS): 1.3 mM	Continuous gas fermentation column bioreactor with hollow fiber membranes	168 days Day 0-43: No inhibition Day 43-66: 1.3 mM TDS Day 63-77: Recovery period Day 77-91: 1.3 mM TDS Day 91-106: Recovery period Day 106-121: 1.3 mM TDS Day 121-168: No inhibition	Day 0-43: 0.7 g L^{-1} d^{-1} (average) Day 43-66: from 0.8 g L^{-1} d^{-1} to 0.1 g L^{-1} d^{-1} Day 63-77: 0.3 g L^{-1} d^{-1} Day 77-91: from 0.3 g L^{-1} d^{-1} to 0.1 g L^{-1} d^{-1} Day 91-106: from 0.1 g L^{-1} d^{-1} to 0.3 g L^{-1} d^{-1} Day 106-121: from 0.3 g L^{-1} d^{-1} to 0 g L^{-1} d^{-1} Day 121-168: 0.2 g L^{-1} d^{-1} from days 133-168 (at 0.5 mM of TDS)	Ntagia et al., 2021
Clostridium aceticum (DSM 1496)	CO_2:H_2:N_2 = 3:12:10	H_2	x	Continuous modified tank bioreactors 2: Trickle-bed biofilm reactor	Packed-bed biofilm Reactor → Dilution rate exp.= 21 days H_2 pressure exp.= 24 days Trickle-bed biofilm reactor → Liquid flow rate exp.= 23 days Gas flow rate exp.= 43 days	**Packed-bed biofilm reactor** Dilution rate exp.→ Max 4.6 g L^{-1} (Prod. Rate: 0.267 g L^{-1} h^{-1}) Hydrogen pressure exp.→ Max 2.66 g L^{-1} (Prod. Rate: 0.41 g L^{-1} h^{-1}) **Trickle-bed biofilm reactor** Liquid flow rate exp.→ Max 8.86 g L^{-1} (Prod. Rate: 0.80 g L^{-1} h^{-1}) Gas flow rate exp.→ Max 4.5 g L^{-1} (Prod. Rate: 0.70 g L^{-1} h^{-1})	Riegler et al., 2019

Inoculum	Carbon source	Electron donor	Inhibition	Exp. mode	Duration	Acetate production	References
Enriched anaerobic sludge (from a wastewater treatment plant acclimatized for 48 days)	100% CO_2 Set 1: 500 ml CO_2 Set 2: 600 ml CO_2 (recirculation)	Graphite electrodes (0.197 V vs. SHE)	x	Two-chamber MES system Set 1: Batch experiment Set 2: Continuous feed batch experiment	Set 1: 3 batches - 22 days Set 2: 3 batches - 20 days	**Set 1** → Prod. Rate: 61mg L^{-1} d^{-1} (average) Max: 1687 mg L^{-1} (after 7 days at batch 1) **Set 2** → Prod. Rate: 109 mg L^{-1} d^{-1} (average) Max: 1957 mg L^{-1} (after 20 days at batch 3) ** The reported acetic acid accumulations did not account for the acetic acid already present in the system from a previous batch.* **Real acetic acid →** Set 1-batch 1: ~ 487 mg L^{-1} Set 2-batch 3: ~ 857 mg L^{-1}	Mateos et al., 2019
Acetogenic enriched anaerobic sludge from MES	CO_2: Flow rate 10 ml min^{-1}	Graphite stick electrode (−1.0 V vs. Ag/AgCl)		Two-chamber MES system Continuous feed batch experiment	116 days	First batch (0-54 days) → 5656 mg L^{-1} after 26 days without power interruption (Prod. Rate: 217.6 mg L^{-1} d^{-1}) 6201 mg L^{-1} at the end of batch with 3 power interruptions	Rojas et al., 2018

Inoculum	Carbon source	Electron donor	Inhibition	Exp. mode	Duration	Acetate production	References
Anaerobic sludge inoculated with *Clostridium ljungdahlii*	Main experiments 80% CO_2	Graphite felts with graphite stick (-0.9 – -1 V vs. Ag/AgCl)	Thermal (90 °C for 1 h) 2 mM BES	Two-chamber MES system Continuous feed batch experiment	Batch 1: 79 days (day 127-206) Batch 2: 41 days (day 205-246) Batch 3: 86 days (day 246-332)	Batch 1: 4500 mg L^{-1} B1 - Prod. Rate: 248 mg L^{-1} (day 127-134) Batch 2: 3000 mg L^{-1} B2 - Prod. Rate: 400 mg L^{-1} (day 225-227) Batch 3: 7000 mg L^{-1} B3 - Prod. Rate: 340 mg L^{-1} (day 251-255)	Bajracharya et al., 2017
Environmental sample - River sludge	CO_2: Flow rate 800 ml min^{-1}	Waste iron (Fe-w)	Phase A&B: 4mM BES Phase-C: Thermal (121 °C for 15 min) and 4mM BES Phase-D: 4 mM BES	Two reactors connected in a series Continuous feed batch experiment	Phase-A: 60 days Phase-B: 60 days Phase-C: 60 days Phase-D: 60 days	Ph. A → Reactor A: 4722 mg L^{-1} Reactor B: 7050 mg L^{-1} (Max prod. Rate: 709 mg L^{-1} – Reactor B – day 37-39) Ph. B → Reactor A: 3018 mg L^{-1} Reactor B: 3957 mg L^{-1} (Max prod. Rate: 267 mg L^{-1} – Reactor A – day 119-120) Ph. C → Reactor A: 4497 mg L^{-1} Reactor B: 1500 mg L^{-1} (Max prod. Rate: 243 mg L^{-1} – Reactor A – day 27-29) Ph. D → Reactor A: 0 mg L^{-1} Reactor B: 3245 mg L^{-1} (Max prod. Rate: 135 mg L-1 – Reactor B – day 31-33)	Present study

3.5.6 Conclusion of Experimental Set-Up 5

This study investigates the potential of using acetogen-enriched inoculum to produce acetic acid in a continuous CO_2-feeding mode in a bioreactor system, incorporating waste iron (Fe-W).

In Phase-A, both reactors exhibited high acetic acid accumulation, with Reactor-B reaching a maximum concentration of 7050 mg L^{-1} after 60 days and demonstrating the highest acetic acid production rate of 709 mg L^{-1} during days 35–37. *Sporomusa* was Reactor A's predominant genus, whereas Acetobacterium exhibited the highest relative abundance in Reactor B.

In Phase-B, the growth medium was replaced with a new one, and reactors contained processed Fe-W. Reactor-B exhibited significant acetic acid production (5440 mg L^{-1}), although at a lower level compared to Phase A, likely due to Fe-W passivation. The maximum acetic acid production rate was observed at the end of the experimental duration of Phase-B, reaching 267 mg L^{-1} in Reactor A, during days 119–120. During this phase, *Sporomusa* significantly decreased in Reactor A, while *Acetobacterium* concurrently increased.

Thermal treatment of Reactor-A at the beginning of Phase-C effectively inhibited methanogenesis; however, *Clostridium sensu stricto* was identified as the predominant strain, resulting in high acetic acid levels in the system, reaching 4497 mg L^{-1}. The maximum acetic acid production rate was observed at Reactor-A, reaching 243 mg L^{-1} during days 147-149.

In the final Phase-D, where Reactor-A served as the ex-situ H_2 producer and supplier for Reactor-B, Firmicutes in the liquid phase of Reactor-B comprised 83% of the microbial phyla. *Acetobacterium* was identified as the most abundant genus, representing 68.49%. However, lower acetate acid production rates were observed compared to previous Phases (Max 135 mg L-1 during days 211-213).

Furthermore, maximum bioethanol accumulations of 1.53 g L^{-1} were observed at the end of Phase-B in Reactor-B, indicating enhanced solventogenesis under the prevailing experimental conditions.

4. CONCLUDING REMARKS

The experimental procedures of this innovative study demonstrated that CO_2 can be bioconverted into acetic acid and/or bioethanol through a mixed microbial consortium action under mild aqueous anaerobic conditions in systems supplemented with solid metals. The study highlights that the necessary H_2 gas, serving as an electron donor and facilitating biological reactions, can be produced *in-situ* via the oxidation of metals under aqueous and carbonated conditions. However, various inhibition methods were explored to address the challenges posed by consuming reactants (CO_2 and H_2) by methanogenic archaea predominant in such systems. The proposed methodologies presented in this study provide significant insights that could guide future research in optimizing this process.

Experimental Set-Up 1: Abiotic Hydrogen Production

The first experimental group investigated the production of abiotic hydrogen through the oxidation of Fe^0 under aqueous and anaerobic conditions. The results revealed that CO_2 gas plays a critical role in H_2 generation by Fe^0, both with and without the addition of $NaHCO_3$. Notably, faster CO_2 utilization and high H_2 accumulation (98%) were observed at elevated temperatures (50°C), even though lower temperatures favor CO_2 dissolution in the aqueous phase. Additionally, pH significantly influenced H_2 production, with slightly acidic conditions (pH 5-6) promoting higher H_2 accumulation. The particle size of Fe_0 was another important factor, with finer particles yielding more H_2. However, excessively fine particles posed the risk of agglomeration, thereby reducing the active surface area and inhibiting H_2 production. It was also observed that carbonated solutions could be achieved using NaOH solutions for CO_2 capture, which were then introduced into systems with Fe^0. The oxidation by-product of Fe^0 was identified as siderite, and the study demonstrated that oxidized Fe^0 could be treated with acid to dissolve siderite, enabling Fe^0 to be reused. Parameters such as agitation mode, *in-situ* mechanical action, and air-water interface area exhibited minimal influence on H_2 production acceleration.

Experimental Set-Up 2: Fe^0 in Microbial Systems with Methanogenesis Inhibition

In the second experimental group, Fe^0 was used *in-situ* within microbial systems, and several methanogenesis inhibition techniques were applied. The use of BES (2-bromoethanesulfonate) as an inhibitor at a high concentration (50 mM), as recommended in the literature, effectively inhibited methanogenesis for several days. However, this study revealed the need to optimize BES concentrations in such a system, as excessive

BES not only inhibited methanogenesis but also acetogenesis. Thermally pre-treated inoculum inhibited methanogenesis, though the effect was not sustained over time. Similarly, applying low pH as a methane inhibition strategy was ineffective due to the pH increase caused by *in-situ* Fe^0 oxidation. Using NaCl as a more economical alternative also inhibited both methanogenesis and acetogenesis.

Experimental Set-Up 3: Magnesium ribbon and acetic acid production

In the third experimental group, similar methodologies were employed as in experimental group 2, with minimal alteration; however, magnesium was used instead of Fe^0. Magnesium reacted rapidly with the aqueous medium, resulting in high H_2 production. As a result, elevated pressures were recorded in the systems; this shift influenced metabolic pathways, favoring the production of higher-value fatty acids such as butyric acid.

Experimental Set-Up 4: response of Inoculum Sources to acetate production

In the fourth experimental group, various inocula were examined. Environmental samples derived from a river and wetland exhibited higher acetic acid productivity than other sludge samples. For methanogenesis inhibition, 4 mM of BES was sufficient for complete inhibition in most systems, whereas anaerobic granular sludge required a higher dosage (10 mM). Additionally, this study demonstrated that pressurized CO_2 prolonged and increased the H_2 production by Fe^0 and that Fe^0 positively affected acetic acid production by promoting direct interspecies electron transfer. Thermal treatment revealed the presence of spore-forming bacteria, such as *Clostridium sensu stricto*, in high relative abundance, suggesting that this methodology inhibits methanogenesis and supports robust microbial communities that enhance acetate production.

Experimental Set-Up 5: Continuous CO_2 Feeding and Waste Metal Utilization

The fifth experimental group explored acetic acid production under continuous CO_2 feeding. Microbial reactions were carried out in two interconnected reactors utilizing waste iron. The results demonstrated that acetic acid could be produced using waste metal, emphasizing circularity and sustainability. Both *in-situ* and *ex-situ* applications of waste iron in reactors were effective, with *in-situ* systems yielding higher acetate accumulation. Interestingly, higher H_2 production in the reactor system corresponded to lower acetic acid concentrations, indicating the need to optimize H_2 release. *Sporomusa* and *Acetobacterium* species were consistently the most abundant throughout all experimental phases.

5. FUTURE DIRECTIONS AND PERSPECTIVES

The findings of this study provide a robust foundation for understanding the practical application of CO_2 bioconversion in systems involving bacteria supplemented with metals under mild aqueous anaerobic conditions. Despite the significant insights gained, further exploration is essential to enhance this process's efficiency, scalability, and sustainability.

Key Future Directions:

1. *Optimization of H_2 Production and Fe^0 Supplementation*

A critical direction is optimizing H_2 production in systems supplemented with metals. Future studies should investigate the effects of various particle sizes on acetogenesis, particularly concerning Fe ion concentrations and H_2 production. Continuous implementation of low dosages of Fe^0 during experimental runs should also be explored to maintain low H_2 partial pressures, which could further enhance acetogenesis by minimizing the inhibitory effects of H_2 accumulation.

2. *Exploration of Alternative Metals in a Circular Economy Approach*

Expanding research to include other metals, such as zinc, aluminum, metal alloys, and electronic waste, could uncover novel pathways for *in-situ* H_2 production in bacterial systems. Investigating the impact of these metals on acetogenesis would support the application of this process within a circular economy framework. Success in this area could lead to broader implementation in metal management industries, enabling waste-to-energy concepts or acetate production.

3. *Regeneration and Reusability of Oxidized Metals*

Developing cost-effective regeneration methods for oxidized Fe^0 and other metals is critical for system sustainability. Alternative treatments for siderite dissolution, including the use of weaker acids or organic compound-derived extractions, should be systematically explored to enhance the recyclability of metals and reduce costs.

4. *Targeted Methanogenesis Inhibition*

Addressing methanogenesis in mixed microbial consortia is essential for maintaining acetogenic activity. Although BES application, pH control, thermal pre-treatment, and salt addition demonstrated varying levels of success, more targeted approaches are needed to preserve acetogenesis while selectively suppressing methanogenesis. Future research should investigate the role of Fe ion concentrations and optimize Fe^0 dosages as a dual strategy to inhibit methanogenesis and support acetogenesis.

5. *Incorporation of Conductive Materials*

Materials such as stainless steel, which do not produce H_2 through oxidation, should be examined to explore the Direct Interspecies Electron Transfer (DIET) mechanism. Additionally, biochar supplementation in these systems could be studied for its potential to immobilize acetogenic bacteria and enhance acetogenesis or even solventogenesis.

6. *Application of High-Pressure Conditions*

Investigating the application of high-pressure conditions could provide insights into chain elongation mechanisms and the production of higher-value compounds, such as medium-chain fatty acids (e.g., caproate), which hold greater market potential.

7. *Use of Real Waste Gases and Continuous Reactor Systems*

Future work should explore the use of real waste gases in continuous feeding modes, integrating reactors with industrial chimneys. The inhibitory effects of waste gas components, such as H_2S, on acetogens and system performance should be systematically evaluated. Furthermore, syngas containing CO_2 and CO should also be tested to determine its suitability for these systems.

8. *Isolation of High-Performing Acetogenic Strains*

Isolating pure acetogenic strains with enhanced productivity for acetogenesis or solventogenesis is another crucial avenue. These strains should be tested under the parameters discussed, including Fe supplementation, alternative metals, high-pressure conditions, and waste gas integration, for optimum production potential.

The recommendations outlined above will play a pivotal role in developing cost-effective and environmentally sustainable methods for CO_2 utilization. These advancements could simultaneously enable the production of value-added products or platform chemicals. Furthermore, the proposed methodologies in this study could facilitate H_2 “storage” in liquid forms, offering improved storage and transportation solutions.

While these directions provide a roadmap for future research, numerous other parameters remain unexplored. Combining these strategies could significantly enhance the productivity and applicability of this method, contributing to a more sustainable and circular bioeconomy.

REFERENCES

- Abdin, Z. et al. (2020). Hydrogen as an energy vector. *Renewable and sustainable energy reviews*, *120*, 109620. https://doi.org/10.1016/j.rser.2019.109620

- ACS. (2025). *Global Climate Change*. https://www.acs.org/policy/publicpolicies/sustainability/globalclimatechange.html

- Agne, M. et al. (2021). The missing enzymatic link in syntrophic methane formation from fatty acids. *Proceedings of the National Academy of Sciences*, *118*(40), e2111682118. https://doi.org/10.1073/pnas.2111682118

- Ajanovic, A. et al. (2022). The economics and the environmental benignity of different colors of hydrogen. *International Journal of Hydrogen Energy*, *47*(57), 24136-24154. https://doi.org/10.1016/j.ijhydene.2022.02.094

- Al-Mamoori, A. et al. (2017). Carbon capture and utilization update. *Energy Technology, 5(6)*, 834-849. https://doi.org/10.1002/ente.201600747

- Alsalem, M. M. et al. (2023). Modelling of CO_2 corrosion and $FeCO_3$ formation in NaCl solutions. *Chemical Engineering Journal*, *451*, 138966. https://doi.org/10.1016/j.cej.2022.138966

- Al-Shetwi, A. Q. (2022). Sustainable development of renewable energy integrated power sector: Trends, environmental impacts, and recent challenges. *Science of The Total Environment*, *822*, 153645. https://doi.org/10.1016/j.scitotenv.2022.153645

- Ameen, F. et al. (2019). Effect of electroactive biofilm formation on acetic acid production in anaerobic sludge driven microbial electrosynthesis. *ACS Sustainable Chemistry & Engineering, 8(1),* 311-318. https://doi.org/10.1021/acssuschemeng.9b05420

- Ammam, F. et al. (2016). Effect of tungstate on acetate and ethanol production by the electrosynthetic bacterium Sporomusa ovata. *Biotechnology for biofuels*, *9*, 1-10. https://doi.org/10.1186/s13068-016-0576-0

- Andrei, A. Ş. et al. (2012). Living with salt: metabolic and phylogenetic diversity of archaea inhabiting saline ecosystems. *FEMS microbiology letters*, *330*(1), 1-9. https://doi.org/10.1111/j.1574-6968.2012.02526.x

- Andronikou, M. et al. (2022). Magnesium ribbon and anaerobic granular sludge for conversion of CO_2 to CH_4 or biogas upgrading. *Chemical Engineering Journal*, *435*, 134888. https://doi.org/10.1016/j.cej.2022.134888

- Ang, T. Z. et al. (2022). A comprehensive study of renewable energy sources: Classifications, challenges and suggestions. *Energy Strategy Reviews*, *43*, 100939. https://doi.org/10.1016/j.esr.2022.100939

- Angelidaki, I. et al. (2009). Defining the biomethane potential (BMP) of solid organic wastes and energy crops: a proposed protocol for batch assays. *Water science and technology*, *59*(5), 927-934. https://doi.org/10.2166/wst.2009.040

- Angelidaki, I. et al. (2018). Biogas upgrading and utilization: Current status and perspectives. *Biotechnology advances*, *36*(2), 452-466. https://doi.org/10.1016/j.biotechadv.2018.01.011

- Appel, A. M. et al. (2013). Frontiers, opportunities, and challenges in biochemical and chemical catalysis of CO_2 fixation. *Chemical reviews*, *113*(8), 6621-6658. https://doi.org/10.1021/cr300463y

- Arslan, K. et al (2019). Solventogenesis in *Clostridium aceticum* producing high concentrations of ethanol from syngas. *Bioresource Technology*, *292*, 121941. https://doi.org/10.1016/j.biortech.2019.121941

- Aryal, N. et al. (2017). Performance of different *Sporomusa* species for the microbial electrosynthesis of acetate from carbon dioxide. *Bioresource technology*, *233*, 184-190. https://doi.org/10.1016/j.biortech.2017.02.128

- Aryal, N. et al. (2018). An overview of microbial biogas enrichment. *Bioresource technology*, *264*, 359-369. https://doi.org/10.1016/j.biortech.2018.06.013

- Ashassi-Sorkhabi, H. et al. (2014). Effects of solution hydrodynamics on corrosion inhibition of steel by citric acid in cooling water. *Journal of materials engineering and performance*, *23*, 2992-3000. https://doi.org/10.1007/s11665-014-1047-z

- Askari, M. et al. (2019). A comprehensive review on internal corrosion and cracking of oil and gas pipelines. *Journal of Natural Gas Science and Engineering*, *71*, 102971. https://doi.org/10.1016/j.jngse.2019.102971

- Bae, J. et al. (2022). Valorization of C1 gases to value-added chemicals using acetogenic biocatalysts. *Chemical Engineering Journal*, *428*, 131325. https://doi.org/10.1016/j.cej.2021.131325

- Bae, S. & Hanna, K. (2015). Reactivity of nanoscale zero-valent iron in unbuffered systems: effect of pH and Fe (II) dissolution. *Environmental science & technology*, *49*(17), 10536-10543. https://doi.org/10.1021/acs.est.5b01298

- Baek, G. et al. (2019). A review of the effects of iron compounds on methanogenesis in anaerobic environments. *Renewable and Sustainable Energy Reviews*, *113*, 109282. https://doi.org/10.1016/j.rser.2019.109282

- Bajpai, P. (2017). *Anaerobic technology in pulp and paper industry* (pp. 7-13). Singapore: Springer Singapore. http://link.springer.com/10.1007/978-981-10-4130-3

- Bajracharya, S. et al. (2017). Biotransformation of carbon dioxide in bioelectrochemical systems: State of the art and future prospects. *Journal of Power Sources*, *356*, 256-273. https://doi.org/10.1016/j.jpowsour.2017.04.024

- Bajracharya, S. et al. (2017). Long-term operation of microbial electrosynthesis cell reducing CO_2 to multi-carbon chemicals with a mixed culture avoiding methanogenesis. *Bioelectrochemistry*, *113*, 26-34. https://doi.org/10.1016/j.bioelechem.2016.09.001

- Barker, R. et al. (2017). Internal corrosion of carbon steel pipelines for dense-phase CO_2 transport in carbon capture and storage (CCS)–a review. *International Materials Reviews*, *62*(1), 1-31. https://doi.org/10.1080/09506608.2016.1176306

- Barker, R. et al. (2018). A review of iron carbonate ($FeCO_3$) formation in the oil and gas industry. *Corrosion Science*, *142*, 312-341. https://doi.org/10.1016/j.corsci.2018.07.021

- Basilico, E. et al. (2021). The effect of chemical species on the electrochemical reactions and corrosion product layer of carbon steel in CO_2 aqueous environment: A review. *Materials and Corrosion*, *72*(7), 1152-1167. https://doi.org/10.1002/maco.202012118

- Bayar, B. et al. (2022). Bioproduction of acetic acid from carbon dioxide as single substrate and zero valent iron (ZVI) by clostridia. *Journal of CO_2 Utilization*, *58*, 101915. https://doi.org/10.1016/j.jcou.2022.101915

- Bhattad, U. et al. (2017). Activity of methanogenic biomass after heat and freeze drying in air. *Environmental Science: Water Research & Technology*, *3*(3), 462-471. https://doi.org/10.1039/c7ew00049a

- Böer, T. et al. (2024). Isolation and characterization of novel acetogenic strains of the genera Terrisporobacter and Acetoanaerobium. *Frontiers in Microbiology*, *15*, 1426882. https://doi.org/10.3389/fmicb.2024.1426882

- Boretti, A. (2021). There are hydrogen production pathways with better than green hydrogen economic and environmental costs. *International Journal of Hydrogen Energy*, *46*(46), 23988-23995. https://doi.org/10.1016/j.ijhydene.2021.04.182

- Boretti, A. (2021). White is the color of hydrogen from concentrated solar energy and thermochemical water splitting cycles. *International Journal of Hydrogen Energy*, *46*(39), 20790-20791. https://doi.org/10.1016/j.ijhydene.2021.03.178

- Braga Nan, L. et al (2020). Biomethanation processes: new insights on the effect of a high H_2 partial pressure on microbial communities. *Biotechnology for biofuels*, *13*, 1-17. https://doi.org/10.1186/s13068-020-01776-y

- Brannon, J. H., & Asmus, J. F. (1981). Citric acid augmented flashlamp cleaning of corroded steel surfaces. *Applications of Surface Science*, *9*(1-4), 14-21. https://doi.org/10.1016/0378-5963(81)90022-2

- Bricker, O. P. et al. (2004). Bog iron formation in the Nassawango Creek watershed, Maryland, USA. In: *First International Conference on Monitoring, Management, Simulation and Remediation of the Geological Environment (Geo-Environment), Segovia, Spain, J. Martin-Deque, C. Brebbia, A. Godfrey, and J. Diaz de Teran (Editors). WIT Press, Southampton, United Kingdom* (pp. 13-23).

- Cai, Y. et al. (2019). Effects of adding EDTA and Fe^{2+} on the performance of reactor and microbial community structure in two simulated phases of anaerobic digestion. *Bioresource technology*, *275*, 183-191. https://doi.org/10.1016/j.biortech.2018.12.050

- Cao, X. et al. (2020). A new environmentally-friendly route to in situ form a high-corrosion-resistant nesquehonite film on pure magnesium. *RSC advances*, *10*(58), 35480-35489. https://doi.org/10.1039/d0ra04423g

- Capurso, T. et al. (2022). Perspective of the role of hydrogen in the 21st-century energy transition. *Energy Conversion and Management*, *251*, 114898. https://doi.org/10.1016/j.enconman.2021.114898

- Castro-Fernandez, A. et al. (2024). Scale-up and economic assessment of volatile fatty acids production from food waste. *Biomass and Bioenergy*, *182*, 107112. https://doi.org/10.1016/j.biombioe.2024.107112

- Chaikitkaew, S. et al. (2024). Conversion of carbon dioxide in biogas into acetic acid by Clostridium thailandense immobilized on porous support materials. *Heliyon*, *10*(4). https://doi.org/10.1016/j.heliyon.2024.e26378

- Charalambous, P. et al. (2020). Anaerobic digestion of industrial dairy wastewater and cheese whey: performance of internal circulation bioreactor and laboratory batch test at pH 5-6. *Renewable Energy*, *147*, 1-10. https://doi.org/10.1016/j.renene.2019.08.091

- Charalambous, P., & Vyrides, I. (2021). In situ biogas upgrading and enhancement of anaerobic digestion of cheese whey by addition of scrap or powder zero-valent iron (ZVI). *Journal of Environmental Management*, *280*, 111651. https://doi.org/10.1016/j.jenvman.2020.111651

- Chen, B. et al. (2022). A redox-based strategy to enhance propionic and butyric acid production during anaerobic fermentation. *Bioresource Technology*, *361*, 127672. https://doi.org/10.1016/j.biortech.2022.127672

- Chen, K. F. et al. (2011). Renewable hydrogen generation by bimetallic zero valent iron nanoparticles. *Chemical Engineering Journal*, *170*(2-3), 562-567. https://doi.org/10.1016/j.cej.2010.12.019

- Chen, L. et al. (2022). Improvement of direct interspecies electron transfer via adding conductive materials in anaerobic digestion: mechanisms, performances, and challenges. *Frontiers in Microbiology*, *13*, 860749. https://doi.org/10.3389/fmicb.2022.860749

- Chen, Y. et al. (2008). Inhibition of anaerobic digestion process: a review. *Bioresource technology*, *99*(10), 4044-4064. https://doi.org/10.1016/j.biortech.2007.01.057

- Chen, Y. T. et al. (2020). Acclimation improves methane production from molasses wastewater with high salinity in an upflow anaerobic filter reactor: performance and microbial community dynamics. *Applied Biochemistry and Biotechnology*, *191*, 397-411. https://doi.org/10.1007/s12010-020-03236-7

- Cheng, D. et al. (2022). Enhanced photo-fermentative biohydrogen production from biowastes: an overview. *Bioresource Technology*, *357*, 127341. https://doi.org/10.1016/j.biortech.2022.127341

- Choudhury, P. K. et al. (2023). Isolation and characterization of reductive acetogens from rumen fluid samples of Murrah buffaloes. *3 Biotech*, *13*(8), 265. https://doi.org/10.1007/s13205-023-03688-8

- Christman, G. D. et al. (2020). Methanogens within a high salinity oil reservoir from the Gulf of Mexico. *Frontiers in Microbiology*, *11*, 570714. https://doi.org/10.3389/fmicb.2020.570714

- Cole, I. S. et al. (2011). Corrosion of pipelines used for CO_2 transport in CCS: Is it a real problem?. *International Journal of Greenhouse Gas Control*, *5*(4), 749-756. https://doi.org/10.1016/j.ijggc.2011.05.010

- Conrad, R. (2020). Importance of hydrogenotrophic, aceticlastic and methylotrophic methanogenesis for methane production in terrestrial, aquatic and other anoxic environments: a mini review. *Pedosphere*, *30*(1), 25-39. https://doi.org/10.1016/S1002-0160(18)60052-9

- Conrad, R. et al. (2000). Phosphate inhibits acetotrophic methanogenesis on rice roots. *Applied and environmental microbiology*, *66*(2), 828-831. https://doi.org/10.1128/AEM.66.2.828-831.2000

- Constantinou, D. et al. (2023). Hydrogen generation by soluble CO_2 reaction with zero-valent iron or scrap iron and the role of weak acids for controlling $FeCO_3$ formation. *Sustainable Energy Technologies and Assessments*, *56*, 103061. https://doi.org/10.1016/j.seta.2023.103061

- Crane, R. A., & Scott, T. B. (2012). Nanoscale zero-valent iron: future prospects for an emerging water treatment technology. *Journal of hazardous materials*, *211*, 112-125. https://doi.org/10.1016/j.jhazmat.2011.11.073

- Dai, K. et al. (2020). Production of chemicals in thermophilic mixed culture fermentation: mechanism and strategy. *Critical Reviews in Environmental Science and Technology*, *50*(1), 1-30. https://doi.org/10.1080/10643389.2019.1616487

- Daniels, L. et al. (1987). Bacterial methanogenesis and growth from CO_2 with elemental iron as the sole source of electrons. Science, 237(4814), 509-511. https://doi.org/10.1126/science.237.4814.509

- De Motte, R. A. et al. (2018). The early stages of $FeCO_3$ scale formation kinetics in CO_2 corrosion. *Materials Chemistry and Physics*, *216*, 102-111. https://doi.org/10.1016/j.matchemphys.2018.04.077

- De Motte, R. et al. (2020). A study by electrochemical impedance spectroscopy and surface analysis of corrosion product layers formed during CO_2 corrosion of low alloy steel. *Corrosion Science*, *172*, 108666. https://doi.org/10.1016/j.corsci.2020.108666

- Debabov, V. G. (2021). Acetogens: biochemistry, bioenergetics, genetics, and biotechnological potential. *Microbiology*, *90*(3), 273-297. https://doi.org/10.1134/S0026261721030024

- Dessì, P. et al. (2021). Microbial electrosynthesis: towards sustainable biorefineries for production of green chemicals from CO_2 emissions. *Biotechnology Advances*, *46*, 107675. https://doi.org/10.1016/j.biotechadv.2020.107675

- Dong, D. et al. (2019). Effects of nanoscale zero valent iron (nZVI) concentration on the biochemical conversion of gaseous carbon dioxide (CO_2) into methane (CH_4). *Bioresource technology*, *275*, 314-320. https://doi.org/10.1016/j.biortech.2018.12.075

- Dong, H. et al. (2019). Microstructure and carbon storage capacity of hydrated magnesium carbonates synthesized from different sources and conditions. *Journal of CO_2 Utilization*, *34*, 353-361. https://doi.org/10.1016/j.jcou.2019.07.016

- Doyle, D. A. et al. (2022). *Clostridium muellerianum* sp. nov., a carbon monoxide-oxidizing acetogen isolated from old hay. International Journal of Systematic and Evolutionary Microbiology, 72(3), 005297. https://doi.org/10.1099/ijsem.0.005297

- Drake, H. L. et al. (2002). Ecological consequences of the phylogenetic and physiological diversities of acetogens. *Antonie Van Leeuwenhoek*, *81*, 203-213. https://doi.org/10.1023/A:1020514617738

- Drake, H. L. et al. (2008). Old acetogens, new light. *Annals of the New York Academy of Sciences*, *1125*(1), 100-128. https://doi.org/10.1196/annals.1419.016

- Dubey, A., & Arora, A. (2022). Advancements in carbon capture technologies: A review. *Journal of Cleaner Production*, *373*, 133932. https://doi.org/10.1016/j.jclepro.2022.133932

- Dyksma, S. et al. (2020). Syntrophic acetate oxidation replaces acetoclastic methanogenesis during thermophilic digestion of biowaste. *Microbiome*, *8*(1), 105. https://doi.org/10.1186/s40168-020-00862-5

- Eba, H. et al. (2020). Progress of hydrogen gas generation by reaction between iron and steel powder and carbonate water in the temperature range near room temperature. *International Journal of Hydrogen Energy*, *45*(27), 13832-13840. https://doi.org/10.1016/j.ijhydene.2020.03.087

- Elgaddafi, R. et al. (2021). Corrosion of carbon steel in CO_2 saturated brine at elevated temperatures. *Journal of Petroleum Science and Engineering*, *196*, 107638. https://doi.org/10.1016/j.petrol.2020.107638

- Eljamal, O. et al. (2018). Chemical pathways of nanoscale zero-valent iron (NZVI) during its transformation in aqueous solutions. *Journal of environmental chemical engineering*, *6*(5), 6207-6220. https://doi.org/10.1016/j.jece.2018.09.012

- Eryildiz, B., & Taherzadeh, M. J. (2020). Effect of pH, substrate loading, oxygen, and methanogens inhibitors on volatile fatty acid (VFA) production from citrus waste by anaerobic digestion. *Bioresource technology*, *302*, 122800. https://doi.org/10.1016/j.biortech.2020.122800

- Esmaily, M. et al. (2017). Fundamentals and advances in magnesium alloy corrosion. *Progress in Materials Science*, *89*, 92-193. https://doi.org/10.1016/j.pmatsci.2017.04.011

- Esposito, A. et al. (2019). Insights into the genome structure of four acetogenic bacteria with specific reference to the Wood–Ljungdahl pathway. *Microbiologyopen*, *8*(12), e938. https://doi.org/10.1002/mbo3.938

- European Commission. (2025). *Delivering the European Green Deal*. https://commission.europa.eu/strategy-and-policy/priorities-2019-2024/european-green-deal/delivering-european-green-deal_en

- Fang, Z. et al. (2020). Synthesis of the morphology-controlled porous Fe 3 O 4 nanorods with enhanced microwave absorption performance. *Journal of Materials Science: Materials in Electronics*, *31*, 3996-4005. https://doi.org/10.1007/s10854-020-02947-1

- Fazal, B. R. et al. (2022). A review of plant extracts as green corrosion inhibitors for CO_2 corrosion of carbon steel. *npj Materials Degradation*, *6*(1), 5. https://doi.org/10.1038/s41529-021-00201-5

- Feng, J. et al. (2023). Recent advances in engineering heterotrophic microorganisms for reinforcing CO_2 fixation based on Calvin–Benson–Bassham cycle. *ACS Sustainable Chemistry & Engineering*, *11*(26), 9509-9522. https://doi.org/10.1021/acssuschemeng.2c06627

- Ferraren-De Cagalitan, D. D. T., & Abundo, M. L. S. (2021). A review of biohydrogen production technology for application towards hydrogen fuel cells. *Renewable and Sustainable Energy Reviews*, *151*, 111413. https://doi.org/10.1016/j.rser.2021.111413

- Franchi, O. et al. (2020). Correlations between microbial population dynamics, bamA gene abundance and performance of anaerobic sequencing batch reactor (ASBR) treating increasing concentrations of phenol. *Journal of biotechnology*, *310*, 40-48. https://doi.org/10.1016/j.jbiotec.2020.01.010

- Frankel, G. S. et al. (2013). Evolution of hydrogen at dissolving magnesium surfaces. *Corrosion Science*, *70*, 104-111. https://doi.org/10.1016/j.corsci.2013.01.017

- Frolov, E. N. et al. (2023). Obligate autotrophy at the thermodynamic limit of life in a new acetogenic bacterium. *Frontiers in Microbiology*, *14*, 1185739. https://doi.org/10.3389/fmicb.2023.1185739

- Fu, B. et al. (2018). Potential contribution of acetogenesis to anaerobic degradation in methanogenic rice field soils. *Soil Biology and Biochemistry*, *119*, 1-10. https://doi.org/10.1016/j.soilbio.2017.10.034

- Fu, B. et al. (2019). Competition between chemolithotrophic acetogenesis and hydrogenotrophic methanogenesis for exogenous H_2/CO_2 in anaerobically digested sludge: impact of temperature. *Frontiers in Microbiology*, *10*, 2418. https://doi.org/10.3389/fmicb.2019.02418

- Fu, F. et al. (2014). The use of zero-valent iron for groundwater remediation and wastewater treatment: a review. *Journal of hazardous materials*, *267*, 194-205. https://doi.org/10.1016/j.jhazmat.2013.12.062

- Gagliano, M. C. et al. (2017). Biofilm formation and granule properties in anaerobic digestion at high salinity. *Water research*, *121*, 61-71. https://doi.org/10.1016/j.watres.2017.05.016

- Galdames, A. et al. (2020). Zero-valent iron nanoparticles for soil and groundwater remediation. *International journal of environmental research and public health*, 17(16), 5817. https://doi.org/10.3390/ijerph17165817

- Gao, M. et al. (2022). Deep insights into the anaerobic co-digestion of waste activated sludge with concentrated leachate under different salinity stresses. *Science of the Total Environment*, *838*, 155922. https://doi.org/10.1016/j.scitotenv.2022.155922

- Georgiou, S. et al. (2022). Microbial Electrosynthesis Inoculated with Anaerobic Granular Sludge and Carbon Cloth Electrodes Functionalized with Copper Nanoparticles for Conversion of CO_2 to CH_4. *Nanomaterials*, *12*(14), 2472. https://doi.org/10.3390/nano12142472

- Giddings, C. G. et al. (2015). Simplifying microbial electrosynthesis reactor design. *Frontiers in microbiology*, *6*, 468. https://doi.org/10.3389/fmicb.2015.00468

- González-Pabón, M. J. et al. (2021). Hydrogen production in two-chamber MEC using a low-cost and biodegradable poly (vinyl) alcohol/chitosan membrane. *Bioresource Technology*, *319*, 124168. https://doi.org/10.1016/j.biortech.2020.124168

- Graber, J. R., & Breznak, J. A. (2004). Physiology and nutrition of *Treponema primitia*, an H_2/CO_2-acetogenic spirochete from termite hindguts. *Applied and environmental microbiology*, 70(3), 1307-1314. https://doi.org/10.1128/AEM.70.3.1307-1314.2004

- Grinter, R., & Greening, C. (2021). Cofactor F420: an expanded view of its distribution, biosynthesis and roles in bacteria and archaea. *FEMS microbiology reviews*, *45*(5), fuab021. https://doi.org/10.1093/femsre/fuab021

- Gu, P. et al. (2024). Application of Acetate as a Substrate for the Production of Value-Added Chemicals in Escherichia coli. *Microorganisms*, *12*(2), 309. https://doi.org/10.3390/microorganisms12020309

- Guan, Q. et al. (2023). Enhancement of methane production in anaerobic digestion of high salinity organic wastewater: The synergistic effect of nano-magnetite and potassium ions. *Chemosphere*, *318*, 137974. https://doi.org/10.1016/j.chemosphere.2023.137974

- Guan, X. et al. (2015). The limitations of applying zero-valent iron technology in contaminants sequestration and the corresponding countermeasures: the development in zero-valent iron technology in the last two decades (1994–2014). *Water research*, *75*, 224-248. https://doi.org/10.1016/j.watres.2015.02.034

- Hache, E. et al. (2019). Critical raw materials and transportation sector electrification: A detailed bottom-up analysis in world transport. *Applied Energy*, *240*, 6-25. https://doi.org/10.1016/j.apenergy.2019.02.057

- Han, J. et al. (2011). Effect of bicarbonate on corrosion of carbon steel in CO_2 saturated brines. *International Journal of Greenhouse Gas Control*, *5*(6), 1680-1683. https://doi.org/10.1016/j.ijggc.2011.08.003

- Han, W. et al. (2019). A methanogenic consortium was active and exhibited long-term survival in an extremely acidified thermophilic bioreactor. *Frontiers in microbiology*, *10*, 2757. https://doi.org/10.3389/fmicb.2019.02757

- Harirchi, S. et al. (2022). Microbiological insights into anaerobic digestion for biogas, hydrogen or volatile fatty acids (VFAs): a review. *Bioengineered*, *13*(3), 6521-6557. https://doi.org/10.1080/21655979.2022.2035986

- He, Y. et al. (2021). Bioethanol production from H_2/CO_2 by solventogenesis using anaerobic granular sludge: effect of process parameters. *Frontiers in Microbiology*, *12*, 647370. https://doi.org/10.3389/fmicb.2021.647370

- He, Y. et al. (2022). Enhanced solventogenesis in syngas bioconversion: role of process parameters and thermodynamics. *Chemosphere*, *299*, 134425. https://doi.org/10.1016/j.chemosphere.2022.134425

- He, Y. et al. (2023). Enrichment of homoacetogens converting H_2/CO_2 into acids and ethanol and simultaneous methane production. *Engineering in life sciences*, *23*(2), e2200027. https://doi.org/10.1002/elsc.202200027

- He, Z. W. et al. (2022). Roles of zero-valent iron in anaerobic digestion: mechanisms, advances and perspectives. *Science of The Total Environment*, *852*, 158420. https://doi.org/10.1016/j.scitotenv.2022.158420

- Hengsbach, J. N. et al. (2022). Microbial electrosynthesis of methane and acetate—comparison of pure and mixed cultures. *Applied Microbiology and Biotechnology*, *106*(12), 4427-4443. https://doi.org/10.1007/s00253-022-12031-9

- Herlekar, M. et al. (2014). Plant-mediated green synthesis of iron nanoparticles. *Journal of Nanoparticles*, *2014*(1), 140614. https://doi.org/10.1155/2014/140614

- Hoag, G. E. et al. (2009). Degradation of bromothymol blue by 'greener'nano-scale zero-valent iron synthesized using tea polyphenols. *Journal of Materials Chemistry*, *19*(45), 8671-8677. https://doi.org/10.1039/b909148c

- Hua, Y. et al. (2019). The formation of $FeCO_3$ and Fe_3O_4 on carbon steel and their protective capabilities against CO_2 corrosion at elevated temperature and pressure. *Corrosion Science*, *157*, 392-405. https://doi.org/10.1016/j.corsci.2019.06.016

- Huang, C. et al. (2020). A novel acetogenic bacteria isolated from waste activated sludge and its potential application for enhancing anaerobic digestion performance. J*ournal of Environmental Management*, 255, 109842. https://doi.org/10.1016/j.jenvman.2019.109842

- Huang, H. W. et al. (2019). Weak magnetic field significantly enhances methane production from a digester supplemented with zero valent iron. https://doi.org/10.1016/j.biortech.2019.03.013

- Igarashi, K. & Kato, S. (2017). Extracellular electron transfer in acetogenic bacteria and its application for conversion of carbon dioxide into organic compounds. *Applied microbiology and biotechnology*, *101*, 6301-6307. https://doi.org/10.1007/s00253-017-8421-3

- Igarashi, K. & Kato, S. (2021). Reductive transformation of Fe (III)(oxyhydr) oxides by mesophilic homoacetogens in the genus Sporomusa. *Frontiers in Microbiology*, *12*, 600808. https://doi.org/10.3389/fmicb.2021.600808

- Im, H. S. et al. (2023). Zero-valent Iron Enhances Acetate and Butyrate Production from Carbon Monoxide by Fonticella tunisiensis HN43. *Biotechnology and Bioprocess Engineering*, *28*(5), 835-841. https://doi.org/10.1007/s12257-023-0033-4

- IPCC, 2023: Sections. In: *Climate Change 2023: Synthesis Report. Contribution of Working Groups I, II and III to the Sixth Assessment Report of the Intergovernmental Panel on Climate Change* [Core Writing Team, H. Lee and J. Romero (eds.)]. IPCC,
  Geneva, Switzerland, pp. 35-115.
  https://doi.org/10.59327/IPCC/AR6-9789291691647

- Jadhav, D. A. et al. (2019). Suppressing methanogens and enriching electrogens in bioelectrochemical systems. *Bioresource technology*, *277*, 148-156. https://doi.org/10.1016/j.biortech.2018.12.098

- Jain, R. et al. (2024). Bio-hydrogen production through dark fermentation: an overview. *Biomass Conversion and Biorefinery*, *14*(12), 12699-12724. https://doi.org/10.1007/s13399-022-03282-7

- Jiang, Y. et al. (2019). Ammonia inhibition and toxicity in anaerobic digestion: A critical review. *Journal of Water Process Engineering*, *32*, 100899. https://doi.org/10.1016/j.jwpe.2019.100899

- Jiang, Y. et al. (2019). Carbon dioxide and organic waste valorization by microbial electrosynthesis and electro-fermentation. *Water research*, *149*, 42-55. https://doi.org/10.1016/j.watres.2018.10.092

- Jiang-xue, L. et al. (2019). Study on production of organic acid rust remover from passion fruit fermented by Aspergillus Niger. *In:* IOP Conference Series: Earth and Environmental Science (Vol. 369, No. 1, p. 012007). IOP Publishing. https://doi.org/10.1088/1755-1315/369/1/012007

- Jin, F. et al. (2011). High-yield reduction of carbon dioxide into formic acid by zero-valent metal/metal oxide redox cycles. *Energy & Environmental Science*, *4*(3), 881-884. https://doi.org/10.1039/c0ee00661k

- Jin, F. et al. (2014). Highly efficient and autocatalytic H_2O dissociation for CO_2 reduction into formic acid with zinc. *Scientific reports*, *4*(1), 1-8. https://doi.org/10.1038/srep04503

- Joshi, G. R. et al. (2018). Temporal evolution of sweet oilfield corrosion scale: Phases, morphologies, habits, and protection. *Corrosion Science*, *142*, 110-118. https://doi.org/10.1016/j.corsci.2018.07.009

- Kahyarian, A. et al. (2017). Electrochemistry of CO_2 corrosion of mild steel: Effect of CO_2 on iron dissolution reaction. *Corrosion Science*, *129*, 146-151. https://doi.org/10.1016/j.corsci.2017.10.005

- Kahyarian, A., & Nesic, S. (2019). A new narrative for CO_2 corrosion of mild steel. *Journal of the Electrochemical Society*, *166*(11), C3048. https://doi.org/10.1149/2.0071911jes

- Kahyarian, A., & Nesic, S. (2020). On the mechanism of carbon dioxide corrosion of mild steel: Experimental investigation and mathematical modeling at elevated pressures and non-ideal solutions. *Corrosion science*, *173*, 108719. https://doi.org/10.1016/j.corsci.2020.108719

- Kallistova, A. et al. (2020). Methanogenesis in the Lake Elton saline aquatic system. *Extremophiles*, *24*, 657-672. https://doi.org/10.1007/s00792-020-01185-x

- Karekar, S. et al. (2022). Homo-acetogens: their metabolism and competitive relationship with hydrogenotrophic methanogens. *Microorganisms*, *10*(2), 397. https://doi.org/10.3390/microorganisms10020397

- Kato, S. (2016). Microbial extracellular electron transfer and its relevance to iron corrosion. *Microbial biotechnology*, *9*(2), 141-148. https://doi.org/10.1111/1751-7915.12340

- Kato, S. et al. (2020). An iron corrosion-assisted H_2-supplying system: a culture method for methanogens and acetogens under low H_2 pressures. *Scientific Reports, 10(1),* 19124. https://doi.org/10.1038/s41598-020-76267-z

- Katsyv, A. & Müller, V. (2020). Overcoming energetic barriers in acetogenic C1 conversion. *Frontiers in Bioengineering and Biotechnology*, *8*, 621166. https://doi.org/10.3389/fbioe.2020.621166

- Ken, D. S., & Sinha, A. (2020). Recent developments in surface modification of nano zero-valent iron (nZVI): Remediation, toxicity and environmental impacts. *Environmental Nanotechnology, Monitoring & Management*, *14*, 100344. https://doi.org/10.1016/j.enmm.2020.100344

- Khaleel, M. et al. (2024). Towards hydrogen sector investments for achieving sustainable electricity generation. *Journal of Solar Energy and Sustainable Development*, *13*(1), 71-96. https://doi.org/10.51646/jsesd.v13i1.173

- Khemkhao, M. et al. (2024). Chemical and biological effects of zero-valent iron (ZVI) concentration on in-situ production of H_2 from ZVI and bioconversion of CO_2 into CH_4 under anaerobic conditions. *Environmental Research*, 119230. https://doi.org/10.1016/j.envres.2024.119230

- Kiefer, D. et al. (2021). From acetate to bio-based products: underexploited potential for industrial biotechnology. *Trends in Biotechnology*, *39*(4), 397-411. https://doi.org/10.1016/j.tibtech.2020.09.004

- Kim, J. Y. et al. (2023). Acetogen and acetogenesis for biological syngas valorization. *Bioresource Technology*, *384*, 129368. https://doi.org/10.1016/j.biortech.2023.129368

- Kim, Y. et al. (2021). Acetate as a potential feedstock for the production of value-added chemicals: metabolism and applications. *Biotechnology Advances*, *49*, 107736. https://doi.org/10.1016/j.biotechadv.2021.107736

- Kong, X. et al. (2018). Enhancing syntrophic associations among Clostridium butyricum, Syntrophomonas and two types of methanogen by zero valent iron in an anaerobic assay with a high organic loading. *Bioresource technology*, *257*, 181-191. https://doi.org/10.1016/j.biortech.2018.02.088

- Kong, X. et al. (2021). Mini art review for zero valent iron application in anaerobic digestion and technical bottlenecks. *Science of the Total Environment*, *791*, 148415. https://doi.org/10.1016/j.scitotenv.2021.148415

- Kong, X. et al. (2023). Metabolic effects of Fe^0 on simultaneously eliminating excessive acidification and upgrading biogas in mesophilic or thermophilic anaerobic reactor. *Journal of Cleaner Production*, *389*, 136079. https://doi.org/10.1016/j.jclepro.2023.136079

- Kotsyurbenko, O. R. et al. (2001). Competition between homoacetogenic bacteria and methanogenic archaea for hydrogen at low temperature. *FEMS microbiology ecology*, *38*(2-3), 153-159. https://doi.org/10.1016/S0168-6496(01)00179-9

- Kremp, F. et al. (2022). A third way of energy conservation in acetogenic bacteria. *Microbiology Spectrum*, *10*(4), e01385-22. https://doi.org/10.1128/spectrum.01385-22

- Krige, A. et al. (2021). 3D bioprinting on cathodes in microbial electrosynthesis for increased acetate production rate using *Sporomusa ovata*. *Journal of Environmental Chemical Engineering*, *9*(5), 106189. https://doi.org/10.1016/j.jece.2021.106189

- LaBelle, E. V., & May, H. D. (2017). Energy efficiency and productivity enhancement of microbial electrosynthesis of acetate. *Frontiers in microbiology*, *8*, 756. https://doi.org/10.3389/fmicb.2017.00756

- Laguillaumie, L. et al. (2023). Controlling the microbial competition between hydrogenotrophic methanogens and homoacetogens using mass transfer and thermodynamic constraints. *Journal of Cleaner Production*, *414*, 137549. https://doi.org/10.1016/j.jclepro.2023.137549

- Lamberts-Van Assche, H., & Compernolle, T. (2022). Economic feasibility studies for carbon capture and utilization technologies: a tutorial review. *Clean Technologies and Environmental Policy*, 1-25. https://doi.org/10.1007/s10098-021-02128-6

- Latif, M. A. et al. (2017). Influence of low pH on continuous anaerobic digestion of waste activated sludge. *Water Research*, *113*, 42-49. https://doi.org/10.1016/j.watres.2017.02.002

- Laura, M., & Jo, P. (2023). No acetogen is equal: Strongly different H_2 thresholds reflect diverse bioenergetics in acetogenic bacteria. *Environmental Microbiology*, *25*(10), 2032-2040. https://doi.org/10.1111/1462-2920.16429

- Lee, H. et al. (2022). Engineering acetogenic bacteria for efficient one-carbon utilization. *Frontiers in Microbiology*, *13*, 865168. https://doi.org/10.3389/fmicb.2022.865168

- Lee, H. S. et al. (2022). Microbial electrolysis cells for the production of biohydrogen in dark fermentation–a review. *Bioresource Technology*, *363*, 127934. https://doi.org/10.1016/j.biortech.2022.127934

- Lemaire, O. N. et al. (2020). CO_2-fixation strategies in energy extremophiles: what can we learn from acetogens?. *Frontiers in Microbiology*, *11*, 486. https://doi.org/10.3389/fmicb.2020.00486

- Li, J. et al. (2019). Characterization methods of zerovalent iron for water treatment and remediation. *Water research*, *148*, 70-85. https://doi.org/10.1016/j.watres.2018.10.025

- Li, L. et al. (2023). Acclimation of anaerobic fermentation microbiome with acetate and ethanol for chain elongation and the biochemical response. *Chemosphere*, *320*, 138083. https://doi.org/10.1016/j.chemosphere.2023.138083

- Li, M. T. et al. (2022). Bioaugmentation with syntrophic volatile fatty acids-oxidizing consortia to alleviate the ammonia inhibition in continuously anaerobic digestion of municipal sludge. *Chemosphere*, *288*, 132389. https://doi.org/10.1016/j.chemosphere.2021.132389

- Li, P. et al. (2022). Effect of applying potentials on anaerobic digestion of high salinity organic wastewater. *Science of the Total Environment*, *822*, 153416. https://doi.org/10.1016/j.scitotenv.2022.153416

- Li, S. et al. (2019). CO_2 corrosion of low carbon steel under the joint effects of time-temperature-salt concentration. *Frontiers in Materials*, *6*, 10. https://doi.org/10.3389/fmats.2019.00010

- Li, S. et al. (2019). Regulating secretion of extracellular polymeric substances through dosing magnetite and zerovalent iron nanoparticles to affect anaerobic digestion mode. *ACS Sustainable Chemistry & Engineering*, *7*(10), 9655-9662. https://doi.org/10.1021/acssuschemeng.9b01252

- Li, Y. et al. (2022). Controlled fabrication and characterization of α-FeOOH nanorods. *Journal of Inorganic and Organometallic Polymers and Materials*, *32*(4), 1400-1408. https://doi.org/10.1007/s10904-021-02190-z

- Lins, P. et al. (2015). Impact of several antibiotics and 2-bromoethanesulfonate on the volatile fatty acid degradation, methanogenesis and community structure during thermophilic anaerobic digestion. *Bioresource Technology*, *190*, 148-158. https://doi.org/10.1016/j.biortech.2015.04.070

- Liou, J. S. C. et al. (2005). *Clostridium carboxidivorans* sp. nov., a solvent-producing clostridium isolated from an agricultural settling lagoon, and reclassification of the acetogen *Clostridium scatologenes* strain SL1 as *Clostridium drakei* sp. nov. *International journal of systematic and evolutionary microbiology*, 55(5), 2085-2091. https://doi.org/10.1099/ijs.0.63482-0

- Litty, D. & Müller, V. (2021). Acetogenic bacteria for biotechnological applications. In: *Enzymes for Solving Humankind's Problems: Natural and Artificial Systems in Health, Agriculture, Environment and Energy*, 109-130.Cham: Springer International Publishing. https://doi.org/10.1007/978-3-030-58315-6_4

- Liu, C. et al. (2021). Electron transfer and mechanism of energy production among syntrophic bacteria during acidogenic fermentation: A review. *Bioresource technology*, *323*, 124637. https://doi.org/10.1016/j.biortech.2020.124637

- Liu, H. et al. (2011). Chemical inhibitors of methanogenesis and putative applications. *Applied microbiology and biotechnology*, *89*, 1333-1340. https://doi.org/10.1007/s00253-010-3066-5

- Liu, H. et al. (2018). Microbial electrosynthesis of organic chemicals from CO_2 by *Clostridium scatologenes* ATCC 25775T. *Bioresources and Bioprocessing*, *5*(1), 1-10. https://doi.org/10.1186/s40643-018-0195-7

- Liu, H. et al. (2018). Full-scale production of VFAs from sewage sludge by anaerobic alkaline fermentation to improve biological nutrients removal in domestic wastewater. *Bioresource technology*, *260*, 105-114. https://doi.org/10.1016/j.biortech.2018.03.105

- Liu, Y. et al. (2019). Effects of adding osmoprotectant on anaerobic digestion of kitchen waste with high level of salinity. *Journal of bioscience and bioengineering*, *128*(6), 723-732. https://doi.org/10.1016/j.jbiosc.2019.05.011

- Liu, Y. et al. (2020). Thermodynamic analysis of direct interspecies electron transfer in syntrophic methanogenesis based on the optimized energy distribution. *Bioresource Technology*, *297*, 122345. https://doi.org/10.1016/j.biortech.2019.122345

- Liu, Y., & Boone, D. R. (1991). Effects of salinity on methanogenic decomposition. *Bioresource Technology*, *35*(3), 271-273. https://doi.org/10.1016/0960-8524(91)90124-3

- Liu, Y., & Wang, J. (2019). Reduction of nitrate by zero valent iron (ZVI)-based materials: a review. *Science of the Total Environment*, *671*, 388-403. https://doi.org/10.1016/j.scitotenv.2019.03.317

- Logroño, W. et al. (2022). Physiological effects of 2-bromoethanesulfonate on hydrogenotrophic pure and mixed cultures. *Microorganisms*, *10*(2), 355. https://doi.org/10.3390/microorganisms10020355

- Lohani, S. P., & Havukainen, J. (2017). Anaerobic digestion: factors affecting anaerobic digestion process. In: *Waste bioremediation* (pp. 343-359). Singapore: Springer Singapore. https://doi.org/10.1007/978-981-10-7413-4_18

- Lopes, S. R., & Ahring, B. (2023). Enhancing acetic acid production in in vitro rumen cultures by addition of a homoacetogenic consortia from a kangaroo: unravelling the impact of inhibition of methanogens and effect of almond biochar on rumen fermentations. *Fermentation*, 9(10), 885. https://doi.org/10.3390/fermentation9100885

- Lorowitz, W. H. et al. (1992). Anaerobic oxidation of elemental metals coupled to methanogenesis by Methanobacterium thermoautotrophicum. *Environmental science & technology*, *26*(8), 1606-1610. https://doi.org/10.1021/es00032a018

- Lou, T. et al. (2024). Promotion of medium-chain fatty acids and long-chain alcohols production by zero-valent iron: Effect of particle sizes. *Journal of Environmental Chemical Engineering*, *12*(1), 111652. https://doi.org/10.1016/j.jece.2023.111652

- Lv, N. et al. (2020). Novel strategy for relieving acid accumulation by enriching syntrophic associations of syntrophic fatty acid-oxidation bacteria and H_2/formate-scavenging methanogens in anaerobic digestion. *Bioresource technology*, *313*, 123702. https://doi.org/10.1016/j.biortech.2020.123702

- Lyu, Z. et al. (2018). Methanogenesis. *Current Biology*, *28*(13), R727-R732. https://doi.org/10.1016/j.cub.2018.05.021

- Madjarov, J. et al. (2022). Sporomusa ovata as catalyst for bioelectrochemical carbon dioxide reduction: a review across disciplines from microbiology to process engineering. *Frontiers in Microbiology, 13,* 913311. https://doi.org/10.3389/fmicb.2022.913311

- Maegaard, K. et al. (2019). Biogas upgrading with hydrogenotrophic methanogenic biofilms. *Bioresource technology*, *287*, 121422. https://doi.org/10.1016/j.biortech.2019.121422

- Malik, S. N., & Kumar, S. (2021). Enhancement effect of zero-valent iron nanoparticle and iron oxide nanoparticles on dark fermentative hydrogen production from molasses-based distillery wastewater. *International Journal of Hydrogen Energy*, *46*(58), 29812-29821. https://doi.org/10.1016/j.ijhydene.2021.06.125

- Mancini, G. et al. (2018). Trace elements dosing and alkaline pretreatment in the anaerobic digestion of rice straw. *Bioresource Technology, 247,* 897-903. https://doi.org/10.1016/j.biortech.2017.10.001

- Martin, W. F., & Thauer, R. K. (2017). Energy in ancient metabolism. *Cell*, *168*(6), 953-955. https://doi.org/10.1016/j.cell.2017.02.032

- Matamoros-Veloza, A., et al. (2020). Iron calcium carbonate instability: structural modification of siderite corrosion films. *ACS Applied Materials & Interfaces*, *12*(43), 49237-49244. https://doi.org/10.1021/acsami.0c14513

- Mateos, R. et al. (2019). Enhanced CO_2 conversion to acetate through microbial electrosynthesis (MES) by continuous headspace gas recirculation. *Energies*, *12*(17), 3297. https://doi.org/10.3390/en12173297

- Melchers, R. E. (2014). Microbiological and abiotic processes in modelling longer-term marine corrosion of steel. *Bioelectrochemistry*, *97*, 89-96. https://doi.org/10.1016/j.bioelechem.2013.07.002

- Meng, X. et al. (2018). Endogenous ternary pH buffer system with ammonia-carbonates-VFAs in high solid anaerobic digestion of swine manure: an alternative for alleviating ammonia inhibition?. *Process Biochemistry*, *69*, 144-152. https://doi.org/10.1016/j.procbio.2018.03.015

- Menzel, T. et al. (2020). Role of microbial hydrolysis in anaerobic digestion. *Energies*, *13*(21), 5555. https://doi.org/10.3390/en13215555

- Michiels, K. et al. (2015). Production of hydrogen gas from water by the oxidation of metallic iron under mild hydrothermal conditions, assisted by in situ formed carbonate ions. *Fuel*, *160*, 205-216. https://doi.org/10.1016/j.fuel.2015.07.061

- Mikhelkis, L. & Govindarajan, V. (2020). Techno-economic and partial environmental analysis of carbon capture and storage (CCS) and carbon capture, utilization, and storage (CCU/S): case study from proposed waste-fed district-heating incinerator in Sweden. *Sustainability*, *12*(15), 5922. https://doi.org/10.3390/SU12155922

- Mishra, P. et al. (2020). Electrochemical impedance spectroscopy analysis of corrosion product layer formation on pipeline steel. *Electrochimica Acta*, *346*, 136232. https://doi.org/10.1016/j.electacta.2020.136232

- Mockaitis, G. (2020). Acidic and thermal pre-treatments for anaerobic digestion inoculum to improve hydrogen and volatile fatty acid production using xylose as the substrate. *Renewable Energy*, *145*, 1388-1398. https://doi.org/10.1016/j.renene.2019.06.134

- Modestra, J. A. et al. (2020). CO_2 fermentation to short chain fatty acids using selectively enriched chemolithoautotrophic acetogenic bacteria. *Chemical Engineering Journal*, *394*, 124759. https://doi.org/10.1016/j.cej.2020.124759

- Mohanakrishna, G. et al. (2020). Microbial electrosynthesis feasibility evaluation at high bicarbonate concentrations with enriched homoacetogenic biocathode. *Science of The Total Environment*, *715*, 137003. https://doi.org/10.1016/j.scitotenv.2020.137003

- Mukherjee, R. et al. (2016). A review on synthesis, characterization, and applications of nano zero valent iron (nZVI) for environmental remediation. *Critical reviews in environmental science and technology*, *46*(5), 443-466. https://doi.org/10.1080/10643389.2015.1103832

- Müller, V. (2019). New horizons in acetogenic conversion of one-carbon substrates and biological hydrogen storage. *Trends in Biotechnology*, *37*(12), 1344-1354. https://doi.org/10.1016/j.tibtech.2019.05.008

- Muñoz, R. et al. (2015). A review on the state-of-the-art of physical/chemical and biological technologies for biogas upgrading. *Reviews in Environmental Science and Bio/Technology*, *14*, 727-759. https://doi.org/10.1007/s11157-015-9379-1

- Murugaiyan, J. et al. (2022). An overview of microbial electrolysis cell configuration: Challenges and prospects on biohydrogen production. *International Journal of Energy Research*, *46*(14), 20811-20827. https://doi.org/10.1002/er.8494

- Mutyala, S., & Kim, J. R. (2022). Recent advances and challenges in the bioconversion of acetate to value-added chemicals. *Bioresource Technology*, *364*, 128064. https://doi.org/10.1016/j.biortech.2022.128064

- Mystrioti, C. et al. (2015). Assessment of polyphenol coated nano zero valent iron for hexavalent chromium removal from contaminated waters. *Bulletin of environmental Contamination and Toxicology*, *94*, 302-307. https://doi.org/10.1007/s00128-014-1442-z

- Nazari, M. H. et al. (2010). The effects of temperature and pH on the characteristics of corrosion product in CO_2 corrosion of grade X70 steel. *Materials & Design*, 31(7), 3559-3563. https://doi.org/10.1016/j.matdes.2010.01.038

- Nazari, M. H. et al. (2010). The effects of temperature and pH on the characteristics of corrosion product in CO_2 corrosion of grade X70 steel. *Materials & Design*, *31*(7), 3559-3563. https://doi.org/10.1016/j.matdes.2010.01.038

- Neerup, R. et al. (2023). Measurements and modelling of $FeCO_3$ solubility in water relevant to corrosion and CO_2 mineralization. *Chemical Engineering Science*, 270, 118549. https://doi.org/10.1016/j.ces.2023.118549

- Neri, A. et al. (2023). An overview of anaerobic digestion of agricultural by-products and food waste for biomethane production. Energies, 16(19), 6851. https://doi.org/10.3390/en16196851

- Nguyen, T. T. et al. (2016). Impact of Organic Acid Addition on The Formation of Precipitated Iron Compounds. *Acta Metallurgica Slovaca*, *22*(4), 259-265. https://doi.org/10.12776/ams.v22i4.831

- Nikolaidis, P., & Poullikkas, A. (2017). A comparative overview of hydrogen production processes. *Renewable and sustainable energy reviews*, *67*, 597-611. https://doi.org/10.1016/j.rser.2016.09.044

- Ntagia, E. et al. (2021). Continuous H_2/CO_2 fermentation for acetic acid production under transient and continuous sulfide inhibition. *Chemosphere*, *285*, 131536. https://doi.org/10.1016/j.chemosphere.2021.131536

- Ogata, Y. et al. (2016). Effect of increasing salinity on biogas production in waste landfills with leachate recirculation: a lab-scale model study. *Biotechnology Reports*, *10*, 111-116. https://doi.org/10.1016/j.btre.2016.04.004

- Oliveira, C. A. et al. (2021). Increasing salinity concentrations determine the long-term participation of methanogenesis and sulfidogenesis in the biodigestion of sulfate-rich wastewater. *Journal of Environmental Management*, *296*, 113254. https://doi.org/10.1016/j.jenvman.2021.113254

- Omar, B. et al. (2018). Simultaneous biogas upgrading and biochemicals production using anaerobic bacterial mixed cultures. *Water research*, *142*, 86-95. https://doi.org/10.1016/j.watres.2018.05.049

- Osman, A. I. et al. (2023). Cost, environmental impact, and resilience of renewable energy under a changing climate: a review. *Environmental chemistry letters*, *21*(2), 741-764. https://doi.org/10.1007/s10311-022-01532-8

- Ouyang, L. et al. (2020). Magnesium-based hydrogen storage compounds: A review. *Journal of Alloys and Compounds*, *832*, 154865. https://doi.org/10.1016/j.jallcom.2020.154865

- Palacios, P. A. et al. (2019). Baltic Sea methanogens compete with acetogens for electrons from metallic iron. *The ISME Journal*, *13*(12), 3011-3023. https://doi.org/10.1038/s41396-019-0490-0

- Palacios, P. A. et al. (2025). Temperature tactics: Targeting acetate or methane production in autotrophic H_2/CO_2 conversion with mixed cultures. *Biochemical Engineering Journal*, *214*, 109574. https://doi.org/10.1016/j.bej.2024.109574

- Pan, X. et al. (2019). Impact of nano zero valent iron on tetracycline degradation and microbial community succession during anaerobic digestion. *Chemical Engineering Journal*, *359*, 662-671. https://doi.org/10.1016/j.cej.2018.11.135

- Pan, X. et al. (2021). Carbon-and metal-based mediators modulate anaerobic methanogenesis and phenol removal: Focusing on stimulatory and inhibitory mechanism. *Journal of hazardous materials*, *420*, 126615. https://doi.org/10.1016/j.jhazmat.2021.126615

- Pan, X. et al. (2021). Deep insights into the network of acetate metabolism in anaerobic digestion: focusing on syntrophic acetate oxidation and homoacetogenesis. *Water Research*, *190*, 116774. https://doi.org/10.1016/j.watres.2020.116774

- Pandey, A. K. et al. (2022). Dark fermentation: Production and utilization of volatile fatty acid from different wastes-A review. *Chemosphere*, *288*, 132444. https://doi.org/10.1016/j.chemosphere.2021.132444

- Park, J. H. et al. (2022). Review of recent technologies for transforming carbon dioxide to carbon materials. *Chemical Engineering Journal*, *427*, 130980. https://doi.org/10.1016/j.cej.2021.130980

- Pendyala, B. et al. (2012). Pretreating mixed anaerobic communities from different sources: Correlating the hydrogen yield with hydrogenase activity and microbial diversity. *International journal of hydrogen energy*, *37*(17), 12175-12186. https://doi.org/10.1016/j.ijhydene.2012.05.105

- Peres, C. B. et al. (2022). Advances in carbon capture and use (CCU) technologies: a comprehensive review and CO_2 mitigation potential analysis. *Clean technologies*, *4*(4), 1193-1207. https://doi.org/10.3390/cleantechnol4040073

- Peters, K., & Sargent, F. (2023). Formate hydrogenlyase, formic acid translocation and hydrogen production: Dynamic membrane biology during fermentation. *Biochimica et Biophysica Acta (BBA)-Bioenergetics*, *1864*(1), 148919. https://doi.org/10.1016/j.bbabio.2022.148919

- Philips, J. (2020). Extracellular electron uptake by acetogenic bacteria: does H_2 consumption favor the H_2 evolution reaction on a cathode or metallic iron?. *Frontiers in Microbiology*, *10*, 2997. https://doi.org/10.3389/fmicb.2019.02997

- Philips, J. et al. (2019). An Acetobacterium strain isolated with metallic iron as electron donor enhances iron corrosion by a similar mechanism as Sporomusa sphaeroides. *FEMS microbiology ecology*, *95*(2), fiy222. https://doi.org/10.1093/femsec/fiy222

- Polaris Market Research. (2024). *Acetic Acid Market Share, Size, Trends, Industry Analysis Report, By Application (Vinyl Acetate Monomer, Purified Terephthalic Acid, Acetate Esters, Acetic Anhydride); By End Use; By Region; Market size & Forecast To, 2024 – 2032.* https://www.polarismarketresearch.com/industry-analysis/acetic-acid-market/request-for-sample

- Prévoteau, A. et al. (2020). Microbial electrosynthesis from CO_2: forever a promise?. *Current opinion in biotechnology*, *62*, 48-57. https://doi.org/10.1016/j.copbio.2019.08.014

- Pullin, H. et al. (2017). The effect of aqueous corrosion on the structure and reactivity of zero-valent iron nanoparticles. *Chemical Engineering Journal*, *308*, 568-577. https://doi.org/10.1016/j.cej.2016.09.088

- Pushcharovsky, D. Y. (2019). Iron and its compounds in the Earth's core: New data and ideas. *Geochemistry International*, *57*, 941-955. https://doi.org/10.1134/S0016702919090088

- Putatunda, C. et al. (2023). Current challenges and future technology in photofermentation-driven biohydrogen production by utilizing algae and bacteria. *International Journal of Hydrogen Energy*, *48*(55), 21088-21109. https://doi.org/10.1016/j.ijhydene.2022.10.042

- Pyne, M. E. et al. (2014). Technical guide for genetic advancement of underdeveloped and intractable Clostridium. *Biotechnology advances*, *32*(3), 623-641. https://doi.org/10.1016/j.biotechadv.2014.04.003

- Qiu, S. et al. (2023). Effect of extreme pH conditions on methanogenesis: Methanogen metabolism and community structure. *Science of The Total Environment*, *877*, 162702. https://doi.org/10.1016/j.scitotenv.2023.162702

- Ragsdale, S. W., & Pierce, E. (2008). Acetogenesis and the Wood–Ljungdahl pathway of CO_2 fixation. *Biochimica et Biophysica Acta (BBA)-Proteins and Proteomics*, *1784*(12), 1873-1898. https://doi.org/10.1016/j.bbapap.2008.08.012

- Rahman, A. et al. (2022). Environmental impact of renewable energy source based electrical power plants: Solar, wind, hydroelectric, biomass, geothermal, tidal, ocean, and osmotic. *Renewable and Sustainable Energy Reviews*, *161*, 112279. https://doi.org/10.1016/j.rser.2022.112279

- Rawool, S. A. et al. (2021). Direct CO_2 capture and conversion to fuels on magnesium nanoparticles under ambient conditions simply using water. *Chemical science*, *12*(16), 5774-5786. https://doi.org/10.1039/d1sc01113h

- Riegler, P. et al. (2019). Continuous conversion of CO_2/H_2 with Clostridium aceticum in biofilm reactors. *Bioresource technology*, *291*, 121760. https://doi.org/10.1016/j.biortech.2019.121760

- Rizzioli, F. et al. (2024). Production, purification and recovery of caproic acid, Volatile fatty acids and methane from Opuntia ficus indica. *Renewable and Sustainable Energy Reviews, 190,* 114083. https://doi.org/10.1016/j.rser.2023.114083

- Rizzo, R. et al. (2020). An electrochemical and X-ray computed tomography investigation of the effect of temperature on CO_2 corrosion of 1Cr carbon steel. *Corrosion Science*, *166*, 108471. https://doi.org/10.1016/j.corsci.2020.108471

- Rocamora, I. et al. (2023). Inhibitory mechanisms on dry anaerobic digestion: Ammonia, hydrogen and propionic acid relationship. *Waste Management*, *161*, 29-42. https://doi.org/10.1016/j.wasman.2023.02.009

- Rojas, M. D. P. A. et al. (2018). Microbial electrosynthesis (MES) from CO_2 is resilient to fluctuations in renewable energy supply. *Energy conversion and management*, *177*, 272-279. https://doi.org/10.1016/j.enconman.2018.09.064

- Romans-Casas, M. et al. (2023). Boosting ethanol production rates from carbon dioxide in MES cells under optimal solventogenic conditions. *Science of The Total Environment*, *856*, 159124. https://doi.org/10.1016/j.scitotenv.2022.159124

- Rosencrantz, D. et al. (1999). Culturable populations of *Sporomusa* spp. and *Desulfovibrio* spp. in the anoxic bulk soil of flooded rice microcosms. *Applied and environmental microbiology*, 65(8), 3526-3533. https://doi.org/10.1128/AEM.65.8.3526-3533.1999

- Rovira, M. et al. (2007). Interaction of uranium with in situ anoxically generated magnetite on steel. *Journal of hazardous materials*, *147*(3), 726-731. https://doi.org/10.1016/j.jhazmat.2007.01.067

- Rovira-Alsina, L. et al. (2022). Thermodynamic approach to foresee experimental CO_2 reduction to organic compounds. *Bioresource Technology*, *354*, 127181. https://doi.org/10.1016/j.biortech.2022.127181

- Roy, A., & Pramanik, S. (2024). A review of the hydrogen fuel path to emission reduction in the surface transport industry. *International Journal of Hydrogen Energy*, *49*, 792-821. https://doi.org/10.1016/j.ijhydene.2023.07.010

- Roy, M. et al. (2021). Direct utilization of industrial carbon dioxide with low impurities for acetate production via microbial electrosynthesis. *Bioresource Technology*, *320*, 124289. https://doi.org/10.1016/j.biortech.2020.124289

- Roy, M. et al. (2024). Brewery CO_2 conversion into acetic acid at an optimized set of microbial electrosynthesis process parameters. *Journal of Environmental Chemical Engineering*, *12*(6), 114436. https://doi.org/10.1016/j.jece.2024.114436

- Ruiz-Fernández, P. et al. (2020). Autotrophic carbon fixation pathways along the redox gradient in oxygen-depleted oceanic waters. *Environmental microbiology reports*, *12*(3), 334-341. https://doi.org/10.1111/1758-2229.12837

- Saji, V. S. (2019). Progress in rust converters. *Progress in Organic Coatings*, *127*, 88-99. https://doi.org/10.1016/j.porgcoat.2018.11.013

- Salkuyeh, Y. K. et al. (2017). Techno-economic analysis and life cycle assessment of hydrogen production from natural gas using current and emerging technologies. *International Journal of hydrogen energy*, *42*(30), 18894-18909. https://doi.org/10.1016/j.ijhydene.2017.05.219

- Samanides, C. G. et al. (2020). Methanogenesis inhibition in anaerobic granular sludge for the generation of volatile fatty acids from CO_2 and zero valent iron. *Frontiers in Energy Research*, *8*, 37. https://doi.org/10.3389/fenrg.2020.00037

- Samanides, C. G., & Vyrides, I. (2023). CO_2 conversion to volatile fatty acids by anaerobic granular sludge and Mg0. *Biochemical Engineering Journal*, *191*, 108799. https://doi.org/10.1016/j.bej.2022.108799

- Sarangi, P. K., & Nanda, S. (2020). Biohydrogen production through dark fermentation. *Chemical Engineering & Technology*, *43*(4), 601-612. https://doi.org/10.1002/ceat.201900452

- Sarkar, O. et al. (2020). Salinity induced acidogenic fermentation of food waste regulates biohydrogen production and volatile fatty acids profile. *Fuel*, *276*, 117794. https://doi.org/10.1016/j.fuel.2020.117794

- Schink, B. (1994). Diversity, ecology, and isolation of acetogenic bacteria. In: *Acetogenesis* (pp. 197-235). Boston, MA: Springer US. https://doi.org/10.1007/978-1-4615-1777-1_7

- Schmidt, A. et al. (2018). Development of a production chain from vegetable biowaste to platform chemicals. *Microbial cell factories*, *17*, 1-12. https://doi.org/10.1186/s12934-018-0937-4

- Schoelmerich, M. C., & Müller, V. (2019). Energy conservation by a hydrogenase-dependent chemiosmotic mechanism in an ancient metabolic pathway. *Proceedings of the National Academy of Sciences*, *116*(13), 6329-6334. https://doi.org/10.1073/pnas.1818580116

- Schuchmann, K., & Müller, V. (2016). Energetics and application of heterotrophy in acetogenic bacteria. *Applied and environmental microbiology*, *82*(14), 4056-4069. https://doi.org/10.1128/AEM.00882-16

- Senatore, E. V. et al. (2021). Effects of pre-filmed $FeCO_3$ on flow-induced corrosion and erosion-corrosion in the absence and presence of corrosion inhibitor at 60° C. *Wear*, *480*, 203927. https://doi.org/10.1016/j.wear.2021.203927

- Serna-García, R. et al. (2023). Unraveling prevalence of homoacetogenesis and methanogenesis pathways due to inhibitors addition. *Bioresource Technology*, *376*, 128922. https://doi.org/10.1016/j.biortech.2023.128922

- Shrestha, S. et al. (2023). Competitive reactions during ethanol chain elongation were temporarily suppressed by increasing hydrogen partial pressure through methanogenesis inhibition. *Environmental Science & Technology*, *57*(8), 3369-3379. https://doi.org/10.1021/acs.est.2c09014

- Sibhat, M. et al. (2024). Advancement in sodium carbonation pathways for sustainable carbon capture and utilization: A review. *Results in Engineering*, 102536. https://doi.org/10.1016/j.rineng.2024.102536

- Sierra, J. D. M. et al. (2019). Comparative performance of upflow anaerobic sludge blanket reactor and anaerobic membrane bioreactor treating phenolic wastewater: Overcoming high salinity. *Chemical engineering journal*, *366*, 480-490. https://doi.org/10.1016/j.cej.2019.02.097

- Simankova, M. V. et al. (2000). *Acetobacterium tundrae* sp. nov., a new psychrophilic acetogenic bacterium from tundra soil. *Archives of Microbiology*, 174, 440-447. https://doi.org/10.1007/s002030000229

- Singh, A. et al. (2023). Syntrophic entanglements for propionate and acetate oxidation under thermophilic and high-ammonia conditions. *The ISME Journal*, *17*(11), 1966-1978. https://doi.org/10.1038/s41396-023-01504-y

- Singh, N. K., & Singh, R. (2021). Modeling and statistical analysis of heat-shocked sulfate-reducers and methanogens rich consortiums for hydrogen and methane production in a bio-electrochemical cell. *International Journal of Hydrogen Energy*, *46*(51), 25819-25831. https://doi.org/10.1016/j.ijhydene.2021.05.097

- Song, G. L., & Atrens, A. (2023). Recently deepened insights regarding Mg corrosion and advanced engineering applications of Mg alloys. *Journal of Magnesium and Alloys*. https://doi.org/10.1016/j.jma.2023.08.012

- Soosaiprakasam, I. R., & Veawab, A. (2008). Corrosion and polarization behavior of carbon steel in MEA-based CO_2 capture process. *International journal of greenhouse gas control*, *2*(4), 553-562. https://doi.org/10.1016/j.ijggc.2008.02.009

- Sorokin, D. Y. et al. (2016). Syntrophic associations from hypersaline soda lakes converting organic acids and alcohols to methane at extremely haloalkaline conditions. *Environmental microbiology*, *18*(9), 3189-3202. https://doi.org/10.1111/1462-2920.13448

- Staley, B. F. et al. (2011). Effect of spatial differences in microbial activity, pH, and substrate levels on methanogenesis initiation in refuse. *Applied and environmental microbiology*, *77*(7), 2381-2391. https://doi.org/10.1128/AEM.02349-10

- Stams, A. J., & Plugge, C. M. (2009). Electron transfer in syntrophic communities of anaerobic bacteria and archaea. *Nature Reviews Microbiology*, *7*(8), 568-577. https://doi.org/10.1038/nrmicro2166

- Stefaniuk, M. et al. (2016). Review on nano zerovalent iron (nZVI): from synthesis to environmental applications. *Chemical Engineering Journal*, *287*, 618-632. https://doi.org/10.1016/j.cej.2015.11.046

- Steinfeld, A. (2002). Solar hydrogen production via a two-step water-splitting thermochemical cycle based on Zn/ZnO redox reactions. *International journal of hydrogen energy*, *27*(6), 611-619. https://doi.org/10.1016/S0360-3199(01)00177-X

- Sun, W. et al. (2009). The effect of temperature and ionic strength on iron carbonate ($FeCO_3$) solubility limit. *Corrosion Science*, *51*(6), 1273-1276. https://doi.org/10.1016/j.corsci.2009.03.009

- Sun, Y. et al. (2016). The influences of iron characteristics, operating conditions and solution chemistry on contaminants removal by zero-valent iron: A review. *Water Research*, *100*, 277-295. https://doi.org/10.1016/j.watres.2016.05.031

- Sun, Y. et al. (2018). Tailoring magnesium based materials for hydrogen storage through synthesis: Current state of the art. *Energy Storage Materials*, *10*, 168-198. https://doi.org/10.1016/j.ensm.2017.01.010

- Sun, Y. P. et al. (2006). Characterization of zero-valent iron nanoparticles. *Advances in colloid and interface science*, *120*(1-3), 47-56. https://doi.org/10.1016/j.cis.2006.03.001

- Takors, R. et al. (2018). Using gas mixtures of CO, CO_2 and H_2 as microbial substrates: the do's and don'ts of successful technology transfer from laboratory to production scale. *Microbial Biotechnology*, *11*(4), 606-625. https://doi.org/10.1111/1751-7915.13270

- Tang, H. et al. (2021). Recent advances in nanoscale zero-valent iron-based materials: Characteristics, environmental remediation and challenges. *Journal of Cleaner Production*, *319*, 128641. https://doi.org/10.1016/j.jclepro.2021.128641

- Tang, R. et al. (2021). Response of anaerobic granular sludge to long-term loading of roxarsone: from macro-to micro-scale perspective. *Water Research*, *204*, 117599. https://doi.org/10.1016/j.watres.2021.117599

- Teramura, K. et al. (2017). Which is an intermediate species for photocatalytic conversion of CO_2 by H_2O as the electron donor: CO_2 molecule, carbonic acid, bicarbonate, or carbonate ions?. *The Journal of Physical Chemistry C*, *121*(16), 8711-8721. https://doi.org/10.1021/acs.jpcc.6b12809

- Tharak, A. et al. (2023). Chemolithoautotrophic reduction of CO_2 to acetic acid in gas and gas-electro fermentation systems: Enrichment, microbial dynamics, and sustainability assessment. *Chemical Engineering Journal*, *454*, 140200. https://doi.org/10.1016/j.cej.2022.140200

- Thiele, J. H., & Zeikus, J. G. (1988). Control of interspecies electron flow during anaerobic digestion: significance of formate transfer versus hydrogen transfer during syntrophic methanogenesis in flocs. *Applied and environmental microbiology*, *54*(1), 20-29. https://doi.org/10.1128/aem.54.1.20-29.1988

- Tirunehe, G., & Norddahl, B. (2016). The influence of polymeric membrane gas spargers on hydrodynamics and mass transfer in bubble column bioreactors. *Bioprocess and biosystems engineering*, *39*, 613-626. https://doi.org/10.1007/s00449-016-1543-7

- Tosca, N. J. et al. (2019). Products of the iron cycle on the early Earth. *Free Radical Biology and Medicine*, *140*, 138-153. https://doi.org/10.1016/j.freeradbiomed.2019.05.005

- Tsapekos, P. et al. (2022). H_2 competition between homoacetogenic bacteria and methanogenic archaea during biomethanation from a combined experimental-modelling approach. *Journal of Environmental Chemical Engineering*, *10*(2), 107281. https://doi.org/10.1016/j.jece.2022.107281

- Tsapekos, P. et al. (2022). Lab-and pilot-scale anaerobic digestion of municipal bio-waste and potential of digestate for biogas upgrading sustained by microbial analysis. *Renewable Energy*, *201*, 344-353. https://doi.org/10.1016/j.renene.2022.10.116

- Uddin, M. M., & Wright, M. M. (2023). Anaerobic digestion fundamentals, challenges, and technological advances. *Physical Sciences Reviews*, *8*(9), 2819-2837. https://doi.org/10.1515/psr-2021-0068

- Valgepea, K. et al. (2017). Maintenance of ATP homeostasis triggers metabolic shifts in gas-fermenting acetogens. *Cell systems*, *4*(5), 505-515. https://doi.org/10.1016/j.cels.2017.04.008

- Van Beek, C. G. E. M. et al. (2021). Concentration of iron (II) in fresh groundwater controlled by siderite, field evidence. *Aquatic Geochemistry*, *27*(1), 49-61. https://doi.org/10.1007/s10498-020-09390-y

- Van Steendam, C. et al. (2019). Improving anaerobic digestion via direct interspecies electron transfer requires development of suitable characterization methods. *Current opinion in biotechnology*, *57*, 183-190. https://doi.org/10.1016/j.copbio.2019.03.018

- Velimirovic, M. et al. (2014). Corrosion rate estimations of microscale zerovalent iron particles via direct hydrogen production measurements. *Journal of Hazardous Materials*, *270*, 18-26. https://doi.org/10.1016/j.jhazmat.2014.01.034

- Voolapalli, R. K., & Stuckey, D. C. (2001). Hydrogen production in anaerobic reactors during shock loads—influence of formate production and H_2 kinetics. *Water Research*, *35*(7), 1831-1841. https://doi.org/10.1016/S0043-1354(00)00441-3

- Vyrides, I. et al. (2018). CO_2 conversion to CH_4 using Zero Valent Iron (ZVI) and anaerobic granular sludge: Optimum batch conditions and microbial pathways. *Journal of CO_2 Utilization*, *27*, 415-422. https://doi.org/10.1016/j.jcou.2018.08.023

- Vyrides, I., & Stuckey, D. C. (2009). Adaptation of anaerobic biomass to saline conditions: Role of compatible solutes and extracellular polysaccharides. *Enzyme and Microbial Technology*, *44*(1), 46-51. https://doi.org/10.1016/j.enzmictec.2008.09.008

- Wang, B. et al. (2021). Transition from pits to stress corrosion cracking of SAE 4120 steel in simulated oilfield environment. *International Journal Of Electrochemical Science*, *16*(2), 21026. https://doi.org/10.20964/2021.02.25

- Wang, C. et al. (2022). Response of methanogenic granules enhanced by magnetite to ammonia stress. *Water Research*, *212*, 118123. https://doi.org/10.1016/j.watres.2022.118123

- Wang, D. et al. (2017). Enhanced treatment of Fischer–Tropsch (FT) wastewater by novel anaerobic biofilm system with scrap zero valent iron (SZVI) assisted. *Biochemical engineering journal*, *117*, 66-76. https://doi.org/10.1016/j.bej.2016.09.012

- Wang, G. et al. (2020). Enhancing microbial electrosynthesis of acetate and butyrate from CO_2 reduction involving engineered Clostridium ljungdahlii with a nickel-phosphide-modified electrode. *Energy & Fuels*, *34*(7), 8666-8675. https://doi.org/10.1021/acs.energyfuels.0c01710

- Wang, R. et al. (2021). Deeper insights into effect of activated carbon and nano-zero-valent iron addition on acidogenesis and whole anaerobic digestion. *Bioresource Technology*, *324*, 124671. https://doi.org/10.1016/j.biortech.2021.124671

- Wang, X. et al. (2018). Evaluation of artificial neural network models for online monitoring of alkalinity in anaerobic co-digestion system. *Biochemical Engineering Journal*, *140*, 85-92. https://doi.org/10.1016/j.bej.2018.09.010

- Wang, Y. et al. (2018). Biomethanation of blast furnace gas using anaerobic granular sludge via addition of hydrogen. *RSC advances*, *8*(46), 26399-26406. https://doi.org/10.1039/c8ra04853c

- Wang, Y. Q. et al. (2021). Microbial community structure and co-occurrence are essential for methanogenesis and its contribution to phenanthrene degradation in paddy soil. *Journal of Hazardous Materials*, *417*, 126086. https://doi.org/10.1016/j.jhazmat.2021.126086

- Wang, Z. et al. (2021). Accelerating anaerobic digestion for methane production: Potential role of direct interspecies electron transfer. *Renewable and Sustainable Energy Reviews*, *145*, 111069. https://doi.org/10.1016/j.rser.2021.111069

- Wang, Z. et al. (2024). Bioconversion of pure CO_2 to caproic acid with zero valent iron: Optimizing carbon flux distribution in co-cultures of Acetobacterium woodii and Megasphaera hexanoica. *Bioresource Technology*, *413*, 131480. https://doi.org/10.1016/j.biortech.2024.131480

- Weber, K. A. et al. (2006). Microorganisms pumping iron: anaerobic microbial iron oxidation and reduction. *Nature Reviews Microbiology*, *4*(10), 752-764. https://doi.org/10.1038/nrmicro1490

- Weng, N. et al. (2024). Catabolism and interactions of syntrophic propionate-and acetate oxidizing microorganisms under mesophilic, high-ammonia conditions. *Frontiers in Microbiology*, *15*, 1389257. https://doi.org/10.3389/fmicb.2024.1389257

- Westerholm, M. et al. (2022). Syntrophic propionate-oxidizing bacteria in methanogenic systems. *FEMS Microbiology Reviews*, *46*(2), fuab057. https://doi.org/10.1093/femsre/fuab057

- Wolf, S. et al. (2021). The European Green Deal—more than climate neutrality. *Intereconomics*, *56*, 99-107. https://doi.org/10.1007/s10272-021-0963-z

- Worm, P. et al. (2011). Growth-and substrate-dependent transcription of formate dehydrogenase and hydrogenase coding genes in Syntrophobacter fumaroxidans and Methanospirillum hungatei. *Microbiology*, *157*(1), 280-289. https://doi.org/10.1099/mic.0.043927-0

- Wu, C. et al. (2020). A quantitative lens on anaerobic life: leveraging the state-of-the-art fluxomics approach to explore clostridial metabolism. *Current opinion in biotechnology*, *64*, 47-54. https://doi.org/10.1016/j.copbio.2019.09.012

- Wu, P. et al. (2023). Deciphering the role and mechanism of nano zero-valent iron on medium chain fatty acids production from CO_2 via chain elongation in microbial electrosynthesis. *Science of The Total Environment*, *863*, 160898. https://doi.org/10.1016/j.scitotenv.2022.160898

- Wu, P. P. et al. (2021). Improvement of intelligent corrosivity-detection and corrosion-protection for reinforcing steel. *Corrosion Science*, *184*, 109396. https://doi.org/10.1016/j.corsci.2021.109396

- Wu, Y. et al. (2020). Conductive materials in anaerobic digestion: From mechanism to application. *Bioresource technology*, *298*, 122403. https://doi.org/10.1016/j.biortech.2019.122403

- Xiao, F. et al. (2024). Research progress in hydrogen production by hydrolysis of magnesium-based materials. *International Journal of Hydrogen Energy*, *49*, 696-718. https://doi.org/10.1016/j.ijhydene.2023.07.085

- Xiao, K. et al. (2021). Effect of concentrations of Fe^{2+} and Fe^{3+} on the corrosion behavior of carbon steel in Cl^- and SO_4^{2-} aqueous environments. *Metals and Materials International*, *27*, 2623-2633. https://doi.org/10.1007/s12540-019-00590-y

- Xiao, L. et al. (2018). Nano-Fe_3O_4 particles accelerating electromethanogenesis on an hour-long timescale in wetland soil. *Environmental Science: Nano*, *5*(2), 436-445. https://doi.org/10.1039/c7en00577f

- Xie, Z. et al. (2023). Power to biogas upgrading: Effects of different H_2/CO_2 ratios on products and microbial communities in anaerobic fermentation system. *Science of The Total Environment*, *865*, 161305. https://doi.org/10.1016/j.scitotenv.2022.161305

- Xu, K. et al. (2010). Effect of classic methanogenic inhibitors on the quantity and diversity of archaeal community and the reductive homoacetogenic activity during the process of anaerobic sludge digestion. *Bioresource Technology*, *101*(8), 2600-2607. https://doi.org/10.1016/j.biortech.2009.10.059

- Xu, S. et al. (2021). On-site CO_2 bio-sequestration in anaerobic digestion: Current status and prospects. *Bioresource Technology*, *332*, 125037. https://doi.org/10.1016/j.biortech.2021.125037

- Xu, X. et al. (2022). The future of hydrogen energy: Bio-hydrogen production technology. *International Journal of Hydrogen Energy*, *47*(79), 33677-33698. https://doi.org/10.1016/j.ijhydene.2022.07.261

- Xu, Y. et al. (2017). Application of zero valent iron coupling with biological process for wastewater treatment: a review. *Reviews in Environmental Science and Bio/Technology*, *16*, 667-693. https://doi.org/10.1007/s11157-017-9445-y

- Yang, C. et al. (2021). Engineering acetogens for biofuel production: from cellular biology to process improvement. *Renewable and Sustainable Energy Reviews*, *151*, 111563. https://doi.org/10.1016/j.rser.2021.111563

- Yang, D. et al. (2019). Functionalization of citric acid-based carbon dots by imidazole toward novel green corrosion inhibitor for carbon steel. *Journal of Cleaner Production*, *229*, 180-192. https://doi.org/10.1016/j.jclepro.2019.05.030

- Yang, H. Y. et al. (2021). Mixed-culture biocathodes for acetate production from CO_2 reduction in the microbial electrosynthesis: Impact of temperature. *Science of the Total Environment*, *790*, 148128. https://doi.org/10.1016/j.scitotenv.2021.148128

- Yang, J. et al. (2024). Ammonia inhibition in anaerobic digestion of organic waste: a review. *International Journal of Environmental Science and Technology*, 1-16. https://doi.org/10.1007/s13762-024-06029-1

- Yang, Y. et al. (2018). Simultaneous removal of nitrate and phosphate from wastewater by siderite based autotrophic denitrification. *Chemosphere*, *199*, 130-137. https://doi.org/10.1016/j.chemosphere.2018.02.014

- Ye, W. et al. (2021). The effects and mechanisms of zero-valent iron on anaerobic digestion of solid waste: A mini-review. *Journal of Cleaner Production*, *278*, 123567. https://doi.org/10.1016/j.jclepro.2020.123567

- Yin, Y. & Wang, J. (2019). Enhanced biohydrogen production from macroalgae by zero-valent iron nanoparticles: Insights into microbial and metabolites distribution. *Bioresource technology*, *282*, 110-117. https://doi.org/10.1016/j.biortech.2019.02.128

- Yin, Y. et al. (2022). Deeper insight into the effect of salinity on the relationship of enzymatic activity, microbial community and key metabolic pathway during the anaerobic digestion of high strength organic wastewater. *Bioresource Technology*, *363*, 127978. https://doi.org/10.1016/j.biortech.2022.127978

- Yoo, M. et al. (2013). Carbon dioxide capture capacity of sodium hydroxide aqueous solution. *Journal of environmental management*, *114*, 512-519. https://doi.org/10.1016/j.jenvman.2012.10.061

- Younas, M. et al. (2022). An overview of hydrogen production: current status, potential, and challenges. *Fuel*, *316*, 123317. https://doi.org/10.1016/j.fuel.2022.123317

- Yu, M. et al. (2021). Insights into low-carbon hydrogen production methods: Green, blue and aqua hydrogen. *International Journal of Hydrogen Energy*, *46*(41), 21261-21273. https://doi.org/10.1016/j.ijhydene.2021.04.016

- Zabranska, J., & Pokorna, D. (2018). Bioconversion of carbon dioxide to methane using hydrogen and hydrogenotrophic methanogens. *Biotechnology advances*, *36*(3), 707-720. https://doi.org/10.1016/j.biotechadv.2017.12.003

- Zeb, I. et al. (2019). Kinetic and microbial analysis of methane production from dairy wastewater anaerobic digester under ammonia and salinity stresses. *Journal of Cleaner Production*, *219*, 797-808. https://doi.org/10.1016/j.jclepro.2019.01.295

- Zhang, A. et al. (2022). Treatment of fracturing wastewater by anaerobic granular sludge: The short-term effect of salinity and its mechanism. *Bioresource Technology*, *345*, 126538. https://doi.org/10.1016/j.biortech.2021.126538

- Zhang, B. et al. (2021). Progress and prospects of hydrogen production: Opportunities and challenges. *Journal of Electronic Science and Technology*, *19*(2), 100080. https://doi.org/10.1016/J.JNLEST.2021.100080

- Zhang, C. et al. (2022). Microbial utilization of next-generation feedstocks for the biomanufacturing of value-added chemicals and food ingredients. *Frontiers in Bioengineering and Biotechnology*, *10*, 874612. https://doi.org/10.3389/fbioe.2022.874612

- Zhang, F. et al. (2016). The survey of key technologies in hydrogen energy storage. *International journal of hydrogen energy*, *41*(33), 14535-14552. https://doi.org/10.1016/j.ijhydene.2016.05.293

- Zhang, J. et al. (2020). Adaptation to salinity: Response of biogas production and microbial communities in anaerobic digestion of kitchen waste to salinity stress. *Journal of bioscience and bioengineering*, *130*(2), 173-178. https://doi.org/10.1016/j.jbiosc.2019.11.011

- Zhang, J. et al. (2020). The bio-chemical cycle of iron and the function induced by ZVI addition in anaerobic digestion: A review. *Water Research*, *186*, 116405. https://doi.org/10.1016/j.watres.2020.116405

- Zhang, M., & Zang, L. (2019). A review of interspecies electron transfer in anaerobic digestion. In *IOP Conference Series: Earth and Environmental Science* (Vol. 310, No. 4, p. 042026). IOP Publishing. https://doi.org/10.1088/1755-1315/310/4/042026

- Zhang, W. et al. (2019). No difference in inhibition among free acids of acetate, propionate and butyrate on hydrogenotrophic methanogen of Methanobacterium formicicum. *Bioresource technology*, *294*, 122237. https://doi.org/10.1016/j.biortech.2019.122237

- Zhang, Y. et al. (2023). Syntrophy mechanism, microbial population, and process optimization for volatile fatty acids metabolism in anaerobic digestion. *Chemical Engineering Journal*, *452*, 139137. https://doi.org/10.1016/j.cej.2022.139137

- Zhao, W. et al. (2021). A review of biochar in anaerobic digestion to improve biogas production: performances, mechanisms and economic assessments. *Bioresource Technology*, *341*, 125797. https://doi.org/10.1016/j.biortech.2021.125797

- Zhen, G. et al. (2015). Influence of zero valent scrap iron (ZVSI) supply on methane production from waste activated sludge. *Chemical Engineering Journal*, *263*, 461-470. https://doi.org/10.1016/j.cej.2014.11.003

- Zhong, Y. et al. (2022). Effects of different particle size of zero-valent iron (ZVI) during anaerobic digestion: performance and mechanism from genetic level. *Chemical Engineering Journal*, *435*, 134977. https://doi.org/10.1016/j.cej.2022.134977

- Zhou, J. et al. (2020). Enhancement of methanogenic activity in anaerobic digestion of high solids sludge by nano zero-valent iron. *Science of the Total Environment*, *703*, 135532. https://doi.org/10.1016/j.scitotenv.2019.135532

- Zhou, L. et al. (2022). Increasing the electron selectivity of nanoscale zero-valent iron in environmental remediation: a review. *Journal of hazardous materials*, *421*, 126709. https://doi.org/10.1016/j.jhazmat.2021.126709

- Zhou, L. et al. (2024). Simultaneous Biogas Upgrading and Valuable Chemical Production Using Homoacetogens in a Membrane Biofilm Reactor. *Environmental Science & Technology*, *58*(28), 12509-12519. https://doi.org/10.1021/acs.est.4c02021

- Zhu, J. et al. (2024). Role of bicarbonate in CO_2 corrosion of carbon steel. *Electrochimica Acta, 478*, 143818. https://doi.org/10.1016/j.electacta.2024.143818

- Zhu, X. et al. (2020). Siderite as a novel reductant for clean utilization of refractory iron ore. *Journal of Cleaner Production*, *245*, 118704. https://doi.org/10.1016/j.jclepro.2019.118704

- Zhu, Y. et al. (2020). Dual roles of zero-valent iron in dry anaerobic digestion: enhancing interspecies hydrogen transfer and direct interspecies electron transfer. *Waste Management*, *118*, 481-490. https://doi.org/10.1016/j.wasman.2020.09.005

- Zinder, S. H. et al. (1984). Selective inhibition by 2-bromoethanesulfonate of methanogenesis from acetate in a thermophilic anaerobic digestor. *Applied and Environmental Microbiology*, *47*(6), 1343-1345. https://doi.org/10.1128/aem.47.6.1343-1345.1984

- Zosel, J. et al. (2011). The measurement of dissolved and gaseous carbon dioxide concentration. *Measurement Science and Technology*, *22*(7), 072001. https://doi.org/10.1088/0957-0233/22/7/072001

- Zupančič, G. D. et al. (2023). Salinity inhibition in thermophilic anaerobic digestion of organic waste. *Applied Sciences*, *13*(11), 6590. https://doi.org/10.3390/app13116590

APPENDIX

App. 1: Supplementary Information Figures

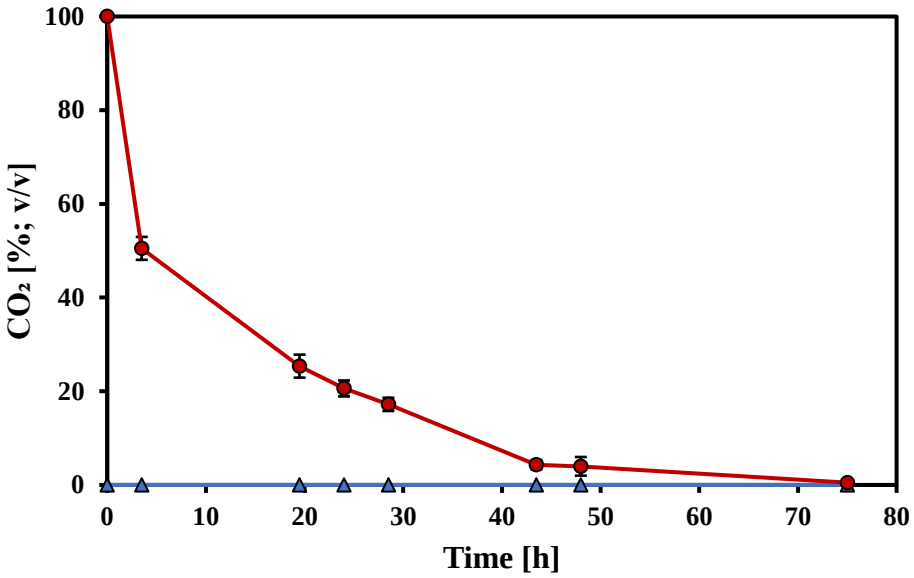

Suppl. Info. Fig. 3.1: CO_2 utilization over time in a system with deionized water and 25 gr L^{-1} of Fe^0.

: N_2-enriched system; : CO_2-enriched system.

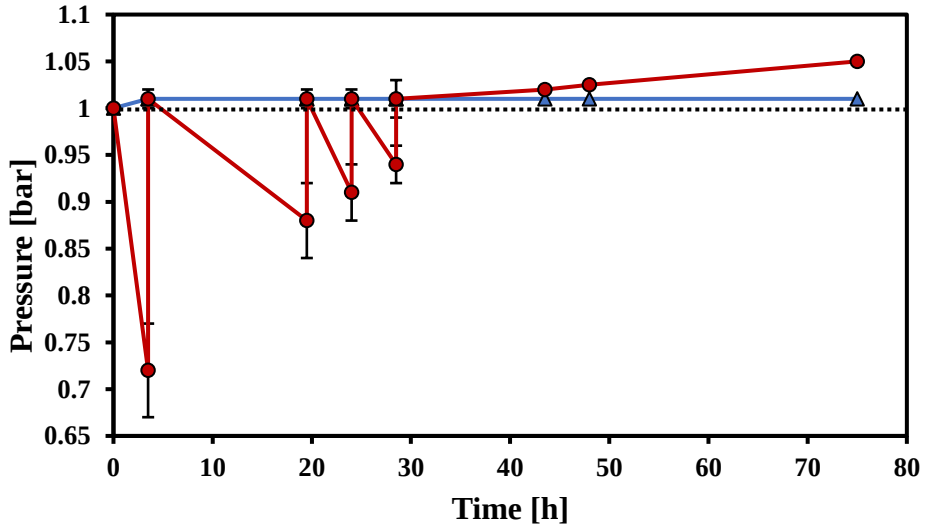

Suppl. Info. Fig. 3.2: The dynamic absolute pressure variations of the N_2-enriched and CO_2-enriched system over time (▪▪▪▪▪: Relative pressure – 0 bar).

: Fe^0-N_2 system; : Fe^0-CO_2 system.

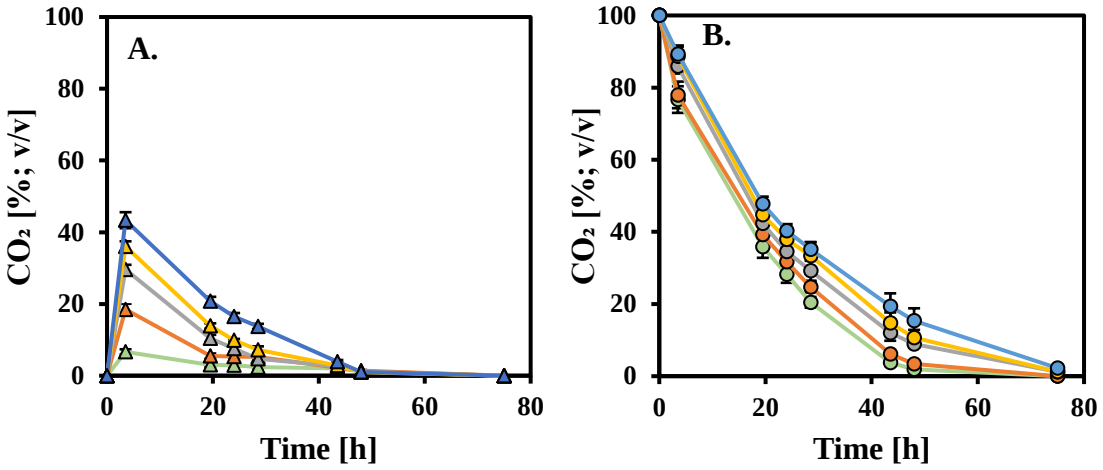

Suppl. Info. Fig. 3.3: The utilization of CO_2 over time in both **A.:** N_2-environment and **B.:** CO_2-environment under various concentrations of $NaHCO_3$.

: 2 g L^{-1} $NaHCO_3$; : 4 g L^{-1} $NaHCO_3$; : 6 g L^{-1} $NaHCO_3$;

: 8 g L^{-1} $NaHCO_3$; : 10 g L^{-1} $NaHCO_3$.

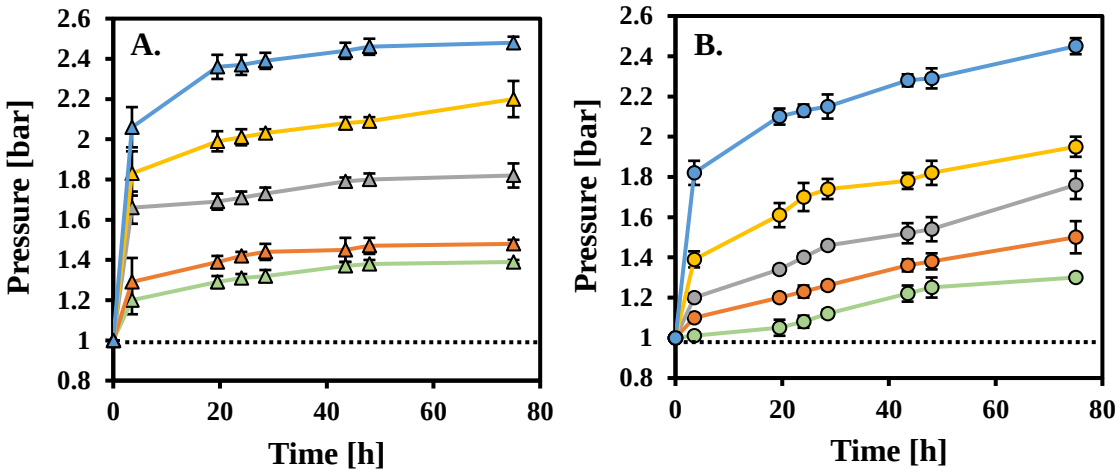

Suppl. Info. Fig. 3.4: The evolution of absolute pressure within the serum bottles over time in both **A.:** N_2-environment and **B.:** CO_2-environment (••••••: Relative pressure – 0 bar).

: 2 g L^{-1} $NaHCO_3$; : 4 g L^{-1} $NaHCO_3$; : 6 g L^{-1} $NaHCO_3$;

: 8 g L^{-1} $NaHCO_3$; : 10 g L^{-1} $NaHCO_3$.

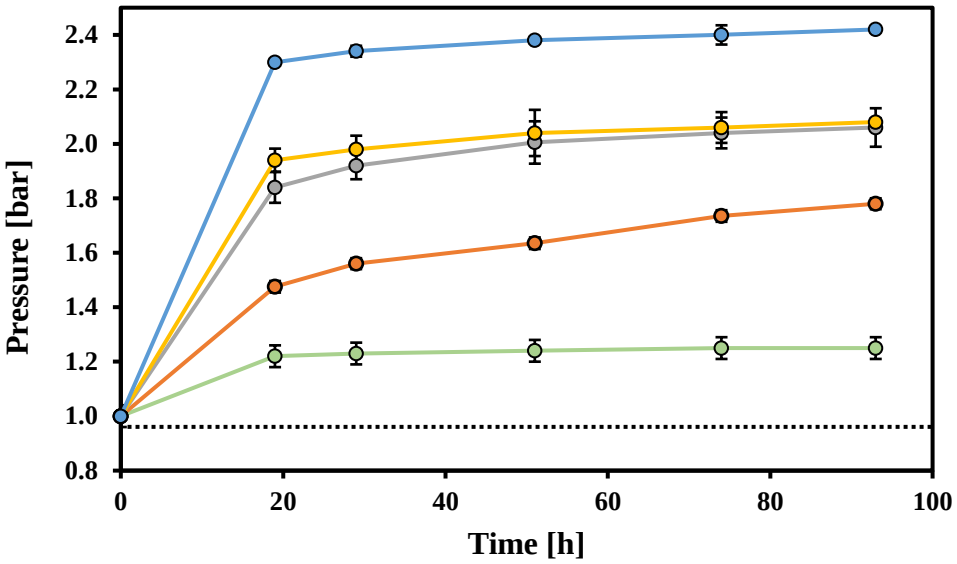

Suppl. Info. Fig. 3.5: The absolute pressure evolution within the serum bottles over time in sup-groups C1-C5 at various temperatures (..... : Relative pressure – 0 bar).

: 2 °C; : 20 °C; : 33 °C; : 40 °C; : 50 °C

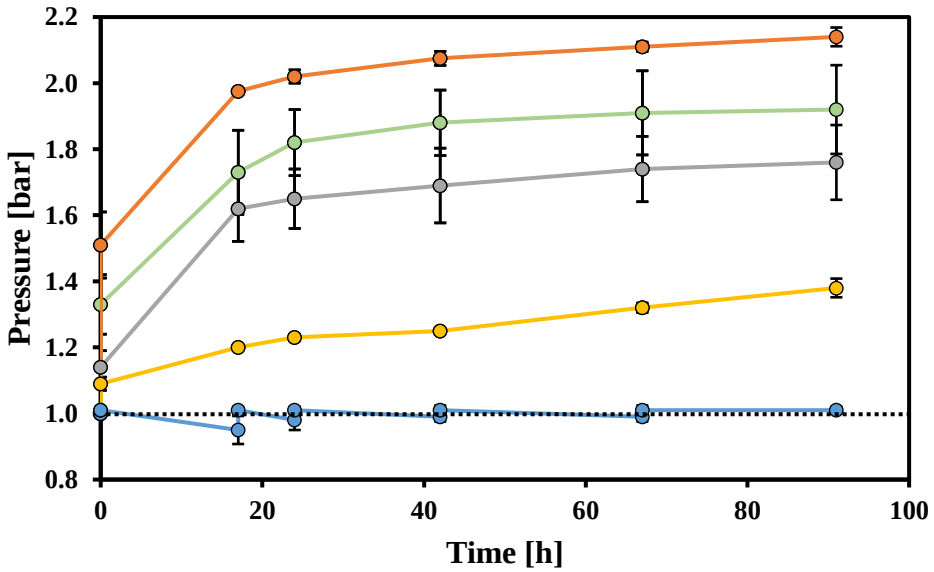

Suppl. Info. Fig. 3.6: The absolute pressure evolution within the serum bottles over time in sup-groups D1-D5 with varied initial pH settings (..... : Relative pressure – 0 bar).

: 4 pH; : 5 pH; : 6 pH; : 7 pH; : 8 pH

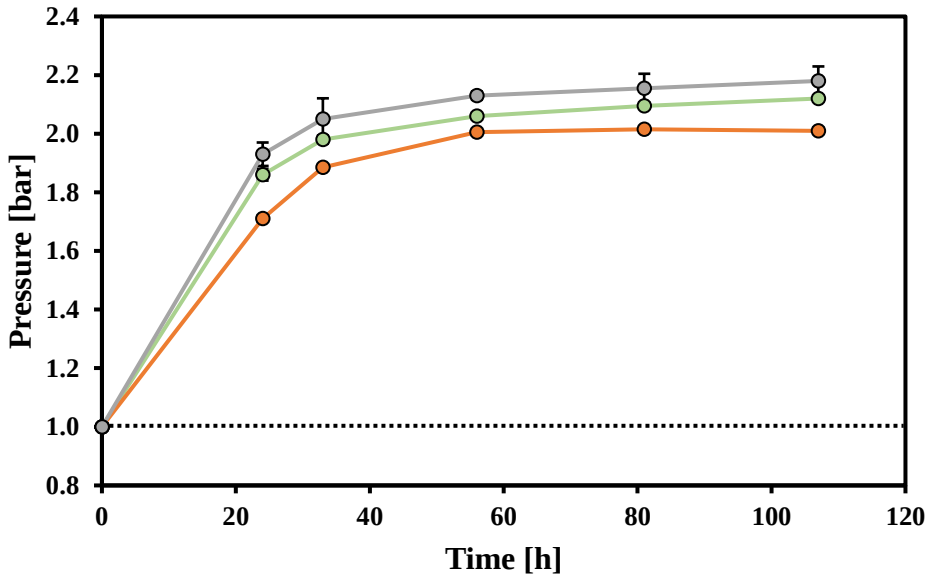

Suppl. Info. Fig. 3.7: The absolute pressure evolution within the serum bottles over time in sup-groups E1-E3, exposed to varied agitation speeds (•••••: Relative pressure – 0 bar).

: 0 rpm; : 100 rpm; : 200 rpm

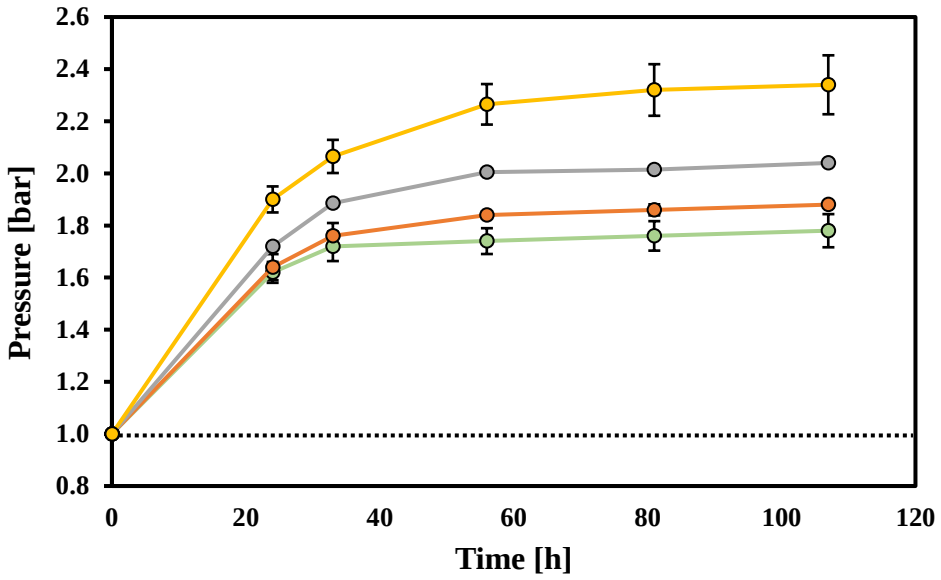

Suppl. Info. Fig. 3.8: Absolute pressure changes in serum bottles over time in Sub-groups F1-F4 with varied Fe^0 concentrations (•••••: Relative pressure – 0 bar).

:5 g L^{-1}; :10 g L^{-1}; :25 g L^{-1}; :50 g L^{-1}

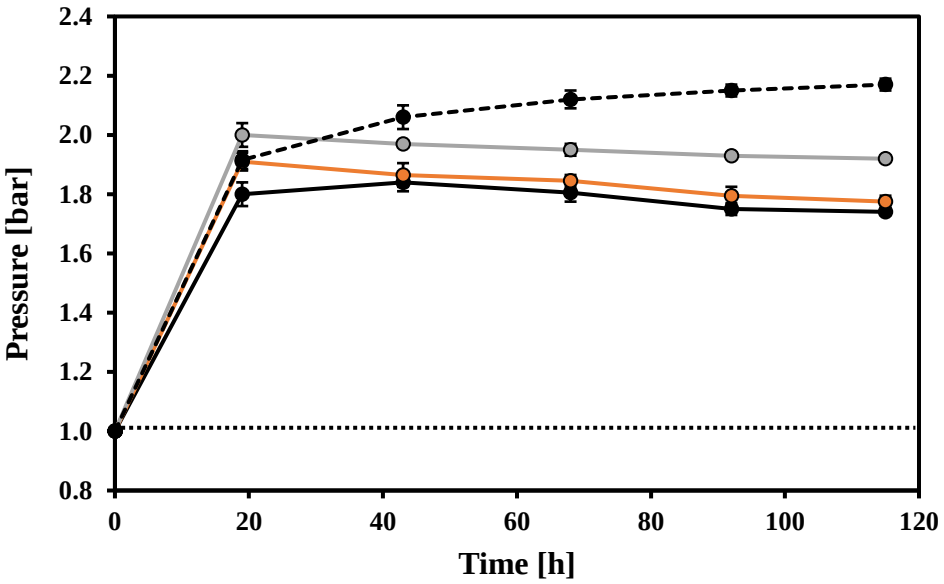

Suppl. Info. Fig. 3.9: Absolute pressure changes in serum bottles over time in Sub-groups G1-G3 (800 µm Fe^0) and G4 (10 µm Fe^0) (•••••: Relative pressure – 0 bar).

: 25 g L^{-1} – 800 µm Fe^0 (G1); : 25 g L^{-1} – 10 µm Fe^0 (Control – G4).

: 100 g L^{-1} – 800 µm Fe^0 (G2); : 200 g L^{-1} – 800 µm Fe^0 (G3).

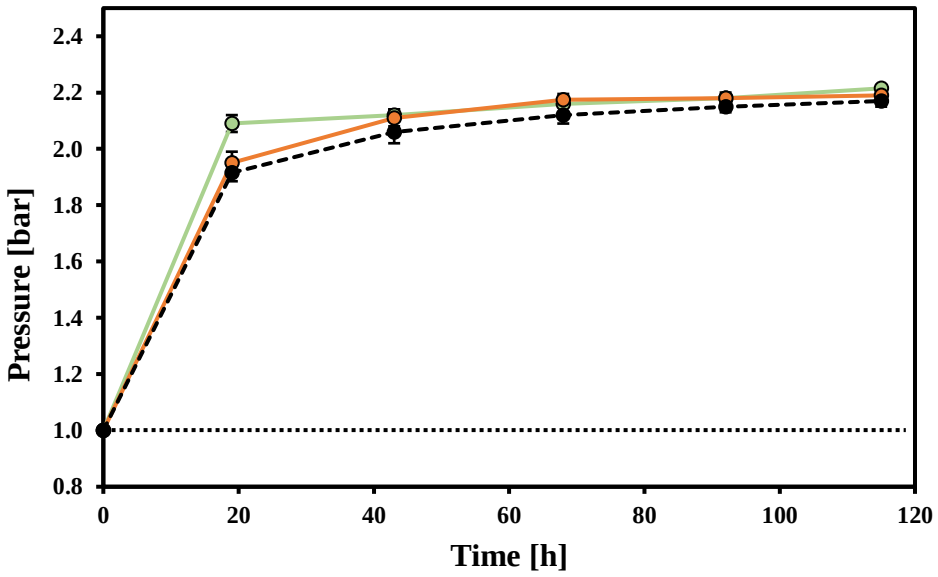

Fig. 3.10: Absolute pressure changes in serum bottles over time in sub-groups H1-H2 subjected to *in-situ* mechanical disruption and no disruption (H3) (••••• Relative pressure – 0 bar).

: Glass beats (145 g L^{-1}); : Boiling chips (145 g L^{-1}); : Control (no mechanical action).

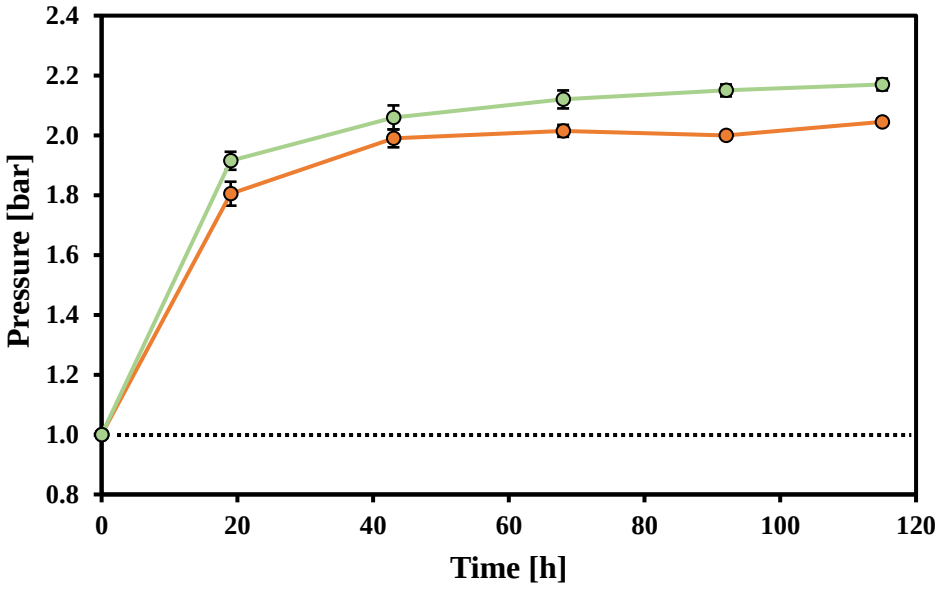

Fig. 3.11: Absolute pressure changes in serum bottles over time in sub-groups I1-I2 (••••• : Relative pressure – 0 bar).

: 28 cm^2 interface area; : 75 cm^2 interface area.

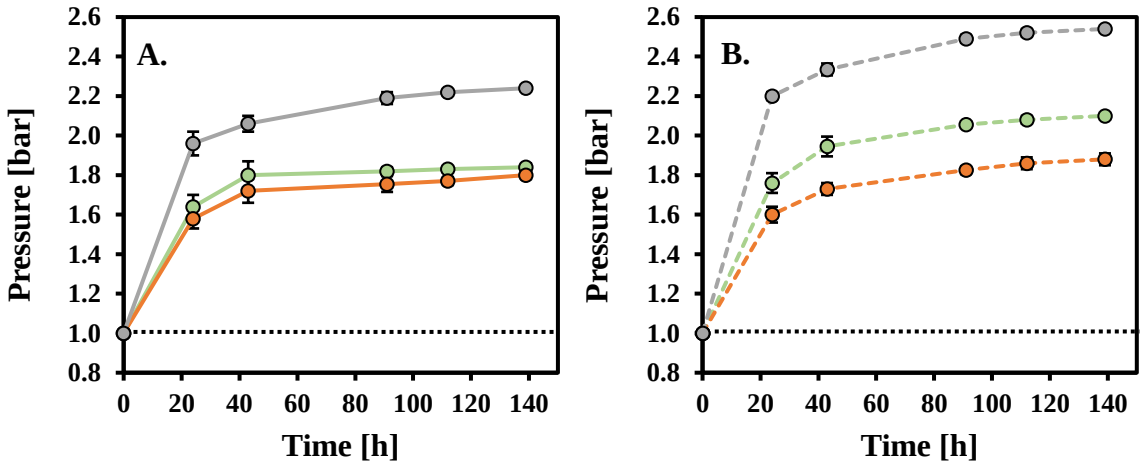

Suppl. Info. Fig. 3.12: Absolute pressure changes in serum bottles over time in systems exposed to various waste Fe^0 materials at two distinguished concentrations (••••• : Relative pressure – 0 bar).

A.: ▬ - $NaHCO_3$-CO_2 system using 25 g L^{-1} of waste Fe^0 (J1; J3; J5)

B.: ▬▬ - $NaHCO_3$-CO_2 system using 100 g L^{-1} of waste Fe^0 (J2; J4; J6)

: 0.05 mm^2; : 5 mm^2; : Steel wool

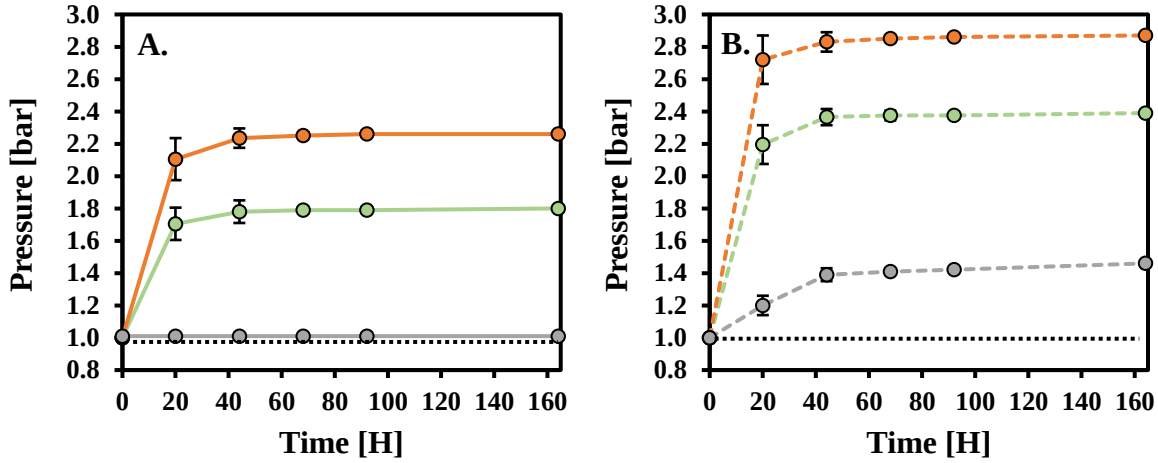

Suppl. Info. Fig. 3.13: Absolute pressure changes in serum bottles over time in systems exposed to various waste Fe^0 materials and NaOH solutions (•••••: Relative pressure – 0 bar).

A.: ▬ - NaOH-CO_2 system using 100 g L^{-1} waste Fe^0 (0.05 mm^2) (K1; K3; K5)

B.: ■■■ - NaOH-CO_2 system using 100 g L^{-1} waste Fe^0 (steel wool) (K2; K4; K6)

▭ : NaOH (0.25 M); ▭ : NaOH (0.75 M); ▭ : Water

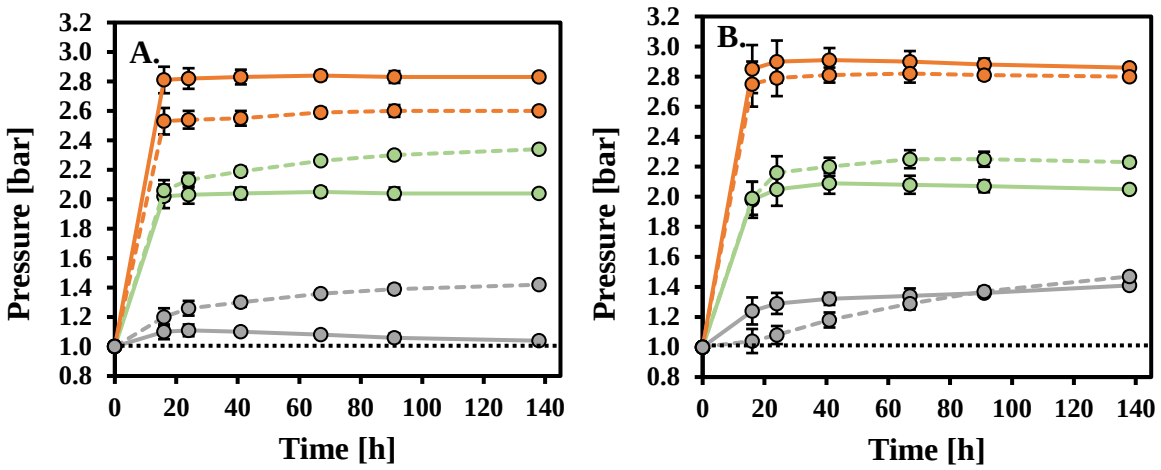

Suppl. Info. Fig. 3.14: Absolute pressure changes in serum bottles over time in systems where various untreated and pre-treated oxidized waste Fe^0 materials were exposed to different NaOH solutions for CO_2 capture (•••••: Relative pressure – 0 bar).

A.: Pressure of systems utilizing untreated oxidized waste Fe^0 materials (L1-L6)

B.: Pressure of systems utilizing pretreated oxidized waste Fe^0 materials (L7-L12)

▬ : 100 g L^{-1} oxidized waste Fe^0 (0.05 mm^2); ■■■ : 100 g L^{-1} oxidized waste Fe^0 (steel wool)

▭ : NaOH (0.25 M); ▭ : NaOH (0.75 M); ▭ : Water

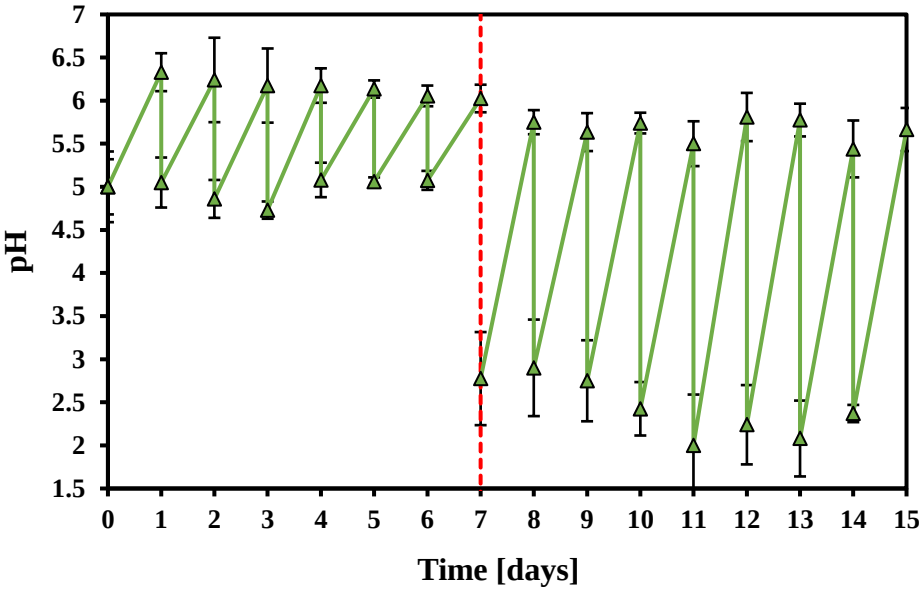

Suppl. Info. Fig. 3.15: pH adjustments and monitoring of the systems throughout the experimental period.

▪▪▪▪ : CO_2 gas purging.

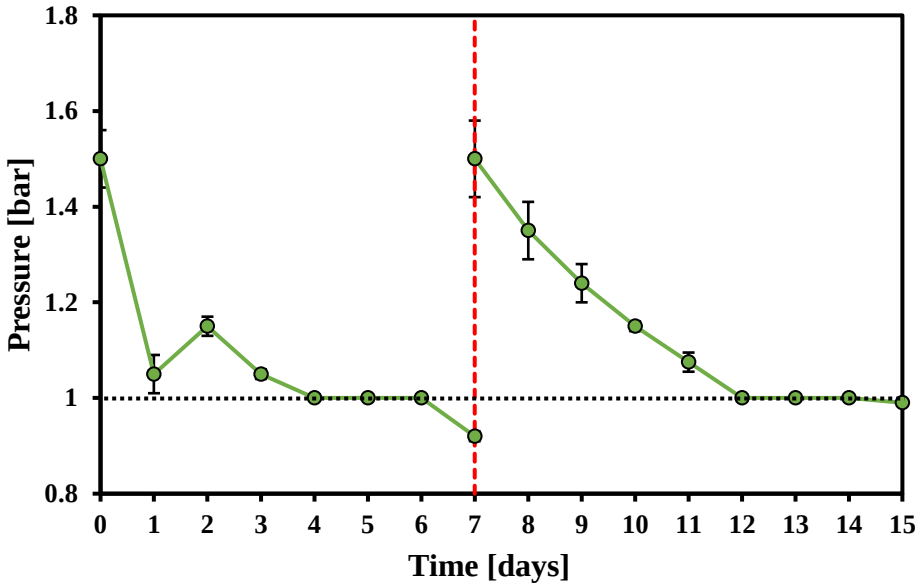

Suppl. Info. Fig. 3.16: Absolute pressure alterations in the systems throughout the experimental period. (▪▪▪▪▪: Relative pressure – 0 bar).

▪▪▪▪ : CO_2 gas purging.

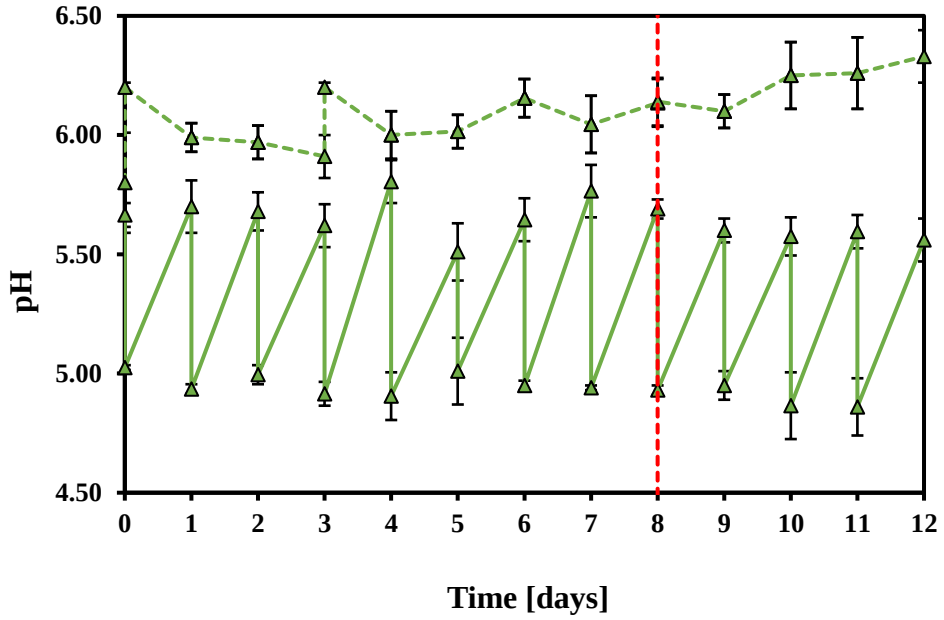

Suppl. Info. Fig. 3.17: pH adjustments and monitoring throughout the experimental period of the systems utilizing thermal pre-treated AnGrSL.

: Sub-group B1 operated at pH 5 – 6; : Sub-group B2 operated at pH 6 – 6,5.

: CO_2 gas purging.

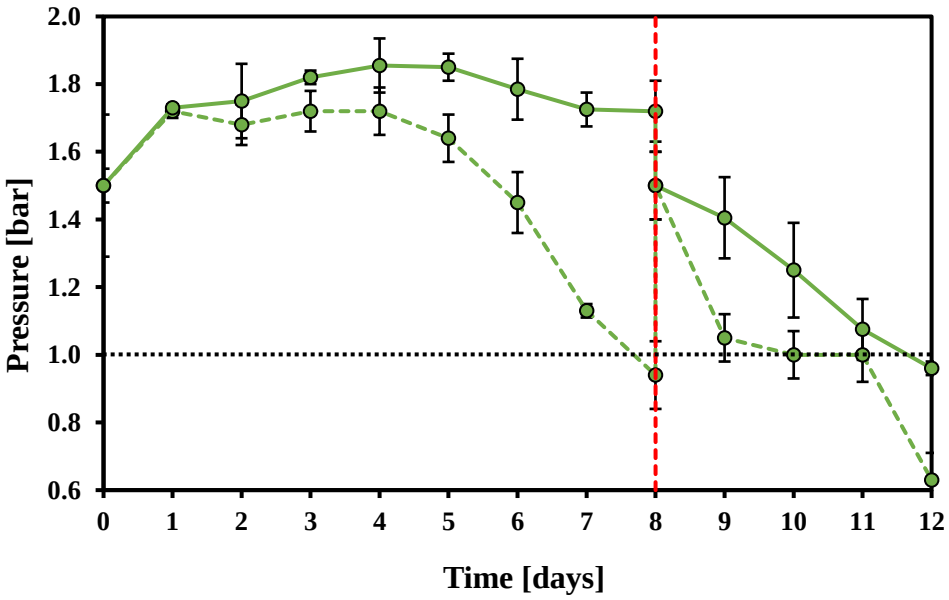

Suppl. Info. Fig. 3.18: Absolute pressure alterations throughout the experimental period systems utilizing thermal pre-treated AnGrSL. (••••• : Relative pressure – 0 bar).

: Sub-group B1 operated at pH 5 – 6; : Sub-group B2 operated at pH 6 – 6,5.

: CO_2 gas purging.

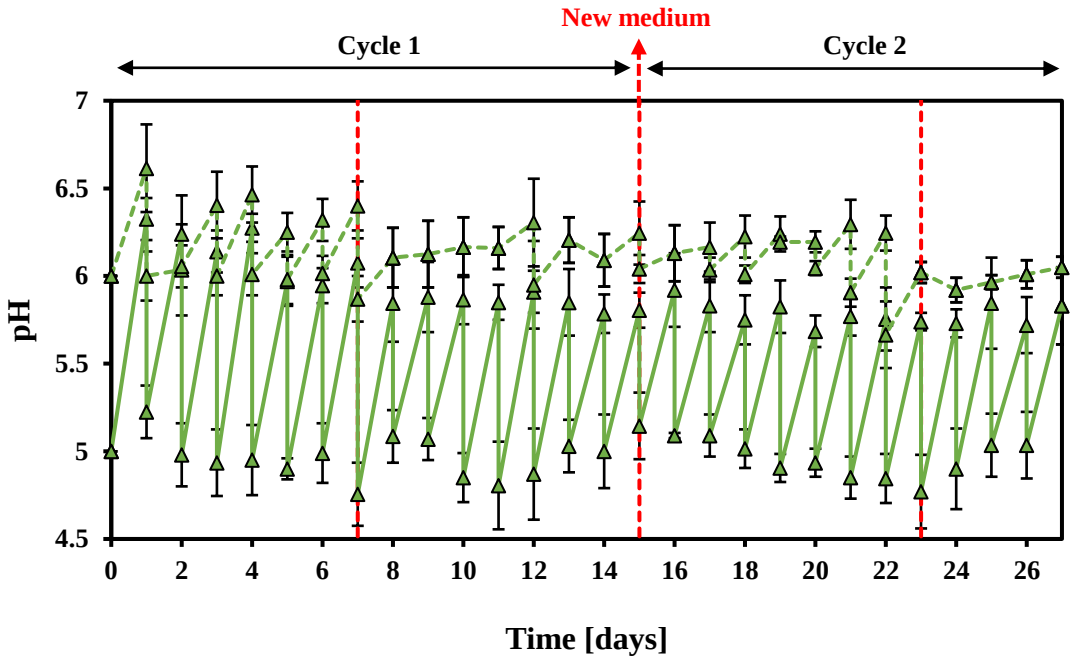

Suppl. Info. Fig. 3.19: pH adjustments and monitoring of the inhibited with 50 mM of BES systems throughout the experimental period.

▬ : Sub-group B1 operated at pH 5 – 6; ▬▬: Sub-group B2 operated at pH 6 – 6,5.

▪▪▪▪ : CO_2 gas purging.

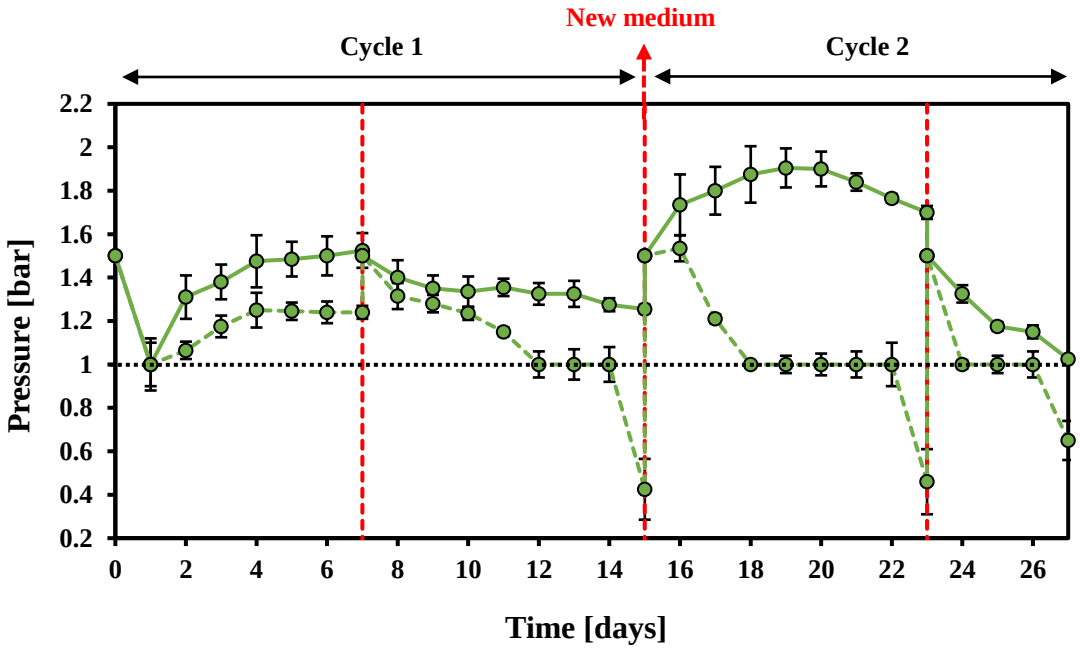

Suppl. Info. Fig. 3.20: Absolute pressure alterations in the inhibited with 50 mM of BES systems throughout the experimental period. (▪▪▪▪▪ : Relative pressure – 0 bar).

▬ : Sub-group B1 operated at pH 5 – 6; ▬▬: Sub-group B2 operated at pH 6 – 6,5.

▪▪▪▪ : CO_2 gas purging.

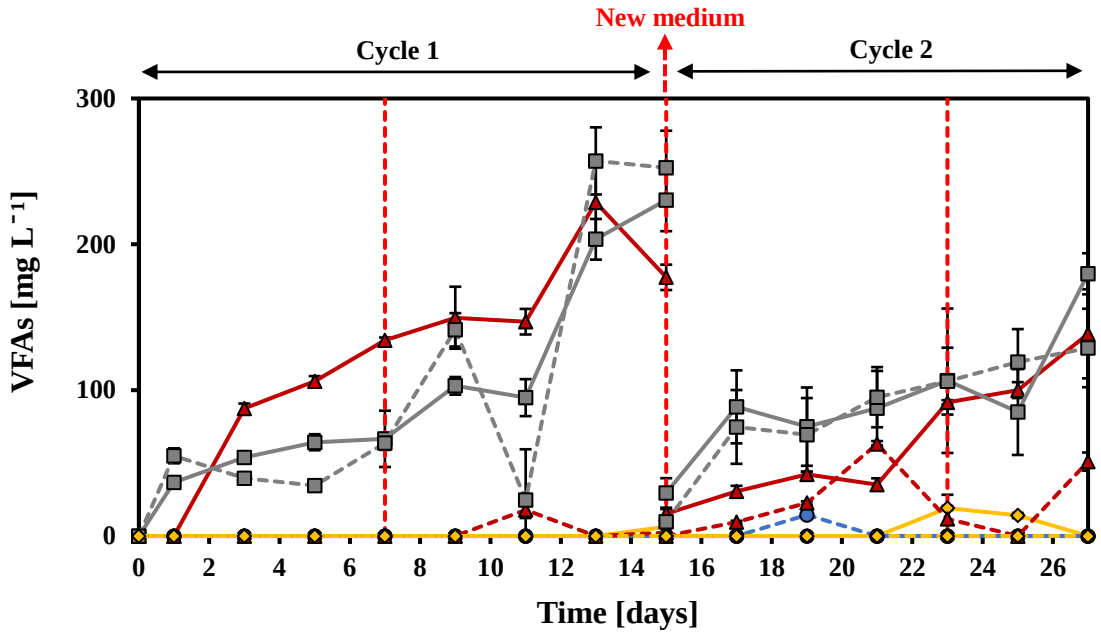

Suppl. Info. Fig. 3.21: VFAs productivity of the control systems where no ZVI (Fe^0) addition over time.

: Sub-group B1 operated at pH 5 – 6; : Sub-group B2 operated at pH 6 – 6,5.

: Formic acid; : Acetic acid; : Propionic acid; : Butyric acid.

: CO_2 gas purging.

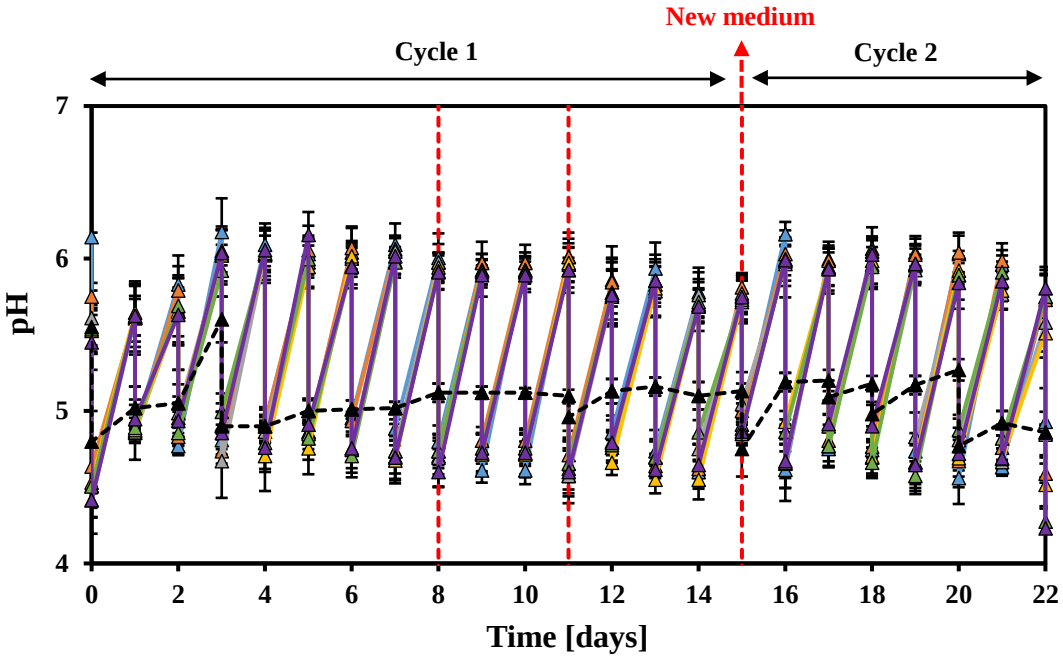

Suppl. Info. Fig. 3.22: pH adjustments and monitoring of the systems throughout the experimental period.

: 1 mM BES; : 2 mM BES; : 4 mM BES; : 6 mM BES; : 8 mM BES; : 10 mM BES; : Control; : CO_2 gas purging.

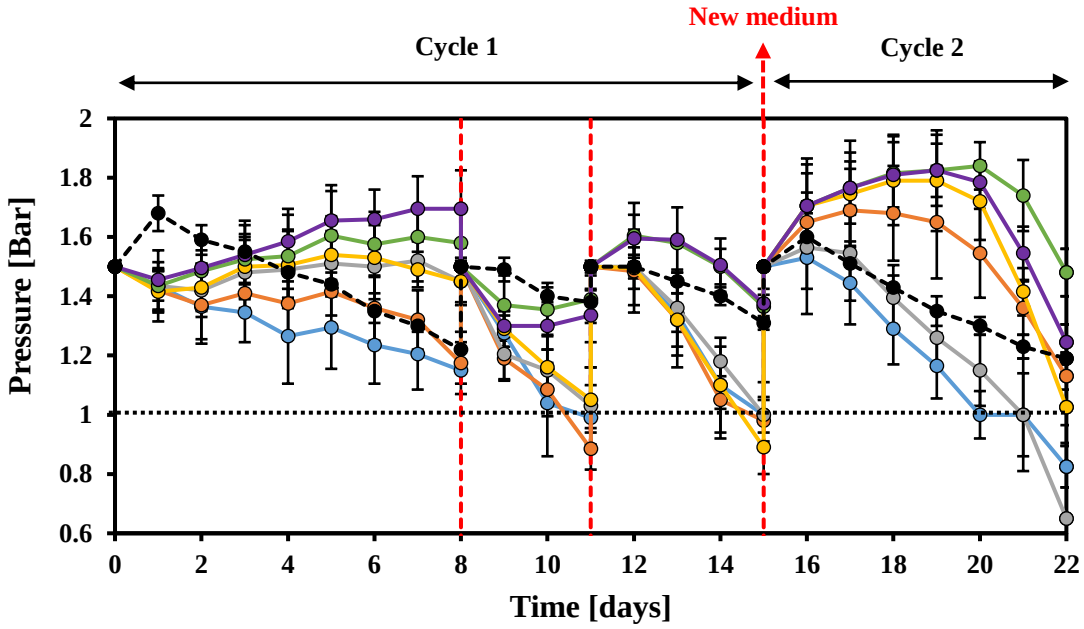

Suppl. Info. Fig. 3.23: Absolute pressure alterations in the systems throughout the experimental period. (••••••: Relative pressure – 0 bar).

: 1 mM BES; : 2 mM BES; : 4 mM BES; : 6 mM BES; : 8 mM BES; : 10 mM BES; : Control; : CO_2 gas purging.

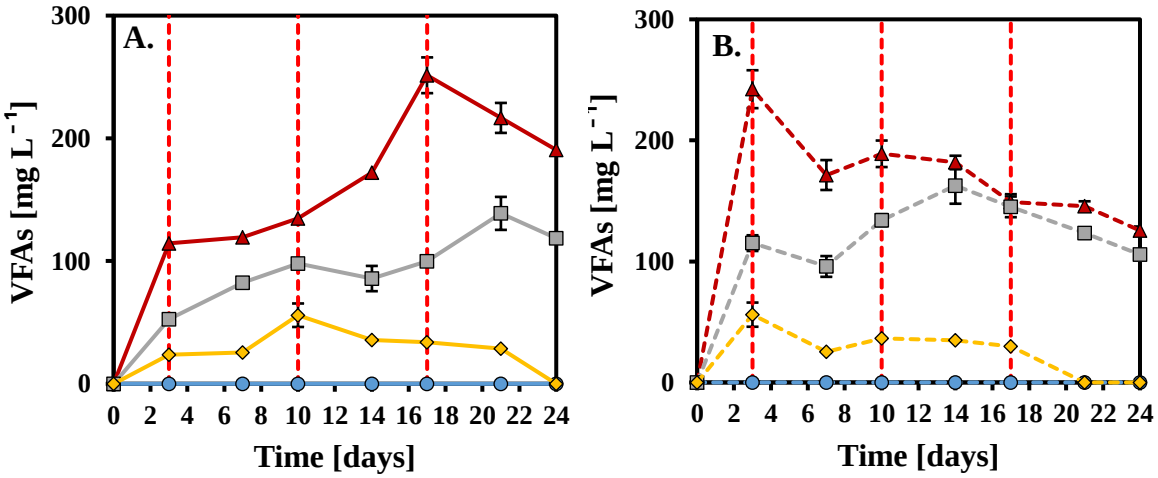

Suppl. Info. Fig. 3.24: VFAs production of the control systems where no ZVI (Fe^0) addition over time.

: 30 gr L^{-1} NaCl ; : 90 gr L^{-1} NaCl; : CO_2 gas purging.

: Formic acid; : Acetic acid; : Propionic acid; : Butyric acid.

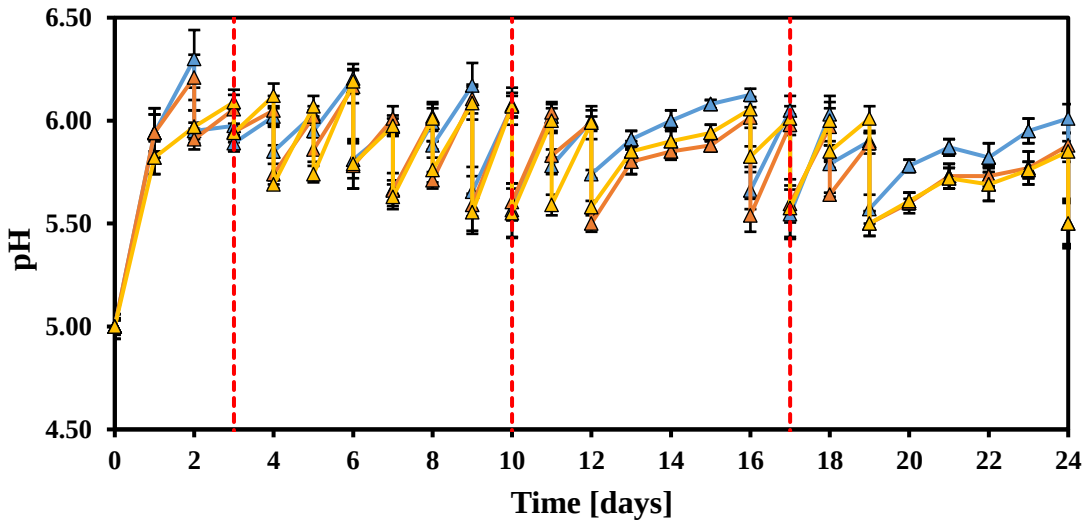

Suppl. Info. Fig. 3.25: pH adjustments and monitoring of the systems throughout the experimental period.

: 30 gr L^{-1} NaCl; : 60 gr L^{-1} NaCl; : 90 gr L^{-1} NaCl; : CO_2 gas purging.

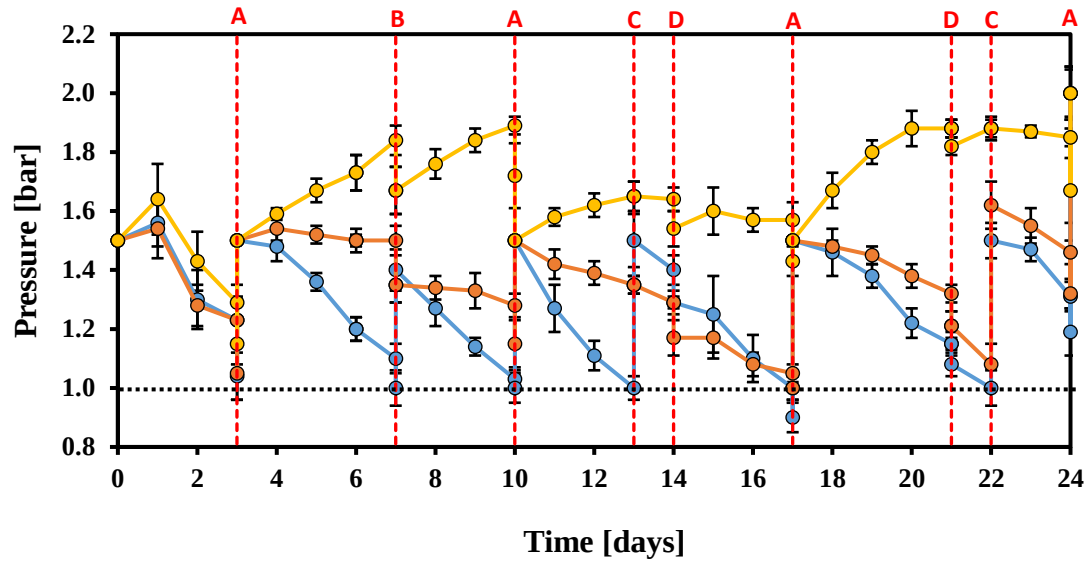

Suppl. Info. Fig. 3.26: Absolute pressure alterations in the systems throughout the experimental period. (••••• : Relative pressure – 0 bar).

A: - 4ml for VFAs analysis / Flash CO_2; B: - 4ml for VFAs analysis / Inert gas addition (N_2);

C: Inert gas addition (N_2); D: - 4ml for VFAs analysis.

: 30 gr L^{-1} NaCl; : 60 gr L^{-1} NaCl; : 90 gr L^{-1} NaCl.

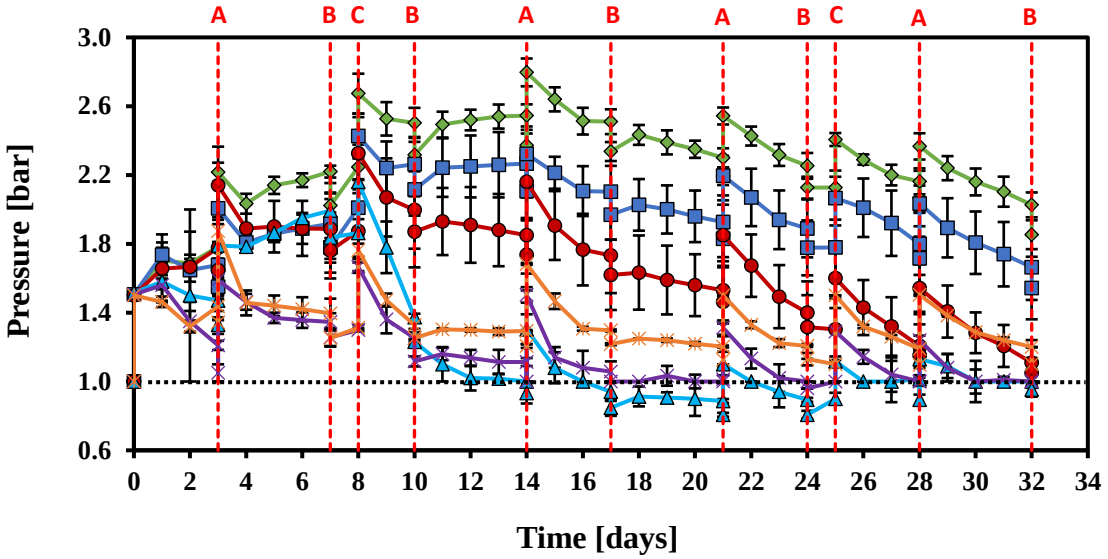

Suppl. Info. Fig. 3.27: Absolute pressure alterations in the systems throughout the experimental period. (▪▪▪▪▪: Relative pressure – 0 bar).

A: - 4ml for VFAs analysis / + 60 ml CO_2; **B:** - 4ml for VFAs analysis; **C:** + 60 ml CO_2

: 90 gr L^{-1} NaCl; : 70 gr L^{-1} NaCl; : 50 gr L^{-1} NaCl ; : Thermal inhibition; : 4mM BES; : CH_4 production system.

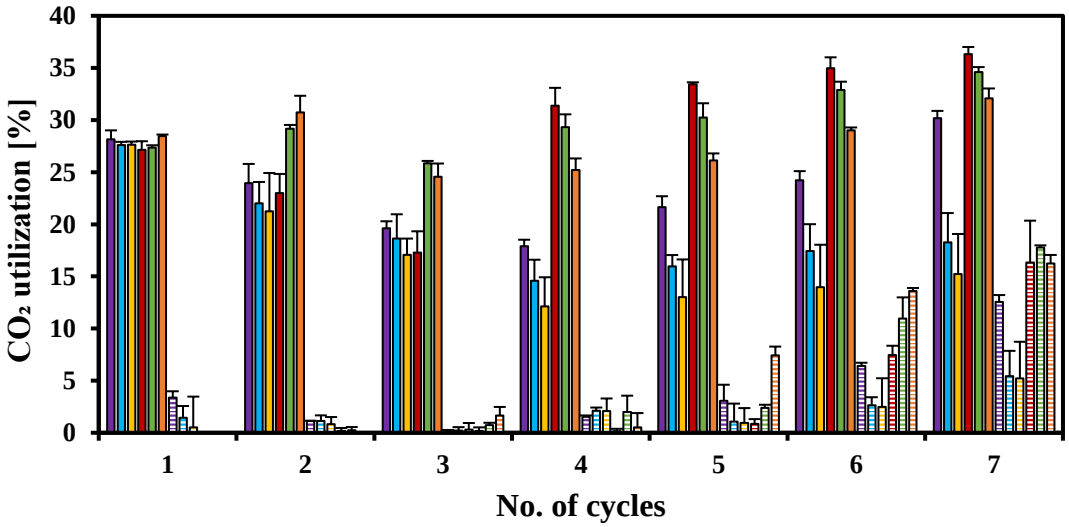

Suppl. Info. Fig. 3.28: The percentage of CO_2 injected and utilized in all systems during each cycle. : CO_2 injection; : CO_2 utilization.

: 90 gr L^{-1} NaCl; : 70 gr L^{-1} NaCl; : 50 gr L^{-1} NaCl; : Thermal inhibition; : 4mM BES; : CH_4 production system.

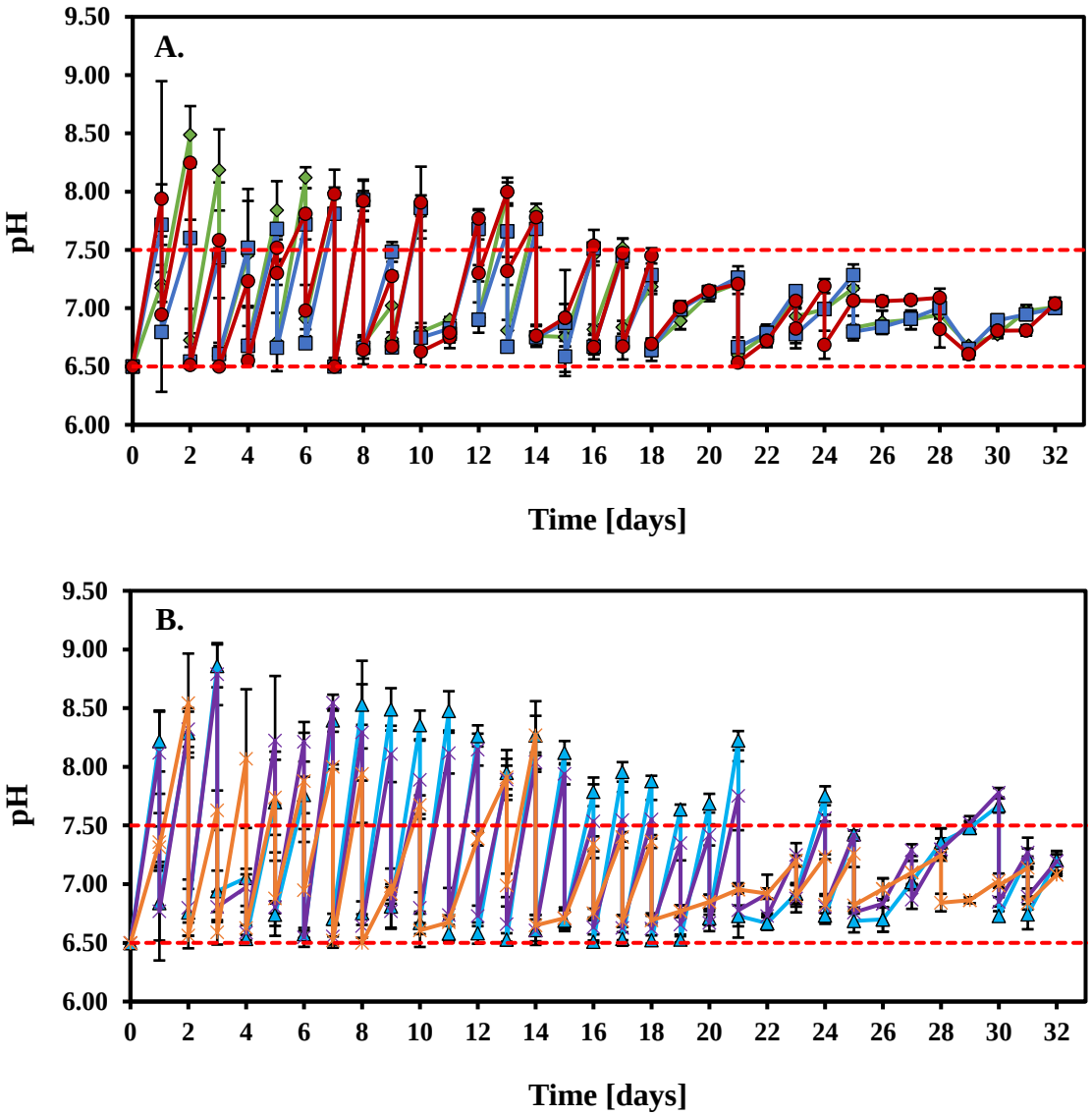

Suppl. Info. Fig. 3.29: pH fluctuations and adjustments between 6.5 and 7.5 for all systems over time.

: 90 gr L^{-1} NaCl; : 70 gr L^{-1} NaCl; : 50 gr L^{-1} NaCl ; : Thermal inhibition; : 4mM BES; : CH_4 production system.

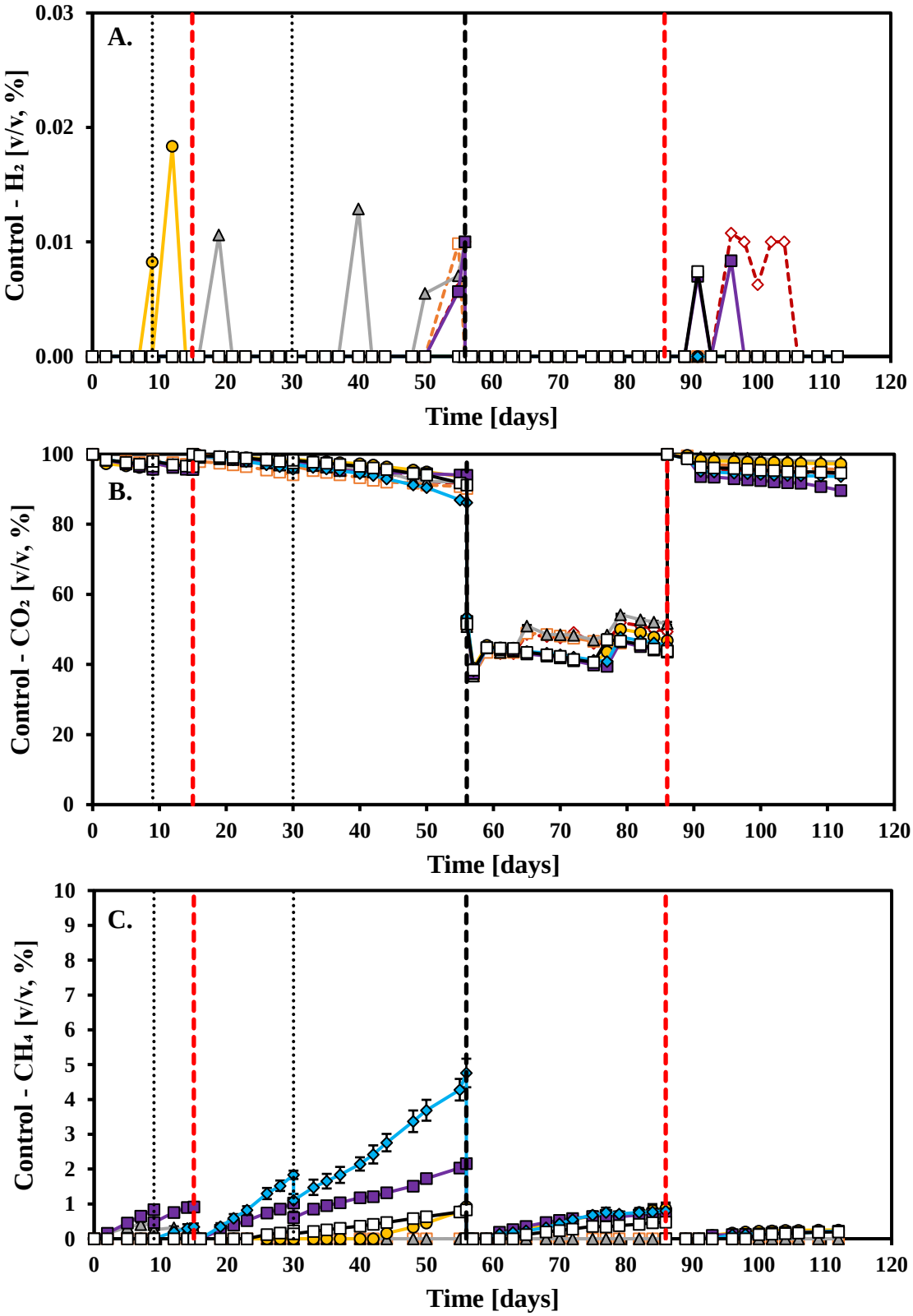

Suppl. Info. Fig. 3.30: Gas composition over time of all control systems. (A.) H_2 production by bacteria (B.) CO_2 utilization by the systems, and (C.) CH_4 productivity of the systems.

: River-SL; : Wetland-SL; : AnGr.-SL; : Comp.-SL; : Anaer.-SL; : Actv.-SL; : Dr.Cuts-SL; : CO_2 flashing / CO_2 feeding; : N_2 flashing / CO_2 feeding; : CO_2 feeding.

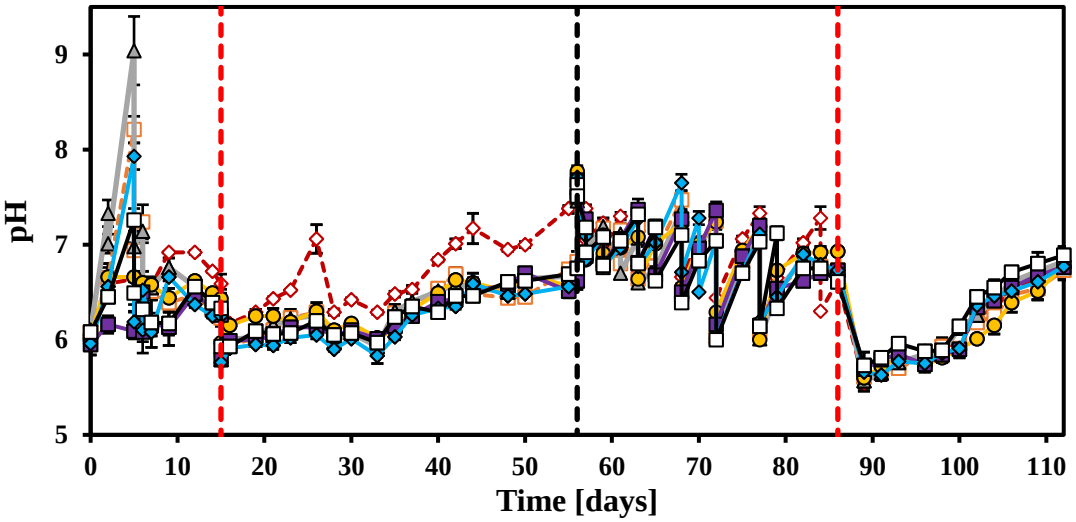

Suppl. Info. Fig. 3.31: pH fluctuations in systems exposed to various sludge inocula, over time.

: River-SL; : Wetland-SL; : AnGr.-SL; : Comp.-SL; : Anaer.-SL; : Actv.-SL; : Dr.Cuts-SL

CO_2 flashing / CO_2 feeding; : N_2 flashing / CO_2 feeding.

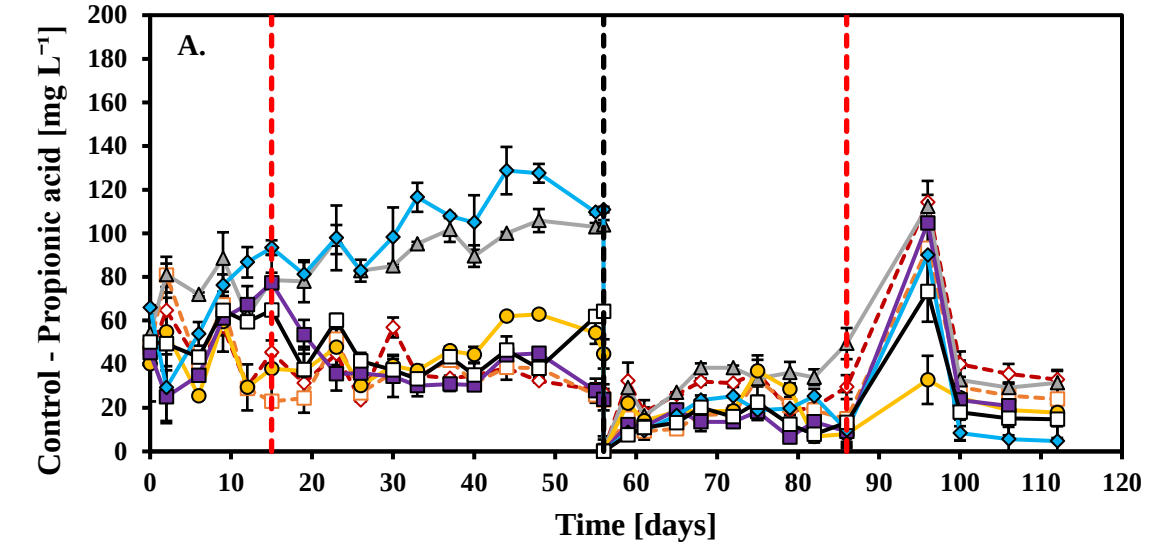
A.
Control - Propionic acid [mg L⁻¹]
Time [days]

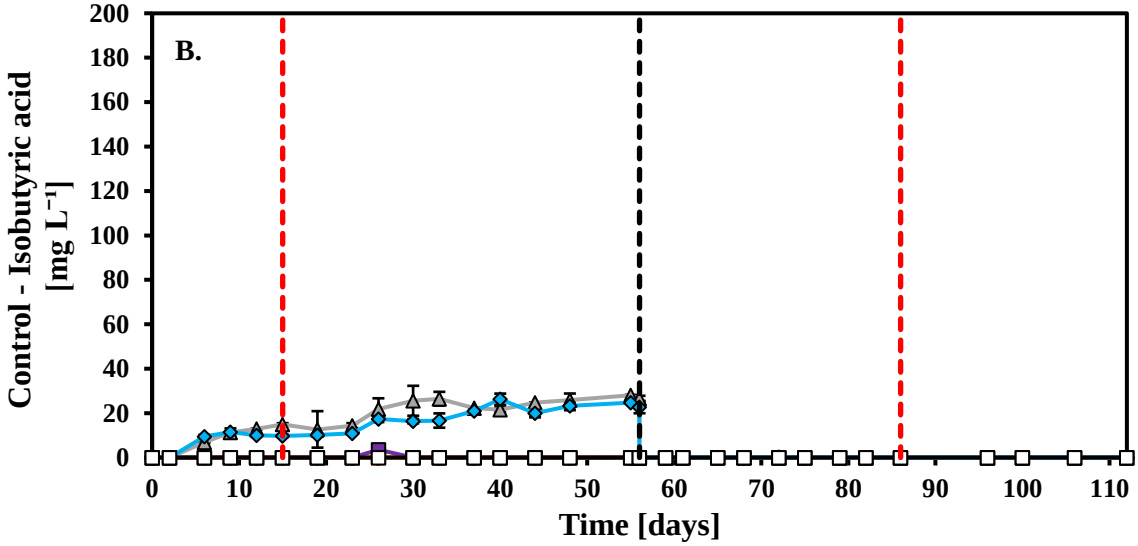
B.
Control - Isobutyric acid [mg L⁻¹]
Time [days]

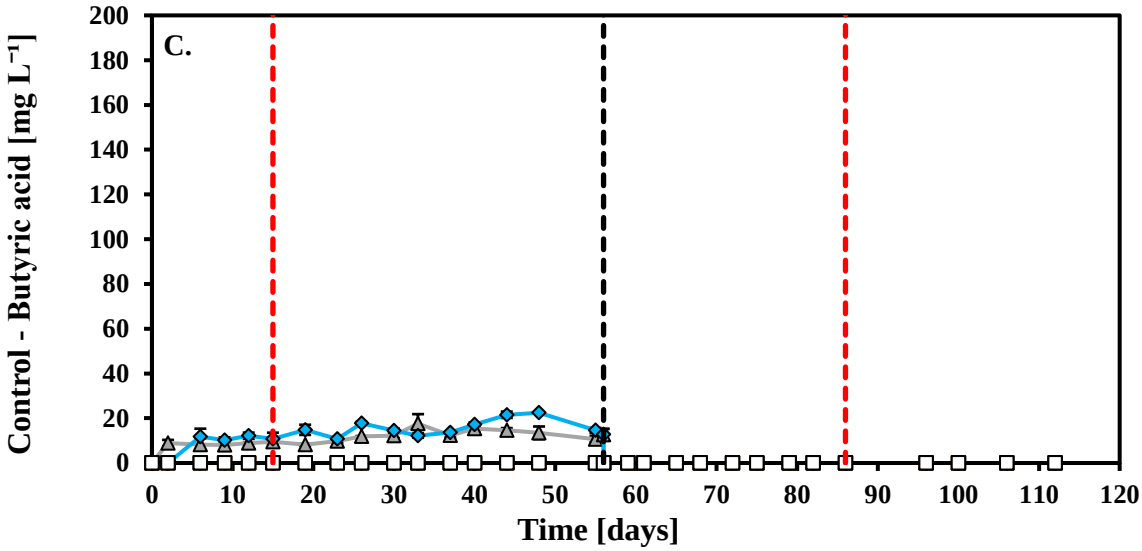
C.
Control - Butyric acid [mg L⁻¹]
Time [days]

Suppl. Info. Fig. 3.32: Accumulations of (A.) propionic, (B.) isobutyric, and (C.) butyric acid for all control systems without ZVI, over time.

: River-SL; : Wetland-SL; : AnGr.-SL; : Comp.-SL; : Anaer.-SL; : Actv.-SL; : Dr.Cuts-SL.

: CO_2 flashing / CO_2 feeding; : N_2 flashing / CO_2 feeding.

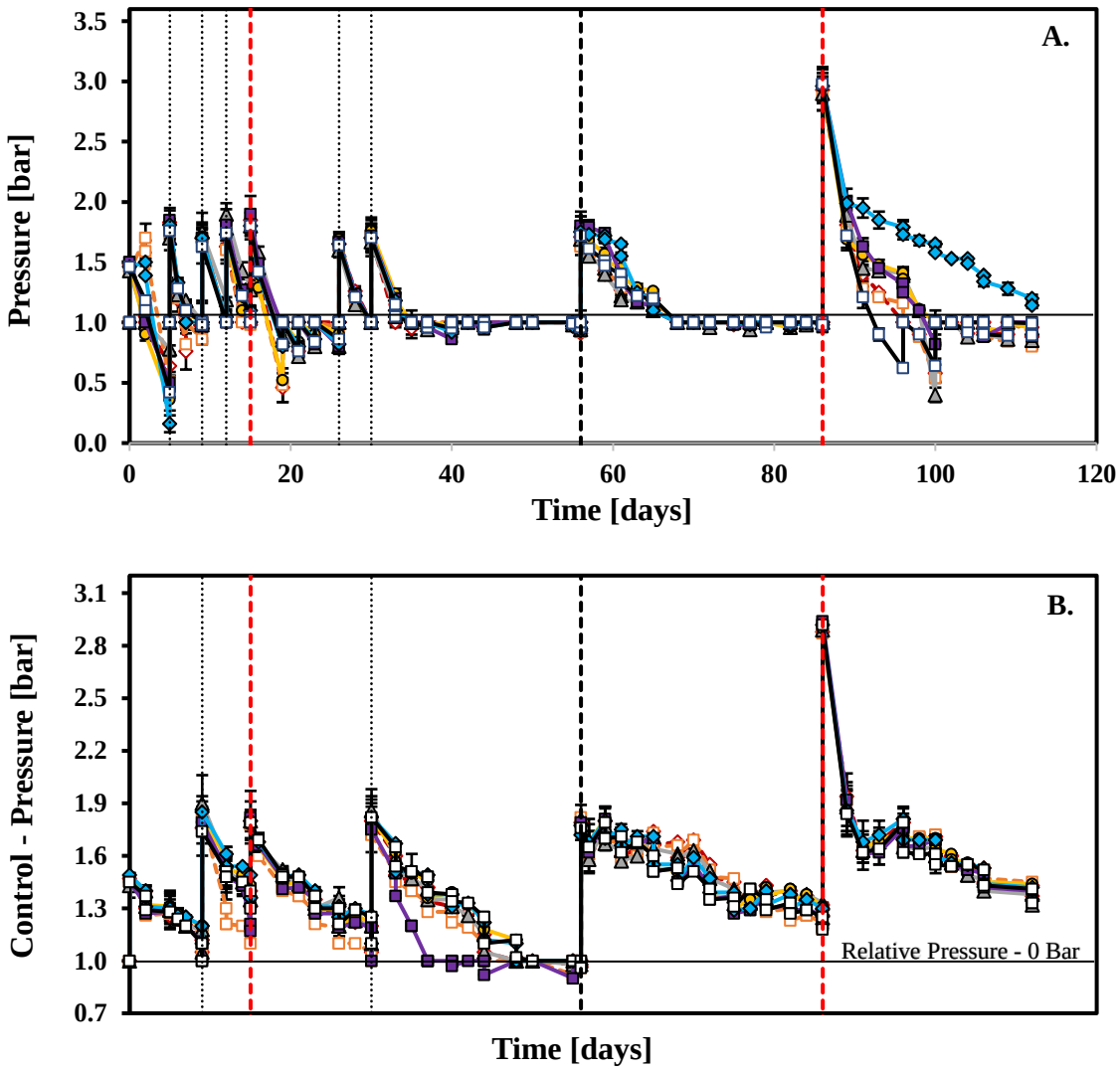

Suppl. Info. Fig. 3.33: Relative pressure alterations in (A.) experimental systems and (B.) control samples exposed to various sludge inocula over time.

: River-SL; : Wetland-SL; : AnGr.-SL; : Comp.-SL; : Anaer.-SL; : Actv.-SL; : Dr.Cuts-SL; : CO_2 flashing / CO_2 feeding; : N_2 flashing / CO_2 feeding; ····· : CO_2 feeding.